



University
of Glasgow

Torney, Clare (2011) *Mineral eyes : lessons from the natural world*.
PhD thesis.

<http://theses.gla.ac.uk/2331/>

Copyright and moral rights for this thesis are retained by the author

A copy can be downloaded for personal non-commercial research or
study, without prior permission or charge

This thesis cannot be reproduced or quoted extensively from without first
obtaining permission in writing from the Author

The content must not be changed in any way or sold commercially in any
format or medium without the formal permission of the Author

When referring to this work, full bibliographic details including the
author, title, awarding institution and date of the thesis must be given

Mineral Eyes - Lessons from the Natural World

Clare Torney
BSc. (Hons) University of Glasgow

Submitted in fulfilment of the requirements for the
Degree of Doctor of Philosophy

School of Geographical and Earth Sciences
College of Science and Engineering
University of Glasgow

September 2010

Abstract

The compound eyes of trilobites, which appeared in the Early Cambrian, represent one of the first preserved visual systems. Application of state-of-the-art microscopy techniques in the present study has revealed fine details of the microstructure and chemistry of these unusual calcite eyes that, until now, have been inaccessible and this has facilitated new insights into their growth and function.

Six species from three families of trilobite with holochroal eyes, ranging from Early Ordovician to Middle Carboniferous, and 21 species from three families of trilobite with schizochroal eyes, ranging from Early Ordovician to Middle Devonian, were investigated. High-resolution microscopy techniques, including Electron Backscatter Diffraction, Transmission Electron Microscopy and Electron Probe Micro-analysis have made it possible to ‘see’ through the diagenesis of trilobite lenses to reveal the likely original lens microstructure and chemistry. Computer-based optical modelling has further shown how original lens microstructure and chemistry enhanced lens function.

The discovery of sub-micron sized crystals that display a gradual and precise change in orientation shows that in many lenses much of the original microstructure has remained intact despite exposure to pore fluids and elevated temperatures and pressures during diagenesis. Although microstructure varies slightly with lens shape, there is often exceptionally precise crystal orientation. In holochroal eyes there is a direct relationship between lens shape and microstructure; where lens surfaces are planar, crystals are of uniform orientation, but where lens surfaces are convex, *c* axis orientation fans out, away from the lens axis. Several microstructural patterns have been identified in

schizochroal lenses. However, a single original microstructural pattern, in which *c* axis orientation fans out at lens surfaces but remains parallel to the lens axis in the centre of the lens, may be applicable to all schizochroal lenses.

The original chemical composition of the lenses, in particular those of schizochroal type, is less commonly preserved. However, the unravelling of a diagenetic pathway of change, through understanding the intricacies of relationships between different minerals in the lenses, has made possible a better understanding of how these lenses were altered during diagenesis. Lenses in holochroal eyes are invariably low-magnesium calcite, like the rest of the exoskeleton, as has been established for some time. The present study clarifies the original structures of schizochroal lenses and in doing so, ends the controversy over lens function; lenses were originally constructed as doublets, as suggested by Clarkson and Levi-Setti, and were not gradient index lenses, as was suggested by Campbell and Bruton and Haas. Lenses in schizochroal eyes, were constructed of high-magnesium calcite, with highest concentrations of magnesium in the lower 'intralensar bowl' and central 'core' regions of the lens. The degree of partitioning of high levels of magnesium, of up to 8 mole % MgCO_3 , in the schizochroal eyes is remarkable given the magnesium-poor 'calcite seas' in which they were formed. This is perhaps the first example of element partitioning within biominerals for a specific function.

Based on the growth sequence of modern arthropod exoskeletons lenses in trilobite eyes are likely to have grown from the outer surface in, one lamella at a time, with microstructure and chemical composition controlled by an organic matrix.

Assessment of the trilobite optical structures, using Code V optical modelling software, leads to the conclusions that the trilobite eyes functioned in a similar manner to the apposition eyes of modern animals. Code V modelling of holochroal and schizochroal eyes, and the subsequent determination of their resolution and sensitivity, shows that both eye types probably had a single optically isolated photoreceptor beneath each lens. Using a combination of specific lens size, shape, spacing, microstructure and composition, the schizochroal eye was adapted to low light intensities, similar to the eye of the

modern isopod *Cirolana*. These adaptations would have provided the trilobite with light and dark detection of a resolution sufficient to identify movement, allowing it to detect prey and defend itself against predators. The birefringent properties of the calcite from which these lenses were made could be a hindrance, resulting in double refraction of light rays and the formation of 'ghost' images. Fascinatingly however this property provides the lenses with the refractive power required to make full use of the light available to them, vital for an organism with a crystalline lens with a fixed focal length.

Study of the calcified lenses of ostracods and brittlestars and comparison to lenses in schizochroal trilobite eyes confirms that these modern organisms do not provide accurate analogues for trilobite eyes. No other organism that shares all characteristics of schizochroal trilobite eyes has yet been found; the eyes of the phacopine trilobites remain unique in the natural world.

Table of Contents

Abstract	ii
List of Tables	x
List of Figures	xiii
List of Equations	xviii
Acknowledgements	xix
Declaration	xxii
Abbreviations	xxiii
 Chapter 1 Introduction	 25
1.1 Aims	25
1.2 The Significance of Visual System Studies	26
1.3 Types of Eye	27
1.3.1 Simple Eyes	27
1.3.2 Compound Eyes	28
1.3.2.1 Apposition Eyes	28
1.3.2.1.1 Neural Superposition Eyes	30
1.3.2.2 Superposition Eyes	31
1.3.2.2.1 Refracting superposition	32
1.3.2.2.2 Reflecting Superposition	33
1.3.2.2.3 Parabolic Superposition	33
1.4 Eye function: Requirement, Adaptation, Compromise	34
1.4.1 The Field of View of <i>Daphnia</i>	35
1.5 Trilobite Eyes	35
1.5.1 Holochroal Eyes	36
1.5.1.1 Lens Arrangement	37
1.5.1.2 Lens Structure	38
1.5.1.3 Lens Function	39
1.5.2 Schizochroal Eyes	39
1.5.2.1 Lens Arrangement	41
1.5.2.2 Lens Structure	43
1.5.2.3 Lens Function	49
1.5.3 Abathochroal Eyes	52
1.5.3.1 Eye Structure	52
1.5.3.2 Eye Function	52
1.5.4 Biomineralisation and the Construction of the Trilobite Eye	53
1.6 Calcite in Modern Optical Systems	55
1.6.1 Ostracods	55
1.6.2 Brittlestars	57
1.7 Detailed Aims of the Present Study	60

Chapter 2 Techniques	61
2.1 Optical Microscopy.....	61
2.2 Cathodoluminescence	61
2.2.1.1 Cathodoluminescence of Carbonates	62
2.2.1.1.1 Activators and Quenchers	62
2.2.2 Optical Cathodoluminescence.....	63
2.2.3 Hyperspectral Cathodoluminescence	63
2.3 Scanning Electron Microscopy.....	64
2.3.1 Scanning Electron Microscopy Technique Development.....	66
2.3.2 High Vacuum Secondary Electron Imaging	66
2.3.3 Low Vacuum Secondary Electron Imaging	66
2.3.4 Backscattered Electron Imaging	67
2.4 Energy Dispersive X-Ray Spectroscopy	67
2.4.1 Representation of EDS Data	68
2.5 Electron Probe Micro-Analysis	68
2.6 Transmission Electron Microscopy.....	69
2.6.1 Representation of TEM Results	70
2.7 Electron Backscatter Diffraction	71
2.7.1 What Is Electron Backscatter Diffraction?.....	71
2.7.2 The History of Electron Backscatter Diffraction.....	72
2.7.2.1 Introduction of Automated Electron Backscatter Diffraction..	73
2.7.3 Applications of Electron Backscatter Diffraction.....	74
2.7.3.1 Identification of Microstructure in Materials	74
2.7.3.1.1 Application of Electron Backscatter Diffraction in Biomineral Studies.....	74
2.7.4 Representation of EBSD Data	75
2.7.4.1 Electron Backscatter Diffraction Image Quality Maps.....	75
2.7.4.2 Electron Backscatter Diffraction Orientation Maps.....	75
2.7.4.3 Tolerance Angle Maps	77
2.7.4.4 Pole Figures and Texture Plots	78
2.7.4.5 Grain Boundary Maps	79
2.7.4.6 Misorientation	80
2.7.5 Chemistry Assisted Indexing: ChI scanning	82
2.7.6 ‘Cleaning’ and Partitioning of Data	83
2.8 Code V Optical Modelling.....	85
2.8.1 Introduction to Code V	85
2.8.1.1 Applications of Code V Software	85
2.8.2 Code V Data Input	85
2.8.2.1 Determining Lens Shape	86
2.8.2.2 Determining Field of View.....	86
2.8.2.3 Modelling Intralensar Structures	87
2.8.2.4 Refractive Indices.....	87
2.8.3 Representation of Results.....	88
2.8.4 Limitations of Code V.....	90
Chapter 3 Materials and Sample Preparation	91
3.1 Sources of Specimens	91
3.1.1 Trilobites	91
3.1.2 Preservation of Specimens.....	93
3.1.2.1 Specimens with Holochroal Eyes	95
3.1.2.1.1 English Material	95
3.1.2.1.2 Swedish Material	95

3.1.2.1.3	Scottish Material	95
3.1.2.1.4	Spitsbergen Material.....	96
3.1.2.2	Specimens with Schizochroal Eyes	97
3.1.2.2.1	German Material	97
3.1.2.2.2	Bohemian Material.....	97
3.1.2.2.3	Material from the U.S.A.....	98
3.1.2.2.4	Canadian Material.....	98
3.1.2.2.5	Moroccan Material	99
3.1.2.2.6	Estonian Material	100
3.1.2.2.7	Australian Material	101
3.1.3	Ostracods	102
3.1.4	Brittlestars	102
3.2	Sample Preparation.....	103
3.2.1	Thin Sectioning of Trilobite Eyes	104
3.2.1.1	Orientation of Thin Sections	105
3.2.1.2	Acid Etching of Thin Sections	106
3.2.2	TEM Sample Preparation	106
3.2.2.1	TEM Preparation by FIB	107
3.2.2.2	TEM Preparation by Argon Ion Milling.....	107
3.2.3	Fracture Surface Preparation	108
3.2.4	Preparation of Ostracod and Brittlestar samples	108
Chapter 4	Holochroal Eyes.....	110
4.1	Results	110
4.1.1	Light Microscopy.....	110
4.1.1.1	Transmitted Light.....	110
4.1.1.2	Reflected Light Microscopy.....	113
4.1.2	Cathodoluminescence	114
4.1.2.1	Optical Cathodoluminescence	114
4.1.3	Electron Backscatter Diffraction.....	114
4.1.3.1	Microstructure of Holochroal Lenses.....	114
4.1.4	Scanning Electron Microscopy	118
4.1.4.1	Backscattered Electron Imaging of Thin Sections	118
4.1.4.2	Secondary Electron Imaging of Etched Thin Sections	119
4.1.5	Energy Dispersive X-Ray Spectroscopy	120
4.2	Interpretation	123
4.2.1	Original Lens Microstructure.....	123
4.2.2	Optical Modelling.....	123
4.2.2.1	Modelling Results	124
4.2.2.2	Sublensar Structures and Photosensitive Components.....	126
4.3	Summary	128
Chapter 5	Schizochroal Eyes	129
5.1	Results	129
5.1.1	Light Microscopy.....	129
5.1.1.1	Transmitted Light Microscopy.....	129
5.1.1.2	Reflected Light Microscopy.....	136
5.1.2	Cathodoluminescence	137
5.1.2.1	Optical Cathodoluminescence	137
5.1.2.2	Hyperspectral Cathodoluminescence	138
5.1.3	Scanning Electron Microscopy	139
5.1.3.1	Secondary Electron Imaging of Fractured Surfaces.....	139
5.1.3.2	Backscattered Electron Imaging of Thin Sections	140

5.1.3.3	Secondary Electron Imaging of Etched Thin Sections	142
5.1.3.3.1	Point Counting of Microdolomite Crystals.....	144
5.1.3.4	Charge Contrast Imaging.....	145
5.1.4	Transmission Electron Microscopy	146
5.1.5	Chemical Analysis: EDS and EPMA	147
5.1.5.1	Qualitative Chemical Analysis	147
5.1.5.1.1	Silicified Trilobites.....	150
5.1.5.2	Quantitative Chemical Analysis.....	153
5.1.6	Electron Backscatter Diffraction.....	163
5.1.6.1	Pole Figure Analysis of Lens Features	163
5.1.6.2	Microstructural arrangements in lenses	163
5.1.6.2.1	The Relationships between Calcite and Dolomite in the Lenses.....	169
5.1.6.2.2	Misorientation of the radial fringe	171
5.1.7	EBSD of the Interlensar Sclera	173
5.1.8	Sublensar Structures	173
5.2	Interpretation	176
5.2.1	Calcite Diagenesis	176
5.2.1.1	Neomorphism - Replacement and Recrystallisation	176
5.2.1.1.1	Recognising Neomorphism	176
5.2.2	Determining Original Lens Construction	177
5.2.2.1	Microstructure of lenses	177
5.2.2.2	Chemistry of Lenses	181
5.2.2.2.1	Magnesium content of the lenses	184
5.2.2.3	Correlation with Conodont Alteration Index.....	188
5.3	Optical Modelling	191
5.3.1	Modelling Results	191
5.3.1.1	Photoreceptive Components	197
5.3.2	Summary	197
Chapter 6	Other Animals with Calcite Lenses	200
6.1	Ostracods.....	200
6.1.1	Results	201
6.1.1.1	Secondary Electron Imaging.....	201
6.1.1.2	Backscattered Electron Imaging.....	202
6.1.1.3	Electron Backscatter Diffraction	202
6.1.1.4	Energy Dispersive X-Ray Spectroscopy.....	204
6.1.2	Interpretation.....	204
6.1.2.1	Carapace Microstructure and Chemistry	204
6.1.2.2	Code V Optical Modelling.....	205
6.1.2.3	Sublensar Structures.....	207
6.1.3	Summary	208
6.2	Brittlestars	208
6.2.1	Results	208
6.2.1.1	Backscattered Electron Imaging of Rough Samples.....	209
6.2.1.2	Backscattered Electron Imaging of Polished Surfaces	210
6.2.1.3	Electron Backscattered Diffraction	210
6.2.1.4	Energy Dispersive X-Ray Spectroscopy.....	211
6.2.2	Interpretation.....	214
6.2.2.1	Code V Optical Modelling.....	214
6.2.2.2	Sublensar Structures.....	217
6.2.3	Summary	219

Chapter 7 Discussion	220
7.1 Eye Function	220
7.1.1 Resolution and Sensitivity.....	220
7.1.2 F-number	222
7.1.3 Eye parameter	223
7.1.4 Holochroal Eye Function	223
7.1.5 Schizochroal Eye Function	226
7.1.5.1 Model 1: Single Receptor per Lens System (Ommatidia-Type Eye).....	231
7.1.5.1.1 Resolution and Sensitivity	232
7.1.5.2 Model 2: Multiple Receptor per Lens System ('Eyelet' Eye) .	233
7.1.5.2.1 Resolution and Sensitivity	233
7.1.5.3 Comparison with Modern Visual Systems.....	234
7.1.5.3.1 F- number	235
7.1.5.3.2 Eye Parameter (p)	236
7.1.5.4 Proposed Model	237
7.2 Biomineralisation	242
7.2.1 Biomineral Growth	242
7.2.2 Ecdysis and Biomineralisation of the Trilobite Exoskeleton	245
Chapter 8 Conclusions	251
References	256

Appendices

Appendix A Specimen Log.....	276
Appendix B Point Counting Data.....	293
Appendix C Microdolomite Size Distribution Data.....	297
C.1 <i>Austerops smoothops</i>	298
C.2 <i>Barrandeops granulops</i>	299
C.3 <i>Boeckops boeckii</i>	301
C.4 <i>Geesops schlotheimi</i>	303
C.5 <i>Odontochile hausmanni</i>	304
C.6 <i>Phacops</i> sp.	307
C.7 <i>Reedops</i> cf. <i>cephalotes</i>	309
C.8 <i>Dalmanites</i> sp.....	311
Appendix D EDS Data [CD-ROM].....	314
D.1 Holochroal Eye Results.....	315
D.2 Schizochroal Eye Results.....	320
D.3 Brittlestar DAP Results.....	332
Appendix E EPMA Data [CD-ROM].....	334
E.1 Strathclyde EPMA Raw Data.....	335
E. 2 Edinburgh EPMA Raw Data.....	380
Appendix F Code V Data.....	408
F.1 Input Data.....	409
F.2 Results.....	411

List of Tables

Table 2.1- Calibration standards and detection limits for quantitative EDS analysis.	68
Table 2.2 - Calibration standards, detection limits and operating conditions for EPMA analysis.	69
Table 4.1 - Shape and typical sizes of holochroal lenses.	111
Table 4.2 - Quantitative chemical analysis of lenses in holochroal eyes- Mole % MgCO_3	122
Table 4.3 - Optical modelling of holochroal lenses.	126
Table 5.1 - Intralensar features in schizochroal lenses by species.	133
Table 5.2 - The occurrence of elements in schizochroal lenses.	148
Table 5.3 - Quantitative chemical analysis data of lenses, sclera and exoskeleton in schizochroal eyes.	157
Table 5.4 - Taxonomic distribution of microstructural arrangements in schizochroal lenses.	167
Table 5.5- Correlation between diagenetic alteration of schizochroal lenses and conodont alteration index.	189
Table 5.6 - Optical modelling of <i>Phacops</i> sp. with a low-magnesian calcite intralensar bowl.	194
Table 5.7- Optical modelling of <i>Phacops</i> sp. with a high-magnesian calcite intralensar bowl.	195
Table 5.8 - Code V optical modelling of <i>Ingriops</i> sp. nov.	196
Table 6.1 - Quantitative chemical analysis of the dorsal arm plate of the brittlestar <i>Ophiocoma wendtii</i>	213
Table 6.2 - Code V modelling results for lenses in the brittlestar <i>Ophiocoma wendtii</i>	217
Table 7.1 - Resolution, sensitivity, F-number and eye parameters of holochroal trilobite eyes.	224
Table 7.2 - Resolution and sensitivity of photoreceptors in modern animal eyes and schizochroal trilobite eyes.	235
Table 7.3 - F-numbers of lenses in schizochroal eyes.	236
Table A.1 - Taxonomic and locality source information for all specimens.	277
Table A.2 - Stratigraphical information for all specimens.	280
Table A.3 - Age data for all specimens.	283
Table A.4 - Specimen Sources and Museum numbers.	286
Table A.5 - Analysis carried out on each specimen.	289
Table B.1 - Point counting of schizochroal lenses and echinoderm fragments.	294

Table B.2 - Volume % values of schizochroal lenses and echinoderm fragments.....	295
Table B.3 - Mole % values of schizochroal lenses and echinoderm fragments...	296
Table C.1 - Microdolomite crystal size distribution in AM65 Lens 2.....	298
Table C.2 - Microdolomite crystal size distribution in PM28 Lens 3.....	299
Table C.3 - Microdolomite crystal size distribution in PM28 Lens 4.....	300
Table C.4 - Microdolomite crystal size distribution in BB3aR Lens 1.....	301
Table C.5 - Microdolomite crystal size distribution in BB3aR Lens 2.....	302
Table C.6 - Microdolomite crystal size distribution in G31R Lens 1.....	303
Table C.7 - Microdolomite crystal size distribution in G41 Lens 1.....	304
Table C.8 - Microdolomite crystal size distribution in OB24LB Lens 2.....	305
Table C.9 - Microdolomite crystal size distribution in OB24LB Lens 3.....	306
Table C.10 - Microdolomite crystal size distribution in PM27 Lens 1.....	307
Table C.11 - Microdolomite crystal size distribution in PM27 Lens 3.....	308
Table C.12 - Microdolomite crystal size distribution in RB2B Lens 1.....	309
Table C.13 - Microdolomite crystal size distribution in RB2B Lens 4.....	310
Table C.14 - Microdolomite crystal size distribution in TS1 Lens 1.....	311
Table C.15 - Microdolomite crystal size distribution in TS1 Lens 2.....	312
Table C.16 - Microdolomite crystal size distribution in TS1 Lens 2 repeat.....	313
Table D.1 - Weight % element EDS data for holochroal eyed trilobites.....	315
Table D.2 - Weight % carbonate EDS data for holochroal eyed trilobites.....	316
Table D.3 - Normalised Weight % carbonate EDS data for holochroal eyed trilobites.....	317
Table D.4 - Mole % carbonate EDS data for holochroal eyed trilobites.....	319
Table D.5 - Weight % element EDS data for schizochroal eyed trilobites.....	320
Table D.6 - Weight % carbonate EDS data for schizochroal eyed trilobites.....	323
Table D.7 - Normalised Weight % carbonate EDS data for schizochroal eyed trilobites.....	326
Table D.8 - Mole % carbonate EDS data for schizochroal eyed trilobites.....	329
Table D.9 - Weight % element EDS data for the Brittlestar DAP.....	332
Table D.10 - Weight % carbonate EDS data for the Brittlestar DAP.....	332
Table D.11 - Normalised weight % carbonate EDS data for the Brittlestar DAP.....	332
Table D.12 - Mole% carbonate EDS data for the Brittlestar DAP.....	333
Table E.1 - Weight % element EPMA data (Strathclyde) for trilobites with schizochroal eyes.....	335
Table E.2 - Weight % carbonate EPMA data (Strathclyde) for trilobites with schizochroal eyes.....	345
Table E.3 - Normalised weight % carbonate EPMA data (Strathclyde) for trilobites with schizochroal eyes.....	357
Table E.4 - Mole % carbonate EPMA data (Strathclyde) for trilobites with schizochroal eyes.....	369
Table E.5 - Weight % element EPMA data (Edinburgh) for trilobites with schizochroal eyes.....	380
Table E.6 - Weight % carbonate EPMA data (Edinburgh) for trilobites with schizochroal eyes.....	387
Table E.7 - Normalised weight % carbonate EPMA data (Edinburgh) for trilobites with schizochroal eyes.....	394
Table E.8 - Mole % carbonate EPMA data (Edinburgh) for trilobites with schizochroal eyes.....	401
Table F.1. - Code V data input; surface types and characteristics.....	409
Table F.2 - Code V input data continued; surface thicknesses and apertures, and FOV angles.....	410

Table F.3 - Code V modelling results; back and effective focal lengths and F-numbers.....	411
Table F.4 - Code V modelling results continued; aberration values and approximate receptor areas.....	412

List of Figures

Figure 1.1 - The human eye - an example of a simple eye.	27
Figure 1.2 - Light and dark adapted states of the apposition eye.	29
Figure 1.3 - The arrangement of receptors in the neural superposition eye.....	30
Figure 1.4 - Light and dark adapted states of the superposition eye.	32
Figure 1.5 - The refracting superposition system.....	33
Figure 1.6 - The reflecting superposition system.....	33
Figure 1.7 - The parabolic superposition system.	34
Figure 1.8 - The compound eye of the translucent water flea, <i>Daphnia</i>	35
Figure 1.9 - Temporal distribution of trilobite Orders.....	36
Figure 1.10 - The holochroal eye of <i>Scutellum campaniferum</i>	37
Figure 1.11 - Lens arrangements in holochroal eyes.	38
Figure 1.12 - Internal structure of the lenses in the holochroal trilobite eye.....	38
Figure 1.13 - The schizochroal eye of <i>Phacops rana milleri</i>	40
Figure 1.14 - Lens arrangement in the schizochroal eye.	42
Figure 1.15 - The lens of <i>Dalmanites</i> sp. in thin section.	44
Figure 1.16 - The internal structure of lenses and the surrounding sclera in the schizochroal eyes of <i>Phacops rana milleri</i>	45
Figure 1.17 - Shapes of intralensar bowls in lenses of schizochroal eyes.....	47
Figure 1.18 - Sublensar structures in schizochroal eyes.	48
Figure 1.19 - The function of the intralensar bowl.....	51
Figure 1.20 - The bifocal lens of <i>Dalmanitina socialis</i>	51
Figure 1.21 - The lens arrangement in the abathochroal eye of <i>Pagetia</i>	52
Figure 1.22 - Growth of holochroal lenses by addition of trabeculae.	54
Figure 1.23 - Biomineralisation of the schizochroal trilobite eye - Post-ecdysial lens development.	55
Figure 1.24 - Primitiopsid ostracods.	56
Figure 1.25 - Structure and function of the naupliar ostracod eye.....	57
Figure 1.26 - Night- and day-time images of the Brittlestar <i>Ophiocoma wendtii</i>	58
Figure 1.27 - The internal structure of the dorsal arm plates of light-sensitive brittlestars.	59
Figure 2.1 - Optical cathodoluminescence microscopy.	63
Figure 2.2 - Hyperspectral cathodoluminescence.	64
Figure 2.3 - FEG-SEM chamber set-up for SE and BSE imaging and EDS chemical analysis.	65
Figure 2.4 - Representation of Energy Dispersive X-ray Spectroscopy data.	68
Figure 2.5 - Representation of Transmission Electron Microscopy results.	71

Figure 2.6 - Scanning Electron Microscope set-up for Electron Backscatter Diffraction.	72
Figure 2.7 - Automated indexing of Kikuchi bands in calcite.	73
Figure 2.8 - Inverse quality (IQ) map.	75
Figure 2.9 - Reference directions of Electron Backscatter Diffraction maps.	76
Figure 2.10 - Electron Backscatter Diffraction orientation maps.	76
Figure 2.11 - Electron Backscatter Diffraction tolerance maps.	77
Figure 2.12 - Electron Backscatter Diffraction pole figures and texture plots. ..	78
Figure 2.13 - Grain boundary mapping	79
Figure 2.14 - Misorientation of a crystal.	80
Figure 2.15 - Representation of misorientation data.	81
Figure 2.16 - Chemistry assisted indexing of Electron Backscattered Diffraction data.	82
Figure 2.17 - Effects of 'cleaning' and partitioning Electron Backscattered Diffraction data.	84
Figure 2.18 - Refractive indices of calcite.	87
Figure 2.19 - Representation of Code V modelling results.	89
Figure 3.1- Spatial and temporal distribution of specimens investigated.	94
Figure 3.2 - Holochroal trilobite eyes.	96
Figure 3.3 - Specimens with schizochroal eyes.	101
Figure 3.4 - <i>Primitiopsis planifrons</i> Jones, 1887.	102
Figure 3.5 - <i>Ophiocoma wendtii</i> Müller and Troschel, 1842.	103
Figure 3.6 - Thin section orientations and corresponding lens arrangements. .	105
Figure 3.7 - Sample orientation of ostracods in polished stubs.	108
Figure 3.8 - Sample orientation of brittlestars in polished stubs.	109
Figure 4.1 - Transmitted light microscopy of lenses in holochroal eyes.	112
Figure 4.2 - Reflected light microscopy of holochroal lenses.	113
Figure 4.3 - Cathodoluminescence of holochroal lenses.	114
Figure 4.4 - Microstructure in holochroal lenses.	115
Figure 4.5 - Lens recrystallisation in <i>Telephina mobergi</i>	116
Figure 4.6 - Crystal growth patterns in holochroal lenses.	117
Figure 4.7 Tolerance mapping and misorientation in the holochroal lens of <i>Telephina mobergi</i>	118
Figure 4.8 - Backscattered Electron imaging of holochroal lenses.	119
Figure 4.9 - Secondary Electron image of an acid etched holaspis Paladin lens.	120
Figure 4.10 - Energy Dispersive X-ray mapping of holochroal lenses.	121
Figure 4.11 - Code V ray tracing in holochroal lenses.	125
Figure 4.12 - The effect of screening pigment in the holochroal eye.	127
Figure 4.13 - Summary of microstructure arrangements in holochroal lenses. .	128
Figure 5.1 - Intralensar features in <i>Dalmanites</i> sp. viewed in plane polarised transmitted light.	130
Figure 5.2 - Intralensar features in <i>Austerops</i> and <i>Eldredgeops</i> viewed in transmitted light.	131
Figure 5.3 - Trabeculae, growth lamellae and cleavage in lenses of schizochroal eyes.	132
Figure 5.4 - Extinction patterns in lenses of schizochroal eyes.	135
Figure 5.5 - Extinction patterns in the cornea of lenses in schizochroal eyes. .	136
Figure 5.6 - Reflected light microscopy of lenses in schizochroal eyes.	136
Figure 5.7 - Intralensar structures in lenses of schizochroal eyes viewed using optical cathodoluminescence microscopy.	137
Figure 5.8 - Hyperspectral CL and X-ray maps of a <i>Geesops</i> lens.	138

Figure 5.9 - Secondary Electron images of fracture surfaces of <i>Geesops schlotheimi</i>	139
Figure 5.10 - Backscattered electron imaging of non-carbonate minerals in lenses of schizochroal eyes.	141
Figure 5.11 - Backscattered Electron imaging of pores and dissolution pits in a lens of <i>Barrandeops granulops</i>	142
Figure 5.12 - Secondary electron and backscattered electron imaging of acid etched lenses.	143
Figure 5.13 - Relationship between Mg concentration and mean microdolomite size in acid etched schizochroal lenses.	144
Figure 5.14 - Charge Contrast images of lenses in schizochroal eyes.	145
Figure 5.15 - Transmission Electron Microscopy of lenses in schizochroal eyes.	146
Figure 5.16 - Transmission Electron Microscopy diffraction patterns in a schizochroal lens.	147
Figure 5.17 - Magnesium distribution patterns in lenses of schizochroal eyes.	149
Figure 5.18 - <i>Barrandops</i> cf. <i>granulops</i>	151
Figure 5.19 - Element distribution patterns within samples with silicified exoskeletons.	152
Figure 5.20 - Electron Probe Micro-Analysis traverses through lenses of <i>Dalmanites</i> sp.	155
Figure 5.21 - Electron Probe Micro-Analysis traverses through lenses of <i>Eldregeops rana</i>	156
Figure 5.22 - Magnesium concentrations of lenses, interlensar sclera and exoskeleton in trilobites with schizochroal eyes.	160
Figure 5.23 - Trace element chemistry of lenses, sclera and the exoskeleton in trilobites with schizochroal eyes.	162
Figure 5.24 - Orientation relationships of cleavage, trabeculae and lens surfaces.	163
Figure 5.25 - Microstructure in the lenses of schizochroal eyes, determined using EBSD.	165
Figure 5.26 - Tangential view of the microstructure in the lenses of schizochroal lenses.	166
Figure 5.27 - Microstructure of lenses and cements identified by tolerance angle mapping.	168
Figure 5.28 - Orientation relationships of calcite and dolomite crystals in lenses, cements and limestone.	170
Figure 5.29 - Misorientation in the 'radial fringe' of lenses in schizochroal eyes.	172
Figure 5.30 - Microstructure of the sclera determined using Electron Backscatter Diffraction.	173
Figure 5.31 - Sub-lensar capsules in the schizochroal eyes of <i>Geesops</i>	174
Figure 5.32 - Sub-lensar calcite cements in schizochroal eyes.	175
Figure 5.33 - Relative timing of epitaxial cement growth and diagenetic change in schizochroal lenses.	178
Figure 5.34 - Alteration of microstructure during diagenesis in lenses of schizochroal eyes.	180
Figure 5.35 - Changes in chemistry during diagenesis in lenses of schizochroal eyes.	182
Figure 5.36 - Continuity between intralensar structures and cement overgrowth in altered lenses in schizochroal eyes.	183
Figure 5.37 - Conversion of high-magnesian calcite to low-magnesian calcite and microdolomite during diagenesis of lenses in schizochroal eyes.	184

Figure 5.38 - Conversion of volume% dolomite derived by point counting to mole% MgCO ₃ in precursor HMC.	185
Figure 5.39 - Magnesium content of lenses in schizochroal eyes determined by point counting and quantitative chemical analysis.	186
Figure 5.40 - Molar Ca/Mg ratio of lens calcite in schizochroal eyes.	188
Figure 5.41 - Degrees of diagenetic alteration in schizochroal lenses.	190
Figure 5.42 - The effects of an intralensar bowl on aberration in lenses of schizochroal eyes.	193
Figure 5.43 - Original chemical composition of the lenses in schizochroal trilobite eye.	198
Figure 5.44 - The original microstructure of lenses in the schizochroal trilobite eye.	198
Figure 6.1 - Secondary Electron image of the ostracod <i>Primitiopsis planifrons</i>	201
Figure 6.2 - Microstructure of the carapace of the ostracod <i>Primitiopsis planifrons</i>	203
Figure 6.3 - Energy Dispersive X-Ray mapping of the carapace of the ostracod <i>Primitiopsis planifrons</i>	204
Figure 6.4 - Surface curvatures of the ostracod lens used in optical modelling.	206
Figure 6.5 - Code V modelling of a lens of the ostracod <i>Primitiopsis planifrons</i>	206
Figure 6.6 - Code V modelling of a tapetum in the eye of the ostracod <i>Primitiopsis planifrons</i>	207
Figure 6.7 - Backscattered electron images of the brittlestar <i>Ophiocoma wendtii</i>	209
Figure 6.8 - Backscattered Electron image of lenses within the dorsal arm plate of the brittlestar <i>Ophiocoma wendtii</i>	210
Figure 6.9 - Electron Backscatter Diffraction of a lens in the brittlestar <i>Ophiocoma wendtii</i>	211
Figure 6.10 - Misorientation in a lens of the brittlestar <i>Ophiocoma wendtii</i> . ..	211
Figure 6.11 - Energy Dispersive X-Ray mapping of lenses in the brittlestar <i>Ophiocoma wendtii</i>	212
Figure 6.12 - Surface curvatures of the brittlestar lens used in Code V optical modelling.	214
Figure 6.13 - Code V modelling results for lenses in the brittlestar <i>Ophiocoma wendtii</i>	216
Figure 6.14 - Code V modelling results for lenses in the brittlestar <i>Ophiocoma wendtii</i> , with overlying epidermis.	217
Figure 6.15 - Microstructure of lenses in the brittlestar <i>Ophiocoma wendtii</i>	219
Figure 7.1 - Terms used in calculating resolution and sensitivity in compound eyes.	222
Figure 7.2 - Determination of the lens nodal point in a biconvex lens.	222
Figure 7.3 - Intersection angles of lens axes in superposition and apposition eyes.	227
Figure 7.4 - The internal structure of a unit within an ocellar-like trilobite eye.	228
Figure 7.5 - Internal structure of the neural superposition trilobite 'hyper-eye'.	229
Figure 7.6 - Schematic cross-section through a 'single receptor per lens' system.	232
Figure 7.7 - Schematic cross-section through a 'multiple receptor per lens' system.	233
Figure 7.8 - The effects of birefringence in schizochroal lenses.	238

Figure 7.9 - The proposed arrangement of sublensar structures in the schizochroal trilobite eye.	240
Figure 7.10 - Field of view and depth perception in trilobite eyes.....	241
Figure 7.11 - Classical and non-classical mineral crystallisation pathways.	243
Figure 7.12 - Layered structure of the organic matrix onto which minerals crystallise in mollusc shells.	244
Figure 7.13 - Layering in the modern crustacean cuticle.	246
Figure 7.14 - Stages of growth and moulting in the crustacean cuticle.	248
Figure 7.15 - Post-ecdysial growth sequence of the schizochroal eye.	250
Figure 8.1 - Original microstructure of holochroal lenses.....	251
Figure 8.2 - Microstructure, chemistry and function of lenses in the schizochroal trilobite eye.	253
Figure 8.3 - Effects of diagenesis on original lens microstructure.....	254
Figure 8.4 - Effects of diagenesis on original lens chemistry.	255
Figure C.1 - Size distribution of microdolomite crystals in AM65 Lens 2.....	298
Figure C.2 - Size distribution of microdolomite crystals in PM28 Lens 3.....	299
Figure C.3 - Size distribution of microdolomite crystals in PM28 Lens 4.....	300
Figure C.4 - Size distribution of microdolomite crystals in BB3aR Lens 1.....	301
Figure C.5 - Size distribution of microdolomite crystals in BB3aR Lens 2.....	302
Figure C.6 - Size distribution of microdolomite crystals in G31R Lens 1.....	304
Figure C.7 - Size distribution of microdolomite crystals in G41R Lens 1.....	305
Figure C.8 - Size distribution of microdolomite crystals in OB24LB Lens 2.....	306
Figure C.9 - Size distribution of microdolomite crystals in OB24LB Lens 3.....	306
Figure C.10 - Size distribution of microdolomite crystals in PM27 Lens 1.....	307
Figure C.11 - Size distribution of microdolomite crystals in PM27 Lens 3.....	309
Figure C.12 - Size distribution of microdolomite crystals in RB2B Lens 1.....	310
Figure C.13 - Size distribution of microdolomite crystals in RB2B Lens 4.....	310
Figure C.14 - Size distribution of microdolomite crystals in TS1 Lens 1.....	311
Figure C.15 - Size distribution of microdolomite crystals in TS1 Lens 2.....	312
Figure C.16 - Size distribution of microdolomite crystals in TS1 Lens 2 (repeat).....	313

List of Equations

Equation 1 - Resolution in a compound eye with hexagonal lens packing.....	221
Equation 2 - Resolution in a compound eye with square lens packing.	221
Equation 3 - Sensitivity of receptors in a compound eye.....	221
Equation 4 - F-number.	223
Equation 5 - Eye parameter (p) of a compound eye.	223
Equation 6 - Resolution of a single receptor per lens system.	232
Equation 7 - Sensitivity of receptors in a 'single receptor per lens' system. ...	232
Equation 8 - Resolution of a multi-receptor per lens system.....	234
Equation 9 - Sensitivity of a multi-receptor per lens system.	234
Equation 10 - Eye parameter (p) of <i>Phacops</i> sp.....	237

Acknowledgements

The list of people that have helped me during the course of my Ph.D is never ending, so I should begin by apologising to anyone I have missed.

Firstly, The Leverhulme Trust, for funding this work, and to the Department (now School) of Geographical and Earth Sciences for providing financial support for conference attendance on so many occasions.

I owe so much to my supervisors at Glasgow University, Alan Owen and Martin Lee, for putting up with me for the last few years. For giving me such a great undergrad project, and then giving in to my constant nagging about extending it to a Ph.D. The effort they put into the initial funding applications and the support and guidance they have given me since has been phenomenal. There are no two other people I would rather have been supervised by...whoever would have thought a palaeontologist and a meteorite fanatic would make such a great team!

Thanks are also due to Rob Martin, my supervisor at Strathclyde University, and to Paul Edwards (Strathclyde University), who went way beyond his role of introducing me to optical modelling. Without his help I would have never got to grips with the modelling software and we would be none the wiser as to the workings of trilobite eyes.

Professor Richard Fortey and Professor Maggie Cusack are sincerely thanked for reviewing this thesis, for their helpful discussion during the viva, and for their advice and suggestions with regards to corrections and future research.

This project would never have yielded so many results if it wasn't for all the generous people who supplied me with specimens (in no particular order): Helje Pärnaste, Richard Fortey, Brian Chatterton, Ryan McKellar, Cristian Klug, David Holloway, David Rudkin, Thijs Vandenbroucke, Pter Budil, Per Ahlberg, Clare Pannell, David Bruton, Gordon Hendler, Cathy Groves and David Siviter. A special thank you is owed to Mike Keen, for assistance with ostracod collection (despite a 100% fail rate during sample preparation!), Brigitte Schoenemann for sample donation and helpful discussion and to Euan Clarkson, for sample donation, helpful discussion during the early stages of my work, uncontrollable enthusiasm and the hugs and kisses!

The success of analysis and sample preparation is due to the training and assistance provided by many people: John Gilleece, Les Hill, Peter Chung, Robert McDonald, Paul Edwards, Dominique Tobler, Brian Miller, Billy Smith and Chris Hayward.

Rachel Jamison and Kate Klajmon are thanked for allowing me to analyse samples prepared for their Undergrad projects, Tom Quinn for providing great training and assistance with 3D imaging and Kate Dobson for always being on hand with IT assistance.

I'm sure the past three years wouldn't have been half as much fun if it wasn't for some great office mates. Too many have come and gone to list them all but in particular Suzie, just for being herself (an absolutely fantastic friend who has made my time in the postgrad office so enjoyable and has always been on hand to provide encouragement and celebrate with me), Daniel, for provoking the odd controversial discussion and introducing me to the Handbook of Biomineralisation, Joanne for teaching me about shell structure and livening up conferences and Neil and Laura for the great banter.

A massive thank you is also due to Alberto for making intensive discussions about biominerals seem like good fun and provoking lots of research ideas through constant questions as well as reminding me how cool this project actually is! Also to Nick for providing regular reading from a certain book that kept me

smiling in the last 6 months or so as well as occasional help with SEM and EPMA stuff.

Heather Maxwell, my diabetes specialist nurse at Gartnavel. Thank you for getting me my pump and making my final year run smoothly!

To my family, who although baffled by my love of trilobite eyes, all supported me in their own ways. It should be acknowledged that my Dad went to considerable lengths to develop an understanding of Electron Backscatter Diffraction so he could tell his work colleagues about it. Mum, Dad, Emer and Stephen (and my little Bird), I hope I've made you proud.

Finally to Graeme, the person who has stood by me since day one of this Ph.D, through all the rants, emotional outbursts, times of frustration and days when I just couldn't face it. For believing I could do it even when I didn't think I could and for checking that all my 3D diagrams worked! Without his constant love and support, and the occasional reality check, this work would have taken a whole lot longer and would have seemed much harder. He gave me the motivation to get this thesis finished on time so we can get on with our future.

Declaration

The material presented in this thesis is the result of three years independent research carried out at the School of Geographical & Earth Sciences at the University of Glasgow and the Department of Physics at the University of Strathclyde. The research was supervised by Dr. Alan Owen, Dr. Martin Lee and Prof. Robert Martin. This thesis represents my own research and any published or unpublished work by other authors has been given full acknowledgement in the text.

.....

Clare Torney

Abbreviations

BFL: Back Focal Length

BSE: Backscattered Electron

CAI: Conodont Alteration Index

ChI: Chemistry Assisted Indexing

CI: Confidence Index

CL: Cathodoluminescence

DAP: Dorsal Arm Plate

EBSD: Electron Backscatter Diffraction

EBSP: Electron Backscatter Pattern

EDS: Energy Dispersive X-Ray Spectroscopy

EFL: Effective Focal Length

EPD: Entrance Pupil Diameter

EPMA: Electron Probe Micro-Analysis

EPT: Expanded Peripheral Trabeculae

FEG: Field Emission Gun

FIB: Focused Ion Beam

FOV: Field of View

HMC: High-magnesian Calcite

IPF: Inverse Pole Figure

IQ: Image Quality

LMC: Low-magnesian Calcite

MD: Microdolomite

ND: Normal Direction

OIM: Orientation Imaging Microscope

RD: Rolling Direction

RI: Refractive Index

RL: Reflected Light

SE: Secondary Electron

SEM: Scanning Electron Microscope

TEM: Transmission Electron Microscope

TD: Transverse Direction

TL: Transmitted Light

WDS: Wave Dispersive X-Ray Spectroscopy

3D- μ CT: 3-dimensional X-Ray Tomography

1

Introduction

1.1 Aims

The first investigations of trilobite eyes were published over 120 years ago by Clarke (1889) and Lindström (1901). Subsequent work (e.g. Campbell, 1975; Clarkson and Levi-Setti, 1975; Clarkson, 1979; Fortey, 1985; Gál *et al.*, 2000; Bruton and Haas, 2003a; Bruton and Høyberget, 2006; Clarkson *et al.*, 2006) has had the aim of clarifying the internal structures in lenses, which were identified in these early works, and ultimately determining how the trilobite eyes would have functioned.

The present study aims to provide a better understanding of the trilobite visual system by determining how representative of trilobites as a whole the currently available literature is. This work aims to specifically resolve the debate over schizochroal eye function (see Clarkson *et al.*, 2006; Bruton and Haas, 2003a) by assessing the internal structures of the lenses, and will also assess the lens chemistry model proposed by Lee *et al.*, (2007a) by providing specific information on the concentration and distribution of elements within the lenses of a number of species.

Many of the state-of-the-art analytical techniques used in the present study are recent developments and are therefore applied to the study of trilobites for the first time. These techniques will be used to reveal the fine details of microstructure and chemistry of the two main types of trilobite eyes (termed holochroal and schizochroal) and an assessment can be made of whether these are representative of the lens architecture and composition *in-vivo*. Computer

based optical modelling will provide an insight into how lens chemistry and internal features within lenses affected their function and will allow a model of overall eye function to be constructed to which other currently published models (e.g. Clarkson and Levi-Setti, 1975; Campbell, 1975; Gál et al., 2000; Bruton and Haas, 2003; Schoenemann, 2007; Schoenemann and Clarkson 2008) may be compared.

The present study also compares trilobite eyes with calcite lenses in ostracods and brittlestars to allow some conclusions to be drawn as to their suitability as analogues. However, the main emphasis of the present study is on the detailed microstructure of trilobite eyes, in particular those of schizochroal type.

1.2 The Significance of Visual System Studies

The first evidence of visual systems is from the Early Cambrian and includes the eyes of the bivalved arthropod *Isoxys* (see Vannier *et al.*, 2009), lobopods such as *Anomalocaris*, *Opabinia* (see Conway-Morris, 1998) and *Miraluolishania haikouensis* (see Schoenemann *et al.*, 2009) as well as the compound eyes of trilobites (e.g. Schoenemann *et al.*, 2010). The trilobite eye differs from the other eyes of this time as they represent some of the early signs of mineralised skeletons (Parker, 2003). The commonly preserved calcite lenses of trilobites may have been preceded by soft forms; based on the interpreted size, form and mode of life of Precambrian animals in general, it is likely that these earlier visual systems consisted of a simple array of directional photoreceptors (Land and Nilsson, 2002).

The complexity of an organism's visual system can provide a considerable amount of information on the palaeobiology of the animal. Study of the trilobite eye enables interpretation of habitat and mode of life (e.g. McCormick and Fortey, 1998; Bruton and Høyberget, 2006). Analysis of the architecture of this visual system and the capabilities of the lenses and inferred photoreceptors within it, allows a better understanding to be built up of how these animals may have lived and how vision has evolved over time.

Vukusic and Sambles' (2003) review of natural photonic phenomena in both fauna and flora, including iridescence in butterflies and plant leaves, outlines how the use of photonics in nature is providing the inspiration for applications in

a variety of industries, and is having a notable impact on today's technology. The review by Vukusic and Sambles (2003) also provides insights into the potential applications of studies on the trilobite visual system. The compound eye of insects has already been the inspiration for the construction of an artificial 'compound eye' visual sensor with a wider field of view than can be achieved from a single lens system (Ogata *et al.*, 1994). The brittlestar lens has also been artificially constructed, and may too prove to have applications in electronics and optics (Aizenberg and Hendler, 2004). It is reasonable to suggest that similar advancements might result from the detailed understanding of trilobite eyes that this study aims to provide.

1.3 Types of Eye

Many different forms of eye are found across the animal kingdom, and fall into two sub-divisions; simple eyes and compound eyes. Understanding the mechanisms by which modern visual systems work is vital for applying these modern 'analogues' to understanding trilobite eyes and ultimately determining the likelihood of similar mechanisms being present in trilobite eyes *in-vivo*.

1.3.1 Simple Eyes

Simple eyes consist of a single lens composed of soft cells or fibres, positioned at the front of a 'capsule' (eye socket) that contains various components including a cornea, retina and photosensitive cells (Figure 1.1).

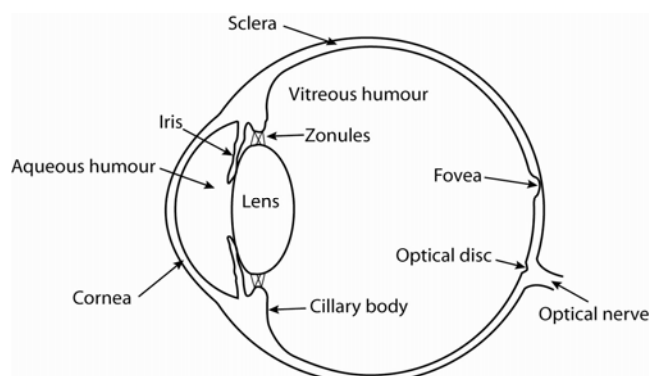


Figure 1.1 - The human eye – an example of a simple eye.
Modified from Atchison and Smith (2000, figure 1.1).

This type of eye is found in vertebrates and cephalopods (Land and Nilsson, 2002). Within simple eyes, there are numerous eye structures and photoreceptor

arrays, often determined by the lifestyle and therefore the requirements of the animal (Ott, 2006). A pelagic animal, for example, exposed to predators from all angles, may benefit more from a wide field of view than from high sensitivity to light. Muscles provide the eye with the ability to react to changes in the surrounding environment. They allow the eye to move within its socket changing the field of view; control the opening and closing of the iris providing the system with light and dark adapted states; and perhaps most importantly, control the accommodation of the lens i.e. allowing it to change shape and thickness to achieve focus on objects at any number of distances (Ott, 2006).

1.3.2 Compound Eyes

Compound eyes consist of two or more ‘optical systems’. These ‘optical systems’ may contain lenses, or in basic forms may consist of eye spots or simple light detecting pits (Land and Nilsson, 2002, p.126). Present day compound eyes are found in the Phylum Arthropoda and also in some annelids and bivalve molluscs (Land and Nilsson, 2002). Compound eyes have been in existence since the Early Cambrian. Their presence is noted in the lobopods *Miraluolishania haikouensis* (see Schoenemann, 2006, Schoenemann *et al.*, 2009) and *Anomalocaris* (in *Anomalocaris* they are inferred based on eye shape, despite the lack of preserved facet structure (Conway-Morris, 1998)) and clearly identified in numerous groups of trilobites (Clarkson *et al.*, 2006).

It is important to note that compound eyes do not always form multiple images (see section 1.3.2.2). In some compound eyes each lens may be capable of forming its own image, although this is not necessarily what the animal will see as its perception of an image is governed by the capabilities of the photoreceptive cells and neural networks as well as the optical components. Below are described the various types of compound eyes that are distinguished by lens type and architecture, and photoreceptor arrangement.

1.3.2.1 Apposition Eyes

Apposition eyes are found in most modern diurnal (active during daylight hours) insects (Land and Nilsson, 2002, p. 125) and adapted forms are used by some nocturnal animals (Greiner, 2006). The eye consists of a number of radially arranged ommatidia each of which is like a pillar or capsule extending from the

visual surface down to the neural network below (Figure 1.2A) (Land and Nilsson, 2002, pp. 128-130).

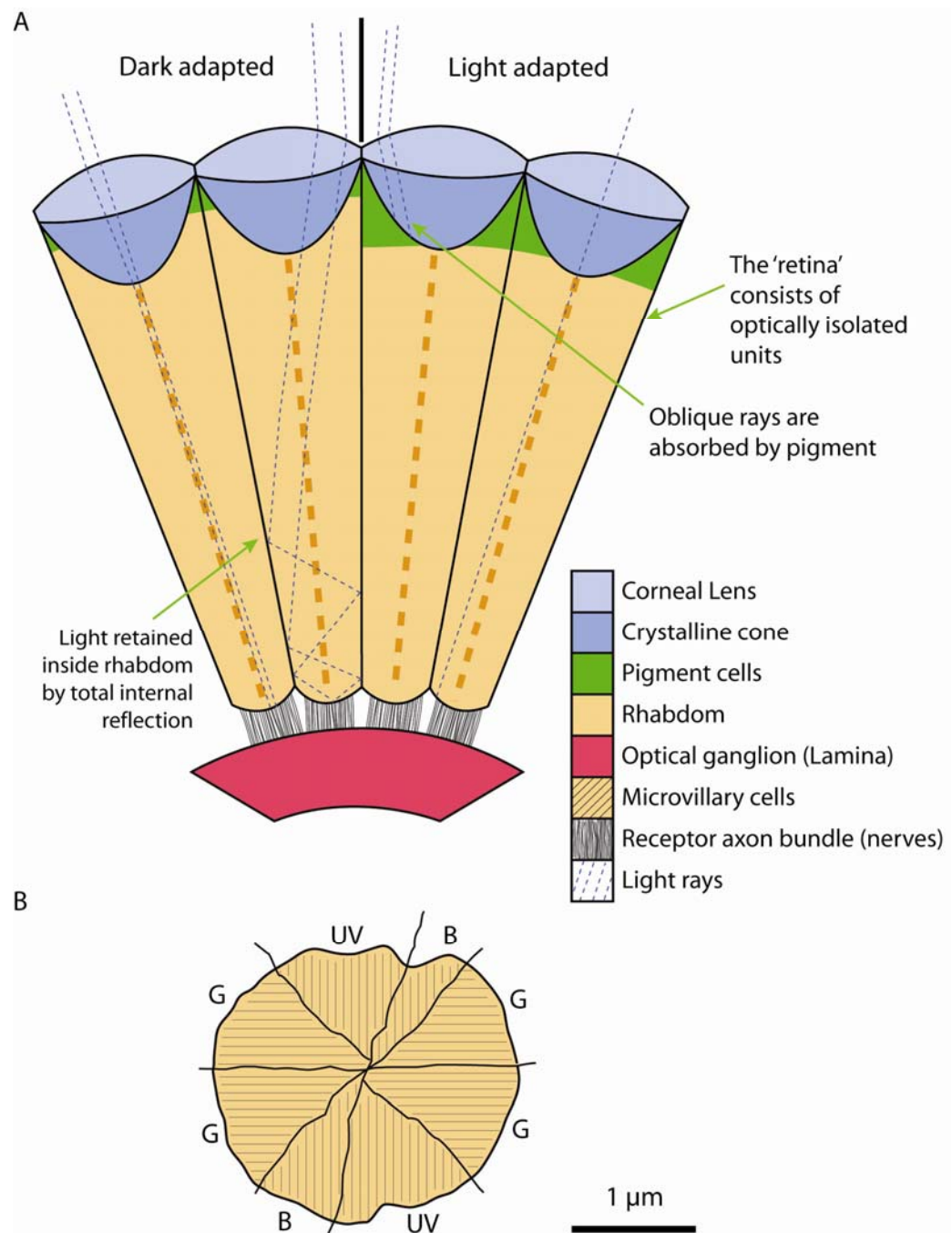


Figure 1.2 – Light and dark adapted states of the apposition eye.

A. Schematic diagram showing the internal structure of the apposition eye for dark and light adapted states. Orange dashed lines in the rhabdom indicate the presence of different receptor cells, i.e. the fused cells. Blue dashed lines represent light rays. Notice how some parts of the rhabdom are shielded from light by pigment in the light adapted state. **B.** A cross section of the rhabdom of a worker bee showing the eight fused receptor cells and the wavelengths of light they respond to: UV=ultra violet; B=blue light; G=green light. Images modified from Land and Nilsson (2002, figure 7.3 and figure 7.4b respectively).

A single ommatidium consists of a corneal lens underlain by a crystalline cone which is partially enveloped in pigment cells isolating it from neighbouring

ommatidia. Migration of these pigment cells enables the eye to adopt light and dark-adapted states; in some insects this involves the screening of photoreceptive units in light conditions in a similar manner to an iris in a simple eye (Land and Nilsson, 2002, pp. 138-139). Beneath the crystalline cone is the rhabdom onto which the lens projects an inverted image. The rhabdom is the photosensitive component of the system consisting of eight fused receptor cells, each composed of a microvillar membrane. Although the rhabdom acts as a single unit, the eight receptor cells may react to different types of light; in the case of a worker bee there are two for UV, two for blue and four for green light (Land and Nilsson, 2002, p. 129) (Figure 1.2B). The relatively high refractive index of the rhabdom allows it to act as a guide, trapping light by total internal reflection (Nilsson, 1990). The repeated reflection of the light inside the rhabdom results in loss of spatial information and ‘averaging’ of light, some (~20%) incident light can be lost in this process (Nilsson, 1990). The eight receptor cells transmit their information to the same area of the optical ganglion below, this is called the lamina (Figure 1.2A). The final output is a single pixel per ommatidium in a mosaic-style upright, or erect, image (Land and Nilsson, 2002).

1.3.2.1.1 Neural Superposition Eyes

Neural superposition eyes (Kirschfeld, 1967; Hardie, 1986) are a sub-type of apposition eye that have a different rhabdomeric construction. Here, the eight receptors, each termed a rhabdomere, are not fused (Figure 1.3A).

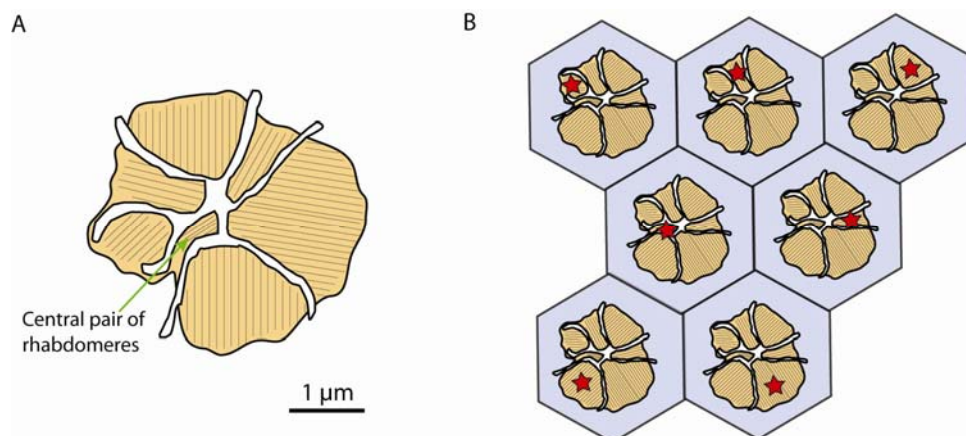


Figure 1.3 – The arrangement of receptors in the neural superposition eye.

A. Cross section of the ‘rhabdom’ in a neural superposition eye showing the separation of rhabdomeres. **B.** Each rhabdomere in an ommatidium samples a different area in space but shares this with one rhabdomere in each of the six neighbouring ommatidia. Rhabdomeres viewing the same area are indicated by a red star. Blue hexagons represent the lenses which lie above the rhabdoms. **A.** modified from Land and Nilsson (2002, figure 7.4d). **B.** modified from Kirschfeld (1967, figure 4).

The rhabdomeres are arranged in such a way that there are six peripheral individuals and a central pair, one overlying the other. Each rhabdomere 'sees' a slightly different area of space to each of its immediate neighbours but shares this field of view with a single rhabdomere in the surrounding six ommatidia (Figure 1.3B) (Hardie, 1986; Kirschfeld, 1967; Nilsson, 1990; Land and Nilsson, 2002). The six peripheral rhabdomeres send signals to different parts of the lamina where the corresponding signals of neighbouring ommatidia will also be transmitted. The central rhabdomeres bypass this area and are received in the next layer, the medulla. It is a 180° 'twist' of the receptor axon bundles at the base of the rhabdomeres that allows the signals to meet up in this way. The result of this system is an image of the same type as in an apposition eye but with the capability of a seven fold greater photon capture, most advantageous to crepuscular animals (Land and Nilsson, 2002, p. 131), active at dusk and dawn. However due to the greater angle of light acceptance, spatial resolution is compromised (Kirschfeld, 1971).

1.3.2.2 Superposition Eyes

On first appearance, superposition eyes look very similar to apposition eyes (Nilsson, 1990; Land and Nilsson, 2002). A series of corneal lenses is arranged radially on a curved outer surface and each is underlain by a crystalline cone. Below this level however the two types of eye differ significantly. Superposition eyes are not of ommatidial type. Instead, beneath the crystalline cones is a 'clear zone'; a layer of clear cells through which light rays from various optical facets are focused to a single spot on the retina (Figure 1.4). The retina in superposition eyes is a continuous sheet at depth rather than discrete units, immediately below the crystalline cones, as in apposition eyes (Land and Nilsson, 2002, pp.156-157). The pigment cells in superposition eyes have the ability to migrate towards the retina allowing the system to screen off light from adjacent lenses; this allows the eye to adapt to different light levels, acting as an apposition eye in daylight reducing image brightness (Nilsson, 1990 and references therein) (Figure 1.4). This adaptation is necessary due to the high sensitivity of the eye that makes it suitable for vision in low light levels; superposition eyes have sensitivity values as much as 100 times that of an apposition eye of the same size (Land and Nilsson, 2002, p.163). Image formation in superposition eyes consists of a single erect image on the retina.

The optics in superposition eyes keep light rays parallel, but transmit them to the opposite side of the lens axis on exiting the lens rather than making them converge as in conventional lenses preventing inversion of the image. This ‘dog-leg’ bending of light can be achieved by refracting light with lenses, reflecting it using mirrors or using a combination of both. These three methods give rise to three different types of superposition eye (see below).

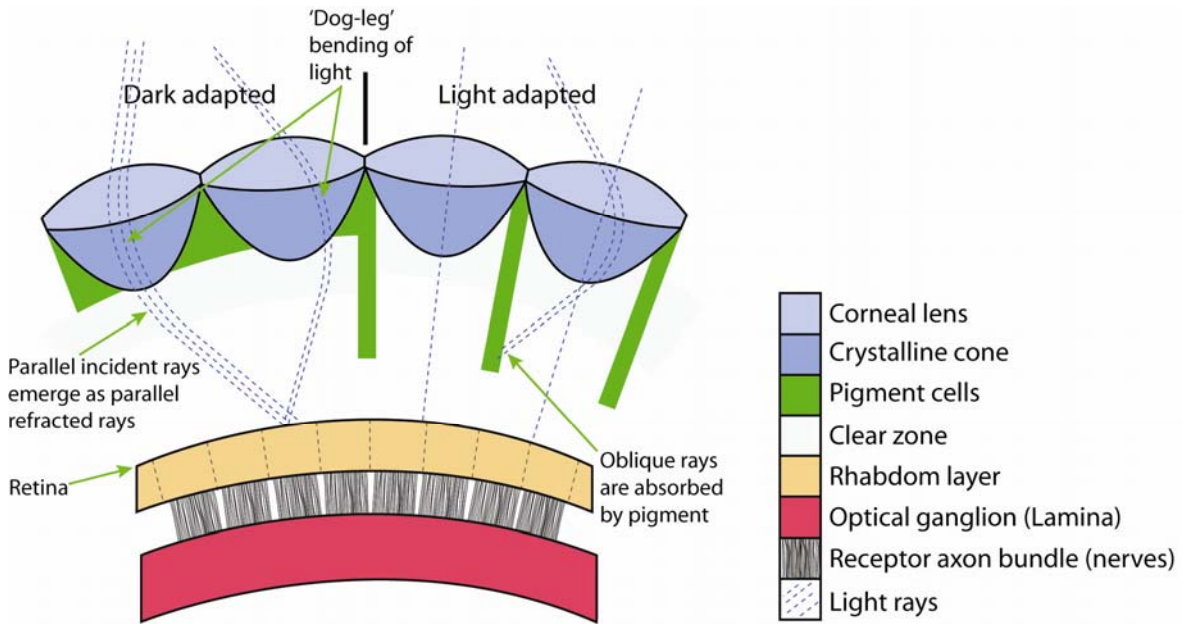


Figure 1.4 – Light and dark adapted states of the superposition eye.

Migration of pigment enables superposition eyes to adapt to light and dark conditions. In the light adapted state, the superposition eye acts as an apposition eye, light passing through each lens is focused on a different area of the retina. Blue dashed lines show the paths of light rays. Note how light is absorbed by pigment cells in the light adapted state preventing it from hitting the rhabdom beneath the adjacent lens. Image based on description in Land and Nilsson (2002, pp.156-157).

1.3.2.2.1 Refracting superposition

Refracting superposition systems can achieve ‘dog-ray’ bending of light in two ways (Nilsson, 1990; Land and Nilsson, 2002): (1) using two lenses, one positioned below the other at a distance of twice the focal length of the lens, to redirect the light ray back across the lens axis (Figure 1.5A), or (2) using a single ‘lens cylinder’ with a radial parabolic refractive index gradient (Figure 1.5B). The latter is found in the eyes of euphausiids crustaceans (Land and Burton, 1979), beetles (Caveney and McIntyre, 1981) and moths (Exner, 1891); the double lens system is used by some copepods and has been adopted in the design of some types of telescope (Land and Nilsson, 2002).

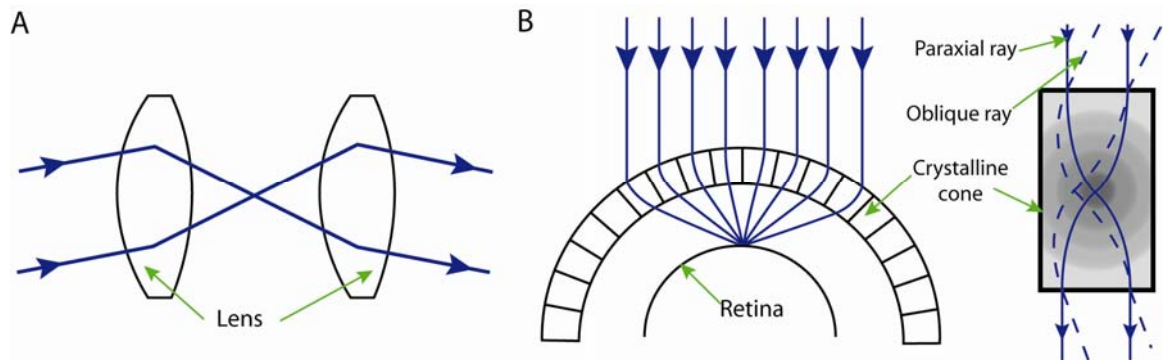


Figure 1.5 – The refracting superposition system.

A. The 'two lens' system used in telescopes. **B.** In refracting superposition eyes, light is refracted by the crystalline cones and brought to focus at a single point on the retina. This is achieved by using a lens with a parabolic refractive index gradient (right) to gradually bend the ray back across the lens axis. The different shades of grey represent a changing refractive index from low (light grey) to high (dark grey). Diagrams modified from Land and Nilsson (2002, figure 8.4, 8.14a and 8.5b).

1.3.2.2.2 Reflecting Superposition

Reflecting superposition systems focus light by using 'mirrors' (Figure 1.6), which in nature are silvered crystalline cones (Vogt, 1980). By positioning the silvered surfaces within the crystalline cones at 90° to one another (Figure 1.6B), oblique light rays are rotated through two right angles. The result of this system is that all rays are directed to a common focus (Figure 1.6A).

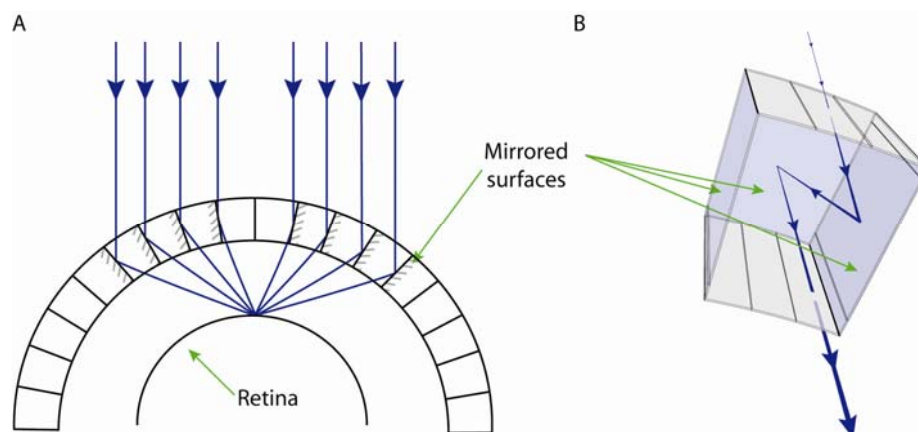


Figure 1.6 – The reflecting superposition system.

A. Mirrored surfaces on all sides of the crystalline cones allow the system to focus light rays onto a single point on the retina. **B.** A 3-dimensional image showing how a light ray is reflected at two surfaces to emerge at the lens base, parallel to the incidence ray. A modified from Land and Nilsson (2002, figure 8.14b). B. based on Vogt (1980, figure 4).

1.3.2.2.3 Parabolic Superposition

Parabolic superposition (Nilsson, 1988) (Figure 1.7) uses a combination of lens and mirror optics. Light rays entering the cone parallel to the optic axis are transmitted to a deep lying rhabdom. Oblique rays are reflected by the mirrored surface of the parabolic crystalline cone and are repeatedly reflected until they emerge from the cone as parallel rays and can cross the clear zone to reach the

retina as in other types of superposition eye (Nilsson, 1988; Land and Nilsson, 2002).

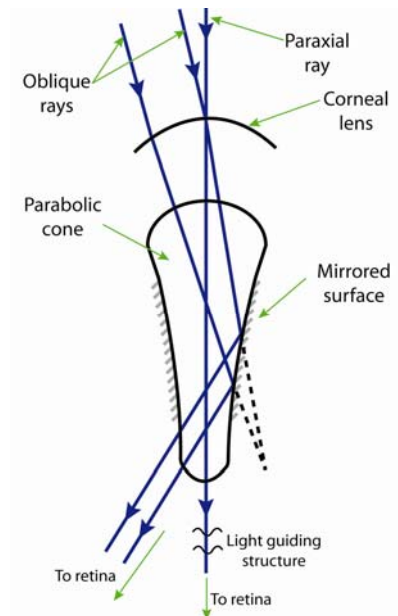


Figure 1.7 – The parabolic superposition system.

This system incorporates features of both refracting and reflecting systems to achieve ‘dog-ray’ bending of light. It is also capable of acting like an apposition eye when light enters parallel to the cone axis. Modified from Land and Nilsson (2002, figure 8.16).

1.4 Eye function: Requirement, Adaptation, Compromise

Light transmission in animals is not exclusively for vision; light transmission rods are constructed by sponges to transmit light to deep lying symbiotic photosynthetic organisms (Brümmer *et al.*, 2008). However, where optical elements are constructed for visual purposes, the required function of an eye very much determines how it is constructed and which of the above models of vision (section 1.3.2.1 and 1.3.2.2) is adopted. Potential functions include navigation, mate selection, communication and predator/prey detection; all of which require different specifications and specialisations in terms of spatial resolution and visual acuity. The internal structure of the eye and the length of the ommatidial capsule are restricted by the size of the organism itself. The required focal length of an optical system and therefore the refractive index of the lens, i.e. the material from which it is constructed, are key. With so many influencing factors, it is inevitable that in some cases at least, compromise comes into play. Compromise and/or adaptation can be seen across the animal kingdom, one example of adaptation of optical structures for specific a role is detailed below.

1.4.1 The Field of View of *Daphnia*

The eye of the primarily planktonic crustacean *Daphnia*, commonly referred to as the water flea, has been the subject of intense study thanks to its unusual structure. The single, approximately hemispherical, compound eye is located centrally on the head and consists of 22 widely separated ommatidia (Frost, 1975; Young and Downing, 1976; Smith and Macagno, 1990) (Figure 1.8). This lens arrangement provides the organism with a field of view of almost 360° with few or no blind spots (Young and Downing, 1976). It is highly adapted for a planktonic mode of life in which the animal is 'exposed' in an open space and therefore prone to attack from all angles. The rhabdoms are 12 µm long but the optics produce images 29 µm behind the lens for distant objects and at an even greater distance for close objects (Young and Downing, 1976). The result of this structure is that the lens in such an eye cannot form a sharp image on the rhabdom; image resolution has been compromised for an increased field of view.

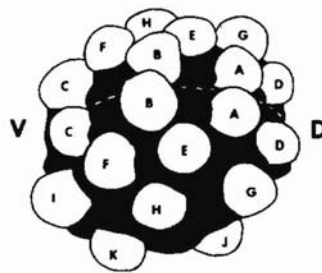


Figure 1.8 - The compound eye of the translucent water flea, *Daphnia*. Schematic diagram showing the widely spaced lenses of *Daphnia*. The total eye diameter is approximately 250 µm. Lenses are labelled A-K. V and D indicate ventral and dorsal sides respectively. The dashed line represents the midplane of the eye. Image from Smith and Macagno (1990, figure 1a).

1.5 Trilobite Eyes

Trilobite eyes are one of the earliest eyes in the fossil record (Parker, 2003, p.221); these compound eyes appear in even the most primitive of trilobites in the Early Cambrian, from about 520 Ma (Clarkson *et al.*, 2006) (Figure 1.9). Three distinct types of compound eye have been identified in trilobites: (1) holochroal, (2) schizochroal and (3) the less common abathochroal eye. In all three cases, the lenses, as well as all other parts of the cuticle, are composed of calcite enabling good preservation in the fossil record, mostly as exuviae (moulted exoskeletons). As trilobite lenses are integrated into the crystalline

exoskeleton, they have a fixed focal length; this is also the case in modern arthropods (e.g. *Limulus* - see Battelle, 2006 for review). Some present-day terrestrial and aquatic crustaceans and echinoderms have calcified corneal lenses (e.g. Dudich, 1931; Aizenberg *et al.*, 2001; Tanaka *et al.*, 2009), but no organisms, past or present, are known to have calcite lenses of such unusual construction as the trilobites.

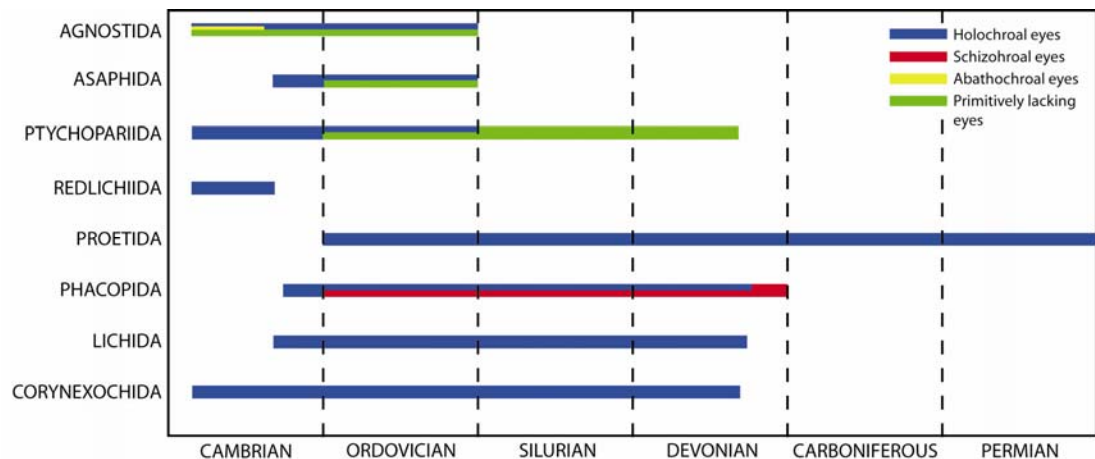


Figure 1.9 - Temporal distribution of trilobite Orders.

Holochroal eyes are found in most taxa. Schizochroal eyes are found in the Order Phacopida only (red) and abathochroal eyes are found in eodiscid trilobites (Agnostida) only. Based on Clarkson *et al.* (2006, figure 1).

Trilobites of the Suborder Agnostina, Conocoryphidae and some trilobite clades within the Order Asaphida typically lacked eyes. Some groups such as the proetids and phacopids display secondary eye loss/reduction (Clarkson *et al.*, 2006). This was particularly common in members of the Ordovician atheloptic deep water trilobite fauna (Fortey and Owens, 1987) and in the Devonian when it is interpreted as an evolutionary response to deepening of the oceans and extensive deposition of mud which obscured light (Feist, 1991). Increased eye size was present in some groups during the Ordovician such as the epipelagic *Carolinites* and Telephinids (Fortey, 1985) and the mesopelagic cyclopygids (Fortey, 1985; Fortey and Owens, 1987).

1.5.1 Holochroal Eyes

Holochroal eyes (Figure 1.10) are the most common type of trilobite eye, present in most taxa from the Early Cambrian to the end Permian. Studies of holochroal eyes reveal that they have a relatively simple construction compared with the schizochroal eye (see section 1.5.2.2).

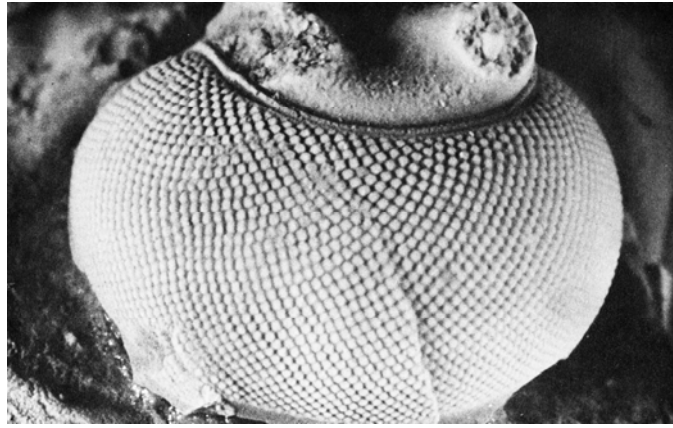


Figure 1.10 - The holochroal eye of *Scutellum campaniferum*.
Each lens is ~100 μm in diameter. Image from Levi-Setti (1975, plate 15a).

1.5.1.1 Lens Arrangement

Holochroal eyes consist of up to many thousand relatively small lenses (usually 30-100 μm in width) generally packed hexagonally and in direct contact with one another (i.e. there is no exoskeleton in between). In the majority of holochroal eyes, the lenses are hexagonal or round as in *Asaphus raniceps* Dalman, 1827 and *Sphaerophthalmus alatus* Boeck, 1838 respectively (Clarkson *et al.*, 2006) (Figure 1.11A, B). However, square lenses are present in *Telephina* (Fortey, 1997; Bruton and Høyberget, 2006). Han (2001) also reported octagonal lenses in some species of *Telephina*, the areas between neighbouring lenses are square. It is unclear whether these areas termed ‘interlenses’ have an optical function or are simply part of the exoskeletal. There is a taxonomic variation in lens shape and thickness as seen in lenses in cross section (Figure 1.11C and D). Lens thickness corresponds to exoskeleton thickness and is not thought to have a significant bearing on lens function, rather the convexity of the lens surface is of more importance optically (Clarkson in Kaesler, 1997 p.120). Both biconvex and plano-convex lenses have been described (Clarkson, 1979). In all holochroal eyes, the lenses are covered by a single common cornea which grades laterally into the outer layer of the exoskeleton (Clarkson in Kaesler, 1997).

The curvature of the visual surface on which the lenses are arranged varies between species and so too does the resultant field of view. A field of view of 35° vertically and 180° horizontally is typical of holochroal lenses (Clarkson *et al.*, 2006). Variation by as much as 60° in the horizontal field of view are evident within a genus (Clarkson, 1979).

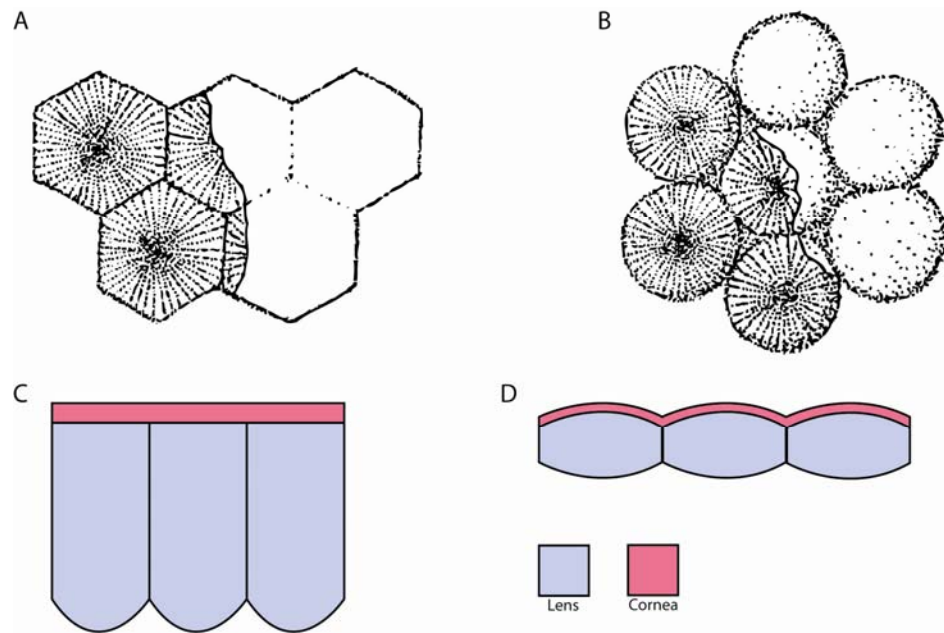


Figure 1.11 - Lens arrangements in holochroal eyes. Hexagonal close packing of A. hexagonal and B. circular lenses. The cornea has been omitted from the left of each image to show the radial arrangement of lamellae (calcite sheets) below. In cross section, both plano-convex (C) and biconvex (D) lenses have been identified. Images from (A, B) and modified from (C, D) Clarkson *et al.* (2006, figure 3).

1.5.1.2 Lens Structure

Holochroal eyes comprise lenses composed of a single calcite crystal consisting of radially arranged lamellae, or calcite sheets (Figure 1.11A,B and Figure 1.12), each consisting of calcite fibres termed trabeculae (Clarkson in Kaesler, 1997). Where the outer surface of the lenses is convex, the trabeculae fan outwards intersecting the visual surface at 90° (Clarkson, 1979); lenses with a planar outer surface do not display fanning of trabeculae. No further structures have been described in holochroal eyes.

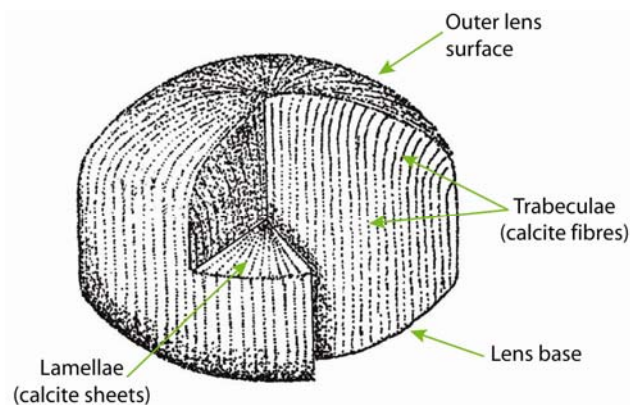


Figure 1.12 - Internal structure of the lenses in the holochroal trilobite eye. Trabeculae in the lens of *Paladin eichwaldi shunnerensis* fan outwards along the upper surface of the lens. Image from Clarkson *et al.*, (2006, figure 3a).

1.5.1.3 Lens Function

The lenses in holochroal eyes are often compared with those of the apposition eyes of modern animals (e.g. Clarkson *et al.*, 2006). The holochroal lenses may have had a function of both the corneal lens and crystalline cone in modern animals (i.e. to focus light onto the photoreceptive components below) (section 1.3.2.1, Figure 1.2).

The square lenses of *Telephina* have been compared to the reflecting superposition eyes of modern crustaceans (Fortey, 1997) (section 1.3.2.2.2, Figure 1.6), but this is based on lens morphology alone and Fortey noted that in true reflecting superposition eyes the eye is spherical whereas this is not the case in *Telephina*.

Arrangement and sizing of the lenses as well as the morphology of the whole holochroal eye has been used to determine mode of life in some deep water genera (e.g. Bruton and Høyberget, 2006). Eye parameter values (see section 7.1.3) calculated by McCormick and Fortey (1998) have been used to determine, more precisely, the palaeobathymetry of pelagic forms.

1.5.2 Schizochroal Eyes

The schizochroal eye (Figure 1.13) is restricted to trilobites of the Suborder Phacopina (Order Phacopida), ranging from the Ordovician to Devonian (Kaesler, 1997) (Figure 1.9). The presence of a similar eye in the juvenile stages of some species with holochroal eyes at adult stages (Clarkson, 1979; Clarkson and Zhang, 1991; Clarkson and Taylor, 1995) suggests that the schizochroal eye originated by paedomorphosis, the evolutionary process by which an adult stage descendant displays characteristics of the juvenile form of its ancestor. McNamara (1978) suggested, in relation to paedomorphosis in olenellid trilobites, that this process is an adaptation to changing environmental conditions.

The schizochroal eyes of trilobites are often compared to the euchelicerate ‘horseshoe crab’, *Limulus polyphemus* (e.g. Fordyce and Cronin, 1989; Clarkson

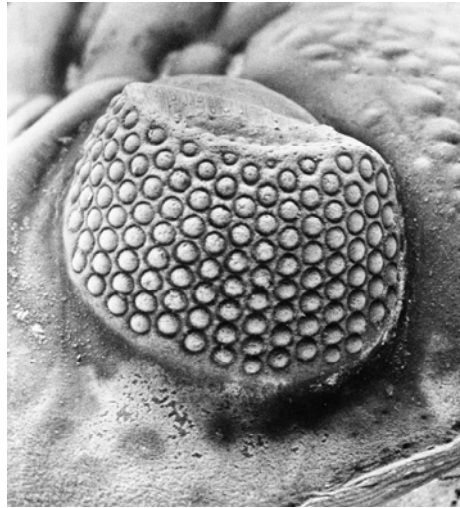


Figure 1.13 - The schizochroal eye of *Phacops rana milleri*.
Each lens is ~500 μm in diameter. Image from Levi-Setti (1975, plate 26).

et al., 2006). These modern arthropods have three types of eye: lateral compound eyes; a median eye; and a pair of ventral eyes located on the cuticle in front of the mouth (Battelle, 2006). The positioning of each of these three sensory organs suggests that they may be the equivalent of schizochroal eyes, the maculae and the 'median eye' (Ruedemann, 1916) or 'glabellar tubercle' (Fortey and Clarkson, 1976) respectively. The lens shape and size, and the spacing of lens axes in schizochroal eyes (see section 1.5.2.1) are similar to the lateral compound eyes of *Limulus* (Clarkson, 1966; Campbell, 1975; Fordyce and Cronin, 1989). However, the lenses/cuticular cones on each lateral eye of *Limulus* reach over 1000 in number and function as apposition eyes, with a single ommatidium behind each lens (e.g. Battelle, 2006) (section 1.3.2.1), which is more consistent with the interpreted function of holochroal eyes (section 1.5.1.3). Lenses in *Limulus* are 'packed' in a less organised manner (e.g. Battelle, 2006), to the hexagonal or square arrays (see section 1.5.2.1, Figure 1.14) seen in schizochroal eyes and as a result, the inter-ommatidial angles vary across the eye, ranging from -2° (overlap in lens axes) to 15° (Waterman, 1954; Von Campenhausen, 1967). Lenses in the eyes of *Limulus* focus light by means of a gradient in refractive index (Clarkson *et al.*, 2006), this has been suggested as a mechanism in schizochroal eyes (Bruton and Haas, 2003) (see section 1.5.2.3), but has yet to be confirmed. Despite the eyes of some other modern animals, such as deep sea ostracods, scallops and male strepsipteran insects, being considered as 'counterparts' to the schizochroal eye, none have been found in which all typical schizochroal eye characteristics are present (Horváth *et al.*, 1997) (see section 1.5.2.1 and 1.5.2.2).

Studies of the schizochroal eye began over 120 years ago with the work of Clarke (1889) and Lindström (1901) providing detailed descriptions of both external and internal features of the lenses. Major advances were made in the 1960's and 1970's when studies were published by Clarkson (e.g. 1967, 1979), Towe (1973), Clarkson and Levi-Setti (1975) and Campbell (1975), providing considerable detail of the internal structure of the lenses by light microscopy. This work continued into the next decade when Miller and Clarkson (1980) proposed a growth mechanism model for schizochroal lenses (see section 1.5.4, Figure 1.23) based on Scanning Electron Microscope (SEM) imaging of acid etched thin sections. Work on the optics of the lenses (Campbell, 1975; Clarkson and Levi-Setti, 1975; Horvath, 1989; Horvath and Clarkson, 1993; Gál *et al.*, 2000) and studies of lens arrangement and field of view (Cowen and Kelley, 1976; Stockton and Cowen, 1976) as well as comparison with modern animals (Fordyce and Cronin, 1989, 1993) provided insights into how the schizochroal eye as a whole may have functioned. More recent work by Bruton and Haas (2003a), Schoenemann (2007) and Schoenemann and Clarkson (2008b) provide alternative suggestions to these earlier studies (see Chapter 7 for details). Questions raised by Bruton and Haas (2003a) as to the origin of the intralensar structures described in earlier work (e.g. Campbell, 1975; Clarkson and Levi-Setti, 1975) were addressed by Lee *et al.* (2007a). In the pilot study that led to the present work, Lee *et al.* (2007) found that intralensar structures in at least some schizochroal eyes are of primary origin. Understanding the detailed structure and composition of the lenses is vital in accurately modelling how they worked.

1.5.2.1 Lens Arrangement

Schizochroal eyes differ from other trilobite eye types in lens shape, size and spacing (Figure 1.13). Lenses are biconvex, large in diameter, ranging from approximately 200 μm to 500 μm and occasionally as much as 750 μm (Clarkson, 1975) and few in number, typically 70-150 with a maximum of 770 (Roy, 1933). Lenses are arranged in diagonal rows and dorso-ventral files (Figure 1.14A); the number of lenses is dependant on the species of trilobite and its ontogenetic stage. Tall cylindrical eyes have been identified in *Erbenochile erbeni*, which have as many as 18 lenses per file (Fortey and Chatterton, 2003). Possible sexual dimorphism has also been identified in some species with schizochroal eyes; different morphs show differences in the number of lenses per file, number of

files, lens sizes and structures and, in some cases, thickness and height of the surrounding cuticle (Campbell, 1975). Lenses are packed hexagonally (Figure 1.14B left) in most species. *Barrandeops forteyi* Chatterton *et al.*, 2006 and *Phacops turco* aff. *Praecedens* Haas (Fortey and Morris, 1977) are exceptions to this, as they exhibit cubic packing (Figure 1.14B right). Each lens in the schizochroal eye has an individual calcite cornea that plunges below the visual surface into the cuticular material separating the lenses (Figure 1.14C); this interlensar sclera extends below the base of the lens and is also composed of calcite.

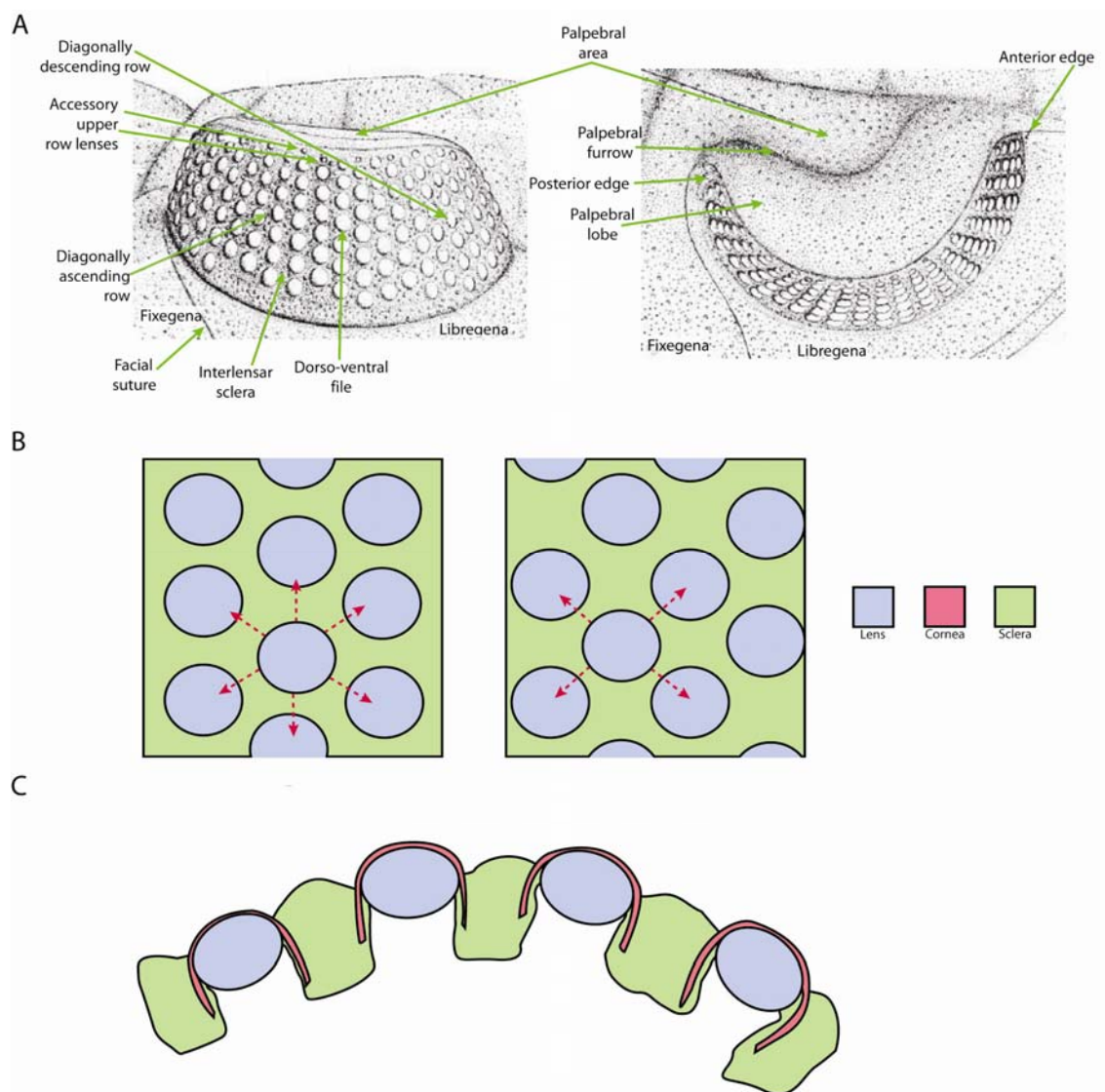


Figure 1.14 – Lens arrangement in the schizochroal eye.

A. A 3D reconstruction of a schizochroal eye. Image modified from Clarkson (1966, figure 1)
B. Different lens packing arrangements in schizochroal eyes. In hexagonal packing (left), each lens has six equally spaced neighbours (red arrows), in cubic packing (right) each lens has only four equally spaced neighbours. For simplicity, the cornea is not included but would cover the entire outer surface of each lens only, not the surrounding sclera.
C. Schematic diagram showing a horizontal section through a few lenses of the schizochroal eye of *Geesops schlotheimi*.

Lenses first appeared at the protaspis stage, increasing in number at each moult by “row by row” addition (Clarkson, 1975, see Harzsch and Hafner, 2006 for brief review). This growth occurred at the generative zone of the eye, initially located below the palpebral suture (Clarkson, 1975). During growth, this zone progressively moved away from the palpebral region (see Figure 1.13A) and the form of the generative zone, an anteriorly expanding logarithmic spiral, resulted in the addition of new lenses below the previous row, forming the regular sequence of diagonal rows and dorso-ventral files characteristic of the schizochroal eye (Clarkson, 1975) (Figure 1.14A). Stockton and Cowen (1976) suggest that packing lenses in this way and establishing rows early in ontogeny, and simply adding lenses to rows during growth, was neurologically simple. The number and height of dorso-ventral files was controlled by the length of the active section of the generative zone (Thomas, 1998). The mechanism by which lenses were emplaced is clearly separate from that which controls growth of the visual surface, as there are rare instances in which trilobites have a visual surface without lenses (Thomas, 2005). Growth of lenses occurred via a developmental programme rather than being under immediate genetic control (Thomas, 1998, Thomas, 2005).

1.5.2.2 Lens Structure

Even the earliest studies discussed the presence of internal structures within schizochroal lenses (Clarke, 1889; Lindström, 1901). Several features were found to be common to all such lenses (Figure 1.15), although preservation of some features is variable.

(1) The cornea. The cornea (Figure 1.16B) is a thin film which is separate from the sclera but held in place by it (Clarke, 1889). It consists of three layers (Campbell, 1975); the corneal layer is sandwiched between an upper organic cuticle and a lower corneal membrane (Miller and Clarkson, 1980). The organic epicuticle covers both the lens and the sclera, whereas the corneal membrane plunges through the sclera and has been interpreted as lining the lens capsule which would have lain beneath (Miller and Clarkson, 1980). The corneal layer is homologous with the prismatic layer of the cuticle and wedges out where the lens meets the sclera (Miller and Clarkson, 1980). Campbell (1975) was unable to determine crystal orientation in the cornea but speculated that random crystal

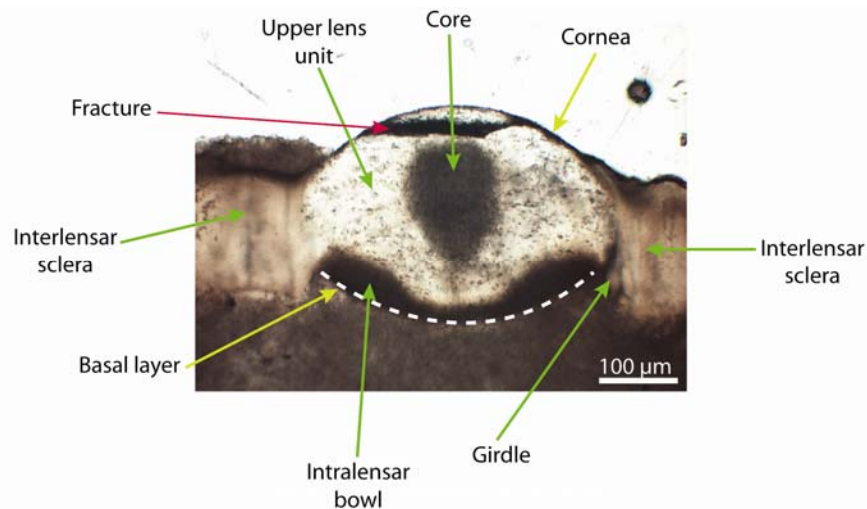


Figure 1.15 – The lens of *Dalmanites* sp. in thin section.

A lens imaged in plane polarised transmitted light showing the features common to all schizochroal lenses. The core and intralensar bowl are easily identified by their dark colour. The cornea and basal layer are not preserved in this lens but their expected locations are indicated (yellow arrows). The white dashed line indicates the base of the lens.

orientation would be most probable. Towe (1973) noted the presence of ‘radially oriented polycrystalline calcite’ in the corneal covering, however comparison of the images from Towe’s study (1973) with images in other studies (Miller and Clarkson, 1980; Bruton and Haas, 2003a; Lee *et al.*, 2007a) and the present study (see section 5.1.1.1) suggests, as noted by Clarkson (1975), that what Towe termed the ‘corneal covering’ may in fact include both the corneal components and the upper unit of the lens as described by Campbell (1975).

(2) The upper lens unit. This area of the lens (Figure 1.15 and Figure 1.16B) has been reported to consist of calcite of uniform orientation, with the *c* axis parallel to the lens axis (Towe, 1973) or of radially arranged calcite crystals, with the *c* axes changing in a regular manner across the lens (Campbell, 1975; Miller and Clarkson, 1980). Laminations present in this area of the lens are curved, but not to the degree of the outer surface of the lens, and are interpreted as growth lines in horizontal sections (i.e. sections cut parallel to the palpebral lobe) (Bruton and Haas, 2003a) along which there may have been organic matter (Miller and Clarkson, 1980). Laminations were also recognised in tangential section (i.e. sections cut perpendicular to the palpebral surface) by Miller and Clarkson (1980) who noted the presence of the calcitic needles termed trabeculae that form the laminae (Figure 1.16A). The needles themselves are only inferred to be present, as it is the turbid areas between them that are visible in transmitted light; it has been suggested that these

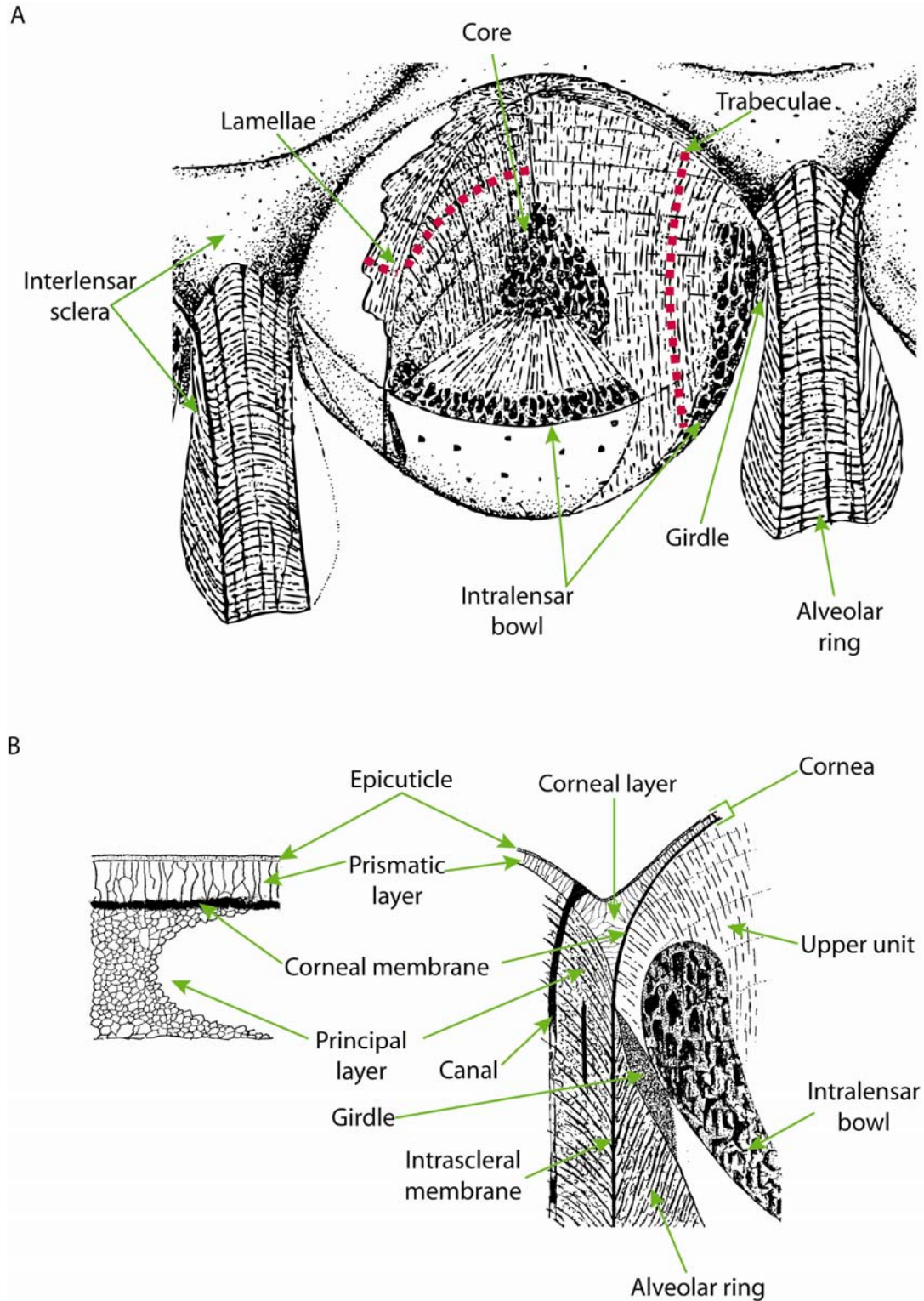


Figure 1.16 – The internal structure of lenses and the surrounding sclera in the schizochroal eyes of *Phacops rana milleri*.

A. Structure of the schizochroal lens of and B. Details of location and extent of corneal components within the lens. Images modified from Miller and Clarkson (1980, figure 3A). The lamellae in A may be the same features termed ‘growth lamellae’ by Bruton and Haas (2003a).

turbid regions represent areas once occupied by organic matter (Schoenemann and Clarkson, 2008b). These structures are parallel with the lens axis in the lower area of the lens but splay outwards at the visual surface up to an angle of

70° (Miller and Clarkson, 1980; Schoenemann 2008a). These features allowed Miller and Clarkson (1980) to speculate on the construction of the schizochroal lens, noting for the first time that lenses had an ‘open mesh construction’ rather than a simple single crystal of calcite as was previously assumed (Towe, 1973).

(3) The core. This structure, of varying size, is located approximately in the centre of the lens and is often ‘pear-drop shaped’ (Campbell, 1975) (Figure 1.15, Figure 1.16). Named ‘the core’ by Campbell (1975), this structure is what was termed the sub-corneal lens by Towe (1973), or is at least located in this area, and the diagenetically altered proximal nucleus identified by Clarkson (1967). It has been found to consist of uniformly oriented calcite, with the *c* axis parallel to the lens axis (Towe, 1973; Campbell, 1975; Lee *et al.*, 2007a). In transmitted light, the core has a speckled appearance due to the presence of inclusions (Campbell, 1975) and micropores (Lee *et al.*, 2007a). The chemistry of the core has for some time been believed to differ from that of the upper unit of the lens; Miller and Clarkson (1980) confirmed the presence of dense ferroan calcite in the core whereas Campbell (1975) showed variation in magnesium content throughout a lens, but with no apparent correlation with the position of the core. Lee *et al.* (2007a) found a direct correlation between position of the core and enrichment of magnesium in *Dalmanites* sp.; the magnesium being present in microdolomite crystals. The variation in size of the core, even within a single specimen, has been attributed to diagenesis, as alteration would result in a growing ‘diagenetic front’, extending from the core in all directions (Miller and Clarkson, 1980).

(4) The intralensar bowl. This feature found along the base of the lens (Figure 1.15 - Figure 1.17) has been documented in many studies (Roy, 1933; Clarkson, 1967; Clarkson and Levi-Setti, 1975; Miller and Clarkson, 1980; Lee *et al.*, 2007a) and is identified by its distinct brown colour when viewed in thin section by plane polarised transmitted light. The intralensar bowl was initially believed to be solid or gelatinous and composed of organic matter (Clarkson, 1975). Miller and Clarkson (1980) noted the similar appearance of the bowl to the ferroan calcite found in the core but noted that this calcite is a coarsely recrystallised replacement material and therefore does not represent the original composition of the bowl and core. Recent electron microprobe data (Lee *et al.*, 2007a) has shown the bowl, like the core, to have elevated levels of magnesium. Lee *et al.*

(2007a) interpreted this as an indication of originally high-magnesian calcite, as was suggested by Miller and Clarkson (1980). The shape of the bowl varies between species (Figure 1.17); some are thin and centrally indented by a dimple where as others are thick with a large hemispherical depression (Clarkson and Levi-Setti, 1975).

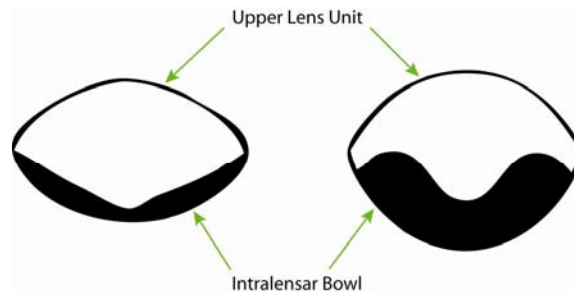


Figure 1.17 - Shapes of intralensar bowls in lenses of schizochroal eyes. Intralensar bowls of *Dalmanitina socialis* (left) and *Crozonaspis struvei* (right) show similarities to Cartesian surfaces (see section 1.5.2.3). Images redrawn from Clarkson and Levi-Setti (1975, figure 4b and 4d).

Clarkson (1975) and Gál *et al.* (2000) noted that in some lenses the intralensar bowl is of the same mineralogy as the host rock. This was assumed to indicate that the basal layer beneath the bowl (see below) had been destroyed and the bowl had ‘fallen out’ (Gál *et al.*, 2000). As the bowl, presumed to be of organic composition, was lost, the infilling matrix was moulded to the upper lens unit. In light of the findings of Lee *et al.* (2007a) it may be the case that the loss of bowl was a result of preferential early dissolution of high-magnesian calcite (see Wollast and Reinhard-Derie, 1977).

Despite the identification of the intralensar bowl and core in numerous species of phacopid trilobite (Lindström, 1901; Clarkson, 1967; Campbell, 1975; Clarkson and Levi-Setti, 1975; Miller and Clarkson, 1980), the authenticity of these structures was questioned by Bruton and Haas (2003a). Their study of *Geesops* lenses, in which optically clear calcite features were identified in place of the core and intralensar bowl, led to the suggestion that such structures could be artefacts of diagenesis in an originally featureless calcite lens which included organic matter in its structure.

(5) The basal layer. Campbell (1975) briefly mentioned this feature, stating that it can be followed around the circumference of the lens, appearing to connect to the corneal membrane. It consists of clear, randomly oriented, calcite

crystals. Miller and Clarkson (1980) noted the presence of a feature termed the 'girdle', consisting of white or pale grey finely crystalline calcite between the lens base and the alveolar ring. Miller and Clarkson (1980) do not suggest a function for the girdle; perhaps this feature represents partial preservation of the basal layer at the lateral margins of the lens only. Bruton and Haas (2003) suggest that this feature is composed of organic material in specimens of *Geesops sparsinodosus*, as it is dark in colour.

The lenses are set at the top of a cylindrical cavity, the sublensar alveola (Clarkson in Kaesler, 1997), the boundary of this cavity is created by the interlensar sclera, which extends beyond the base of the lens. The cornea cuts through the sclera, creating a ring in three dimensions called the interscleral membrane (Clarkson in Kaesler, 1997) (Figure 1.16B).

Sub-lensar structures are rarely preserved as they were not mineralised but have been identified in a few instances in different species. Fibrous appendices (Lindström, 1901; Stürmer and Bergstrom, 1973), cones (Clarkson, 1967) and mesodermal capsules (Bruton and Haas, 2003a) (Figure 1.18A) have all been identified by studying thin sections in transmitted light. Schoenemann *et al.* (2008) has identified sublensar capsules and the stalks of possible light perceiving structures in schizochroal eyes, revealed by the non-destructive technique of 3D X-ray tomography (3D- μ CT). The images showing these structures are somewhat ambiguous and no other techniques have been used to confirm the presence of such structures (Figure 1.18B).

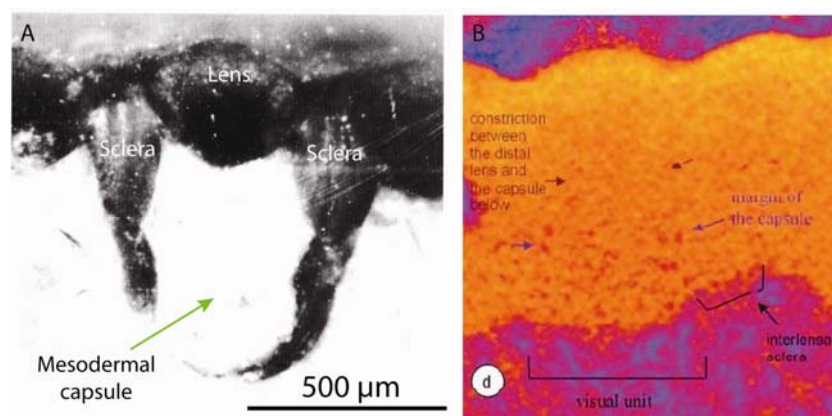


Figure 1.18 - Sublensar structures in schizochroal eyes.

A. The 'mesodermal capsule' identified by Bruton and Haas (2003a, figure 4) and **B.** The 'sublensar capsule' identified by Schoenemann *et al.* (2008, figure 2d). No scale is provided on B, however the depth of the 'capsule' appears to be on a similar scale to that in A based on the width of the visual unit.

1.5.2.3 Lens Function

Towe (1973) interpreted the presence of uniformly orientated calcite as evidence that the trilobite lenses in his study were original, as the precise orientation of the calcite would enable lenses to overcome the effects of birefringence and behave optically like glass, i.e. light entering along the *c* axis would not be doubly refracted. Towe (1973) tested the optical properties of these lenses by embedding them in clear epoxy resin and grinding them from the rear. Sections were positioned on a microscope stage, visual surface down, and objects below brought into focus. An inverted image is reported to have formed on each individual lens; image formation being successful across a large depth of field from a few millimetres up to infinity. Towe took this as evidence that trilobites had a 'significantly better optical system than that of the few living arthropods known to have calcified corneal lenses'. However, by grinding down the rear surface of the lens Towe changed the shape significantly, from biconvex to hemispherical. These results do not therefore accurately represent the focusing capabilities of the lenses, as angle of refraction is partly dependant on surface curvature. Towe (1973) also noted that these results do not indicate whether trilobites were capable of form perception (i.e. could see images and shapes rather than light and dark) because photoreceptors are not preserved and it is therefore unclear how the eye functioned overall.

Clarkson and Levi-Setti (1975) showed how the boundary between the upper lens and the intralensar bowl acted as an aplanatic surface to enhance the focusing capabilities of the lenses. The boundary between the lens calcite and the bowl would have caused significant refraction of rays (Clarkson and Levi-Setti, 1975), reducing the spherical aberration, or blur, of the lens, as is the case in Cartesian ovals, independently designed by DesCartes (1637) and Huygens (1690) (Figure 1.19). An aplanatic surface would only be successful in focusing light if there was a change in refractive index across the boundary. Optical modelling by Horváth (1989) showed that for lenses of *Crozonaspis struvei* and *Dalmanitina socialis* this requires a refractive index (RI) in the bowl of 1.53 and 1.40 respectively; the RI of calcite is approximately 1.66 (see section 2.8.2.4). Based on these figures, Horvath (1989) suggested that this might be achieved by constructing the bowl from an hydrated chitin-like substance in *Crozonaspis struvei* and a wet jelly-like substance in *Dalmanitina socialis*.

Gál *et al.* (2000) proposed that the 'central bulge' in the upper unit of calcite (i.e. the central dimple in the intralensar bowl) may have provided the lens with bifocality; the central area of the lens sampling near objects and the peripheral areas focusing on objects in the distance. This may seem to be a huge advantage to an organism that has no accommodation ability, i.e. cannot flex the lens to achieve different focal lengths, however the authors themselves (Gál *et al.*, 2000) admitted that it is not clear whether such a function was necessary for the trilobites.

An alternative model for schizochroal lens function was proposed by Bruton and Haas (2003a); that of a gradient index (GRIN) lens in which light was focused by continuously refracting the rays as they passed through the lens. This could have been achieved by a gradual change in the refractive index of the lens by incorporating organic matter (Bruton and Haas, 2003a). Light rays passing through the peripheral areas of such a lens are refracted less than in a homogeneous lens allowing light to come to a tighter focus, i.e. spherical aberration is reduced. This mechanism is adopted by fish (Land and Nilsson, 2002) and some modern arthropods (Campbell, 1975). However, there is no evidence that organic matter was incorporated into the trilobite lenses. Despite the significant attention given to the potential function of the intralensar bowl (Clarkson and Levi-Setti, 1975; Gál *et al.*, 2000), no suggestions have been made to explain the presence of the core.

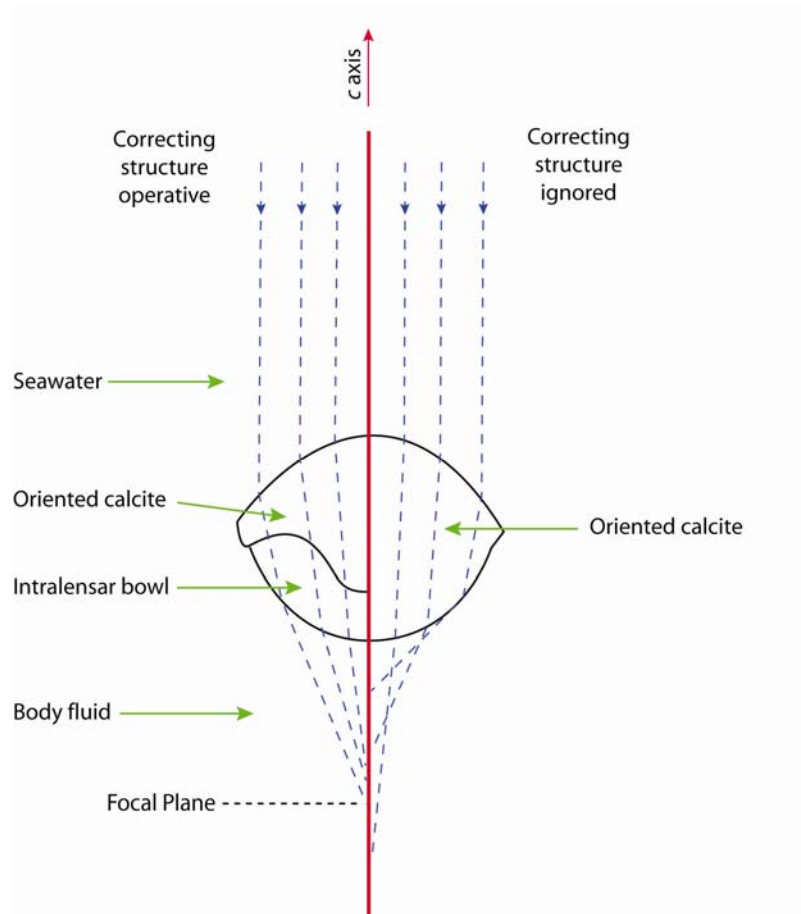


Figure 1.19 – The function of the intralensar bowl.

Light rays entering the lens along the c axis come to a sharp focus only with the assistance of the aplanatic surface created by the insertion of an intralensar bowl. Note that the core is not included in this model. Image redrawn from Clarkson and Levi-Setti (1975, figure 5a).

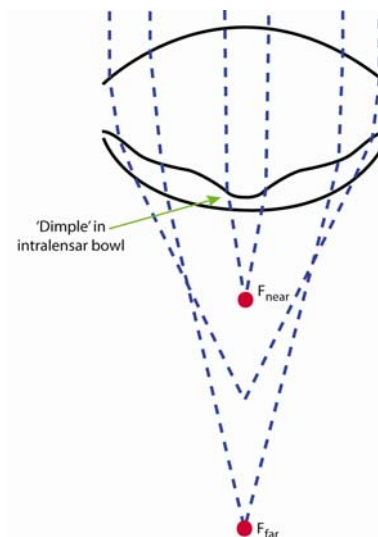


Figure 1.20 - The bifocal lens of *Dalmanitina socialis*.

Gál *et al.* (2000) interpreted the range of focal lengths of the lens (red dots) created by the 'dimple' in the intralensar bowl as bifocality. Blue dashed lines represent light rays, only a few rays have been shown for simplicity. The refractive index was assumed to be 1.66 for the upper lens and 1.40 for the intralensar bowl. Image modified from Gál *et al.* (2000, figure 3).

1.5.3 Abathochroal Eyes

The abathochroal eye is the least common type and is found only in the Early to Middle Cambrian Suborder Eodiscina. Jell (1975) described this type of eye in the trilobite *Pagetia* using the features revealed by internal and external moulds and latex casts to make assumptions on the lens shape and size.

1.5.3.1 Eye Structure

Study of the internal moulds led Jell (1975) to conclude that lenses in the abathochroal eye were thin and biconvex. The lenses are separated by thin exoskeletal material (Figure 1.21) that does not plunge below the base of the lens as in schizochroal eyes (section 1.5.2.1, Figure 1.13C). The similarity in texture between the interlensar areas and the cheek was interpreted as an indication that this area was not covered by a corneal membrane; it is thought that each lens was covered by an individual cornea which terminated at the lens edge. Some species have a 'dimple' in the centre of the lens (Zhang and Clarkson, 1990) making the lens base one of an aplanatic nature. Unlike schizochroal eyes, abathochroal eyes show no evidence of an intralensar bowl below this surface.

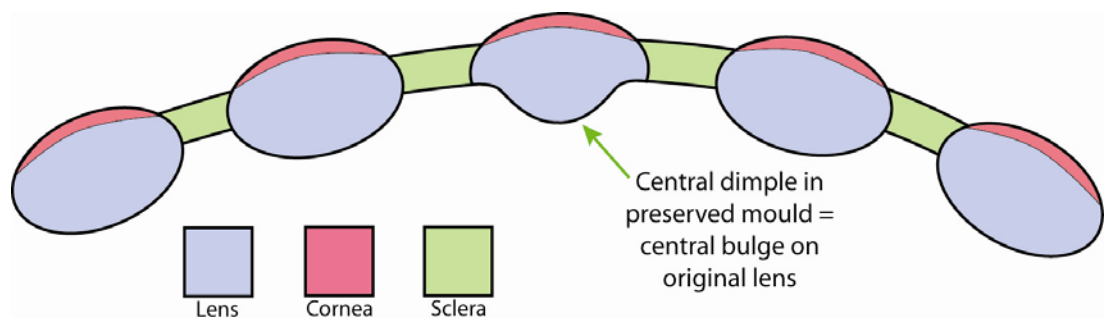


Figure 1.21 – The lens arrangement in the abathochroal eye of *Pagetia*. Schematic diagram based on Jell (1975, figure 1).

1.5.3.2 Eye Function

Based on the lack of deep penetrating sclera, Jell (1975) suggested two possible mechanisms for eye abathochroal function: (1) the eye was of apposition type (section 1.3.2.1) with the movement of pigment enabling isolation of ommatidia or (2) the ommatidia were not isolated from each other and were therefore of superposition type (section 1.3.2.2). Jell (1975) favoured the former mechanism

and speculated that the primary purpose of this eye was to detect changes in light intensity and produce a mosaic image.

1.5.4 Biomineralisation and the Construction of the Trilobite Eye

The trilobite eye, and indeed the whole exoskeleton, was grown by biomineralisation (Towe, 1973); the process whereby an organism exhibits biological control over the secretion of its mineralised skeleton (Dove, 2010). This ‘control’, which is powered by acidic glyco-proteins, dictates the chemistry, crystallographic orientation and microstructure of the mineralised parts and is thought to initiate with the harbouring of amorphous calcium carbonate (ACC), which is crystallised when required (Dove, 2010 and references therein); in the case of arthropods this begins prior to moulting the existing exoskeleton (Roer and Dillaman, 1984; Compère *et al.*, 1998) (see section 7.2.2 for more details), presumably minimising the vulnerability of the organism. This phenomenon is at an advanced level in many terrestrial crustaceans that, unlike marine species, do not have a readily available exogenous source of calcium (Luquet and Marin, 2004).

The biomineralisation processes of modern organisms have been the subject of many studies (Addadi *et al.*, 2006; Dalbeck and Cusack, 2006; Griesshaber *et al.*, 2007; Cusack *et al.*, 2008a; MacDonald *et al.*, 2010). Extraction and analysis of individual proteins provides details on how different components of the skeletal structure are controlled, even revealing the presence of ‘anti-calcifying’ macromolecules; inhibitors used to prevent crystallisation of calcium carbonate enabling organisms such as echinoderms to incorporate porosity into their structure or to prevent spontaneous calcification of soft tissues (Dove, 2010 and references therein). Because of degradation of organic components during diagenesis, such studies are not possible on the trilobite exoskeleton.

The presumed mechanism of trilobite eye construction has only been documented in one study; that of Miller and Clarkson (1980) for the schizochroal eye of *Phacops [=Eldredgeops] rana milleri* (Stewart 1927).

The growth of holochroal eyes may occur by the addition of trabeculae to the lens edges (Clarkson in Kaesler, 1997, p.120), the trabeculae fanning out at the distal edges as the lenses grow (Figure 1.22).

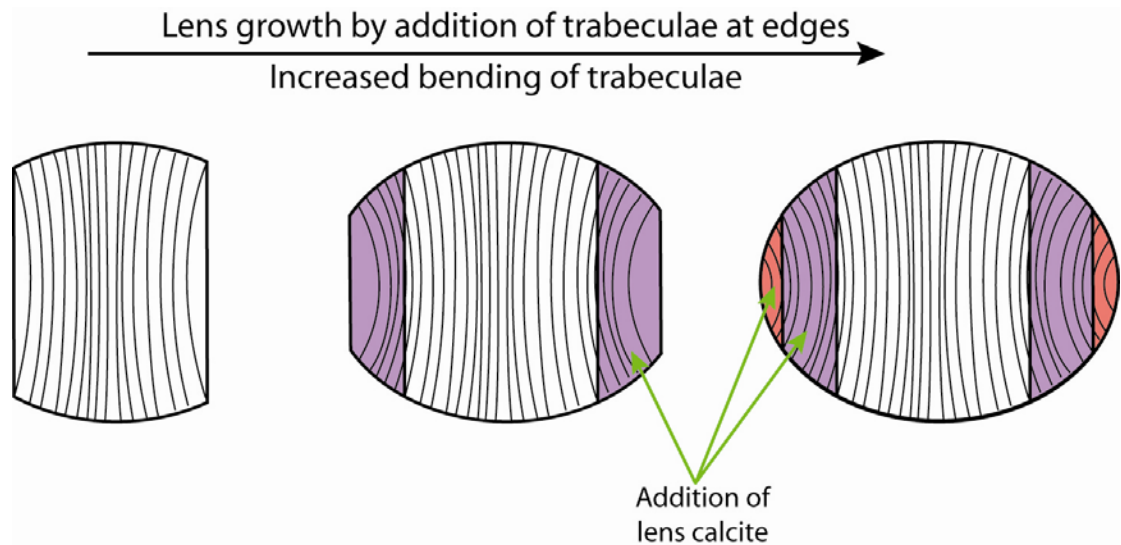


Figure 1.22 - Growth of holochroal lenses by addition of trabeculae. Lenses grow in size by addition of trabeculae at the lens edges, interpreted from Kaesler (1997). Areas of 'new' growth are indicated by the purple and red areas.

Schizochroal lens growth involved a more complex mechanism; four distinct post-ecdysial stages have been identified (Miller and Clarkson, 1980) (Figure 1.23).

Initially growth began from the lower surface of the cornea, with the formation of a simple calcite cone (Figure 1.23 - stage 1). This progressed to a relatively thin biconvex lens (Figure 1.23 - stage 2), then on to a Huygensian-shaped unit of calcite (Figure 1.23 - stage 3), occupying the full width between the scleral projections, themselves not yet fully formed. Finally the lens would reach completion with the growth of a central core and an intralensar bowl, both of massive texture (Figure 1.23 - stage 4).

Miller and Clarkson (1980) did not discuss the details of how the central core may be emplaced in the already existing upper lens unit. The epicuticle and prismatic layer of the new cuticle is thought to have formed above the hypodermis prior to moulting. The sclera between the lenses did not reach completion until after the lenses had matured (Miller and Clarkson, 1980).

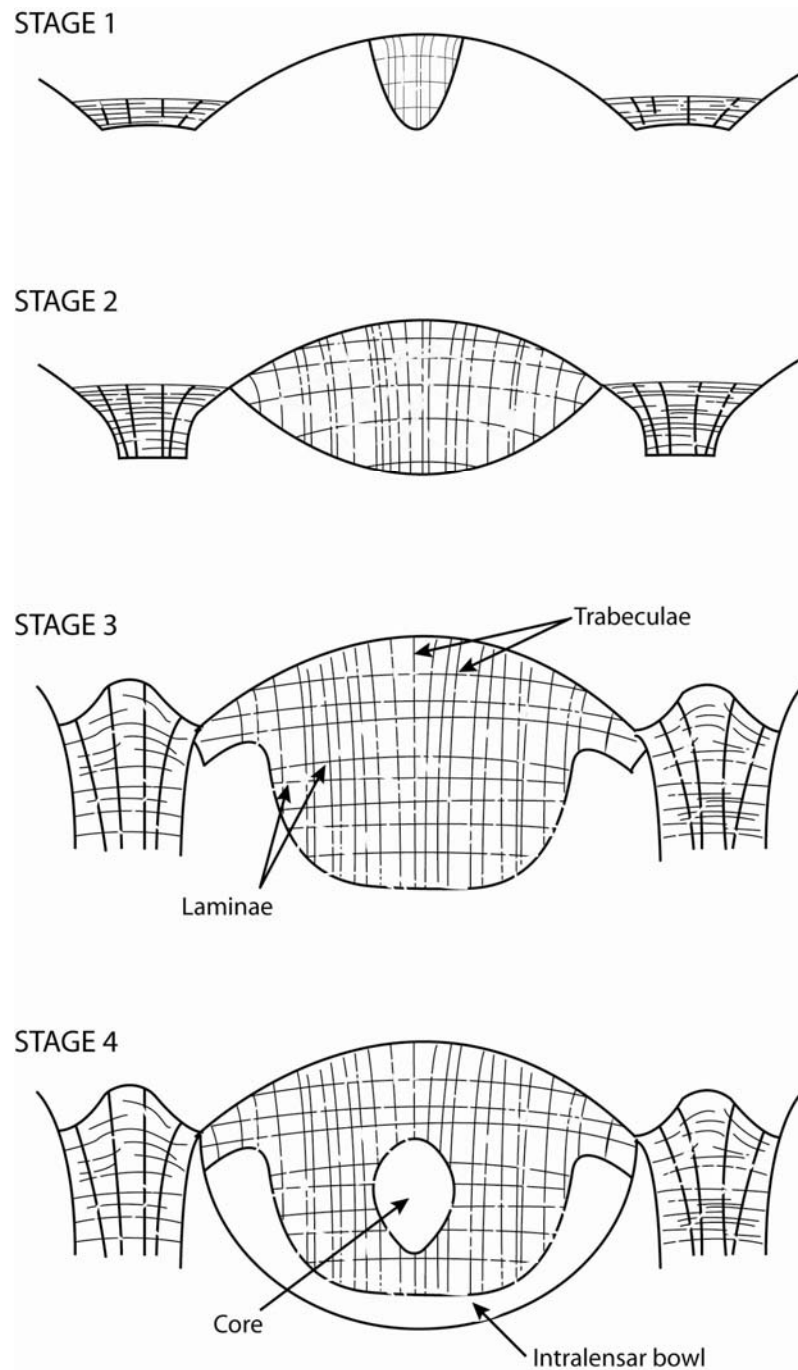


Figure 1.23 – Biomineralisation of the schizochroal trilobite eye - Post-ecdysial lens development.

The four stages of lens formation as described by Miller and Clarkson (1980). Image modified from Miller and Clarkson (1980, figure 2).

1.6 Calcite in Modern Optical Systems

1.6.1 Ostracods

Myodocopid ostracods have laterally positioned compound eyes beneath a transparent area of the carapace (Tanaka *et al.*, 2009). Unlike the compound

eyes of other arthropods, these eyes lack a cuticular lens; each ommatidium is overlain by a crystalline cone only (Tanaka *et al.*, 2009). Other ostracode groups including the modern podocopids (Tanaka, 2006) and the Palaeozoic primitiopsids (Tanaka *et al.*, 2009) (Figure 1.24) possess what is known as a naupliar eye. This type of eye, one of the most common in crustaceans, consists of ocellar-type structures; one found laterally on each valve and a third found ventrally in some species (Andersson and Nilsson, 1981; Tanaka, 2006) covered externally by a strongly calcified cuticular lens which is continuous with the carapace (Figure 1.24A and Figure 1.25A). At this point on the carapace there is a layer of prismatic calcite orientated perpendicular to the outer surface, in contrast to other areas of the carapace which consist of a foliated ultrastructure (Tanaka *et al.*, 2009).

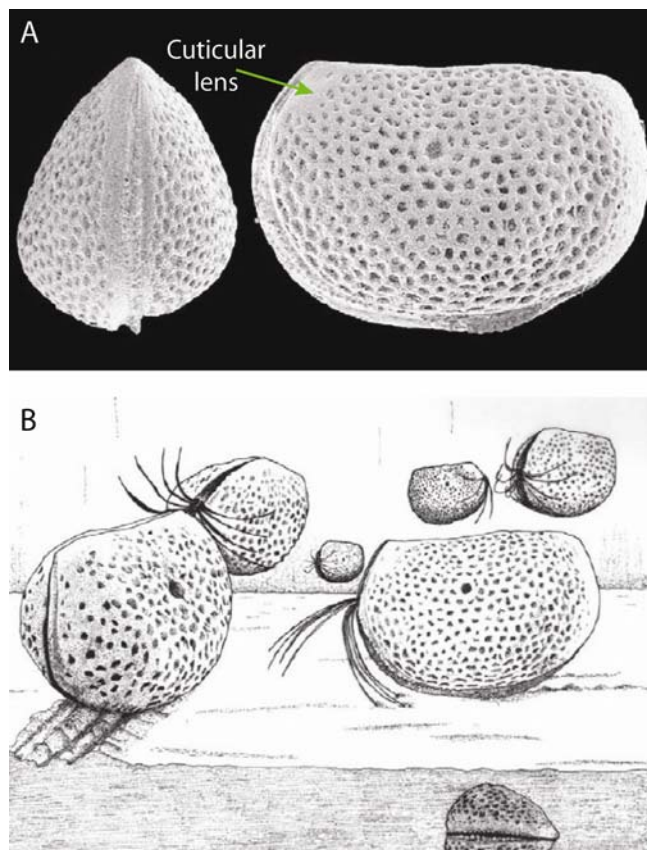


Figure 1.24 - Primitiopsid ostracods.

A. Anterior (left) and left lateral (right) views of the carapace of *Primitiopsis planifrons*. Specimen is approximately 1 mm in length. Note that the lens is a smooth area of the carapace. **B.** Ostracods in their inferred nektonic life position. Images from Tanaka *et al.* (2009, figure 2 (1-2) and figure 10 respectively).

Ray tracing analysis shows that the focal length of the system is extremely long relative to the carapace width (Tanaka *et al.*, 2009). Modern ostracods with naupliar eyes use a mirrored surface, the tapetum, which is positioned below

the photosensitive cells, to reflect light back onto the cells hence optimising light. Tanaka *et al.* (2009) concluded that a similar system was in operation in the eyes of the Silurian ostracod *Primitiopsis planifrons* resulting in a more achievable, focal length (Figure 1.25B).

Tanaka's work (2006) highlighted variations in lenses of different species. Four types of eye have been identified based on lens parameters. These lens types show variation in light-gathering abilities and are thought to be the result of both phylogenetic constraints and ecological demands. Relationships between the different lens types suggest that three types are derived from one initial ancestor (Tanaka, 2006). This ancestral eye is characterised by a lens with wide ranging values of both relative lens thickness and outer surface curvature, and a medium light-gathering ability (Tanaka, 2006).

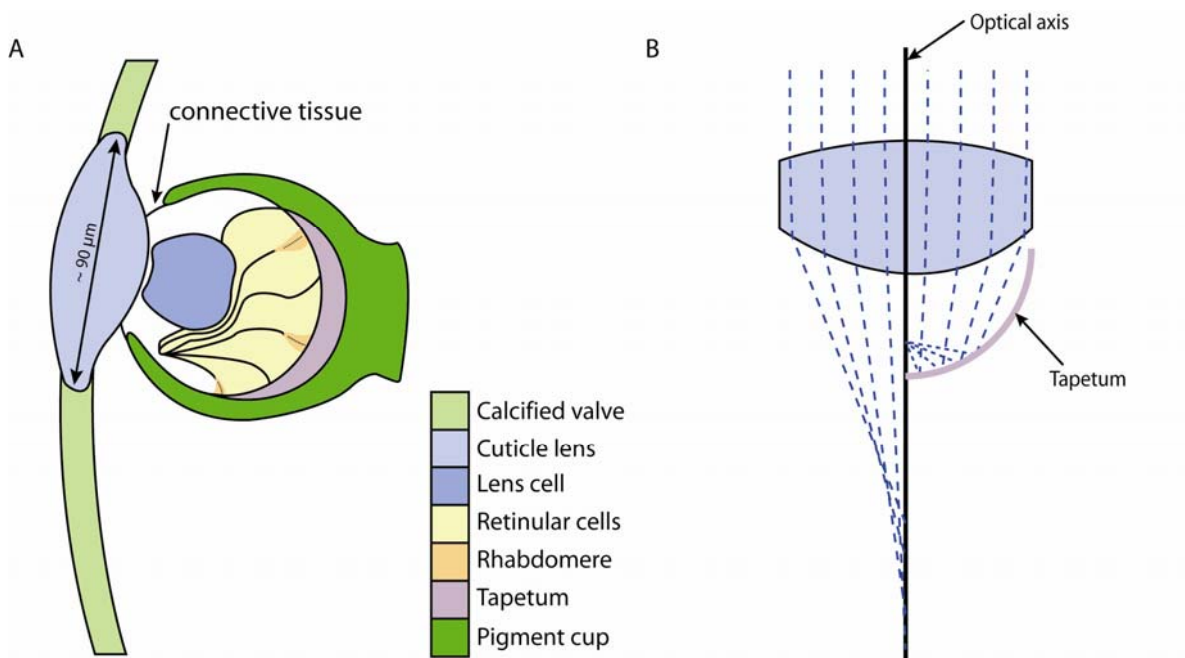


Figure 1.25 - Structure and function of the naupliar ostracod eye.

A. Schematic diagram of the ocellar structure found beneath each cuticular lens. Diagram modified from Tanaka (2006, figure 2) and B. The focusing of light in the ostracod lens with (right) and without (left) the use of a tapetum. Blue dashed lines represent light rays. Diagram modified from Tanaka *et al.* (2009, figure 7).

1.6.2 Brittlestars

The visual structures of brittlestars (Figure 1.26) have been documented by Aizenberg *et al.* (2001) and Aizenberg and Hendler (2004), following the earlier work of Hendler (1984) and Hendler and Byrne (1987).



Figure 1.26 – Night- and day-time images of the Brittlestar *Ophiocoma wendtii*. Photographed during the day (top) and during the night (bottom). Image from Aizenberg and Hendler (2004, figure 1).

These studies have shown that light sensitive species of brittlestar construct visual systems on the dorsal arm plates (DAPs) from three components (Figure 1.27): vast arrays of single-crystal calcite micro-lenses (expanded peripheral trabeculae: EPT); nerve bundles, presumed to be acting as primary photoreceptors; and chromatophores (pigment cells). Combined, these components provide the animal with sufficient ‘vision’ to employ rapid escape responses (Hendler, 1984). Beneath this layer on the DAP, the brittlestar stereom is a three dimensional network of calcite skeleton and pores. This area of ‘labyrinthine stereom’ would not permit the transmission of light due to the huge numbers of pore/skeleton interfaces which effectively make this area opaque (Hendler and Byrne, 1987).

As in the upper lens unit of schizochroal trilobite eyes, the lenses in brittlestar DAPs have an aplanatic lower surface which minimises spherical aberration and focus light on the photosensitive cells beneath them. The lenses are 40-50 μm in diameter and form part of a thick (~40 μm) transparent layer on the external surface of the plates (Aizenberg and Hendler, 2004); this layer is absent in light-

insensitive species. Aizenberg *et al.* (2001) determined the focal length of the lens to be approximately 4-7 μm , which coincide with the first nerve bundles; the spot size of this focal point is 3 μm (Aizenberg and Hendler, 2004), this was determined by experiment using photosensitive paper.

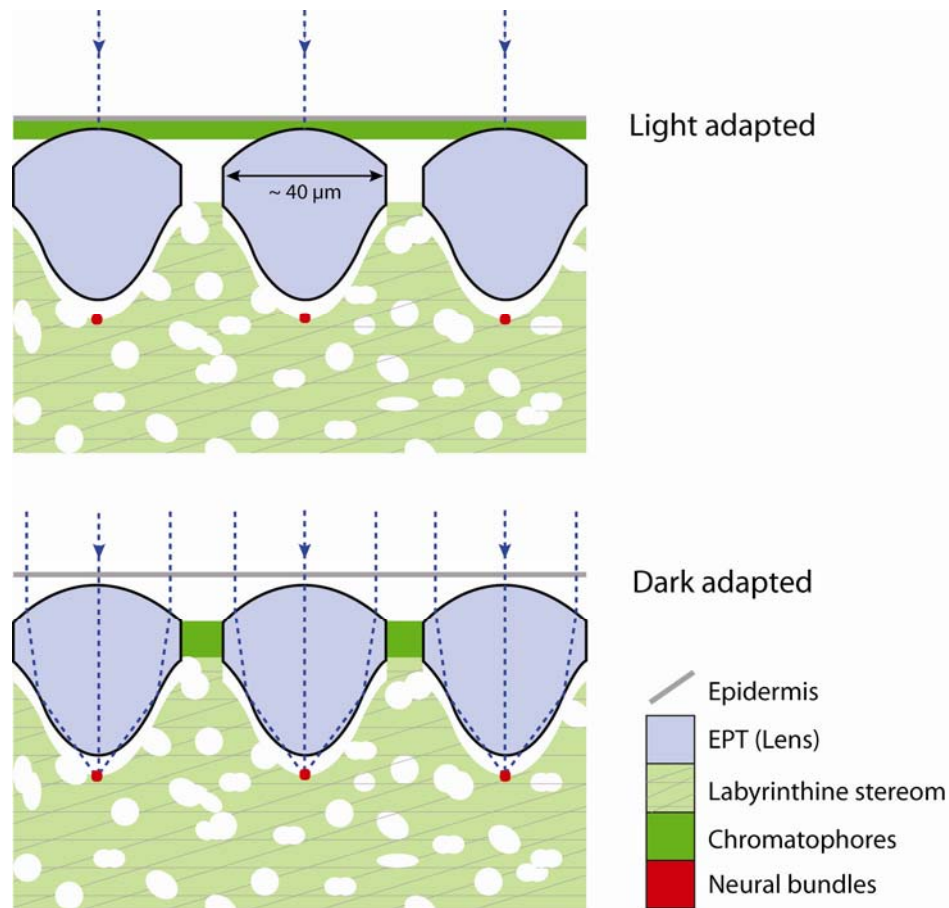


Figure 1.27 - The internal structure of the dorsal arm plates of light-sensitive brittlestars. Schematic cross-sectional view through the dorsal arm plate of a light sensitive brittlestar. Migration of pigment cells (chromatophores) allows the animal to control the amount of light reaching the photoreceptors and so adapt itself to light and dark conditions. Blue dashed lines represent light rays. Images based on Aizenberg and Hendler (2004, figure 4 and 5).

Hendler and Byrne (1987) identified the function of the chromatophores as one of light/dark adaptation. As in ommatidial type eyes, this is achieved by pigment migration (section 1.3.2.1, Figure 1.2). In daylight, the pigment is spread across the uppermost region of the DAP (Figure 1.26 and Figure 1.27 top), directly beneath the epidermis, shielding the EPT and nerve bundles below from light and giving the specimen a fairly uniform colour. In periods of darkness this pigment is concentrated in channels between the EPT allowing maximum light transmission through the lenses (Figure 1.26 and Figure 1.27 bottom), resulting in a black and grey striped pattern (Hendler, 1984). This theory was

experimentally tested by Hendler (1984) who showed that pigment migration is definitely a response to day/night cycles and is not simply a mode of camouflage.

1.7 Detailed Aims of the Present Study

The primary aim of this study is to determine how the lenses in both holochroal and schizochroal trilobite eyes functioned. This will be addressed using a combination of state-of-the-art microscopy techniques, to determine the original chemical composition and microstructure of lenses, and optical modelling to identify how the lenses functioned. These results, in conjunction with published literature on eyes of modern arthropods, will be used to produce a model of schizochroal eye function that will be compared to other published models (see chapter 7).

This work will provide clarification as to which model of lens function is correct, the aplanatic doublet lens proposed by Clarkson and Levi-Setti (1975) or the gradient index lens proposed by Campbell (1975) and later by Bruton and Haas (2003a). These two models will be assessed by determining the following: how common intralensar features are; if intralensar features are consistent across the Suborder Phacopina; how intralensar features influence lens function; and what the impact of diagenesis is on lens chemistry and microstructure.

The present study also aims to highlight the similarities and differences between trilobite eyes and the eyes of other animals that construct calcite lenses (section 1.6). A more in depth understanding of the lenses in trilobite eyes will show if modern calcite lenses can be classed as 'modern analogues' for trilobite vision or if the eyes of trilobites, in particular the schizochroal eyes, really are unique.

2

Techniques

The present study has used a range of techniques to establish a three-dimensional understanding of original chemistry and microstructure in lenses of trilobites. Those of fossil ostracods and modern brittlestars are also investigated. The techniques include light microscopy, cathodoluminescence microscopy and electron microscopy based imaging and analysis methods. This chapter explains the processes involved in using each of these techniques, the theory behind their operation and their intended outcomes.

Chapters 4, 5 and 6 synthesize the outcomes of investigations by these techniques rather than providing a species by species account of all observations. Details of the techniques applied to each sample are presented in Appendix A.

2.1 Optical Microscopy

Optical microscopy was carried out using a Zeiss Axioplan petrological microscope. All thin sections were studied in transmitted light (TL), both plane polarised and in crossed nicols/polars, and in reflected light (RL), at magnifications ranging from x1.5 to x40. Images from the light microscope were captured using a Nikon DN100 Digital Net Camera and camera control unit. This imaging technique may reveal the presence of internal structures in the lenses defined by contrasts in crystallographic orientation, microstructure and inclusions.

2.2 Cathodoluminescence

Cathodoluminescence (CL) is a state of atomic ‘excitement’ achieved by bombarding a sample with an electron beam which results in the emission of

light from the excited substance. CL emission is produced primarily by defects in the crystal lattice, either structural or due to the presence of trace element substitutions (Marshall, 1988). The present study involved both optical and hyperspectral CL analysis and imaging.

2.2.1.1 Cathodoluminescence of Carbonates

CL of the carbonate minerals has been used widely to determine growth histories of crystals. Zoning, common in cements and not visible using transmitted light microscopy, except for samples that have been stained, can be revealed by CL which can in turn be linked to a material's crystallisation and diagenetic history (Reeder, 1983; Reeder *et al.*, 1990).

Calcite typically luminesces in the red-orange part of the spectrum (Smith and Stenstrom, 1965), dolomites also cover this range but occasionally extend to the yellow wavelengths (Sippel and Glover, 1965). Despite this overlap a distinction between different carbonates can usually be achieved using CL as differences are always present between calcite and dolomite within a sample (Marshall, 1988).

2.2.1.1.1 Activators and Quenchers

Activators are impurities within a mineral's structure, usually substitutional, which act as a centre for the production of CL. Quenchers have the opposite effect, preventing CL from occurring, or at least inhibiting CL production to some degree (Marshall, 1988). The ability of an ion to activate or quench CL is related to its energy level within the crystal structure of the host material (Marshall, 1988); activators and quenchers therefore differ between minerals; there can also be more than one activator or quencher within a single mineral.

The primary activator of CL in calcite is Mn^{2+} (Schulman *et al.*, 1947, Medlin, 1968, Medlin, 1959). Medlin (1959) reported iron, in the form of Fe^{3+} , to be the primary quencher of CL in calcite, with Co^{2+} and Ni^{2+} possibly having a similar effect.

Dolomite CL is activated by Mn^{2+} and quenched by Fe^{2+} (Medlin, 1968, Gillhaus *et al.*, 2001 and references therein).

2.2.2 Optical Cathodoluminescence

Optical CL microscopy was carried out using a CITL Technosyn 8200 Mk 4 mounted on a Zeiss Axioplan petrological microscope (Figure 2.1A). Images were digitally captured using a Nikon DN100 Digital Net Camera and camera control unit. This type of imaging is qualitative, producing images of CL intensity and colour in the visible range of the spectrum (Figure 2.1B, C).

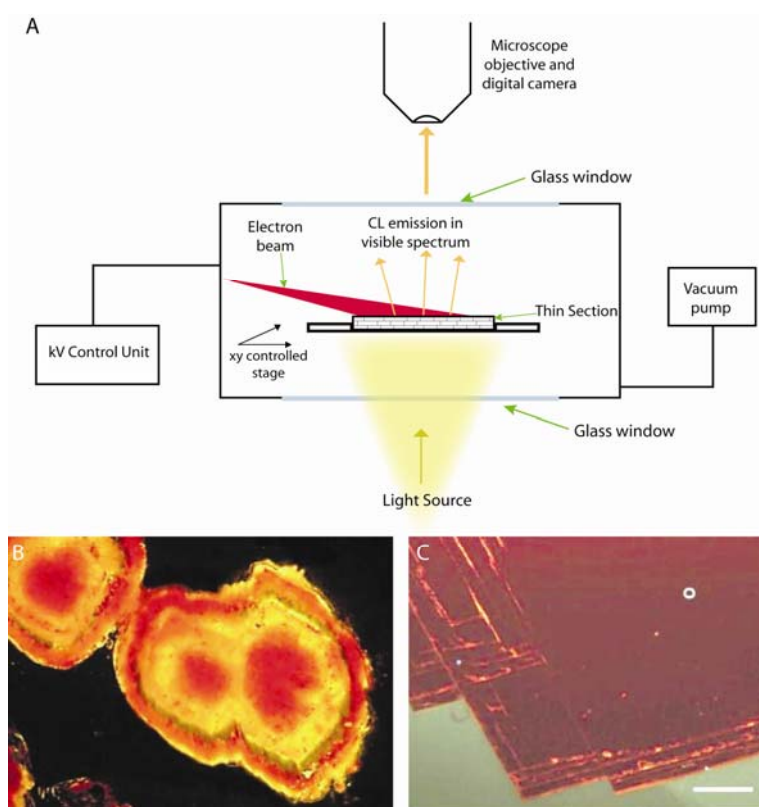


Figure 2.1 - Optical cathodoluminescence microscopy.
A. set-up in a vacuum chamber. **B and C.** Optical CL images of a dolomite crystal and an Fe-rich calcite crystal respectively. Images from Gillhaus *et al.* (2001, plate 1, images 1 and 2).

2.2.3 Hyperspectral Cathodoluminescence

Hyperspectral CL imaging was carried out using a Cameca SX 100 Electron Probe Microanalyser (EPMA) (set up shown in Figure 2.2) at Strathclyde University. The EPMA provides much higher resolution imaging than is possible using optical CL. CL and X-ray spectra can also be simultaneously obtained for each point within a mapped area. The CL data are represented as graphs of emission intensity against wavelength and hyperspectral maps, which show a gradient colour scale for different wavelengths; the orange and ultraviolet to blue regions of the

spectrum being the wavelengths at which calcite and dolomite luminesce (e.g. Reed and Milliken, 2003).

CL can also be carried out on a Scanning Electron Microscope (SEM) but there is clear advantage in using hyperspectral CL rather than optical CL or SEM CL; the problem of phosphorescence (i.e. the continued luminescence of a body after the source of excitement has been removed) and therefore ‘smearing’ of the image evident in SEM CL is overcome, and X-Ray maps can be simultaneously obtained with micron scale spatial resolution (Lee *et al.*, 2005a; 2005b). Hyperspectral CL can also be detected across a much wider wavelength range than is possible using optical methods that only detect luminescence from the visible range of the spectrum.

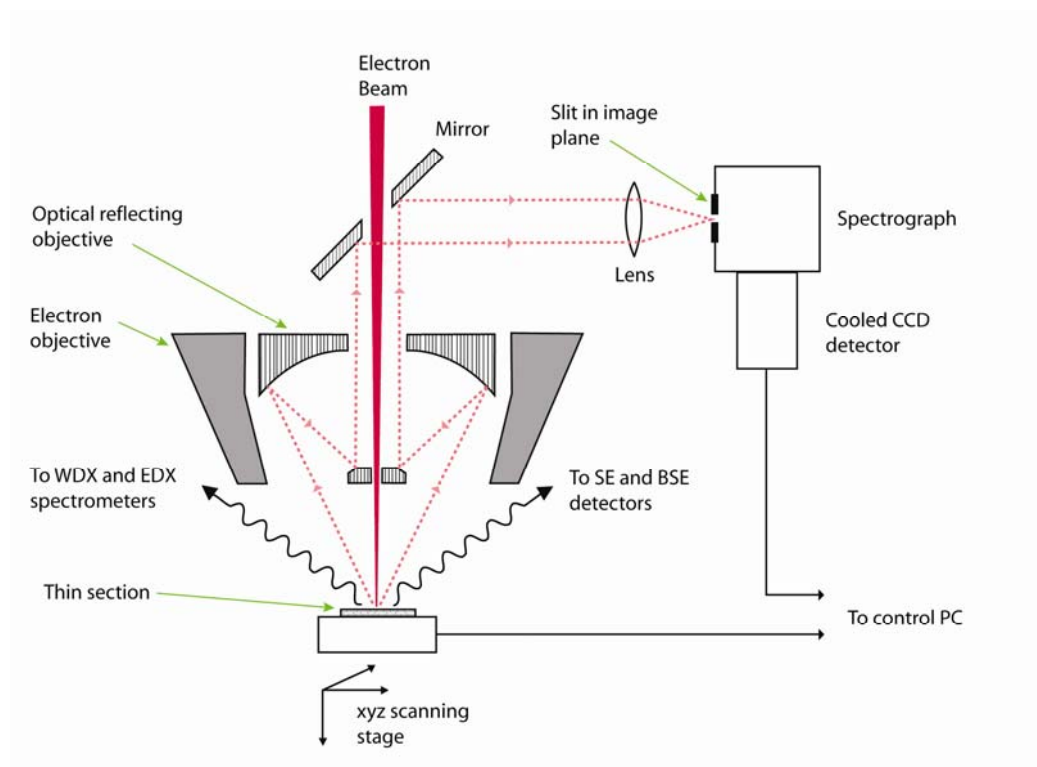


Figure 2.2 – Hyperspectral cathodoluminescence.

CL spectroscopy system of the Cameca SX100 EPMA. Red lines indicate the pathway of electrons in the CL set-up. Image modified from Lee *et al.* (2005b, figure 1).

2.3 Scanning Electron Microscopy

Various types of imaging can be carried out on a SEM, the two most frequently used are secondary electron (SE) imaging and backscattered electron imaging (BSE). SEM imaging techniques were carried out using a Quanta 200F Field Emission Environmental SEM (hereafter referred to as FEG-SEM) that is equipped

with an array of detectors; Figure 2.3 illustrates the chamber set-up as well as the beam interaction with the sample surface which results in emission of electromagnetic radiation of different wavelengths (Figure 2.3B) and in turn permits imaging.

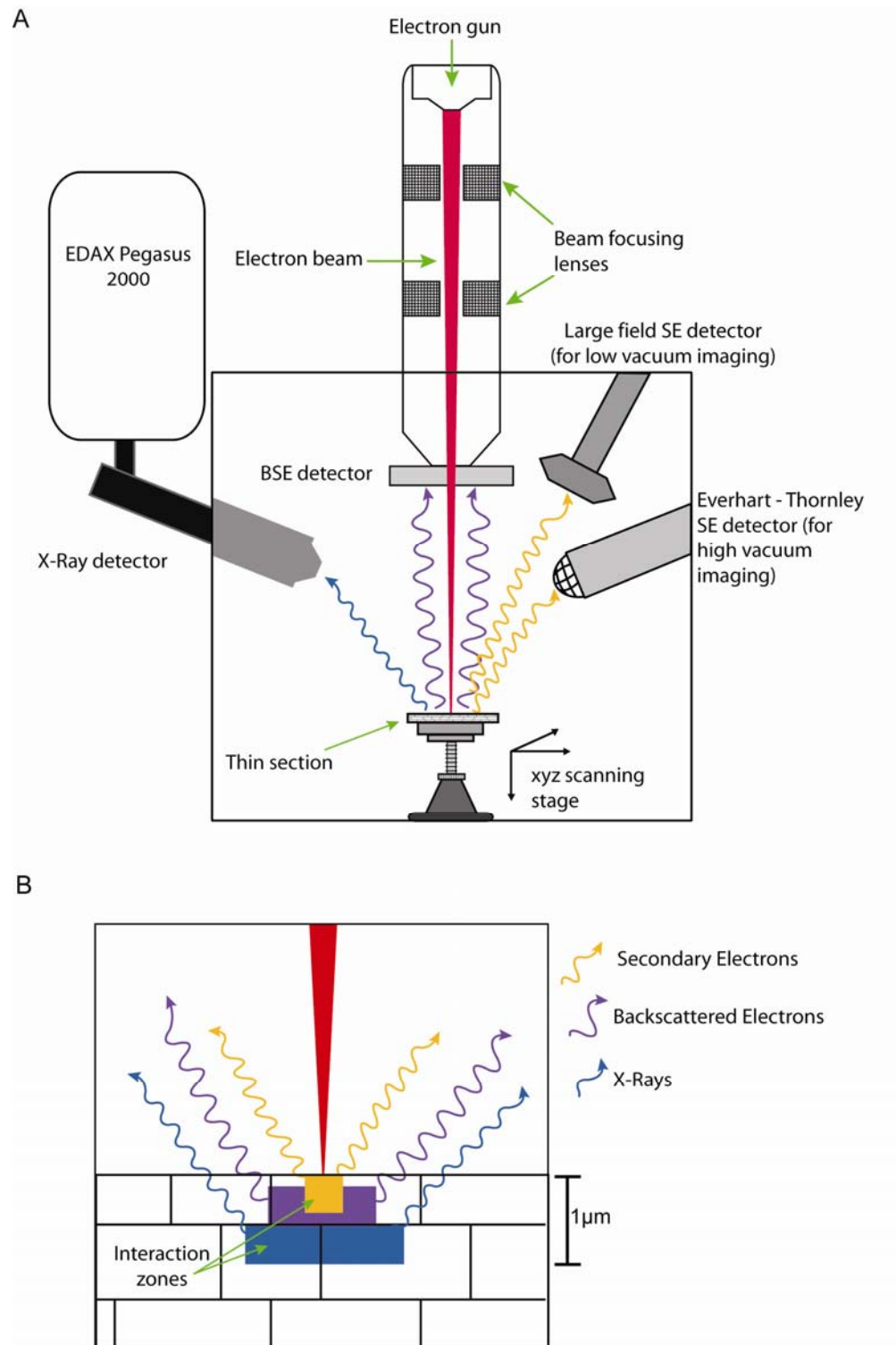


Figure 2.3 – FEG-SEM chamber set-up for SE and BSE imaging and EDS chemical analysis. A. Schematic diagram showing the detectors in use for the various types of imaging B. Beam interaction with sample surface. Note that the different electron types are produced at differing depths within the sample.

2.3.1 Scanning Electron Microscopy Technique Development

Samples have been studied at both high vacuum ($5.5\text{e-}6$ Torr) and low vacuum ($5.2\text{e-}1$ Torr) on the FEG-SEM. High vacuum work was carried out on samples coated with 10-15 nm of carbon using the AGAR SEM carbon coater. Low vacuum analysis has an advantage over high vacuum in terms of time, as samples do not require carbon coating, although this method results in spreading of the electron beam, owing to the interaction of air and water vapour in the chamber and is therefore somewhat experimental. This may reduce resolution of images and spatial accuracy of X-ray analyses as a result of increased data collection area. Experimental Electron Backscatter Diffraction (EBSD) (see section 2.7) carried out at low vacuum proved to be successful, producing results comparable with high vacuum scanning (Torney *et al.*, 2009). Typical operational settings for the FEG-SEM are as follows; accelerating voltage of 20.0 kV; gun pressure of $1.2\text{e-}9$ Torr; emission current ~ 200 μA ; 50 μm aperture; spot size of 4.

2.3.2 High Vacuum Secondary Electron Imaging

Secondary electrons are emitted from very shallow depths within the sample (Figure 2.3B) and are electrons from the sample itself, displaced when sample atoms interact with the high energy primary electron beam. SE imaging provides information on the topography of samples and is carried out using an Everhart-Thornley SE detector. This type of imaging was used to study the trilobite eye prior to thin sectioning as well as for high resolution characterisation of fracture surfaces and etched thin sections.

2.3.3 Low Vacuum Secondary Electron Imaging

Low vacuum secondary electron imaging was carried out on uncoated thin sections. Using low vacuum mode in the FEG-SEM allows variation in the amount of charge that accumulates on a sample surface (Kearns and Orr, 2009 and references therein). This results in the formation of charge contrast (CC) images which show greyscale variations within the sample. The exact cause of these variations is unknown but it may be due to differences in electrical conductivity as well as defects and dislocations in the crystal lattice (Kearns and Orr, 2009). CC images therefore yield contrast analogous to CL (section 2.2) and in the

present study proved most useful in highlighting textural differences between lens components (see section 5.1.3.4).

2.3.4 Backscattered Electron Imaging

Backscattered electron imaging is based on the mean atomic mass of the sample; images are grey scale with minerals of the highest mean atomic number appearing brightest as they have the greatest emission of backscattered electrons. BSE imaging uses a backscattered electron detector capable of high resolution atomic number contrast imaging and is most effective on polished thin sections but can also be used on rough surfaces. Backscattered electrons emit higher energy, and are emitted from a greater depth within the sample than secondary electrons (Figure 2.3B) and as the name suggest, are electrons from the primary electron beam, scattered over 180° by the sample.

2.4 Energy Dispersive X-Ray Spectroscopy

Energy Dispersive X-Ray Spectroscopy (EDS) provides semi-quantitative and quantitative information on the chemical composition of a sample. Semi-quantitative EDS has been carried out primarily on the Quanta 200F FEG-SEM equipped with an EDAX Pegasus 2000 X-Ray detector system (see Figure 2.3A for chamber set-up). On occasion a Cambridge Instruments S360 analytical SEM was also used. Quantitative EDS was carried out on a Zeiss Sigma FEG-SEM equipped with an Oxford Instruments INCA microanalysis system.

X-rays are emitted by a sample when bombardment by an electron beam forces electrons within sample atoms to change energy state; when this is from a high to low state, the energy is emitted as X-rays. X-ray analysis originates from deeper in the sample than secondary electrons and backscattered electrons, down to approximately $1\text{ }\mu\text{m}$ depth depending on its atomic mass (Figure 2.3B).

Quantitative EDS on the Zeiss Sigma required calibration prior to analysis of each sample. Details of calibration and detection limits are listed in Table 2.1. Analysis was carried out manually on a series of points, each at a magnification of $\times 30000$ creating a raster area of $10\text{ }\mu\text{m}$. Acquisition time was 30 seconds.

Table 2.1- Calibration standards and detection limits for quantitative EDS analysis. Calcite (CaCO_3) and Magnesium Oxide (MgO) were used to calibrate for Ca and Mg detection respectively. Detection limits are not relevant as all sample analyses greatly exceed the detection limits for these elements.

ELEMENT	STANDARD FOR CALIBRATION	DETECTION LIMIT (weight %)
Sr	Celestite (SrSO_4)	0.6
Fe	Haematite (Fe_2O_3)	0.6
Mn	Rhodonite (MnSiO_3)	0.6

2.4.1 Representation of EDS Data

EDAX Genesis (Quanta) and Oxford INCA (Cambridge and Sigma) computer software programmes were used for collection and analysis of the data. Data can be represented as spectra and maps in the case of qualitative data (Figure 2.4) and also as numerical values in the case quantitative analyses.

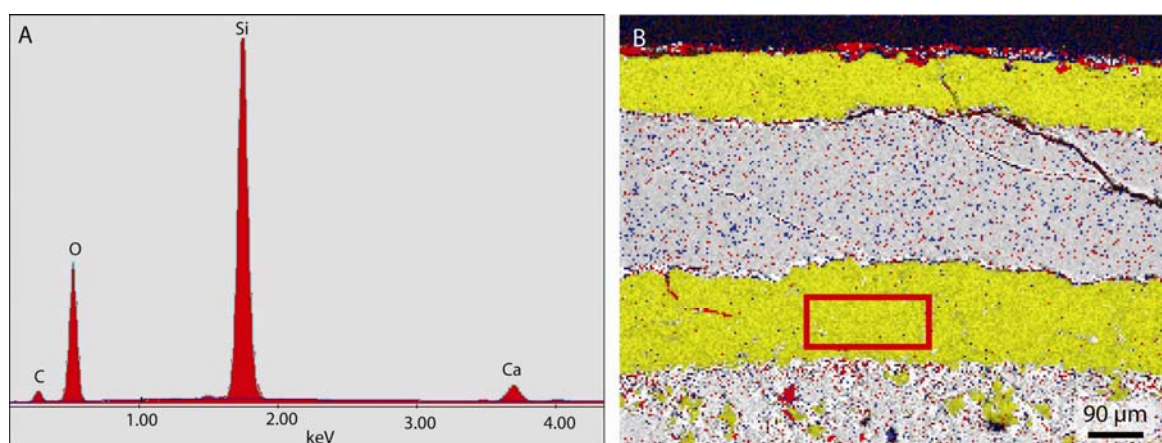


Figure 2.4 - Representation of Energy Dispersive X-ray Spectroscopy data. A. A spectrum, peaks are automatically identified by the software and indicated by element symbols. B. qualitative EDS map showing the distribution of elements in a silicified trilobite exoskeleton. Each element is colour coded: Mg= blue, Ca= grey, Fe= red, Si= yellow. The spectrum in A corresponds to the area in the red box in B.

2.5 Electron Probe Micro-Analysis

Electron Probe Microanalysis (hereafter referred to as EPMA) was carried on a Cameca SX 100 at the Department of Physics, University of Strathclyde and the same instrument in the Department of Geosciences at the University of Edinburgh. Analysis was carried out on two instruments to determine the reliability of the results. Analysis on both instruments involved automatic analysis of a number of points across one or more lenses in a thin section.

Operating conditions, calibration standards and detection limits are listed in Table 2.2.

Table 2.2 - Calibration standards, detection limits and operating conditions for EPMA analysis.

‘ACC. VOLTAGE’ is accelerating voltage of the system, ‘ACQU. TIME’ is the duration for which data was acquired on each point.

	ELEMENT	STANDARD FOR CALIBRATION	DETECT. LIMIT (weight %)	SPOT SIZE (µm)	BEAM CURRENT (nA)	ACC. VOLTAGE (Kv)	ACQU. TIME
EDINBURGH UNIVERSITY	Ca	Calcite-Silicarb	0.25	2	2	15	30
	Mg	Spinel (MgAl ₂ O ₄)	0.01		40		
	Sr	Celestite (SrSO ₄)	0.03				
	Fe	Fayalite (Fe ₂ SiO ₄)	0.02				
	Mn	PuMn (metal)	0.03				
STRATHCLYDE UNIVERSITY	Ca	Calcite (CaCO ₃)	0.03	10	10	15	30
	Mg	Magnesium Oxide (MgO)	0.02				
	Sr	Celestite (SrSO ₄)	0.06				
	Fe	Haematite (Fe ₂ O ₃)	0.06				
	Mn	Rhodonite (MnSiO ₃)	0.06				

In contrast to most SEM microanalysis, EPMA uses wavelength dispersive spectroscopy (hereafter referred to as WDS). WDS employs crystals to diffract X-rays of certain wavelengths into a detector (Goldstein *et al.*, 1989; Çubukçu *et al.*, 2008). The diffracting crystal used in a spectrometer is therefore chosen based on the wavelength of X-rays corresponding to the element to be measured. WDS provides an advantage over EDS in numerous ways. It provides higher precision data as it has high peak to background ratios and can therefore detect elements which are present in very low quantities (Goldstein *et al.*, 1989) and also analyses elements individually, enabling it to resolve peaks on the spectrum which normally overlap (Goldstein *et al.*, 1989). However, the energy resolution of modern EDS detectors is approaching the wavelength resolution of WDS systems (e.g. Çubukçu *et al.*, 2008).

2.6 Transmission Electron Microscopy

Transmission Electron Microscopy (TEM) works on the principle of electron diffraction in electron transparent samples termed ‘foils’, which are generally

<100 nm thick (Lee *et al.*, 2003); sample preparation (see chapter 3 for details) is crucial as the ‘foil’ must be thin enough to allow electrons to pass through it without undergoing considerable scattering or significant loss of initial energy (Lee, 2010). This technique provides high resolution images of a material’s microstructure and can provide information on chemical variations (via EDS), crystal orientations (by electron diffraction) and defects such as dislocations (e.g. Williams and Carter, 2009a). In the present study this techniques has been used to reveal the fine-scale structures within lenses of schizochroal eyes.

TEM work used a FEI Tecnai T20 system at the Kelvin Nanocharacterisation Centre at the University of Glasgow. The system is equipped with a Gatan Image Filter, GIF 2000 for low magnification imaging of microstructure and a SIS Megaview III CCD camera for acquisition of diffraction patterns.

2.6.1 Representation of TEM Results

TEM results are represented in three ways: as bright field images (Figure 2.5A), dark field images (Figure 2.5B) and diffraction patterns (Figure 2.5C). Bright field (BF) and dark field (DF) images are ‘strong-beam’ and ‘weak-beam’ microscopy imaging methods respectively, i.e. the images are formed using strongly or weakly diffracted electrons (Williams and Carter, 2009b). Defects within a sample cause bending in the lattice plane and therefore a change in diffraction conditions (Williams and Carter, 2009a). As these imaging techniques work on the basis of diffraction contrast (Williams and Carter, 2009b) they indicate the presence of micron and sub-micron scale subgrains (Figure 2.5B) and defects such as dislocations (Figure 2.5A). The finer scale features such as sub-micron sub-grains and dislocations are below the resolution limit of most techniques, including the other techniques used in this study.

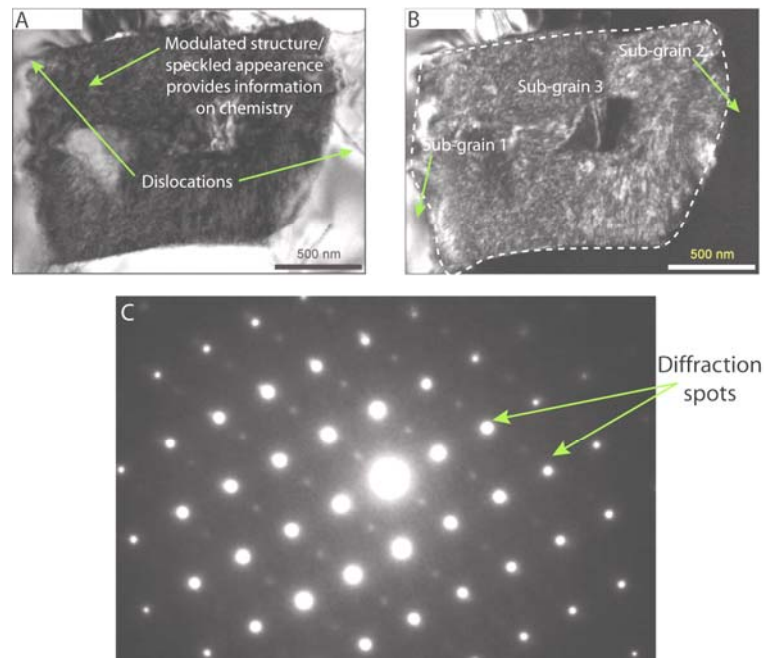


Figure 2.5 - Representation of Transmission Electron Microscopy results.

A. Bright-field and B. Dark field imaging of the same area on a sample. Note the presence of subgrains and dislocations (dark lines). C. The diffraction pattern created by the same sample. Images are from the present study.

2.7 Electron Backscatter Diffraction

2.7.1 What Is Electron Backscatter Diffraction?

Electron Backscatter Diffraction (EBSD) is an SEM based technique in which an electron beam is focused on a polished sample tilted to 70° to the horizontal (Figure 2.6). Electrons are diffracted by planes within the crystal lattice of the sample and are imaged using a phosphor screen and camera. The geometry of the pattern formed by the diffracted electrons, termed a Kikuchi pattern, is determined by unit-cell parameters and crystallographic orientation and so allows precise details of the crystal orientation within a sample, at micrometre scales, to be determined.

The present study used an EDAX OIM 2000 EBSD system on the Quanta 200F FEG-SEM for acquisition of EBSD data with an operating voltage of 20 kV and a spot size of $4\ \mu\text{m}$. This system was used in conjunction with the EDAX Pegasus system for simultaneous acquisition of EDS analyses during ChI scanning (see section 2.7.5).

The resolution of data obtained in EBSD scans varies depending on the individual settings for each scan. Factors such as the step size at which data are recorded

and the speed at which data are obtained and therefore the time allowed for indexing of each point all have an effect. In the present study, the step size for data acquisition was determined based on crystal size in each sample, i.e. step size must be several times smaller than the smallest crystal in order to detect the presence of all crystals; typical step size was 1-2 μm . Data were typically obtained at a speed of 15-25 points per second (pps).

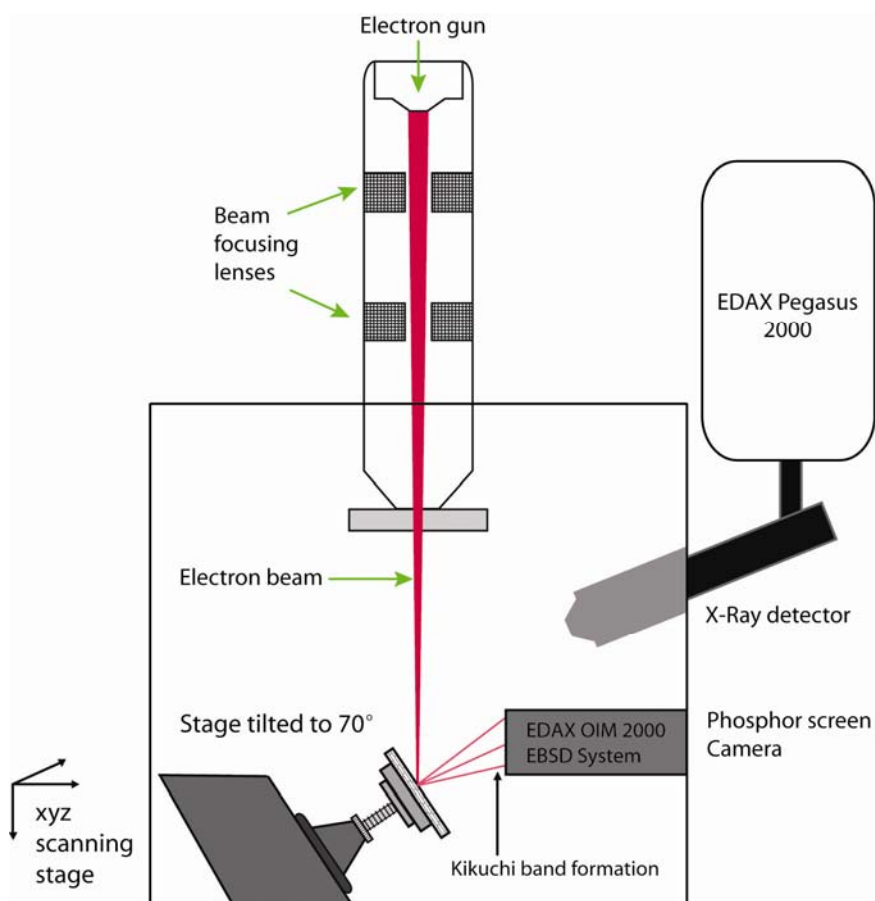


Figure 2.6 – Scanning Electron Microscope set-up for Electron Backscatter Diffraction. The sample is tilted to 70° relative to the horizontal plane for optimum diffraction of electrons. The X-ray detector can be used in conjunction with the EBSD system to obtain qualitative chemical analysis.

2.7.2 The History of Electron Backscatter Diffraction

Some of the first experiments that produced electron backscatter patterns (EBSPs) were reported over 80 years ago by Nishikawa and Kikuchi (1928a; 1928b). In the first of these studies, a ‘net-like pattern’ of intersecting bands was formed by passing an electron beam through mica; the ‘diffraction of short waves by a 2-dimensional lattice placed perpendicular to the incident beam’ (Nishikawa and Kikuchi, 1928a) forming this pattern. The study which followed produced diffracted rays by passing an electron beam through calcite and

imaging these on a photographic plate (Nishikawa and Kikuchi, 1928b). A black and a white line, later to be termed a Kikuchi line, could be identified within each band; these lines being attributed to reflected rays hitting the photographic plate (excess) and a loss of reflected rays (defect).

Later studies by Alam *et al.* (1953) attempted to fine-tune the technique of Kikuchi pattern production by determining the effect on pattern quality of varying tilt angles of the sample with respect to the incident beam. It was here discovered that materials of higher mean atomic number produced stronger patterns at high angles to the incident beam. Although in general optimum diffraction of electrons by a material was found at lower angles (high angle relative to the horizontal), the downside to this is that at these angles background noise, created from ‘electrons with a continuous energy spectrum’ (Alam *et al.*, 1953), is at its maximum and so a compromise must be met. The problem in Kikuchi pattern formation caused by this background ‘noise’ was eased with the development of computer software to automatically detect EBSPs and so to carry out the process of ‘background subtract’ (Lassen, 1996). This is done by obtaining an ‘average’ diffraction pattern of the sample over a relatively large area which is then subtracted from the initial raw and noisy EBSP.

2.7.2.1 Introduction of Automated Electron Backscatter Diffraction

Lassen (1996) also details some of the first attempts to automatically detect and identify the bands in EBSPs, a process known as indexing (Figure 2.7).

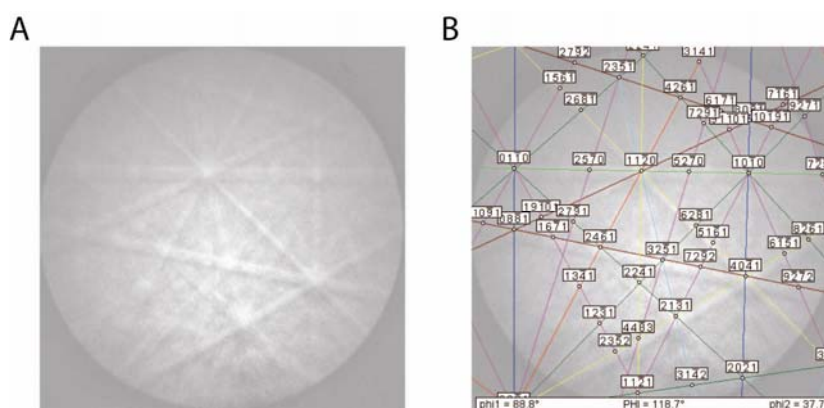


Figure 2.7 – Automated indexing of Kikuchi bands in calcite.

A. Diffraction pattern of inorganic calcite as imaged by the phosphor screen camera. **B.** Superimposed indexing solution suggested by the software. Numbers correspond to the (hkl) planes in the crystal lattice of calcite.

From this point on computers played a vital role in enhancing the detection of EBSPs and furthering the applications of EBSD. Phase files from various databases can now be used on a huge range of materials for accurate indexing (Figure 2.7). This also enables identification of the mineral phase to a certain degree; if several phase files are chosen, the automated system can calculate which is the closest match based on the position of Kikuchi bands, and this technique can assist in the differentiation of polymorphs such as calcite and aragonite (e.g. Cusack *et al.*, 2007).

2.7.3 Applications of Electron Backscatter Diffraction

EBSD has been widely used in studies of metallography (Humphreys *et al.*, 1999) and ceramics (Faryna *et al.*, 2006) and its understanding in these fields is now well established. Over the past decade the use of EBSD in studies of natural materials has become more and more frequent (e.g. Prior *et al.*, 1999; Bestmann and Prior, 2003; Valcke *et al.*, 2006; Mørk and Moen, 2007; Neuser and Richter, 2007), although many aspects of its use in this area of science are still unexplored.

2.7.3.1 Identification of Microstructure in Materials

In geology, EBSD is most commonly used for the analysis and interpretation of micro-structures. Studies on grain and sub-grain boundaries of quartz (Valcke *et al.*, 2006) and calcite (Mørk and Moen, 2007; Neuser and Richter, 2007) respectively have revealed information on crystal growth in non-biological systems.

2.7.3.1.1 Application of Electron Backscatter Diffraction in Biomineral Studies

EBSD is also becoming an increasingly popular tool in studies of biomineralisation (e.g. Griesshaber *et al.*, 2007; Cusack *et al.*, 2008a, 2009), providing a wealth of information on crystal growth in modern and fossil biological systems. EBSD had however, never been used to study the micro-structure of the trilobite exoskeleton until 2007 when Lee *et al.* (2007a) published the findings of the pilot study for the present project; the present study therefore further extends the applications of EBSD in attempting to identify and characterise the microstructures of trilobite exoskeletons, including the eyes.

2.7.4 Representation of EBSD Data

A range of computer software programmes are available that allow EBSD data to be analysed and represented in various forms to provide the user with the maximum amount of information and optimum understanding. The present study used TSL OIM 5.2 Data Collection and Data Analysis software by EDAX. The computer software can be used to display EBSD data in various forms; the orientation maps, pole figures and misorientation graphs employed in this study have been used for some time (e.g. Randle and Caul, 1996). All data in this study is expressed relative to the (0001) plane of calcite.

2.7.4.1 Electron Backscatter Diffraction Image Quality Maps

Image quality (IQ) maps form the background of all other EBSD maps. An IQ map is a grey scale image of the area that has been scanned (Figure 2.8). These maps do not provide any information on crystal orientation of the sample but do enable easy identification of exact location within the scan area, which can become unclear once other information, represented as blocks of colour, is superimposed.

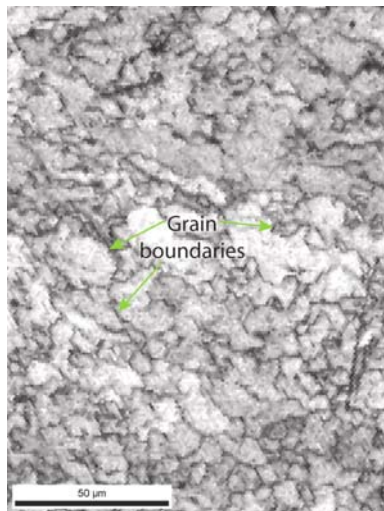


Figure 2.8 - Inverse quality (IQ) map.

All other types of EBSD map are superimposed on the IQ 'base map'. The grey scale gives an indication of how well points were indexed. Darkest areas, which indicate poorly indexed points, often represent grain boundaries.

2.7.4.2 Electron Backscatter Diffraction Orientation Maps

EBSD orientation maps, referred to in OIM software as inverse pole figures (IPF), are a simple, visually attractive way of expressing orientation data. In these

maps, differences in colour represent variations in the crystal orientation within the sample relative to one of three reference directions (Figure 2.9); the normal direction (ND), at 90° to the sample surface; the rolling direction (RD), parallel to the direction in which the sample is tilted, usually 70° to the horizontal; and the transverse direction (TD), running horizontally across the sample surface, at 90° to the rolling direction.

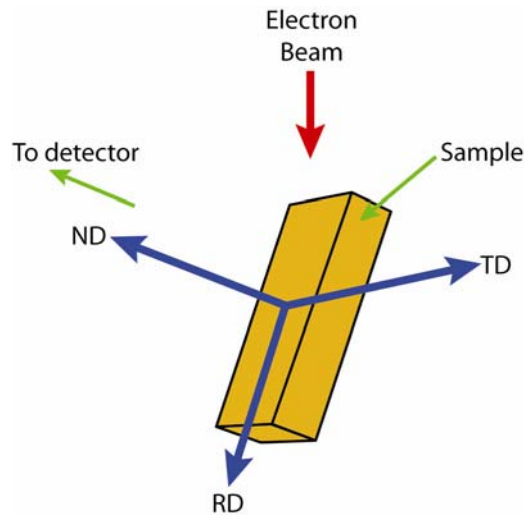


Figure 2.9 - Reference directions of Electron Backscatter Diffraction maps. The normal (ND), rolling (RD) and transverse (TD) directions are shown relative to the sample surface and electron beam. Image modified from OIM users manual.

The subtlety of the colour change across an area in an EBSD map gives an indication as to the extent of the change in crystallographic orientation.

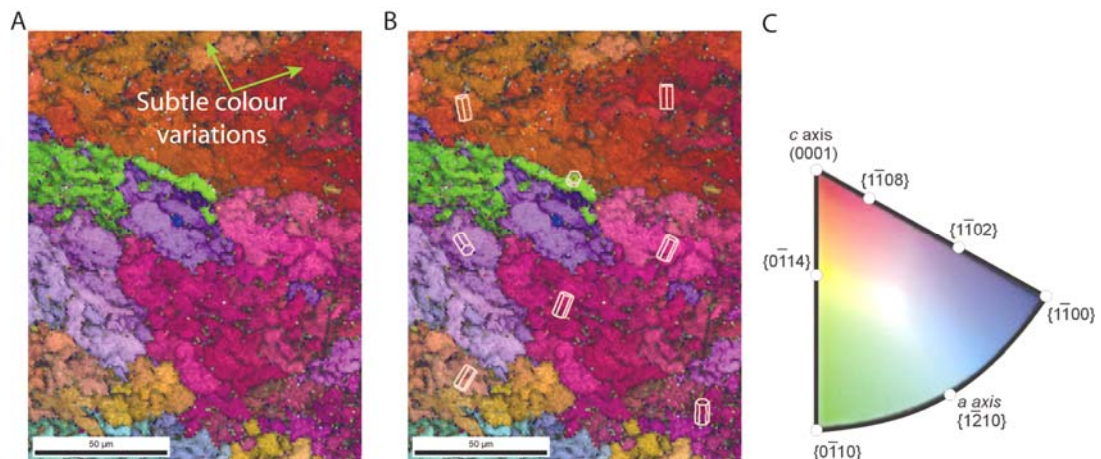


Figure 2.10 – Electron Backscatter Diffraction orientation maps. EBSD maps of limestone (orientation maps superimposed on IQ maps). A. Different colours represent different orientations relative to a reference direction, in this case RD. B. superimposed crystal models highlight crystal orientation. C colour scale for maps A and B. In these maps red indicates that poles to (0001) planes are parallel to RD and green indicates that poles to {0110} planes are perpendicular to RD.

A gradual colour change may be seen where the crystal axis changes gradually throughout a crystal (Figure 2.10A and B), as is the case in radiaxial fibrous calcite (Neuser and Richter, 2007), perhaps due to a series of dislocations in the crystal lattice or the presence of subgrains. Sharp colour changes can be seen along grain boundaries, for example, in the matrix of a sedimentary rock where there is no preferred orientation of crystals and the orientation difference of the neighbouring grains is high (Figure 2.10A). Wire frame crystal models can be superimposed on the maps to further emphasise orientation (Figure 2.10B).

2.7.4.3 Tolerance Angle Maps

This type of map (Figure 2.11) semi-quantitatively shows the change in orientation across a grain from a specific point. Here colour relates to degree of orientation differences (increasing from blue, through green into red) which can be specified by the software user.

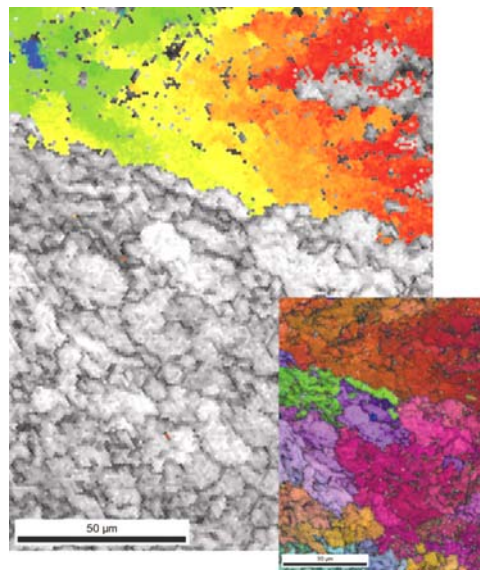


Figure 2.11 – Electron Backscatter Diffraction tolerance maps. Tolerance map overlain on an IQ map of the same limestone sample as Figure 2.10 (also inset). Colour changes, from blue to red, represent increasing deviation in crystal orientation relative to a specified point, indicated by the blue area; the angular difference between blue and red areas in this map is a minimum of 15° . Variations in orientation clearly visible in this type of map are not so easily identified in orientation maps (see inset in which colour change within a grain is very subtle).

Tolerance angle maps highlight subtle variations that are not so easily identified in orientation maps; colour change in all maps presented in the present study indicate a minimum variation of 15° from blue to red; points with a difference greater than 15° from the reference point also appear red.

2.7.4.4 Pole Figures and Texture Plots

Pole figures and texture plots are another way of expressing orientation data. Orientations are plotted on a stereogram and are expressed relative to the reference directions (Figure 2.12A). Data points are plotted in the upper or positive hemisphere of the equal angle pole figure. Pole figures can be plotted simply as a series of points on the stereogram (Figure 2.12B) or as pole figure texture plots (Figure 2.12C), using coloured contours in which colour represents the density of points of a given orientation. All plots presented in this study are equal angle upper hemisphere and are based on a density linear scale.

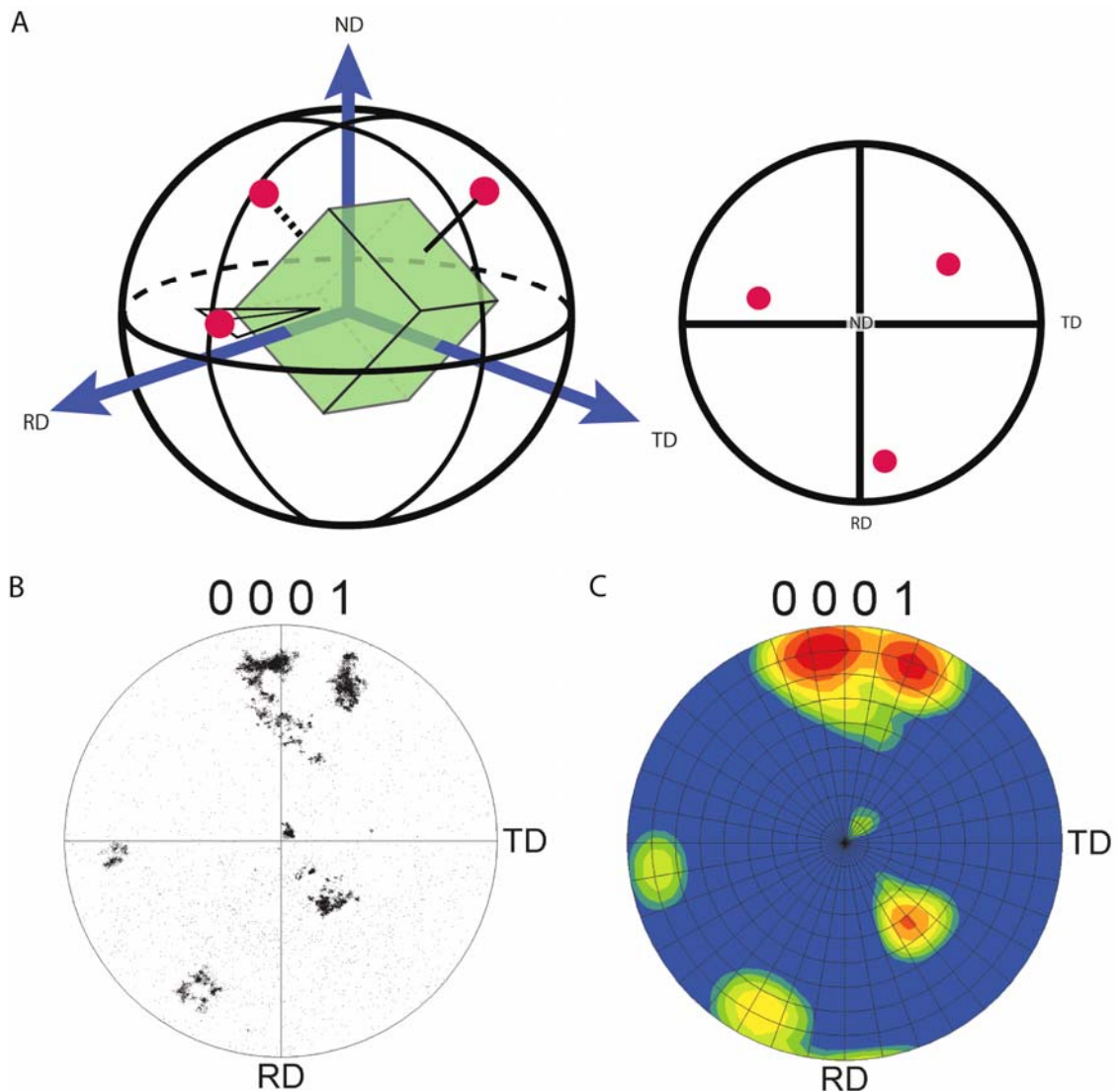


Figure 2.12 – Electron Backscatter Diffraction pole figures and texture plots.

A. Representation of crystal planes on a stereographic projection as poles to the plane. Each plane is represented by a single point on the plot (right). **B.** A scatter plot in which each point corresponds to one orientation measured in the sample mapped. **C.** Pole figure texture plot of B, in which colour represents density of points with a specific orientation. This plot shows that the majority of data points are orientated with the pole to (0001) parallel to RD. A is modified from the OIM user manual.

2.7.4.5 Grain Boundary Maps

Grains can be identified by two methods, either using the ‘unique grain’ mapping or the ‘grain boundary maps’ option in the OIM software.

Unique grain maps differentiate between grains using a computer algorithm that groups points of similar orientation, below a user-specified tolerance angle, and identifies grains where the angular difference between points exceeds this tolerance value (Figure 2.13A).

Grain boundary maps provide similar information, but simply highlight boundaries between grains of user-specified angular difference. This type of mapping is useful in showing the locations of both high angle grain boundaries (angular difference $>10^\circ$) and low angle boundaries (angular difference $<10^\circ$) which may indicate the presence of sub-grains within a larger grain (Figure 2.13B).

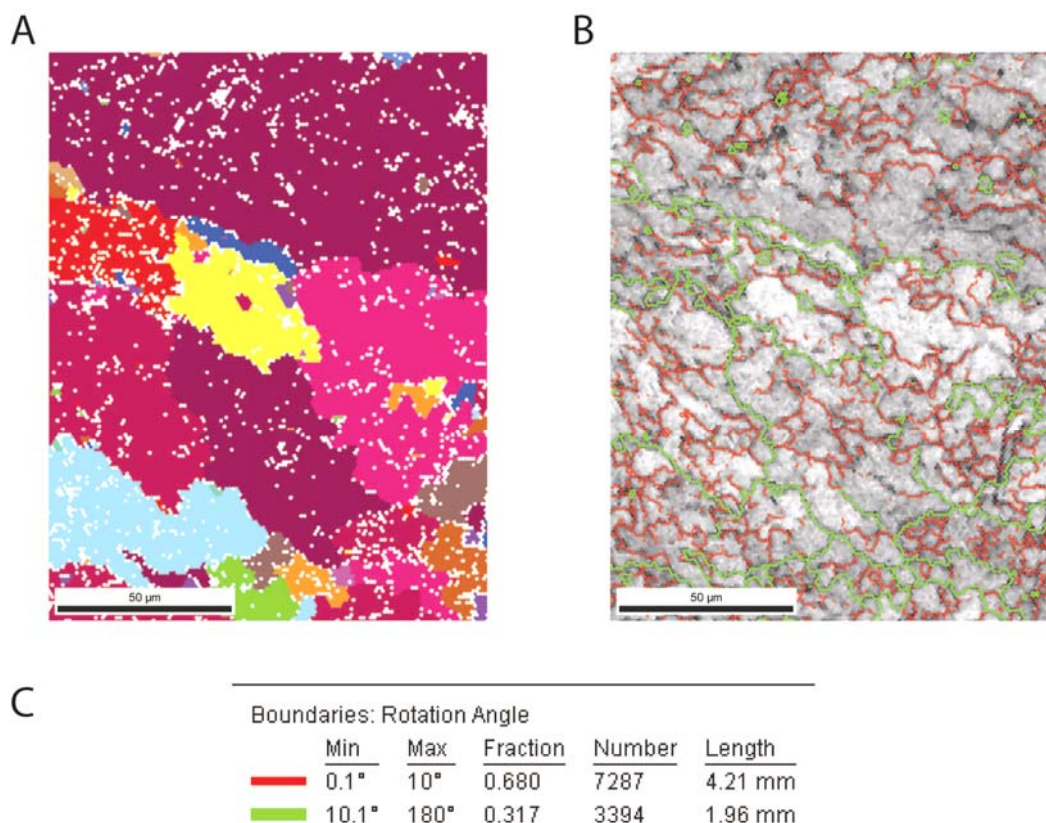


Figure 2.13 - Grain boundary mapping

A. Unique grain colour map and **B.** Grain boundary map (overlain on an IQ map) of the same area showing the presence of both subgrains (red) and grains (green) within a sample of limestone. **C.** Scale showing the user-specified minimum and maximum rotation angles for both boundary types. The scale also indicates the relative proportion of boundaries of a given angle.

2.7.4.6 Misorientation

Regardless of the number and combination of rotations of a rigid body, one axis will always remain in the same position as it was originally (Frank, 1988). Misorientation is the difference in crystal orientation between two neighbouring grains of the same crystal system (e.g. both crystals are hexagonal), expressed relative to the common, fixed, axis (Figure 2.14), i.e. the angle of rotation required to bring the two crystal lattices to the same position.

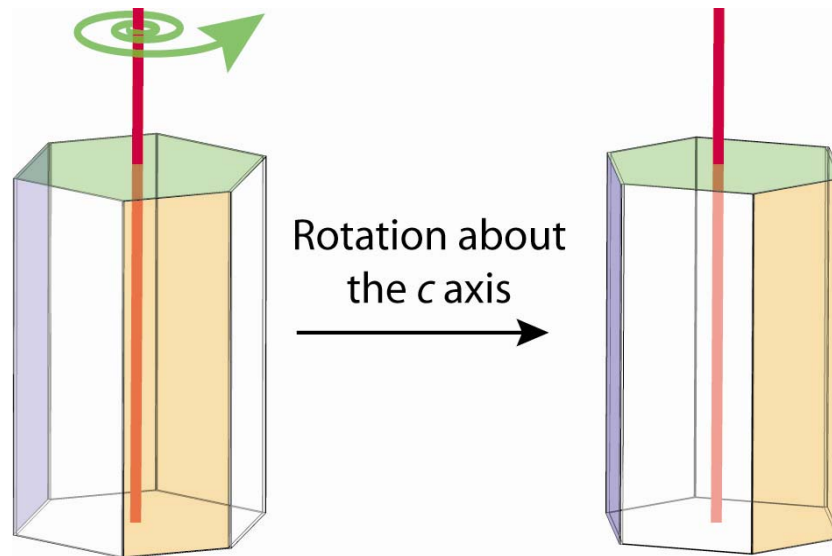


Figure 2.14 - Misorientation of a crystal.

Misorientation is rotation (indicated by the green arrow) about a common axis (indicated by the red line) required to bring two crystals to the same position. Note how in the second image the position of the coloured faces has moved but the direction of the *c* axis has remained the same.

Misorientation can be represented in two ways: firstly in the form of a graph (Figure 2.15A), displaying the change in orientation from point to point, or point to origin along a line across a sample; or secondly as a chart (Figure 2.15B), showing the proportion of points of various misorientations. Misorientation angles of a fraction of a degree may represent dislocations within crystals, angles of $1\text{--}5^\circ$ typically indicate the presence of subgrains (Humphreys *et al.*, 1999) and larger angles are most likely to represent grain boundaries.

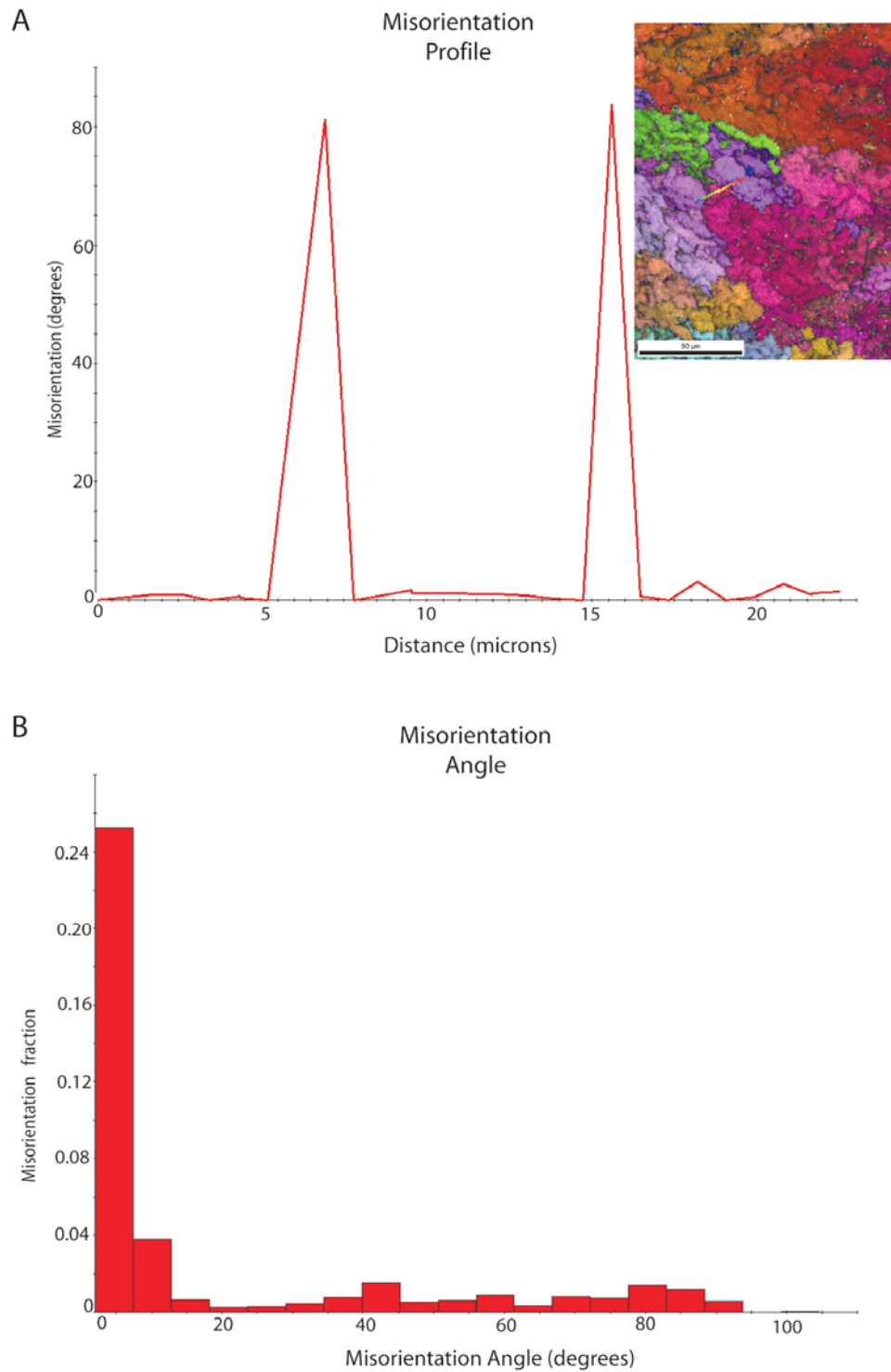


Figure 2.15 – Representation of misorientation data.

A. Graph showing point to point misorientation across the multi-coloured line shown in the inset. Peaks in the graph represent grain boundaries across which there is a change in crystal orientation **B.** A bar chart showing the proportion of grain/sub-grain boundaries of each misorientation angle across the entire area mapped. Misorientation angles over 10° generally represents grain boundaries, lower angles may indicate the presence of sub-domains within a material.

2.7.5 Chemistry Assisted Indexing: ChI scanning

Chemistry assisted indexing (ChI) use simultaneous EBSD and EDS mapping to enable more accurate indexing of samples containing chemically distinct crystals (Figure 2.16). This post-analysis process uses the chemical data gathered to determine where compositionally different materials lie within a scanned area. 'Filters' are added to allow areas of a particular chemical makeup to be indexed in isolation using a pre-selected phase file from a database.

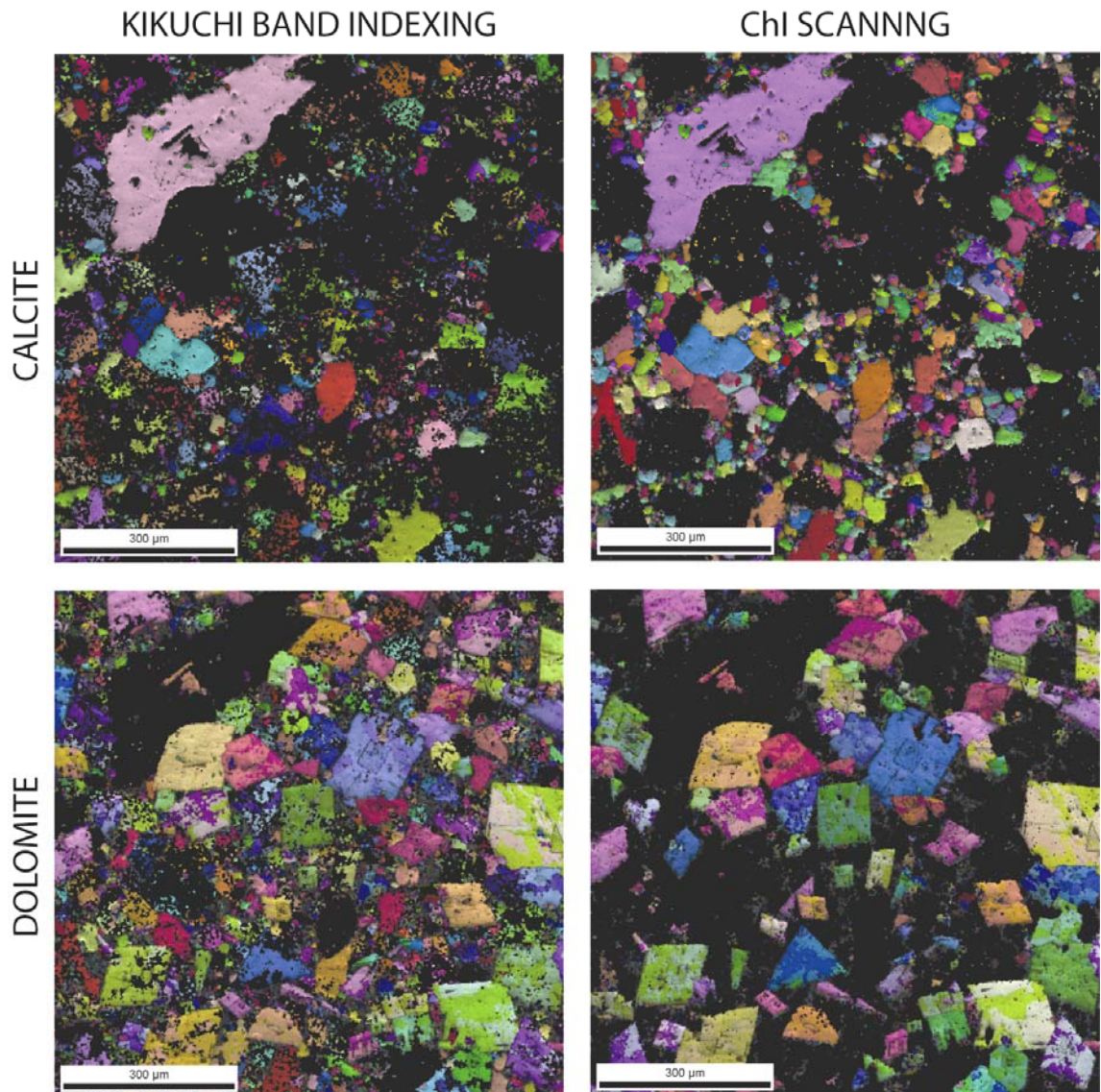


Figure 2.16 - Chemistry assisted indexing of Electron Backscattered Diffraction data. Individual grains of both calcite and dolomite in a sample of dolomitised limestone are significantly better defined in ChI scans (right) as opposed to scans that have been indexed using Kikuchi bands alone (left).

Tolerance levels can be manually altered to further improve accuracy of the scanning, ensuring that the locations of the various principle components (i.e. different minerals) are correctly identified as some overlap of components may

result in scans of low resolution. This scanning method is useful in cases where EBSD indexing alone can not differentiate between two chemically different materials due to similar unit-cell parameters. ChI scanning is a relatively fast process; data is obtained at a rate of up to 450 points per second (pps). In the case of the present study, ChI scanning is used to accurately map the orientation of microdolomite crystals within a low magnesian calcite (LMC) host. Figure 2.16 shows a comparison of ChI scanning (right) and EBSD scanning by indexing of Kikuchi bands alone (left). ChI scanning provides a much clearer map in which dolomite crystals can be easily distinguished from calcite crystals. The accuracy of mineral analysis by pole figure also increases as a result of more accurate indexing and reduction of 'poor' or inaccurate points.

2.7.6 'Cleaning' and Partitioning of Data

The quality of an EBSD scan can be affected by several factors including density of grain boundaries, sample surface deformation, thickness and nature the surface coating (Pérez-Huerta and Cusack, 2009), and the step size of the scan itself. Each point or pixel within a scan is assigned a confidence index (CI), which usually ranges from 0 to 1 but can be -1 when no indexing solution is found. This CI value refers to the degree of 'confidence' with which a particular pattern is indexed, based on the fact that several solutions may be present for a single set of Kikuchi bands.

In order to improve EBSD orientation contrast maps, the data can be 'cleaned' of poorly indexed points (Figure 2.17B); this involves assigning all points of a given CI (generally <0.1) the orientation of their more 'confident' neighbouring points within the grain. Excessive 'cleaning' of data can result in slight alteration of the results so data used to determine angular spread of crystal orientation is 'partitioned' (Figure 2.17C). Removal of points of low CI by 'partitioning' involves complete removal of the 'bad' point from the data set rather than assigning it a neighbouring grains orientation, this ensures that only reliable data are displayed.

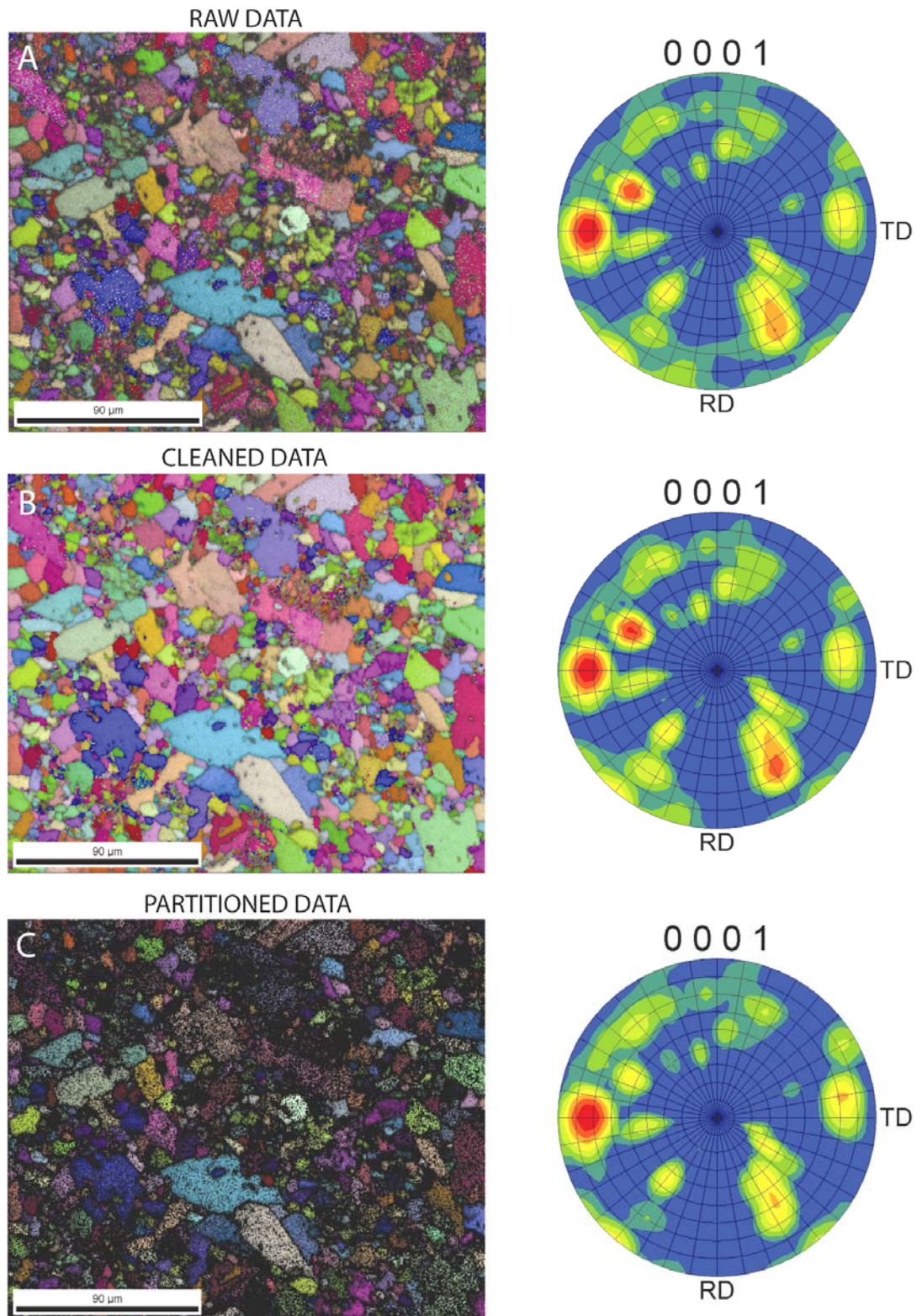


Figure 2.17 - Effects of 'cleaning' and partitioning Electron Backscattered Diffraction data. Orientation maps of a limestone sample showing A. raw data prior to cleaning B. data cleaned by assigning points with $CI < 0.05$ the orientation of their neighbour and C. partitioning of data involving the removal of points with a CI less than 0.05.

2.8 Code V Optical Modelling

Optical modelling was carried out in the Department of Physics at the University of Strathclyde, using the software package Code V, version 10.0 (ORA, 2004).

2.8.1 Introduction to Code V

Code V is a software package manufactured by ORA (Optical Research Associates) and is designed to model, analyse and optimize optical systems by various means. The program has an extensive catalogue of commercially available materials, which can be used to virtually construct optical systems prior to manufacture, as well as a wide-ranging database of patented optical systems. The software also has the ability to optimize any optical system by varying any number of lens characteristics, including the ‘optimisation’ and virtual creation of ‘fictitious glasses’ to best suit the given system.

2.8.1.1 Applications of Code V Software

In this project, Code V was used to assess the capabilities of calcitic lenses/lens components in the optical systems of trilobites, ostracods and brittlestars. The ability of lenses to focus light, as well as the effect of changing refractive index (hereafter referred to as RI), incorporation of intralensar structures and the presence of aplanatic surfaces, was investigated by simple ray tracing. Results provided information on the focal lengths of the lenses, and spot diagrams (see section 2.8.3), illustrate the amount of spherical aberration created by a lens.

2.8.2 Code V Data Input

The data required to model a specific lens include; shape types (e.g. conic, spheric, aspheric) and curvatures of all lens surfaces including conic constants and polynomial factors where relevant, refractive indices of all components, lens thickness, lens aperture and surface properties including refract mode of system elements (i.e. whether the surface reflects or refracts light). The wavelengths at which the system is to be tested must also be specified. Here all modelling used light at 475 nm (blue) unless otherwise stated. Virtually all other wavelengths of light, with the exception of some green, are absorbed by water at depths of 20 m and below (Pain, 2009).

Full details of the data input for each lens are provided in Appendix F.

2.8.2.1 Determining Lens Shape

Accurate determination of lens shape is critical in assessing the capability of an optical system because a small change in surface shape can result in significant changes in refraction. When working with lenses on the micron scale, small inaccuracies in lens shape could therefore result in large errors in determining focal length.

Graphs were constructed to determine accurately the shape of each surface (i.e. visual surface, lens base, intralensar bowl) using background images of lenses in transmitted light to trace the surfaces. For each surface, several points were plotted to provide precise surface coordinates. These data were rotated (and corrected for any tilt present in the original lens image) to correspond to the axis set-up of Code V. A second series of points were superimposed or ‘fitted’ to the original points using a series of formulae in which numerous mathematical functions were varied or ‘solved’ to allow this match. This process enabled the shape of each line (i.e. surface) to be expressed in terms of these mathematical functions; namely the radius of curvature, the conic constant and three polynomial functions x^2 , x^4 and x^6 (only aplanatic surfaces required the use of all five values) all of which are entered into Code V to reconstruct exactly the surface shape. This is the same method that was used by Gál *et al.* (2000).

2.8.2.2 Determining Field of View

The field of view (FOV) of each lens modelled was determined from TL images. Images of the whole eye in thin section were taken and lens axes were superimposed on these. The angle between each pair of adjacent lens axes was measured and an average was taken. This reasonably assumes that all areas within the FOV of the eye are imaged by at least one lens (the 3-dimensional ‘cone’ of view of lenses increases with distance away from the eye so FOVs of adjacent lenses will eventually overlap). In Code V this FOV is expressed as the field angle at which light enters the lens. This value is entered as a \pm value either side of the lens axis, i.e. the FOV measured for each eye was halved. Details of FOV measurements for each lens modelled are presented in Appendix F.

2.8.2.3 Modelling Intralensar Structures

Code V assumes all surfaces to be sequential, i.e. all rays pass through all surfaces. Intralensar bowls can be modelled in the same way as any other surface, as all rays entering the lens will pass through this surface as it is equal in width to the lens. The core cannot be modelled in this way, as peripheral rays would not enter this component; as a result, this surface was not modelled.

Where an intralensar bowl was present, lenses were modelled in three ways:

- (1) Incorporating a bowl with a different RI (see section 2.8.2.4) to the main lens body
- (2) Optimising the bowl to determine the most effective RI.
- (3) Without a bowl

2.8.2.4 Refractive Indices

The RI of a material varies depending on the wavelength of the light that is passing through it; in calcite RI decreases with increasing wavelength (Figure 2.18).

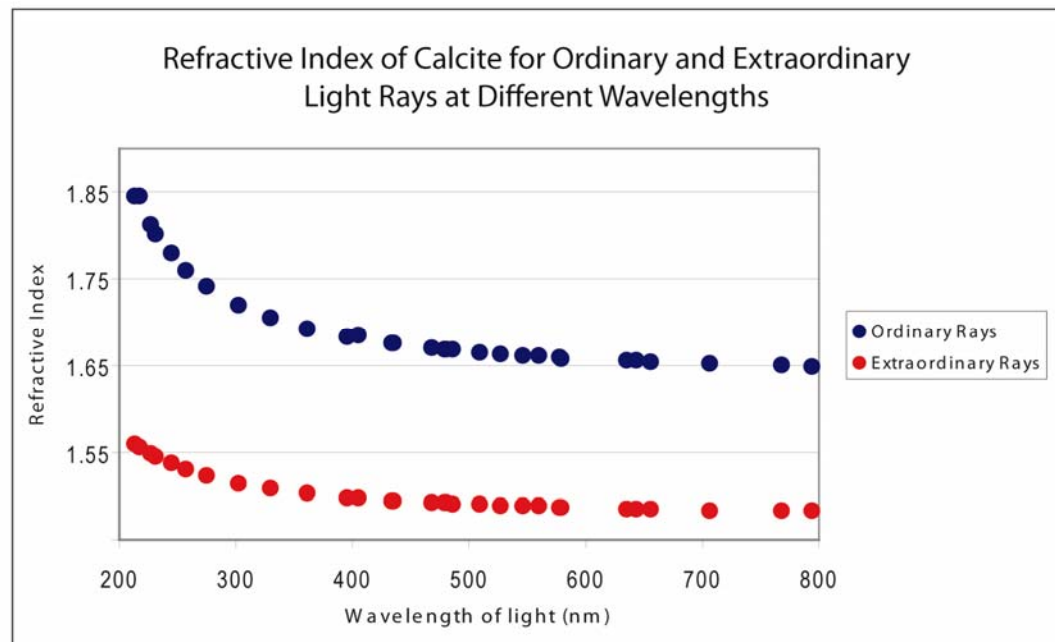


Figure 2.18 - Refractive indices of calcite.

Refractive index changes depending on the wavelength of light and the ray type. Data were obtained from Crystaltechno, manufacturers of synthetic optical calcite. Code V uses this information to determine the RI of calcite, for ordinary and extraordinary rays, at any specified wavelength between the maximum and minimum values on the graph.

The present study assumed a wavelength of 475 nm. RI values for calcite were obtained from Crystaltechno, manufacturers of synthetic optical calcite who state, that ‘in light transmission synthetic calcite is identical to the best sorts of natural crystals’; values provided by Crystaltechno are consistent with values determined by Ghosh (1999). As calcite is birefringent, it has two different indices of refraction (in different directions). Ordinary rays ($RI \approx 1.66$) are those that travel parallel to the calcite c axis and are not doubly refracted (Figure 2.18). Extraordinary rays ($RI \approx 1.49$) travel perpendicular to the c axis and are therefore split into two rays, undergoing refraction at different refractive indices; one ray is the same as the ordinary ray. Crystaltechno values (Figure 2.18) were input directly into Code V when defining the characteristics of low-magnesian calcite (LMC). These values are consistent with those stated by Read (1970).

Lenses originally consisting of high-magnesian calcite (HMC) (see section 5.2.2.2) have an unknown RI, as RI will vary depending on the amount of Mg present in the calcite. For the purposes of optical modelling the RI of HMC is assumed to be the same as dolomite; $RI = 1.68$ for light travelling along the c axis and $RI = 1.50$ for light travelling perpendicular to the c axis (Read, 1970). Refractive index values for seawater ($RI = 1.33$) and trilobite body fluid ($RI = 1.34$) have been taken from Clarkson and Levi-Setti (1975).

2.8.3 Representation of Results

Results of Code V modelling can be represented in various ways (ORA, 2004). For simplicity, results for the present study are represented as ray traces (Figure 2.19A) and spot diagrams (Figure 2.19B).

Ray traces (Figure 2.19A) show how the light rays pass through the lenses, refracting at each surface, converging at the focal point. Spot diagrams show the aberration or ‘blur circle’ at the focal point i.e. the spread of light rays where they are best focused. If a lens focuses well, the spot will be small, if focusing is poor, the spot will be large. Where a lens has been modelled for light entering

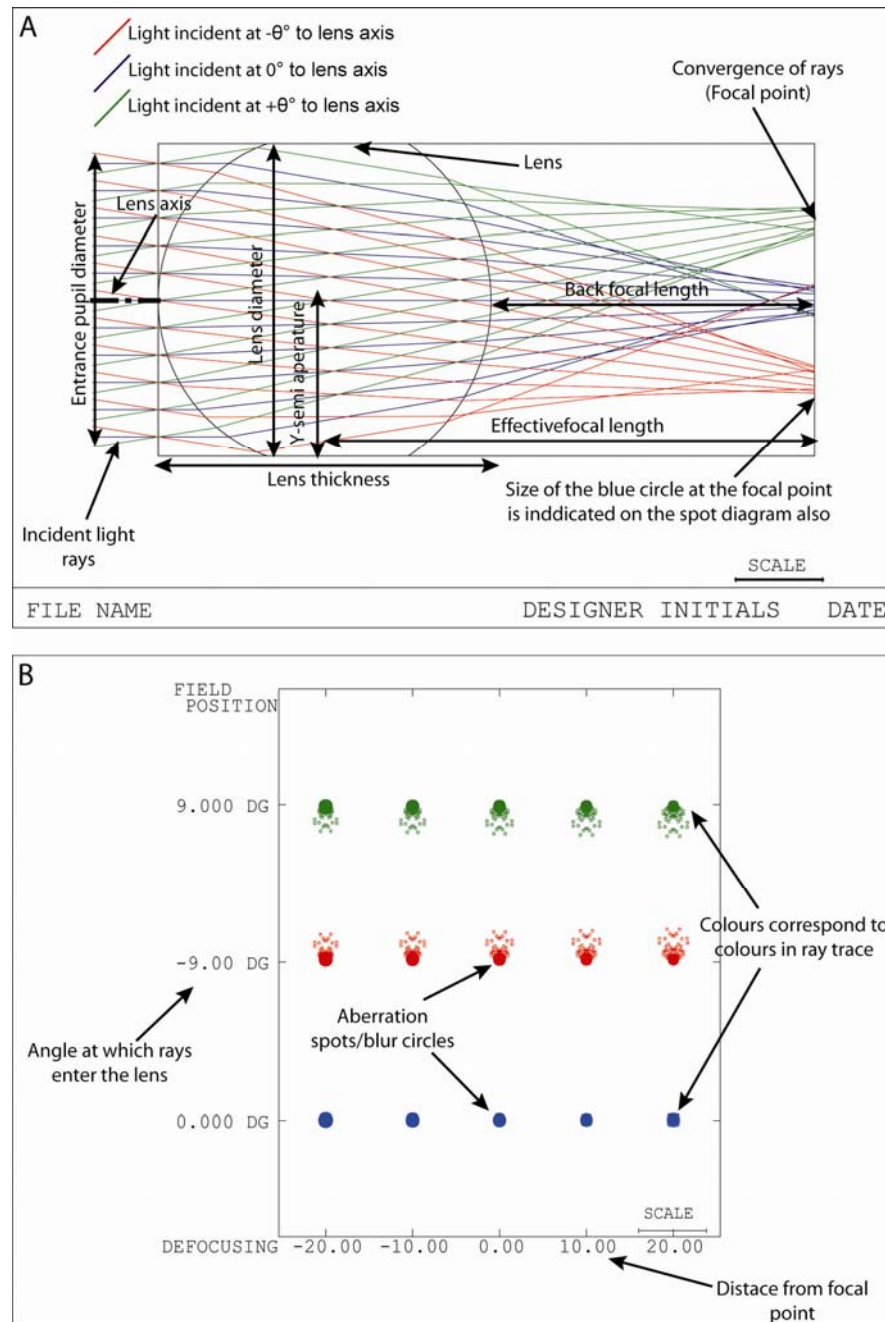


Figure 2.19 - Representation of Code V modelling results.

Results are represented as ray traces (A) and spot diagrams (B). The angle of incidence of light rays as well as all lens characteristics are user defined (see Appendix F for full details).

the system at different angles, a separate spot is created (Figure 2.19B). Spot diagrams can also show the change in aberration with increasing distance from the focal point. Where aberration values are stated in the text, these refer to the aberration of paraxial rays at the focal point, aberration values for ordinary and extraordinary rays are provided alongside these visual representations. The terms ‘back focal length’ (BFL) and ‘effective focal length’ (EFL) (Figure 2.19A) are the equivalent of ‘back vertex distance of the focal point’ and ‘principle focal length’ respectively, used by Gál *et al.* (2000).

2.8.4 Limitations of Code V

As Code V software is primarily used in industry to model optical systems consisting of lenses made of glass (i.e. non-crystalline silica), it does not have the capability to incorporate changes in crystal direction within lenses and so assumes, in all cases, that the crystal *c* axis is parallel to the lens axis. In lenses where this is not the case, identified by EBSD mapping (see section 2.7), modelling results will be less accurate. In an attempt to reduce such inaccuracy, several combinations of ordinary (rays not doubly refracted) and extraordinary rays (rays experiencing double refraction) have been modelled by assigning different two RIs to the lenses (Figure 2.18). Strictly speaking, as extraordinary rays are perpendicular to the optic axis of the medium through which they are travelling, they do not include ‘oblique’ rays entering the material at $>0^\circ$ but $<90^\circ$ to the optic axis. These ‘oblique’ rays will also undergo double refraction, RI ‘experienced’ dependent on the angle at which the rays make with the optic axis. As Code V cannot accommodate variations in *c* axis orientation, all rays at an angle greater than 0° to the lens axis are assumed to be extraordinary and undergo refraction at $RI \approx 1.49$ (from Figure 2.18). This provides a simplified view of refraction and double refraction within the lens but is the closest to refraction in trilobite lenses that can be achieved using this software.

The ‘optimisation’ feature of Code V has been used to determine where the focal point lies behind a lens. Determination of the focal point is calculated by Code V by taking an average of the focal points of all rays entering the lens at the user-specified angles. As the focal points of the different ray types can differ significantly, the aberration for a particular set of rays may be less at some distance away from the chosen focal point. This also occurs where peripheral rays are focused at a different point from that of more central rays.

The software has the ability to model an optical system consisting of up to 99 lenses; however, these must be arranged one behind the other, rather than side by side. Modelling of more than one trilobite lens at a time is therefore not possible, i.e. modelling of the eye as a whole could not be carried out using this software.

3

Materials and Sample Preparation

3.1 Sources of Specimens

3.1.1 Trilobites

Specimens were loaned or donated for research by trilobite workers in several museums and universities. The samples cover a wide geographical and palaeogeographical area, including Germany, the Czech Republic, Estonia, Morocco, Norway, U.S.A, Canada, Australia, England, Sweden and Scotland. The stratigraphical age range of specimens is from the Early Ordovician to Middle Carboniferous for specimens with holochroal eyes and Early Ordovician to Middle Devonian for specimens with schizochroal eyes.

In many instances a number of different species has been obtained from different rock units in a particular region. The wide geographical and stratigraphical range of samples encompasses different diagenetic histories. Diagenetic effects can be expected to vary between specimens from different areas but potentially also between specimens from the same locality due to the spatially and temporally variable nature of the processes involved. This provides a good representation of the changes that lenses undergo during diagenesis and gives an indication of how typical of a taxon the structures might be.

Six species representing four genera and three families of holochroal eyed trilobites were studied:

Class Trilobita Walch, 1771

Order Proetida Fortey and Owens, 1975

Superfamily Proetoidae

Family Proetidae

Genus *Paladin* Weller, 1936Species *Paladin eichwaldi* Fischer von Waldheim in Eichwald, 1825 *shunnerensis* (King, 1914)

Superfamily Bathyuroidea

Family Telephinidae

Genus *Carolinites* Kobayashi, 1940Species *Carolinites sibiricus* Chugaeva, 1964Species *Carolinites angustagena* Ross, 1967Genus *Telephina* Marek, 1952Species *Telephina mobergi* (Hadding, 1913)Species *Telephina bicuspis* (Angelin, 1854)

Order Asaphida

Superfamily Cyclopygoidea

Family Cyclopygidae

Genus *Symphysops* Raymond, 1925Species *Symphysops subarmata* Reed, 1914

Twenty-one species of trilobite with schizochroal eyes were studied and represent 13 genera and three families:

Class Trilobita Walch, 1771

Order Phacopida Salter, 1864

Suborder Phacopina Struve in Moore, 1959

Superfamily Phacopoidea

Family Phacopidae Hawle and Corda, 1847

Genus *Austerops* McKellar and Chatterton, 2009Species *Austerops smoothops* (Chatterton *et al.*, 2006)Genus *Ananaspis* Campbell, 1967Species *Ananaspis macdonaldi* Fletcher, 1950Genus *Barrandeops* McKellar and Chatterton, 2009Species *Barrandeops granulops* (Chatterton *et al.*, 2006)Species *Barrandeops forteyi* McKellar and Chatterton, 2009Genus *Boeckops* Chlupáč, 1972Species *Boeckops boeckii* (Hawle and Corda, 1847)Genus *Eldredgeops* Struve, 1990Species *Eldredgeops rana* (Green, 1832)Genus *Geesops* Struve, 1972Species *Geesops schlottheimi* (Bronn, 1825)Species *Geesops sparsinodosus* (Struve, 1970)Genus *Phacops* Emmerich, 1839Species *Phacops* sp.

- Species *Phacops superstes superstes* Barrande, 1852
- Genus *Reedops* Richter and Richter, 1925
- Species *Reedops bronni* (Barrande, 1846)
- Species *Reedops prospiciens* Chlupáč, 1977
- Species *Reedops* cf. *sternbergi* (Hawle and Corda, 1847)
- Species *Reedops cephalotes* (Hawle and Corda, 1847)
- Family Pterygometopidae Reed, 1905
- Genus *Chasmops* McCoy, 1849
- Species *Chasmops* sp.
- Species *Chasmops* cf. *musei* Öpik, 1937
- Genus *Estoniops* Männil, 1958
- Species *Estoniops exilis* (Eichwald, 1858)
- Genus *Ingriops* Jaanusson and Ramsköld, 1993
- Species *Ingriops* sp. nov.
- Species *Ingriops trigonocephalus* (Schmidt, 1881)
- Superfamily Dalmanitacea Vodges, 1890
- Family Dalmanitidae Vodges, 1890
- Genus *Dalmanites* Barrande, 1852
- Species *Dalmanites* sp.
- Genus *Odontochile* Hawle and Corda, 1847
- Species *Odontochile hausmanni* (Brongniart, 1822)

The geographical and temporal distribution of specimens is summarised in Figure 3.1. For full details of all thin sections produced, including an explanation of the specimen numbering system, as well as a list of the techniques applied to each specimen, see Appendix A.

3.1.2 Preservation of Specimens

Where details of conodont alteration index (CAI) (Epstein *et al.*, 1976) are available in the literature, these have been specified in the descriptions below to give an indication of the degree of heating the specimens have undergone. It should be noted that although CAI values are provided for the general region in which samples were sourced, data are not always available for the exact site. These values may therefore not be a precise reflection of the post-deposition thermal history of the trilobites.

AGE (Ma)	EPOCH/STAGE		REGION / REGIONAL SUBDIVISION	SPECIES
299.0 ± 0.8	CARBONIFEROUS	Gzelian	ENGLAND Arnsbergian Stage	<i>Paladin eichwaldi shunnerensis</i> (King, 1914)
		Kasimovian		
		Moscovian		
		Bashkirian		
		Serpukhovian		
359.2 ± 2.5	DEVONIAN	Viséan	UNITED STATES & CANADA Silica Formation / Hamilton Formation	<i>Eldredgeops rana</i> (Green, 1832)
		Tournaisian		
		Famennian	GERMANY Flesten Member, Ahrdorf Formation	<i>Geesops schlotheimi</i> (Bronn, 1825) <i>Geesops sparsinodosus</i> (Struve, 1970)
		Frasnian		
		Givetian	MOROCCO Timrharrhart Fm./Teratite Fm./Kess-Kess Fm.	<i>Phacops</i> sp. <i>Austerops smoothops</i> (Chatterton et al., 2006) <i>Barrandeops granulops</i> (Chatterton et al., 2006) <i>Barrandeops cf. granulops</i> (Chatterton et al., 2006) <i>Barrandeops forteyi</i> Chatterton et al., 2009
		Eifelian		
		Emsian	CZECH REPUBLIC Praha Formation	<i>Phacops superstes superstes</i> Barrande, 1852 <i>Reedops bronni</i> (Barrande, 1846) <i>Boeckops boeckii</i> (Hawle & Corda, 1847) <i>Reedops prospiciens</i> Chlupáč, 1977 <i>Reedops cf. sternbergi</i> Hawle & Corda, 1847 <i>Reedops cf. cephalotes</i> (Hawle & Corda, 1847) <i>Odontochile hausmanni</i> (Brongniart, 1822)
		Pragian		
		Lochkovian		
416.0 ± 2.8	SILURIAN	Ludfordian	AUSTRALIA Boree Creek Formation	<i>Ananaspis macdonaldi</i> (Fletcher, 1950)
		Gorstian		
		Homerian		
		Sheinwoodian		
		Telychian		
		Aeronian		
443.7 ± 1.5	ORDOVICIAN	Ruddanian		
		Hirnantian	SCOTLAND Upper Whitehouse Subgroup	<i>Symphysops subarmata</i> Reed, 1914
		Katian	ESTONIA Oandu stage	<i>Chasmops aff. musei</i> Öpik, 1937
		Sandbian	ESTONIA Kukuse stage	<i>Estoniops exilis</i> (Eichwald, 1858)
		Darwillian	SWEDEN Lower Anderson Shale	<i>Telephina bicuspis</i> (Angelin, 1854) <i>Telephina mobergi</i> (Hadding, 1913)
		Dapingian	ESTONIA Aseri stage	<i>Ingriops</i> sp. nov.
		Floian	ESTONIA Kunda stage	<i>Ingriops trigonocephalus</i> (Schmidt, 1881)
488.3 ± 1.7	CAMBRIAN	Tremadocian	SPITSBERGEN Valhålfonna Formation	<i>Carolinites sibiricus</i> Chugaeva, 1964 <i>Carolinites angustagena</i> Ross, 1967

Figure 3.1- Spatial and temporal distribution of specimens investigated.

In addition specimens of *Dalmanites* sp. were studied; specimen age and locality are unknown. Species names in blue indicate those with holochroal eyes, all others have schizochroal eyes. Age dates are taken from Gradstein *et al.* (2004).

3.1.2.1 Specimens with Holochroal Eyes

3.1.2.1.1 English Material

Numerous specimens of *Paladin eichwaldi shunnerensis* (King, 1914) were donated by Prof. Euan Clarkson, University of Edinburgh. The specimens are from the type locality; the Shunner Fell Limestone of North Yorkshire and are from the base of the Arnsbergian stage (Late Carboniferous, Serpukhovian stage) (Rowell and Scanlon, 1957; Zhang and Clarkson, 1990). Specimens are disarticulated, but individual sclerites are fairly well preserved (Figure 3.2A).

3.1.2.1.2 Swedish Material

Specimens of *Telephina mobergi* (Hadding, 1913) and *Telephina bicuspis* (Angelin, 1854) (Figure 3.2B) were donated by Prof. Per Ahlberg of Lund University. The specimens are from the lower Andersön Shale (Upper Dariwillian Stage of the Middle Ordovician) in the Storsjön area of the Jämtland region of Sweden (Ahlberg, 1995). The material consists of isolated free cheeks. The eyes are intact but identification of individual lenses was only possible in one specimen (Figure 3.2B).

CAI values of 4.5 - 5.0 in allochthonous units and 3 - 5 in autochthonous deposits in Jämtland have been recorded by Bergström (1980) indicating considerable heating to temperatures of 110 - 400°C and perhaps even in excess of this.

3.1.2.1.3 Scottish Material

Two specimens of *Symphysops subarmata* Reed, 1914 were sourced from the Upper Whitehouse Subgroup, Girvan, Scotland and are Upper Katian in age, from around the Caradoc-Ashgill boundary in terms of Anglo-Welsh chronostratigraphy. Both specimens consist of a single eye on which only part of the visual surface was preserved (Figure 3.2C). Specimens were provided by Dr Alan Owen, University of Glasgow.

CAI values for the Girvan area range from 1.5 - 2.5 (Aldridge, 1986; Bergström, 1980, 1990) indicating burial temperatures of approximately 50 - 140°C.

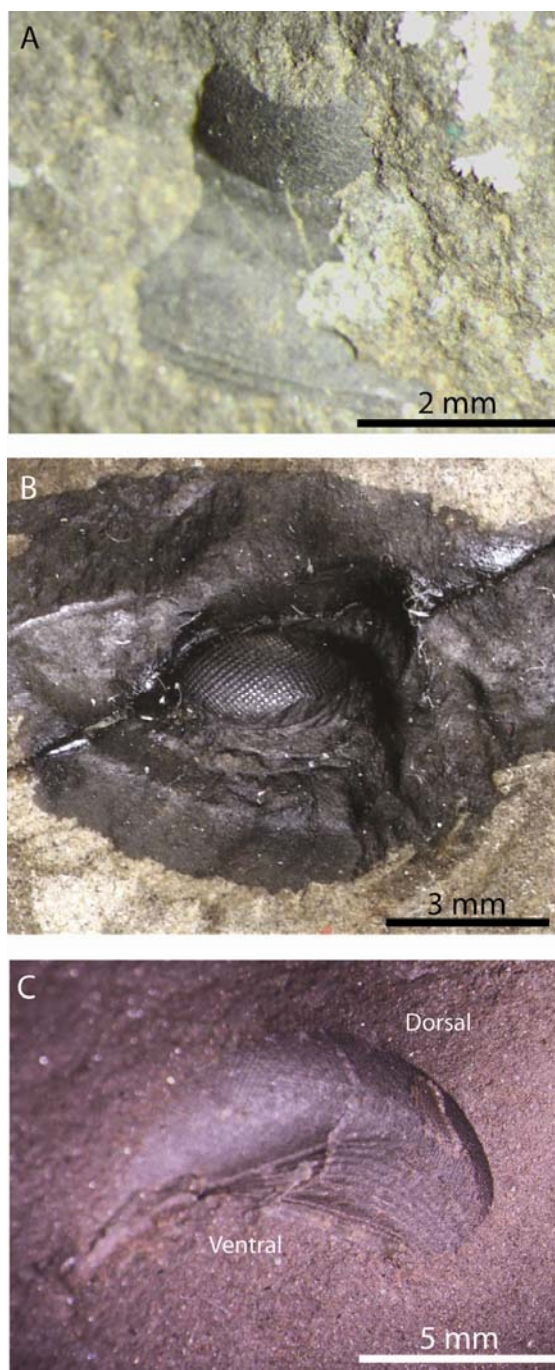


Figure 3.2 - Holochroal trilobite eyes.

A. *Paladin shunnerensis* (specimen 82), **B.** *Telephina bicuspis* (specimen 97) and **C.** *Symphysops subarmata* (specimen 93 - oblique view image of a negative impression on which part of the visual surface has been retained).

3.1.2.1.4 Spitsbergen Material

Thin sections containing one specimen each of *Carolinites sibiricus* Chugaeva, 1964 of Fortey, 1975 and *Carolinites angustagena* Ross, 1967 were loaned for analysis by Dr. Thijs Vandenbroucke of the Université Lille in conjunction with his study of oxygen isotopes in the lenses of these trilobites (Vandenbroucke *et al.*, 2010). The specimens were originally provided by Prof. Richard Fortey of the Natural History Museum and are from the Arenig (Lower Ordovician) Vallhalfonna

Formation (more precisely unit V4b of the Profilbekken Member (type section) in the case of *C. angustagena*) (Fortey, 1975) .

A CAI value of 1 has been determined for this region (Bergström, 1980), this corresponds to a burial temperature of <50 - 80 °C.

3.1.2.2 Specimens with Schizochroal Eyes

3.1.2.2.1 German Material

Specimens of *Geesops schlotheimi* (Bronn, 1825) and *Geesops sparsinodosus* (Struve, 1970) from the Eifelian Trilobitenfelder near to the town of Gees in the German region of Eifel were provided for analysis by Dr. Brigitte Schoenemann (Universität Bonn) and Prof. David Bruton (University of Oslo); the latter being specimens collected by Mr Harald Presher. The precise locality in Gees for the *G. schlotheimi* specimens is not known but the *G. sparsinodosus* material is from 'The Trench' Salmer Weg, Gees; the same locality as material studied by Bruton and Haas (2003a). Bruton and Haas (1997) noted that specimens of *G. sparsinodosus* from the Gees Trilobitenfelder are restricted to the central 2-3m of the 28 m Flesten Member of the Ahrdorf Formation, which is lower Eifelian in age; this information was obtained from an unpublished masters thesis (Schüngel, 1988). Preservation of the visual system in the specimens of *G. schlotheimi* is good. However most of the eyes are exposed (i.e. not enclosed by the host rock) and as a result some weathering and post-sampling damage has occurred. In a few cases this involves the partial loss of the visual surface. Eyes typically have 12-13 files consisting of a maximum of 5-6 lenses each. There is minimal damage to the visual surfaces of the *G. sparsinodosus* specimens which are excellently preserved (Figure 3.3A); the eyes typically consist of 16 files of lenses with 5 lenses each.

CAI values for conodonts in the Lower to Middle Devonian carbonates in the Eifel hills are low, 1.5 - 2.0, indicating temperatures of ~60 - 110 °C showing 'little, if any, effect of heating' (Helsen and Königshof, 1994). Conodonts in dolomitised rocks in the Eifel region have a higher CAI of 6.0 (Helsen and Königshof, 1994), indicating temperatures in excess of 300 °C.

3.1.2.2.2 Bohemian Material

A wide variety of material from the Bohemia region of the Czech Republic was provided by Dr. Petr Budil from the Czech Geological Survey. A single specimen

is from the Royal Museum of Scotland. The majority of material is from the Praha Formation: *Reedops prospiciens* Chlupáč, 1977 from the Silvenec Limestone Facies; *Reedops* cf. *cephalotes* (Hawle and Corda, 1847) and *Odontochile hausmanni* (Brongniart, 1822b), from the Dvorce-Prokop Limestone Facies (Royal Museum of Scotland collection number 1963.15.69); *Reedops* cf. *sternbergi* Hawle and Corda, 1847 from the transition layers between the two previously mentioned facies; *Reedops bronni* (Barrande, 1852b) and *Boeckops boeckii* (Hawle and Corda, 1847) from the Loděnice Limestone Facies. A single specimen of *Phacops superstes superstes* Barrande, 1852 is from the Daleje Shale of the Daleje-Trebator Formation. All the material is Pragian in age, with the exception of *P. superstes superstes* which is upper Emsian. Only cephalons are present in this material. The condition of the visual surfaces varies somewhat between specimens; some eyes are embedded in matrix, presumably with intact visual surfaces, whereas others show considerable damage as a result of their exposure during collection or curation. Many eyes consist of very pale coloured calcite with the exception of specimens from the Dvorce-Prokop Facies and the Daleje Shale which are much darker in colour.

Extensive work on conodont biostratigraphy at the Pragian/Emsian boundary of the Barrandian area has been carried out by Slavík (Slavík, 2001, 2004; Slavík *et al.*, 2007). However, these studies do not discuss CAI values.

3.1.2.2.3 Material from the U.S.A

Specimens of *Eldredgeops rana* (Green, 1832) from the Silica Formation (Unit 7-9) at the Martin-Marietta Quarry in Milan, Michigan were provided by Mr. David Rudkin of the Royal Ontario Museum. This material is of Middle Devonian age (Givetian). The specimen chosen for analysis consists of a cephalon only (Figure 3.3B); the exoskeleton is pale red/brown in colour. The visual surface has about 80 lenses preserved (approximately 16 files of lenses, 7 lenses per file at the largest part). There is fracturing along the glabella and palpebral lobe which extends to the eye surface resulting in the loss of, or damage to, some lenses. However, many remain in good condition.

3.1.2.2.4 Canadian Material

Specimens of *Eldredgeops rana* (Green, 1832) from the Middle Devonian Hamilton Formation of the Theoford-Arkona Area of Ontario were provided by Mr. David Rudkin of the Royal Ontario Museum. The specimen chosen for

analysis, a cephalon only, has a very dark brown/black exoskeleton; fracturing is prominent through the glabella but does not affect the eyes. The eyes have a maximum of 6 lenses per file and approximately 14 files of lenses. A few files of lenses are missing but the lenses which remain are well preserved.

3.1.2.2.5 Moroccan Material

A number of specimens, primarily of *Phacops* and *Barrandeops*, were donated for research by Prof. Richard Fortey and Claire Mellish (Natural History Museum, London), Professor Brian Chatterton and Mr Ryan McKellar (Department of Earth and Atmospheric Sciences, University of Alberta, Canada) and Dr. Christian Klug (Paläontologisches Institut und Museum der Universität Zürich).

Of the numerous specimens provided a small number with excellently preserved eyes were selected for analysis: *Phacops* sp. of the Terarine Formation; *Barrandeops granulops* (Chatterton *et al.*, 2006) and *Austerops smoothops* (Chatterton *et al.*, 2006) from the Timhanrrhart Formation of Jbel Gara el Zguilma, south of Foug Zguid; and *Barrandeops cf. granulops* (Chatterton *et al.*, 2006) from the Kess-Kess Formation of the Red Cliffs (Klug *et al.*, 2009), Hamar Laghdad, Tafilalt, eastern Anti-Atlas. One specimen of *Phacops* sp. also selected for analysis was purchased from Mr Wood's Fossils, Edinburgh; the sample is from the Erfoud area of Morocco but the exact location is not known. Most specimens are intact and enrolled, but various parts of the exoskeleton are no longer present due to abrasion. In all cases the visual surface is well preserved, most notably in *A. smoothops* (Figure 3.3C) in which all lenses are intact; trilobites from the Timhanrrhart Formation at this locality were protected from compaction by the formation of calcareous nodules during early diagenesis (Chatterton *et al.*, 2006). This material is Early Devonian, more specifically Late Emsian to upper Eifelian (Wendt *et al.*, 1997; Chatterton *et al.*, 2006; McKellar and Chatterton, 2009). These specimens typically have 14 files of lenses with 5 lenses per file. Material from Morocco also includes specimens of *Barrandeops forteyi* McKellar and Chatterton, 2009 from the Psychopyge horizon of the Tazoulart Formation. Eyes of this species differ from other schizochroal eyes in the packing arrangement of the lenses. Rather than a hexagonal packing arrangement, lenses of *B. forteyi* show a cubic pattern identified in other species by Fortey and Morris (1977) (section 1.5.2.1); each lens has four direct neighbours rather than six. Specimen 98 consists of a cephalon with a single eye

only. Specimen 62 is complete and enrolled. In both cases lenses are, in part, concealed by debris, but what is exposed seems to be well preserved. Exposed eyes typically have 12 files of lenses each consisting of a maximum of 3 lenses. Significant silicification events in Morocco have been well documented (Lang *et al.*, 1990; Thiry and Benbrahim, 1990) as well as dolomitisation (Klug *et al.*, 2009), these events are not thought to have affected the lenses (Klug *et al.*, 2009).

CAI values of 3 - 5 in the Devonian rocks of the Anti-Atlas rocks indicate heating to temperatures of 210 - 310°C (Belka, 1991); values from the Tafilalt area are at 4 - 4.5 (Belka, 1991) indicating temperatures of approximately 190 - 300°C.

3.1.2.2.6 Estonian Material

Four species, each from a different stratigraphical unit in the North of Estonia, were loaned for research by Dr. Helje Pärnaste of Tallinna Tehnikaülikooli Geoloogia Instituut.

The specimens belong to: *Ingriops trigonocephalus* (Schmidt, 1881) from the Middle Ordovician Kunda stage (Darriwilian) at Paldiski; *Ingriops. sp nov.* from the Middle Ordovician Aseri stage (Darriwilian) on Vaike-Pakri Island; *Estoniops exilis* (Eichwald, 1858) from the Late Ordovician Kukruse stage (Sandbian) at Kohtla kaevandus and Narva karjaar; *Chasmops cf. musei* (Öpik, 1937) from the Late Ordovician Oandu stage (Katian) at Kunda-Aru Karjaar. These four baltoscandian stages correspond to the Fennian-Abereiddian, Abereiddian-Llandeilian, Aurelucian and Cheneyan stages of the Anglo-Welsh chronostratigraphy respectively (Bergström *et al.*, 2009). The lithologies are predominantly bioclastic limestones with argillaceous limestone and calcareous sandstones also present. The material comprises cephalia only and in some cases only the eye and free cheek are present (Figure 3.3D). Preservation is however very good; there has been some damage to the visual surfaces in a few cases but the lenses that remain are in good condition. A few of the specimens have one or both eyes embedded in matrix so the quality of preservation could not be assessed prior to thin section preparation.

A CAI of 1.0 - 1.5 has been reported in the Cambrian-Ordovician beds at Tõnismägi, Tallinn, North Estonia (Kaljo *et al.*, 1988) indicating low temperatures in the region of <50 - 90°C.

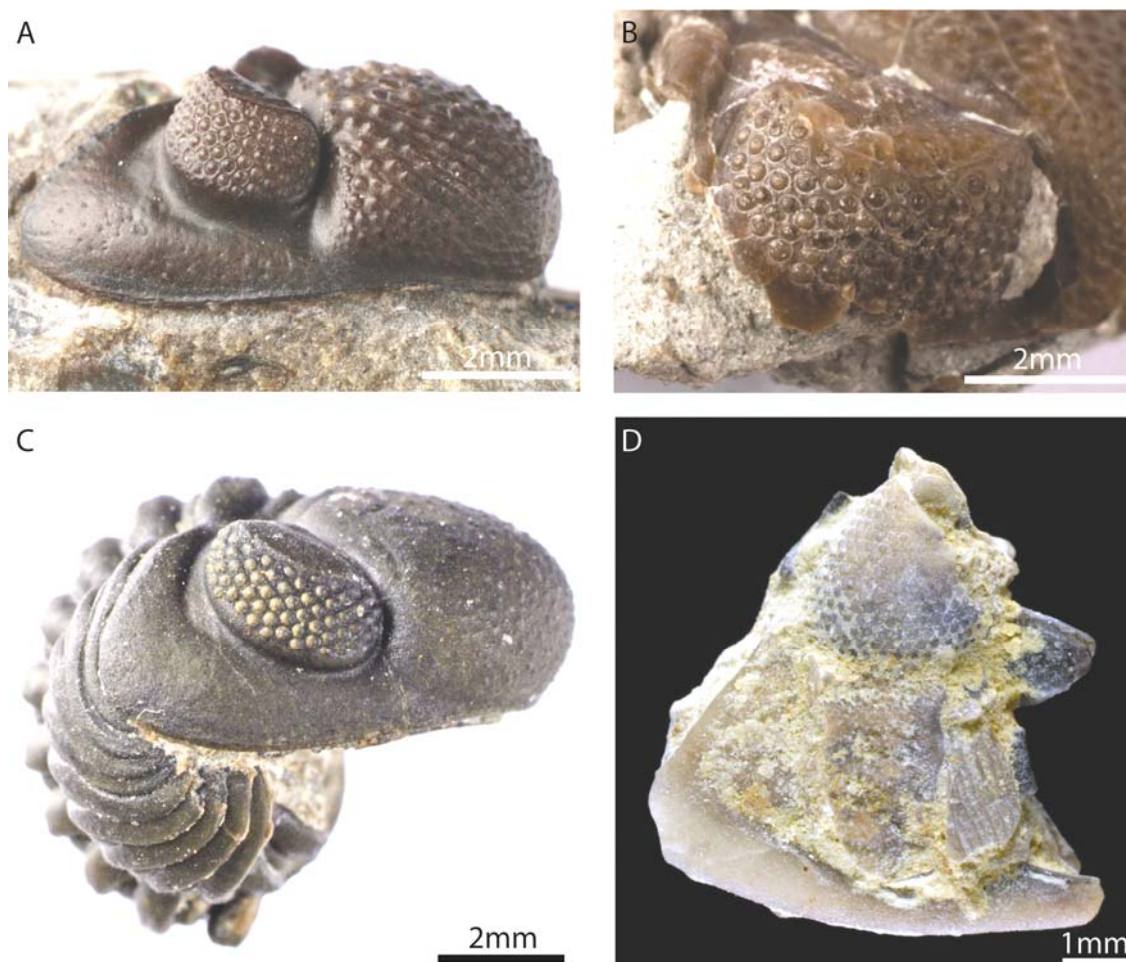


Figure 3.3 – Specimens with schizochroal eyes.

The schizochroal eyes of A. *Geesops sparsinodosus* (specimen 57), B. *Eldredgeops rana* (specimen 22), C. *Austerops smoothops* (specimen 65) and D. *Chasmops cf. musei* (specimen 53). Note the range in preservation quality.

3.1.2.2.7 Australian Material

Specimens of *Ananaspis macdonaldi* (Fletcher, 1950) were provided by Dr. David Holloway of the Royal Museum Victoria (Museum numbers NMV P312897-NMV P312899). They were collected from the Boree Creek Formation, Borenore-Molong District of New South Wales, Australia, which is Silurian (upper Telychian - lowermost Sheinwoodian) in age (Valentine and Brock, 2003). The specimen chosen for thin sectioning is well preserved; the left eye was partially exposed and the right eye was entirely encased in a matrix of grey limestone.

CAI values of 2 - 3 are reported in the Boree Creek Formation at a locality 3 - 4.5 km south-east of where the trilobites were collected (Cockle, 1999a). These values indicate temperatures of 60 - 200°C.

3.1.3 Ostracods

Numerous specimens of the ostracod *Primitiopsis planifrons* Jones, 1887 (Figure 3.4) were provided for study by Prof. David Siveter (Department of Geology, University of Leicester). This material was collected at the type location of the Mulde Member (Halla Formation, Silurian Wenlock Series) in the Mulde area (Gotland region), Sweden (Tanaka *et al.*, 2009).

Modern ostracods were collected from the intertidal zone of the Firth of Clyde (Largs) on the West coast of Scotland under the supervision of Dr. Mike Keen (University of Glasgow). Unfortunately due to the small size of the specimens (maximum ~3 mm in length), preparation of polished blocks (in which specimens were encased) for analysis was unsuccessful. It was noted that the ostracod eye spots *in-vivo* ‘glow’ brightly, this is indicative of a reflecting surface, the tapetum, below the carapace (section 1.6.1).

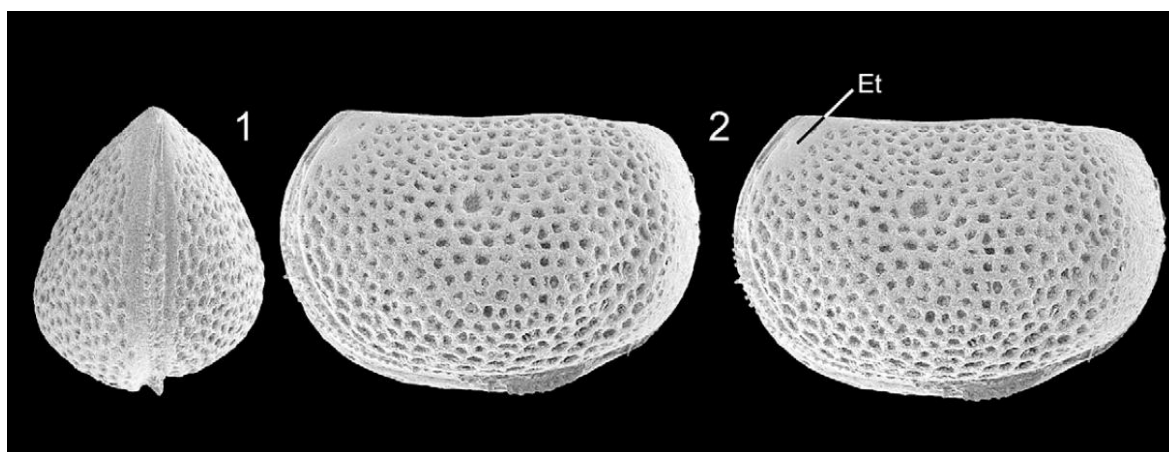


Figure 3.4 - *Primitiopsis planifrons* Jones, 1887. Anterior view (left) and stereo pair of left lateral views (right) of the carapace of *Primitiopsis planifrons*. ‘Et’ marks the eye tubercle. Specimens are approximately 1 mm in length. Image from Tanaka *et al.*, 2009.

3.1.4 Brittlestars

A single specimen of *Ophiocoma wendtii* Müller and Troschel, 1842 (Natural History Museum of Los Angeles County museum number CBC-08-09) (Figure 3.5) was donated by Dr Gordon Hendler. This species was chosen as previous studies have shown that the calcite ‘micro-lenses’ on the dorsal surface of this brittlestar are light detecting units (Hendler, 1984; Hendler and Byrne, 1987; Aizenberg *et al.*, 2001; Aizenberg and Hendler, 2004; Aizenberg and Hendler,

2005). The sample is from Carries Cow Bay, Belize and is preserved in 95% alcohol.

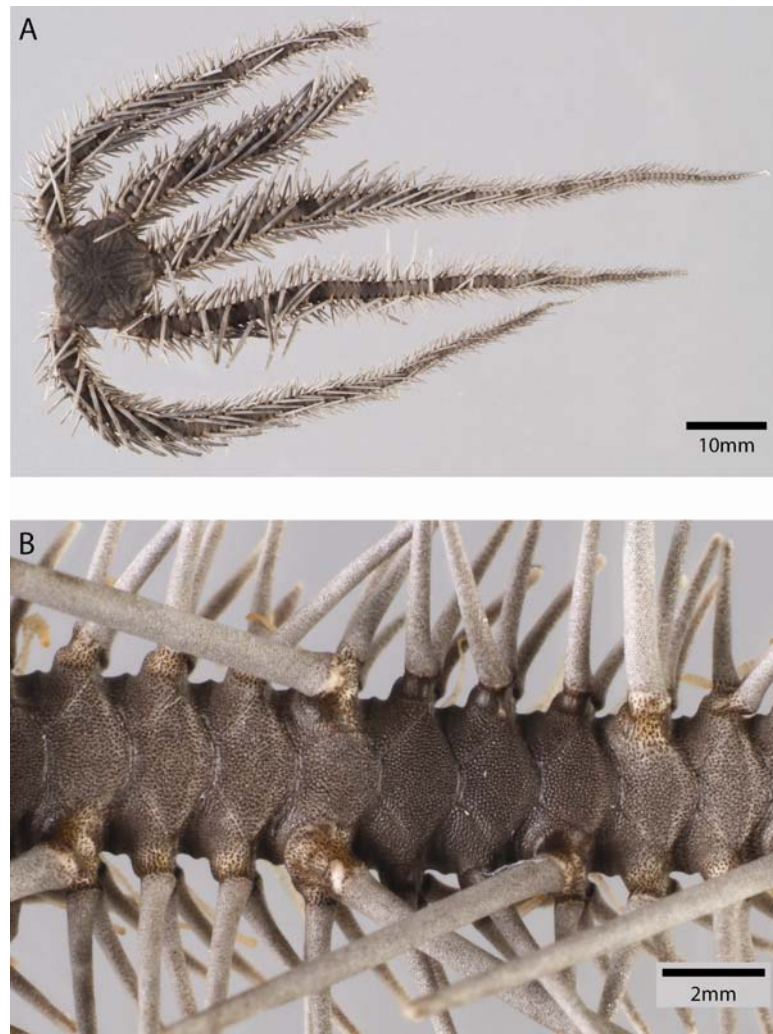


Figure 3.5 - *Ophiocoma wendtii* Müller and Troschel, 1842.

Photographs of the dorsal view of the entire specimen (A) and of a single arm at higher magnification (B). Several dorsal arm plates can be seen in B, each of these is covered with small raised lenses which are just visible to the naked eye.

3.2 Sample Preparation

Polished thin sections were prepared for EBSD and other microscopy techniques. Etched thin sections and fractured surfaces were imaged in the SEM using secondary electrons. It should be noted that preparation of thin sections presented significant challenges; producing a thin section at the desired orientation and at the correct level within the eye was often difficult due to the uneven shape of the specimens. Innovative measures were often taken to ensure success of sample preparation but, unavoidably, preparation of some samples was unsuccessful.

3.2.1 Thin Sectioning of Trilobite Eyes

Polished thin sections were prepared in a series of steps, the first of which was application of EpoThin resin (3 parts resin to 1.2 parts hardener) to any exposed areas of the trilobite visual surface; this provided a layer of protection to minimise any potential damage during subsequent sample preparation.

Large specimens and those held within a rock matrix were trimmed, using a Husqvarna TS 230F high speed saw, to a more manageable size prior to embedding in resin. A mixture of EpoxiCure resin and hardener was prepared in the ratio 5 parts to 1 part and poured into moulds in which specimens had been placed in the desired orientation.

Once hardened, resin blocks were ground using silicon carbide abrasive paper discs of decreasing grade (68 μm - 15 μm) on a Buehler® Beta Grinder-Polisher until the lenses were exposed. Blocks were mounted, exposed surface down, onto pre-ground glass slides of standard size (47 mm x 25 mm) using a small amount of EpoThin resin, mixed in a ratio of 3 parts resin to 1.2 parts hardener, and placed in a press to set. The grinding of glass slides ensures a completely flat surface on which to bond the sample, minimising any deviation from the intended orientation when the section is cut.

Glass slides with sample blocks were attached to a Buehler® PetroThin® thin sectioning system and were trimmed to approximately 3 mm using the integrated diamond blade. The remaining block was ground down to a thickness of 50 μm using the system's grinding plate.

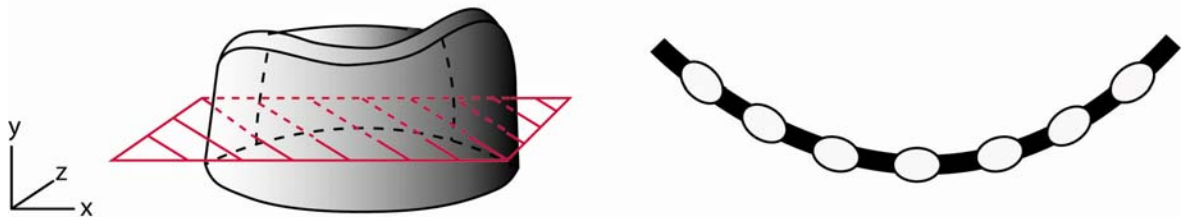
Thin sections underwent further grinding using 8 μm , 6 μm and 3 μm diamond lapping plates and lubricant on a Kemet 300 Series lapping unit after which polishing was carried out. Two stages of polishing using decreasing grades of Alpha Alumina (1 μm and 0.3 μm) preceded the final stage of polishing using 0.4 μm colloidal silica solution; polishing with colloidal silica is necessary to give the high quality polish required for analysis by EBSD. These three final stages of polishing were carried out mechanically using a Kent 3 automatic lapping and polishing unit fitted with soft polishing clothes. The time required on each stage of polishing varied depending on the hardness of the materials within the thin section.

The final thickness of the thin sections produced was approximately 30 μm .

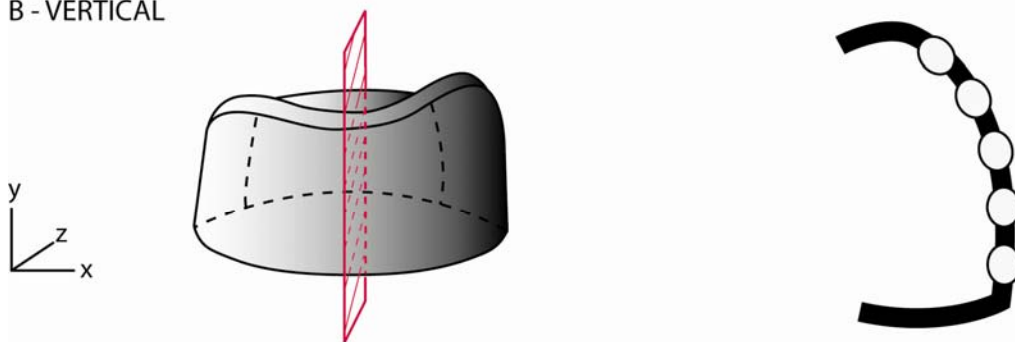
3.2.1.1 Orientation of Thin Sections

Sections were cut in three orientations, horizontal, vertical and tangential (Figure 3.6). Viewing the lenses in different orientations enables the construction of three-dimensional models from two-dimensional imaging.

A - HORIZONTAL



B - VERTICAL



C - TANGENTIAL

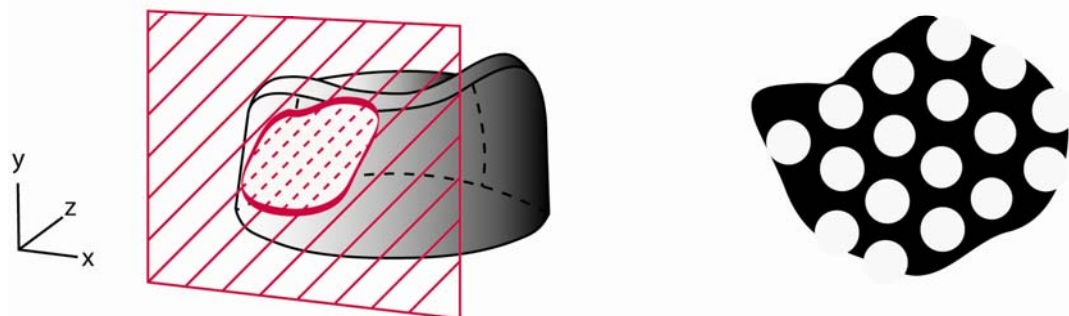


Figure 3.6 - Thin section orientations and corresponding lens arrangements. Schematic diagrams of A. horizontal, B. vertical and C. tangential lines of section. Any line of section between these three is termed 'oblique'. For simplicity the visual surface has been drawn without lenses. In lens arrangement diagrams the black areas represent sclera.

(1) Horizontal: sections cut the visual surface parallel to the palpebral lobe, sectioning a horizontal row of lenses; it should be noted that such a 'horizontal row' parallel to the palpebral lobe, crosscuts several diagonal rows. This type of

row should not be confused with the diagonal rows referred to in studies of external eye morphology and lens distribution (section 1.5.2.1). Sections cut in this plane contain up to 20 lenses, the exact number determined by the number of lens files in a particular specimen and the depth in the eye at which the section is cut.

(2) Vertical: sections cut the visual surface perpendicular to the palpebral lobe. This results in the sectioning of a file of lenses, which consists of usually no more than 6 or 7 lenses, determined by the number of lenses per file in a given specimen and the point in the eye at which the section is cut.

(3) Tangential: sections are cut in the plane of the visual surface, providing a 'plan view' of the lenses but curvature of the visual surface results in lenses being sectioned at varying depths and angles.

Difficulties were faced in achieving the desired orientation of thin sections because of the uneven shape of specimens. As a result many thin sections have been produced a few degrees off the intended line of section. In a small number of cases where this deviation is significant, sections have been termed 'oblique'. Curvature of the visual surface both in the horizontal and vertical planes means that lenses within a section will be cut at slightly different orientations and depths. These variations are identified in EBSD and are noted as artefacts of the sectioning process.

3.2.1.2 Acid Etching of Thin Sections

Thin sections were etched using 1% aqueous HCl. Polished sections were dipped into a beaker of this solution for 20 seconds; this treatment time allowed sufficient dissolution of calcite giving dolomite crystals a topographic elevation of approximately 100 nm above the calcite. Prior to SE imaging on the FEG-SEM the sections were coated with gold, using an AGAR sputter coater, for 120 seconds.

3.2.2 TEM Sample Preparation

Electron transparent samples, 'foils', were produced for TEM work, at a thickness of less than 100 nm. Samples were produced by two methods: Focused Ion Beam milling (hereafter referred to as FIB), carried using a FEI Nova 200

Dualbeam FIB system and argon ion milling carried out on a Gentlemill system, both held at the Kelvin Nanocharacterisation Centre at the University of Glasgow. Both methods were applied to polished thin sections.

3.2.2.1 TEM Preparation by FIB

This preparation method was used on a thin section of *Geesops sparsinodosus* (GG58) cut in the horizontal plane. Foils from both the upper lens and lens centre were prepared.

This process, carried out by Mr William Smith (FIB sample preparation technician at the Kelvin Nanocharacterisation Centre at the University of Glasgow) involved various stages of platinum deposition and gallium ion milling. A small (~15 x 5 µm) area of the sample was selected for analysis onto which platinum was deposited, using a Ga⁺ ion beam, prior to fine scale milling, providing protection from the ion beam and therefore minimising deformation during preparation; Vicenzi and Heaney (1999) showed that structural integrity is not always retained when materials are bombarded with high-energy Ga⁺ ions, Lee *et al* (2007b) overcame this problem by coating samples with a >85 nm layer of gold prior to FIB work. However, this was not required in the present study as no significant damage was detected during FIB work on uncoated samples. 'Trenches' were milled along two sides of the area of interest which was attached to a fine glass needle using an Omniprobe 100 micromanipulator before the final edge was cut, separating the site of interest from the thin section. The sample was transferred to a holder for later analysis. This method has been successfully used on minerals including kaolinite and feldspar (Lee *et al.*, 2007b; Lee and Smith, 2006). A more detailed description of this process can be found in Heaney *et al.* (2001).

3.2.2.2 TEM Preparation by Argon Ion Milling

This sample preparation method was used on a thin section of *Reedops cf. cephalotes* (RB2B) cut in the horizontal plane.

TEM 'foils' were prepared by this method by Mr Brian Miller (sample preparation technician Kelvin Nanocharacterisation Centre at the University of Glasgow). Argon ion milling involves preparation of foils using a low-energy Technoorg-Linda Gentlemill system (see Scott *et al.*, 2006 for details), bombarding the

sample, from above and below at low angles, with a ≤ 5 kV Ar^+ ion beam under vacuum so it gradually thins by ‘sputtering’ (Lee *et al.*, 2003 and references therein, Lee, 2010). Milling is terminated once holes are formed in the sample, the areas around these being electron transparent (Lee, 2010). Although an effective sample preparation method, ion milling can result in damage of the sample; a thin amorphous and ion implanted layer can form on the milled surfaces resulting in degradation of high-resolution images and electron diffraction patterns (Lee, 2010 and references therein).

3.2.3 Fracture Surface Preparation

‘Rough’ samples were prepared by applying a point load on an area on or near the visual surface, usually the palpebral lobe, using long-nose pliers. This resulted in cracking along the visual surface, exposing the interior of lenses. Samples were mounted on SEM stubs and gold coated using an AGAR sputter coater for 180 seconds.

3.2.4 Preparation of Ostracod and Brittlestar samples

Ostracod (Figure 3.7) and brittlestar (Figure 3.8) specimens were prepared as polished SEM stubs. In the case of the ostracods, the entire specimen was mounted, for brittlestars, individual dorsal arm plates were removed from the specimen using a scalpel and adhered to a stub. Specimens were covered with a small amount of Epothin resin (3:1.2 of resin to hardener) which once set was ground down to the desired level within the specimen using silicon carbide abrasive paper and polished using alpha alumina in the same sequence as for the thin sections (section 3.2.1).

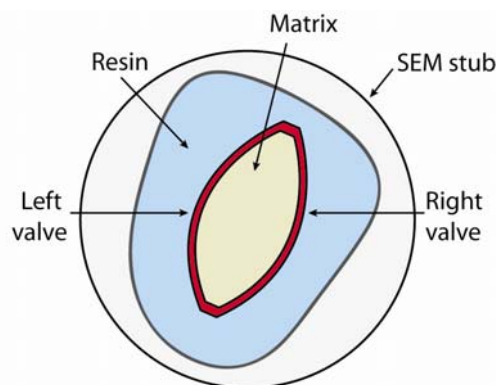


Figure 3.7 - Sample orientation of ostracods in polished stubs.
Samples were produced in horizontal section.

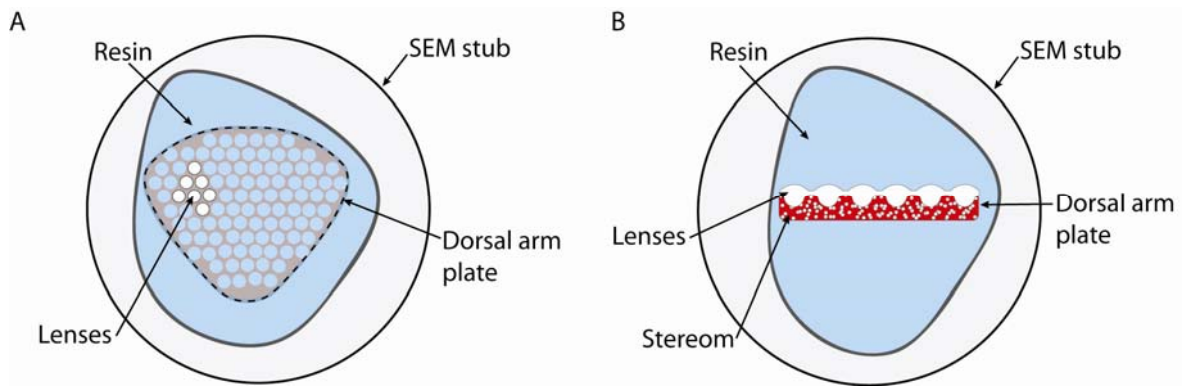


Figure 3.8 – Sample orientation of brittlestars in polished stubs.

Samples were prepared in tangential (A) and transverse (B) lines of section. Note that in A not all lenses in the dorsal arm plate are sectioned, this is due to the slight curvature of the plate surface.

4

Holochroal Eyes

4.1 Results

Thin sections of *Paladin eichwaldi shunnerensis*, *Symphysops subarmata*, *Telephina bicuspis*, *Telephina mobergi*, *Carolinites angustagena* and *Carolinites sibiricus* were analysed by light microscopy, optical CL, EBSD and EDS. *Symphysops*, *Telephina* and *Carolinites* are Ordovician in age, *Paladin* is Carboniferous (section 3.1.1).

4.1.1 Light Microscopy

4.1.1.1 Transmitted Light

Holochroal lenses vary considerably in shape both between species, and between ontogenetic stages within a single species (Table 4.1). Lenses of *S. subarmata* and holaspid specimens of *P. shunnerensis* are plano-convex; they have flat outer surfaces and convex bases. Lenses of *T. bicuspis*, *T. mobergi*, *C. angustagena* and *C. sibiricus* as well as juvenile specimens of *P. eichwaldi shunnerensis* are biconvex. Convexity varies between species; juvenile *Paladin* lenses are the most convex of those analysed. Unlike schizochroal eyes, adjacent lenses in holochroal eyes including those that are biconvex, are in direct contact, with the exception of juvenile *P. eichwaldi shunnerensis* in which lenses are spaced by ~5 µm. Lens shapes and sizes are summarised in Table 4.1.

Holaspid *Paladin* lenses (Figure 4.1A) range in thickness from ~80 µm to 150 µm, increasing from one side of the eye to the other. This is most likely to be due to a gradual change in the angle at which lenses have been sectioned, as a result of the curvature of the eye. Lenses are composed of optically clear calcite with

Table 4.1 - Shape and typical sizes of holochroal lenses.

GENUS	LENS SHAPE	LENS SIZE	
		THICKNESS (µm)	WIDTH (µm)
<i>Paladin eichwaldi shunnerensis</i> (HOLASPIS)	Plano-convex	90	70
<i>Paladin eichwaldi shunnerensis</i> (MERASPIS)	Biconvex	45	45
<i>Symphysops subarmata</i>	Plano-convex	130	155
<i>Telephina mobergi</i>	Biconvex	74	160
<i>Telephina bicuspis</i>	Biconvex	80	180
<i>Carolinites angustagena</i>	Biconvex - Rectangular	60	105
<i>Carolinites sibiricus</i>	Biconvex	65	100

varying abundances of inclusions, which are randomly distributed in the majority of lenses. However, in one or two cases they form faint lines that can be traced part way through the lens; equivalent to the trabeculae described in other studies (e.g. Clarkson *et al.*, 2006). One thin section shows a brown staining on the lenses across the entire eye (Figure 4.1A), penetrating more than half the thickness of the lenses, and the adjacent exoskeleton. The size of the biconvex lenses of the juvenile of *P. shunnerensis* analysed (Figure 4.1B) is consistent with holaspis lenses, however the shape is consistent with meraspis lenses (Clarkson and Zhang, 1991). Based on the number (>10 in a single row) and spacing of the lenses it is unlikely that this specimen is a degree 0 meraspis, and is probably a later stage, approaching the early holaspid period. The diameter of holaspis lenses also exceeds the range stated by Clarkson and Zhang (1991) this may at least in part reflect differences in the measuring technique; thickness and width measurements were determined in the present study from TL images of thin sections rather than intact eyes. Meraspis lenses are almost in contact, with just a small bridge between them. This is not thick enough to be classed as intralensar sclera, nor does it have the fibrous appearance of the cuticle, it appears more like an extension of the lenses themselves. Lenses are relatively clear with few inclusions. Rotation of the microscope stage in crossed nicols shows that the extinction angle varies along the lens base in holaspis *Paladin eichwaldi shunnerensis* (the upper area of the lens extinguishes uniformly) and

along both the outer surface and lens base in meraspis lenses of this species. This indicates a change in crystal orientation within lenses from meraspis to holaspis.

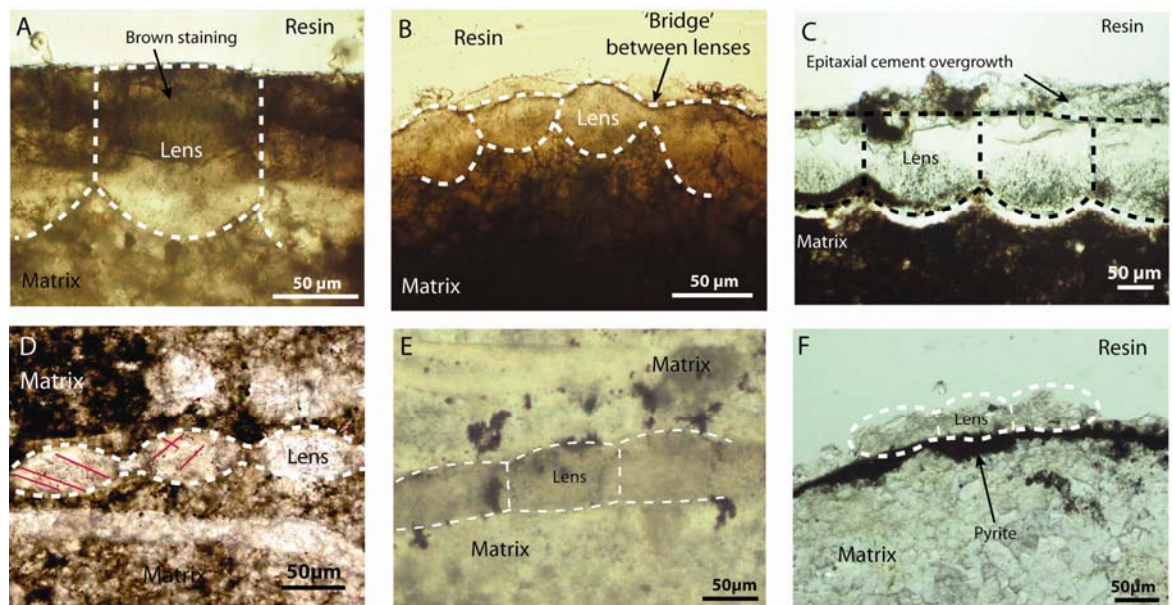


Figure 4.1 – Transmitted light microscopy of lenses in holochroal eyes.

A. Holaspis *Paladin shunnerensis* (PE79), **B.** Meraspis *Paladin shunnerensis* (PE92), **C.** *Symphysops subarmata* (SS93), **D.** *Telephina mobergi* (T95), red lines highlight cleavage, optically clear areas above and below the lenses represent recrystallised sclerites **E.** *Carolinites angustagena* (C2.6) and **F.** *Carolinites sibiricus* (C1B). Dashed lines denote lens boundaries.

The lenses of *Symphysops subarmata* (Figure 4.1C) are composed of optically clear calcite, with few inclusions. Where inclusions are present, they are restricted to the lower portion of the lens but are randomly distributed within this area. No trabeculae have been identified using light microscopy.

Lenses of both analysed species of *Telephina* are similar in TL (Figure 4.1D). They are inclusion rich and cleavage is often prominent (indicated by red lines in Figure 4.1D); some cracking has occurred along these lines. Rotation of the microscope stage in crossed polarisers shows that the extinction angle varies only slightly across the outer surface of the lens indicating a fairly consistent *c* axis orientation of the calcite. Some lenses of *T. mobergi* consist of several coarse crystals in which cleavage and twinning is prominent; the angle of extinction within the coarse crystals is uniform but does vary between crystals, possibly indicating recrystallisation.

Lens surfaces of both species of *Carolinites* are very slightly convex, some lenses are almost rectangular (Figure 4.1E-F). The *C. angustagena* lenses are easily

distinguishable from the enclosing rock as they are slightly darker in colour than the coarse calcite cement (Figure 4.1E). Lenses in the sample of *C. sibiricus* are heavily fractured along the calcite cleavage planes and so difficult to distinguish from calcite cement in the matrix (Figure 4.1F). Examination of the lenses in crossed nicols shows that there is a slight variation in crystal orientation along the outer lens surface, identified by a very subtle sweeping of extinction angle as the microscope stage is rotated.

4.1.1.2 Reflected Light Microscopy

RL microscopy (Figure 4.2) indicates that the ‘inclusions’ found in some of the holochroal lenses are micropores, identified by depressions in the lens calcite rather than elevations, which would be expected if crystals of dolomite or pyrite were present. This microporosity may be indicative of recrystallisation. Pyrite is found along the base of the lenses the *Carolinites angustagena* specimen (Figure 4.2F); this may have entered along a fracture between the lenses and the underling matrix, and small amounts of pyrite are found in the lenses themselves.

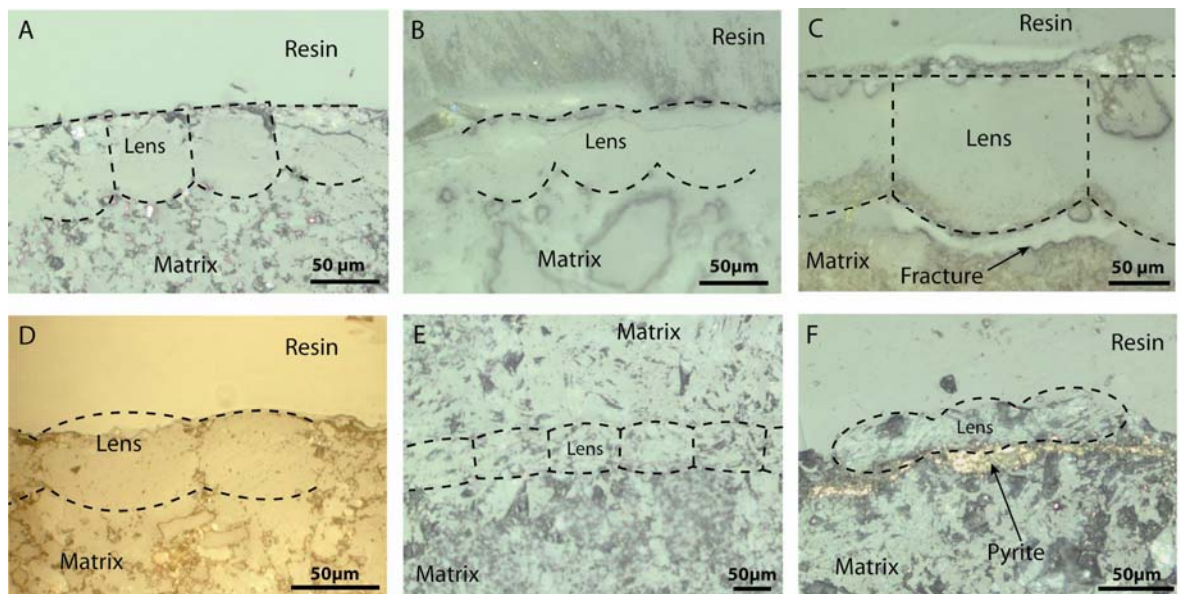


Figure 4.2 – Reflected light microscopy of holochroal lenses.

A. *Holaspis Paladin shunnerensis* (PE79), **B.** *Meraspis Paladin shunnerensis* (PE92), **C.** *Symphysops subarmata* (SS93), **D.** *Telephina mobergi* (T95), **E.** *Carolinites angustagena* (C2.6) and **F.** *Carolinites sibiricus* (C1B). Dashed lines denote lens boundaries. Note the presence of pyrite below the lenses in F.

4.1.2 Cathodoluminescence

4.1.2.1 Optical Cathodoluminescence

In the cases of *P. shunnerensis*, *S. subarmata* and both *Carolinites* species analysed, CL intensity within the lenses is homogeneous and is consistent across the eye. The brown staining seen on the lenses of one *Paladin* specimen (Figure 4.1A) luminesces much more brightly than the lenses, suggesting it is a later diagenetic overprint. There is a two-fold structure to the CL pattern of *Telephina mobergi* lenses (Figure 4.3) with a dull top layer and a brighter lower layer, and a distinct boundary between the two. The depth to which the dull layer extends from the visual surface down varies between lenses; there are four lenses in a row along which the extent of the dull region increases progressively (Figure 4.3). This distribution of luminescence may be indicative of penetration of fluids during diagenesis, as the difference in calcite CL intensity is likely to arise from subtle differences in the chemistry (e.g. Mn^{2+} concentrations - section 2.2.1.1.1).

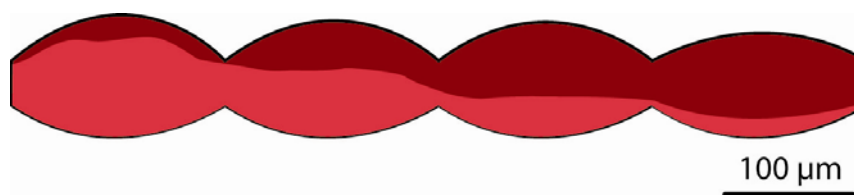


Figure 4.3 - Cathodoluminescence of holochroal lenses. Schematic illustration of the two-fold structure to the CL pattern in the lenses of *Telephina mobergi* (T95).

4.1.3 Electron Backscatter Diffraction

4.1.3.1 Microstructure of Holochroal Lenses

EBSD reveals several microstructural patterns within holochroal lenses (Figure 4.4). Differences are evident between the meraspis and holaspis *Paladin* lenses. Lenses of the meraspid specimen have a variation in *c* axis orientation along both the outer lens surface and the lens base whereas in holaspid specimens this variation is present only along the lens base (Figure 4.4A-B). *Symphysops* lenses display a similar pattern to holaspis *Paladin* lenses but with a more constrained *c* axis orientation (Figure 4.4C); pole figures show this to be in the region of 30° whereas in holaspis *Paladin* the variation is as much as 60°. *Telephina* and

Carolinites lenses show a small variation in *c* axis orientation along both the outer lens surface and the lens base (Figure 4.4D-E); the variation is slight at 20–30° and is too subtle to be identified in most EBSD maps but is revealed by the pole figures.

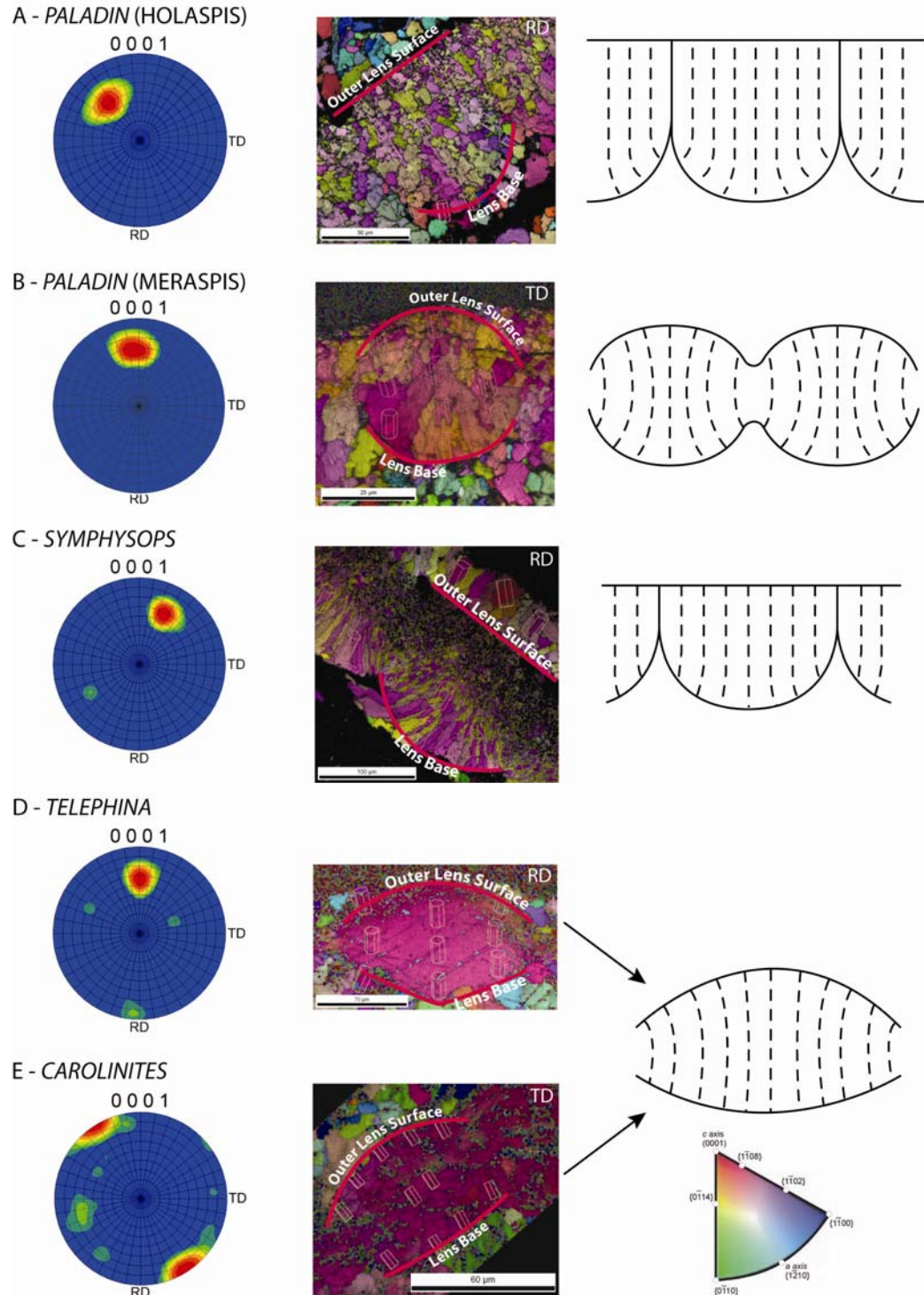


Figure 4.4 – Microstructure in holochroal lenses.

Pole figures, EBSD maps and corresponding schematic diagrams illustrating the *c* axis orientation in lenses of A. *Paladin* (holaspis) (PE93), B. *Paladin* (meraspis) (PE92), C. *Symphysops* (SS93), D. *Telephina* (T95) and E. *Carolinites* (C1B). Grid line divisions on pole figures represent 10°. White letters on maps (top right) indicate reference directions (section 2.7.4).

EBSD mapping of *T. mobergi* lenses confirms that some have been recrystallised. The lenses are now composed of a number of coarse crystals, tens of microns in size, that differ significantly in orientation to the host lens (Figure 4.5). This is an indication that some of the original microstructure has been lost as the preferred orientation resulting from biomineralisation has been lost. The lens with the most altered microstructure is that in which the dull CL region was most extensive (section 4.1.2.1).

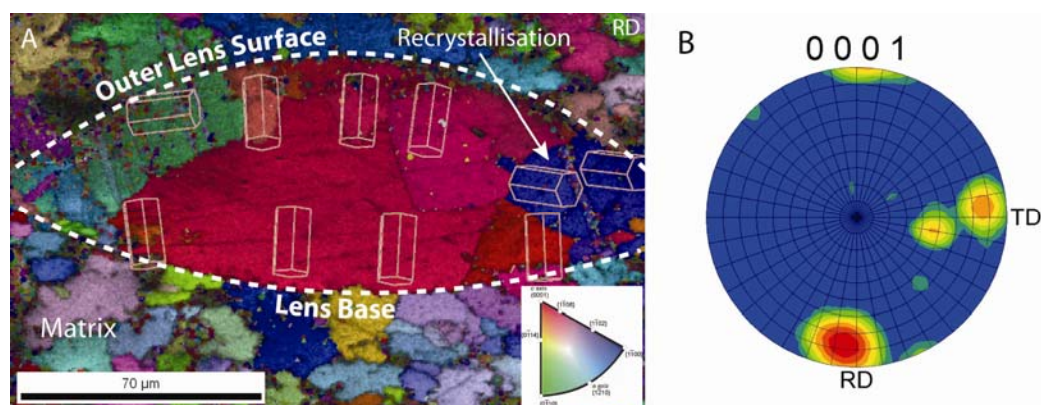


Figure 4.5 – Lens recrystallisation in *Telephina mobergi*.

A. EBSD map of a lens in section T95 with superimposed crystal models. Note how crystal orientation at the lateral parts of the lens is different to that in the central areas; the latter are inferred to have retained the original microstructure. White lines in A highlight the boundaries of the lens. **B.** Plot showing crystal orientation in the lens shown in A. Grid line divisions represent 10°.

EBSD mapping has revealed the presence of multiple grains in the lenses of *Symphysops* (Figure 4.6A). The lower portion of the lens, in which there is variation in *c* axis orientation, consists of ~50 µm long, thin, calcite crystals. These crystals fan out along the lens base, and at approximately 4-12 µm in width may be consistent with trabeculae, although none were identified in TL in this sample (section 4.1.1.1). The upper uniformly orientated region of the lenses consists of an aggregate of 1-2 µm diameter equidimensional crystals. The change in crystal size is gradual as illustrated in Figure 4.6A, fining towards the outer lens surface. A comparable gradation in crystal size is also present in some lenses of holaspis *Paladin* but the size range is narrower. Variation in *c* axis orientation and fanning out of crystals along the lens base is seen even in lenses that appear to have undergone coarse recrystallisation and now consist only of a series of elongate subgrains (Figure 4.6B). Misorientation between subgrains in both *Symphysops* and holaspis *Paladin* vary; values range from approximately 20° to 50° and 5° to 75° respectively, this inconsistency could be the result of recrystallisation. Meraspis *Paladin* lenses consist of numerous approximately

equidimensional crystals in the region of 5-20 μm ; crystal size is not related to position within the lens (Figure 4.6C).

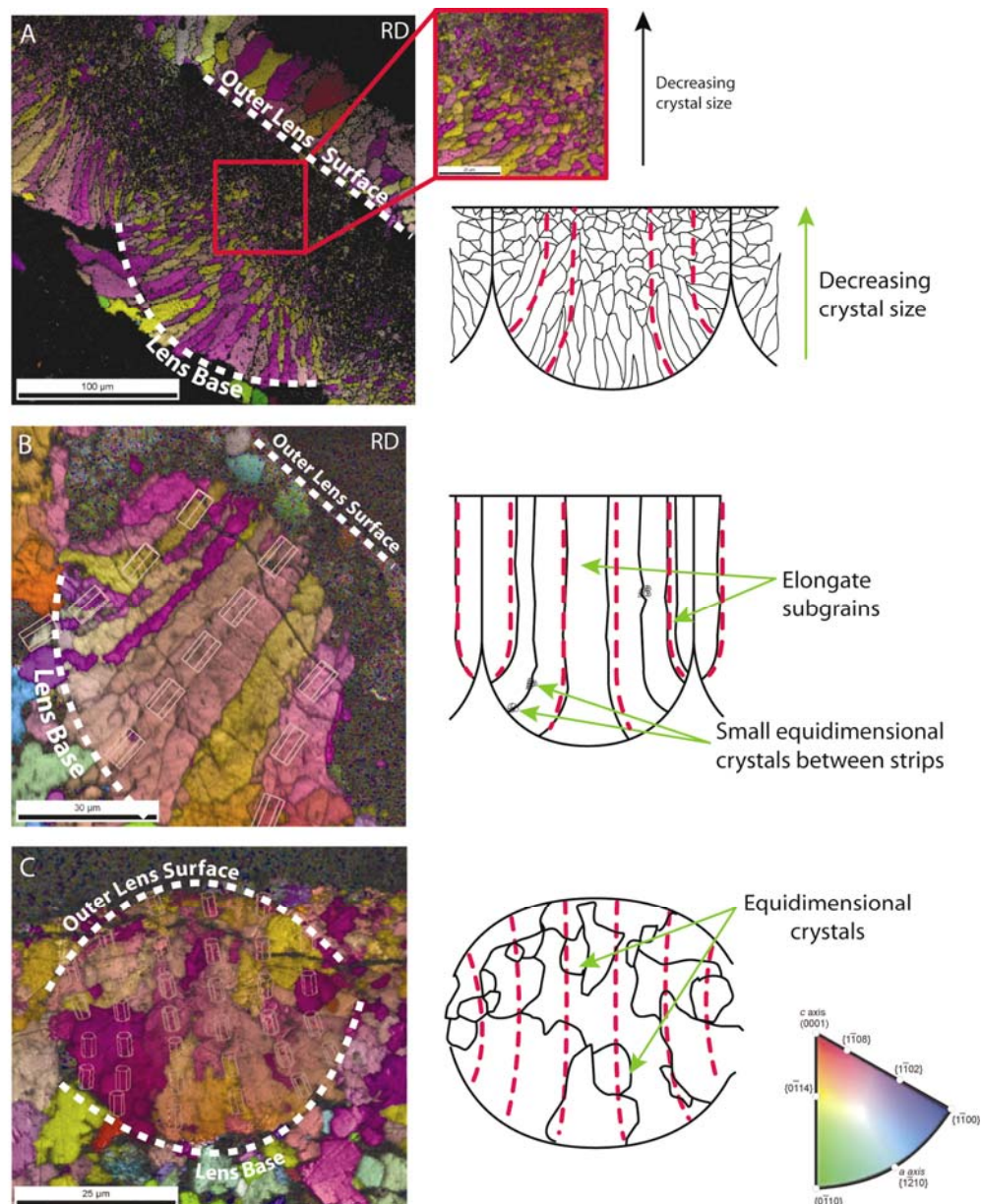


Figure 4.6 – Crystal growth patterns in holochroal lenses.

EBSD maps and corresponding schematic diagrams showing A. the gradual decrease in crystal size from the lens base up to the outer lens surface in lenses of *Symphysops subarmata* (SS93). This microstructure is also seen in lenses of *Paladin* (holaspis) although to a lesser extent and B. crystal subgrains are present in some coarsely recrystallised *Paladin* lenses (PE79). Note how subgrains fan out, mirroring *c* axis orientation. The outer surface of the lens in the EBSD map is partially obscured by leached barite. C. Relatively coarse, equidimensional crystals in lenses of the meraspis stage *Paladin* (PE92). Red dashed lines show *c* axis orientation.

Telephina lenses, which have not been affected by coarse recrystallisation, do not show this microstructure. These lenses initially appear to be a single calcite crystal with changing *c* axis orientation, highlighted by tolerance maps (Figure 4.7A) but misorientation graphs (Figure 4.7B) reveal the presence of micron

scale sub-domains or sub-grains. It is likely to be the gradual change in orientation of the sub-grains that gives the lens this ‘single crystal’ appearance. *Carolinites* lenses also show this misorientation within each component of their fractured crystal lenses. These sub-domains may suggest that the lens consists of many sub-crystals however as the size of these sub-domains is, like those in *Telephina* lenses, in the region of 1-3 μm , close to the limits of EBSD detection, there is some uncertainty as to the authenticity of these structures.

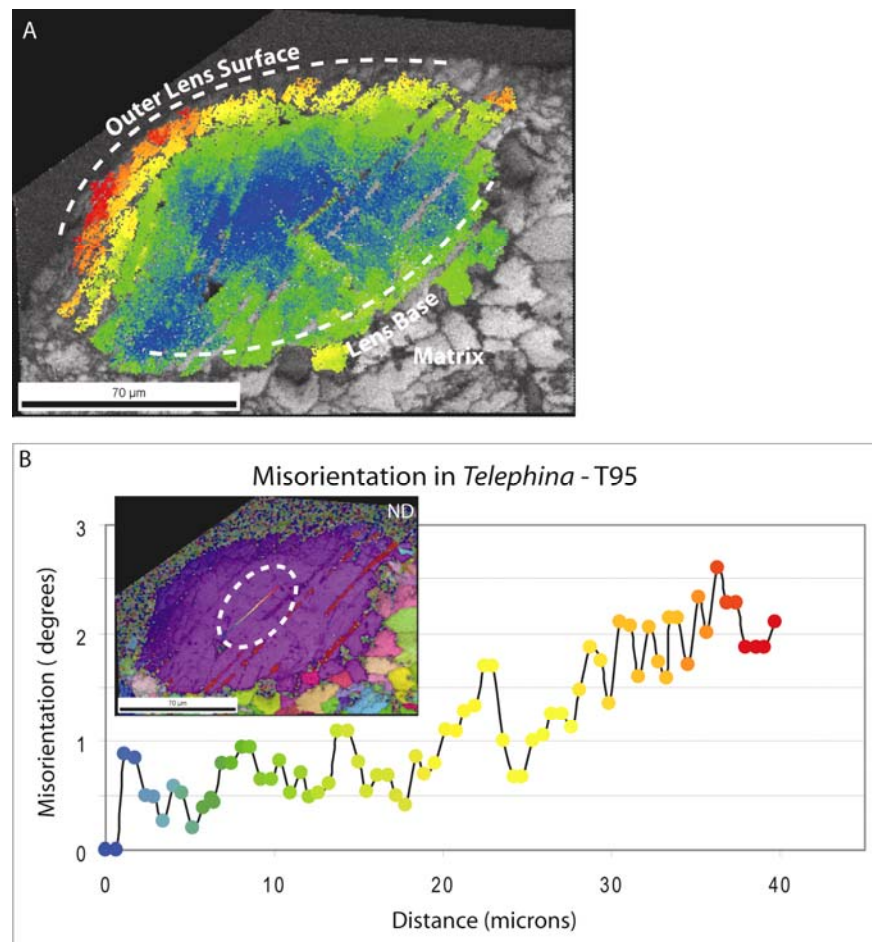


Figure 4.7 Tolerance mapping and misorientation in the holochroal lens of *Telephina mobergi*.

A. Tolerance mapping shows that there is a gradual change in *c* axis orientation across the outer surface and B. Point to origin misorientation graphs show that the lens consists of numerous sub-grains, each in the region of 1-3 μm in width. (Section T95).

4.1.4 Scanning Electron Microscopy

4.1.4.1 Backscattered Electron Imaging of Thin Sections

BSE imaging of polished thin sections shows that the calcite in the lenses of *Paladin*, *Symphysops* and *Telephina* is not homogeneous. The lenses have a patchy appearance that suggests a subtle variation in the chemistry of the

calcite, possibly arising during diagenesis (Figure 4.8A-C). In lenses of *Paladin* and *Telephina* this does not have any particular structure whereas in lenses of *Symphysops* there is a striped appearance, with stripes fanning out along the lens base (Figure 4.8B). Lenses of *Carolinites* are uniform in mean atomic number in BSE indicating a homogeneous major element chemical composition (Figure 4.8D). BSE imaging also highlights the presence of micropores (Figure 4.8A-C) and faint grain boundaries (Figure 4.8B).

4.1.4.2 Secondary Electron Imaging of Etched Thin Sections

SE imaging of etched sections highlights the grain boundaries identified by EBSD as well as the micropores seen using TL and RL microscopy. Lenses of *Paladin* have very irregular and sutured grain boundaries indicating that recrystallisation has occurred (Figure 4.9).

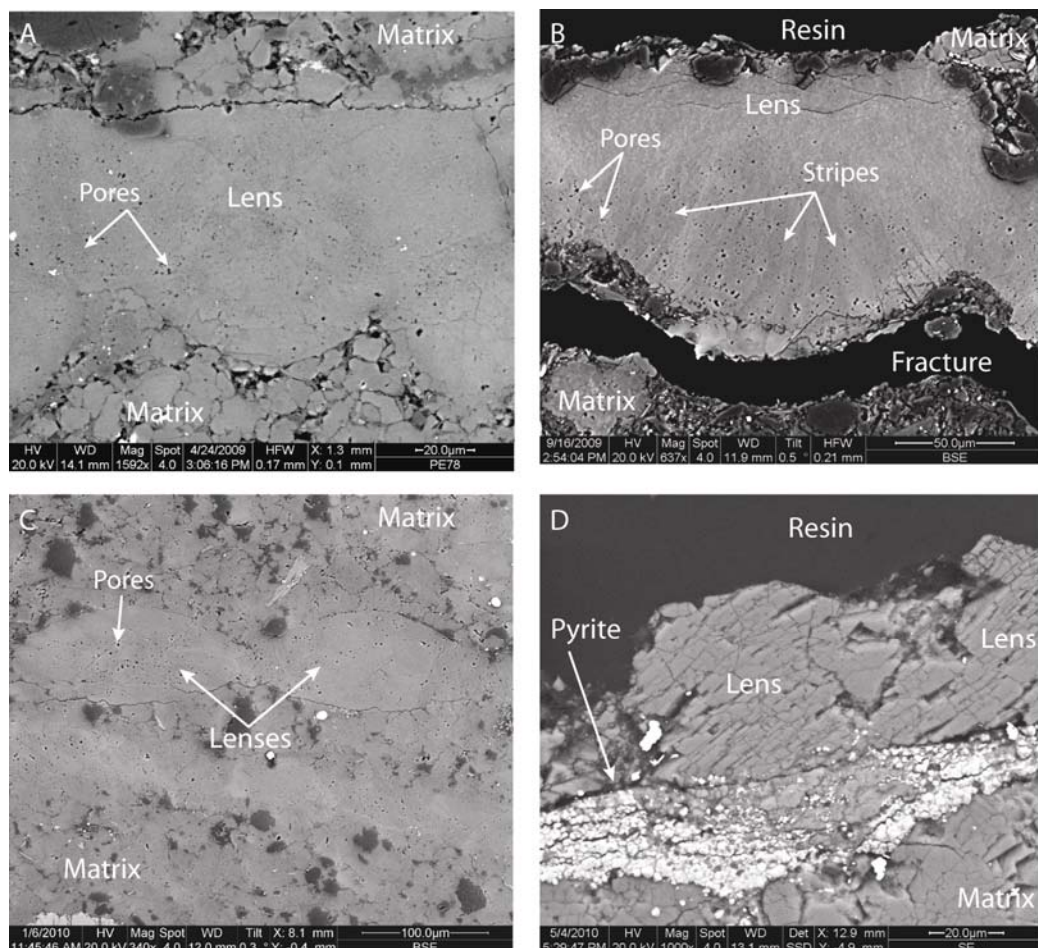


Figure 4.8 – Backscattered Electron imaging of holochoroal lenses.

A. *Paladin shunnerensis* (holaspis) (PE78). B. *Symphysops subarmata* (SS93). C. *Telephina mobergi* (T95). D. *Carolinites sibiricus* (C1B). Note the patchy appearance of the lens calcite and the pores in A-C and the fracturing and presence of pyrite between the lens base and the matrix in D.

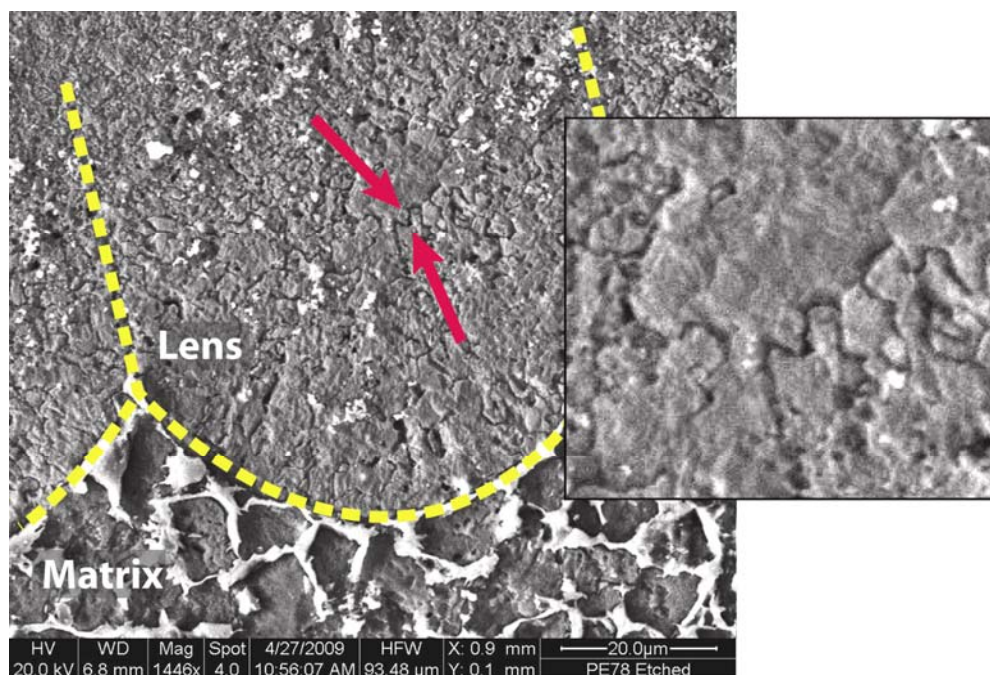


Figure 4.9 – Secondary Electron image of an acid etched holaspis Paladin lens. Note the irregular, or sutured, grain boundaries in the lens (highlighted by red arrows and magnified on the right) (section PE78). Yellow lines indicate lens boundaries.

4.1.5 Energy Dispersive X-Ray Spectroscopy

EDS analysis of holochroal lenses shows that they are composed of LMC; low concentrations of Mg are present in both the lenses and the surrounding matrix (Figure 4.10). The presence of pyrite at the base of *Carolinites sibiricus* lenses indicates input from an external source, probably from interaction with seawater during the very early stages of diagenesis. There is no difference in lens chemistry between holaspis and meraspis *Paladin* specimens.

Quantitative EDS is consistent with these results for the most part. Analysis of one *Paladin* specimen reveals relatively high levels of Mg, putting it in the range of HMC. The entire eye in this sample is coated with a layer of barite (Figure 4.1A), the brown staining identified by TL (section 4.1.1.1). This indicates a strong external influence, such as leaching of fluids rich in barite, as barite is not autochthonous to the eye. These EDS results suggest that the entire lens chemistry has been diagenetically altered.

Table 4.2 summarises quantitative EDS results, a full list of analyses is presented in Appendix D.

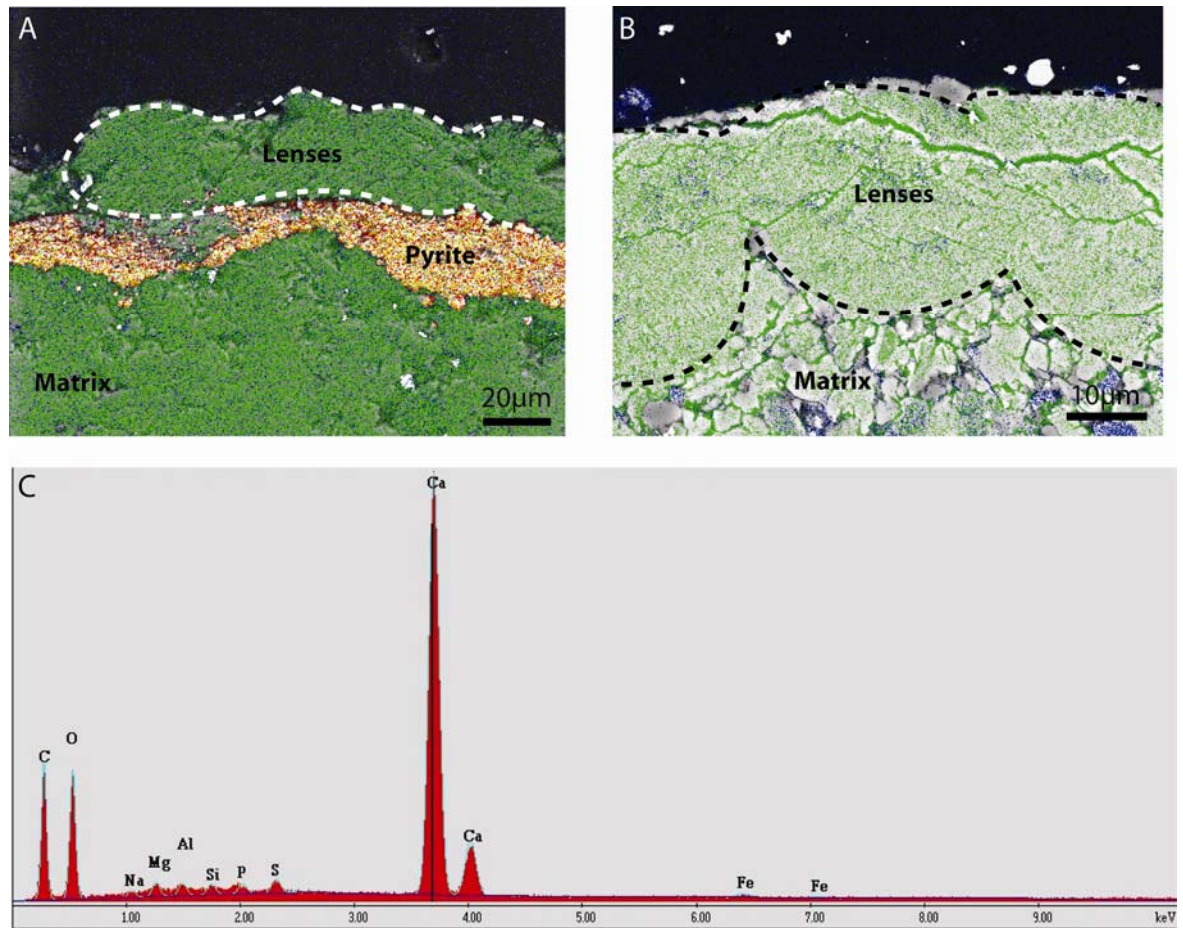


Figure 4.10 – Energy Dispersive X-ray mapping of holochoal lenses.

ESD maps of A. *Carolinites* (C1B) and B. *Paladin shunnerensis* (meraspis) (PE92) in which colour denotes the presence of certain elements (Ca=green, Mg=blue, Fe=red, S=yellow). Note the presence of pyrite beneath the lenses in A. C. EDS spectrum of a *Carolinites sibiricus* lens (one of the lenses shown in A).

Table 4.2 – Quantitative chemical analysis of lenses in holochroal eyes- Mol % MgCO_3 .

'MN' denotes mean and 'STD DEV' denotes standard deviation of the mean value. 'n' indicates the number of samples analysed. Values below the detection limits have been put to zero.

SAMPLE	SPECIES	MOL % CaCO_3				MOL % MgCO_3				MOL % SrCO_3				MOL % FeCO_3				MOL % MnCO_3				n
		MN	MAX	MIN	STD DEV	MN	MAX	MIN	STD DEV	MN	MAX	MIN	STD DEV	MN	MAX	MIN	STD DEV	MN	MAX	MIN	STD DEV	
C1B	<i>Carolinites sibiricus</i>	97.74	98.49	96.48	0.44	1.37	2.10	0.99	0.31	0.07	0.22	0.00	0.07	0.45	2.14	0.13	0.47	0.37	0.59	0.27	0.09	15
SS93	<i>Symphysops subarmata</i>	95.63	92.26	95.63	0.39	0.94	1.49	0.48	0.25	0.03	0.15	0.00	0.05	0.13	0.29	0.00	0.11	3.27	3.93	2.91	0.31	15
PE79	<i>Paladin eichwaldi shunnerensis</i> (holaspis)	93.48	95.87	90.32	1.90	5.17	9.15	2.04	2.35	0.13	0.34	0.00	0.12	1.07	2.10	0.19	0.14	0.15	0.49	0.00	0.14	15

4.2 Interpretation

4.2.1 Original Lens Microstructure

Despite the obvious recrystallisation in many of the holochroal lenses studied (section 4.1.3.1, Figure 4.5 and Figure 4.6), it is possible that the present microstructure of many is, to some degree, representative of the original structure. Aggrading recrystallisation (Bathurst, 1971) is likely to be the origin of the elongate crystal subgrains of holaspis *Paladin* lenses and coarse crystals in meraspis *Paladin* lenses (Figure 4.6B, C). Had the lenses been recrystallised to the point of losing all traces of original microstructure, they would probably appear similar to the surrounding matrix, with a distinct lack of preferred orientation; the early stages of this are seen in the specimen of *Telephina mobergi* (Figure 4.5). The microstructures identified using EBSD (Figure 4.4) are repeated across numerous lenses in each specimen analysed; this repetition further supports the suggestion that these represent original structure, as the spatially variable nature of diagenesis would prevent such consistency.

The range in *c* axis variations across the lens surfaces (Figure 4.4) is not the outcome of recrystallisation, but of differing surface curvatures. Where lens surfaces are planar, the *c* axis is aligned parallel to the optic axis of the lens. Where lens surfaces are strongly convex, the variation in *c* axis orientation is most intense. This is most notable in the plano-convex lenses of holaspis *Paladin* (Figure 4.4A). A similar relationship between surface curvature and direction of trabeculae has been noted in previous studies (see Clarkson *et al.*, 2006 for review). The *c* axis orientations, which generally mirror the trabeculae, are likely to be representative of original microstructure because of the fine scale of recrystallisation.

4.2.2 Optical Modelling

No computer based modelling has been done on holochroal eyes despite the extensive work (e.g. Clarkson, 1975, 1979; McCormick and Fortey, 1998; Clarkson *et al.*, 2006) that has been carried out to provide information on aspects of palaeobiology such as field of view (e.g. Fordyce and Cronin, 1993; Acenolaza *et al.*, 2001) and mode of life (e.g. Bruton and Høyberget, 2006). Holochroal eyes have generally been compared with apposition eyes (e.g.

Clarkson *et al.*, 2006) and occasionally superposition eyes (Fortey, 1997) of modern arthropods. Computer based modelling of lens function in holochroal eyes is undertaken here for the first time.

4.2.2.1 Modelling Results

Code V modelling was carried out on all four genera of holochroal eyed trilobites. In each case a lens, typical of the genus, was used to determine curvatures of the outer lens surface and the lens base. Each lens was modelled in three ways; to determine the effects of refraction on: (1) ordinary light rays and (2) extraordinary light rays, both from a range of angles and (3) paraxial light rays only. Due to the limitations of Code V software, modelling automatically assumes uniform *c* axis orientation throughout the lens, parallel to the lens axis. This means that in modelling, rays entering the lens parallel to the lens axis are not doubly refracted. In reality, the variations in *c* axis orientation revealed through EBSD mapping (section 4.1.3.1) would result in the double refraction of rays, as the *c* axis is not parallel to the lens axis in all parts of the lens. To overcome this, the lenses were modelled in two ways; firstly with the RI of the calcite for ordinary rays and secondly at the RI of calcite for extraordinary rays (section 2.8.2.4), to simulate the refraction path that doubly refracted rays would adopt.

Ray tracing (Figure 4.11) shows that there is a significant difference between the refraction of ordinary and extraordinary light rays due to the different refractive indices they experience. In general, the focal point of extraordinary rays is at approximately twice the depth of the focal point of the ordinary rays.

The plano-convex lenses of *Paladin* (holaspis) and *Symphysops* (Figure 4.11C, D) focus extraordinary rays much more effectively than ordinary rays, however the focal point is at a much greater depth. The biconvex lenses of *Telephina* and *Carolinites* are capable of focusing both sets of rays to an equivalent standard as indicated by similar aberration values. Results are summarised in Table 4.3.

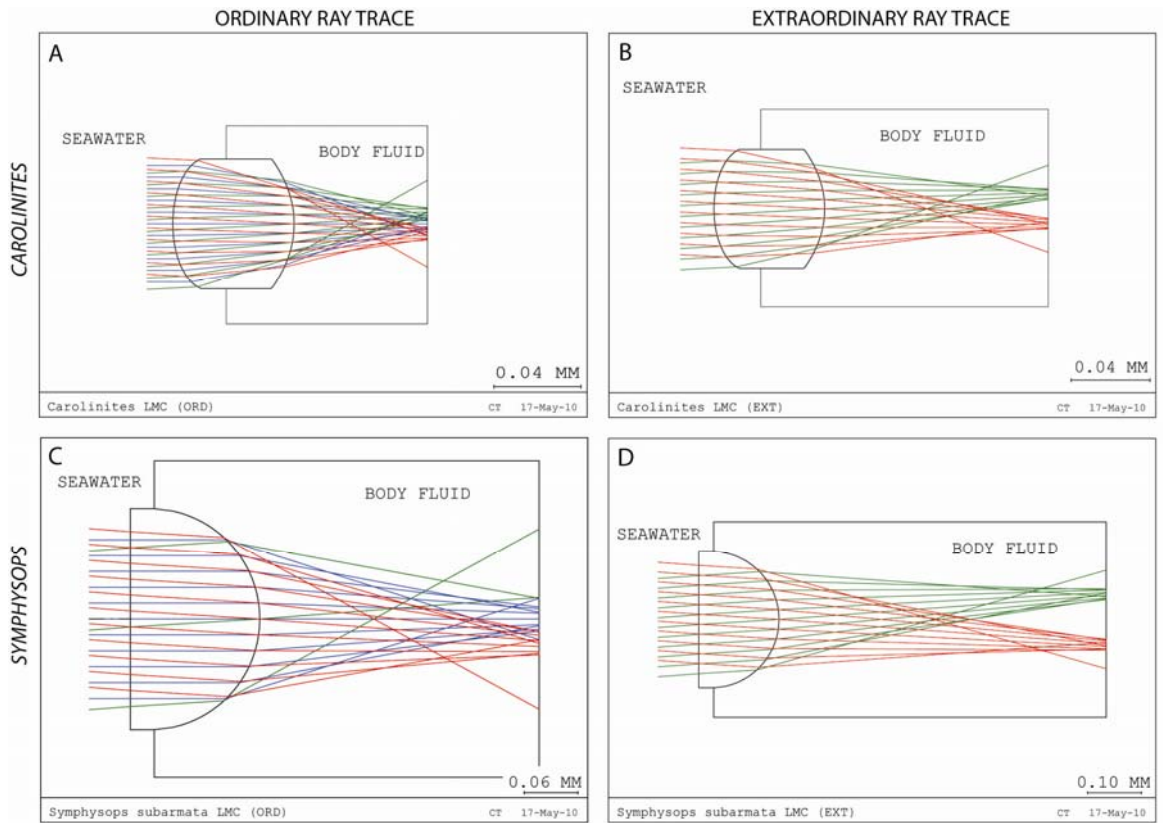


Figure 4.11 – Code V ray tracing in holochroal lenses.

Code V ray tracing of ordinary (left) and extraordinary rays (right) in lenses of *Carolinites angustagena* (A-B) and *Symphysops subarmata* (C-D). Note the greatly increased focal length for extraordinary rays compared to ordinary rays. Paraxial rays (blue lines) are not included in B and D as these rays are parallel to the *c* axis in the majority of the lens and therefore do not experience significant double refraction. Green and red lines represent rays at the extent of the field of view, either side of the lens axis; for values see Appendix F.

Table 4.3 - Optical modelling of holochroal lenses.

Back focal length and aberration (blur) values, for holochroal lenses. Biconvex lenses (purple) have lower aberration values than plano-convex lenses (cream), i.e. these are more effective at focusing light.

GENUS	RAY TYPE	BACK FOCAL LENGTH (μm)	ABERRATION (μm)
<i>Paladin</i> (HOLASPIS) (PE79)	Ordinary	115	24
	Extraordinary	212	29
	Paraxial	117	25
<i>Paladin</i> (MERASPIS) (PE92)	Ordinary	24	9
	Extraordinary	23	9
	Paraxial	24	9
<i>Symphysops</i> (SS93)	Ordinary	309	22
	Extraordinary	584	6
	Paraxial	324	18
<i>Telephina</i> (T95)	Ordinary	291	8
	Extraordinary	392	7
	Paraxial	223	8
<i>Carolinites</i> (C2.6)	Ordinary	69	5
	Extraordinary	126	5
	Paraxial	71	6

4.2.2.2 Sublensar Structures and Photosensitive Components

No evidence of sublensar structures has been found in holochroal eyes in the present study. The lack of cement overgrowths and geopetal structures indicates that all soft parts of the eye had deteriorated prior to matrix infill. Thus, there are no secondary structures to give an indication of how much of the eye was occupied by soft parts or what these structures may have consisted of.

Holochroal eyes are thought to have functioned in a similar manner to modern apposition eyes (Clarkson, 1979; Clarkson *et al.*, 2006); this is based on the shape of the eye and the size and arrangement of the lenses across the visual surface. The present study supports this as ray tracing of lenses showed that ordinary light rays from a range of angles were focused on approximately the same point (Figure 4.11A and C); due to this overlap, having more than one photoreceptor in this location would be of little advantage. Fortey's (1997) suggestion that some holochroal eyes may have function as reflecting

superposition eyes was based on the observation of square lenses. All lenses in the present study are plano-convex or biconvex and so this is not applicable in this instance.

Determination of the back focal length (BFL) of the lenses in the present study by optical modelling provides the location of the photoreceptors, assuming that the lens was used to focus light onto the receptor tip as in modern apposition eyes (1.3.2.1). In the case of the holochroal lenses modelled, this is at a distance of 1.1 to 2.6 times the lens depth below the lenses for paraxial and ordinary light rays. The value varies between genera as would be expected when there are variations in lens shape, size and arrangement on the eye.

The ray tracing results presented above show that light rays entering the peripheral areas of the lenses undergo a greater angle of refraction than those entering central areas of the lenses. This could result in the detection of light by the photoreceptor of an adjacent lens (Figure 4.12), which could ‘mix’ the light coming from two different areas in space and therefore reduce spatial acuity. Trilobites may have used screening pigment (see section 1.3.2.1) to keep receptors optically isolated and prevent this problem from arising.

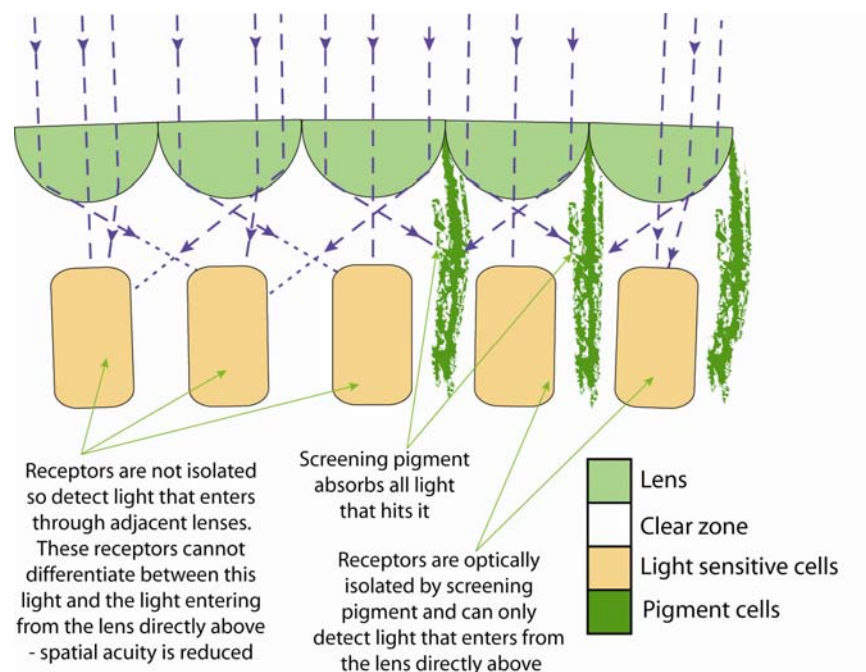


Figure 4.12 - The effect of screening pigment in the holochroal eye.

Ray tracing (Figure 4.11) shows that rays entering the peripheral areas of the lenses could be refracted so that they would penetrate the receptor of a neighbouring lens. Screening pigment may have been used to prevent this. Only paraxial rays are shown for simplicity.

4.3 Summary

Optical microscopy and EBSD has confirmed the existence of two end-member microstructural patterns within holochroal lenses (Figure 4.13). The *c* axis orientation within the lenses is controlled by, or at least occurs in conjunction with, particular surface curvatures. Where lenses have a convex surface, the *c* axes bend outwards at the surface edges and where lenses have planar surfaces, the *c* axes are uniform and parallel with the lens axis. Similar observations have been reported with regards to the orientation of trabeculae in holochroal lenses (Clarkson *et al.*, 2006), however very few convincing trabeculae were identified in the present study. Both qualitative and quantitative EDS analysis indicates that holochroal lenses were composed of LMC *in-vivo*.

Ray tracing of holochroal lenses for both ordinary and extraordinary rays does not provide any insights into why there is a variation of *c* axis orientation across convex lens surfaces; the reduced aberrations of the extraordinary rays in holochroal lenses (Table 4.3) is an unlikely explanation as it is combined with a significant increase in focal length, which in turn limits the space available for rhabdoms within the eye. It is possible that the apparent ‘bending’ of *c* axis along curved lens surfaces, simply represents the most energy efficient pathway of lens growth that the trilobites were capable of producing.

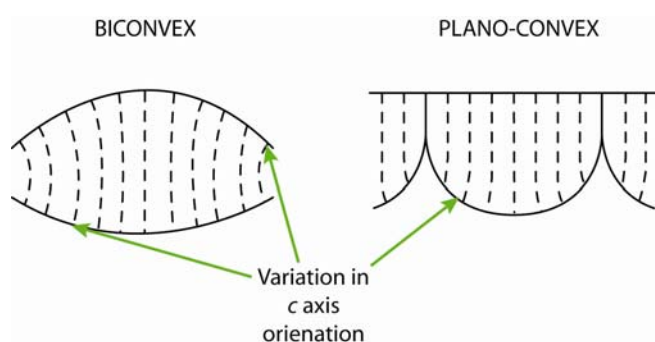


Figure 4.13 - Summary of microstructure arrangements in holochroal lenses. Dashed lines represent *c* axis orientations.

Study of a wider range of holochroal-eyed genera, focusing on different ontogenetic stages, could provide a more detailed understanding of the microstructural changes that occur during ontogeny and where specifically in the life cycle these changes occur. A better understanding of why these changes occur may also be gained from additional work.

5

Schizochroal Eyes

5.1 Results

Trilobites with schizochroal eyes from twenty-one species representing 13 genera were prepared for analysis (section 3.1.1). All thin sections were studied using light microscopy, optical CL, EDS and EBSD. Based on the findings from these techniques, a sub-set of these was chosen for acid etching, EPMA work, hyperspectral CL imaging and TEM.

5.1.1 Light Microscopy

Transmitted light (TL) and reflected light (RL) microscopy provide important details on the internal structure of the lenses. Light microscopy gives an indication as to the microstructure, from cross-polarised light extinction angles, and the presence of inclusions of different minerals, from the variations in light reflectance (e.g. pyrite has a high reflectance under reflected light).

5.1.1.1 Transmitted Light Microscopy

All lenses are biconvex when cut in the horizontal and vertical planes (section 3.2.1.1, Figure 3.6); the surface curvatures vary slightly between taxa. Sectioned *Reedops* lenses range from almost circular to more elliptical. The circular outlines probably result from sectioning close to the outer lens surface or lens base, rather than the central region, which would appear more elliptical in cross section; this is reflected in lens width, which is greatest in elliptical lenses. Different sectioning angles may also contribute to the variations in cut that are inevitable when sectioning a curved surface. *Dalmanites* sp. is an excellent example of this; the difference in lens shape from one edge of the eye to the other is significant, as can be seen in Figure 5.1.

Dalmanites and *Odontochile* lenses are the most oval, typically measuring 550 μm wide by 400 μm thick and 220 μm wide by 150 μm thick respectively and separated by relatively thin interlensar sclera. All the other genera studied have more circular lenses, the sizes of which vary between specimens.

Intralensar bowls and cores can be identified in transmitted light in lenses of *Dalmanites* and *Reedops* as areas of concentrated turbidity. Bowls alone are also found in other genera (e.g. *Barrandeops*) but are not as distinct as in *Dalmanites* and *Reedops* (Table 5.1). Variation in internal features is commonly evident within a row of lenses in a single eye, from very distinct areas of dense turbidity, to more diffuse structures with less prominent boundaries. This is most notable in the case of *Dalmanites* sp. (Figure 5.1).

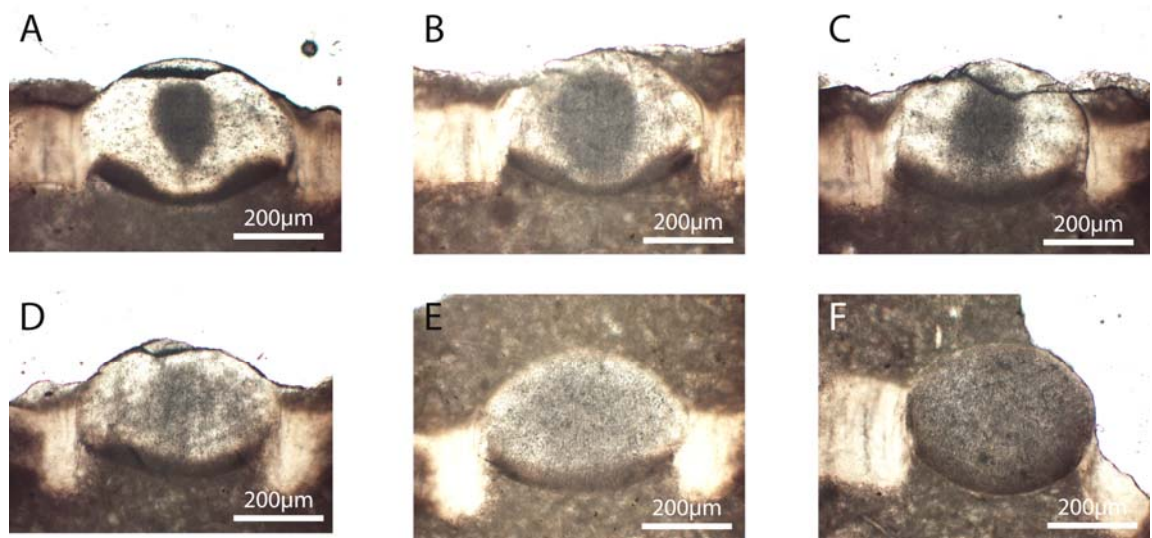


Figure 5.1 - Intralensar features in *Dalmanites* sp. viewed in plane polarised transmitted light.

Note how the intralensar bowl and core, clearly identified in A become gradually less well defined until the lens is uniformly turbid (F). Also, note the difference in lens shape (elliptical to circular) from A-F resulting from different sectioning angles and depths as discussed in the text. All images are from the same eye in section TS1.

Lenses of *Austerops*, *Barrandeops*, *Eldredgeops* and *Phacops* specimens contain two or more components (Figure 5.2). In these samples, the intralensar structures consist of optically clear calcite, within an otherwise turbid lens. These clear zones are not present in all lenses within an eye but when they do occur they are invariably distinct, i.e. they do not become diffuse like the turbid intralensar features discussed above, but have a sharp boundary with the adjacent relatively turbid lens calcite.

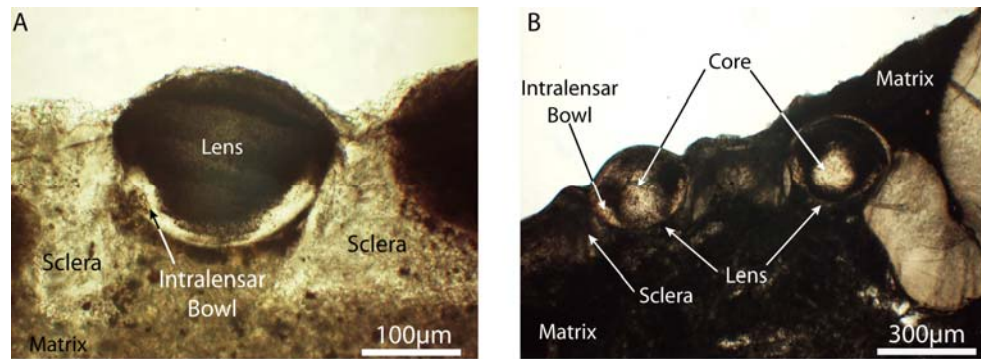


Figure 5.2 - Intralensar features in *Austerops* and *Eldredgeops* viewed in transmitted light. A. Lenses of *Austerops* (AM65) which have intralensar bowls only. B. *Eldredgeops* (E22B) lenses with a thin intralensar bowl and a large droplet-shaped core. In both cases, intralensar bowls are thinnest in the centre.

Table 5.1 summarises the types and appearance of intralensar structures, where present, in each species analysed.

Trabeculae, the calcite fibres that make up the lenses (Clarkson in Kaesler, 1997, p.120) occur in lenses of *Dalmanites*, *Geesops*, *Odontochile* and *Eldredgeops* (Figure 5.3A). These fibres are only identified in TL by the lines of inclusions that trace their boundaries. The clarity of them varies from lens to lens and in many cases they are only traceable part way through the lens. Trabeculae are most obvious in turbid *Dalmanites* lenses, as these lenses are inclusion rich (Figure 5.3A); they are approximately parallel to the lens axis in the central and upper regions of the lens but along the lens base they fan outwards (Figure 5.3A).

Features similar to the ‘growth lamellae’ described by Bruton and Haas (2003a) are visible in a small number of *Reedops* lenses (Figure 5.3B). These are approximately parallel with the outer lens surface in the uppermost area of the lens and become horizontal in the lens centre. Towards the lens base, they curve downwards slightly in sympathy with the lens surface but not to the same degree as in the upper region of the lens. In some lenses these growth lamellae can be traced into the sclera (Figure 5.3B). Lamellae are only seen in lenses in which there is a clear indication of recrystallisation, this raises concerns as to how these were formed and if they actually represent growth lines. In one particular lens (Figure 5.3B), some lines similar to the ‘growth lamellae’ trend in a different direction; these are found in an area of the lens in which there is coarse recrystallisation suggesting that in this case at least, they do not represent growth.

Cleavage is prominent in many of these *Reedops* lenses and appears to curve upwards in a similar manner to the ‘growth lamellae’.

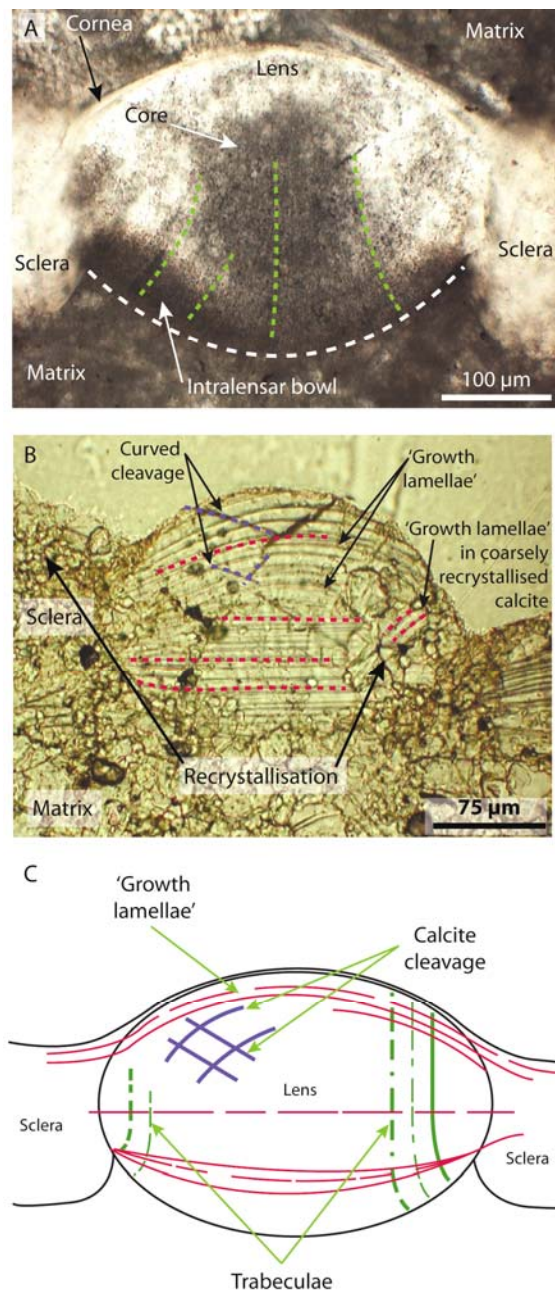


Figure 5.3 - Trabeculae, growth lamellae and cleavage in lenses of schizochroal eyes.

A. TL image of a *Dalmanites* sp. (TS1) lens. Lines of inclusions mark the trabeculae and are most prominent along the base of the lens. Green dashed lines highlight the trabeculae and the white dashed line highlights the lens base. **B.** Lines in *Reedops cephalotes* (RB14L) similar to the features termed growth lamellae by Bruton and Haas (2003a) are highlighted by red dashed lines. Purple lines highlight the curved cleavage. **C** Schematic diagram showing all the above features. Only a few of each feature have been shown for simplicity.

Table 5.1 - Intralensar features in schizochroal lenses by species.

All the lenses analysed in each species have been included and as a result, both turbid and clear features are marked in some instances. Where there is no 'X', no intralensar features are present. 'Both' indicates that some lenses from a given species consist of turbid lens calcite while others are clear.

SECTION CODES	SPECIES	TURBID		CLEAR		LENS CALCITE
		BOWL	CORE	BOWL	CORE	
LB1C	<i>Ananaspis macdonaldi</i>					Turbid
AM65	<i>Austerops smoothops</i>			X		Turbid
BM98	<i>Barrandeops fortleyi</i>	X			X	Both
PM28	<i>Barrandeops granulops</i>	X	X	X		Turbid
BM60, BM61	<i>Barrandeops</i> cf. <i>granulops</i>	X				Turbid
BB3a, BB3aR, BB3b	<i>Boeckops boeckii</i>					Clear
CE51, CE52, CE53	<i>Chasmops</i> cf. <i>musei</i>		X			Both
CE43	<i>Chasmops</i> sp.					Clear
TS1, TS3	<i>Dalmanites</i> sp.	X	X			Clear
E21R, E21L, E22B, E22T	<i>Eldredgeops rana</i>		X	X	X	Both
EE45, EE46	<i>Estoniops exilis</i>		X		X	Both
G29 – G42R	<i>Geesops schlottheimi</i>	X	X			Both
GG58	<i>Geesops sparsinodosus</i>					Both
IE48R	<i>Ingriops</i> sp. nov.					Turbid
IE47	<i>Ingriops trigonocephalus</i>					Clear
OB24R, OB24RB, OB24L, OB24LB	<i>Odontochile hausmanni</i>					Turbid
PB8	<i>Phacops superstes superstes</i>					Turbid
PM27, PM55	<i>Phacops</i> sp.		X	X	X	Turbid
RB12	<i>Reedops bronni</i>					Clear
RB7, RB14L	<i>Reedops cephalotes</i>	X				Both
RB2, RB2B	<i>Reedops</i> cf. <i>cephalotes</i>					Both
RB13L	<i>Reedops</i> cf. <i>sternbergi</i>	X	X			Both
RB1L	<i>Reedops prospiciens</i>					Clear

Lenses show one of four distinct extinction patterns (Figure 5.4) when viewed in TL between crossed polars. Lenses within an eye, and indeed all lenses from specimens of the same genus, tend to show the same extinction pattern. *Reedops* displaying patterns two, three and four and *Barrandeops* and *Phacops* displaying patterns two and three, are exceptions.

Extinction pattern 1: the majority of the lens extinguishes at the same angle suggesting uniform orientation, interpreted by Towe (1973) to indicate that the lens consists of a single calcite crystal. Some variation in extinction angle is seen in a band (maximum 10 μm thick) along the outermost surface of the lens; this area of varying extinction angle is hereafter referred to as the 'radial fringe'. This area appears to lie immediately below the cornea.

Extinction pattern 2: a sweeping extinction occurs along the outer surface of the lens and is underlain by an area of uniform extinction. Rotation of the microscope stage by 60° completes a 'sweep' across the radial fringe in many *Geesops* lenses but this angle varies somewhat between thin sections, presumably due to the differences in sectioning depths between samples (section 1.5.1.2, Figure 1.22 and section 3.2.1.1). The central uniform area extinguishes with the crystals in the middle of the radial fringe. The thickness of the radial fringe is consistent between lenses within an eye but does vary between specimens, reaching a maximum of half the total lens thickness in *Eldredgeops*. This pattern was observed in specimens of *Geesops sparsinodosus* by Bruton and Haas (2003a) who inferred it to indicate the presence of many small crystals.

Extinction pattern 3: a sweeping variation in extinction angle is present in the upper and lower parts of the lens. Only a small area in the centre of the lens extinguishes uniformly. This pattern has been observed in all *Boeckops* lenses, some *Reedops* and *Phacops* lenses, and a single *Barrandeops* lens.

Extinction pattern 4: the different parts of the lens extinguish at different angles indicating that the lens consists of numerous crystals in different orientations.

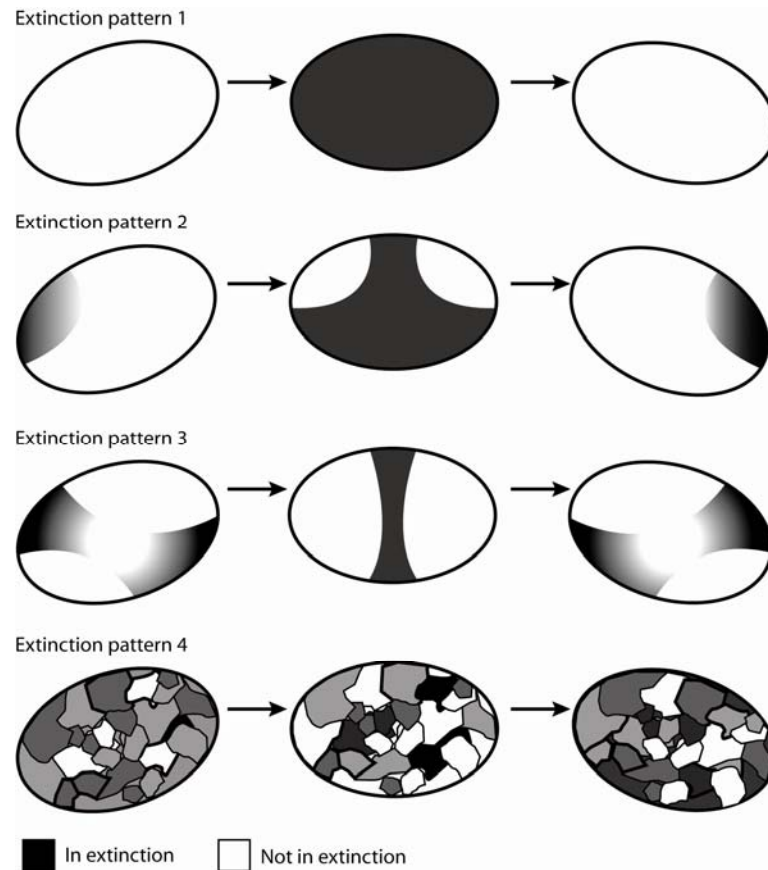


Figure 5.4 - Extinction patterns in lenses of schizochroal eyes. Extinction patterns 1 - 4 as described in the text. Arrows represent a 30° stage rotation in the clockwise direction.

The cornea is rarely preserved but in a small number of lenses it can be identified in TL as a thin (~10 µm) optically clear continuous layer on the outer surface of the lens. In some lenses, upon rotation of the stage in crossed polars, there appears to be a ‘sweeping’ of extinction angle across the cornea (Figure 5.5A), as is seen in the upper region of the lens in extinction patterns 2 and 3. The corneas of other lenses are more consistent with extinction pattern 4 but on a very fine scale (Figure 5.5B).

The sclera between the lenses plunges to varying depths below the lens depending on the species; thickness is consistent within a species. The sclera is usually parallel to the lens axis but on occasion can plunge below the lens off axis. There is variation in this angle within a single eye suggesting that this is not original but reflects compaction during diagenesis or is an artefact of the sectioning process. The sclera also has a varying angle of extinction indicating that it is not made up of a single crystal. There are three vertical ‘strips’ or columns within the sclera, when sectioned in the horizontal plane (section 3.2.1.1), each of which extinguishes separately. Within each strip, there is also a

slight variation in extinction angle indicating the presence of numerous small crystals.

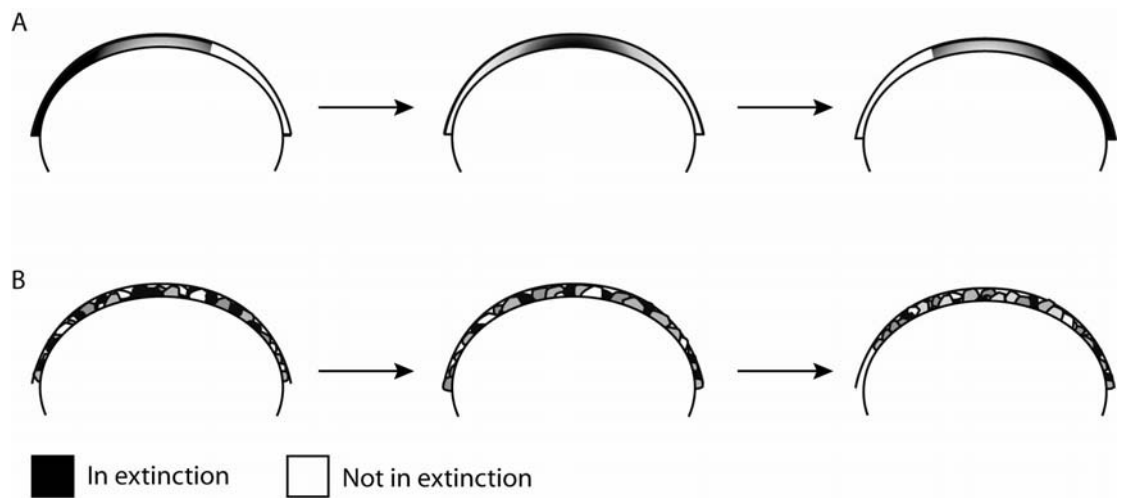


Figure 5.5 - Extinction patterns in the cornea of lenses in schizochroal eyes.

A. sweeping extinction pattern across the cornea and **B.** extinction angles of the different crystals show no particular pattern. Arrows indicate 30° rotation of the microscope stage in the clockwise direction.

5.1.1.2 Reflected Light Microscopy

RL microscopy highlights a textural variation between the different components of the lenses (Figure 5.6). The turbid areas seen in transmitted light are represented in RL as regions containing a high density of sub-micron to micron sized pores and inclusions. A few lenses of *Ananaspis*, *Geesops* and *Eldredgeops* contain small numbers of micron-scale pyrite crystals, identified by their distinctive cubic shape and high contrast and reflectivity in RL.

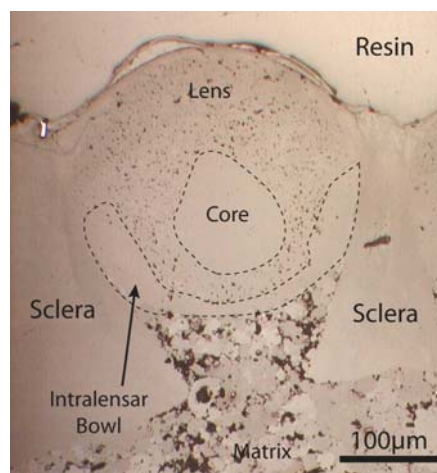


Figure 5.6 - Reflected light microscopy of lenses in schizochroal eyes.

Reflected light image of *Eldredgeops* (E22B) showing that the lens calcite is much more porous than the intralensar bowl and core. There are also distinct textural differences between the calcite of the lens and sclera, and the underlying matrix.

5.1.2 Cathodoluminescence

Preliminary optical CL findings of *Geesops schlotheimi* lenses were published in conference proceedings (Torney *et al.*, 2008) during the course of the present study.

5.1.2.1 Optical Cathodoluminescence

All lenses luminesce within the red/orange region of the electromagnetic spectrum as would be expected for calcite (section 2.2.2). Variation in CL intensity throughout the lenses is common, and in some instances coincides with turbid and clear regions of the lens as observed in TL (Figure 5.7A and B). These differing CL intensities suggest subtle chemical and/or mineralogical differences between the lens components.

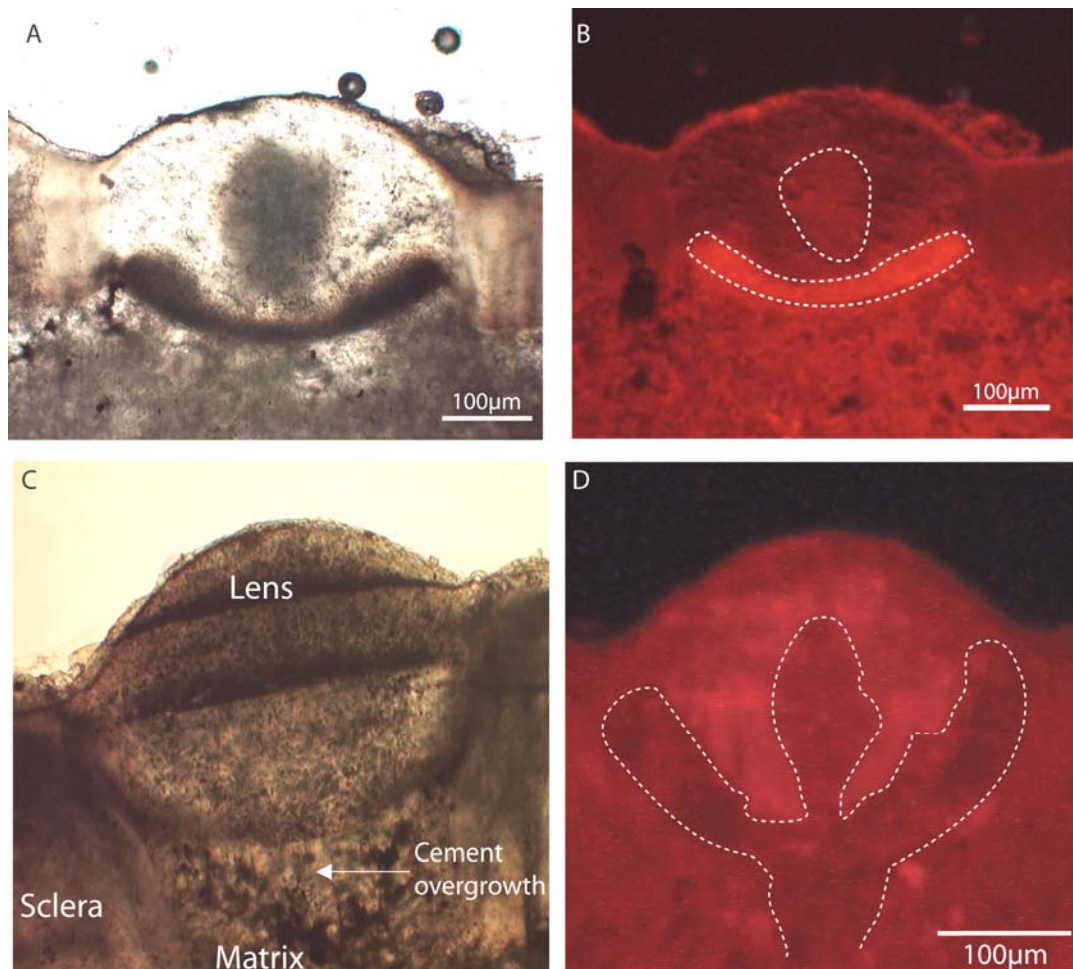


Figure 5.7 - Intralensar structures in lenses of schizochroal eyes viewed using optical cathodoluminescence microscopy.

Transmitted light images and corresponding optical CL images of a lens in *Dalmanites* sp. (TS1) (A and B) and *Geesops schlotheimi* (G33R) (C and D). Note that in the former the bowl luminesces more brightly than the core and in the latter the intralensar bowl and core, which appear dull in CL (outlined in white) are not seen in TL.

Lenses that lack intralensar features in TL are generally homogeneous but anisotropic when viewed using CL; they display patchy luminescence variations. In a small number of *Geesops* lenses differences in CL intensity make visible what appear to be intralensar structures, undetected in TL. As shown in Figure 5.7C and D the intralensar bowl and core are merged and continuous with the underlying cement. This suggests that the bowl and core areas of the lens were being modified (i.e. undergoing diagenetic alteration) at the same time as cement crystallisation.

5.1.2.2 Hyperspectral Cathodoluminescence

Hyperspectral CL analysis was carried out on sample G35, a tangential section of *G. schlotheimi* lenses (Figure 5.8).

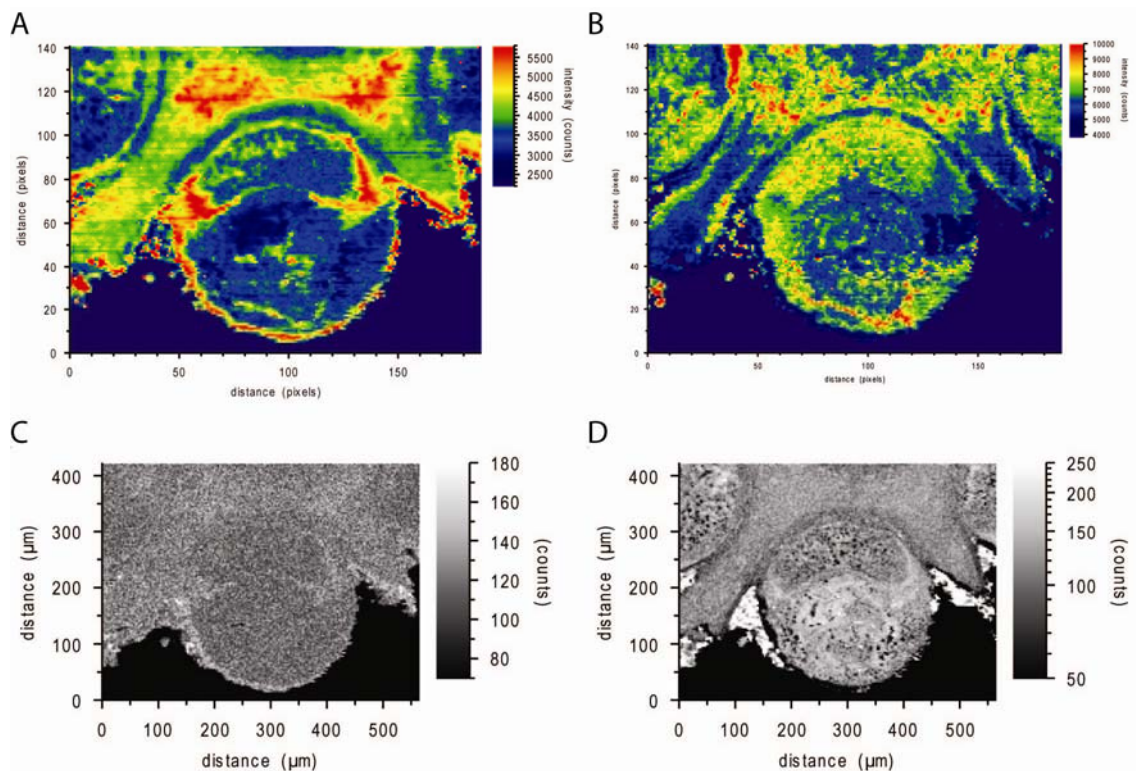


Figure 5.8 - Hyperspectral CL and X-ray maps of a *Geesops* lens.

A. and B. Maps showing CL intensity, of a lens cut in the tangential plane, at the red and blue wavelengths respectively. **C and D.** X-ray maps showing distribution of Mn and Mg respectively. Note the correlation between element distribution and CL intensity in the map above. Images are of section G35.

CL spectra show peaks in both the red (575-660 nm) and blue regions of the spectrum (385-435 nm). Maps of the red peak (Figure 5.8A) show significant differences between the lenses and the surrounding sclera whereas the blue peak (Figure 5.8B) reveals a difference between the centre of the lens and the

surrounding lens calcite. X-ray maps (Figure 5.8C and D) obtained simultaneously reveal variations in Mn and Mg concentrations, which correspond in location to calcite emitting red and blue peaks respectively (Figure 5.8).

5.1.3 Scanning Electron Microscopy

5.1.3.1 Secondary Electron Imaging of Fractured Surfaces

SE images of fractured surfaces of *G. schlotheimi* provide some indication of the growth process of lens calcite. Imaging of the lenses at different angles and along various lines of section reveals the presence of sheets of calcite (Figure 5.9A-C), presumably the structures termed lamellae in previous studies (e.g. Miller and Clarkson, 1980; Clarkson *et al.*, 2006).

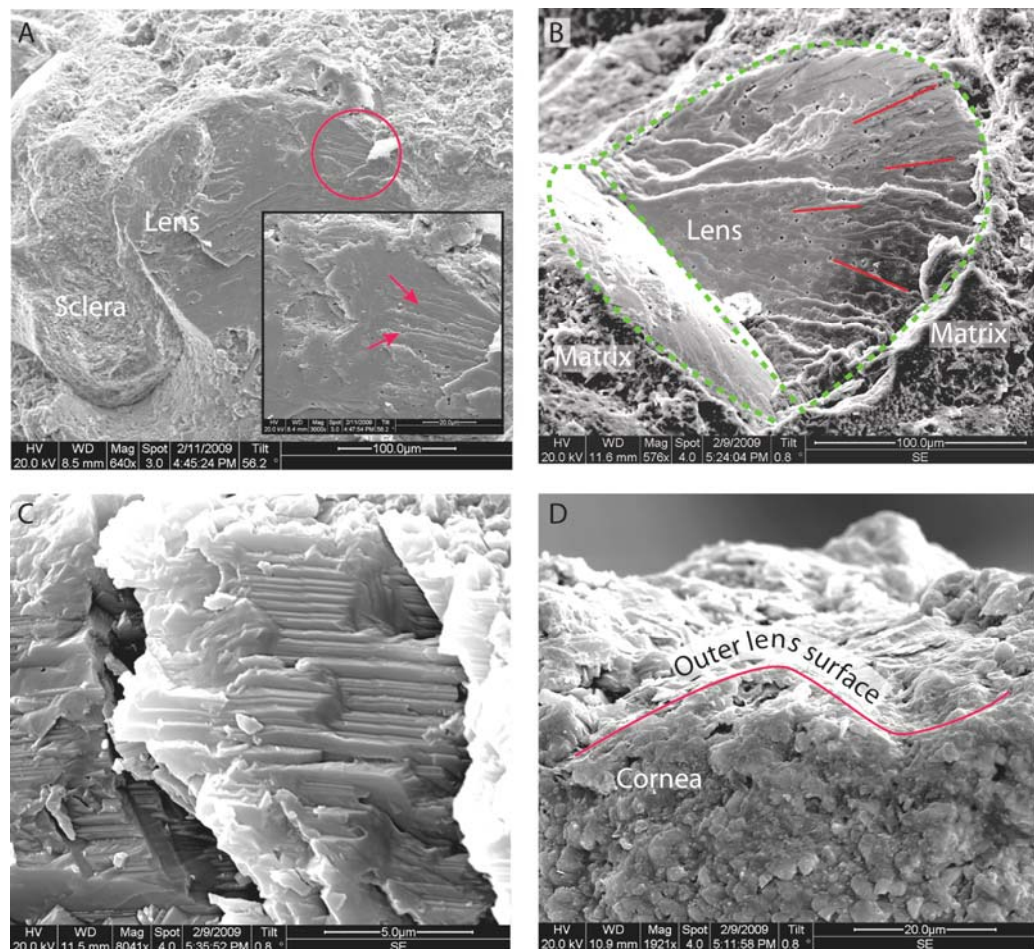


Figure 5.9 - Secondary Electron images of fracture surfaces of *Geesops schlotheimi*. Specimen 32 - Note the curved fracture lines in A highlighted by the red circle and magnified in the inset image. B. A tangential fracture of the lens (outline in green) showing a faint radial pattern to the calcite sheets (highlighted by the red lines). C. High magnification of the calcite sheets or lamellae. D. The polycrystalline cornea.

These stacked calcite sheets are continuous across the width of the lens (Figure 5.9A) and in some lines of section a faint radial pattern is seen (Figure 5.9B),

this microstructure is consistent with the growth model proposed by Miller and Clarkson (1980) in which the lens develops as a three-dimensional mesh of calcite sheets and fibres (section 1.5.2.2). In the upper portion of the lens, curved fractures are evident, possibly due to breaking of the lens perpendicular to the changing *c* axis in the radial fringe (Figure 5.9A). The identification of these calcite sheets in more than one plane of section confirms that this stacking is three-dimensional. Imaging of a fractured inorganic calcite block revealed similar calcite sheets suggesting that this ‘layering’ is simply a product of calcite growth in general and is not unique to biominerals. The curved fractures and radial lamellae, however, have been found only in biogenic calcite; curved fractures may be the result of the changing crystal orientation seen in the lenses when viewed in TL between crossed polarisers (section 5.1.1.1). Imaging of fracture surfaces also reveals the presence of a large number of sub-micron sized crystals lacking any preferred orientation in the uppermost region of the lens; this polycrystalline material is likely to be the cornea (Figure 5.9D).

5.1.3.2 Backscattered Electron Imaging of Thin Sections

BSE imaging has revealed several other minerals within the lens calcite (Figure 5.10). The most abundant is microdolomite (MD), which is found in most, but not all, of the lenses studied and can vary greatly in abundance. Three non-carbonate minerals are also found in the lenses; apatite, celestite and pyrite. The quantities of each of these minerals varies between lenses and they are not always present. Pyrite and celestite are easily identified in BSE imaging against the grey background of the lens calcite, as they appear very bright due to their high mean atomic numbers (FeS and SrSO₄). Apatite and dolomite are less distinctive, appearing as different shades of grey against the calcite (also grey); it is primarily the distinctive habits of these minerals that make their identification possible in BSE imaging (Figure 5.10A and B).

The microdolomite crystals have a considerable size range although most are only a few micrometers in length. Some of the microdolomite crystals found in lenses of *Barrandeops* and *Phacops* are iron-rich. These iron-rich dolomites occur at the lens edge or in the lower region (Figure 5.10A) suggesting that ion exchange with external sources during diagenesis did not penetrate the whole lens. Apatite crystals are generally 1-3 µm in size although some larger grains of

5-15 μm are seen in the lenses of *Barrandeops* and *Phacops* (Figure 5.10B) which were also host to the iron-rich dolomite. Celestite (Figure 5.10C) and pyrite (Figure 5.10D) are both found in lenses of *Geesops schlotheimi*. Crystals are a maximum of 2 μm and 1 μm respectively; a similar scale to apatite crystals found in the same lenses. Where pyrite is present, it is framboidal and is located just below the radial fringe or at the lens edge.

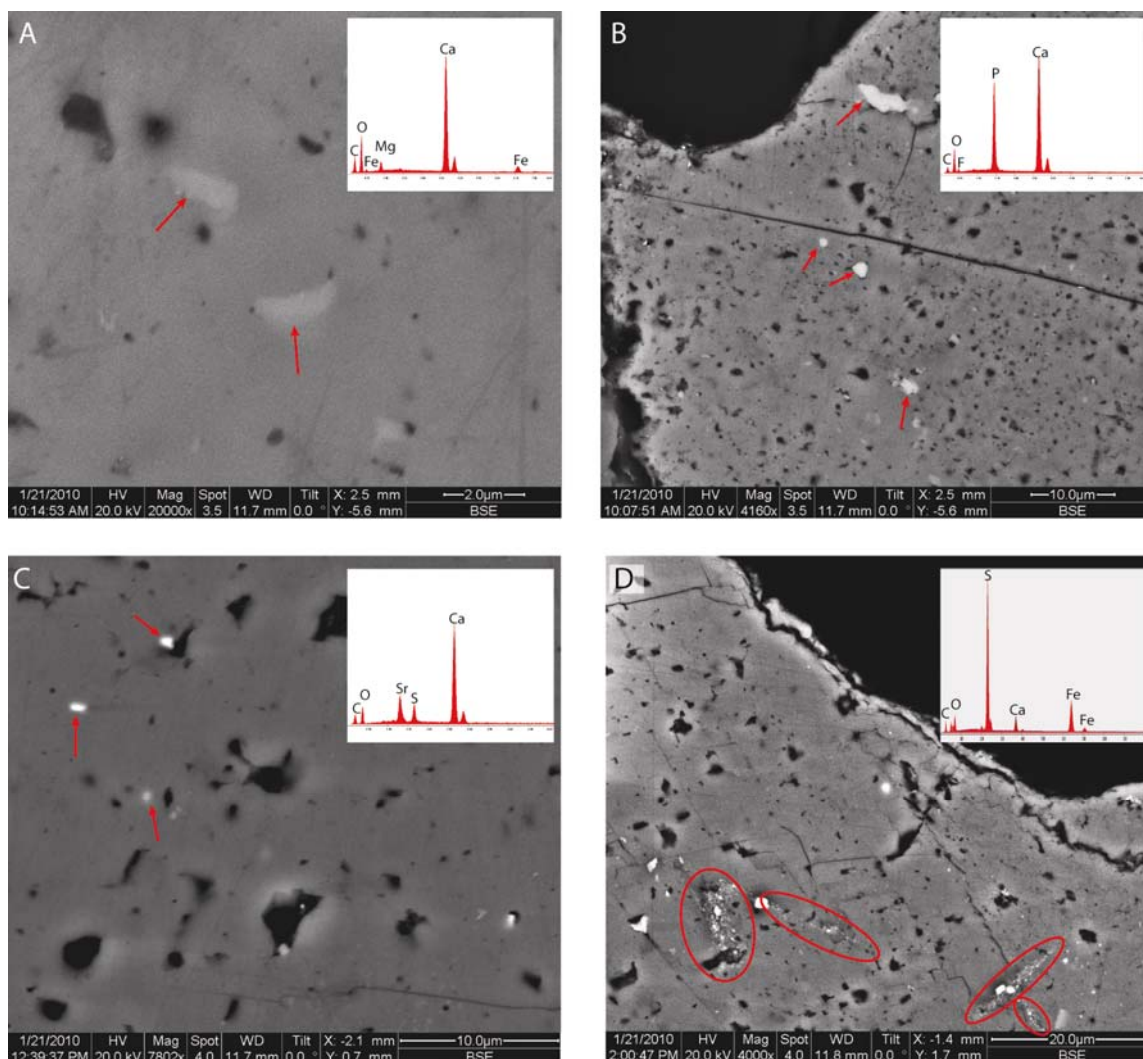


Figure 5.10 – Backscattered electron imaging of non-carbonate minerals in lenses of schizochroal eyes.

A. Fe-rich microdolomite (BM62), **B.** Apatite (PM28), **C.** Celestite (G33R) and **D.** Framboidal pyrite (GG58). Red arrows and circles highlight the location of the mineral of interest. EDS was used to confirm the identity of each mineral (spectrum inset).

BSE imaging also highlights the presence of micropores and areas of dissolution within the lenses (Figure 5.11). The location of the micropores varies between lenses but is coincident with the turbid areas in TL images. Pores are typically round to sub-round and are rarely greater than a few micrometres in size. In lenses where there is evidence of dissolution, the dissolution pits tend to be at the lateral margins or in the lower region of the lens.

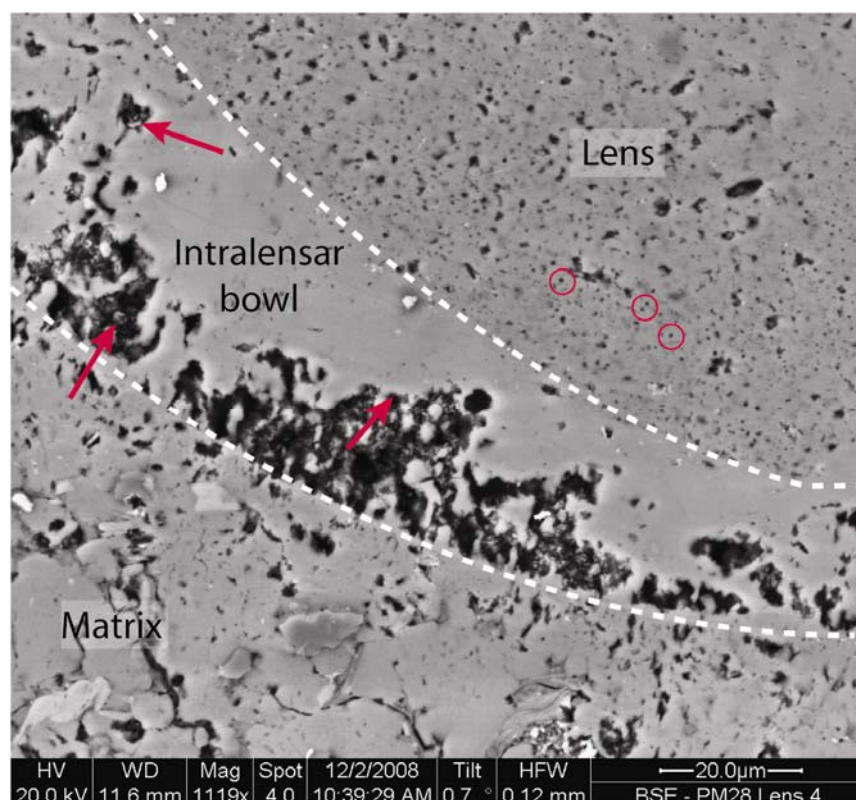


Figure 5.11 – Backscattered Electron imaging of pores and dissolution pits in a lens of *Barrandeops granulops*.

Section PM28 - Rounded pores are found in areas that appear turbid in TL (some are highlighted by red circles). Dissolution pits are located along the base or at the lateral margins of the lens (red arrows).

5.1.3.3 Secondary Electron Imaging of Etched Thin Sections

Acid etching of lenses significantly enhances the definition of microdolomite crystals, highlighting their rhombohedral habit, and revealing the presence of rounded pores (Figure 5.12A-B). The location of microdolomite crystals varies between lenses and corresponds to the turbid regions in TL. The microdolomite crystal size range is 0.26-34.60 μm across the full range of samples analysed with a mean of 2.57 μm (full details are given in Appendix B, crystal size was determined using FEI image analysis software 'XT Docu'). Lenses of *Dalmanites* sp. and *Boeckops boeckii* have a small proportion of larger crystals (20-35 μm). In general, there is no correlation between crystal size and location within the lens; in lenses with a wide range in microdolomite size, large crystals occur amongst smaller ones. *Phacops* sp. is an exception to this with the largest crystals occurring in the centre of the lens (see section 5.1.5.1.1).

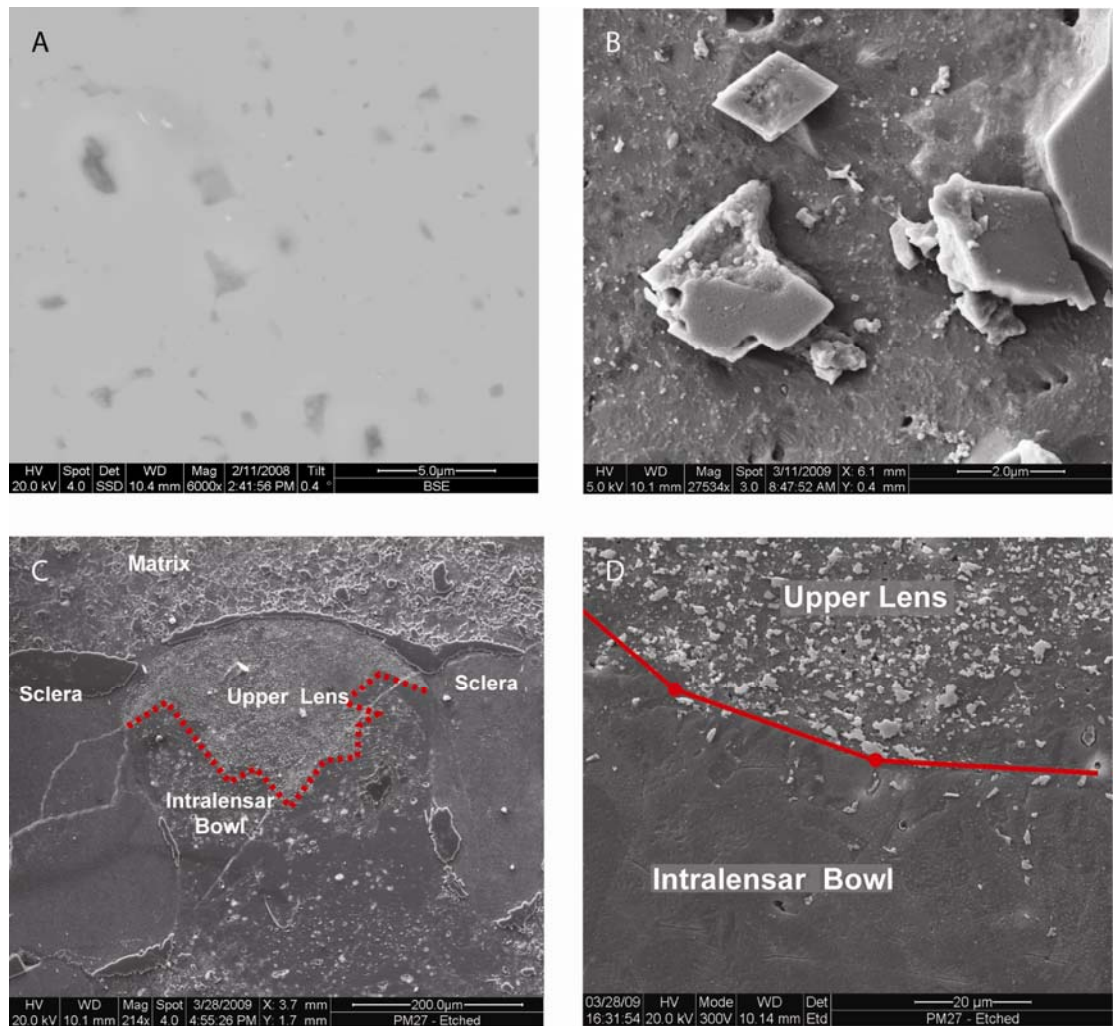


Figure 5.12 – Secondary electron and backscattered electron imaging of acid etched lenses. A. BSE image of dolomite crystals (dark grey) within lens calcite (light grey) (G33R). Note the difficulty in distinguishing between crystals compared with B which is an SE image of microdolomite crystals in an etched lens (G31). Crystals are easily identified due to the elevated topography. C. and D. SE imaging of an etched *Phacops* sp. lens (PM27). Note the marked contrast between the upper lens and the intralensar bowl region, this boundary is cleavage parallel.

Optically clear calcite intralensar bowls (see section 5.1.1.1) are relatively featureless in SE imaging, despite being acid etched, with a distinct lack of both microdolomite crystals and pores (Figure 5.12D). This optically clear calcite may therefore be of a different generation to the turbid calcite occupying the rest of the lens. A faint granoblastic texture is present within the area of clear calcite. This texture indicates that the clear calcite has been recrystallised and may represent areas of originally turbid calcite, which have been replaced by inorganic calcite. The boundary between porous calcite of the main lens and the featureless calcite of the intralensar bowl is parallel to the traces of $\{10\bar{1}4\}$ cleavage planes (Figure 5.12C).

5.1.3.3.1 Point Counting of Microdolomite Crystals

Volume % of microdolomite in the lenses was determined by point counting acid etched thin sections using SE imaging and results were plotted against crystal size (measurements obtained during point counting) (Figure 5.13) to determine any potential relationships between Mg content of lenses and the scale of diagenesis. Recrystallisation, and therefore diagenesis, is ‘measured’ by microdolomite size; the smaller the microdolomite crystal, the smaller the scale of ion transfer during diagenesis (Dickson, 2001a) and so the more closed the system has remained (see Figure 5.37).

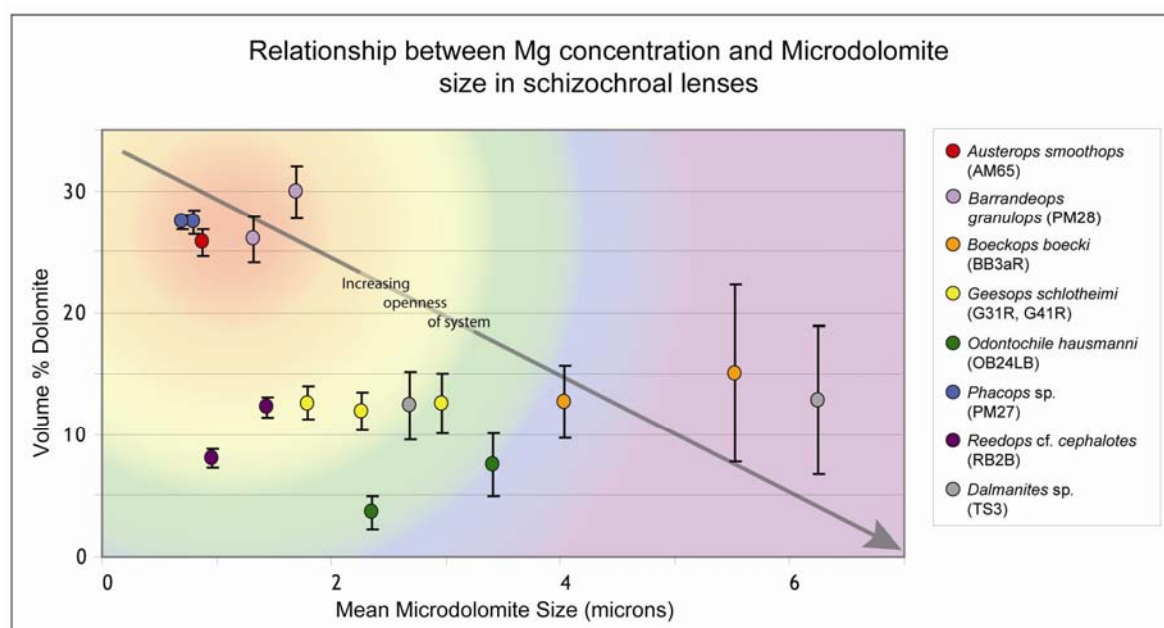


Figure 5.13 - Relationship between Mg concentration and mean microdolomite size in acid etched schizochroal lenses. Vertical bars indicate one standard deviation on each side of each mean value. Note the general trend between increasing openness of the system and increasing standard deviation.

Figure 5.13 shows that there is a weak correlation between volume % microdolomite and mean microdolomite size; lenses with the highest concentration of microdolomite crystals also have the lowest mean crystal size. This combination of characteristics suggests that these lenses (*Phacops*, *Austerops* and *Barrandeops*) have remained a relatively closed system, with ion transfer over a 2-3 μm scale, whereas the others have not and as a result have lost Mg to the surrounding environment, with ion transfer on a larger scale. A large variation in volume % of microdolomite is seen in different species, even when mean microdolomite size is similar. This could be indicative of *in-vivo* variations in Mg content between species. If all schizochroal lenses were to focus

light to the same extent, this is a reasonable assumption. Some variation in chemistry would be expected to compensate for variations in lens shape and size, as different surface curvatures will result in differing degrees of spherical aberration, as will differences in size and shape of intralensar features.

5.1.3.4 Charge Contrast Imaging

A clear textural distinction between lens components is highlighted by charge contrast (CC) imaging. This variation is most evident in *Geesops* and *Eldredgeops* lenses (Figure 5.14). In *Geesops* the upper regions of the lenses are composed of a series of curved structures, fibrous in appearance, which appear to be continuous with the sclera (Figure 5.14A), these may be calcite lamellae (Miller and Clarkson, 1980) (section 1.5.2.2). Below this lies an area of distinctly crystalline texture consisting of relatively coarse crystals, with a range of sizes. This area coincides with the clear calcite bowl seen in TL (section 5.1.1.1). In the case of *Eldredgeops*, there is a sharp distinction between the core and the main body of the lens (Figure 5.14B). The lens centre has a somewhat patchy appearance; this texture is also visible along the base of the lens although to a lesser extent. These CC image variations may be the result of different defects in the crystal lattice and may indicate variations in microstructure and chemical composition within the lens.

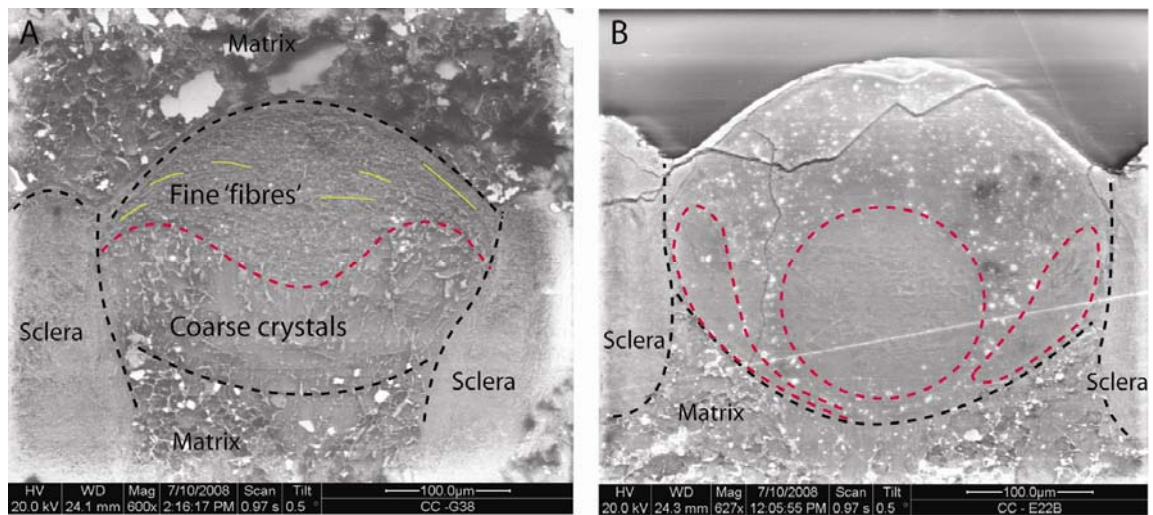


Figure 5.14 – Charge Contrast images of lenses in schizochroal eyes.

A. *Geesops schlotheimi* (G38) lens with a fibrous-coarsely crystalline boundary similar in shape to a Cartesian surface. Fibres are highlighted by yellow lines. **B.** *Eldredgeops rana* (E22B) lens in which areas corresponding to a core and intralensar bowl in TL consist of calcite with a patchy appearance (circled in red).

5.1.4 Transmission Electron Microscopy

Samples for TEM work were extracted from lenses of *Geesops sparsinodosus* and *Reedops* cf. *cephalotes* using the methods described in section 3.2.2. A sample was taken from both the smooth radial fringe and more coarsely crystalline lens centre (*Geesops* only) (Figure 5.15A). TEM imaging and electron diffraction confirm the presence of sub-grains within the lens calcite of both species. Bright field images (Figure 5.15B) show that these sub-grains are on the scale of 1 μm or less. The grains are internally featureless but are bounded by dislocations indicative of strain. A gradual change in orientation from one sub-grain to the next is what gives the lenses the sweeping extinction identified in TL (5.1.1.1, Figure 5.4).

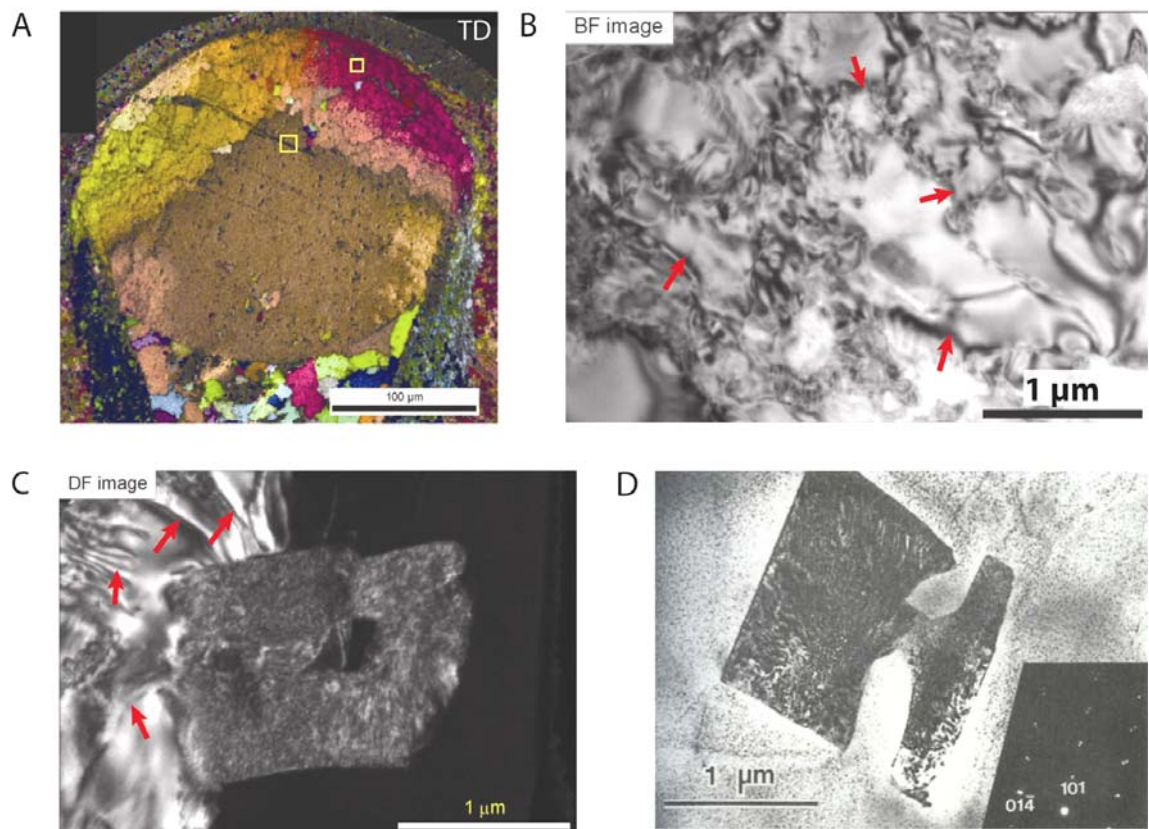


Figure 5.15 – Transmission Electron Microscopy of lenses in schizochroal eyes.

A. EBSD map of a lens in *Geesops sparsinodosus* (GG58) showing the areas from which TEM samples were extracted (yellow boxes). **B.** Bright field image of calcite in the upper region of the lens. Red arrows indicate dislocation rich sub-grain boundaries. **C.** Dark field image of a microdolomite crystal between two calcite sub-grains. Note the dislocations in the calcite sub-grain (indicated by red arrows) and the mottled texture of the microdolomite, which is similar to D, a calcian-rich microdolomite. From Reeder (1992, p. 413 figure 10-24).

Microdolomite crystals have a mottled texture (Figure 5.15C) that is characteristic of calcian dolomites (Reeder, 1992). Some microdolomite crystals cross-cut boundaries between calcite subgrains indicating that the dolomite post

dates the calcite. In Figure 5.15C, the boundary between the dolomite and calcite sub-grain to its right is somewhat blurred, suggesting that the dolomite formed from the calcite. The diffraction pattern created by the lens is a combination of the diffraction patterns of calcite and dolomite (Figure 5.16). This indicates that the minerals formed simultaneously, or at similar times. This suggests that the lens was originally HMC.

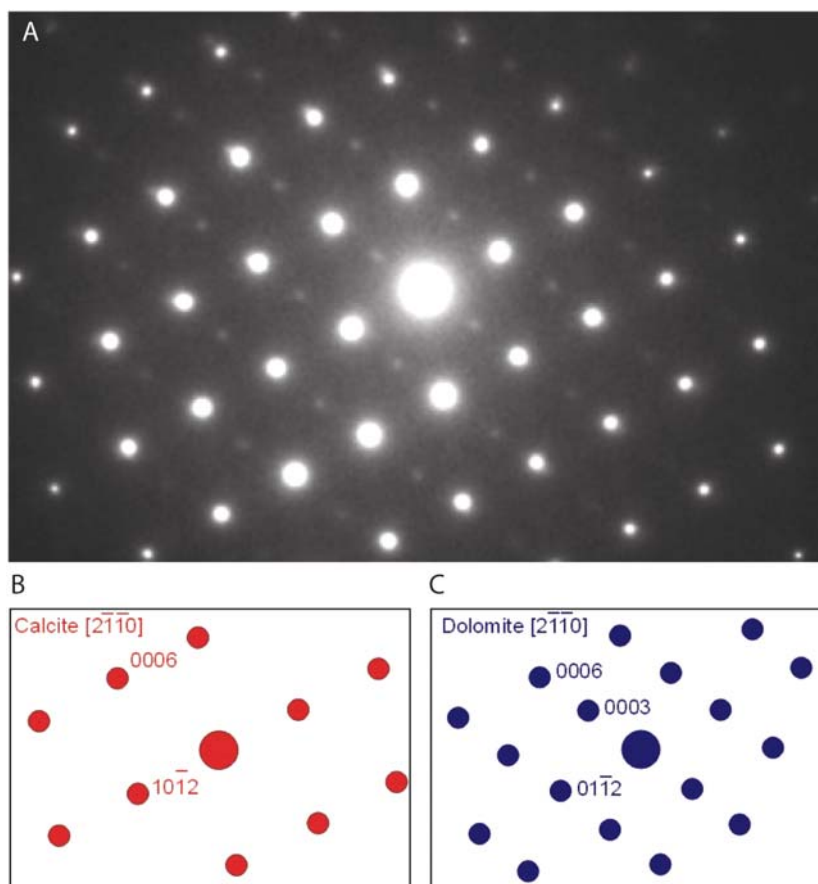


Figure 5.16 – Transmission Electron Microscopy diffraction patterns in a schizochroal lens. A. The electron diffraction pattern created by a lens of *Geesops sparsinodosus* (GG58 – shown in Figure 5.15). This pattern is a combination of calcite and dolomite diffraction patterns, which have been isolated for clarity in B and C respectively. Numbers on ‘spots’ indicate the crystal faces which diffract to produce the pattern.

5.1.5 Chemical Analysis: EDS and EPMA

5.1.5.1 Qualitative Chemical Analysis

The element distribution patterns from EDS analysis confirm and correspond directly to structures identified in lenses using BSE and SE imaging, and TL microscopy. EDS mapping was used to show the distribution of Mg, Mn, Fe, P, Sr and S and to provide quantitative information on their concentrations; Table 5.2

details the minerals in which each element is concentrated, and the significance of it's presence in that mineral.

Table 5.2 - The occurrence of elements in schizochroal lenses.

The elements analysed for using EDS and EPMA, the minerals in which they are present and their significance to lens chemistry.

ELEMENT	HOST MINERAL	SIGNIFICANCE
Ca	Calcite	Derived from original lens
	Dolomite	
	Apatite	
Mg	Dolomite	Indicative of HMC precursor if found within the lens calcite. Indicative of marine diagenesis if present in the cement
	Calcite	If above ~4 Mol% Lens is classed as HMC
P	Apatite	May originate from organic matter in the lens or surrounding soft parts
S	Pyrite	Indicates sea water interaction during early diagenesis
	Celestite	Indicative of HMC precursor as often found in recrystallised HMC
Mn	Calcite	Indicates ion influx from external source as not present in original LMC
	Dolomite	Indicates ion influx from external source as not present in pure dolomite if present in dolomite then influx was after lens recrystallisation
Fe	Calcite	As for Mn
	Dolomite	
	Pyrite	As for S
Sr	Calcite	Present in the lattice of primary calcite, loss occurs during diagenesis
	Celestite	As for S

Magnesium occurs primarily in microdolomite crystals but also at much lower concentrations in the lens calcite. The location of the microdolomite varies between lenses, even within the same eye and although X-ray mapping reveals a range of Mg distribution patterns, there are four end-member states (Figure 5.17).

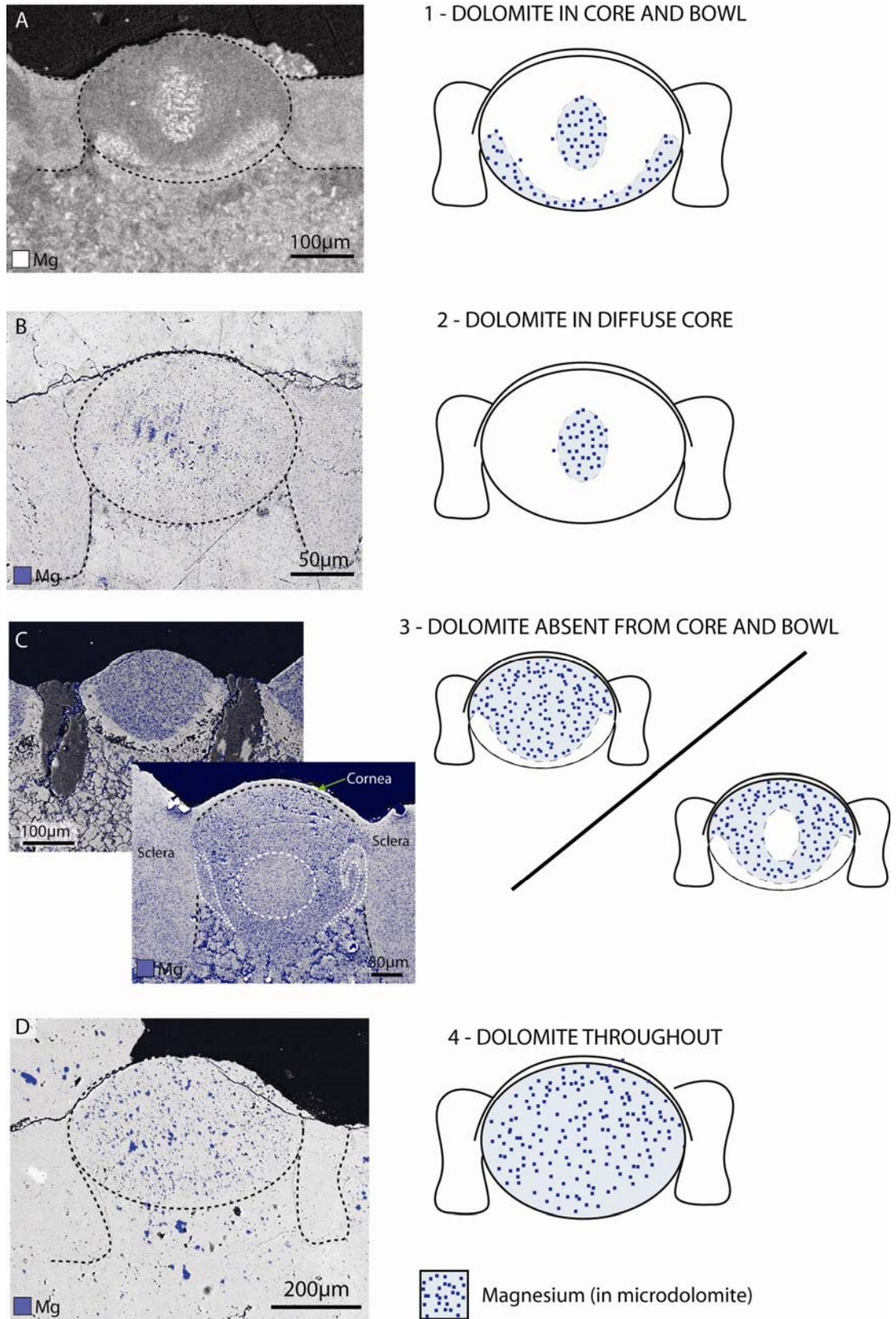


Figure 5.17 - Magnesium distribution patterns in lenses of schizochroal eyes. EDS maps and corresponding interpretative diagrams for **A.** *Dalmanites* sp. (TS1) **B.** *Ananaspis macdonaldi*. (LB1C) **C.** *Barrandeops granulops* (PM28) (top) and *Eldredgeops rana* (E22B) (bottom) and **D.** *Boeckops boeckii* (BB3aR). Black dashed lines in outline the lens and sclera, white dashed lines in C highlight the parts with lowest Mg, these correspond to the bowl and core seen in TL. Note that in D, the surrounding cement contains dolomite, this was original HMC cement.

1. Dolomite concentrated in core and bowl areas (Figure 5.17A) - this is found in some lenses of *Dalmanites* sp. and less clearly in lenses of *Geesops schlotheimi* and *Reedops* cf. *sternbergi*.
2. Dolomite concentrated in the core (Figure 5.17B) - this is seen in lenses of *Ananaspis macdonaldi* only.
3. Dolomite absent from the bowl and core (Figure 5.17C) - this pattern is present in some but not all lenses of the following species: *Austerops smoothops*, *Barrandeops forteyi*, *Barrandeops granulops*, *Geesops schlotheimi*, *Eldredgeops rana* and *Phacops* sp.. Not all lenses have a core. Where the core is present, it is depleted in dolomite. This pattern is the inverse of the core and bowl identified above (pattern 1) and by Lee *et al.* (2007).
4. Dolomite distributed uniformly throughout the lens (Figure 5.17D) - this even distribution is seen in lenses of *Ananaspis macdonaldi*, *Boeckops boeckii*, *Dalmanites* sp., *Geesops schlotheimi*, *Eldredgeops rana*, *Phacops* sp., and *Barrandeops granulops*. The magnesium concentration varies both between specimens, and within a single specimen.

In all cases, the Mg is present mainly in microdolomite crystals, identified by SE imaging of etched thin sections (5.1.3.3). In the few cases where the cornea has been preserved, it consists of calcite with no detectable magnesium (Figure 5.17C).

5.1.5.1.1 Silicified Trilobites

Several episodes of silicification have occurred in the red formations of Morocco (Lang *et al.*, 1990; Thiry and Benbrahim, 1990) which have inevitably affected preservation of fossils in rocks of the area; all five of the Moroccan specimens analysed (*Barrandeops* cf. *granulops* - BM60 and BM61, *Barrandeops granulops* - PM28, *Barrandeops forteyi* - BM98 and *Phacops* sp. - PM27) have been silicified during regional events (Lang *et al.*, 1990; Thiry and Benbrahim, 1990) (section 3.1.2.2.5). EDS maps provide a visual representation of the overall chemistry of these specimens (Figure 5.19), and values stated are only semi-quantitative.

Klug *et al.*, (2009) described the chemistry of *B. cf. granulops* obtained from the same locality (18 km east southeast of Erfoud; N 31°22'37" W4°03'28") as samples BM61 and BM62. Klug *et al.* (2009) found that 'all red parts of the

exoskeleton are silicified while the greenish parts such as the lenses retained the calcitic composition' (Figure 5.18). EDS analyses on the samples from this locality (BM60 and BM61) reveal the lenses to be predominantly calcium carbonate with traces (~1 %wt.) of iron and manganese. The surrounding sclera also remains, for the most part, calcitic. Both lens and sclera do however show some evidence of silicification; an outer crust of quartz has precipitated on parts of the interlensar sclera and other exoskeletal regions (Figure 5.19A). Penetration of silica into the sclera is evident from BSE imaging. There is a clear colour change, from dark grey to lighter grey (Figure 5.19A), in the sclera at 70-90 μm depth (Figure 5.19A); Si content in the sclera decreases with depth from the outer surface. Micron-scale stylolite-like quartz veins are present in the main body of the lenses in a few cases; these areas contain upwards of 3 %wt. Fe and less than 0.5 %wt. Mn.



Figure 5.18 - *Barrandops cf. granulops*.

Anterior (left) and lateral (right) views of a specimen sourced from the Eastern Anti-Atlas region of Morocco. Note that the exoskeleton is red but the lenses are green, this is indicative of differences in chemistry. The cephalon is 10.2 mm wide (anterior view). Image from Klug *et al.* (2009, figure 2A).

Silicification of *Phacops* sp. (PM27) varies considerably throughout the sample. The lenses are not silicified, but consist of two calcite components (Figure 5.19B); an upper part rich in Mg, and a lower 'bowl' region, which has less than half this Mg content, but is enriched, relative to the upper part, in Fe and Mn. The boundary between the upper and lower unit lies parallel to the calcite cleavage planes suggesting that the cleavage planes acted as a barrier to fluid penetration. This chemistry suggests that the upper part best represents the original lens chemistry, the original bowl region having been replaced with LMC during diagenesis. Iron distribution in *Phacops* sp. (PM27) lenses suggest that this alteration may have worked along a gradient from the lens base up with iron being derived from the host rock. Dolomite crystals in the middle of the lenses,

immediately above the centre of the bowl, contain Fe, the quantity decreasing with distance of dolomite crystals from the bowl; this variation does not constitute a core as there is not a significant difference between this area and the upper region of the lens in either TL microscopy or Mg content. Microdolomite size is also indicative of an alteration gradient; the largest crystals are in the middle of the lens, close to the bowl, suggesting that ion transfer was on a larger scale here than in the uppermost parts of the lenses. EDS maps also reveal the presence of small quantities of phosphorus in the upper region of the lens; this suggests that ion transfer was on a very local scale as this phosphorus is more likely to have come from organics within the original lens material than from the host rock.

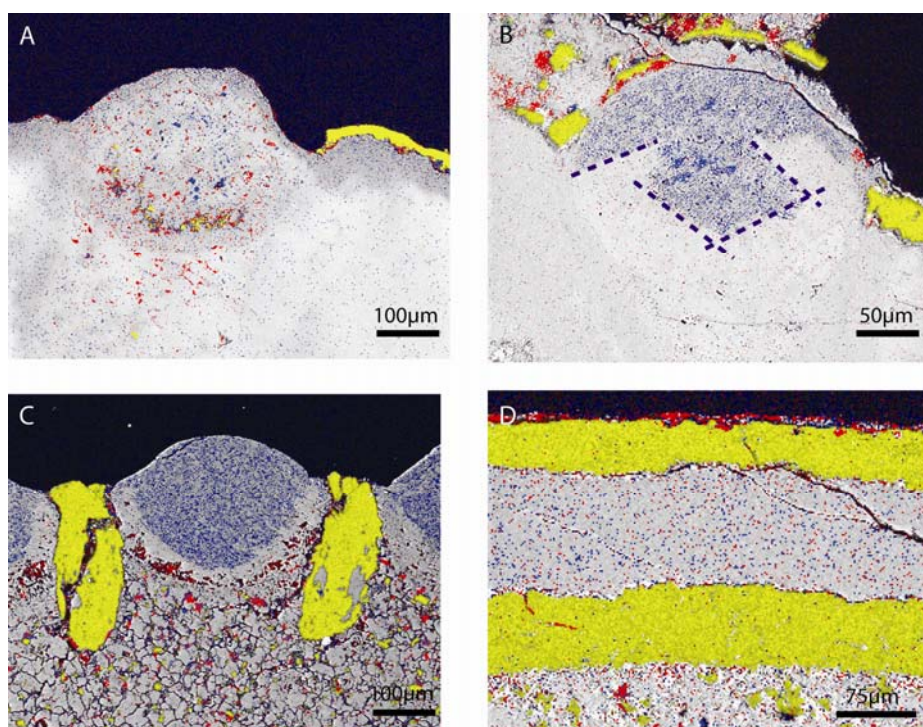


Figure 5.19 – Element distribution patterns within samples with silicified exoskeletons. EDS maps of A. *Barrandeops* cf. *granulops* (BM61) and B. *Phacops* sp. (PM27), with stylolitic (A only) and crust silicification. C. *Barrandeops granulops* (PM28) with preferential silicification of the interlensar sclera and D. *Phacops* sp. (PM27-Glabella), preferential silicification of certain cuticular layers. Colours denote the presence of certain elements: Si (yellow), Mg (blue) and Fe (red). Note how the Mg distribution in B is controlled by or bounded by the {10 $\bar{1}$ 4} calcite cleavage (indicated by blue dashed lines).

The glabella of *Phacops* sp. (PM27) has been silicified to a much greater degree than the eyes and now comprises a single band of calcite sandwiched between two silicified layers (Figure 5.19D). This suggests that the original exoskeleton consisted also of three layers, the central one of which was probably chemically or physically distinct preventing it from being silicified. A three-layered

structure was identified in numerous species, including *Phacops rana*, by Dalingwater and Miller (1977), who recognised differing orientations of lamellae.

The eyes in *Barrandeops granulops* (PM28) and *Barrandeops forteyi* (BM98) have been altered to a greater degree than *Phacops* sp. (PM27). As Figure 5.19C illustrates, the lenses have remained as calcite but the surrounding sclera has been silicified. The presence of iron in the bowl combined with the pitted texture along the lens/matrix interface suggests dissolution of the original bowl and replacement with inorganic calcite, as is likely to be the case for the bowl region in PM27 also. There are two possible explanations for why the bowl was preferentially dissolved: (1) the bowl had elevated Mg content with respect to the main body of the lens (which has in excess of 25% dolomite by volume); (2) it had a similar Mg content to the rest of the lens but was grown as a physically separate component, perhaps separated by an organic interface, allowing it to be altered in isolation. Mechanisms of dissolution of Mg-calcite (i.e. the greater solubility of HMC) favour the first explanation (e.g. Wollast and Reinhard-Derie, 1977).

EDS mapping of these specimens (Figure 5.19) shows no dolomite in the host rock or the sclera, thus indicating that dolomitisation events reported in the region from which samples were sourced (Klug *et al.*, 2009) had no effect on the rocks in which the specimens were preserved. Thus, the magnesium is likely to be autochthons to the lenses.

5.1.5.2 Quantitative Chemical Analysis

Seven species were chosen, based on qualitative EDS maps, for more in-depth analysis using quantitative EDS and EPMA: *Austerops smoothops* (AM65), *Boeckops boeckii* (BB3aR), *Dalmanites* sp. (TS1), *Eldredgeops rana* (E22B and E22T), *Geesops schlotheimi* (G33R, G33RT and G42), *Barrandeops granulops* (PM28) and *Reedops cephalotes* (RB14L). EPMA work involved analysis by automatic traverse of a series of points across the width and depth of one or more lenses in each section. In some instances, the sclera, exoskeleton, matrix and cement were analysed for comparison. EDS results were obtained by 'spot' analysis on a number of different points within each lens analysed and data were also collected for the sclera, exoskeleton, matrix and cements by this method. EPMA work was carried out on instruments at Strathclyde and Edinburgh

Universities. EDS was carried out at The University of Glasgow. Some samples were analysed on all three instruments to ensure comparable results were being obtained. Table 5.3 gives a summary of the results, for full details of all analyses see Appendices D and E.

There is a large variation in overall Mg concentration between lenses (Table 5.3); the lenses with the highest concentrations (8.07 mol % MgCO_3), from Morocco, have seen silicification of the exoskeleton (see section 5.1.5.1.1), although the lenses have remained largely unaffected.

Data show a correlation between lens chemistry and appearance in TL, as suggested by EDS mapping (section 5.1.5.1); areas that are turbid in TL generally have higher Mg concentrations than optically clear areas. Traverses through lenses of *Dalmanites* sp. (TS1) show that it has elevated levels of Mg in both the intralensar structures, most notably in the core (from Figure 5.20A), whereas *Eldredgeops rana* (E22B) has relatively low Mg concentrations in these parts, similar to or, in some cases, lower than the surrounding lens and its adjacent sclera (Figure 5.21A). Variations in concentrations of the trace elements Fe, Sr and Mn are also seen across the lenses. The increase in Fe with Mg in the core of *Dalmanites* sp. (TS1) (Figure 5.20B) suggests that although the intralensar structures are still present, there has been some alteration of chemistry during diagenesis (i.e. import of Fe from the host rock). Despite having low levels of Fe, concentrations of Mn in the lens of *Eldredgeops rana* (E22B) (Figure 5.21B) are marginally higher than in the adjacent sclera. This, combined with the complete loss of Sr in most of the lens, whilst some is retained in the sclera, indicates that this lens has also undergone compositional change.

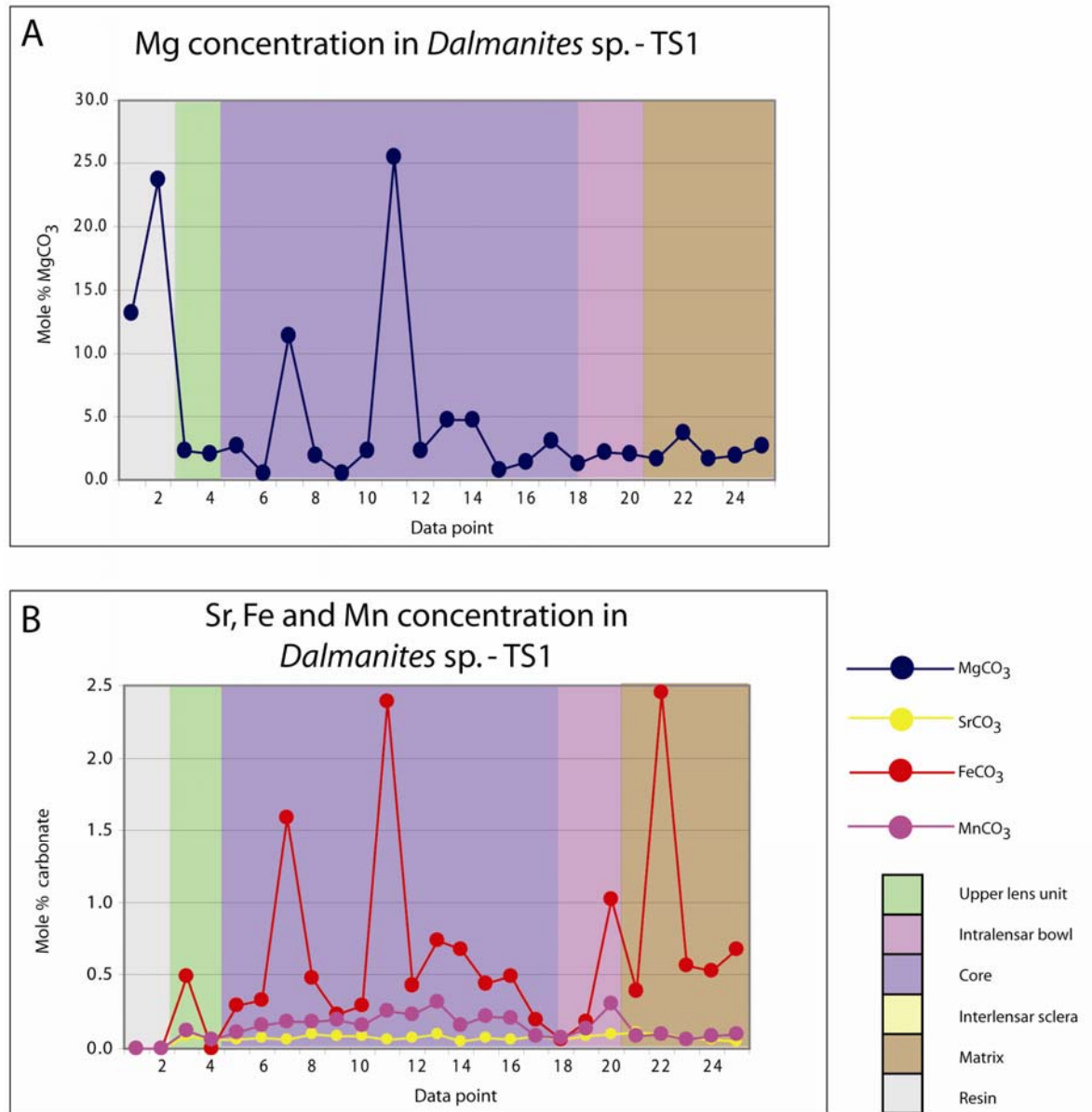


Figure 5.20 - Electron Probe Micro-Analysis traverses through lenses of *Dalmanites* sp. A. Mg and B. Fe, Sr and Mn are seen to vary across the lens. *Dalmanites* sp. (TS1) has turbid intralensar structures. Step size between points approximately 20 μm . Points below the detection limit have been put to zero.

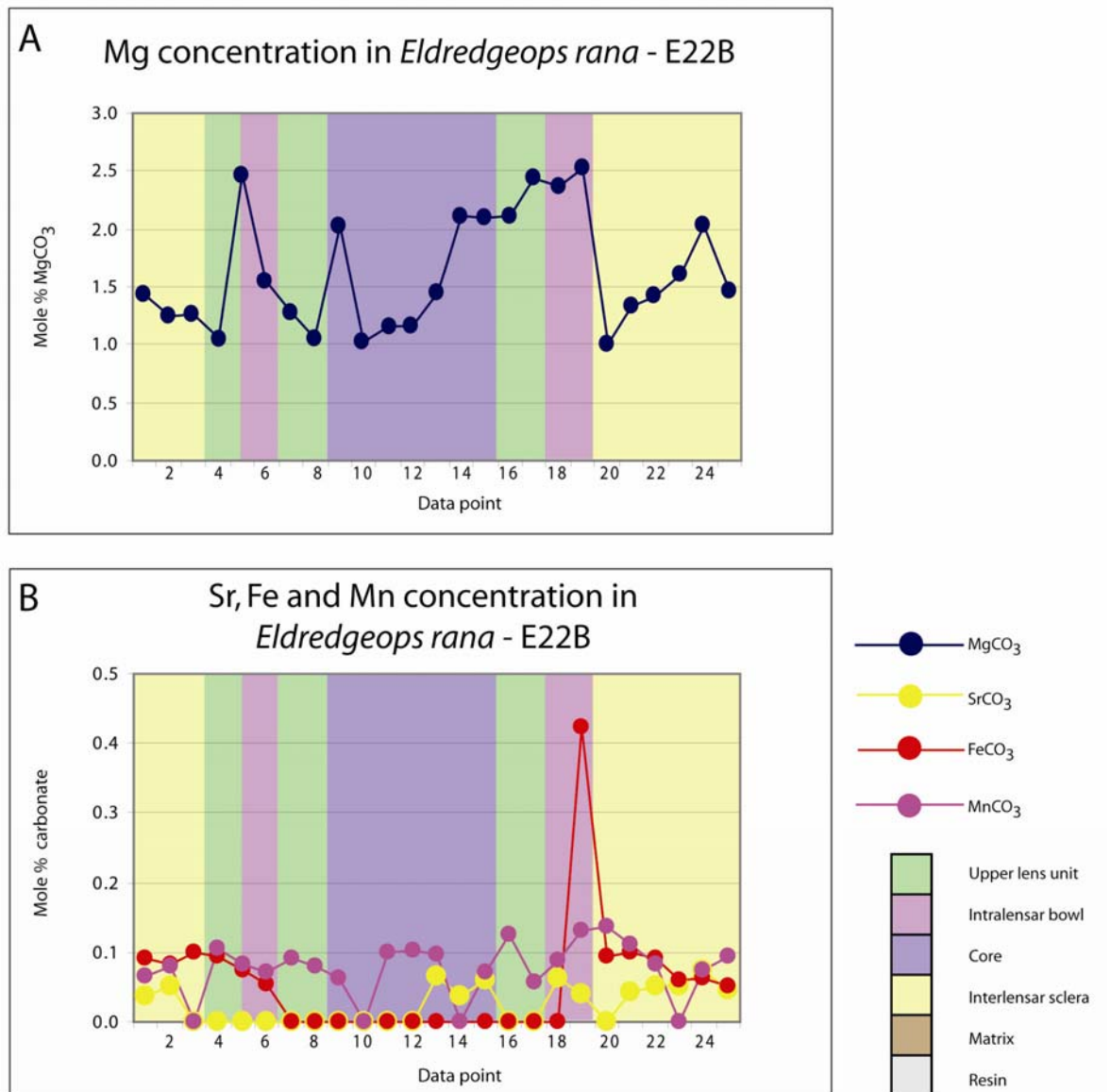


Figure 5.21 - Electron Probe Micro-Analysis traverses through lenses of *Eldredgeops rana*. **A.** Mg and **B.** Fe, Sr and Mn are seen to vary across the lens. *Eldredgeops rana* (E22B) has clear intralensar structures. Step size between points approximately 20 μm . Points below the detection limit have been put to zero.

Table 5.3 continued - Quantitative chemical analysis data of lenses, sclera and exoskeleton in schizochroal eyes.

SPECIES SAMPLE/FEATURE	EDINBURGH EPMA																
	MOL % MgCO ₃				MOL % SrCO ₃				MOL % FeCO ₃				MOL % MnCO ₃				n
	MN	MAX	MIN	SD	MN	MAX	MIN	SD	MN	MAX	MIN	SD	MN	MAX	MIN	SD	
<i>Austerops smoothops</i> AM65/ LENS	-	-	-	-	-	-	-	-	-	-	-	-	-	-	-	-	-
<i>Austerops smoothops</i> AM65/ BOWL	-	-	-	-	-	-	-	-	-	-	-	-	-	-	-	-	-
<i>Boeckops boeckii</i> BB3aR/ CEMENT	0.86	1.86	0.08	0.49	0.02	0.10	0.00	0.03	0.01	0.05	0.00	0.02	0.00	0.00	0.00	0.00	15
<i>Barrandeops granulops</i> PM28/ SCLERA	6.49	22.91	0.51	4.58	0.24	0.37	0.00	0.07	0.53	9.61	0.00	1.45	0.08	1.11	0.00	0.19	58
<i>Barrandeops granulops</i> PM28/ MATRIX	8.09	40.47	0.62	12.84	0.03	0.14	0.00	0.05	7.72	29.01	1.72	9.42	0.91	6.22	0.00	2.00	8
<i>Boeckops boeckii</i> BB3aR/ LENS	2.75	30.40	0.05	6.08	0.03	0.07	0.00	0.02	0.03	0.35	0.00	0.09	0.01	0.35	0.00	0.05	58
<i>Boeckops boeckii</i> BB3aR/ MATRIX	0.85	1.16	0.37	0.27	0.01	0.05	0.00	0.02	0.00	0.00	0.00	0.00	0.00	0.00	0.00	0.00	6
<i>Boeckops boeckii</i> BB3aR/ SCLERA	0.66	0.96	0.45	0.16	0.01	0.07	0.00	0.02	0.13	0.35	0.30	0.10	0.06	0.16	0.00	0.06	11
<i>Boeckops boeckii</i> BB3aR EXOSKELETON	0.72	1.40	0.34	0.28	0.01	0.05	0.00	0.01	0.06	0.26	0.00	0.08	0.04	0.26	0.00	0.07	18
<i>Eldredgeops rana</i> E22B/LENS	1.79	3.34	0.54	0.56	0.03	0.08	0.03	0.03	0.01	0.09	0.00	0.02	0.03	0.22	0.00	0.05	23
<i>Eldredgeops rana</i> E22B/ CORE	1.51	2.28	0.72	0.45	0.03	0.08	0.00	0.03	0.00	0.00	0.00	0.00	0.07	0.18	0.00	0.06	27
<i>Eldredgeops rana</i> E22B/ BOWL	2.07	2.84	1.43	0.50	0.03	0.07	0.00	0.03	0.07	0.42	0.00	0.13	0.10	0.22	0.00	0.05	8
<i>Eldredgeops rana</i> E22B/ SCLERA	1.43	2.02	1.01	0.26	0.04	0.07	0.00	0.02	0.08	0.16	0.03	0.03	0.07	0.14	0.00	0.04	18
<i>Eldredgeops rana</i> E22B/ EXOSKELETON	1.48	1.86	1.20	0.20	0.04	0.07	0.00	0.20	0.05	0.13	0.00	0.04	0.09	0.15	0.00	0.04	12
<i>Eldredgeops rana</i> E22T/ LENS	-	-	-	-	-	-	-	-	-	-	-	-	-	-	-	-	-
<i>Eldredgeops rana</i> E22T/ CORE	-	-	-	-	-	-	-	-	-	-	-	-	-	-	-	-	-
<i>Eldredgeops rana</i> E22T/ BOWL	-	-	-	-	-	-	-	-	-	-	-	-	-	-	-	-	-
<i>Eldredgeops rana</i> E22T/ SCLERA	-	-	-	-	-	-	-	-	-	-	-	-	-	-	-	-	-
<i>Eldredgeops rana</i> E22T/ EXOSKELETON	-	-	-	-	-	-	-	-	-	-	-	-	-	-	-	-	-
<i>Geesops schlotheimi</i> G33R/ LENS	1.81	5.40	0.45	1.09	0.22	0.61	0.07	0.10	0.38	0.91	0.04	0.16	0.10	0.36	0.00	0.08	24
<i>Geesops schlotheimi</i> G33R/ SCLERA	1.95	2.94	1.29	0.48	0.25	0.33	0.16	0.04	0.27	0.35	0.20	0.05	0.06	0.12	0.00	0.04	12
<i>Geesops schlotheimi</i> G33R/ CEMENT	3.29	4.20	2.41	0.67	0.18	0.30	0.07	0.08	0.89	1.21	0.50	0.25	0.04	0.09	0.00	0.04	4
<i>Geesops schlotheimi</i> G33RT/ LENS	-	-	-	-	-	-	-	-	-	-	-	-	-	-	-	-	-
<i>Geesops schlotheimi</i> G33RT/ SCLERA	-	-	-	-	-	-	-	-	-	-	-	-	-	-	-	-	-
<i>Geesops schlotheimi</i> G33RT/ EXOSKELETON	-	-	-	-	-	-	-	-	-	-	-	-	-	-	-	-	-
<i>Geesops schlotheimi</i> G42/ LENS	-	-	-	-	-	-	-	-	-	-	-	-	-	-	-	-	-
<i>Geesops schlotheimi</i> G42/ SCLERA	-	-	-	-	-	-	-	-	-	-	-	-	-	-	-	-	-
<i>Reedops cephalotes</i> RB14L/ LENS	-	-	-	-	-	-	-	-	-	-	-	-	-	-	-	-	-
<i>Dalmanites</i> sp. TS1/ LENS	2.95	17.82	0.36	3.47	0.07	0.17	0.04	0.02	0.22	1.65	0.00	0.33	0.06	0.28	0.00	0.06	48
<i>Dalmanites</i> sp. TS1/ CORE	3.81	26.33	0.40	6.24	0.07	0.10	0.02	0.02	0.53	2.82	0.02	0.61	0.16	0.32	0.03	0.08	32
<i>Dalmanites</i> sp. TS1/ BOWL	2.13	2.22	2.03	0.10	0.09	0.09	0.09	0.00	0.61	1.02	0.19	0.42	0.22	0.31	0.14	0.09	2
<i>Dalmanites</i> sp. TS1/ SCLERA	2.40	6.82	1.51	1.08	0.10	0.16	0.07	0.02	0.37	0.61	0.00	0.15	0.09	0.24	0.00	0.07	21
<i>Dalmanites</i> sp. TS1/ EXOSKELETON	2.31	3.67	1.61	0.77	0.08	0.11	0.05	0.02	0.92	2.45	0.39	0.77	0.09	0.10	0.06	0.01	5

The concentration of Mg in the sclera varies between specimens. *Boeckops boeckii* (BB3aR) lenses have a significant difference in Mg content between the lens and sclera whereas *Geesops schlotheimi* lenses show little difference between the two (Table 5.3). These two examples may represent closed and open systems respectively. Although the data suggest that lenses in *B. boeckii* acted as closed systems, the lack of clearly defined intralensar structures (section 5.1.5.1, Figure 5.17) may indicate that some migration of Mg within each lens has occurred.

Overall, the lenses in schizochroal eyes have higher Mg concentrations than the adjacent sclera, many of these concentrations are well within the range of HMC (Figure 5.22). Lenses that fall within the range of LMC, which have a core and/or bowl, have optically clear rather than turbid intralensar structures; this may be the result of alteration, specifically the replacement by LMC during diagenesis.

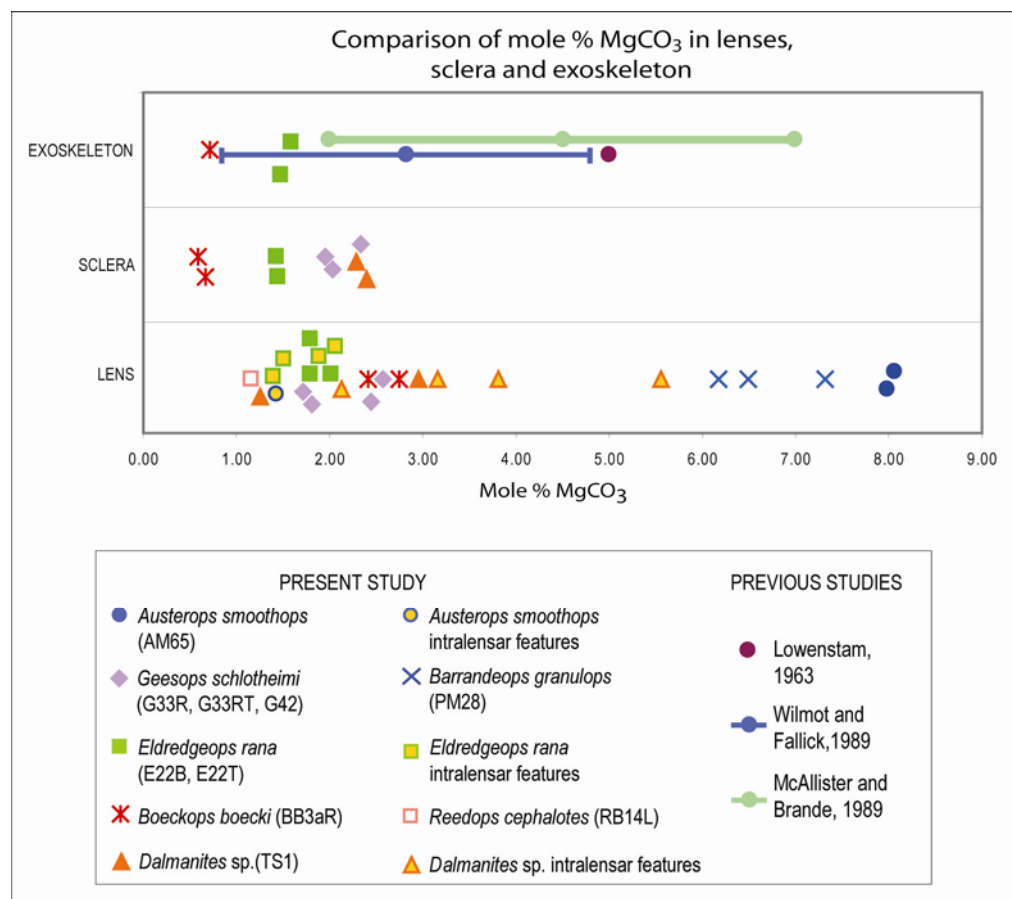


Figure 5.22 – Magnesium concentrations of lenses, interlensar sclera and exoskeleton in trilobites with schizochroal eyes.

Mean magnesium concentrations of all samples analysed. Values correspond to the mean values stated in Table 5.3. For simplicity standard deviation lines have been omitted, values can be found in Table 5.3. Lenses generally have higher Mg content than the sclera and exoskeleton, which are in the same range as each other. Values for exoskeleton chemistry of previous studies are given.

Concentrations of Mg recorded in the sclera are generally lower than found in previous studies (Lowenstam, 1963; McAllister and Brand, 1989, Wilmot and Fallick, 1989) (Figure 5.22). This is most likely a reflection of the different techniques used in obtaining data; previous studies used bulk sampling methods which may result in some 'contamination' by other parts of the exoskeleton, such as the eyes, and the host rock. The present study has analysed individual spots with a maximum diameter of 10 μm .

Variations in the trace element concentration, especially Sr, Fe and Mn, can give an indication of the degree of diagenetic alteration a fossil has undergone (Figure 5.23). In general, the concentration of Sr in calcite is expected to decrease during diagenesis while the concentrations of both Fe and Mn are expected to increase (Bruckschen *et al.*, 1995 and references therein). Based on the concentration of each of these trace elements in the lenses, sclera and exoskeleton, lens chemistry must have undergone some change, as both Fe and Mn are present (Figure 5.23B-C). In many cases however as some Sr has been retained (Figure 5.23A), there has not been complete loss of original composition. Of all lens components, the optically clear intralensar structures have the lowest concentrations of Sr, suggesting that these features are not representative of the original chemistry. The presence of Mn and small concentrations of Fe (Figure 5.22) suggest that these clear features formed during diagenesis.

The sclera and the exoskeleton have similar trace element composition, possibly indicating that they have been subject to an equal degree of alteration (Figure 5.23). There is significant overlap between the concentrations of trace elements in the sclera and exoskeleton, and the lenses. The exception to this is the intralensar structures; those that are turbid in TL (section 5.1.1.1) have higher concentrations of Mn, and some that are optically clear in TL have much higher concentrations of Fe. This disparity is most likely the result of different original compositions; the originally HMC intralensar structures would have been more liable to change due to their less stable composition.

Other than these general observations, it is difficult to draw any conclusions from these results. Figure 5.23 highlights variations in trace element chemistry within a single sample and between samples that have undergone the same diagenetic history (i.e. specimens of *Geesops schlotheimi* that were sourced

from a single locality). As the original trace element composition of the trilobite exoskeleton is unknown, it is not possible to say with certainty, what degree of alteration the specimens have experienced.

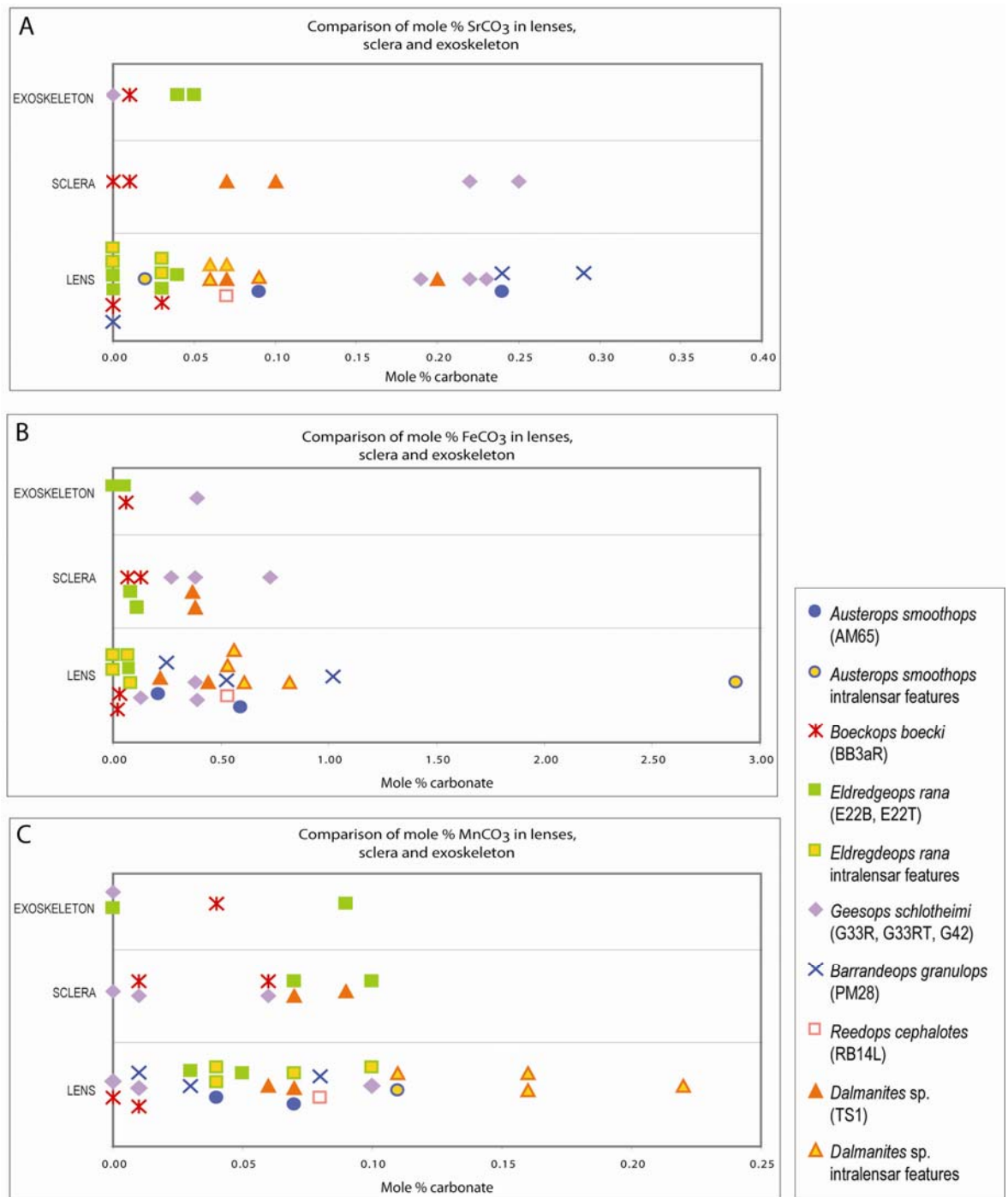


Figure 5.23 - Trace element chemistry of lenses, sclera and the exoskeleton in trilobites with schizochroal eyes.

A. Sr, B. Fe and C. Mn concentrations in the lenses, sclera and exoskeleton. Concentrations are expressed as mean mol % of the carbonate taken from Table 5.3. For simplicity standard deviation lines have been omitted, values can be found in Table 5.3.

5.1.6 Electron Backscatter Diffraction

5.1.6.1 Pole Figure Analysis of Lens Features

Analysis of lens features by pole figures provides quantitative information on feature orientations expressed relative to particular planes, and relative to other features. Pole figures reveal the calcite cleavage to be along the plane $10\bar{1}4$ and highlight the change in orientation of the trabeculae, from the $01\bar{1}1$ plane to the $01\bar{1}2$ plane. The relationships between these different components and the lens surfaces are illustrated in Figure 5.24.

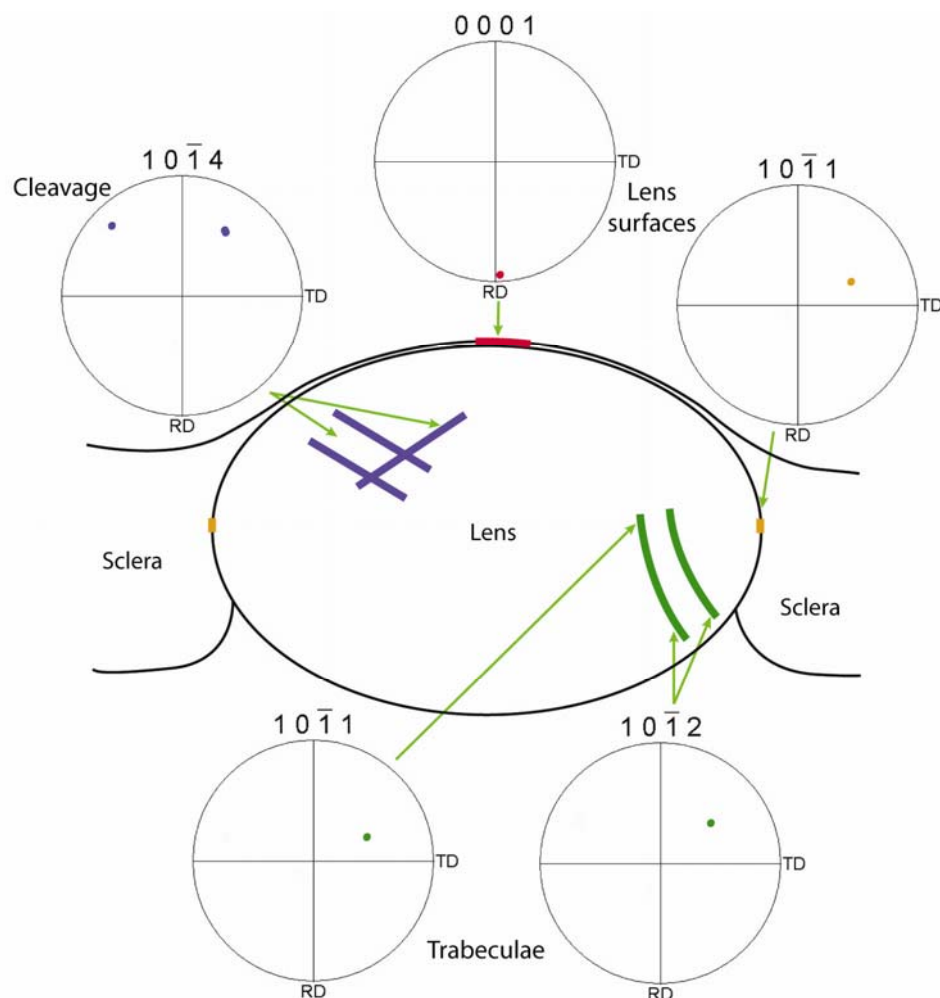


Figure 5.24 - Orientation relationships of cleavage, trabeculae and lens surfaces. Numbers above pole figures indicate the plane of the feature.

5.1.6.2 Microstructural arrangements in lenses

EBSD mapping has revealed the presence of four microstructural patterns within schizochroal lenses; each of these corresponds to a pattern identified at a coarser scale by extinction angles in TL microscopy (see section 5.1.1.1). EBSD

maps show these patterns in two dimensions but mapping of lenses cut in different planes (horizontal, vertical and tangential - section 3.2.1.1) reveals that these microstructural patterns are three-dimensional (Figure 5.25). Some preliminary findings of this analysis were published in conference proceedings (Torney *et al.*, 2008, 2009) in the course of the present study, microstructure arrangements 3 and 4 (below) had not been discovered at the time of these publications.

Microstructure arrangement 1: The entire lens appears uniform in orientation, with the *c* axis parallel to the lens axis (Figure 5.25A). Further analysis of the data using tolerance angle maps reveals a variation of *c* axes along the visual surface of up to $\pm 35^\circ$ about the lens axis however this area occupies only a minor portion of the lens, a very thin 'layer' generally no more than 10 μm in depth. Lenses with this pattern are oval rather than round and consist of a series of sub-grains that fan out along the lens base (Figure 5.25A); the sub-grains may be trabeculae (section 5.1.1.1).

Microstructure arrangement 2: The visual surface of the lens consists of calcite with a radial variation in *c* axis orientation (Figure 5.25B and Figure 5.26). Pole figures show a 'splay' of *c* axes of up to 112° from one side of the lens to the other. This 'radial fringe' reaches a thickness of up to 100 μm ; this is approximately half the depth of the lens in some species. In most cases, the splay of the *c* axis in the fringe is gradual but in some lenses of *Geesops schlotheimi* (G35 and G38) the radial fringe consists of a number of coarse crystals, each with uniform orientation internally but between which there is a change in *c* axis orientation. Below the fringe, the lens contains uniformly orientated calcite, with *c* axis orientation parallel to the lens axis.

Microstructure arrangement 3: Variation in *c* axis orientation is present along both the outer lens surface and the base of the lens (Figure 5.25C). The change in *c* axis orientation is generally not as pronounced along the lens base as it is along the upper surface; a maximum variation of 80° may be present. The angle that the *c* axis makes with the lens surface also differs between the outer surface of the lens and the lens base. At the outer surface this angle is close to or at 90° , as it is in microstructure patterns 1 and 2. At the lens base this angle varies, but is always significantly less than 90° .

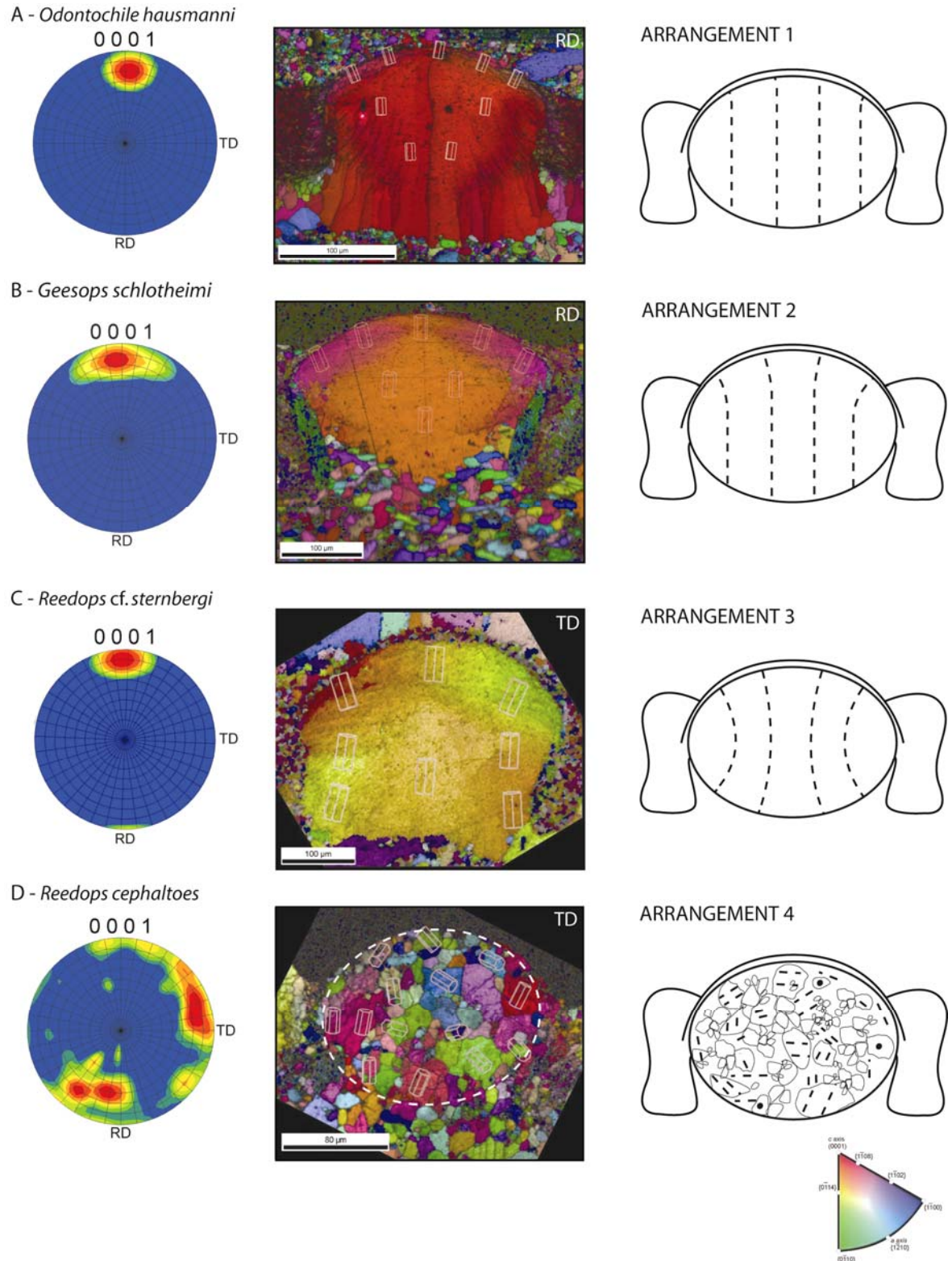


Figure 5.25 - Microstructure in the lenses of schizochroal eyes, determined using EBSD. Pole figure texture plots, EBSD maps and corresponding schematic diagrams in which dashed lines represent *c* axis orientation. Superimposed crystal models on the EBSD maps also show *c* axis orientation. A. *Odontochile hausmanni* (OB24RB), B. *Geesops schlotheimi* (G33R), C. *Reedops cf. sternbergi* (RB13L) and D. *Reedops cephalotes* (RB14L). Crystal orientation in the cornea has not been determined as crystal size is below the detection limits of EBSD. White letters the corners of the maps indicates the reference direction of the EBSD map (section 2.7.4.2). Grid line divisions on pole figures represent 10 °.

Microstructural arrangement 4: The lens consists of numerous crystals ranging from $<10\ \mu\text{m}$ to over $40\ \mu\text{m}$ in size. The crystals show no preferred orientation in any part of the lens (Figure 5.25D).

The angle by which the c axis varies across a lens in microstructural arrangements 1-3 generally remains constant across all lenses of an eye but there are instances where a difference of up to 20° is present within the set of lenses, and this is due to the slight differences in sectioning angles and depths on the curved eye surface (section 3.2.1).

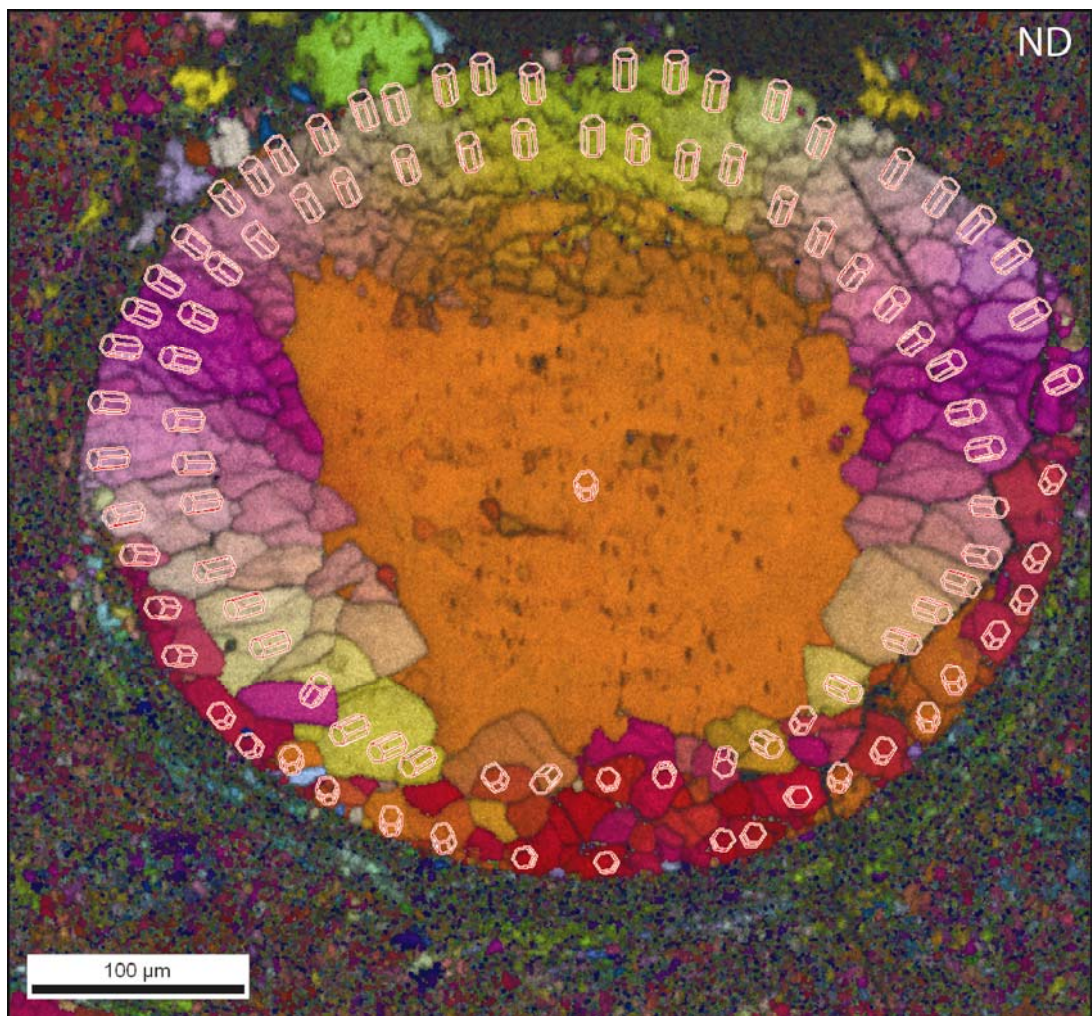


Figure 5.26 - Tangential view of the microstructure in the lenses of schizochroal lenses. EBSD map of a lens of *Geesops schlotheimi* (G35). Comparison of this view with the horizontal view (Figure 5.25B) enables a 3-dimensional understanding of lens microstructure. White letters in the top right indicate the reference direction of the EBSD map (2.7.4.2).

No one microstructural arrangement is unique to a particular taxon. Also more than one arrangement can be present within any given taxon, and indeed within a single specimen. Table 5.4 provides a summary of these findings.

Table 5.4 - Taxonomic distribution of microstructural arrangements in schizochroal lenses. Microstructure determined using EBSD orientation maps. Note that several species have lenses of more than one arrangement. *Boeckops boeckii* is the only species that has lenses solely of arrangement 3.

SECTION CODES	SPECIES	MICROSTRUCTURE ARRANGEMENT			
		1	2	3	4
LB1C	<i>Ananaspis macdonaldi</i>		X		
AM65	<i>Austerops smoothops</i>		X		
BM98	<i>Barrandeops forteyi</i>	X			
PM28	<i>Barrandeops granulops</i>		X	X	
BM60, BM61	<i>Barrandeops cf. granulops</i>		X		
BB3a, BB3aR, BB3b	<i>Boeckops boeckii</i>			X	
CE51, CE52, CE53	<i>Chasmops cf. musei</i>	X			
CE43	<i>Chasmops sp.</i>		X		
TS1, TS3	<i>Dalmanites sp.</i>	X			
E21R, E21L, E22B, E22T	<i>Eldredgeops rana</i>		X		
EE45, EE46	<i>Estoniops exilis</i>		X		
G29 – G42R	<i>Geesops schlotheimi</i>		X		
GG58	<i>Geesops sparsinodosus</i>		X	X	
IE48R	<i>Ingriops sp. nov.</i>	X			
IE47	<i>Ingriops trigonocephalus</i>	X			
OB24R, OB24RB, OB24L, OB24LB	<i>Odontochile hausmanni</i>	X			
PB8	<i>Phacops superstes superstes</i>		X		
PM27, PM55	<i>Phacops sp.</i>		X	X	
RB12	<i>Reedops bronni</i>		X		
RB7, RB14L	<i>Reedops cephalotes</i>		X	X	
RB2, RB2B	<i>Reedops cf. cephalotes</i>		X	X	
RB13L	<i>Reedops cf. sternbergi</i>		X	X	
RB1L	<i>Reedops prospiciens</i>		X		X

Tolerance angle maps (section 2.7.4.3) (Figure 5.27) highlight very subtle changes in the c axis orientation in the lenses that are not easily seen in EBSD orientation maps (Figure 5.25). Arrangement 1 (Figure 5.27A) is similar to arrangement 3 but with more subtle orientation variation, this probably

represents the original microstructure of the oval lenses in which it is restricted to. Arrangement 2 (Figure 5.27B) is simply a variation of arrangement 3 in which the variation in *c* axis orientation in the base of the lens has been overprinted to some extent during diagenesis. Note that the variation is *c* axis orientation along the lens bases extends into the epitaxial cements below Figure 5.27. Dissolution textures along the base of the lens in Figure 5.27C must post-date cement growth as the cement is in crystallographic continuity with the lens calcite above the dissolution pits.

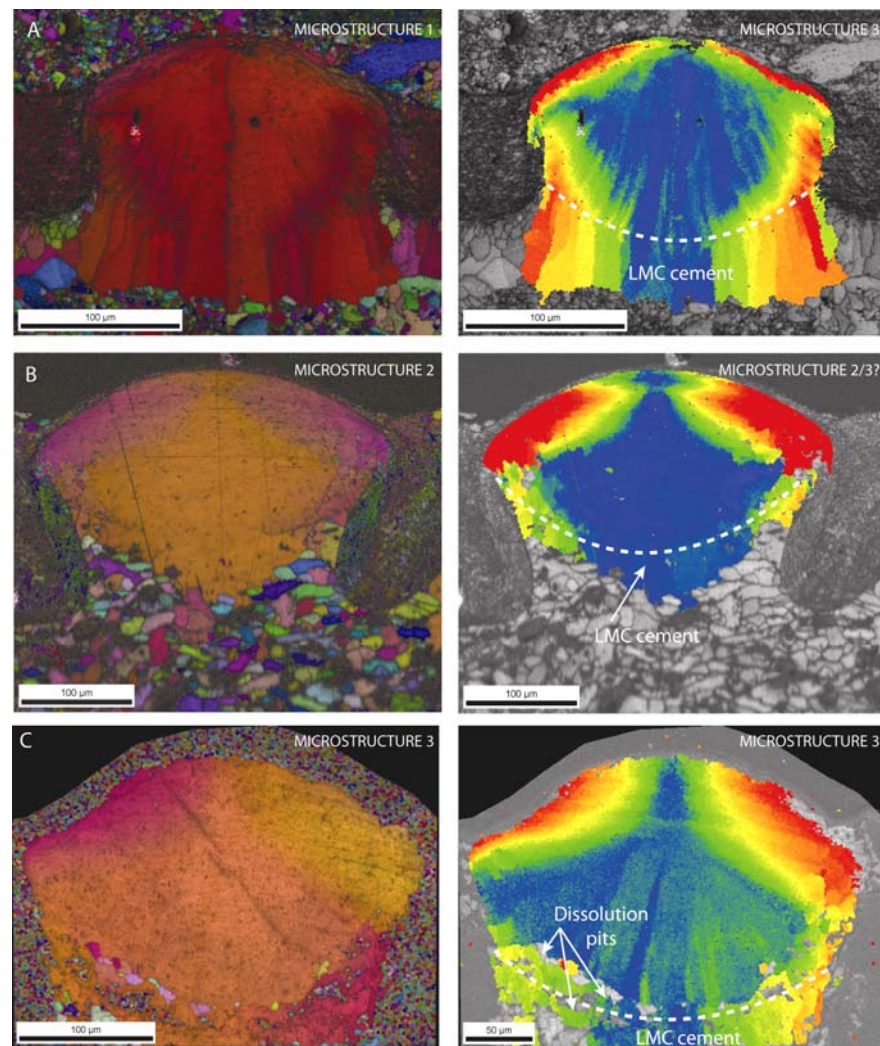


Figure 5.27 - Microstructure of lenses and cements identified by tolerance angle mapping. EBSD orientation maps (left) and corresponding tolerance angle maps (right) (section 2.7.4.3) of A. *Odontochile hausmanni* (OB24RB) B. *Geesops schlotheimi* (G33R) and C. *Barrandeops granulops* (PM28). Tolerance angle maps highlight variation of *c* axis orientation along the lens base and underlying cement (blue-red= minimum 15° variation of *c* axis). These variations were not observed in either TL images (section 5.1.1.1) or EBSD maps (section 5.1.6.2) in the case of B. The dashed white lines indicate the lens base.

5.1.6.2.1 The Relationships between Calcite and Dolomite in the Lenses

Understanding the relationships between calcite and dolomite is vital in determining the original chemistry of the lenses as it can provide information on the relative timing of mineral formation. There are two possibilities with regards to the formation of microdolomite in the lenses. (1) It formed during the early stages of burial (eogenesis) and synchronously with LMC from a HMC precursor or (2) the Mg was imported by fluids during mesogenesis, resulting in the dolomitisation of originally LMC lenses.

The first scenario would result in the simultaneous growth of two minerals in crystallographic continuity replacing the original HMC, the orientation of which was controlled by biomineralisation (e.g. Cusack *et al.*, 2007). The fine scale nature of this recrystallisation would be highlighted by the small size of the dolomite crystals and micro-porosity (Dickson, 2001a). This relationship would also be seen in HMC cements that have reverted to LMC plus microdolomite.

The second hypothesis involves two very separate stages of mineral formation. The initial biomineralisation process would produce the preferred/controlled orientation of calcite crystals within the lenses but later dolomitisation by ingress of fluids would result in the crystallisation of dolomites showing no preferred orientation; their size dependent on the available space created by dissolution of original lens calcite. Replacement by dolomitisation rarely results in epitaxial growth (Braithwaite, 1991).

Production of EBSD maps by indexing of Kikuchi patterns alone (section 2.7) failed to reliably distinguish the two minerals. This is due to the very similar unit-cell parameters of calcite and dolomite. To overcome this problem Chl scanning (section 2.7.5) was used to map the minerals separately, using simultaneously collected EDS data to differentiate between calcite and dolomite. Lenses, HMC cements and dolomitised limestone were analysed by EBSD and subsequently Chl scanned to test the above hypotheses (Figure 5.28). Partitioning of the two sets of data and processing each individually reveals the relationships between the two minerals.

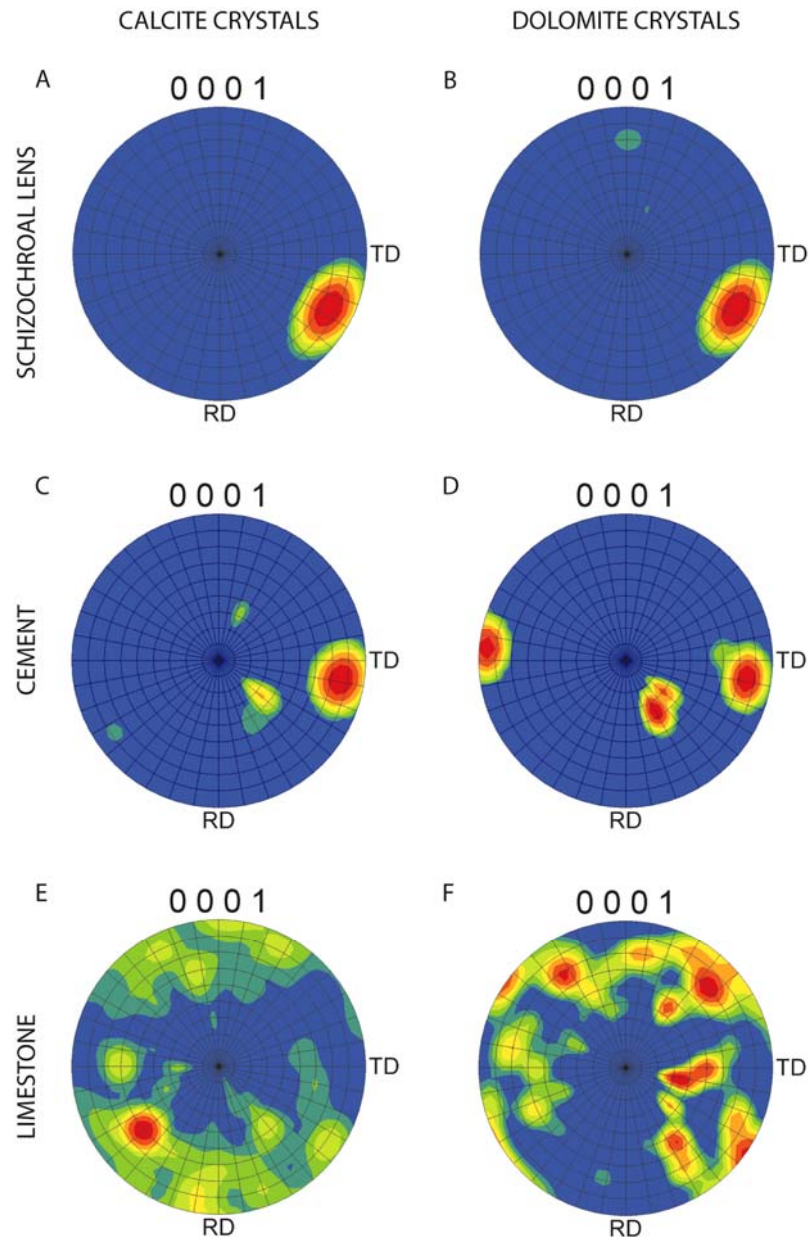


Figure 5.28 - Orientation relationships of calcite and dolomite crystals in lenses, cements and limestone.

Texture plots showing the orientation relationship between calcite and dolomite crystals in: A & B. schizochroal lenses of *Boeckops boeckii* (BB3aR); C & D. HMC cement surrounding the lenses; and E & F. a partially dolomitised limestone from the upper Permian Raisby Fm, Northeast England. Note the very similar orientations of the minerals in the lenses and HMC cement. The limestone does not show this relationship. Line divisions represent 10°.

ChI scanning shows that the dolomite crystals in the lenses have precisely the same orientation as the host calcite (Figure 5.28A and B) indicating that they formed at the same time, and that the Mg in the microdolomite originated from the lens itself rather than by dolomitisation. This mineral relationship is also seen in the cement surrounding the lenses, indicating that it too was originally HMC (Figure 5.28C and D). The dolomitised limestone, analysed for comparison, does not show this relationship; dolomite crystals display no preferred orientation (Figure 5.28E and F). The calcite in the limestone also lacks

preferred orientation but has a significantly different range of orientations to the dolomite (Figure 5.28E and F), which is expected as the two minerals formed at different times; dolomitisation occurs during diagenesis, not by simultaneous precipitation with calcite (e.g. Braithwaite, 1991).

The Moroccan trilobites (details of sample localities in Appendix A), which have undergone silicification of the exoskeleton (section 5.1.5.1.1), have been sourced from a locality in which dolomitisation is known to have occurred (Klug *et al.*, 2009). ChI scanning of these specimens confirms that the dolomite crystals have the same orientation as the lens calcite. This indicates that the lens dolomite formed at the same time as the calcite and is therefore of primary lens origin; EDS mapping showed little effect of dolomitisation in the matrix in which these trilobites are preserved (section 5.1.5.1.1).

5.1.6.2.2 Misorientation of the radial fringe

The microstructure of the radial fringe can be revealed by plotting misorientations approximately perpendicular to the crystal *c* axis; thus, showing rotation about the plane that is 90° to the *c* axis. Within the gradually varying radial fringes, crystal orientation varies from point to point usually by < 1° - 3° (Figure 5.29A). Lenses that have a coarse-grained radial fringe have a very different profile; there is an orientation difference between grains, but little or none within a grain (Figure 5.29B). It is likely that these two different misorientation profiles (Figure 5.29) represent contrasting scales of recrystallisation in the lenses, the former indicating fine scale recrystallisation and the latter indicating coarser recrystallisation with a greater degree of overprint on the original fabric. If the 'smooth' fringes do represent original microstructure, then the low angle of misorientation is likely to represent the presence of subgrains within the lenses, as visible grain boundaries tend to be >10°. This may have implications on the growth mechanism of the lens; a single calcite lens consists of a network of sub-crystals that are fused together i.e. the meshwork of trabeculae identified by Miller and Clarkson (1980).

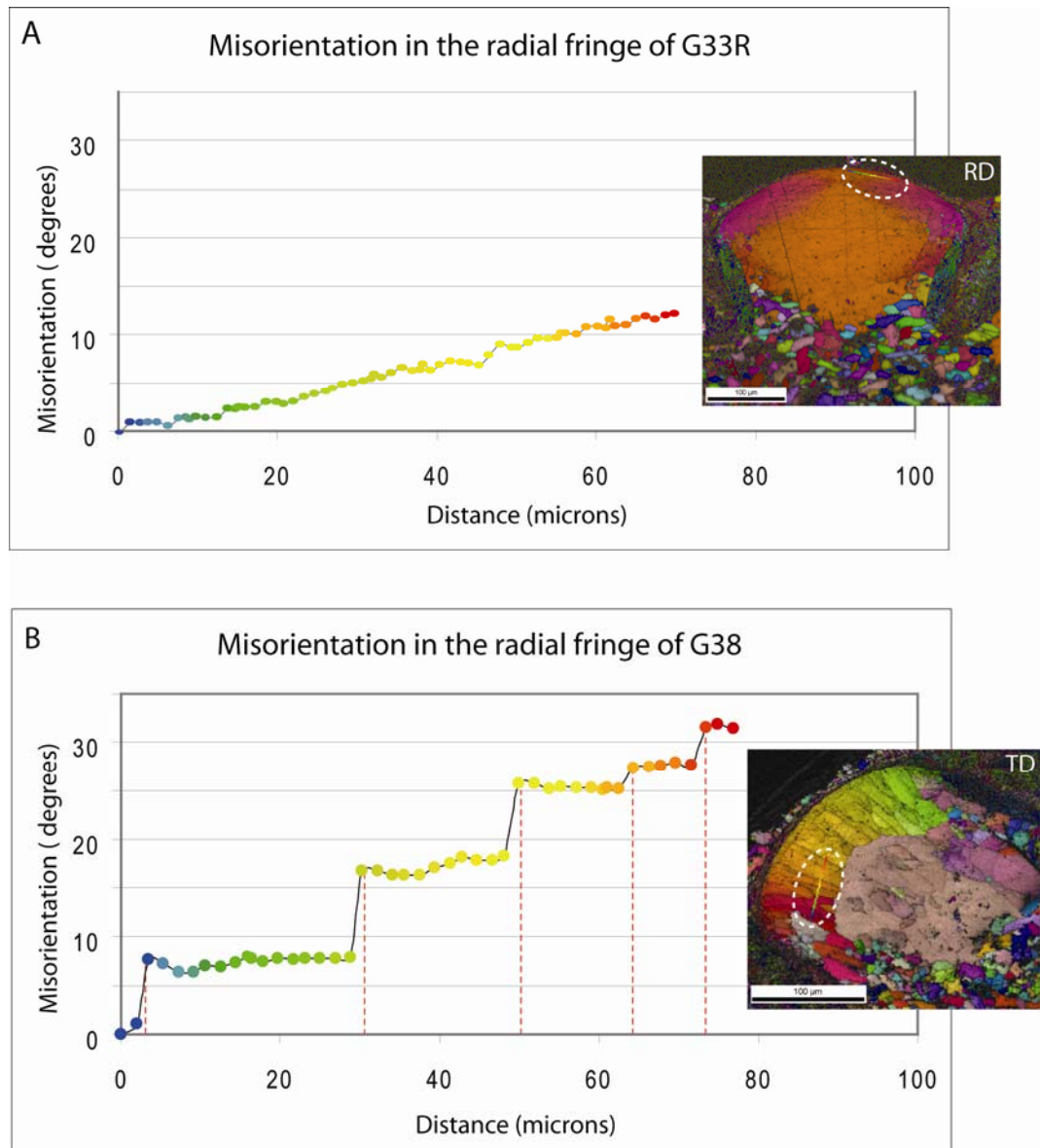


Figure 5.29 - Misorientation in the ‘radial fringe’ of lenses in schizochroal eyes.

A. in the smooth and **B.** the coarse-grained radial fringe of *Geesops schlotheimi* (sections G33R and G38 respectively). Differences in rate of change in orientation are likely to the result of differences in lens sizes and sectioning depths. The inset images show the line along which misorientation was measured (blue – red). The colour of the points on the graphs corresponds to the position along this line. Red dashed lines in **B** indicate the boundaries between grains. White letters indicate the reference direction of EBSD scans.

The disparities in *c* axis splay and depth of the radial fringe between specimens may be due to lens shape, i.e. circular lenses will display a different *c* axis splay compared to that of oval lenses as a result of different surface curvatures, as has been identified for trabeculae (Kaesler, 1997) (section 1.5.4, Figure 1.22). This also explains the variations in *c* axis splay of up to 20° within a sample: lenses cut at slightly different depths will reveal different lens profiles and therefore lens shapes and surface curvatures (section 3.2.1.1), this was seen in TL images of *Dalmanites* sp. (Figure 5.1).

5.1.7 EBSD of the Interlensar Sclera

EBSD maps confirm that the sclera consists of three ‘strips’ or pillars. The crystal orientation within each pillar is generally constant but varies considerable between pillars (Figure 5.30). Crystal orientation is approximately perpendicular to the fabric within the sclera. EBSD confirms the presence of many small crystals that are of the order of 1-5 μm in length. This shows that the sclera differs from the rest of the exoskeleton in which changes in crystal orientation, if present, are seen in layers parallel to the external surface rather than perpendicular to it (Klajmon, unpublished).

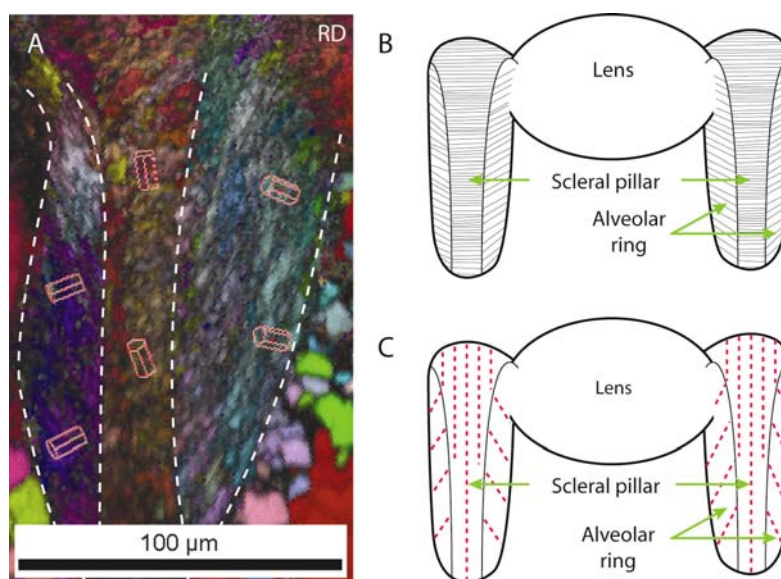


Figure 5.30 - Microstructure of the sclera determined using Electron Backscatter Diffraction. A. EBSD map of the sclera with superimposed models to show *c* axis orientation. White dashed lines highlight the three pillars within the sclera. B and C. schematic diagrams illustrating the direction of the crystal growth fabric and the *c* axis orientation respectively. White letters in A indicate the reference direction of the EBSD map.

5.1.8 Sublensar Structures

Considerable information has been obtained from analysis of the lenses but little is known about the soft tissues beneath them *in-vivo*. Analogy with modern arthropods suggests that a series of photoreceptive cells lay at some distance beneath the lenses; these may have been in direct contact with the lens, ‘lining’ its base, or alternatively may have been positioned at the base of an ommatidial capsule, consisting of cells and pigment (Land and Nilsson, 2002 pp. 100, 128). The former is found in insects with simple eyes (ocelli) rendering the latter the more likely type in trilobites as they had compound eyes.

Clarkson (1967), Miller and Clarkson (1980) and Bruton and Haas (2003a) reported sublensar structures in schizochroal eyes and termed them cones, cylinders and mesodermal capsules respectively. Bruton and Haas (2003a) suggested that the mesodermal capsule identified in their study may have housed a retina with numerous photoreceptors or a series of rhabdoms (Figure 5.31A). Schoenemann *et al.* (2008) and Schoenemann and Clarkson (2010) reported a stalk-like structure protruding from the base of a capsule in *Geesops schlotheimi* (Figure 5.31B), determined by 3D-X-ray tomography and suggested that this may be some kind of ‘efferent’ structure of a light sensing unit (i.e. a nerve or similar structure that carries impulses away from the visual unit). Images of this feature are however somewhat unconvincing (Figure 5.31B). It would be informative to image these specimens using light microscopy to clarify the presence of these structures.

Despite the numerous trilobite taxa analysed in the present study and the range of localities, and therefore diagenetic histories, from which they were obtained, no intralensar structures or any other preserved soft parts were identified.

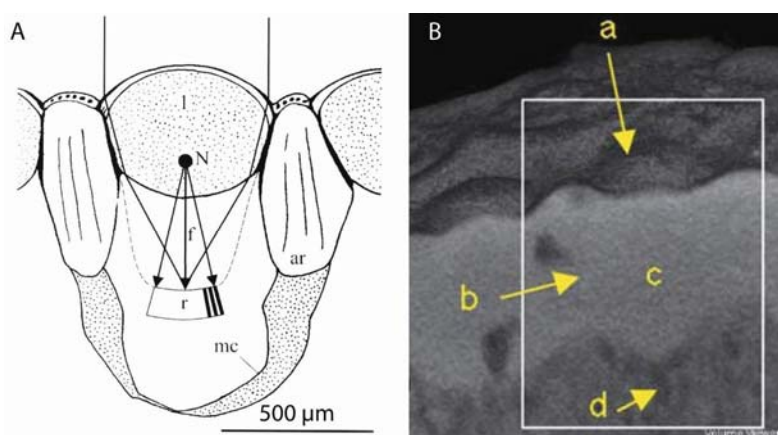


Figure 5.31 - Sub-lensar capsules in the schizochroal eyes of *Geesops*.

The interpreted location of the retina in the mesodermal capsule of *Geesops sparsinodus* (Bruton and Haas, 2003a, figure 4). 3D- µCT scan showing a possible ‘efferent’ or light directing structure below the lens(d) in the eye of *Geesops schlotheimi*: a indicates the lens, b the intralensar sclera and c the visual unit (Schoenemann *et al.*, 2008, figure 1c).

Many of the lenses studied have calcite overgrowths extending from the base of the lens into the matrix (Figure 5.32A), these cements could be misinterpreted as sublensar structures but are probably the result of nucleation and growth of crystals very soon after the decay of the internal soft parts. Sections through *Ananaspis macdonaldi* and *Odontochile hausmanni* (Figure 5.33) show that crystals grew into ‘free’ space. It is not clear if the space in either of these

examples was 'free' owing to the former presence of soft parts preventing matrix infill. If this was the case and these soft parts decayed after matrix infill then the shape of the cement overgrowths in *Ananaspis* and *Odontochile* would suggest the presence of an ommatidial-type capsule and an ocellar-like capsule respectively.

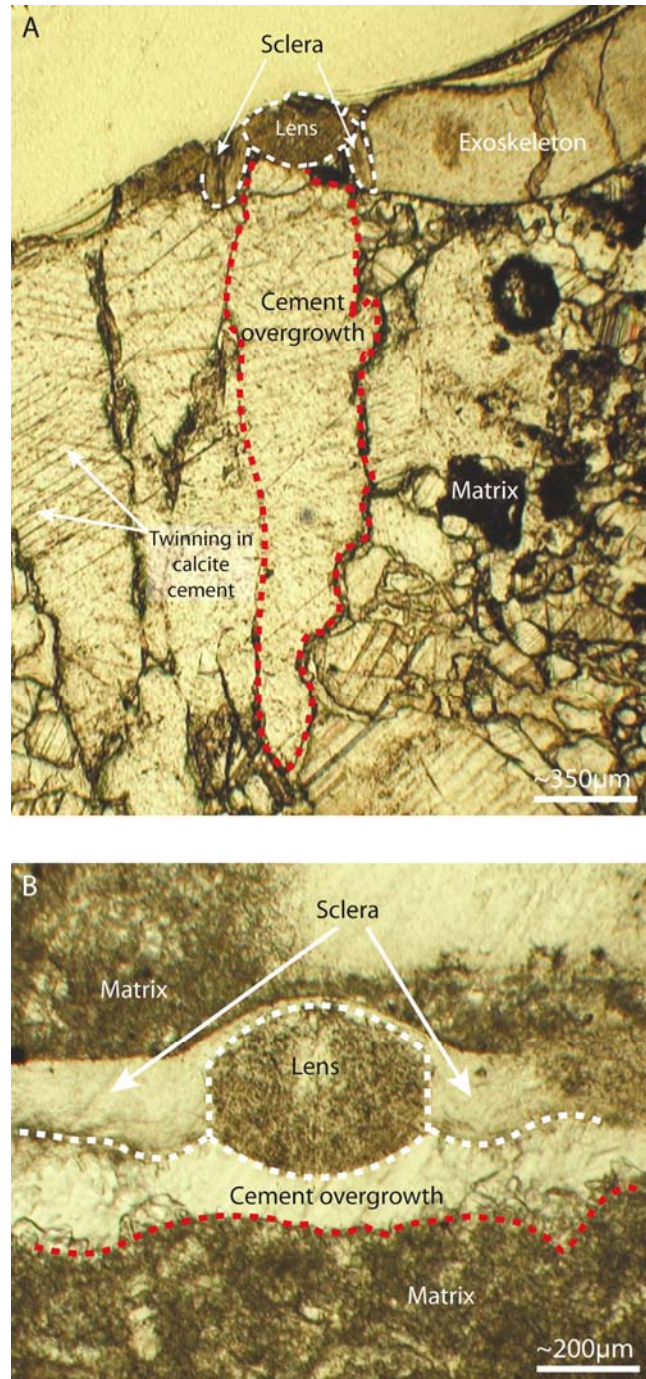


Figure 5.32 - Sub-lensar calcite cements in schizochroal eyes. Cements that have grown epitaxially on lenses, A. *Ananaspis macdonaldi* (LB1C) and B. *Odontochile hausmanni* (OB24RB). In B the cement has produced a geopetal structure due to formation after sediment infill. White lines indicate the extent of the lenses and surrounding sclera. Red dashed lines show the extent of the calcite cement.

5.2 Interpretation

5.2.1 Calcite Diagenesis

One of the primary aims of this study is to determine whether the microstructures revealed through TL, EBSD and TEM, and the chemical signatures identified by EDS and EPMA are primary, and then representative of original structures, or solely the products of neomorphism during diagenesis.

5.2.1.1 Neomorphism – Replacement and Recrystallisation

Neomorphism, as described by Folk (1965), involves two main processes, recrystallisation and replacement. Recrystallisation produces a change in fabric, without altering mineralogy; this can result in formation of larger crystals (aggrading neomorphism) or smaller crystals (degrading neomorphism). Replacement describes a change in chemistry. Both neomorphic reactions are mediated by water and are termed ‘wet processes’. Despite diagenesis, the schizochroal lenses remain, for the most part, composed of calcite indicating that changes in the lenses are solely due to the process of recrystallisation.

5.2.1.1.1 Recognising Neomorphism

Several changes occur in calcium carbonate rocks during neomorphism making it possible to determine if the rock chemistry has been altered. These changes include (from Tucker and Wright, 1990): formation of microporosity; formation of syntaxial overgrowths and burial cements; and conversion of high-magnesian calcite (HMC) to low magnesian calcite (LMC) + microdolomite. Dickson (2001b) recognised similar chemical changes in the plates of modern echinoderm skeletons (originally ~14 mol% MgCO_3) when they were subjected to heating at 300°C for just 20 hours; subsequent heating did not result in any further chemical changes. In addition, formation of microporosity was noted (Dickson, 2001b). Lohmann and Meyers (1977) commented on the presence of microdolomite in echinoderm grains, arguing that their restricted existence within the grains implies an autochthonous source and therefore an HMC precursor. These studies, and in particular Dickson (2001b), highlight the ease with which an HMC precursor will ‘split’ into calcite and dolomite. This ‘fractionation’ may provide an explanation for the presence of microdolomite in

the schizochroal lenses if these were either partly or wholly composed of HMC *in-vivo* (Lee *et al.*, 2007a).

5.2.2 Determining Original Lens Construction

The task of determining whether microstructure and chemistry are primary or diagenetic artefacts is less of an obstacle in organisms such as echinoids, which can be studied in both fossil and recent forms (e.g. Dickson, 2001b). With no close modern analogue for the schizochroal eye, determining *in-vivo* chemistry and microstructures of the lenses must rely heavily upon comparisons to the sclera and the surrounding matrix and/or cements where present. The occurrence of intralensar structures and the orientation relationships between the minerals in the lens, sclera and cements sheds light on the formation mechanisms and timing of each of these structures.

5.2.2.1 Microstructure of lenses

Variability in the microstructure of lenses is present at the genus and species level, and even within a single specimen (section 5.1.6.2). There is little evidence of taxonomic control on lens microstructure (section 5.1.6.2, Table 5.4) unless the variation seen across the eye of a single specimen represents an original characteristic. Tolerance angle maps (Figure 5.27A) show that lenses which appear to have microstructure arrangements 1 (identified by TL and EBSD orientation maps) are similar to those with microstructure 3 but with a more subtle variation in *c* axis orientation. Tolerance angle maps also show that lenses with microstructure 2 also have some variation in *c* axis orientation in the peripheral areas (Figure 5.27B).

Study of the epitaxial cement overgrowths on the lenses also indicates that microstructure pattern 3 is most representative of the original lens microstructure. In most instances these epitaxial cements are of LMC, indicating formation during burial diagenesis. In some thin sections (of different species from different localities), the cement beneath the lens has the appearance of HMC that has converted to LMC and MD, i.e. significant turbidity in TL and radiaxial fibrous extinction (see Bathurst, 1971) in crossed-polarised light. This original HMC chemistry may indicate that the calcite grew at a very early stage in diagenesis when interaction with Mg-rich seawater, found in the uppermost

layers of the sediment pile only, was possible. As these epitaxial HMC overgrowths formed prior to neomorphism they will have ‘locked in’ the crystallographic orientation of the original host lens (Figure 5.33A). Tolerance angle maps showed that this is also the case for LMC cements (Figure 5.27) indicating that although this LMC probably crystallised later than HMC, its growth may have preceded lens recrystallisation (Figure 5.33B).

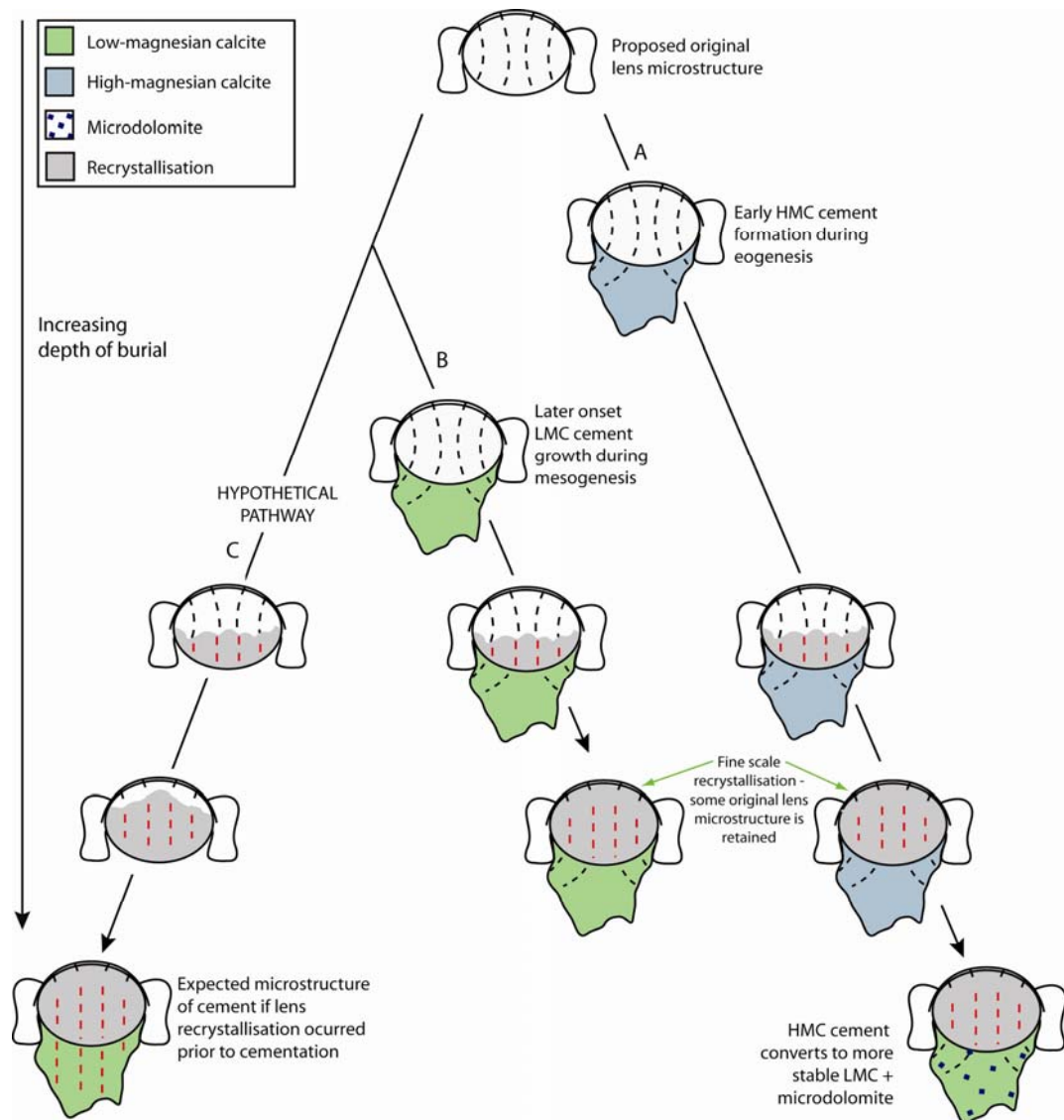


Figure 5.33 - Relative timing of epitaxial cement growth and diagenetic change in schizochroal lenses.

A. HMC and B. LMC cementation has occurred prior to diagenetic changes in the lenses; the cement adopts the same orientation of the lens, which is later recrystallised losing all or part of the original microstructure. C. shows the expected microstructure should lens recrystallisation occur prior to cement growth. Grey areas represent secondary lens calcite. Red dashed lines indicate secondary c axis orientation adopted after recrystallisation. This diagram relates to lenses with microstructural pattern 1 and 2 only as lenses showing pattern 3 have retained their original structure, and those with pattern 4 have completely lost original microstructure. The assumption that lens alteration occurs from the lens base up is based on the alteration gradient seen in *Phacops* sp. (section 5.1.5.1.1). Lens chemistry has been omitted for simplicity but it discussed in the following section.

EBSD also highlighted variation in crystal size between lenses (section 5.1.6.2.2); lenses displaying the same overall crystal arrangement in terms of *c* axis orientation can still exhibit differences in grain size. Lenses of *Geesops schlotheimi* show this trend well. Although the lenses conform to model B in Figure 5.25 (radial fringe underlain by uniformly orientated calcite), some consist of a series of small micron-scale sub-crystals that result in a gradual change in the *c* axis orientation, while other lenses consist of a relatively small number of coarser grains up to several tens of microns in size. In the latter, *c* axis orientation varies between grains but is uniform, or at least has a very narrow range, within a grain. The formation of this coarse-grained radial fringe may be the result of aggrading neomorphism (see Folk, 1965) (section 5.2.1.1.1) on an originally 'smooth' fringe (Figure 5.34a-c), suggesting that these variations in microstructure may simply be the result of diagenesis-induced degradation of a single original microstructure (Figure 5.34a). An extreme case of this degradation would result from total dissolution and recrystallisation of the lenses and would lead to complete loss of original structure and formation of crystals lacking preferred orientation (Figure 5.34e); this extreme degree of alteration is evident in lenses of a *Reedops cephalotes* specimen (RB14L) (Figure 5.34D inset). Within a single eye of this specimen, both end member models B and D from Figure 5.25 (section 5.1.6.2) are present; this shows that microstructure arrangement 4 (section 5.1.6.2) is not original.

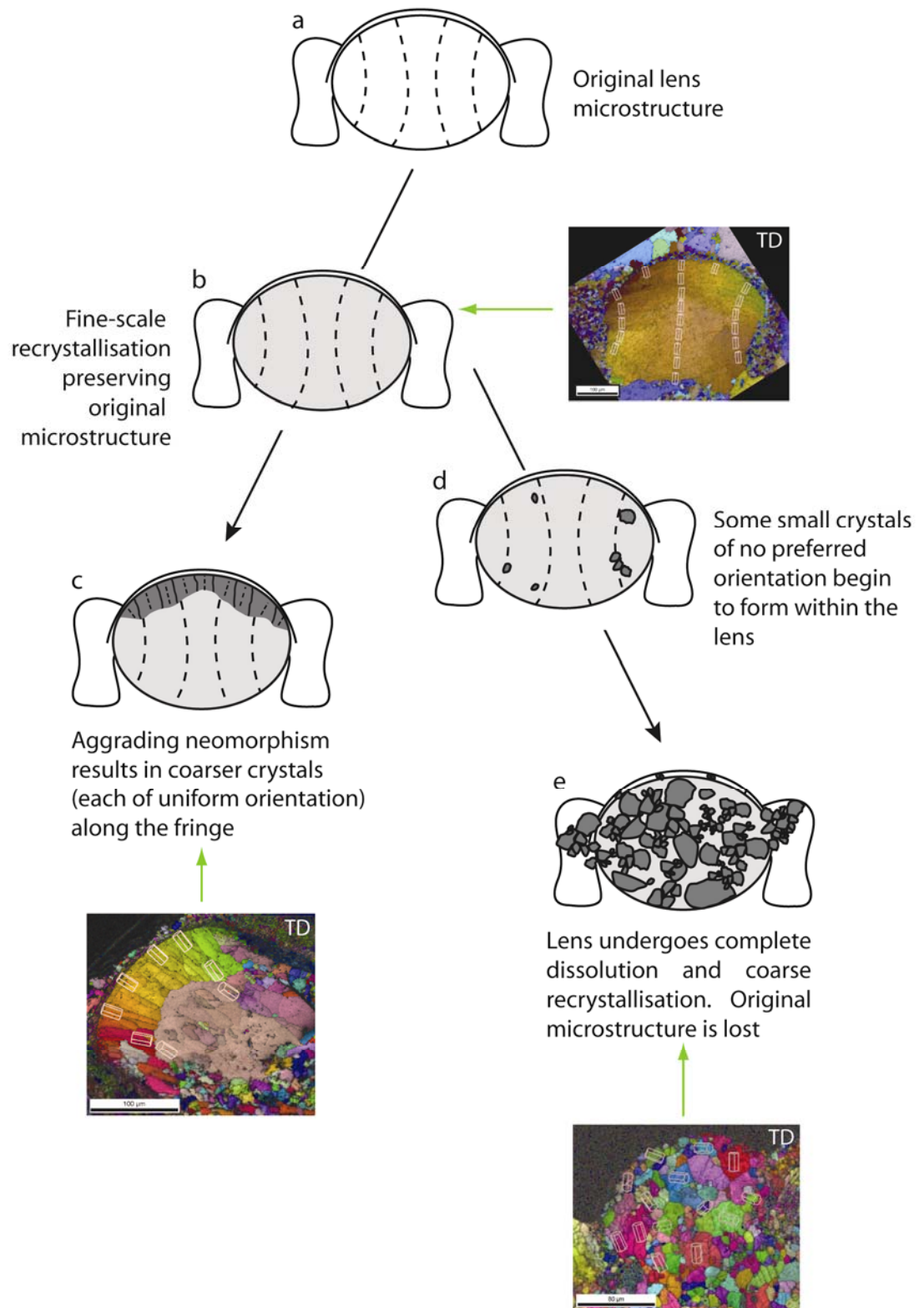


Figure 5.34 - Alteration of microstructure during diagenesis in lenses of schizochroal eyes. All patterns originated from a single original microstructure (a). The most extreme case being coarse recrystallisation (e), in which the replacement grains show no preferred orientation. Aggrading neomorphism (c) is seen along the radial fringe of some lenses. Grey shading indicates the extent of lens recrystallisation. Corresponding EBSD scans are of *Reedops* cf. *sternbergi* (RB13L), *Geesops schlotheimi* (G38) and *Reedops cephalotes* (RB14L) for stages b, c and e respectively. White letters indicate the reference direction of EBSD scans.

5.2.2.2 Chemistry of Lenses

Although EDS indicates that many lenses are rich in Mg, which occurs in microdolomite crystals, such crystals, as well as the pores now present (section 5.1.1.2 and 5.1.3.2), cannot be original as they would have significantly inhibited the transmission of light through the calcite and therefore the ability of the lens to function. In order to determine how and when the microdolomite formed, its occurrence and relationship with the adjacent calcite has been studied.

Lens chemistry shows a considerable range (section 5.1.5.1). Magnesium distribution patterns vary between lenses of different genera and species but significant differences are also present within an eye. *Dalmanites* sp. is a prime example of this; several lenses have very distinct intralensar features but within the same row there are lenses of uniform turbidity which corresponds to homogeneous distribution of Mg throughout the lenses (section 5.1.1.1).

The patterns identified in Mg distribution (section 5.1.5.1, Figure 5.17) could each represent several original configurations. However, it seems more plausible that the patterns were formed as the result of differing styles and degrees of diagenetic alteration of a single original configuration; that of a HMC intralensar bowl and core within an otherwise lower magnesian calcite lens (Figure 5.35). It is unlikely that the upper lens unit consisted of pure LMC as microdolomite has been found within it, in some cases, in high concentration (section 5.1.5.2). Diagenesis resulted in the dissipation of the HMC structures; the most extreme instance being where, in a closed system, Mg became homogeneously resident in microdolomite crystals across the lens (Figure 5.35e) or, in an open system, Mg was completely lost to the surrounding environment (Figure 5.35f). Optically clear intralensar structures (section 5.1.1.1, Figure 5.2) represent areas of the lens that were dissolved and replaced by LMC (Figure 5.35i). This dissolution occurred as a result of these areas containing highest concentrations of Mg; dissolution is a sequential process, areas of highest Mg concentration are altered first (Wollast and Reinhard-Derie, 1977).

Further evidence of HMC intralensar structures has been found in the cases of *Ingriops* sp. nov., *Barrandeops granulops* and *Geesops schlotheimi*. It is clear from the shape of the *Ingriops* lenses (e.g. Figure 5.35h) that they have not been

preserved intact. The basal surfaces of the lenses are very similar in shape to the sinuous second surface of Huygens' model of an aplanatic lens (section 1.5.2.3); this leads to the conclusion that the intralensar bowl has been lost prior to matrix infill (Figure 5.35g-h), as was noted by Clarkson (1967) in a specimen of *Phacops* [now *Eldredgeops*] *rana*. Again, the most feasible hypothesis for such a process is the preferential, early dissolution of the intralensar bowl due to its high magnesian concentration.

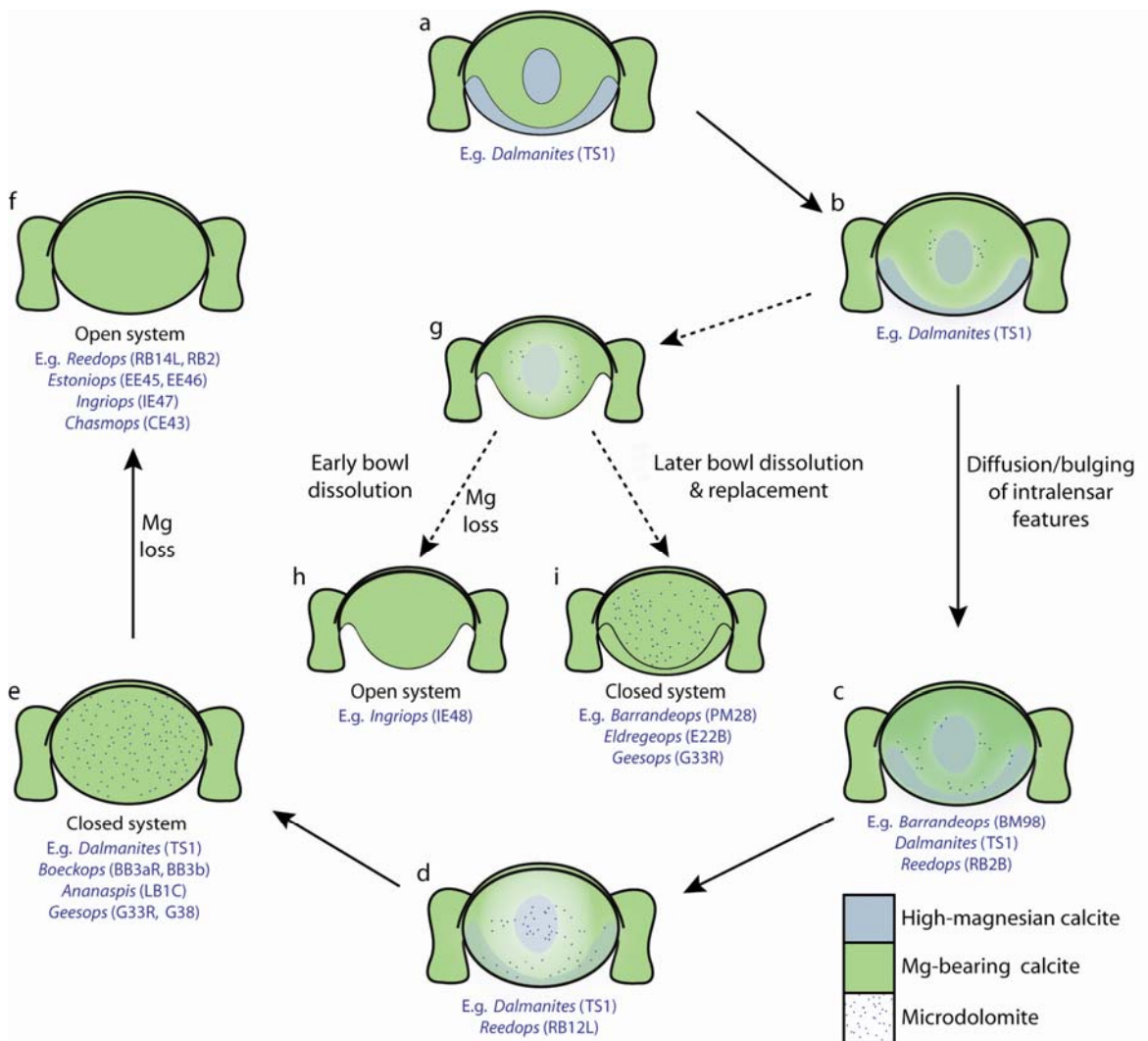


Figure 5.35 - Changes in chemistry during diagenesis in lenses of schizochroal eyes. Gradual diffusion or 'bulging' of the intralensar bowl and core eventually result in a lens with homogeneous Mg distribution (f). Early dissolution of the intralensar bowl leads to either an 'incomplete' lens (h), or one with a secondary LMC bowl (i).

A lens of *Barrandeops granulops* (PM28) displays very prominent evidence of dissolution along the interface between the lens base and the cement below (section 5.1.3.2, Figure 5.11; Figure 5.27C). The lower region of the lens is now depleted in Mg with respect to the main body of the lens. The granoblastic

texture identified using BSE imaging (section 5.1.3.2) indicates that this is due to recrystallisation of LMC in place of the originally HMC bowl. The main body of the lens also has a high concentration of Mg although this must be lower than the bowl as it has been less susceptible to dissolution. EDS analysis of a *G. schlotheimi* lens (G33R) yields similar results; in this case, both the intralensar core and bowl are devoid of Mg. These features are inconspicuous in TL and appear only as dull regions in CL (section 5.1.2.1, Figure 5.7). Both lens components appear as a single unit continuous with the cement overgrowth below (Figure 5.36). CL patterns suggest that both original structures were replaced at the time of cement formation (Figure 5.35i); the chemistry and microstructure of the cement indicate that this was during mesogenesis (Figure 5.33B).

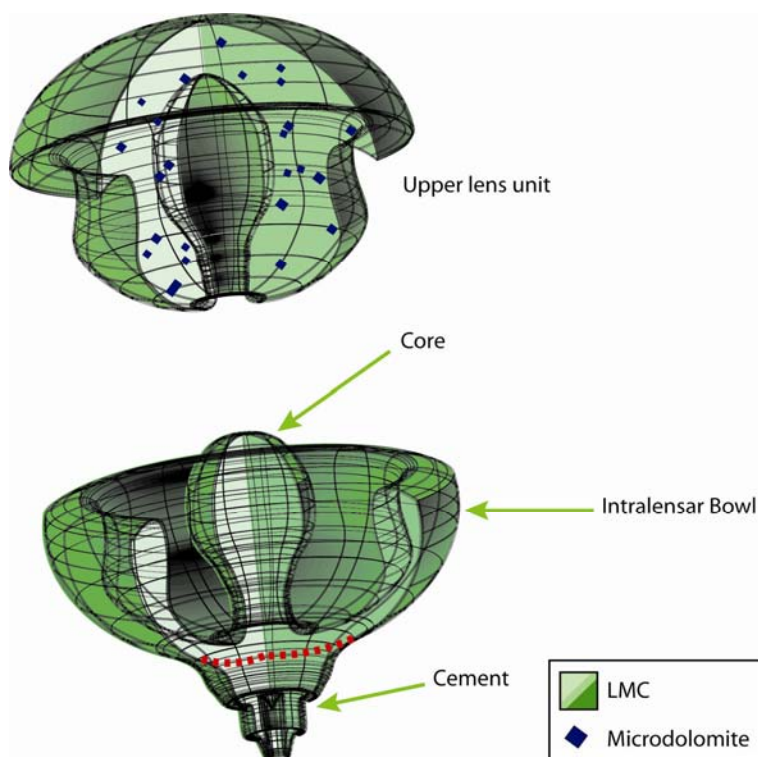


Figure 5.36 - Continuity between intralensar structures and cement overgrowth in altered lenses in schizochroal eyes.

This continuity is the result of alteration during diagenesis. Intralensar structures are preferentially dissolved due to their elevated Mg content, replacement is with LMC. The continuity of the core and bowl suggest some diffusion prior to dissolution, as these units are usually separate (section 1.5.2, Figure 1.15). The red dashed line indicates the base of the bowl.

The mechanism by which HMC converts to LMC + MD is illustrated in Figure 5.37. This process is likely to be a fluid-mediated reaction. The final combination of minerals in the lens is determined by the openness of the system. An open system (Figure 5.37b), in which there is ion transfer on a relatively large scale,

would result in iron entering the system from the host rock, the formation of large iron-rich dolomite crystals, and pyrite forming by interaction with external fluids. In a closed system (Figure 5.37c), ion transfer on a local scale would result in the formation of micro-sized dolomite crystals in a LMC host and formation of apatite crystals derived from original organic components. Blake *et al.* (1984) identified similar micro-dissolution-precipitation of primary HMC echinoderm calcite in which magnesium from the original skeleton was retained as dolomite. In practice many of the schizochroal lenses fall somewhere between these two end member states (Figure 5.37d).

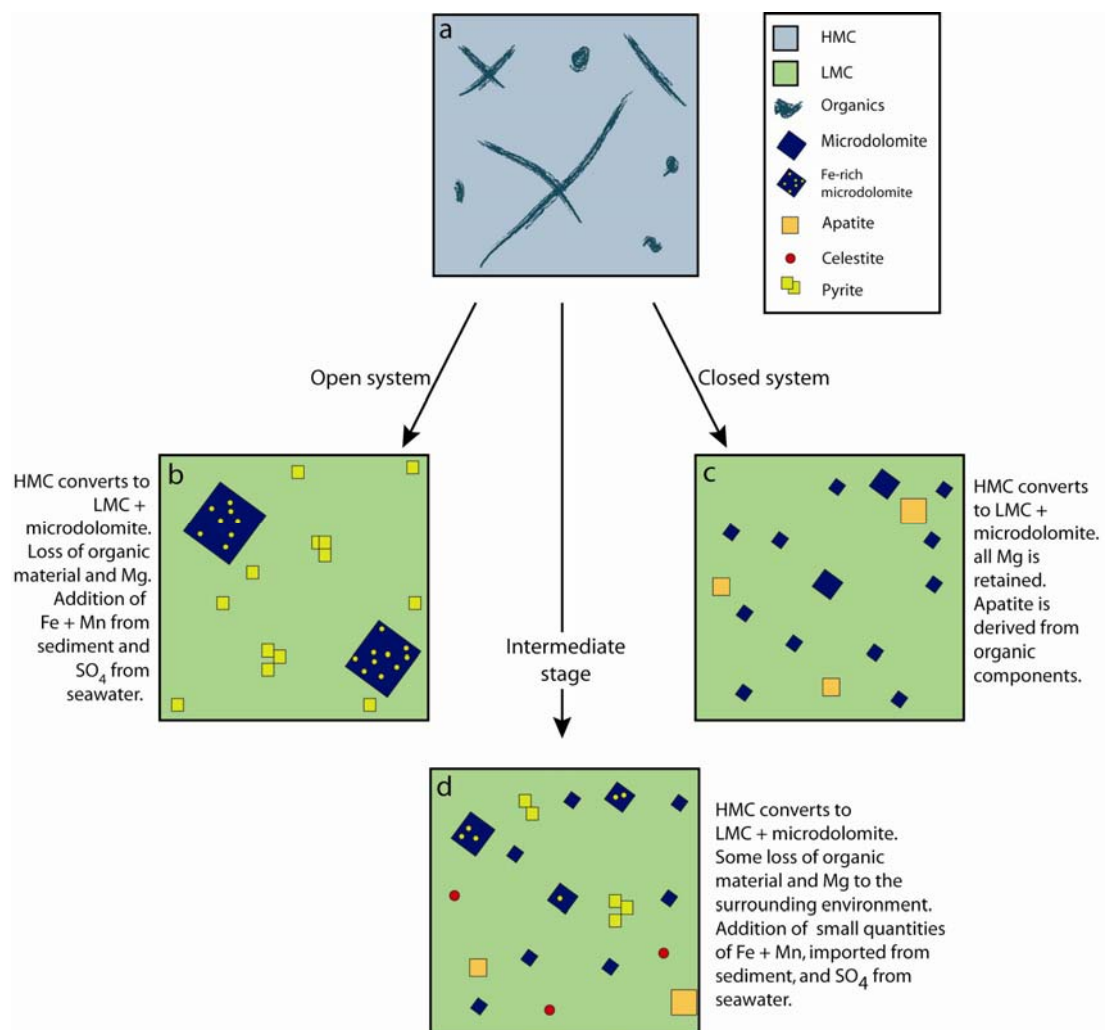


Figure 5.37 - Conversion of high-magnesian calcite to low-magnesian calcite and microdolomite during diagenesis of lenses in schizochroal eyes.

Open and closed systems result in the formation of different suites of minerals. Crystal size also gives an indication of openness of the system, as ion transfer on a large scale will produce larger crystals. Many schizochroal lenses fall in between these two states (intermediate stage d).

5.2.2.2.1 Magnesium content of the lenses

Magnesium concentrations within the lenses were quantified by EPMA (section 5.1.5.2) and point counting of microdolomite using SE imaging of etched thin

sections (section 5.1.3.3). These methods provide the concentration of Mg in the fossil lenses. In the case of EPMA, data were obtained for each lens component (upper lens, and bowl and core where present), whereas point counting data incorporate the whole lens. For the purposes of comparison, EPMA data for all lens components of a given sample were combined and the mean value calculated. Point counting data (expressed as volume%) were converted to Mol % Mg calcite using information from Bischoff *et al.* (1983) (Appendix B), which yields values very similar to the conversion graph of Dickson (2001a) (Figure 5.38).

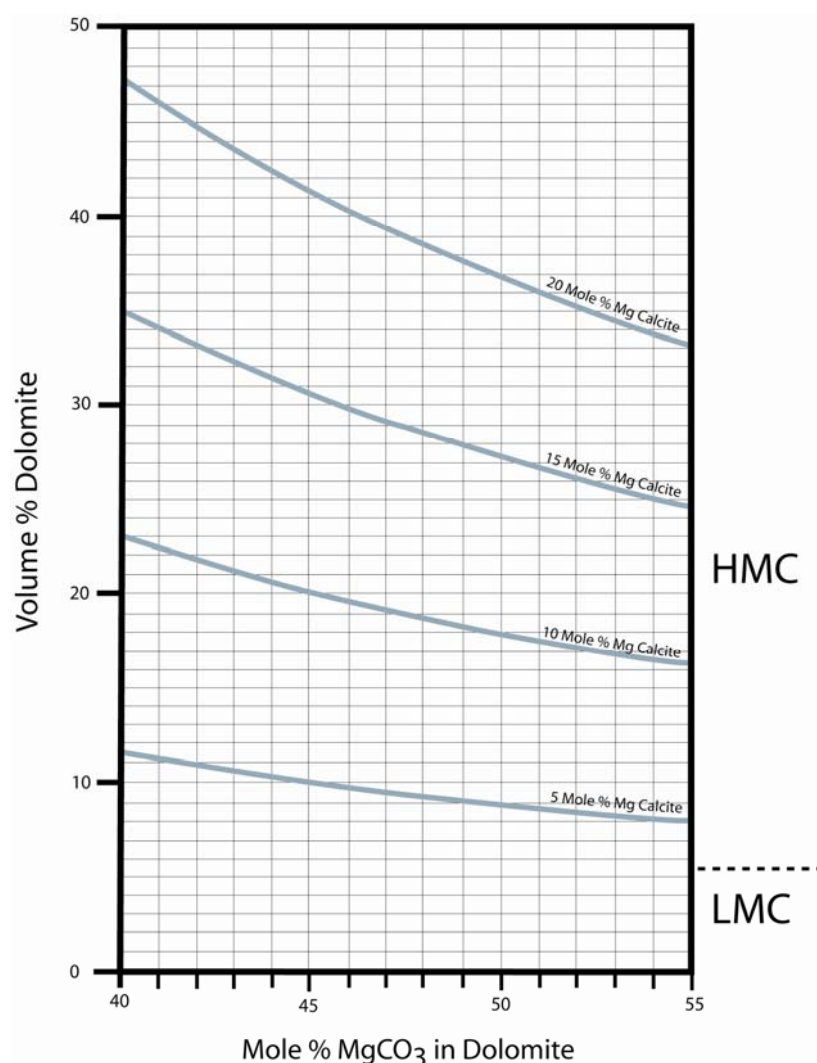


Figure 5.38 - Conversion of volume% dolomite derived by point counting to mol % MgCO₃ in precursor HMC.

This graph assumes the system to be closed. Numerous values have been reported to indicate the LMC/HMC boundary (see Bathurst, 1971 and references therein for details), here a value of 4 mol % MgCO₃ is assumed. Modified from Dickson (2001a, figure 4).

Point counting results are not consistent with the EPMA/EDS analyses detailed in section 5.1.5.2; the mean mol % MgCO₃ determined by EPMA is approximately

half of the value calculated using point counting values in all lenses (Figure 5.39). The small size of the crystals compared with the relatively large beam interaction volume on the sample, in EPMA, would result in significant ‘dilution’ of the dolomite chemistry by the surrounding LMC. Although, the acid etching process used for point counting may also have resulted in enhanced exposure of dolomite crystals. However, as all samples were etched for the same length of time using the same concentration of acid (section 3.2.1.2) values can be used for relative comparisons.

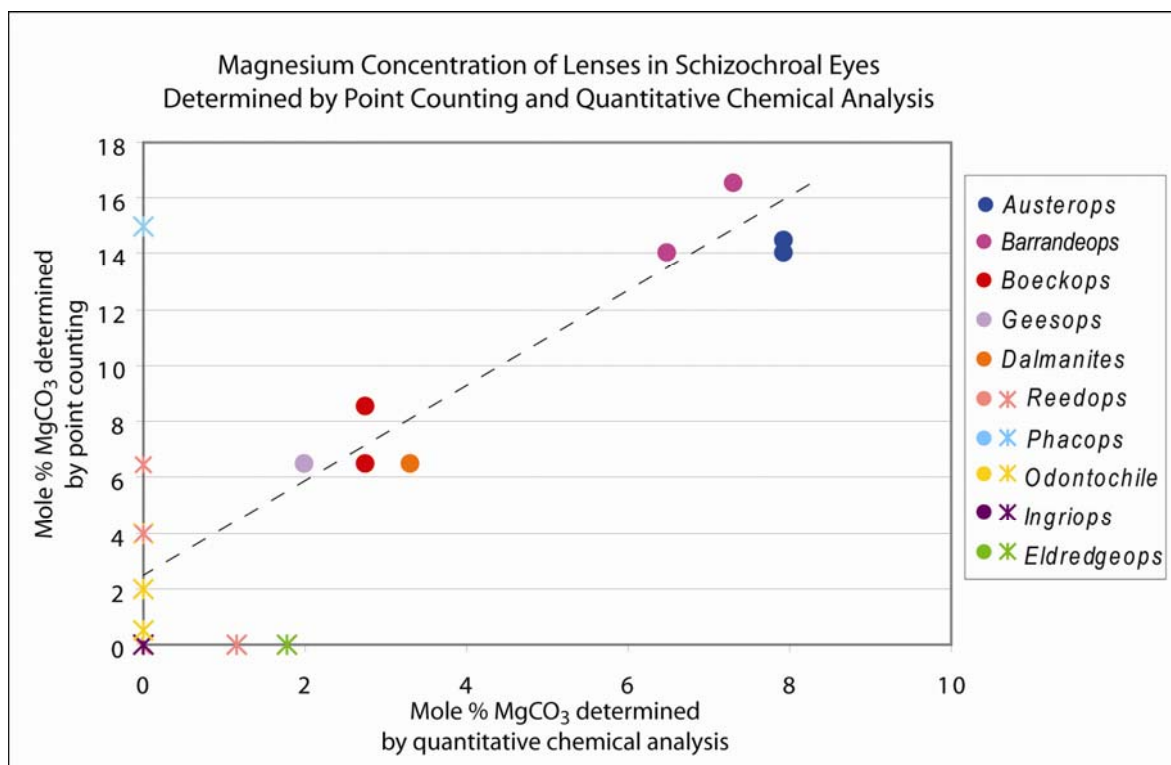


Figure 5.39 - Magnesium content of lenses in schizochroal eyes determined by point counting and quantitative chemical analysis.

Volume % dolomite obtained from point counting acid etched thin sections has been converted into mol % Mg Calcite using data from Bischoff *et al.* (1983). Quantitative chemical analyses are mean values from (Table 5.3), where lenses have intralensar features, an average of the lens, bowl and core has been used. Stars indicate samples that have been analysed by one method only – points lie on the axis of the method used.

The above data (Figure 5.39) provide an average across the whole lens and assume that the lenses acted as closed systems during diagenesis. Mg was more highly concentrated in the intralensar bowl and core *in-vivo* (5.2.2.2), so in reality these areas would have had even higher concentrations of Mg, whereas the main lens body would have had less. As many of the lenses appear to have acted as open systems to some degree (section 5.1.3.3.1), the *in-vivo* Mg concentrations in the core and bowl may have been even greater than the values determined by EPMA (section 5.1.5.2).

Based on these findings (Figure 5.13), it appears that the present Mg concentrations of *Austerops*, *Barrandeops* and *Phacops* lenses best represent the original lens chemistry; lenses from these genera range from 6.49 - 7.89 mean mol % MgCO_3 in the upper lens unit (by EPMA - section 5.1.5.2, Table 5.3) (intralensar structures in these specimens consist of replacement calcite). Variations in mol % MgCO_3 between specimens would be expected as partitioning of Mg is influenced by seawater temperature (Dickson, 2002, Ries, 2004) and therefore the palaeoenvironment at each sample locality. From the material analysed, 8 mol % MgCO_3 is the limit of Mg concentration in the upper lens. Preferential dissolution of intralensar structures in these lenses indicates that Mg concentration would have been higher in these areas, possibly exceeding 8 mol % MgCO_3 .

Although there are difficulties in determining the exact *in-vivo* MgCO_3 concentration of the intralensar structures, it is clear from quantitative chemical analysis (section 5.1.5.2) and EBSD ChI scanning (section 5.1.6.2.1) that both the original chemistry of the core and bowl fall into the category of HMC; in some genera (*Austerops*, *Barrandeops* and *Phacops*) this is true of the upper lens unit also. These schizochroal eyed trilobites must have exhibited a considerable degree of control over the chemistry of their exoskeleton in their ability to partition HMC in an ocean which preferentially precipitated LMC (Dickson, 2004; Ries, 2004).

TEM imaging revealed features characteristic of calcium rich dolomite in material from Gees (section 5.1.4, Figure 5.15C), however this does not provide an accurate composition. Analysis of EPMA data, and subsequent determination of molar CaCO_3 : MgCO_3 ratios, shows that the calcian composition of the dolomite in *Geesops* samples is very slight, at 51:49 Ca:Mg (Figure 5.40A) . All other samples analysed show a stoichiometric value for dolomite (Figure 5.40B), i.e. a 50:50 mixing of molar Ca and Mg.

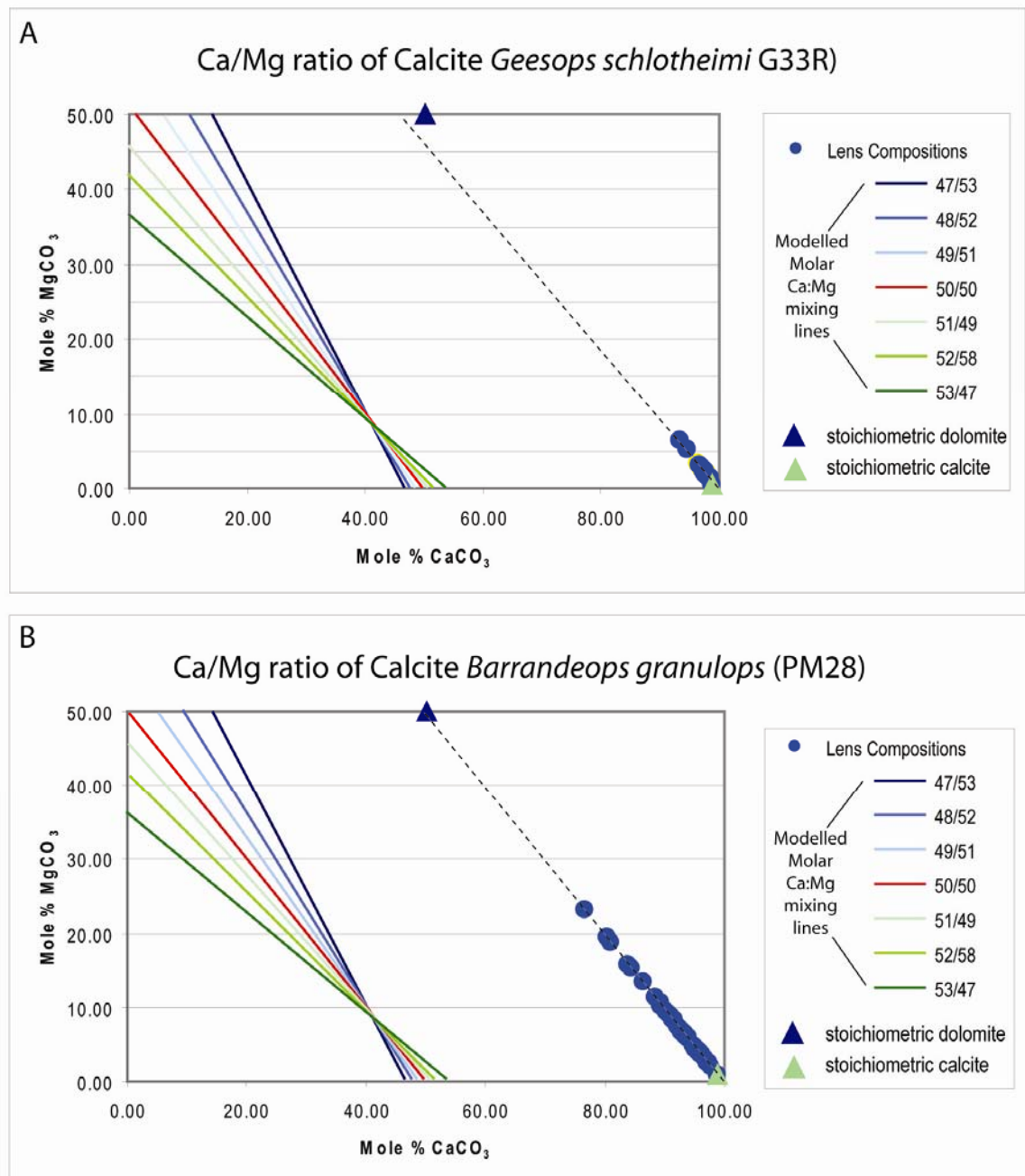


Figure 5.40 – Molar Ca/Mg ratio of lens calcite in schizochroal eyes.

Extrapolation of the lens calcite composition values and comparison with different calcite/dolomite mixing values shows that dolomite in the lenses in samples of *Geesops schlotheimi* (A) is slightly calcitic whereas all other samples analysed including *Barrandeops granulops* (B) are stoichiometric, trending parallel to the 50:50 line.

5.2.2.3 Correlation with Conodont Alteration Index

Diagenetic pathways have been identified in schizochroal lenses with regards to both alteration of microstructure (section 5.2.2.1, Figure 5.34) and chemistry (section 5.2.2.2, Figure 5.35). Here, conodont alteration index (CAI), which provides information on the thermal history of an area, is compared to stages within the diagenetic pathways of schizochroal eyes to determine if the degree of alteration in lenses corresponds to thermal history.

Each of the stages in the diagenetic pathways for lens microstructure and chemistry has been assigned a number or letter respectively to indicate the degree of change from the interpreted original lens structure; '1' or 'a' indicating the least change and '4' or 'd' indicating the most extensive changes in each case (Figure 5.41).

The assigned values (Figure 5.41) have been compared to conodont alteration index (CAI) values to determine if a similar temperature zoning system could be developed based on schizochroal eyes (Table 5.5).

Table 5.5- Correlation between diagenetic alteration of schizochroal lenses and conodont alteration index.

Numbers correspond to stages of alteration in Figure 5.41; 1 and a indicate least change, 4 and d indicate most extensive change from the original lens microstructure and chemistry.

SPECIES	SOURCE LOCATION	CAI VALUE	MICRO-STRUCTURE STAGE	CHEMISTRY STAGE
<i>Barrandeops granulops</i> <i>Barrandeops fortayi</i> <i>Phacops</i> sp.	MOROCCO (ANTI-ATLAS REGION)	3-5 (Belka, 1991)	1-3	c
<i>Geesops schlotheimi</i> <i>Geesops sparsinodosus</i>	GERMANY (EIFEL REGION)	1.5-2.0 (Helsen and Königshof, 1994)	1-2	c-d
<i>Ananaspis macdonaldi</i>	AUSTRALIA (BOREE CREEK FM.)	2-3 (Cockle, 1999b)	1	b-d
<i>Estoniops exilis</i> <i>Chasmops</i> cf. <i>musei</i> <i>Ingriops</i> sp. nov. <i>Ingriops trigonocephalus</i>	ESTONIA (NORTH)	1.0-1.5 (Kaljo <i>et al.</i> , 1988)	1	d

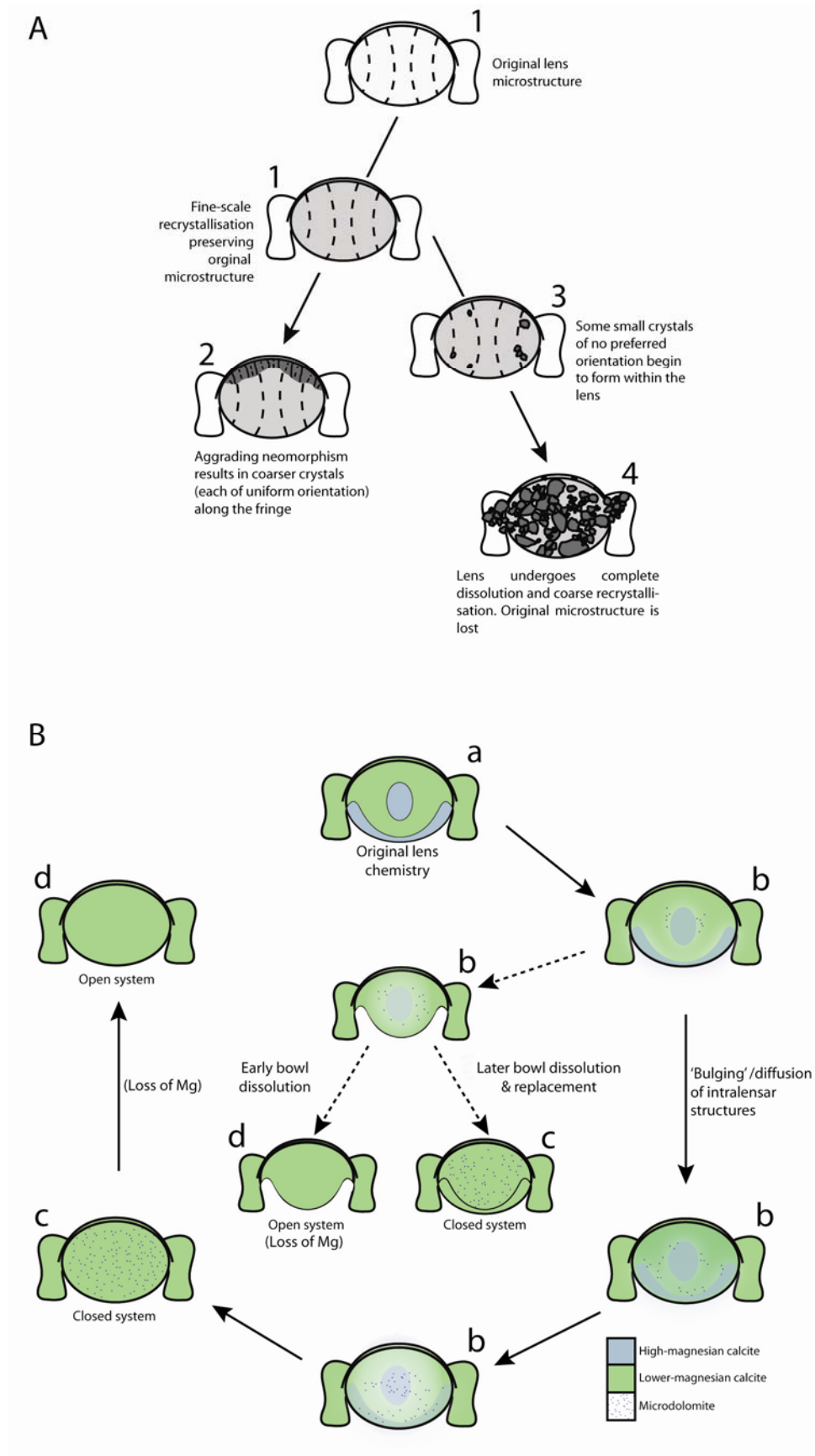


Figure 5.41 - Degrees of diagenetic alteration in schizochroal lenses.

Numbers and letters assigned to different stages in the diagenetic pathway models for purposes of correlation with CAI values. Numbers in A. Microstructure pathway (section 5.2.2.1) and letters in B. Chemistry pathway (section 5.2.2.2) are not directly comparable. Grey areas in A represent lens recrystallisation.

The results (Table 5.5) show that in general, there is positive correlation between CAI and the upper value for microstructure changes, i.e. the higher the CAI and therefore temperature experienced during diagenesis, the more extreme the changes in the lens microstructure can be. Despite this, even in zones of high CAI, some lenses can retain traces of their original microstructure. This trend does not apply to variations in chemistry of the lenses; lenses displaying the most altered chemical arrangement are present within areas of relatively low CAI. Alteration of lens chemistry would occur at very low temperature, early in diagenesis, due to the instability of HMC. It is unlikely that there were two separate stages of lens modification (i.e. one for chemistry and another for microstructure) suggesting that these trends may be coincidental.

5.3 Optical Modelling

5.3.1 Modelling Results

Ray tracing of schizochroal lenses in previous studies (Campbell, 1975; Clarkson and Levi-Setti, 1975; Gál *et al.*, 2000) has provided information on focal lengths and focusing capabilities of the lenses in several different species. Of particular interest is the study by Gál *et al.* (2000), in which it is proposed that the central dimple in the intralensar bowl provided the trilobite with bifocal vision, allowing it to sharply image objects at a range of distances from infinity to closer than half the head diameter. Previous studies, are based on lenses with uniform crystal orientation parallel to the lens axis, and in the cases of Clarkson and Levi-Setti (1975) and Gál *et al.* (2000), assume all light to travel parallel to the *c* axis, avoiding double refraction. Restriction of light to this direction is unlikely and EBSD in the present study has shown that crystal orientation in the lenses is not uniform. Also, EDS and EPMA analyses from the present study and from Lee *et al.* (2007a) have provided new insights into the original composition of the intralensar bowl which was unknown at the time of these previous studies. Therefore, results presented by Campbell (1975), Clarkson and Levi-Setti (1975) and Gál *et al.* (2000) come with limitations.

In the present study, optical modelling of schizochroal lenses was carried out in order to assess the focusing capabilities of the lenses and the influence of intralensar structures on lens function. Ray tracing was carried out in numerous

ways (see the following sections) in an attempt to overcome the limitations prevalent in other studies. The following sections provide an overview of modelling results, full details of these results are presented on Appendix F.

Ray tracing of biconvex lenses of uniform refractive index shows that the difference in refraction between rays passing through the lens centre and the lens edge is such that light is not focused on a single point but rather across a large region in the vertical plane below the lens (Figure 5.42A); light rays passing through the edge of the lens are refracted much more than light rays passing through more central areas of the lens. In such a scenario, the numerous convergence points that lie along the focal plane result in the formation of a blurred image. Therefore, the lenses *in-vivo* must have been more complicated than this, if they were to function efficiently.

The introduction of an aplanatic surface, beyond which lies an optical element of a different refractive index (i.e. the intralensar bowl), alleviates this problem to a significant degree (Figure 5.42B). This architecture results in the enhanced refraction of rays upon intersection with the aplanatic surface and in turn, a more tightly clustered set of convergence points. Modelling of *Phacops* sp. lenses in which the refractive index has been ‘optimised’ to provide the best focus of light shows that where an intralensar bowl is present, the refractive index must change from high (in the upper lens) to low (in the intralensar bowl) to enable the lens to focus better than a biconvex lens of uniform LMC or HMC composition. The ‘best’ values obtained for each component of the lens by optimisation are 1.66 for the upper unit and 1.53 for the lower unit; the same RI value was calculated by Horváth (1989) for the intralensar bowl of *Crozonaspis struvei*. These values are very close to those stated by Reed (1970) for calcite and dolomite respectively. Modelling of *Phacops* sp. assumes the maximum field of view of each lens to be $\pm 9.00^\circ$ about the lens axis (section 2.8.2.2).

As calcite is a birefringent mineral, light that does not travel parallel to the *c* axis of the crystal will undergo double refraction, i.e. rays refract at different angles as the material has two different refractive indices, one value for ‘ordinary’ rays and a lower value for ‘extraordinary’ rays. A lens of *Phacops* sp. was modelled for various compositional states: uniform LMC; uniform HMC; LMC upper lens with HMC bowl; HMC upper lens with LMC bowl for all combinations of

ordinary and extraordinary rays to determine which combination gives the best result, i.e. the result closest to the optimised lens (Table 5.6, Table 5.7).

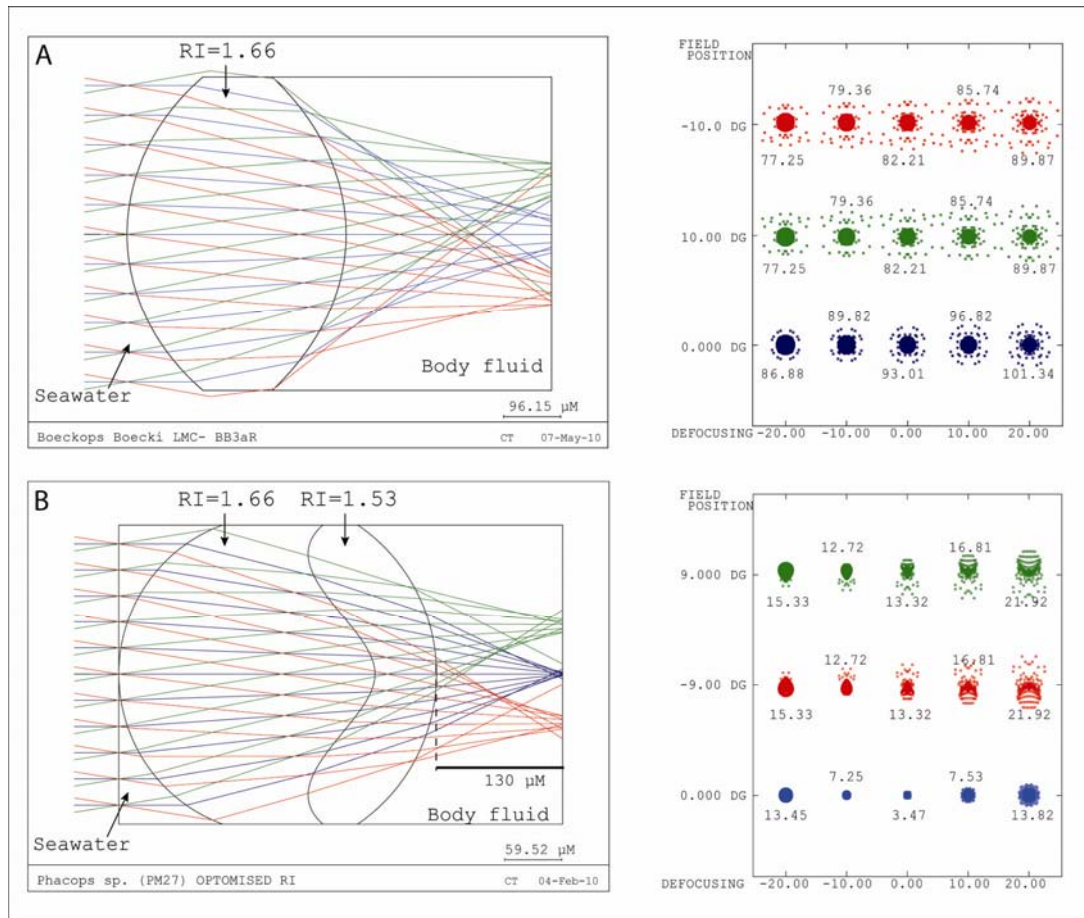


Figure 5.42 – The effects of an intralensar bowl on aberration in lenses of schizochroal eyes. A. Ray trace and corresponding spot diagram for a lens of *Boeckops boeckii* (BB3aR) of uniform composition. Note that the focus of rays is poor. **B.** 'Optimisation' of refractive index in the lens of *Phacops* sp. (PM27). Code V optimisation determines that the ideal refractive indices for the upper lens and bowl are 1.66 and 1.53 respectively. Back focal length (BFL) and aberration are also indicated.

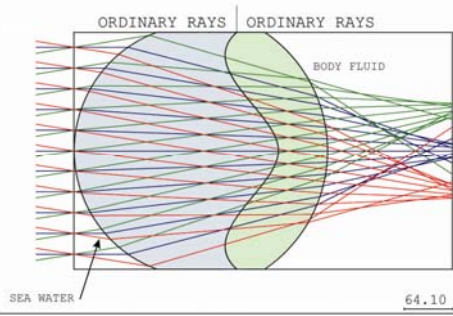
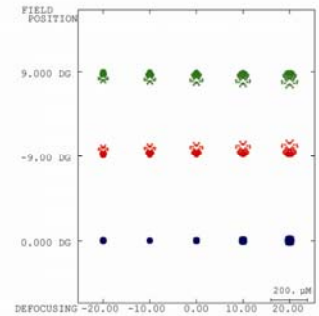
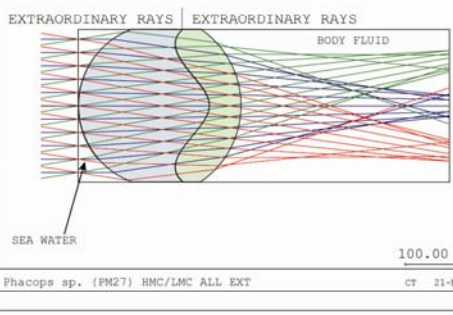
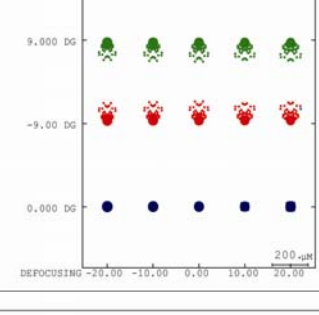
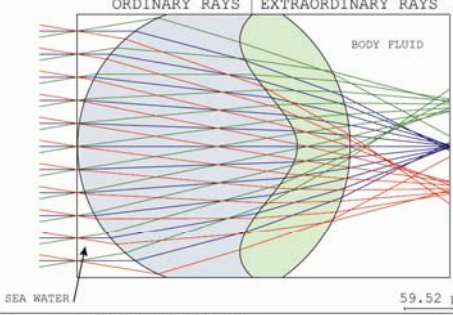
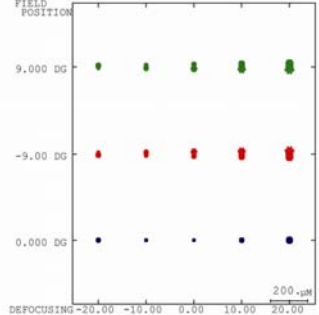
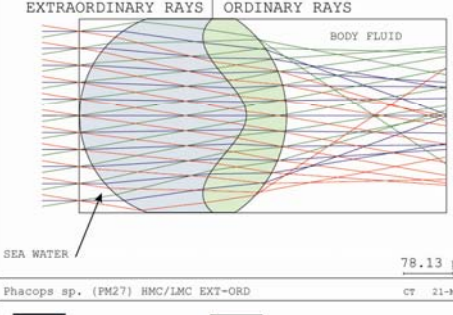

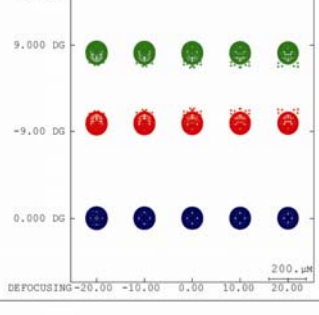
Ray Trace	Spot Diagram	BFL (microns)	Aberration (RMS microns)
 <p>ORDINARY RAYS ORDINARY RAYS</p> <p>SEA WATER</p> <p>64.10 μm</p> <p>Phacops sp. (PM27) HMC/LMC ALL ORD CT 21-May-10</p>	 <p>FIELD POSITION</p> <p>9.000 DG</p> <p>-9.00 DG</p> <p>0.000 DG</p> <p>DEFOCUSING -20.00 -10.00 0.00 10.00 20.00</p> <p>200 μm</p>	163	16
 <p>EXTRAORDINARY RAYS EXTRAORDINARY RAYS</p> <p>SEA WATER</p> <p>100.00 μm</p> <p>Phacops sp. (PM27) HMC/LMC ALL EXT CT 21-May-10</p>	 <p>FIELD POSITION</p> <p>9.000 DG</p> <p>-9.00 DG</p> <p>0.000 DG</p> <p>DEFOCUSING -20.00 -10.00 0.00 10.00 20.00</p> <p>200 μm</p>	425	32
 <p>ORDINARY RAYS EXTRAORDINARY RAYS</p> <p>SEA WATER</p> <p>59.52 μm</p> <p>Phacops sp. (PM27) HMC/LMC ORD-EXT CT 21-May-10</p>	 <p>FIELD POSITION</p> <p>9.000 DG</p> <p>-9.00 DG</p> <p>0.000 DG</p> <p>DEFOCUSING -20.00 -10.00 0.00 10.00 20.00</p> <p>200 μm</p>	121	3
 <p>EXTRAORDINARY RAYS ORDINARY RAYS</p> <p>SEA WATER</p> <p>78.13 μm</p> <p>Phacops sp. (PM27) HMC/LMC EXT-ORD CT 21-May-10</p> <p>  </p>	 <p>FIELD POSITION</p> <p>9.000 DG</p> <p>-9.00 DG</p> <p>0.000 DG</p> <p>DEFOCUSING -20.00 -10.00 0.00 10.00 20.00</p> <p>200 μm</p>	256	85

Table 5.6 - Optical modelling of *Phacops* sp. with a low-magnesian calcite intralensar bowl. Code V results for a lens in section PM27. Columns from right to left: ray traces; corresponding spot diagrams; back focal length; aberration. Rows from top to bottom: ordinary rays; extraordinary rays; ordinary rays in upper lens-extraordinary rays in bowl; extraordinary rays in upper lens-ordinary rays in bowl.

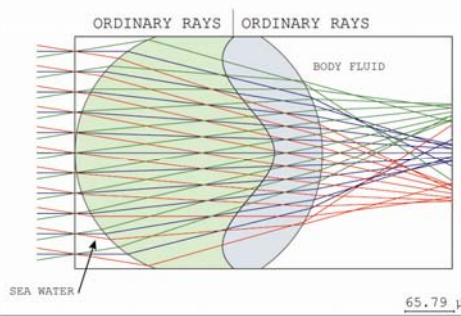
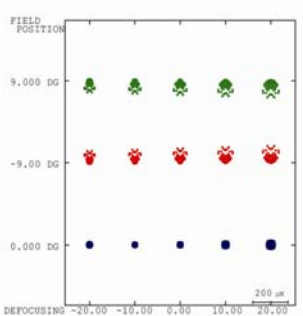
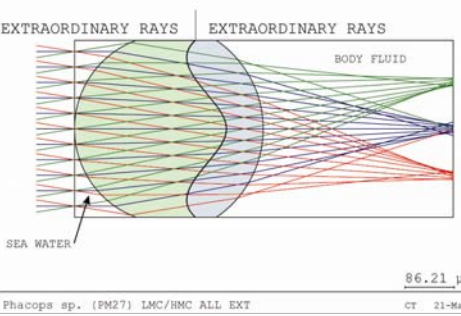
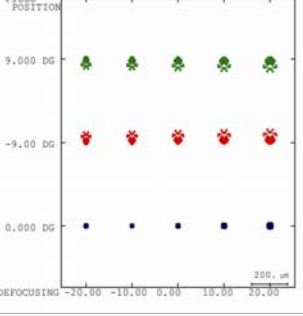
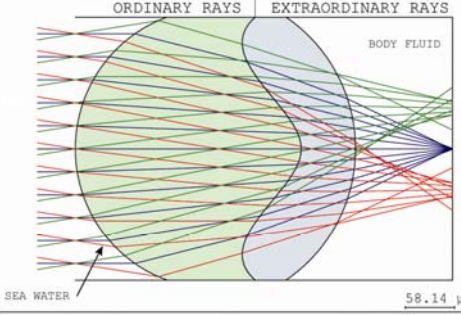
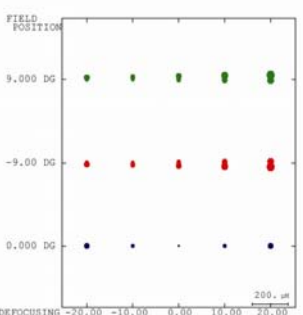
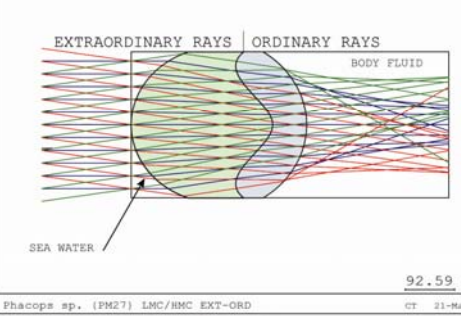
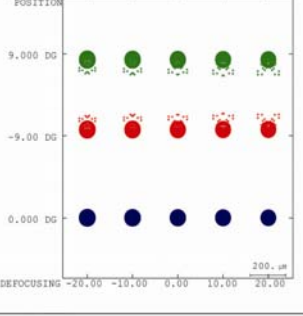

Ray Trace	Spot Diagram	BFL (microns)	Aberration (RMS microns)
 <p>ORDINARY RAYS ORDINARY RAYS</p> <p>SEA WATER</p> <p>BODY FLUID</p> <p>65.79 μm</p> <p>Phacops sp. (PM27) LMC/HMC ALL ORD CT 21-May-10</p>	 <p>FIELD POSITION</p> <p>9.000 DG</p> <p>-9.00 DG</p> <p>0.000 DG</p> <p>DEFOCUSING -20.00 -10.00 0.00 10.00 20.00</p>	173	18
 <p>EXTRAORDINARY RAYS EXTRAORDINARY RAYS</p> <p>SEA WATER</p> <p>BODY FLUID</p> <p>86.21 μm</p> <p>Phacops sp. (PM27) LMC/HMC ALL EXT CT 21-May-10</p>	 <p>FIELD POSITION</p> <p>9.000 DG</p> <p>-9.00 DG</p> <p>0.000 DG</p> <p>DEFOCUSING -20.00 -10.00 0.00 10.00 20.00</p>	333	10
 <p>ORDINARY RAYS EXTRAORDINARY RAYS</p> <p>SEA WATER</p> <p>BODY FLUID</p> <p>58.14 μm</p> <p>Phacops sp. (PM27) LMC/HMC ORD-EXT CT 21-May-10</p>	 <p>FIELD POSITION</p> <p>9.000 DG</p> <p>-9.00 DG</p> <p>0.000 DG</p> <p>DEFOCUSING -20.00 -10.00 0.00 10.00 20.00</p>	114	1
 <p>EXTRAORDINARY RAYS ORDINARY RAYS</p> <p>SEA WATER</p> <p>BODY FLUID</p> <p>92.59 μm</p> <p>Phacops sp. (PM27) LMC/HMC EXT-ORD CT 21-May-10</p>	 <p>FIELD POSITION</p> <p>9.000 DG</p> <p>-9.00 DG</p> <p>0.000 DG</p> <p>DEFOCUSING -20.00 -10.00 0.00 10.00 20.00</p>	267	62
 <p>HMC LMC</p>			

Table 5.7- Optical modelling of Phacops sp. with a high-magnesian calcite intralensar bowl. Code V results for a lens in section PM27. Columns from right to left: ray traces; corresponding spot diagrams; back focal length; aberration. Rows from top to bottom: ordinary rays; extraordinary rays; ordinary rays in upper lens-extraordinary rays in bowl; extraordinary rays in upper lens-ordinary rays in bowl.

The results show that the lens with both the best focusing capability and shortest focal length is one in which the upper lens unit is composed of LMC (RI = ~1.66) and the intralensar bowl is composed of HMC (RI = 1.50) (Table 5.7). These results also show that microstructure is crucial as it is a combination of ordinary rays and extraordinary rays that provides the best focus. EBSD results show that there is variation in *c* axis orientation along the lens base of up to 40° either side of the lens axis in microstructure 3 (section 5.1.6.2), believed to best represent original lens microstructure (section 5.2.2.1). Providing light does not reach the intralensar bowl at this angle, it will always experience double refraction. The so-called extraordinary rays that are refracted at the lower value are brought into a sharp focus beneath the lens. This result supports the diagenetic pathway detailed in section 5.2.2.2 (Figure 5.35) as the LMC composition of the bowl identified in EDS analysis and presumed to be replacement calcite (section 5.2.2.2, Figure 5.19B) has been shown not to be as effective as an HMC bowl in focusing light.

In the case of *Ingrriops*, in which the intralensar bowl is interpreted as having been dissolved (5.2.2.2, Figure 5.35h), the sinuous nature of the apparent ‘lens base’ alone is not sufficient to tightly focus light. However, the addition of a ‘virtual’ bowl of HMC composition significantly reduces both spherical aberration and focal length of the lens (Table 5.8).

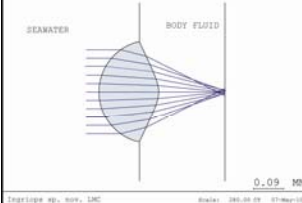
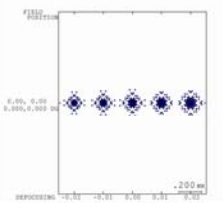
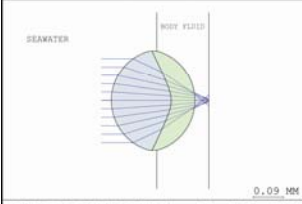
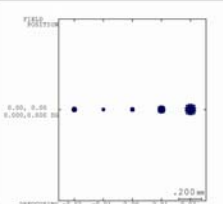
Ray Trace	Spot Diagram	Back focal length (μm)	Aberration (RMS)
 <p>0.09 mm</p> <p>Topolops sp. nov., LMC</p> <p>01-May-11</p>	 <p>0.00, 0.00 0.000, 0.000 μm</p> <p>0.200 mm</p> <p>01-May-11</p>	200	56
 <p>0.09 mm</p> <p>Topolops sp. nov., LMC lens + HMC bowl</p> <p>01-May-11</p>	 <p>0.00, 0.00 0.000, 0.000 μm</p> <p>0.200 mm</p> <p>01-May-11</p>	40	11
<div style="display: flex; justify-content: space-around;"> LMC HMC </div>			

Table 5.8 – Code V optical modelling of *Ingrriops* sp. nov.

Code V results for a lens in section IE48. Columns from right to left: ray traces of paraxial rays; corresponding spot diagrams; back focal length; aberration. Rows from top to bottom: LMC lens; LMC upper lens with HMC intralensar bowl. Note that the lens that focuses best is that with the LMC upper lens and HMC intralensar bowl.

5.3.1.1 Photoreceptive Components

As no sublensar structures have been identified in the studied material, the location of the photoreceptive components cannot be determined with certainty. It is reasonable to assume that the back focal length, i.e. the point beneath the lens at which light comes to focus, indicates the location of the photoreceptive components.

In the case of *Phacops* sp. (PM27), the back focal length is approximately 114 μm in the 'best case scenario' (Table 5.7). If light for the assumed field of view is to be detected (i.e. $\pm 9^\circ$ about the lens axis), the photoreceptor would need to be approximately 140 μm in diameter. If only paraxial light is to be detected, the size of the receptor is assumed to be, at a minimum, equal to the diameter of the blur circle created by these rays, i.e. 1 μm . The latter value is comparable to the width of the rhabdom of modern bees (Land and Nilsson, 2002 p. 129). The size of lenses in the bee eye is however significantly smaller than schizochroal lenses. The former value of 140 μm is comparable with the deep-sea isopod *Cirolana* (Nilsson and Nilsson, 1981) and would fit within the mesodermal capsule found by Bruton and Hass in the schizochroal eyes of *Geesops sparsinodosus* (2003b).

Code V results of all lenses modelled are presented in Appendix F.

5.3.2 Summary

The array of techniques used in the present study has revealed new information on the microstructure and chemistry of the lenses analysed, at a level of detail not possible before now. This analysis has allowed original lens features to be distinguished from diagenetic artefacts and lens function to be assessed by 'seeing through' the diagenesis that they have undergone.

The original composition of lenses in the schizochroal eye exhibited partitioning of Mg (Figure 5.43), however the present study has yielded results different to those of Lee *et al.* (2007a). The upper unit of the lens was composed of Mg-bearing calcite; variations in Mg concentration between species or genera may have been evident to account for differences in lens shape but an upper limit of ~8 mol % MgCO_3 is probable. The intralensar features, the core and bowl, were

composed of HMC, the exact concentration is unknown however in each case, these features would have contained more Mg than the surrounding lens calcite.

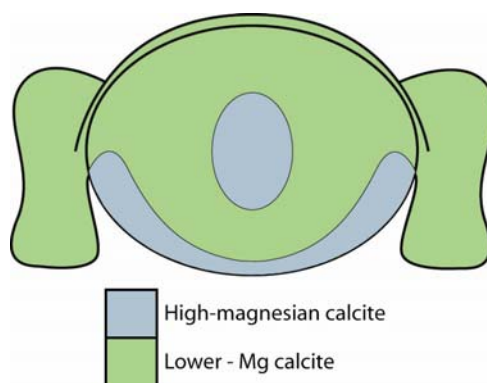


Figure 5.43 - Original chemical composition of the lenses in schizochroal trilobite eye. This interpretation is based on TL, RL and CL microscopy as well as EBSD ChI scanning, TEM and chemical analysis by EDS and EPMA.

EBSD of schizochroal lenses and the epitaxial diagenetic cements beneath them leads to the conclusion that the original lens microstructure (Figure 5.44) consisted of a variation in *c* axis orientation along the outer fringe of the lens and along the lens base; creating an angle close to 90° with the lens surfaces. Although the general shape of the trabeculae in lenses is similar to the trend of the *c* axis, they do not mirror it exactly. This may either suggest that (1) crystal orientation has been overprinted to some degree during diagenesis or (2) that crystal orientation *in-vivo* could vary independently of trabeculae orientation. If lens growth occurred via addition of trabeculae (Clarkson in Kaesler, 1997), the former seems the more likely suggestion.

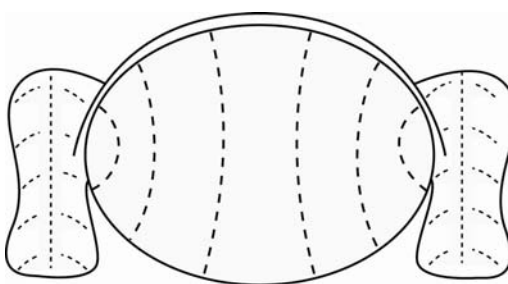


Figure 5.44 - The original microstructure of lenses in the schizochroal trilobite eye. Dashed lines represent *c* axis orientation. This interpretation is based on TL microscopy and EBSD analysis.

The results (Table 5.6-Table 5.8) show that the lenses in schizochroal trilobite eyes were capable of focusing light however, perhaps more importantly, they show that the birefringent properties of the calcite used to construct the lenses, which has been long thought of as a problem, is actually what enables the lenses

to focus light so well. Without this characteristic, the change in RI across the lens/bowl boundary would be low to high ($RI=1.66$ for ordinary rays in calcite and $RI=1.68$ for ordinary rays in dolomite), resulting in slight divergence of light rays rather than greater convergence. It is the combination of ordinary rays in the upper lens that undergo double refraction upon entering the intralensar bowl, due to the change in c axis orientation (section 5.1.6.2), and their resultant extraordinary rays, that produce the sharpest focal point below the lens (Table 5.7).

Further work involving the analysis of a full ontogenetic sequence of schizochroal eyes would enable the identification of any changes in lens structure through growth that have not been possible in the material analysed in the present study.

6

Other Animals with Calcite Lenses

The use of calcite in construction of natural lenses is not restricted to trilobite eyes. Modern animals including isopods, amphipods, ostracods and brittlestars use calcite, to some degree, in the lenses of their visual systems (section 1.6.1 and 1.6.1). In the case of the isopods and amphipods, this is restricted to the corneal covering (Dudich, 1931), but in ostracods (Anderson and Nilsson, 1981; Myers and Kontrovitz, 1988; Kontrovitz and Slack, 1995; Kontrovitz and Puckett, 1998; Tanaka *et al.*, 2009) and brittlestars (Aizenberg *et al.*, 2001) the entire lens is calcified, and is an extension of the stereom or carapace in a similar manner to the lenses in trilobites which are part of the exoskeleton (section 1.5).

The lenses of brittlestars in particular have been concluded to be analogues to trilobite eyes (Aizenberg and Hendler, 2004). Ostracods and brittlestars have been investigated in the present study to clarify the similarities and differences between these lenses and trilobite lenses, and in the case of brittlestars, assess their suitability as modern analogues.

6.1 Ostracods

Samples of the Silurian ostracod *Primitiopsis planifrons* were analysed in the SEM by SE and BSE imaging, EBSD and EDS analysis. Light microscopy was not carried out, as samples were prepared as polished stubs, not in thin section (section 3.2.4).

6.1.1 Results

Intact specimens and polished stubs were studied by SE and BSE imaging respectively. Stubs were prepared to reveal a transverse line of section (Figure 3.7, section 3.2.4).

6.1.1.1 Secondary Electron Imaging

SE imaging of intact *Primitiopsis planifrons* specimens enabled the identification of the eyespot. This feature is characterised by a smooth outer surface in marked contrast with the textured surface of the adjacent carapace (Figure 6.1).

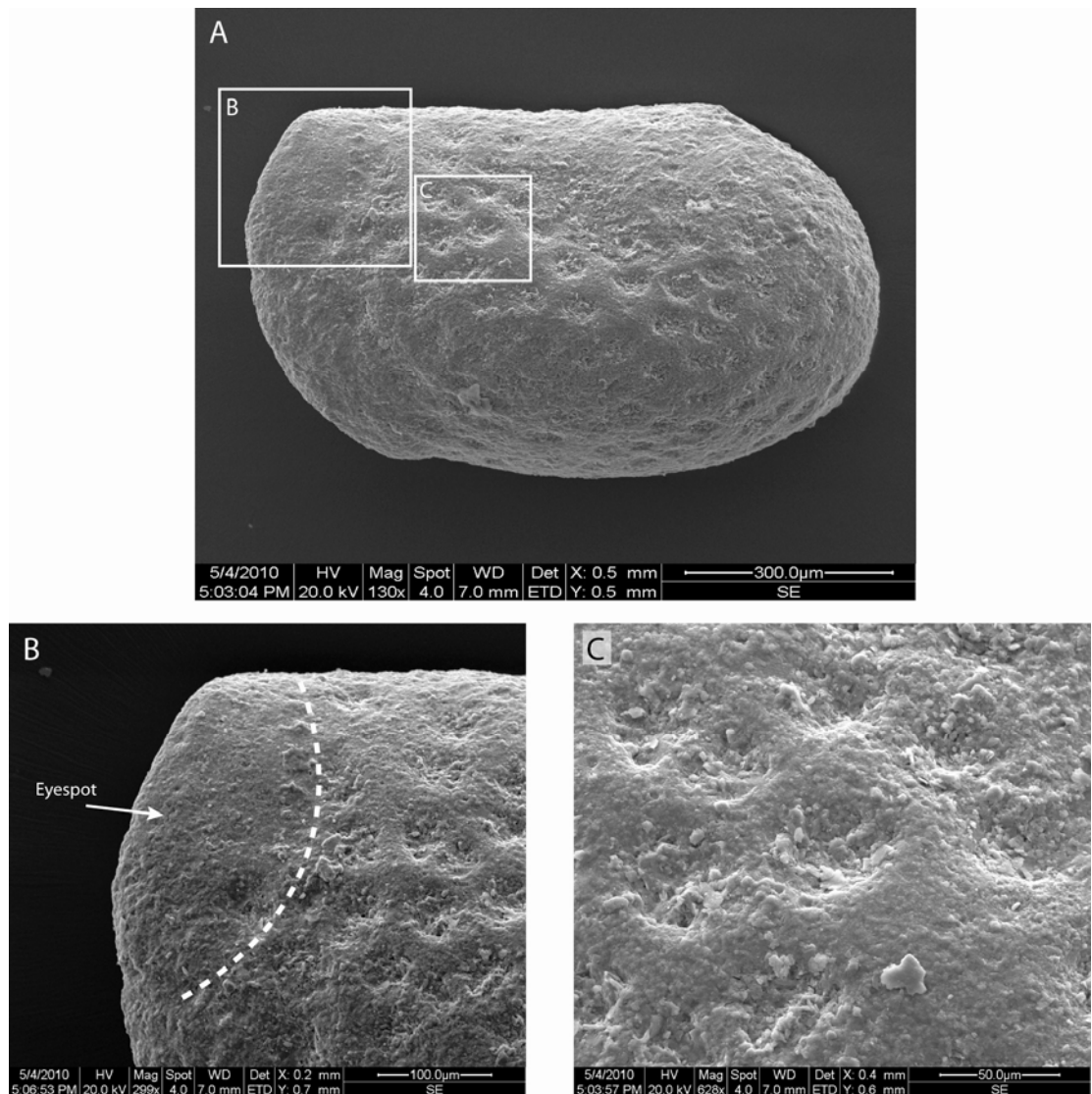


Figure 6.1 – Secondary Electron image of the ostracod *Primitiopsis planifrons*.

A. Low magnification image of the left valve. **B and C.** High magnification images of the eyespot and the carapace respectively. These images correspond to the highlighted areas in A. Note the relatively smooth external surface of the eyespot.

6.1.1.2 Backscattered Electron Imaging

BSE imaging of the polished sections of carapaces revealed a homogeneous, dense structure and invariant BSE signal intensity indicating uniform major element distribution. Despite the careful preparation of samples, the location of the eyespots in the sections is somewhat unclear. Based on the description by Tanaka *et al.* (2009) of the lens in section as having ‘a prominent convex inner surface’ it is clear that the line of section, in all samples, has gone beyond the level of the eyespot. This highlights the difficulties involved when working with small samples in which the site of interest (i.e. the eyespot) occupies an area of just a few tens of microns.

6.1.1.3 Electron Backscatter Diffraction

EBSD of the ostracod specimens reveals that the carapace, in general, consists of numerous irregularly shaped crystals ranging in size from 1-2 μm in diameter to >20 μm . In some instances the grain size increases from the outer carapace surface inwards (Figure 6.2A) and crystal orientation is constrained; the calcite *c* axis is aligned at approximately 90° to the outer carapace surface (Figure 6.2A). In other regions there is no preferred crystal orientation (Figure 6.2B, C) although layering is identified by different grain sizes (Figure 6.2B). Regardless of the orientation of the grains, irregular shaped, sutured inter-granular boundaries are commonly present (Figure 6.2A, B).

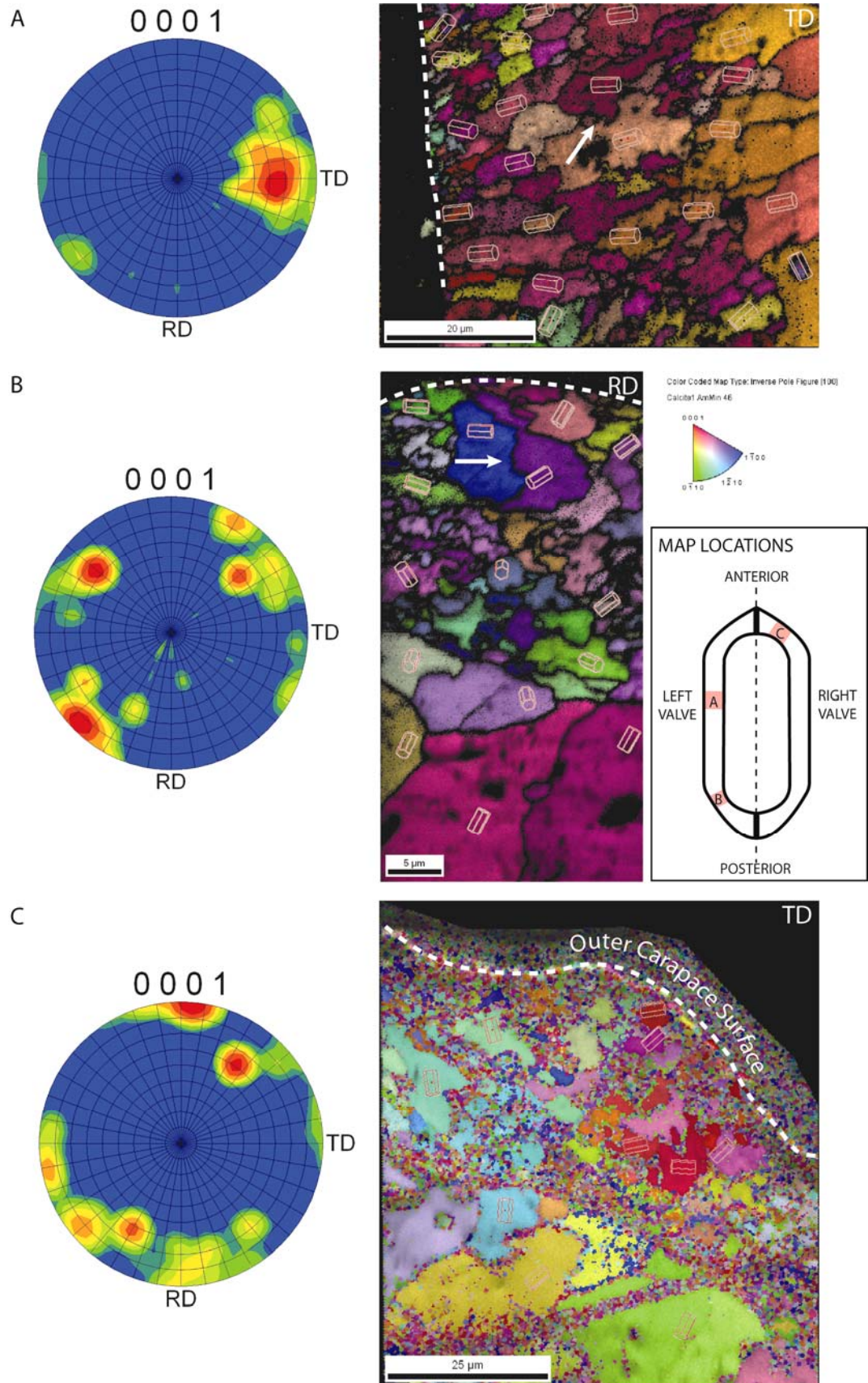


Figure 6.2 - Microstructure of the carapace of the ostracod *Primitiopsis planifrons*. Pole figure plots and corresponding EBSD maps of the carapace. Superimposed crystal models indicate crystal orientation. Dashed white lines indicate the outer surface of the carapace. Arrows in A and B highlight sutured grain boundaries. Grid line divisions in pole figures represent 10° . The inset map shows the approximate locations of each scan. White letters indicate reference direction of EBSD scans (section 2.7.4.2).

6.1.1.4 Energy Dispersive X-Ray Spectroscopy

EDS mapping of the ostracod carapace shows that low concentrations of Mg are present throughout (Figure 6.3). This Mg is incorporated into the calcite itself but is not present in sufficient quantity for this to be HMC; the carapace consists of LMC.

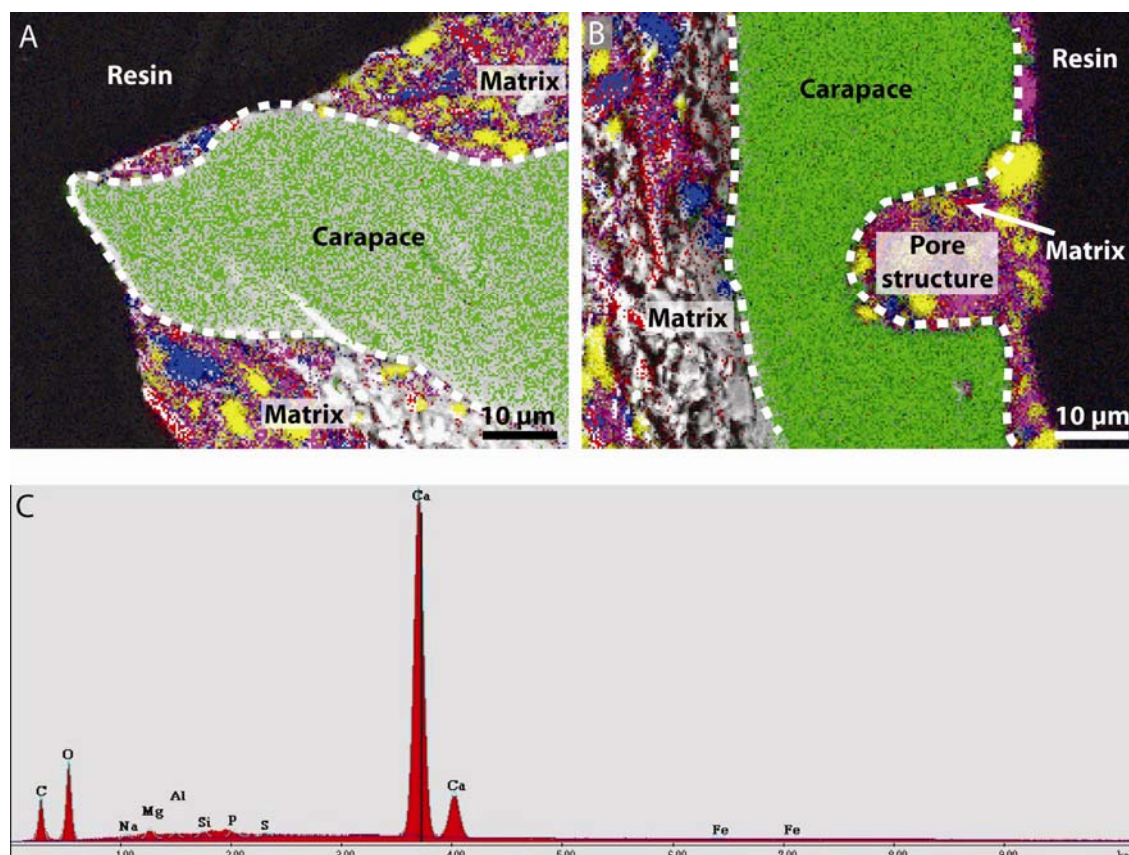


Figure 6.3 – Energy Dispersive X-Ray mapping of the carapace of the ostracod *Primitiopsis planifrons*.

A - B. Distribution of Ca (green), Mg (blue) in the carapace. Si (yellow), Al (pink) and Fe (red) are found in the surrounding matrix only. C. A spectrum showing the typical chemical composition of the ostracod carapace.

6.1.2 Interpretation

6.1.2.1 Carapace Microstructure and Chemistry

The carapace of *P. planifrons* as reported by Tanaka *et al.* (2009) consists of a foliated grain structure with the exception of the lens, which has a distinct prismatic structure. BSE imaging and EBSD maps reveal that the carapace of the samples analysed consists of a crystalline framework with sutured grain boundaries. These boundaries, which are indicative of neomorphism (see Bathurst, 1971), imply that this microstructure is not original.

Tanaka *et al.* (2009) chose *P. planifrons* for study because of the ‘potential presence of an eye’. The ambiguity of this feature is unavoidable due to the lack of soft parts in fossil specimens however based on comparison with modern ostracods in which photo-components are found below these smooth areas (Andersson and Nilsson, 1981), it is most likely that this area of the carapace in *P. planifrons* does indicate the presence of an eyespot. The distinct difference in reported microstructure between this area and the rest of the carapace can only act as further support for the suggestion by Tanaka *et al.* (Tanaka *et al.*, 2009) that this area is an eyespot/lens. The prismatic structure and orientation of the crystals within the ‘lens’ implies a functional capacity and a degree of biological control over growth. As sectioning of the eyespot was unsuccessful, the degree of recrystallisation of this part of the carapace has not been determined. Further work on sample preparation may yield positive results. The fact that the rest of the carapace appears to have been recrystallised does not mean that the lens too has lost its original microstructure. The grain size in the carapace implies fine scale recrystallisation so it is possible that this does not extend to the lens; the microstructure identified by Tanaka *et al.*, (2009), i.e. aligned prisms of calcite, may be original.

6.1.2.2 Code V Optical Modelling

Surface curvatures of the eye spot were determined using an image from Tanaka *et al.* (2009) (Figure 6.4) as no successful cross-sections through the lens were made in the present study. The ostracod lens was modelled assuming the wavelength of light to be 475 nm; this corresponds to light in the blue part of the spectrum. This assumption was based on the inferred depth of habitat as 50-60 m (Tanaka *et al.*, 2009). It is unclear whether all ordinary rays are also paraxial as the microstructure of the lens is unknown. Ordinary rays are therefore modelled in addition, at an angle of $\pm 2^\circ$ about the lens axis so they can be distinguished from the paraxial rays (Figure 6.5A).

Code V ray tracing shows that paraxial and ordinary rays are focused at a depth of 168 μm and extraordinary rays are focused at 305 μm . Aberration values are 9 μm and 7 μm respectively (Figure 6.5).

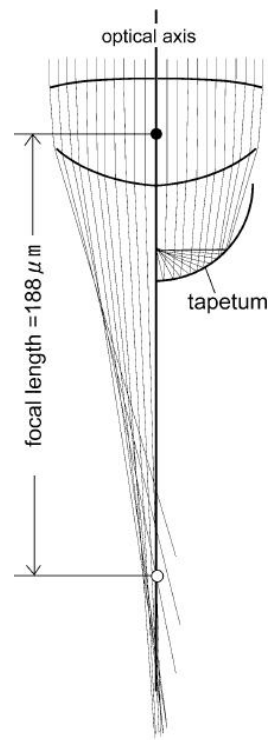


Figure 6.4 - Surface curvatures of the ostracod lens used in optical modelling. Modelling results from the study by Tanaka *et al.* (2009) for a lens with and without a reflecting tapetum. Image from Tanaka *et al.* (2009, figure 7).

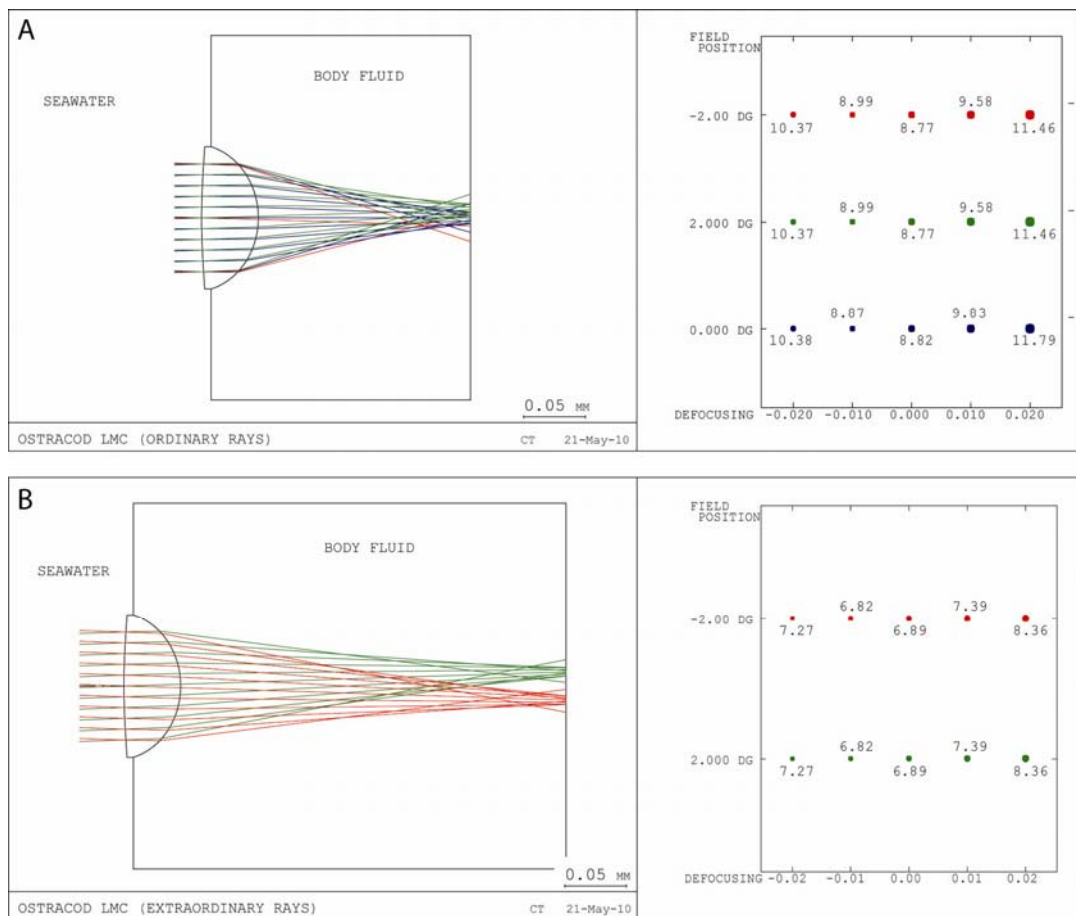


Figure 6.5 – Code V modelling of a lens of the ostracod *Primitiopsis planifrons*. Ray traces and corresponding spot diagrams for A. ordinary lights rays (including paraxial rays) and B. extraordinary light rays.

6.1.2.3 Sublensar Structures

The focal lengths of both ordinary, paraxial and extraordinary rays determined by Code V ray tracing are extremely long relative to the thickness of the carapace and the lens itself, it is therefore unlikely that any photoreceptive components were positioned at this level; the carapace is approximately 45 μm thick at the eyespot, determined from Figure 6.4. An optical system with a tapetum (reflecting surface composed of pigment cells) positioned below the lens is thought to have been present *in-vivo* (Tanaka *et al.*, 2009). Similar reflecting surfaces are commonly found in the eyes of modern vertebrates, which are nocturnal or live in dim habitats (Ollivier *et al.*, 2004). For the purposes of modelling this structure, the surface shape and width of the ostracod tapetum have been assumed to be the same as the base of the lens (Figure 6.6).

The introduction of a tapetum reduces the back focal length to 75 μm and the aberration to 4 μm (Figure 6.6). The position of the tapetum was assigned by the process of ‘optimisation’ (section 2.8.1) i.e. the assigned position is that which results in the best focus; this was calculated as 98 μm below the lens.

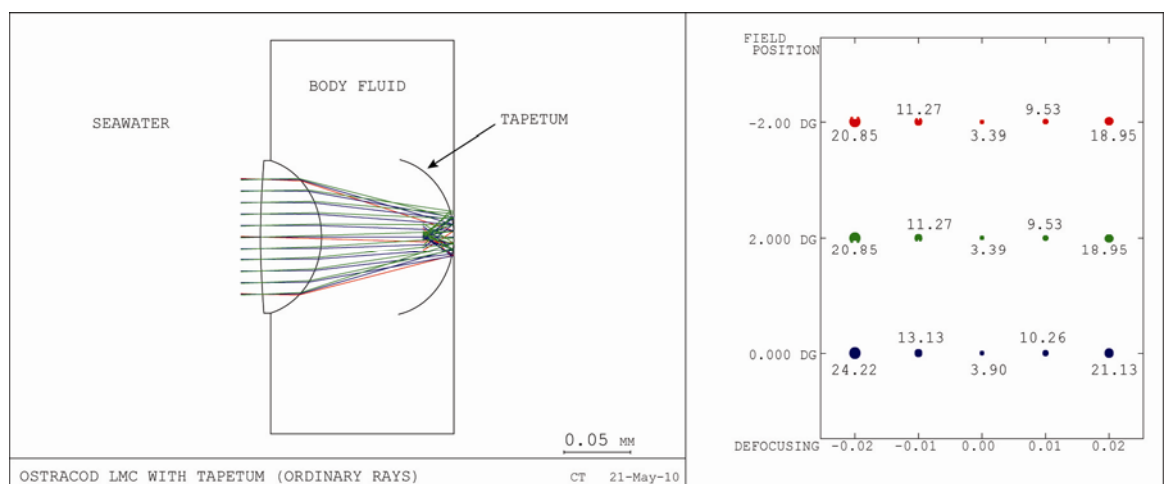


Figure 6.6 - Code V modelling of a tapetum in the eye of the ostracod *Primitiopsis planifrons*.

The tapetum reduces both the back focal length and the aberration of the optical system.

These results imply that a reflecting structure, the tapetum, was used to minimise the focal length of the system, scaling it down to a more appropriate size for the host; this structure is present in many podocopid ostracods (Tanaka *et al.*, 2009). In addition, the tapetum results in tighter focusing of light rays, which would be beneficial if photoreceptive units were small.

A full list of Code V modelling results of *Primitiopsis planifrons* can be found in Appendix F.

6.1.3 Summary

Standard grinding and polishing with silicon carbide abrasives and alpha alumina polishing agents is clearly not appropriate for the preparation of ostracod samples. Alternative techniques such as acetate peels may be more appropriate for the preparation of such small samples (e.g. Frank, 1965), however this type of sample is not suitable for EBSD work.

The chemical composition of the carapace is LMC, this may also represent the composition of the eyespot. However, as partitioning of Mg has been identified in the schizochroal eyes of trilobites, it would be unwise to make assumptions.

The carapace of the ostracods analysed has been recrystallised, possibly altering the original microstructure.

Optical modelling of the ostracod lens, based on shape and size details from Tanaka *et al.* (2009), leads to the conclusion that a tapetum, a reflecting surface, was present beneath the lens *in-vivo*, to reduce the focal length and enable focusing of light.

6.2 Brittlestars

Brittlestar samples were analysed in the SEM by SE and BSE imaging, EBSD and qualitative and quantitative EDS analysis; optical microscopy was not carried out as samples were prepared as polished stubs, not in thin section (section 3.2.4).

6.2.1 Results

Rough samples and polished stubs of brittlestar dorsal arm plates (DAPs) (Figure 3.8, section 3.2.4) were studied by SE and BSE imaging. Stubs were prepared to show DAPs in both tangential and transverse lines of section (Figure 3.8, section 3.2.4)

6.2.1.1 Backscattered Electron Imaging of Rough Samples

BSE imaging was carried out on the dorsal surface of a transverse section through a brittlestar arm. This imaging has revealed a significant difference between the lens structures on the DAP and the labyrinthine stereom below (Figure 6.7). In this instance, BSE imaging proved more successful in highlighting detail than SE imaging (used for rough samples of trilobites).

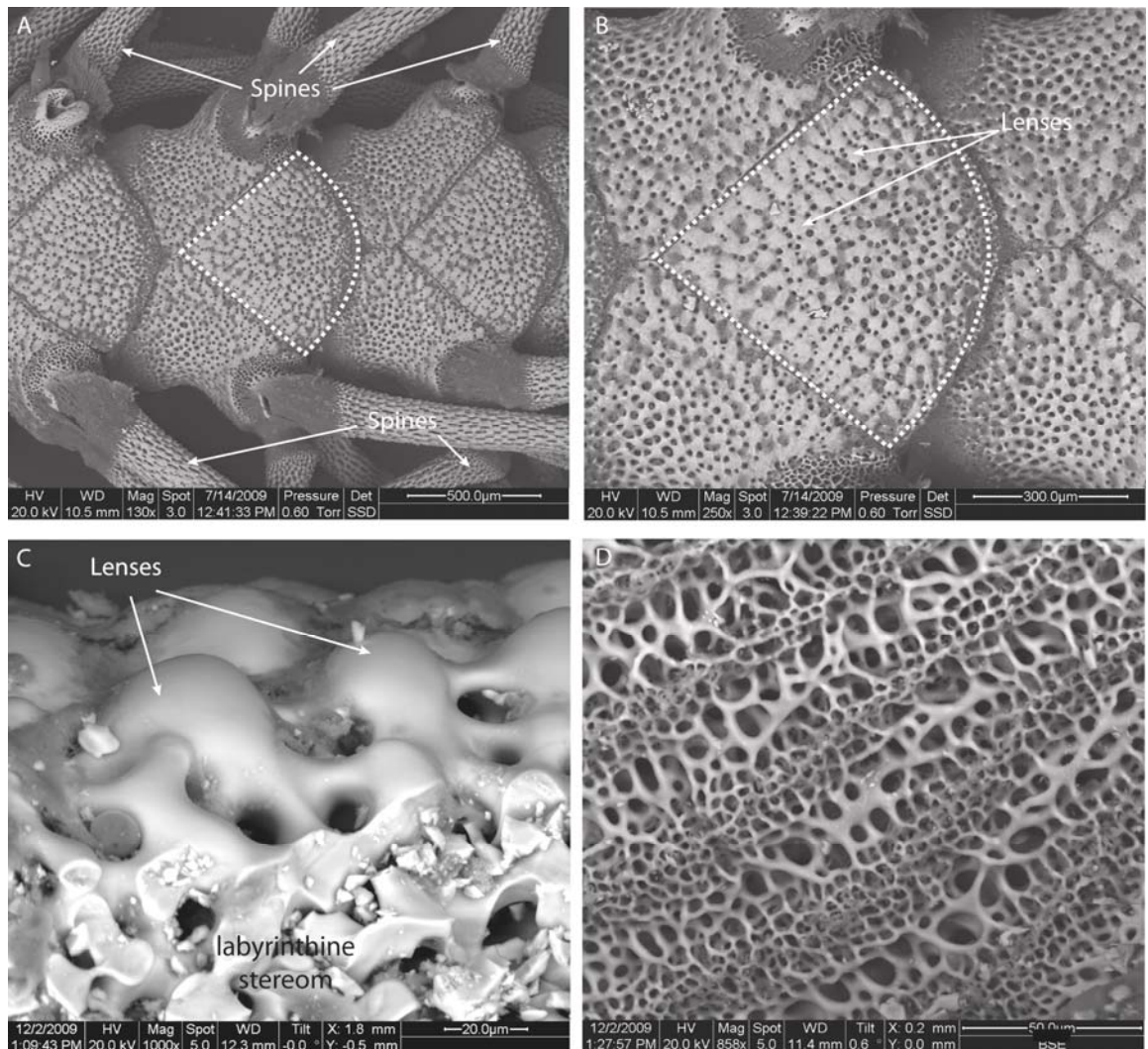


Figure 6.7 - Backscattered electron images of the brittlestar *Ophiocoma wendtii*.

A-B. Lenses cover the dorsal arm plates (highlighted by dashed white line) but not the spines or the areas to which they are attached. Note the smooth appearance of the lenses (C) compared to the rest of the stereom that has a very porous structure (D).

The stereom has a porous structure (Figure 6.7D) whereas the lenses on the dorsal surface are more compact (Figure 6.7C). The lenses are small, reaching only ~40 μm in diameter, and have very rounded outer surfaces.

6.2.1.2 Backscattered Electron Imaging of Polished Surfaces

Lenses are internally featureless in BSE images (Figure 6.8); the uniform greyscale indicating a homogeneous major element chemical composition throughout the lens and the indeed the rest of the stereom. Lenses are free of micropores and inclusions.

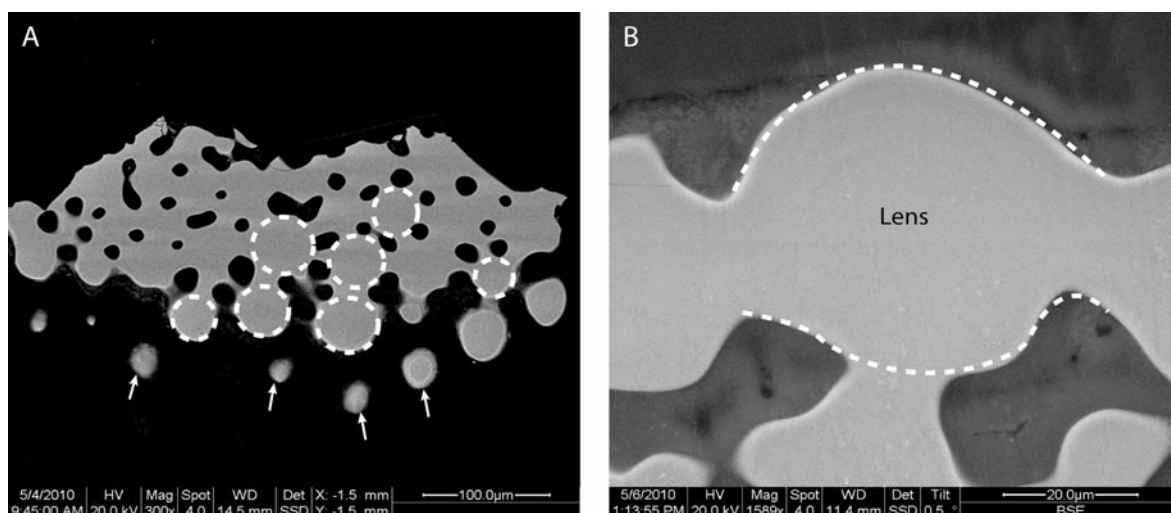


Figure 6.8 – Backscattered Electron image of lenses within the dorsal arm plate of the brittlestar *Ophiocoma wendtii*.

Lenses have been cut in the tangential (A) and vertical (B) planes. A. Lenses that have been sectioned close to their outer surfaces appear small and detached (arrowed). Lenses cut through the centre are connected to one another (circled). The uniform greyscale of the lenses in BSE imaging indicates a homogeneous major element chemical composition.

6.2.1.3 Electron Backscattered Diffraction

EBSD of lenses and the surrounding stereom show that there is no detectable variation in crystallographic orientation within the brittlestar skeleton. The *c* axis of calcite lies parallel with the lens axis across the whole skeleton (Figure 6.9).

Misorientation graphs (Figure 6.10) show that although the lens appears to be of uniform *c* axis orientation, there is a slight variation in orientation across the sample surface. This misorientation, which occurs in steps of 1-5 μm , reaches a maximum of 1.2° between any two points. This misorientation would be expected if the apparent ‘single crystal’ of the echinoderm stereom consisted of numerous sub-domains as was suggested by Towe (1967) and supported by the work of Blake *et al.* (1984). However, these values are too close to the limits of EBSD detection to be taken with any degree of certainty and this suggestion would require clarification by other techniques such as TEM.

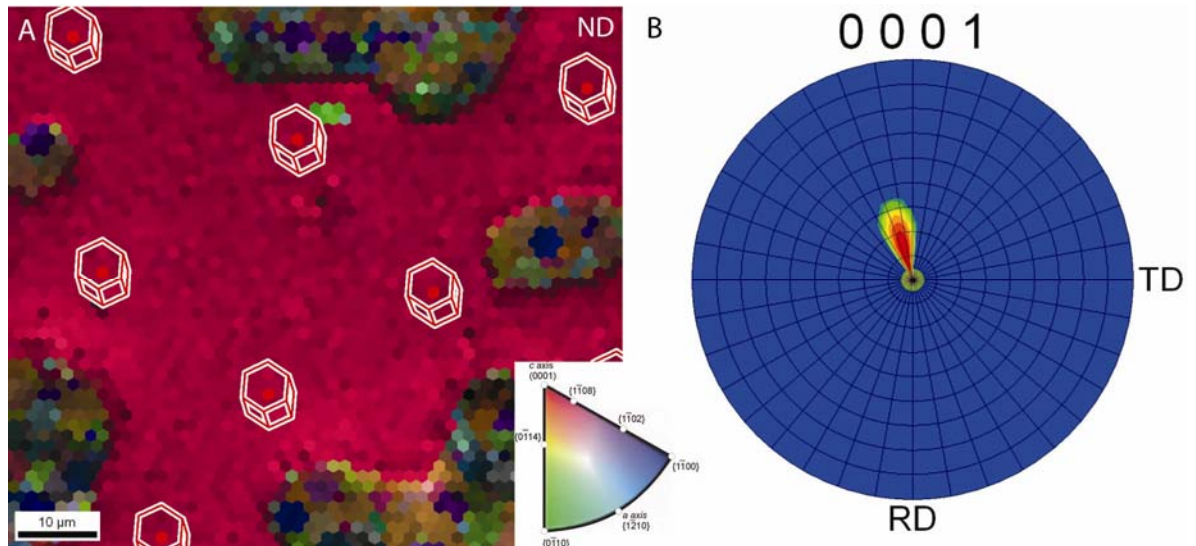


Figure 6.9 – Electron Backscatter Diffraction of a lens in the brittlestar *Ophiocoma wendtii*. A. EBSD map and B. pole figure plot of a lens cut in the tangential plane. Superimposed crystal models in A show that the whole lens is of uniform crystal orientation. The slight spread of angles in the pole figure plot (B) indicates that the lens has not quite been sectioned perpendicular to the lens axis as was intended. White letters in A indicate the reference direction of the EBSD map (section 2.7.4.2).

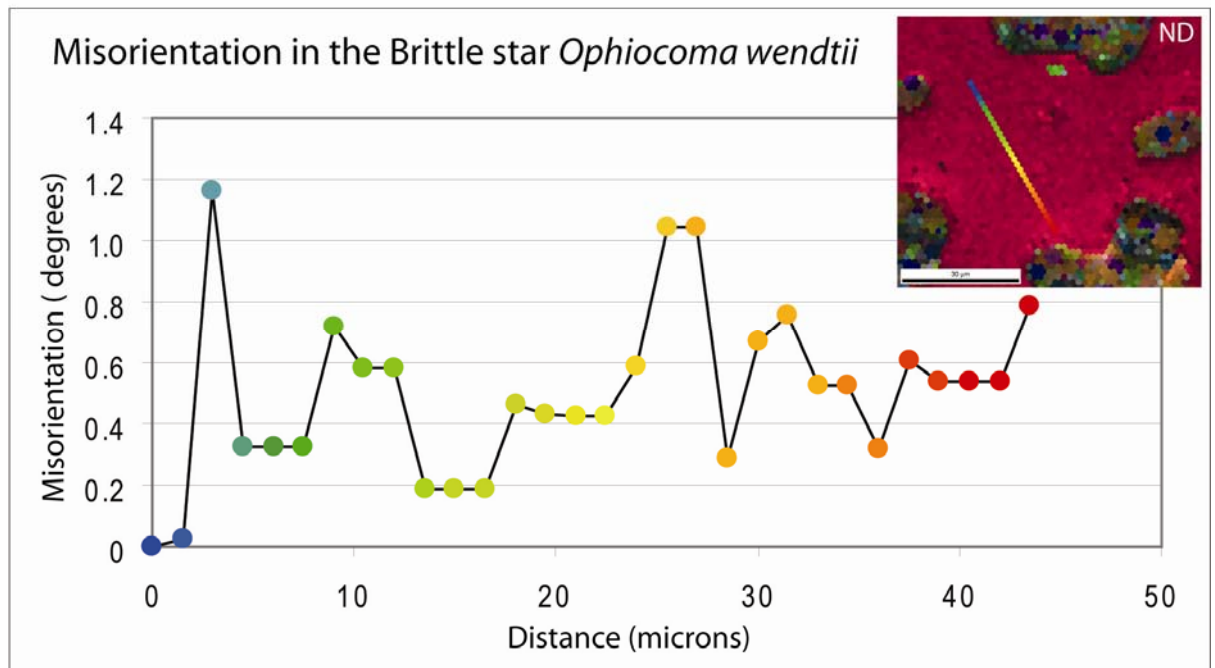


Figure 6.10 - Misorientation in a lens of the brittlestar *Ophiocoma wendtii*. Misorientation shows that the single crystal of the brittlestar stereom is composed of numerous micron-scaled subgrains. Misorientation of each point is relative to the first point. Colour of points on the graph corresponds to their position along the line in the inset image.

6.2.1.4 Energy Dispersive X-Ray Spectroscopy

EDS work on the DAPs show that Mg is present in both the lenses and the labyrinthine stereom in the form of HMC; its distribution is homogeneous (Figure 6.11). EDS analysis shows that the Mg content of the lens is in the region of 17.6

mol % MgCO_3 (Table 6.1); analyses by atomic absorption is consistent with this yielding a value of 16.9 mol % MgCO_3 .

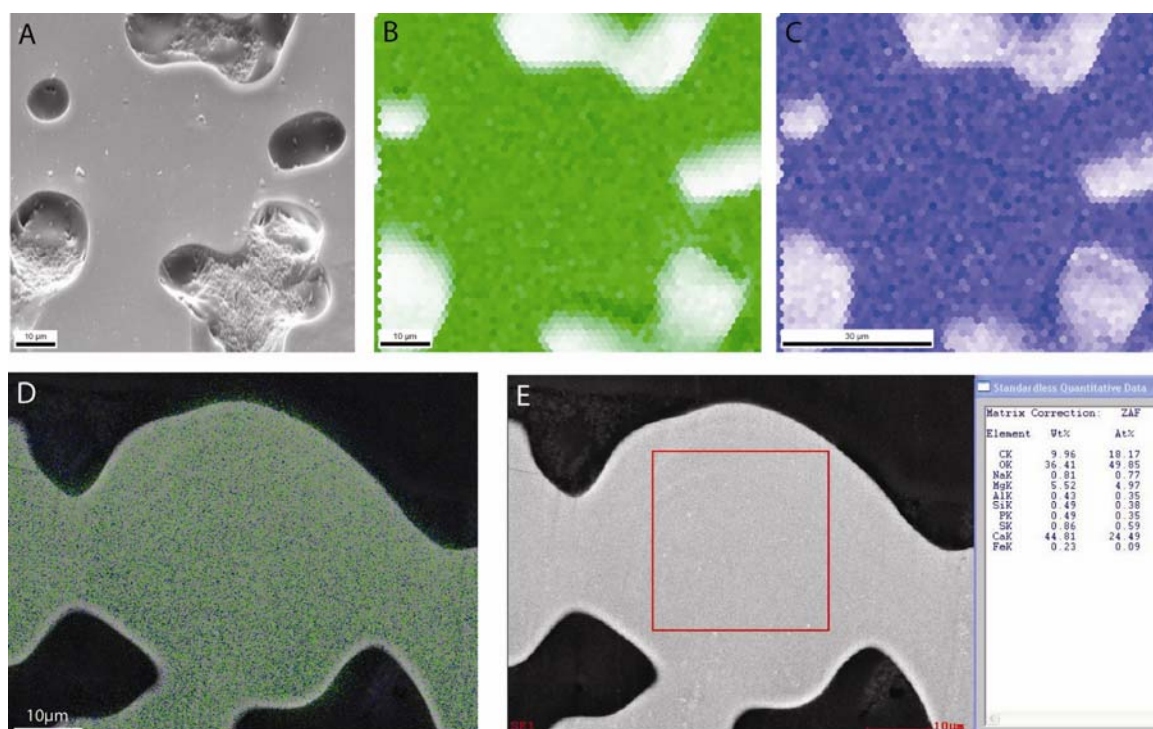


Figure 6.11 – Energy Dispersive X-Ray mapping of lenses in the brittlestar *Ophiocoma wendtii*.

EDS analysis carried out simultaneously with EBSD provides a qualitative indication of lens chemistry; calcium, magnesium, carbon and oxygen are detected. A. SE image of the lens mapped, B. location of Ca (green) within the sample. C. location of Mg (blue) within the sample. D-E. Semi-quantitative EDS analysis shows the same result. Colours in map D denote the presence of Ca (green) and Mg (blue). Values in E correspond to the area within the red box. Lenses are cut in A. the tangential plane and D. The horizontal plane.

Table 6.1 - Quantitative chemical analysis of the dorsal arm plate of the brittlestar *Ophiocoma wendtii*. 'MN' and 'SD' denote mean and standard deviation respectively.

SAMPLE	FEATURE	MOL % CaCO ₃				MOL % MgCO ₃				MOL %SrCO ₃				MOL % FeCO ₃				MOL % MnCO ₃				n
		MN	MAX	MIN	SD	MN	MAX	MIN	SD	MN	MAX	MIN	SD	MN	MAX	MIN	SD	MN	MAX	MIN	SD	
Brittlestar	Lens	82.22	82.45	81.94	0.23	17.60	17.82	17.38	0.18	0.09	0.13	0.07	0.02	0.07	0.16	0.00	0.07	0.03	0.11	0.00	0.05	4

6.2.2 Interpretation

6.2.2.1 Code V Optical Modelling

Optical modelling was used to assess how effective the brittlestar lenses are at focusing light and what affect the aplanatic surface has on the aberration of the lens. Although Aizenberg *et al.* (2001) and Aizenberg and Hendler (2004) have commented on the aplanatic nature of the lens base and the position of photoreceptors (section 1.6.1), and determined focal length and lens aberration experimentally, no computer based optical modelling was carried out.

Surface curvatures were determined from a SEM image from Aizenberg *et al.* (2001) (Figure 6.12) and using the method detailed in section 2.8.2.1. This image was used, rather than SEM images obtained during the present study, as it appears to provide a more central cross sectional view than any of the samples prepared for this study. Ray tracing analysis of the brittlestar lens was carried out using two different sets of surface curvatures. Firstly, the lens shape outlined (in red/orange) by Aizenberg *et al.* (2001) (Figure 6.12), which does not follow the line of the lens exactly but was stated to be the profile of a lens compensated for spherical aberration (hereafter referred to as shape 1).

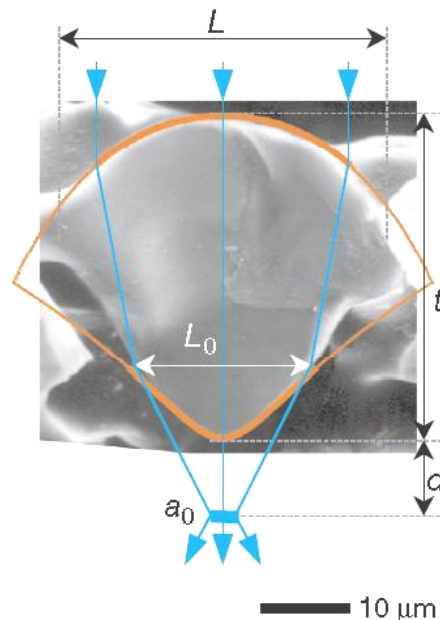


Figure 6.12 - Surface curvatures of the brittlestar lens used in Code V optical modelling. The red/orange line denotes the shape of a lens compensated for spherical aberration (Aizenberg *et al.*, 2001) (shape 1). Note how this does not exactly match the shape of the brittlestar lens (shape 2). Blue lines represent light rays, the blue rectangle where they converge indicates the position of the photoreceptors. Image from Aizenberg *et al.* (2001, figure 1g).

Secondly, the actual shape of the lens determined by tracing the lens outline in the same image (hereafter referred to as shape 2). This will allow an assessment of brittlestar lens (shape 2) function to be made as it can be compared to a lens of optimum shape (shape 1).

As EBSD has confirmed that brittlestar lenses have uniform *c* axis orientation parallel to the lens axis (see section 6.2.1.3), all paraxial rays will also be ordinary. Ray tracing was executed for paraxial/ordinary rays and extraordinary rays (Figure 6.13).

Ray tracing results of shape 1 show that paraxial rays are focused at approximately one quarter of the depth of extraordinary rays with an aberration of less than half (Figure 6.13A-B). Here the RI of the HMC lens has been assumed to be the same as dolomite (section 2.8.2.4) however in reality, the RI will vary depending on the concentration of Mg in the calcite. Code V ‘optimisation’ of the RI for this lens shape shows that it will be most efficient at focusing light when RI=1.73. This RI, which is closer to that of dolomite (RI=1.68) than calcite (RI=1.66), may be an appropriate value for HMC. This ‘optimised’ RI will result in a focal point 12 μm below the lens with an aberration, or blur circle, of 2 μm .

Ray tracing results of shape 2 (Figure 6.13C-D) also show a significant difference between the focal lengths of paraxial/ordinary rays and extraordinary rays. Ordinary rays are focused at approximately one third of the depth of the extraordinary rays and create an aberration, or blur circle, of less than half that of the extraordinary rays. Aberration of the paraxial rays by a lens of shape 2 is greater than that of shape 1 at 5 μm , this is expected as the actual shape of the lens (shape 2) is slightly off the shape of a lens compensated for spherical aberration (shape 1) (Figure 6.12).

The addition of a thin (5 μm) virtual layer of organic matter (RI= 1.46) (value from Aizenberg *et al.*, 2001), to mimic the presence of the epidermis that covers the endoskeleton, increases both the back focal length and the aberration of the lenses relative to those modelled without an epidermis (Figure 6.14).

Results are summarised in Table 6.2. A full list of Code V modelling results for *Ophiocoma wendtii* are listed in Appendix F.

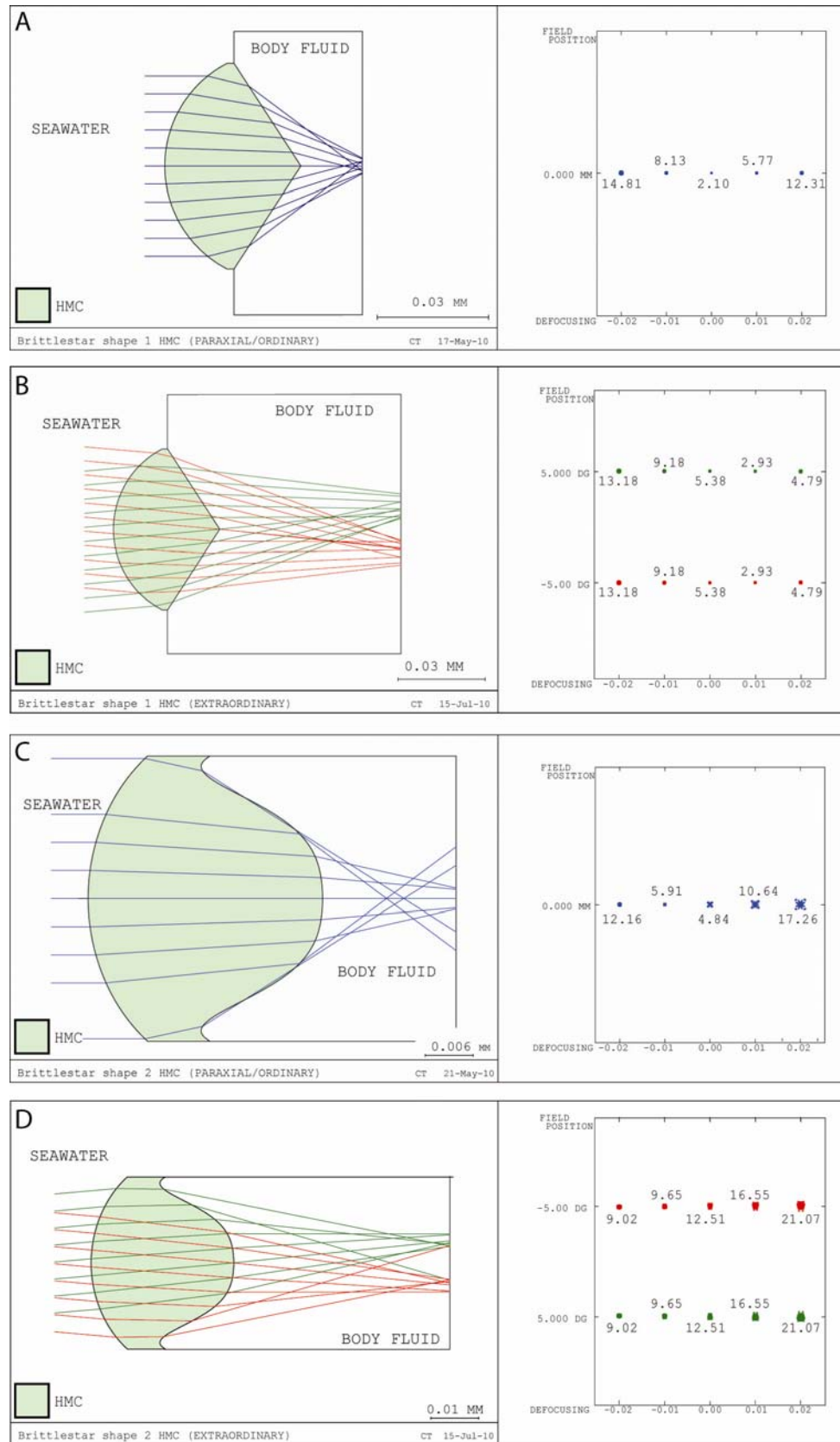


Figure 6.13 – Code V modelling results for lenses in the brittlestar *Ophiocoma wendtii*.

A. Paraxial rays for a lens of shape 1, B. Extraordinary rays for a lens of shape 1, C. Paraxial rays for a lens of shape 2 and D. Extraordinary rays for a lens of shape 2.

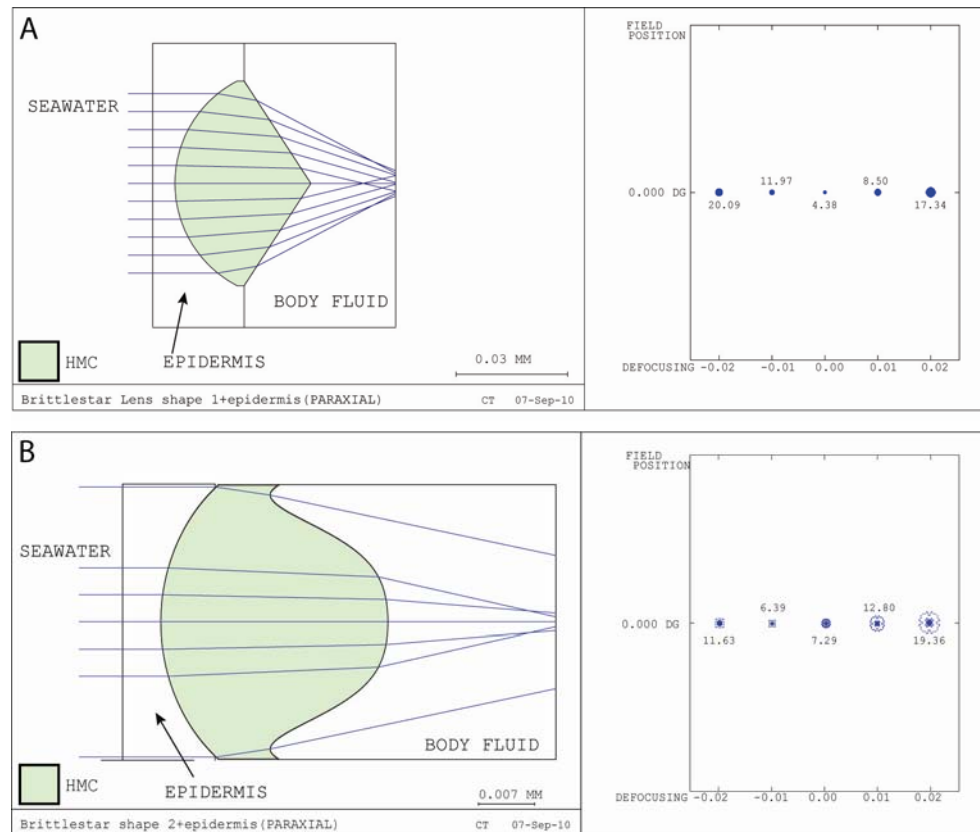


Figure 6.14 - Code V modelling results for lenses in the brittlestar *Ophiocoma wendtii*, with overlying epidermis.
Ray traces and corresponding spot diagrams for lenses of shape 1 (A) and shape 2 (B).

Table 6.2 – Code V modelling results for lenses in the brittlestar *Ophiocoma wendtii*.
Focal lengths and aberration values for brittlestar lenses of the two shapes modelled for both paraxial/ordinary and extraordinary rays.

LENS SHAPE	LENS COMPOSITION	RAY TYPE	BACK FOCAL LENGTH (μm)	ABERRATION (μm)
SHAPE 1	HMC	Paraxial/Ordinary	14	2
		Extraordinary	52	5
	HMC with organic epidermis	Paraxial/Ordinary	19	4
		Extraordinary	75	14
SHAPE 2	HMC	Paraxial/Ordinary	17	5
		Extraordinary	45	13
	HMC with organic epidermis	Paraxial/Ordinary	22	7
		Extraordinary	52	15

6.2.2.2 Sublensar Structures

Assuming the photosensitive components of the brittlestar ‘visual’ system are positioned to maximise the use of light transmitted by the lens they will be

located at the focal point of the lens, i.e. the back focal length, and will occupy an area equal to the spread of light rays at this point, i.e. the aberration value. For lenses of shape 1, with an epidermis, the receptor is calculated to be positioned 19 μm below the lens with a diameter of 4 μm and for shape 2, with an epidermis, 2 μm below the lens with a diameter of 7 μm .

Aizenberg and Hendler (2004) determined the focal point to be only 4-7 μm below the lens and aberration of light rays at this depth to be approximately 3 μm . This was determined by 'collecting' light on photosensitive films positioned at different depths below the lenses (Aizenberg and Hendler, 2004) and by TEM study of thin sections of decalcified DAPs (Aizenberg *et al.*, 2001). However, Code V modelling results of lenses alone, and lenses with an overlying epidermis, are not consistent with this. There are two potential explanations for these disparities (1) the value used for refractive index of the lens is not correct; one possible explanation for this is that the lens calcite contains trace elements or organic components (Aizenberg and Hendler, 2004) that would effect the RI. It should be noted that the RI of the lenses assumed by Aizenberg *et al.* (2001) was 1.66, this is the correct value for calcite, Aizenberg *et al.* (2001) do not consider that the lenses are HMC, which has been determined in the present study by EDS analysis (section 6.2.1.4) and so assumed for optical modelling. (2) Only a small central portion of the lens is responsible for focusing light, Aizenberg *et al.* (2001) determined an operational diameter of 20 μm , this is approximately half the lens diameter.

Optimisation of the brittlestar lens with an overlying organic epidermis (RI=1.46) indicates that in order of the lens to focus light at a depth of 4-7 μm below the lens base, the optimum RI for the lens is 1.79. This RI value would produce an aberration of 7 μm and 5 μm at depths of 4 μm and 7 μm respectively. Despite optimisation of the system to produce these aberration values, they are greater than those determined by Aizenberg *et al.* (2001) and Aizenberg and Hendler (2004). This suggests that a combination of the two explanations above has resulted in these inconsistent modelling results.

The aberration value determined by Aizenberg and Hendler (2004) and by Code V modelling, show that the brittlestar lenses are very effective at focusing light. Although the lenses may be capable of producing images, what the animal 'saw' is determined by the photoreceptive and neural components. Behavioural studies

of brittlestars (e.g. Hendler, 1984) indicate that the visual system was used for detecting variations in illumination levels rather than actually imaging the surrounding environment.

6.2.3 Summary

Brittlestar lenses consist of HMC orientated parallel to the lens axis. The precisely orientated crystals that make up the complex stereom highlight the degree of control that was exhibited during biomineralisation.

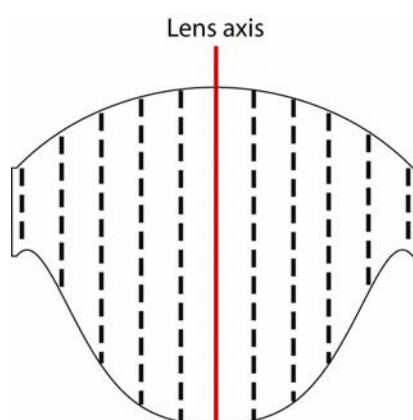


Figure 6.15 - Microstructure of lenses in the brittlestar *Ophiocoma wendtii*. Calcite c axis (indicated by dashed lines) is parallel to the lens axis in all parts of the lens and skeleton.

Other than being composed of HMC calcite with an aplanatic base, the brittlestar lenses bear little resemblance to lenses in the schizochroal eyes of trilobites, which display partitioning of magnesium in different regions of lens calcite and have variations in c axis orientation. The aplanatic base of the lenses does aid focusing of light but there are no intralensar structures to enhance focusing unlike in schizochroal eyes. At best, using aberration values from Aizenberg et al. (2001), brittlestar lenses create a blur circle of 7.5% the lens width; the blur circle of the trilobite *Phacops* sp. (section 5.3.1) is less than 1% of the lens width.

To overcome the problem of RI uncertainty, precise determination of the refractive index in brittlestars, and indeed ostracods, could be carried out using a refractometer. Analysis of Raman spectroscopy would also provide information on the inclusion of organics in the lenses.

7

Discussion

7.1 Eye Function

As members of the Arthropoda, both crustaceans (specifically *Limulus*) and insects are obvious choices for a comparison of trilobite eyes to extant groups and for allowing assumptions to be made as to the functioning of the trilobite visual system. High-resolution imaging may seem advantageous in any eye but in the compound eye there are other requirements, which may rank higher up a list of functional priorities (section 1.4.1). High-resolution imaging is often compromised so that functions warranted by particular environmental conditions or modes of life can be achieved (Young and Downing, 1976; Cronin 1986). Thus, for example, pelagic animals may require a wider field of view (FOV) as they are exposed from all angles and deep-sea dwellers require high sensitivity to light as they inhabit environments with low levels of illumination. The function of an eye is not only reflected in its external morphology, but also in the photoreceptors below.

In order to determine the number, size and arrangement of photoreceptors in the trilobite eye, there are several variables of importance in animal vision that must be understood. These variables are resolution, sensitivity, F-number, and eye parameter.

7.1.1 Resolution and Sensitivity

Resolution, or ‘sampling frequency’ is the ‘precision with which an eye splits up light according to its direction of origin’ (Land and Nilsson, 2002, p.34). It is determined by two factors: (1) the quality of the optics, i.e. how well the lens can focus light rays and (2) the fineness of the mosaic of retinal detectors,

which is determined by the size of the individual detectors and the area they occupy (Land and Nilsson, 2002).

Sensitivity is a measure of how good an eye is at making full use of its potential resolution and is defined by Land and Nilsson (2002, p.51) as ‘the number of photons caught per receptor when the eye views a scene of standard radiance’. In order to reach its maximum potential, the eye must get a sufficient amount of light to the receptors (Land and Nilsson, 2002). Sensitivity is therefore important for animals living in dim environments.

Resolution and sensitivity values were determined for both holochroal eyes and schizochroal eyes using the following equations.

$$\text{Resolution (sampling frequency)} = 1 / \sqrt{3}\Delta\theta \text{ (cycles per radian)}$$

Equation 1 – Resolution in a compound eye with hexagonal lens packing.
(Equation from Snyder, 1977).

$$\text{Resolution (sampling frequency)} = 1 / 2\Delta\theta \text{ (cycles per radian)}$$

Equation 2 – Resolution in a compound eye with square lens packing.
(Equation from Snyder, 1977).

Where $\Delta\theta$ is the interommatidial angle, i.e. the angle between lens axes.

$$\text{Sensitivity} = (\pi/4)^2 A^2 (d/f)^2 1 - e^{-kL} (\mu\text{m}^2.\text{sr.})$$

Equation 3 - Sensitivity of receptors in a compound eye.
(Equation from Land, 1981a).

Where A is the diameter of the lens, or the entrance pupil diameter (EPD - the width of the aperture through which light enters the lens) (section 2.8) (Figure 7.1) defined from optical modelling, whichever is smaller; d is the receptor diameter; f is the effective focal length; k is the absorption coefficient for light rays absorbed by tissues, (0.01 for invertebrate receptors made of microvilli); and L is the length of the receptors (Figure 7.1).

The length of receptors (i.e. the rhabdom length) in modern animals varies significantly. Some mesopelagic crustaceans have rhabdoms as short as 70 μm (Meyer-Rochow and Walsh, 1978) whereas other species have rhabdoms that reach 350 μm (Land, 1981b). Variations are even seen between eyes within the same animals when both medial and lateral eyes are present (Land, 1981b).

Sensitivity is, in part, determined by the effective focal length (EFL) of the lens (Equation 3). Code V modelling provided the back focal length (BFL) of the lens only. The EFL includes part of the lens thickness, from the nodal point to the

lens base. The nodal point of each lens has been determined by extrapolating the incident rays and their resultant refracted rays and noting the line of intersection; the nodal point is in the centre of this line (Figure 7.2). In plano-convex lenses, this is the lens base as there is no refraction of paraxial rays at the planar surface.

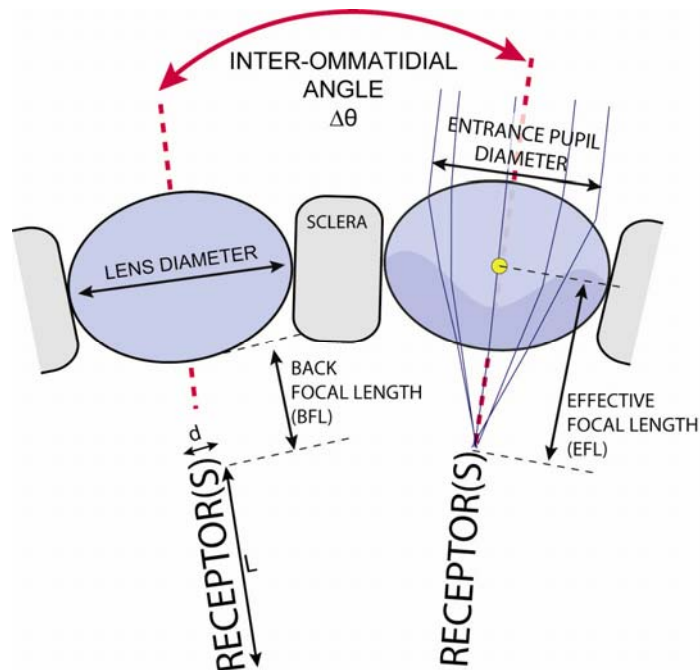


Figure 7.1 - Terms used in calculating resolution and sensitivity in compound eyes. The yellow point indicates the nodal point of the lens, the point from which the effective focal length is measured.

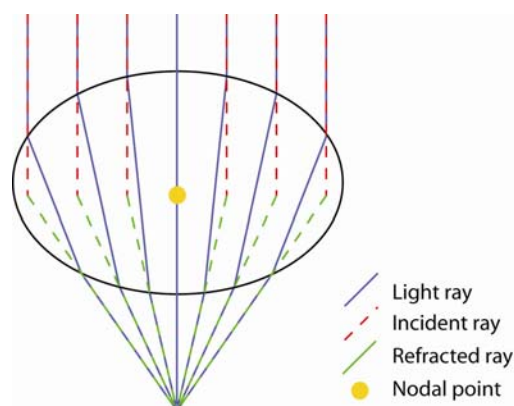


Figure 7.2 - Determination of the lens nodal point in a biconvex lens. Blue lines represent the actual pathway of light. Incident rays and their resultant refracted rays are extrapolated to reveal the line along which the nodal point lies, the nodal point is the central point along this line.

7.1.2 F-number

F-number (or $f\#$) (Kirschfeld, 1974; Land, 1981a) is a dimensionless number that gives a quantitative indication of the amount of light that a lens will transmit to

the image plane behind it. The higher the F-number of a lens, the less light per unit area will reach the image plane. F-number is calculated using Equation 4.

$$\text{F-number} = \text{focal length} / \text{entrance pupil diameter}$$

Equation 4 - F-number.

(Equation from Land, 1981a)

7.1.3 Eye parameter

The eye parameter (p) is a dimensionless number used to indicate the illumination level for which a compound eye is optimised. Optimisation of visual systems to particular light levels was first proposed by Snyder (1977), who termed it ‘optimum compound design theory’. The greater the value of p , the lower the illumination level to which the eye is suited. Diurnal insects living in bright environments have very low values ranging from 0.5 to 1.0 and insects active in dim-light have values reaching 2.0 (Fordyce and Cronin, 1989). Deeper water (100m) animals, such as the isopod *Cirolana*, have been shown to have relatively high p values (4-14), showing that their eyes are adapted to dark conditions (Nilsson and Nilsson, 1981). Modern crustaceans inhabiting similar environments to those suggested for phacopid trilobites (Bruton and Haas, 2003b) (i.e. on or near the sea floor where light levels were low) have mid-range values of between 2 and 4 (Fordyce and Cronin, 1989). The p values of some holochroal eyed trilobite species have been used as an indication of palaeobathymetry (McCormick and Fortey, 1998) (see Table 7.1 for values). The eye parameter is calculated using the following equation:

$$p = D \times \sqrt[3]{\Delta\theta} \text{ (rad-}\mu\text{m)}$$

Equation 5 - Eye parameter (p) of a compound eye.

(Equation from Snyder, 1977)

Where D is lens diameter and $\Delta\theta$ is interommatidial angle. Eye parameters in the present study are measured in the antero-posterior direction, i.e. the horizontal plane of vision, as this is the orientation in which most specimens were cut (section 3.2.1.1) and modelled in Code V.

7.1.4 Holochroal Eye Function

Holochroal eyes, in general, are thought to function in a similar manner to many modern insect and crustacean eyes (Clarkson, 1979); i.e. as an apposition eye with a radial system of ommatidia (Clarkson *et al.*, 2006). This interpretation is

based on the morphology of the eye, optical modelling of the lenses (Clarkson, 1979) and comparisons with modern animals, as no evidence of sublensar structures have been found in holochroal eyes. The findings of the present study are consistent with this, as ray tracing showed that ordinary rays entering the lens across a range of angles are focused to approximately the same point below the lens (section 4.2.2.1) and are likely to have been focused on the tip of a rhabdom as in apposition eyes (section 1.3.2.1). The overall result of an apposition-type holochroal eye would be that of a mosaic image (Clarkson, 1979); the number of pixels dependant on the number of lenses, over 15,000 per eye in some species (Clarkson in Kaesler, 1997).

Table 7.1 – Resolution, sensitivity, F-number and eye parameters of holochroal trilobite eyes.

Sensitivity, like eye parameter, appears to be linked to mode of life. Mode of life has been taken from the literature where available. Values for some holochroal eyed trilobite species and *Cirolana*, a modern isopod are given for comparison (blue). Where two values are given for eye parameter, these correspond to the median values of the two eyes of the specimen as calculated by McCormick and Fortey (1998). Genera are listed in order of presumed increasing depth in the water column.

GENUS	RESOLUTION (cycles per radian)	SENSITIVITY ($\mu\text{m}^2\cdot\text{sr.}$)	F#	EYE PARAMETER (rad- μm)	MODE OF LIFE
<i>Paladin (Meraspis)</i> PE92	4.00	116	1.14	0.73	Planktonic (Clarkson and Zhang, 1991)
<i>Carolinites angustagena</i> C2.6	2.53	407	1.52	2.70	Epipelagic (McCormick and Fortey, 1998)
<i>Carolinites killaryensis utahensis</i>	-	-	-	3.17 / 4.16	Epipelagic (McCormick and Fortey, 1998)
<i>Paladin (Holaspis)</i> PE93	2.48	371	1.92	2.80	Benthic (Clarkson and Zhang, 1991)
<i>Cirolana borealis</i>	1.9	4200	1.0	4-14	Benthic 100m (Nilsson and Nilsson, 1981)
<i>Symphysops subarmata</i> SS93	2.13	5110	2.13	9.20	Mesopelagic (Fortey and Owens, 1987)
<i>Pricyclopyge binodosa</i>	-	-	-	7.06 / 8.31	Mesopelagic (McCormick and Fortey, 1998)
<i>Telephina bicuspis</i> T95	1.69	6054	1.33	17.02	Mesopelagic

Assuming that photoreceptors are positioned at the lens focal point, determined by Code V modelling, the retina in a holochroal apposition eye would be found at a depth of 0.6 to 2.6 times the lens thickness. Values of resolution and sensitivity in holochroal eyes have been calculated using Equation 1 and Equation 3 (section 7.1.1), and the results vary greatly (Table 7.1). Values of both resolution and sensitivity are however still consistent with the modern animals from mid-water to deep-sea habitats or of nocturnal and crepuscular (active during dusk and dawn) activity (Land and Nilsson, 2002).

Sensitivity may provide information on the palaeobiology of these trilobites. Variations in sensitivity would be expected between animals of different habitats. For example, epipelagic forms would require less sensitivity to light than mesopelagic forms due to greater illumination in their environment. Similar trends were noted by McCormick and Fortey (1998) in terms of eye parameters (values are listed in Table 7.1), which have also been calculated here (Table 7.1) using Equation 5 (section 7.1.3). F-number (Table 7.1), calculated using Equation 4 (section 7.1.2), of holochroal lenses is higher but on the same scale as the modern isopod *Cirolana*. These relatively low F-numbers indicate that the lenses were constructed in such a way as to maximise light capture.

Resolution values and F-number for meraspid stage *Paladin* eyes (Table 7.1) are the highest and lowest respectively for all the holochroal eyes modelled. Across the range of holochroal eyes modelled, there is a general trend between resolution, sensitivity and eye parameter. An increase in sensitivity goes hand in hand with an increase in eye parameter, which is expected as animals with eyes of high sensitivity tend to live in dim environments (Land and Nilsson, 2002, pp.51-52) as they require eyes that are optimised for low light levels (i.e. have a high eye parameter value). Resolution is often compromised in favour of sensitivity in these animals (Land and Nilsson, 2002, pp.52) explaining the negative correlation between the two factors in holochroal eyes. Mode of life also ties in with the general trend of resolution, sensitivity, F-number and eye parameter as it is directly linked with illumination levels. Although the mode of life of the Telephinid *Carolinites* is well established (Fortey, 1985), that of *Telephina* is less well constrained, simply being described as 'pelagic' (Bruton and Høyberget, 2006). The high sensitivity and eye parameter, combined with

the low resolution of this eye (Table 7.1), suggests that it adopted a mesopelagic mode of life.

Clear differences in both resolution and sensitivity exist between the holaspis and meraspis forms of *Paladin* (Table 7.1); the juvenile forms compromising on sensitivity in order to achieve better resolution. This strategy may have played an important role in the survival of juveniles, which could not enrol (Clarkson and Zhang, 1991); with fewer lenses, increased resolution would provide better detection of predators than increased sensitivity. Adults, with a greater number of lenses, would already have better motion detection across the field of view and so increasing sensitivity would be more advantageous. The switch in resolution and sensitivity from meraspis to holaspis may also reflect a change in mode of life from planktonic to benthic (Clarkson and Zhang, 1991). This change in mode of life would result in a decrease in light levels, which in turn is reflected in the eye parameter values, which are significantly lower in the meraspis form. The F-number of the meraspis lenses suggests that these were more efficient at directing light to the photoreceptors than the adult lenses, this again may have been necessary for the survival of the more vulnerable juveniles.

7.1.5 Schizochroal Eye Function

As for holochroal eyes, the soft parts of the visual system in schizochroal eyes have yet to be found and so it is unclear what the overall structure of the eye may have been and how it would have functioned *in-vivo*. Interpretations have been made in previous studies, based on lens microstructure and arrangement as to what the most likely internal eye structures are; three distinct models have been proposed:

(1) Apposition eye: Clarkson (1967) proposed that the schizochroal eye was one of ommatidial type, specifically apposition (section 1.3.2.1). The option of a superposition-type eye (section 1.3.2.2) is ruled out (Clarkson, 1967) based on the intersection point of lens axes relative to the centre of curvature of the eye (Figure 7.3). Modern arthropods with superposition eyes have a convergence point close to the centre of curvature of the eye (Figure 7.3A), those with apposition eyes have a convergence point half way between the eye surface and its centre of curvature (Figure 7.3B); the latter is what is seen in schizochroal eyes (Clarkson, 1979). Clarkson (1979) argued that the ommatidia would be large

and ‘moderately long’ as ommatidial size is related to lens size. Such an arrangement would result in the production of an ‘image’ consisting of a mosaic of dots, the number determined by the number of lenses (Clarkson, 1979).

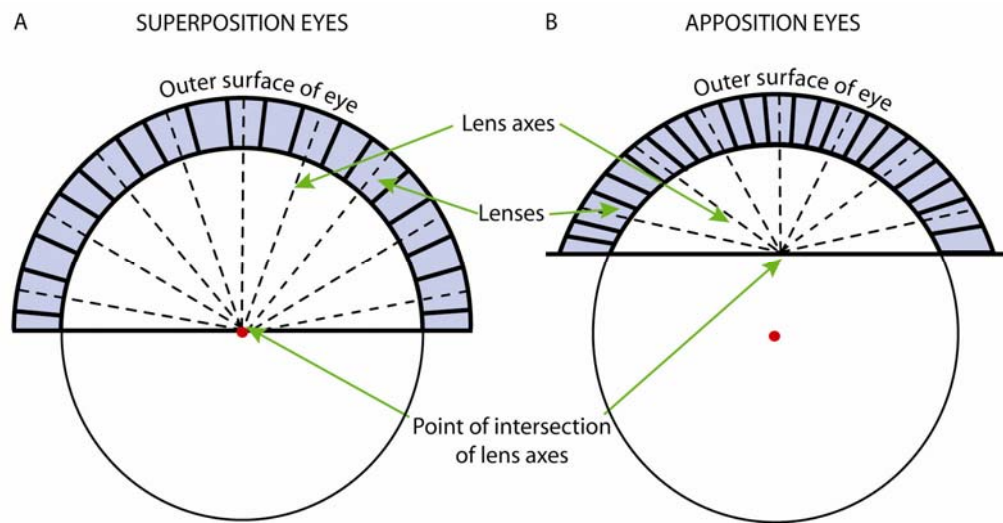


Figure 7.3 - Intersection angles of lens axes in superposition and apposition eyes. Schematic diagrams of A. superposition eyes and B. apposition eyes. Note that the convergence point in A. is close to the centre of curvature of the visual surface (red point) whereas in B. it is approximately half way between the centre of curvature and the visual surface. Image modified from Clarkson (1967, figure 3c-d).

(2) Ocellar-like eye: Campbell (1975) suggested that phacopid trilobites may have possessed an eye similar to the ocellar eyes found in modern slow-moving terrestrial and aquatic arthropods (Figure 7.4); this was later supported by Clarkson (1979). The ocellar eye is a simple eye rather than a compound eye. The ocellar eyes of spiders, consists of six or eight ocelli (Land and Nilsson, 2002, p.95). These ocelli, which are paired according to different FOVs (e.g. antero-median and postero-lateral), have different photoreceptor arrangements (Land and Nilsson, 2002, p.95). Campbell (1975) suggested this model, not on any direct evidence but based on the fact that in the schizochroal eye both lens diameter and inter-ommatidial angles are much larger than in any known apposition eyes. Campbell (1975) claimed that the schizochroal eye is therefore unlikely to be of apposition-type. The ocellar eye consists of a lens at the apex of a capsule that is host to numerous rhabdoms that are positioned below a layer of ‘corneogeneous material’. The top of the reticular layer (i.e. the rhabdoms) is assumed to be at the depth of the focal plane; calculated by Campbell (1975) to be approximately 1.6 times the lens thickness for an ordinary beam parallel to the lens axis. Campbell (1975) commented that the rhabdoms themselves are assumed to be relatively short so as not to obstruct the muscle bundles of the

palpebral region. This optical system was thought to be an adaptation to movement perception. Campbell's (1975) ray tracing analysis of lenses showed that acute vision is only achieved in the most central rhabdoms raising questions as to the effectiveness and therefore presence of peripheral rhabdoms. Campbell (1975) did not discuss the possibility of different photoreceptor arrays below lenses with different FOVs.

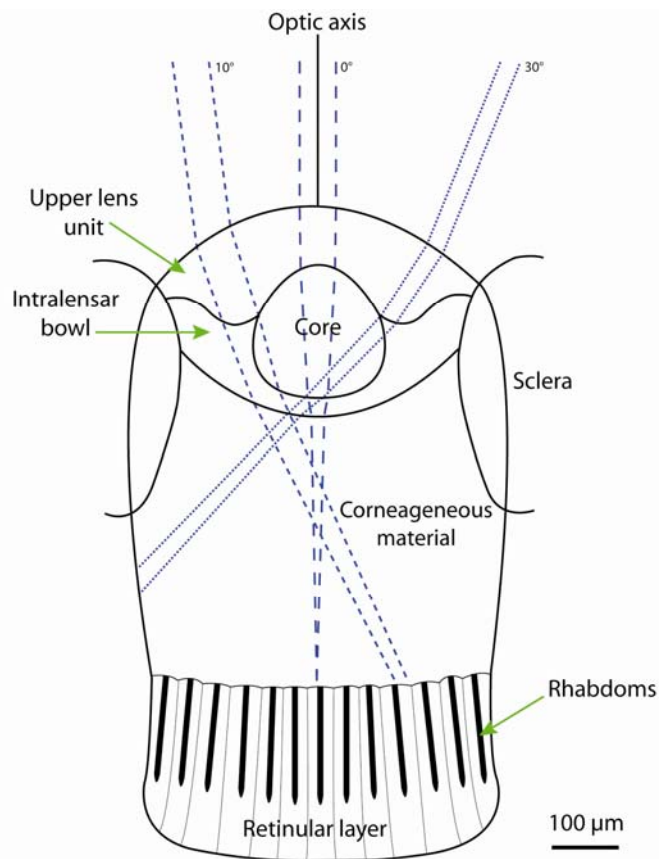


Figure 7.4 - The internal structure of a unit within an ocellar-like trilobite eye. Blue lines indicate light rays. Values beside them indicate the angle of incidence relative to the optic axis. Modified from Campbell (1975, figure 8). The corneogeneous layer is comparable to the clear zone in superposition eyes (section 1.3.2.2, Figure 1.4).

Neural superposition eye: Schoenemann (2007) proposed a new type of neural superposition eye (section 1.3.2.1.1) in which each lens acts as an 'eyelet' similar to that which is seen in the strepsipteran insect *Xenos peckii* (Buschbeck *et al.*, 1999, Buschbeck, 2005, Buschbeck *et al.*, 2003) (Figure 7.5A). This insect has numerous rhabdomeres (about 100) a short distance below each lens (Buschbeck *et al.*, 1999, 2003; Buschbeck, 2005). Schoenemann (2007) suggested that rhabdomeres in the schizochroal eyelets did not lose resolution as is the case in modern neural superposition eyes (Kirschfeld, 1971), but that each individual rhabdomere contributed a single pixel in an image that consisted

potentially of many thousands of pixels; Schoenemann (2007) calculated that there could be up to 2200 receptors below each lens. When information from both eyes is combined, this 'hyper-eye' construction would be capable of producing high resolution stereoscopic images.

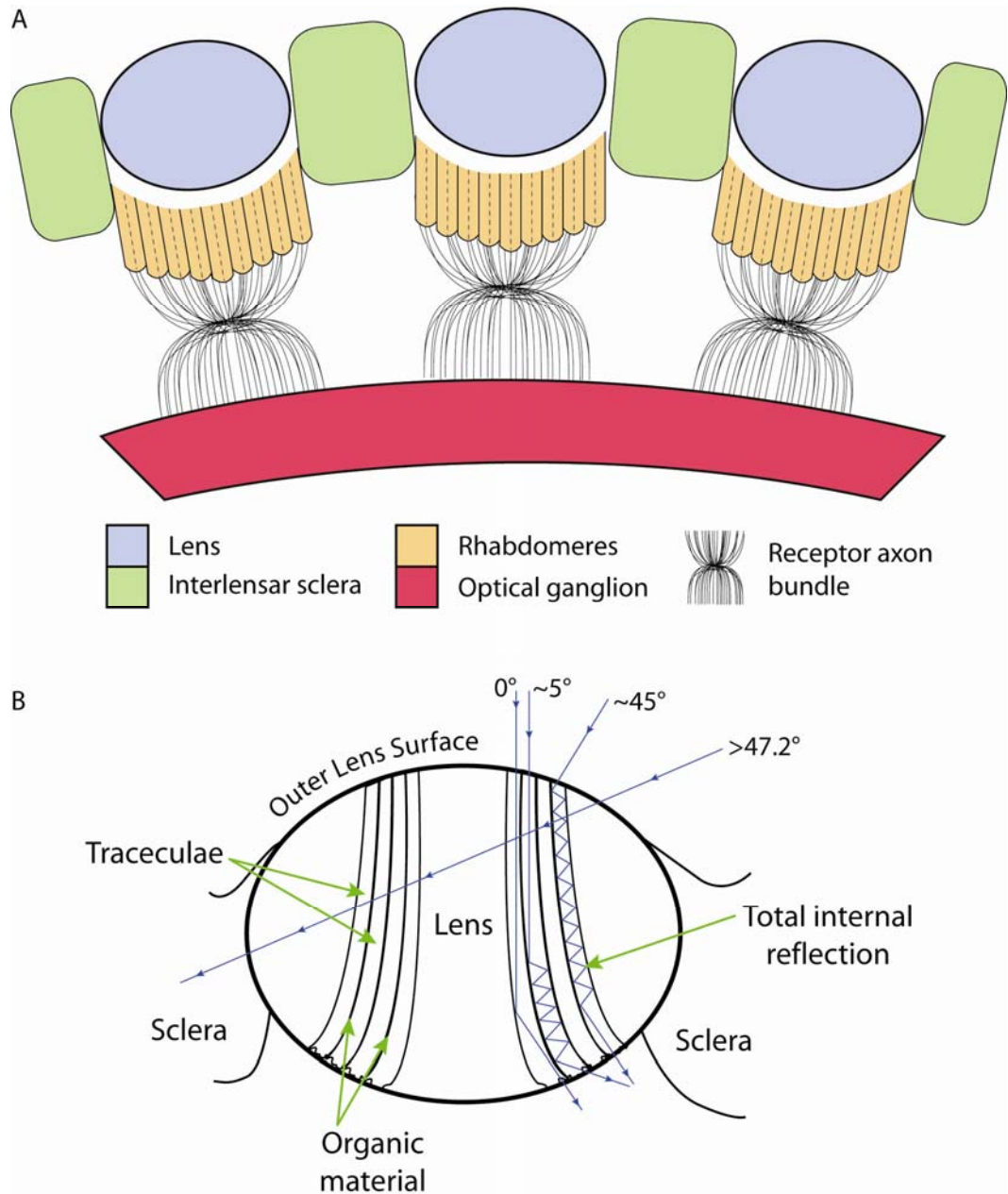


Figure 7.5 - Internal structure of the neural superposition trilobite 'hyper-eye'. Schematic diagram showing A. The interpreted understanding of the sublensar structure of the hyper-eye based on descriptions by Schoenemann (2007). The cornea has been omitted from this diagram for simplicity. B. Total internal reflection within the light-guiding structures in the lenses. Blue lines represent light rays. Values beside them indicate the angle of incidence relative to the optic axis. Modified from Schoenemann and Clarkson (2008a, figure 3d).

Schoenemann and Clarkson (2008a) suggested that the trabeculae in the schizochroal lenses may have acted as light guides, channelling rays, by total

internal reflection (Nilsson, 1990) to the retinal layer below (Figure 7.5B). Oblique rays entering the lens at more than 42.7° relative to the optic axis would pass directly through the lens, escaping at the other side (Schoenemann and Clarkson, 2008a). Schoenemann's (2007) model (Figure 7.5) is a more detailed depiction of the 'micromosaic' suggestion posed by Clarkson and Levi-Setti (1975), in which there was a thin retina consisting of numerous sub-units beneath each lens, and the neurophysiological model put forward by Stockton and Cowen (1976) in which sufficient overlap between lens fields of view (Cowen and Kelley, 1976) and neural connections between lenses in vertical files resulted in stereoscopic vision.

As no sublensar structures have been identified in the present study, or conclusively in any previous studies, assessment of photoreceptive components and eye function remains difficult. There are two possible end-member models for schizochroal eye function. A single receptor per lens, ommatidial-type system as was suggested by Clarkson (1967) (Figure 7.3) or a multi-receptor per lens system or 'eyelet' eye similar to that found in the Strepsipteran wasp parasite *Xenos peckii* (Buschbeck *et al.*, 1999, 2003; Buschbeck, 2005), proposed as a model of schizochroal eye function by Schoenemann (2007) (Figure 7.5). The following discussion aims to test both models and assess the likelihood of either operating in the schizochroal trilobite eye. The lens dimensions and optical properties (focal length, aberration etc) for this assessment are taken from a specimen of *Phacops* sp. (PM27) as this sample has a distinctive intralensar bowl and has been used most extensively for optical modelling.

Resolution and sensitivity have been calculated for eyes consistent with both models and are based on several assumptions:

- (1) The lens functions to its best ability, i.e. as determined by Code V optimisation (section 5.3.1, Figure 5.42).
- (2) The length of the ommatidium/capsule in each model is $400\text{ }\mu\text{m}$. This is the same depth, relative to lens thickness, to which the cones or mesodermal capsules reported in other studies extend (Clarkson, 1967; Bruton and Haas, 2003a) (section 1.5.2.2, Figure 5.31).

(3) Rhabdom length is 270 μm . This is based on the rhabdom being positioned at the focal point of the lens (130 μm) (section 5.3.1) and extending, from this depth, to the base of the capsule. Assuming the rhabdom is positioned at this depth also assumes that there is a significant space above each rhabdom (see section 1.3.2.2). This may have been occupied by corneogeneous cells (i.e. forming a clear zone) or alternatively may have been occupied by a soft equivalent to the crystalline cone (section 1.3.2) that was not preserved.

(4) Rhabdom width is 145 μm , the lateral extent of light rays along the image plane. This is partially controlled by the angular field of view of the lens, which in the case of PM27 is $\pm 9^\circ$ about the lens axis. This assumed width is large relative to rhabdoms in modern eyes however, increase in rhabdom width by 4-5 times has been reported in insects with dark adapted apposition eyes (Greiner *et al.*, 2004). Also, the rhabdom in the apposition eye of the isopod *Cirolana borealis*, which lives at a depth of 100 m, occupies the same width as the lens that sits above it, approximately 150 μm (Nilsson and Nilsson, 1981, figure 2).

7.1.5.1 Model 1: Single Receptor per Lens System (Ommatidia-Type Eye)

A single receptor per lens, or ommatidial system, would compromise resolution of images in favour of sensitivity (Figure 7.6). The resolution of an eye is constrained by lens size and inter-ommatidial angle (Land and Nilsson, 2002); in order to produce an image of high-resolution a small inter-ommatidial angle is vital. This requirement imposes a restriction on lens diameter, as the larger the lens, the greater the angle between neighbouring lenses. To maximise sensitivity however, the lens in an ommatidial system is presumed to be relatively large with a wide FOV/light intake angle and is perhaps most beneficial in dimly lit environments where lower photon levels make it more important to use the available light efficiently. The size of the photoreceptive unit in such a system would be determined by the focusing capability of the lens above. Where the lens focuses light to a well-constrained convergence point, a small receptor would be appropriate. However, where the lens does not focus light well, a larger receptor would be more beneficial in order to maximise the capture of light. Resolution and sensitivity values for the receptor in this system were calculated using the values in Figure 7.6.

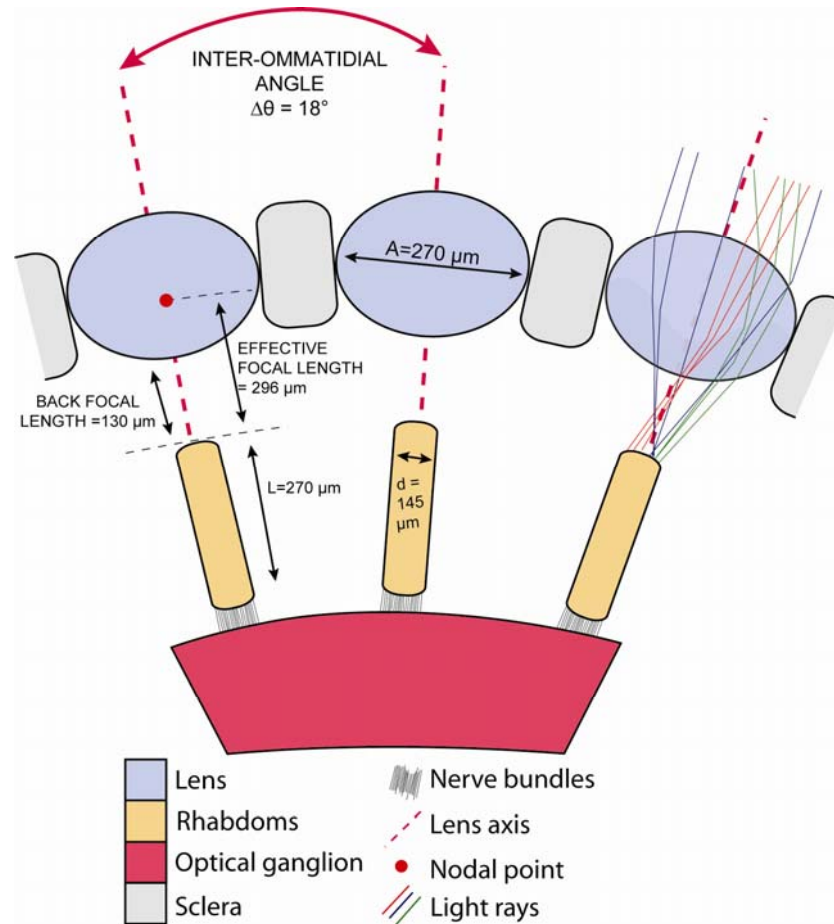


Figure 7.6 – Schematic cross-section through a ‘single receptor per lens’ system. Lens measurements were made from TL images; focal length measurements are taken from Code V modelling results. Receptor diameter is assumed to be equal to the total area onto which light is focused at the focal point. For simplicity, the intralensar bowl and a few light rays are shown on one lens only.

7.1.5.1.1 Resolution and Sensitivity

Resolution of this system is based on the inter-ommatidial angle ($\Delta\theta$) of 18° , the average field of view calculated for lenses in sample PM27 (section 2.8.2.2). Values are expressed in radians.

$$\begin{aligned}\text{Resolution (sampling frequency)} &= 1 / \sqrt{3\theta} \text{ (in radians)} \\ &= 1 / \sqrt{3 \times 0.31} \\ &= 1.04 \text{ cycles per radian}\end{aligned}$$

Equation 6 - Resolution of a single receptor per lens system.

(Equation from Snyder, 1977).

$$\begin{aligned}\text{Sensitivity} &= (\pi/4)^2 A^2 (d/f)^2 1 - e^{-kL} \\ &= 0.62 \times 270^2 \times 0.49^2 \times 0.93 \\ &= 10,092 \mu\text{m}^2 \cdot \text{sr}.\end{aligned}$$

Equation 7 - Sensitivity of receptors in a ‘single receptor per lens’ system.

(Equation from Land, 1981a).

7.1.5.2 Model 2: Multiple Receptor per Lens System ('Eyelet' Eye)

A multiple receptor system is able to produce an image with a greater number of pixels. Where there are numerous lenses each with multiple receptors, the culmination of pixels results in the formation of a relatively high-resolution image. The result of 'dividing' light between a large number of receptors is an overall duller image i.e. sensitivity is compromised. Resolution and sensitivity values given below are for each receptor in the eyelet and have been determined using the values in Figure 7.7.

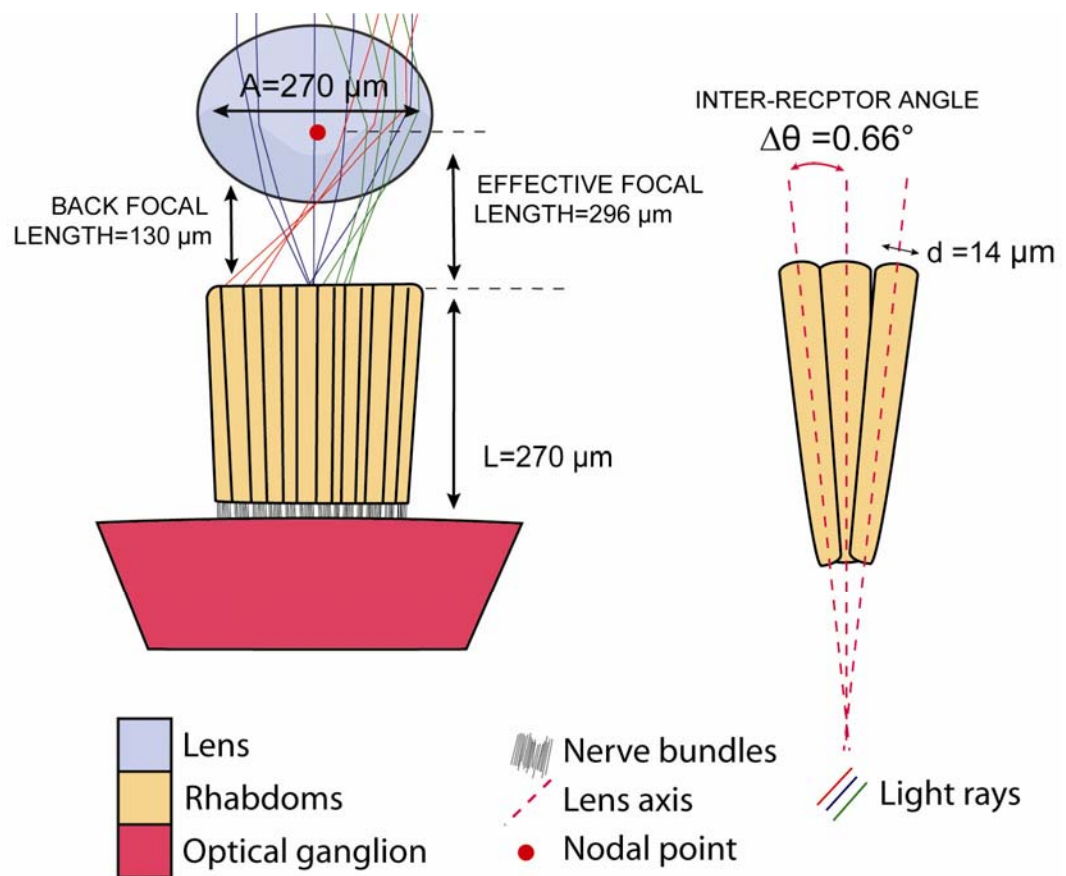


Figure 7.7 – Schematic cross-section through a 'multiple receptor per lens' system. Lens measurements have been obtained from TL images; focal length measurements are taken from Code V modelling results. Light entering the lens from different areas in space are transmitted to receptors on different parts of the rhabdom/retinal surface.

7.1.5.2.1 Resolution and Sensitivity

The equivalent for inter-ommatidial angle in a multiple receptor system is the angle between receptors. Each receptor can only work to its full potential if it can capture all light transmitted by the lens, the diameter of the receptors is therefore assumed equal to the largest blur circle (section 2.8.3) created by light at the focal depth (assumption based on Land and Nilsson (2002, p.34). In

the case of *Phacops* this has been determined by Code V modelling and is 14 μm for light entering the lens at the edge of the FOV, i.e. $\pm 9^\circ$ about the lens axis.

$$\begin{aligned}\text{Resolution (sampling frequency)} &= 1 / \sqrt{3\theta} \text{ (in radians)} \\ &= 1 / \sqrt{3 \times 0.012} \\ &= 5.27 \text{ cycles per radian}\end{aligned}$$

Equation 8 - Resolution of a multi-receptor per lens system.

(Equation from Snyder, 1977).

The position of the receptors in a multiple receptor per lens system is assumed to be the same as in a single receptor per lens system as this value is governed by the focusing capabilities of the lens, which is the same in both models. d/f in this system is reduced by a factor of 10 compared with the previous scenario, as the receptor area is much smaller. The proportion of light absorbed by the receptors ($1 - e^{-kL}$) remains the same, as despite a reduction in diameter of receptors, the same depth within the eye is available so the receptors are assumed to use this.

$$\begin{aligned}\text{Sensitivity} &= (\pi/4)^2 A^2 (d/f)^2 1 - e^{-kL} \\ &= 0.62 \times 270^2 \times 0.05^2 \times 0.93 \\ &= 105.08 \mu\text{m}^2 \cdot \text{sr}.\end{aligned}$$

Equation 9 - Sensitivity of a multi-receptor per lens system.

(Equation from Land, 1981a).

Calculation of resolution and sensitivity value for the two schizochroal eye end-member models enables comparison with modern animals.

7.1.5.3 Comparison with Modern Visual Systems

Some degree of error is involved in all values determined for resolution and sensitivity due to the assumptions that were made (section 7.1.5). The resolution and sensitivity values calculated (Equation 6 - Equation 9), although given to two decimal places (Table 7.2), simply give an indication of the scale of resolution and sensitivity in each model. Most importantly, these values allow for comparison with modern animals in which the photoreceptors have been studied. Comparison with modern animals of varying habitats and modes of life give these numbers (Table 7.2) some meaning. Model 1, the ommatidial-type eye, puts the schizochroal eye on par with the modern isopod *Cirolana borealis* in terms of resolution. Sensitivity, although much higher than this crustacean, is still in the range for nocturnal and deep-water (~100m) animals (Land and Nilsson, 2002 pp. 53). Model 2, the 'eyelet' eye, is more consistent with coastal animals such as *Limulus* in terms of resolution and sensitivity (Land and Nilsson, 2002, pp.52) which may be somewhat low given the benthic mode of life of

phacopid trilobites in often turbid water (Bruton and Haas, 2003b). Based on Equation 2, resolution in the eye of *Barrandeops forteyi*, in which lenses are arranged in a square lattice (section 1.5.2.1, Figure 1.14B) with an interommatidial angle of approximately 13° , would be marginally higher, than that of *Phacops* sp. in Model 1 and an order of magnitude higher in Model 2. In the latter, this would put the schizochroal eye on par with that of the worker bee (Land and Nilsson, 2002 p.38), again this seems unlikely for animals living in dim environments where light may often be obscured. Some comparisons to modern animals are given in Table 7.2.

Table 7.2 - Resolution and sensitivity of photoreceptors in modern animal eyes and schizochroal trilobite eyes.

Results of both schizochroal eye models are highlighted in red. Values for other animals have been obtained from Land and Nilsson (2002, pp. 38,52).

ANIMAL	RESOLUTION	SENSITIVITY	LIGHT HABITAT
Worker bee	30	0.32	Diurnal
<i>Leptograpsus</i> (shore crab)	19	0.5	Diurnal
<i>Pecten</i> (scallop)	18	4.0	Coastal sea floor
<i>Phacops</i> (multiple receptors per lens)	5.27	105	Benthic – turbid waters
<i>Limulus</i> (horseshoe crab)	4.8	83-317	Coastal mainly nocturnal
<i>Cirolana</i> (isopod)	1.9	4200	Deep sea
<i>Phacops</i> (single receptor per lens)	1.04	10100	Benthic – turbid waters

7.1.5.3.1 F- number

F-numbers of schizochroal lenses that were optically modelled are listed in Table 7.3. Values have been calculated for lenses of both LMC and HMC composition and lenses with an intralensar bowl where applicable.

Results show that the F-numbers for all schizochroal lenses modelled are on the same scale as the modern isopod *Cirolana borealis* (Nilsson and Nilsson, 1981). Lenses that have an intralensar bowl have a significantly lower F-number than lenses of the same shape with homogeneous composition. This shows that the inclusion of an intralensar bowl in the schizochroal lens enhances the ability of lenses to transmit light and to focus it, therefore increasing sensitivity.

Table 7.3 - F-numbers of lenses in schizochroal eyes.

Lens and bowl chemistry are indicated by LMC and HMC. EFL is the effective focal length of the lens. Note that F# in *Phacops* and *Ingriops* is at its lowest where there is a HMC intralensar bowl (yellow). A modern arthropod is given for comparison (blue); values are from Nilsson and Nilsson (1981).

GENUS	INCIDENT RAY ANGLE	LENS	BOWL	EFL (microns)	F-NUMBER
<i>Phacops</i> sp. PM27	$\pm 9.00^\circ$	LMC	-	328	1.21
		HMC	-	586	2.17
		LMC	HMC	280	1.04
		HMC	LMC	422	1.56
<i>Ingriops</i> sp. nov. IE48	$\pm 4.42^\circ$	LMC	-	244	0.97
		HMC	-	236	0.94
		LMC	HMC	167	0.67
<i>Boeckops boeckii</i> BB3aR	$\pm 10.00^\circ$	LMC	-	512	1.02
		HMC	-	505	1.02
<i>Geesops schlotheimi</i> G40	$\pm 9.16^\circ$	LMC	-	233	1.17
		HMC	-	230	1.15
<i>Ananaspis macdonaldi</i> LB1C	$\pm 8.6^\circ$	LMC	-	275	1.10
		HMC	-	266	1.06
<i>Odontochile hausmanni</i> OB24RB	$\pm 2^\circ$	LMC	-	2.16	1.44
		HMC	-	2.09	1.39
<i>Cirolana borealis</i>	-	-	-	-	1.0

7.1.5.3.2 Eye Parameter (p)

Previous work reveals eye parameter values of some trilobites with schizochroal eyes to be in excess of 100 (Fordyce and Cronin, 1989, 1993). This was considered to be an indication that optimum compound design theory (section 7.1.3) is not applicable to this type of eye (Fordyce and Cronin, 1989) as the theory is based on the assumption that there is a single ommatidium per lens (Snyder, 1977), which, although generally accepted for the holochroal eye (Clarkson *et al.*, 2006), has not yet been confirmed for phacopid trilobite eyes (Fordyce and Cronin, 1989).

The p value for *Phacops* sp. (PM27) is calculated as follows:

$$\begin{aligned}
 p &= D \times \sqrt[3]{\frac{1}{2} \theta \Delta} \\
 &= 309 \times \sqrt[3]{\frac{1}{2} \times 0.31} \\
 &= 82.96 \text{ rad-}\mu\text{m}
 \end{aligned}$$

Equation 10 - Eye parameter (p) of *Phacops* sp.

(Equation from Snyder, 1977).

The calculated value falls within the range reported for other species with schizochroal eyes (Fordyce and Cronin, 1989) and is almost twice that of the deep sea isopod *Cirolana* (Nilsson and Nilsson, 1981). Whether this indicates that the schizochroal eye of *Phacops* sp. was better suited to even lower light intensities or that it simply does not fit the model of optimum compound design theory is unclear. However, as the present study has determined that a single receptor per lens in the schizochroal eye was probable (see section 7.1.5.4), the former suggestion is favoured.

7.1.5.4 Proposed Model

Calculation of resolution and sensitivity as well as F-number, favour the single receptor per lens model of schizochroal eye function. Resolution and sensitivity are consistent with modern marine arthropods living in dimly lit environments and the F-number indicates that the doublet lens maximises the transmission of light. Given that the chosen optical material in schizochroal eyes is birefringent, this model maximises the collection of light on the receptor, with the effect of double refraction being minimised. All light that is focused on the rhabdoms is averaged as it travels through them by total internal reflection, producing a single signal at the base of the ommatidium (Land and Nilsson, 2002, pp.129-130). If the schizochroal eye consisted of ‘eyelets’, each with their own reticular layer, two different parts of the retina would detect light from the same position in space as a result of double refraction of the rays (Figure 7.8). The only other way to overcome the problem of birefringence would be if the lens acted as a series of ‘light-guides’ as was proposed by Schoenemann (2008a), however such a model provides no explanation for the presence of an aplanatic surface or intralensar bowl, nor would it require the change in RI achieved from the presence of the intralensar bowl.

Compromising the resolution of images in favour of sensitivity by positioning a single receptive unit beneath each lens and keeping it optically isolated from its neighbours using screening pigment (Figure 7.9), as in modern apposition eyes (section 1.3.2.1) including that of *Limulus* (Battelle 2006), would have allowed

schizochroal eyed trilobites to make full use of the available light in a generally dim environment. It is impossible to determine the exact structure of the light sensitive rhabdoms within the eye but these may have been fused forming a single unit, as in apposition eyes, separated as in the neural superposition eye (Land and Nilsson, 2002), or semi-fused as in the eye of the isopod *Cirolana borealis* (Nilsson and Nilsson, 1981). In addition, photoreceptors may have been sensitive to UV light possibly allowing them to enhance sensitivity even further, as is evident in the night active *Limulus* (Herzog and Barlow, 1991). The spacing required between the lens base and the rhabdom tip, for light to be focused, suggests that the eye also had a 'clear zone' like those found in modern superposition eyes (section 1.3.2.2).

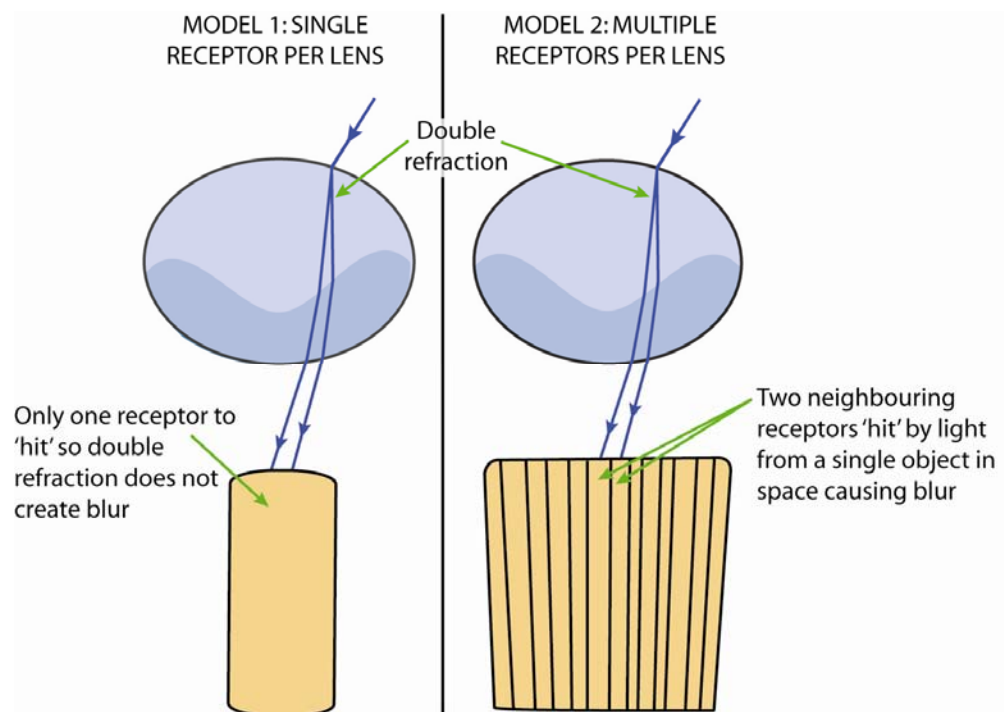


Figure 7.8 - The effects of birefringence in schizochroal lenses.

Although resolution may be lower in model 1 (see Equation 6 and Equation 8), its construction using a single receptor means that in this model the birefringent properties of calcite and the resultant double refraction of rays do not cause a problem. In model 2, light from the same point in space is focused on two different receptors effectively creating a 'ghost' pixel on the overall 'image'.

The proposed eye structure would result in the formation of a pixellated 'image', each ommatidium contributing a single pixel. The primary function of the large lenses in schizochroal eyes and the intralensar bowls within the lenses in such a system was not for image formation *per se* but to maximise the intake of light, thus enhancing the efficiency of the photoreceptors below indicated by the very low F-numbers (section 7.1.5.3.1). If the optics in this eye did not focus

light so well it would reduce the efficiency of the receptors by reducing sensitivity (see Equation 3). Movement of objects across the field of view of this type of eye would be 'seen' as changing areas of light and dark across the whole visual field, the contrast increased by the high sensitivity of the system. This movement perception would be sufficient to allow the trilobite to employ defence mechanisms such as enrolment when the approach of a predator was detected and equally to detect prey, if indeed phacopids were hunters as suggested by Fortey and Owens (1999). Used in combination with other sensory organs, such as antennae and a 'median eye' (Ruedemann, 1916) or 'glabellar tubercle' (Fortey and Clarkson, 1976), these schizochroal eyes would have given the phacopids significant advantage over other organisms with the same life habit.

Limiting the overlap of individual lenses by minimising FOV of each lens would limit the chances of two different photoreceptors within the same eye imaging the same area in near space, the result of this would be the accurate determination of the location of a near object. As the 3-dimensional field, or 'cone' of view of each lens increases with distance from the lens, far objects may have been viewed by more than one lens/photoreceptor. By determining the combination of receptors that were being stimulated by an object, the trilobite may have been able to gain some information on the size and distance of the object. However, as the overlap of lens FOV increases with distance from the lens, precise determination of the objects location would decrease with distance. The combined use of both eyes may have minimised this problem and enhanced depth perception in the most central areas of the trilobites' FOV. Overlap between eyes in these regions, i.e. at the anterior and, in some cases, posterior areas of the head, which results in binocular vision, allows even more lenses/photoreceptors to 'image' the same area in space, reducing error by dividing the FOV into smaller sections. This is not possible in lateral regions of the eye, thus peripheral vision would not have been as well developed.

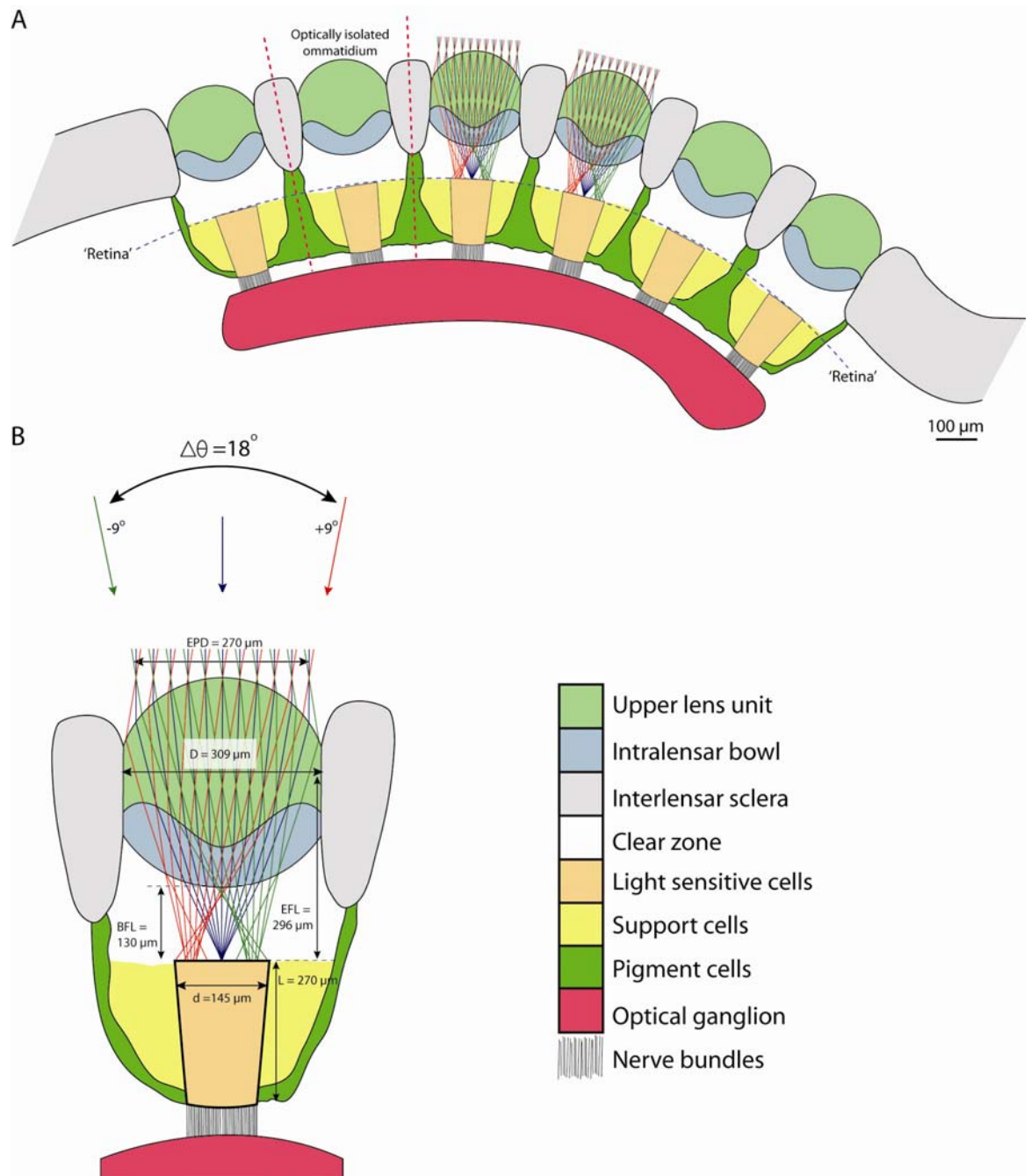


Figure 7.9 - The proposed arrangement of sublensar structures in the schizochroal trilobite eye.

A. Cross-section through the eye. B. Cross-section of an individual ommatidium showing the approximate position and size of sublensar components based on analysis of thin sections and Code V modelling of *Phacops* sp. (PM27). Green, blue and red lines represent light rays entering the lens from different angles within the field of view.

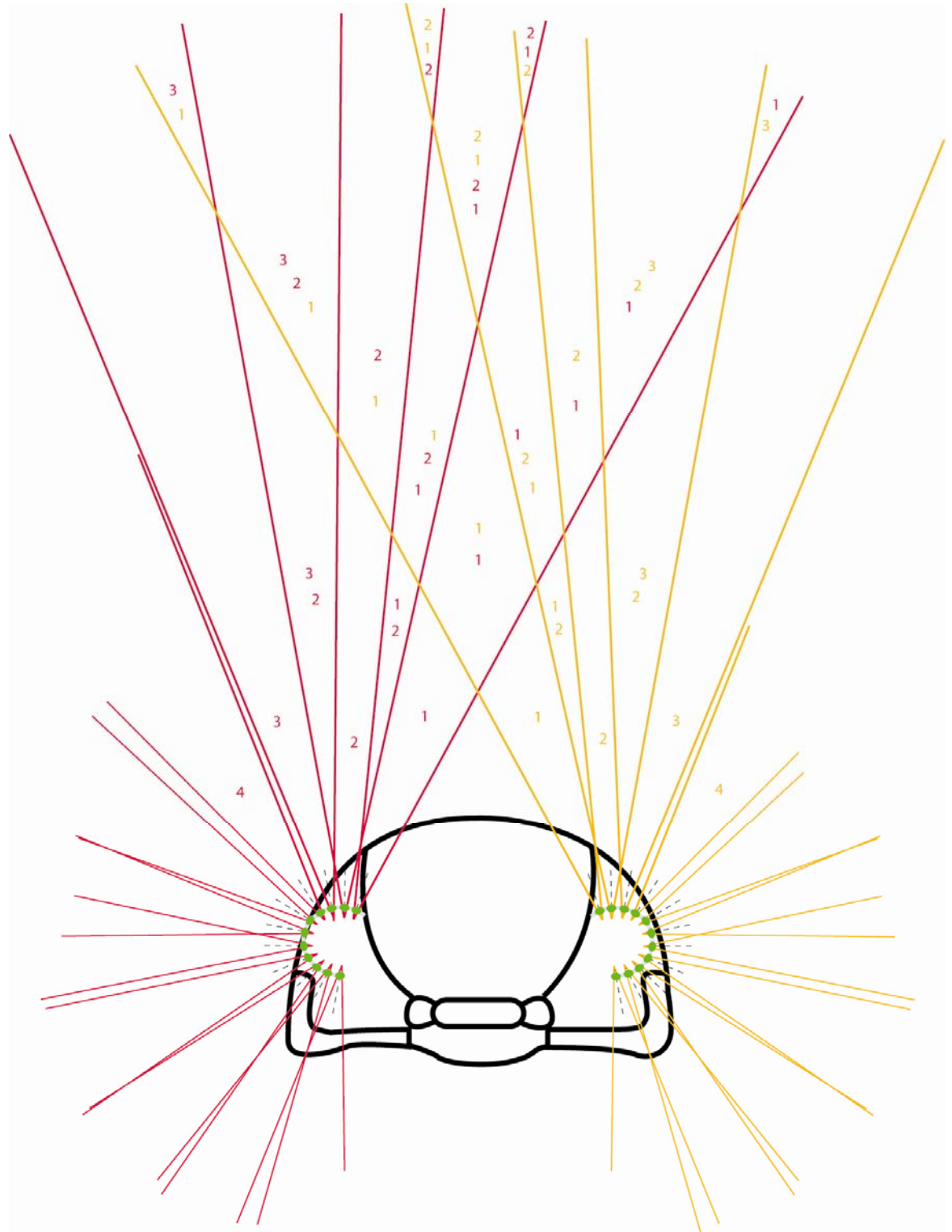


Figure 7.10 - Field of view and depth perception in trilobite eyes.

Schematic diagram showing how overlapping FOV of lenses and eyes may have provided the trilobite with depth perception as different areas in space are imaged by different combinations of lenses. The degree of FOV overlap between lenses and between eyes would be dependant on the size and curvature of the eyes and thus, different species would have different degrees of depth perception. Red and yellow lines represent the FOV of lenses in the left and right eyes respectively. Black dashed lines represent lens axes; lenses are green. Numbers indicate the lenses that image that particular area, number colour also corresponds to eye (red=right, yellow=left).

7.2 Biomineralisation

The precise crystal orientation seen in holochroal and schizochroal trilobite eyes highlights the degree of the control that the organism exhibited during biomineralisation of its exoskeleton. Controlled crystal orientation is reported in members of the Phyla Echinodermata (e.g. Towe, 1967), Mollusca (e.g. Weiner *et al.*, 1984; MacDonald *et al.*, 2010) and Brachiopoda (e.g. Cusack *et al.*, 2007, 2009; Griesshaber *et al.*, 2007, 2009). This control of crystal orientation by means of organic templates is thought to enhance the mechanical properties of the skeleton, optimising it for functions such as structural support, light transmission and filtration (Griesshaber *et al.*, 2007; Raue *et al.*, 2009, Dove, 2010). As well as exhibiting control of crystal orientation, some organisms display control over the minerals used in constructing certain parts of their skeleton. Phase partitioning has been identified in the bimineralic mollusc *Mytilus edulis* (Cusack *et al.*, 2007, 2009) that has a distinct boundary between the outer prismatic calcite layer and the inner nacreous aragonite layer. The same applies in bryozoans (e.g. Smith and Girvan, 2010). Members of the bryozoan Infraorder Flustrina have a dual-calcite skeleton that has discrete areas of LMC and HMC (Smith *et al.*, 1998), however the exact purpose of this partitioning is unclear. Both the present study and work by Lee *et al.* (2007a) have identified the chemical partitioning in lenses of schizochroal eyes (section 5.3.2) as original. This may represent one of the earliest examples of biological control over chemical composition with direct functional application, as optical modelling showed that concentration of magnesium in intralensar bowl significantly enhanced the focusing power of the lens.

7.2.1 Biomineral Growth

Minerals can form by two pathways (Tremel *et al.*, 2007): (1) Classical crystallisation. This involves growth via a process of ion-by-ion addition. (2) Non-classical crystallisation in which arrangement and orientation of nanocrystals coated in organic components occurs prior to their fusion and the creation of a mesocrystal (Figure 7.11). This mesocrystal, although an aggregation of nanocrystals has properties similar to a single crystal (Cölfen, 2007 and references therein). The ‘single’ crystal structure of the echinoderm skeleton for example has been shown to consist of numerous sub-domains (Towe, 1967; Blake *et al.*,

1984), consistent with formation by non-classical crystallisation. Although any traces of organic components that may have been present in trilobite lenses *in-vivo* have degraded, misorientation graphs (section 5.1.6.2.2) and TEM imaging (section 5.1.4 and 5.1.6.2.1) have revealed the presence of micron-scaled sub-domains. This may be an indication that trilobites mineralised their eyes by a mechanism similar to non-classical crystallisation. The presence of trabeculae and lamellae within some lenses could suggest that they did not undergo complete fusion to the single crystal stage if the trabeculae were bounded by organic matter when the trilobite was alive, as was proposed by Schoenemann and Clarkson (2008a). However, no organic matter has been identified in the present study so this suggestion is somewhat speculative.

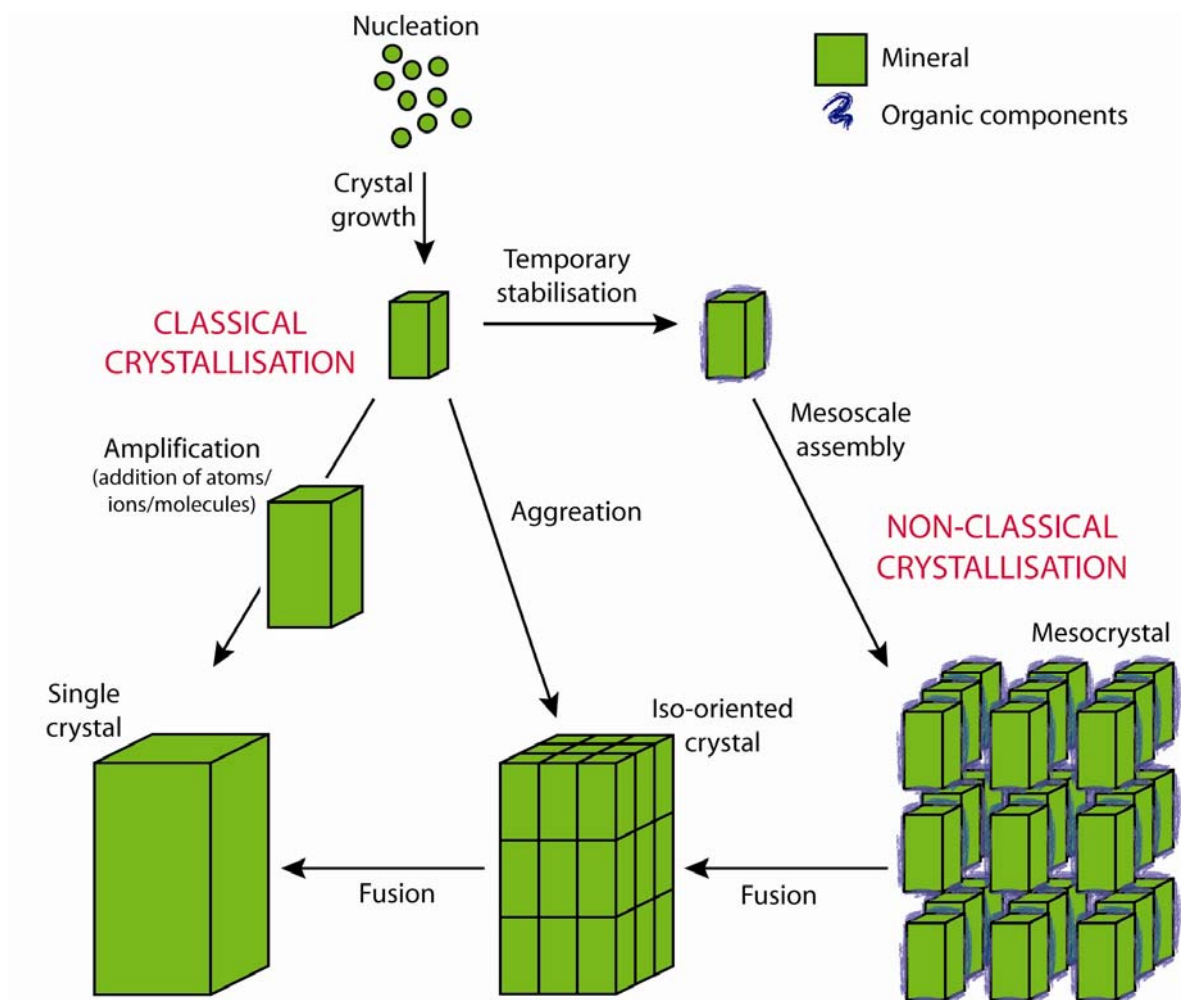


Figure 7.11 - Classical and non-classical mineral crystallisation pathways. Biominerals form by non-classical crystallisation. Image modified from Cölfen (2007, figure 3.1).

Biominerals form via a complex 'organic-matrix mediated' process of crystal growth (Weiner *et al.*, 1984). Studies into the biomineralisation of mollusc shells (Weiner *et al.*, 1984; Addadi *et al.*, 2006) show that minerals grow onto an

organic framework built up from sheets of chitin, proteins and acidic macromolecules (Figure 7.12) which enhance the mechanical properties of the mineral (Tremel *et al.*, 2007). The thickness of these sheets is reported to vary from 12 nm to 300 nm and is in the form of a three dimensional mesh woven around and between nano-crystals (Watabe, 1965). Growth of minerals on the organic 'template' is epitaxial; the orientation is determined by the specific macromolecules within the organic matrix, which can initiate or inhibit growth of particular crystals (Aizenberg *et al.*, 1994; Tremel *et al.*, 2007). The presence of this organic matrix not only provides a template for crystal growth and orientation, but also mineral chemistry. The presence of certain peptides in this matrix has been shown to enhance the magnesium concentration in calcite (Stephenson *et al.*, 2008; Wang *et al.*, 2009); a similar matrix may have been present within the bowl and core regions of the schizochroal lenses.

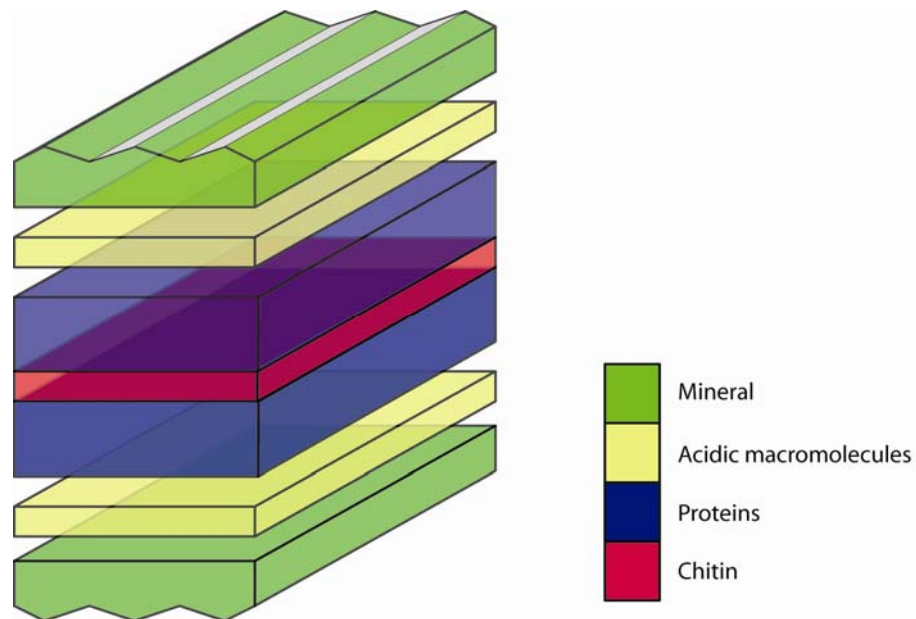


Figure 7.12 - Layered structure of the organic matrix onto which minerals crystallise in mollusc shells.

Modified from Weiner (1984, figure 2). In reality, the mineral and organic matrix are in direct contact, sometimes appearing distinct but commonly indistinguishable (Watabe, 1965).

The growth of biominerals is thought to occur via an amorphous calcite carbonate (ACC) precursor (e.g. Weiner *et al.*, 1984; Addadi *et al.*, 2006). This ACC is harboured prior to the moult stage in terrestrial arthropods, which, unlike marine animals, do not have access to a readily available source of calcium carbonate (Dove, 2010).

7.2.2 Ecdysis and Biomineralisation of the Trilobite Exoskeleton

Without close living relatives with which to make comparisons, understanding the processes of ecdysis and the subsequent biomineralisation of new cuticle in the trilobites is limited. Some studies have provided insights into the mechanisms that may have been used in the act of exuviation of the trilobite exoskeleton (e.g. Henningsmoen, 1975; McNamara and Rudkin, 1984; Speyer, 1985; Brandt, 2002; Bruthansová, 2003). The conclusions drawn in these studies were based on sutures in the exoskeleton, disarticulation of exoskeletal segments and the orientations of moulted sclerites. To gain some understanding of the processes that followed moulting, and the sequence in which the new cuticle was grown, attention must turn to modern day crustaceans for possible explanations. Much of the literature is based on the study of decapod crustaceans (e.g. crabs and lobsters). Modern crab carapaces consist of several layers (all descriptions below are from Roer and Dillaman, 1984 and references therein) (Figure 7.13):

The epicuticle: This is the thinnest and outermost layer. It consists of proteins impregnated with calcite salts and has a distinct lack of chitin and lamellar organisation.

The exocuticle: This layer consists of layers of stacked chitin-protein fibres with changing orientations.

The endocuticle: This is the thickest and most heavily calcified layer of the cuticle. Like the exocuticle, it consists of stacked chitin-protein fibres with continuously changing orientations.

The membranous layer: This layer consists of chitin and protein with no mineralised components. It is the innermost layer of the cuticle.

The hypodermis: This is a layer of cells consisting of three sub-layers. The uppermost layer, the 'outer epithelial layer' is one cell thick and consists of epithelial cells that secrete the cuticle above. Below this lies the 'sub-epithelial connective tissue layer' that consists of various cell types. Finally, the 'inner epithelial layer' is similar to the outer epithelial layer and is bounded, for the most part, by the basement membrane.

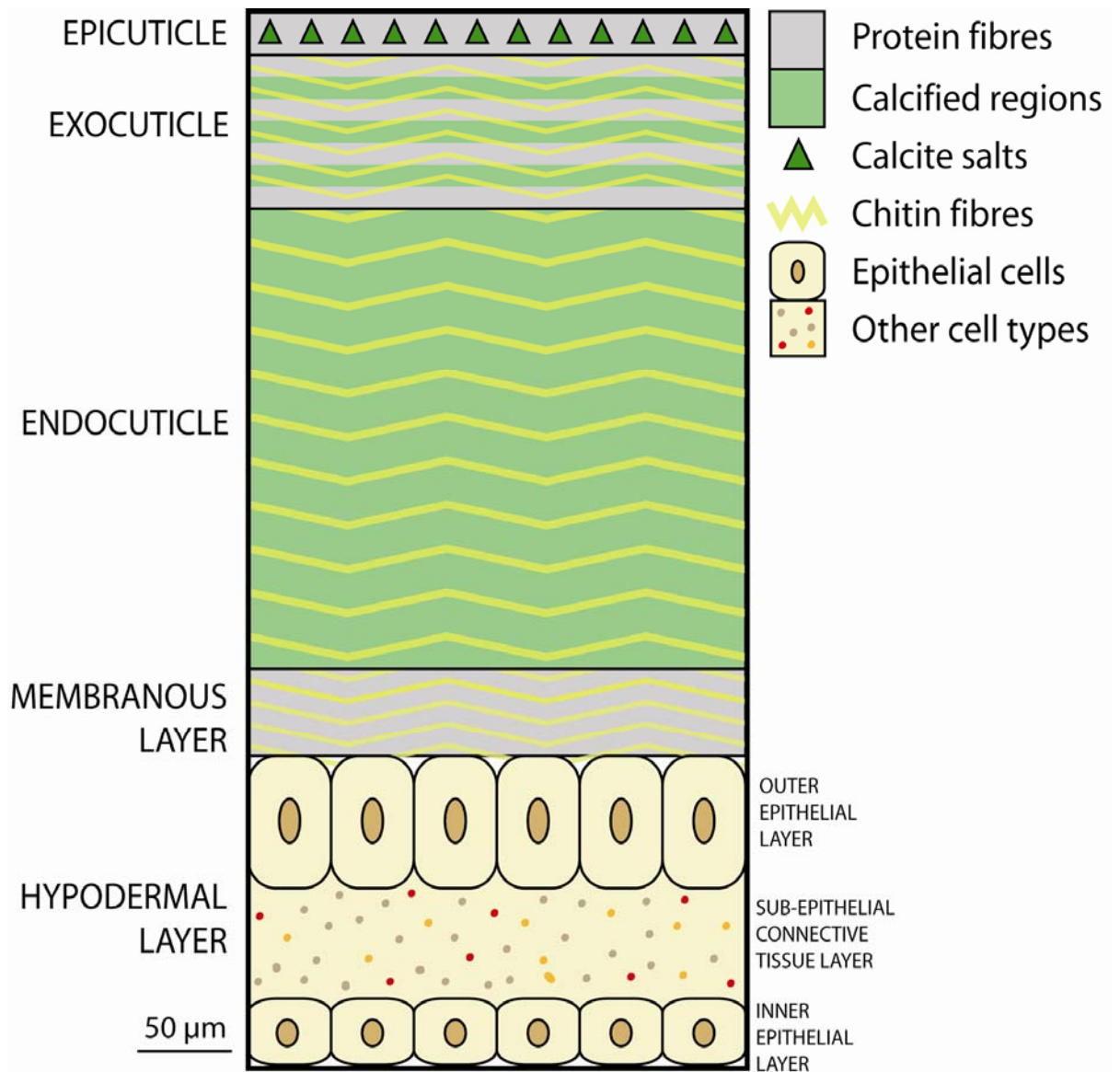


Figure 7.13 - Layering in the modern crustacean cuticle.
Image based on descriptions in Roer and Dillaman (1984).

The various stages of growth of the modern day crustacean carapace and the changes it undergoes during the moult cycle have been well documented (e.g. Roer and Dillaman, 1984; Compère *et al.*, 1998; Taylor *et al.*, 2007). The moult cycle consists of the pre-ecdysial (pre-moult) stage (Compère *et al.*, 1998) and two post-moult stages, the soft stage and the paper shell stage that are followed by the hard stage (Henningsmoen, 1975; Taylor *et al.*, 2007). Within the pre-moult stage there are several changes that occur in the structure of the exoskeleton (Figure 7.14):

Early pre-moult: this stage, which is well documented for the crab *Carcinus maenas*, begins by the secretion of 'ecdysial droplets' from the epidermis which leads to a loss of adherence between the epidermis and the 'old' cuticle above

(Compère *et al.*, 1998) (Figure 7.14A). The subsequent moulding of the epidermal surface, in preparation of growth of the new cuticle causes separation of the epidermis and old cuticle forming what is known as an ‘ecdysial cleft’ (Compère *et al.*, 1998).

Late pre-moult: During these processes, degradation of the chitin-protein microfibers and mineral dissolution of the old cuticle occur and both mineral and organic components are resorbed by the epidermis below (Roer and Dillaman, 1984). At this point in the moult cycle, the epithelial cells are at their largest and formation of the new epi- and exocuticle layers begin by the emplacement of an organic matrix (Roer and Dillaman, 1984) (Figure 7.14B). The old exoskeleton is now shed, leaving the animal in a vulnerable state. It is likely that by now, the animal would have retreated to as safe a place as possible; trilobites may have retreated to sheltered areas such as caves in reefs, burrows or empty shells of other animals (Henningsmoen, 1975; Chatterton and Fortey, 2008).

Post-moult: The immediate post-moult stage is known as the ‘soft-shell’ stage as the carapace is highly flexible (Taylor *et al.*, 2007). Calcification and subsequent hardening of the layers formed prior to exuviation begins (Figure 7.14C). Crystallisation of calcium carbonate initiates at the margins of the epithelial cell walls and progresses inwards, the final result being homogeneous distribution of crystalline calcium carbonate; this process begins at 10 hours post-moult in the crab *Carcinus maenas* and calcium deposition reaches its peak after two days (Roer and Dillaman, 1984). Once this stage is complete, growth of the endocuticle begins and progresses by growth and mineralisation of a single lamella at a time (Roer and Dillaman, 1984), this is known as the ‘paper-shell’ stage (e.g. Henningsmoen, 1975; Taylor *et al.*, 2007) (Figure 7.14D). The final stage is deposition of the membranous layer and cessation of calcification, epithelial cells decrease in size for the remainder of the inter-moult period (Figure 7.14E).

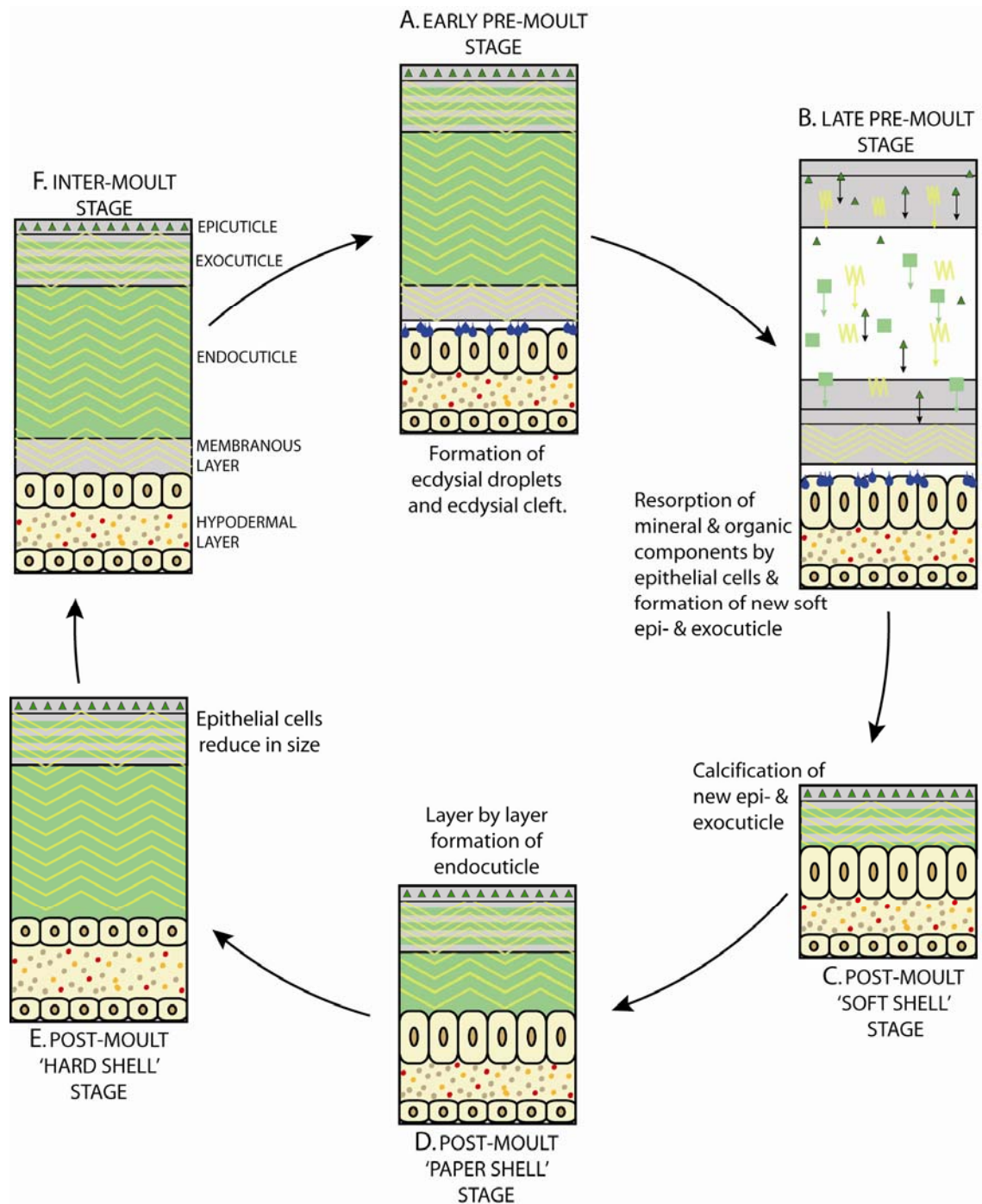


Figure 7.14 - Stages of growth and moulting in the crustacean cuticle.

Changes in the structure of the crustacean cuticle during the moult cycle. Image based on Roer and Dillaman (1984, figure 2) and description from Compère (1998). Symbols are as for Figure 7.13.

Study of the lobster exoskeleton (Raue *et al.*, 2009) has identified enhanced mechanical properties, specifically a high elastic modulus that provides maximum resistance against penetration, in areas where the calcite *c* axis is parallel to outer carapace surface. This may also explain the precise orientation in the trilobite exoskeleton, including the eyes, where the calcite in *c* axis intersects the outer eye surface at an angle close to 90° (section 5.1.6.2). Growth of the trilobite exoskeleton including the calcified parts of the eye

probably proceeded via similar mechanism to the exoskeleton of modern day crustaceans. Studies of the microstructure of the trilobite exoskeleton have identified three layers (Dalingwater, 1973 and references therein; Miller and Clarkson, 1980). A extremely thin outer layer, identified in well preserved specimens by a glossy lustre, a thin middle layer approximately 6-10 % of the total cuticle thickness and a much thicker inner layer (Dalingwater, 1973), which is seen to vary in thickness between specimens (Miller and Clarkson, 1980). These layers probably correspond respectively to the epicuticle, the exocuticle and the endocuticle of modern crustaceans.

In the eyes, the cornea, which itself consists of three layers (Miller and Clarkson, 1980) (section 1.5.2.2) probably grew first, in conjunction with the epi- and exocuticular layers of the exoskeleton (Figure 7.15 stage 1). The cornea, which has been determined by EDS to consist of LMC (section 5.1.5.1) would have provided little refracting power as it overlies a lens of the same curvature and similar RI; this is also the case in some other aquatic animals (e.g. Land and Nilsson, 2002, p.132; Jonasova and Kozmik, 2008). Considering that the lens would produce similar optical results without the cornea, it is likely that this component had a different function, for example acting as protection for the eye, or as a light filter (Jonasova and Kozmik, 2008 and references therein). The lens is likely to have grown post-moult in a similar manner to the endocuticle of modern crustaceans, and the growth lamellae identified by Miller and Clarkson (1980) may be an indication that the lens was grown and mineralised one lamella at a time. Miller and Clarkson (1980) were unable to determine if the growth of the bowl and the core occurred in a particular sequence or simultaneously. If the growth proceeded in a manner similar to the modern crustacean cuticle, the lateral edges of the intralensar bowl would have been formed simultaneously with the lens calcite at the same depth in the lens, the partitioning between HMC and lower-Mg calcite controlled by the organic template (section 7.2.1) (Figure 7.15 stage 3). The lowermost parts of the bowl would have constituted the last additions to the lens. The core, where present, would have formed simultaneously with the calcite at the same depth in the surrounding lens, in a similar manner to the lateral edges of the bowl.

It is impossible to determine the timescale over which growth of the lenses occurred. Based on biomineralisation processes of modern animals it can be

assumed that growth of the lenses reached completion within a matter of hours but hardening may have continued over a period of days; the blue crab, although at a 'soft-shell' stage one hour after moulting, does not reach the 'hard-shell' stage for seven days (Taylor *et al.*, 2007). With the added problem of lack of vision, this moulting timescale would render the trilobites more vulnerable. It may be that light was able to penetrate the thin early ecdysial trilobite 'lens', providing the animal with 'vision' of limited resolution and sensitivity, or trilobites may have been able to mineralise lenses more quickly than modern crustaceans, but there is no way of testing this.

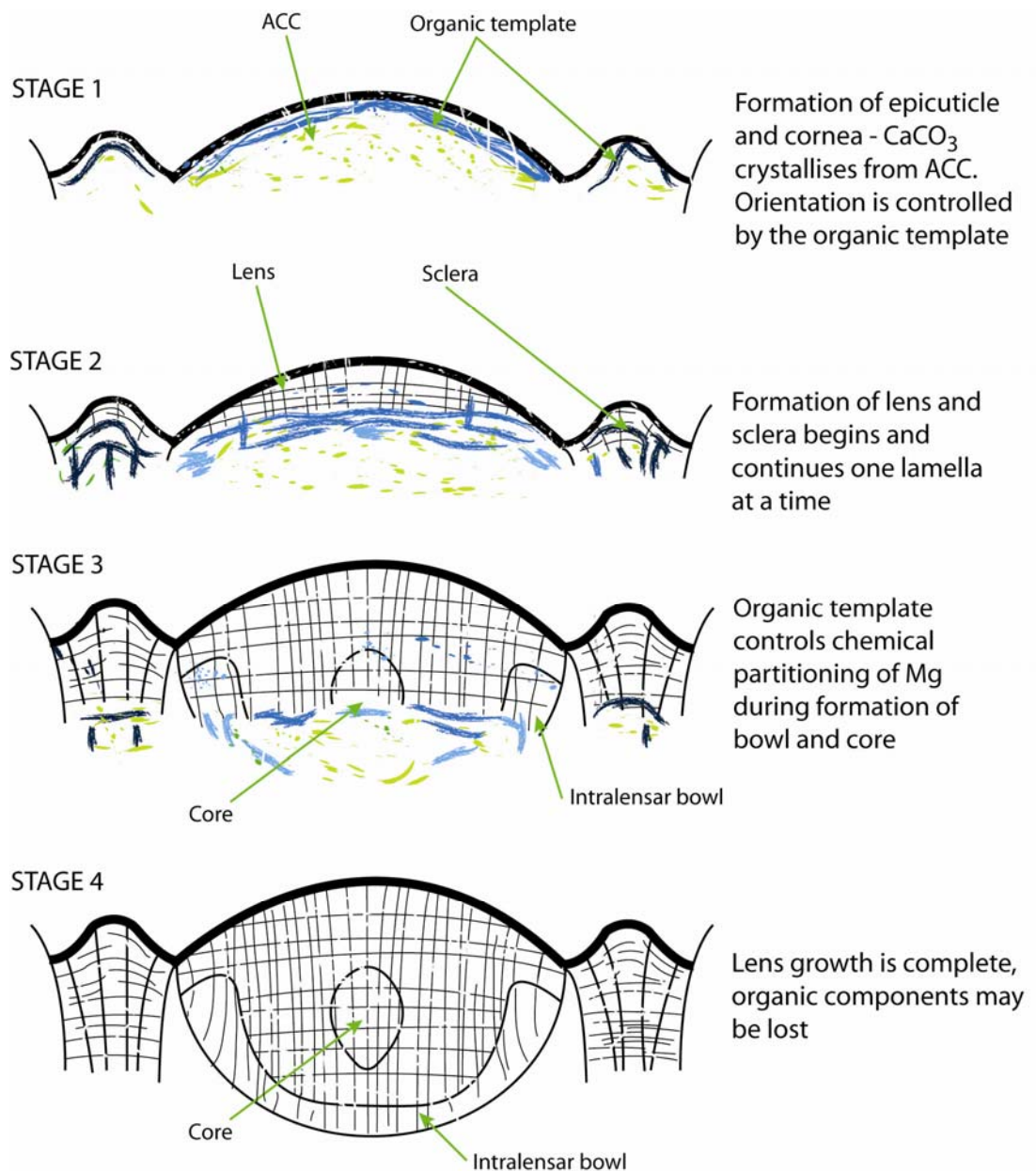


Figure 7.15 - Post-ecdysial growth sequence of the schizochroal eye.
 This growth sequence is based on growth of the modern arthropod cuticle.

Conclusions

The array of high-resolution imaging and analytical techniques used in the present study have enabled a more in-depth understanding of the construction and function of trilobite eyes than was possible in previous studies because of the limitations imposed by the technology available at the time. The study of a wide range of specimens, encompassing trilobites from different palaeographical localities, has allowed the effects of diagenesis to be identified and the original lens structures to be distinguished from diagenetic artefact.

Qualitative and quantitative EDS analysis has confirmed that lenses in holochroal eyes were originally LMC and it is most likely this stable form that has, in many cases, ‘protected’ them from extensive changes in microstructure. EBSD has revealed the original microstructure of holochroal lenses and highlights the changes that lenses undergo during diagenesis. All lenses analysed have retained their original microstructure for the most part; lens microstructure corresponds to surface curvature in holochroal lenses, apparent ‘bending’ of the *c* axis occurring at convex surfaces only (Figure 0.1).

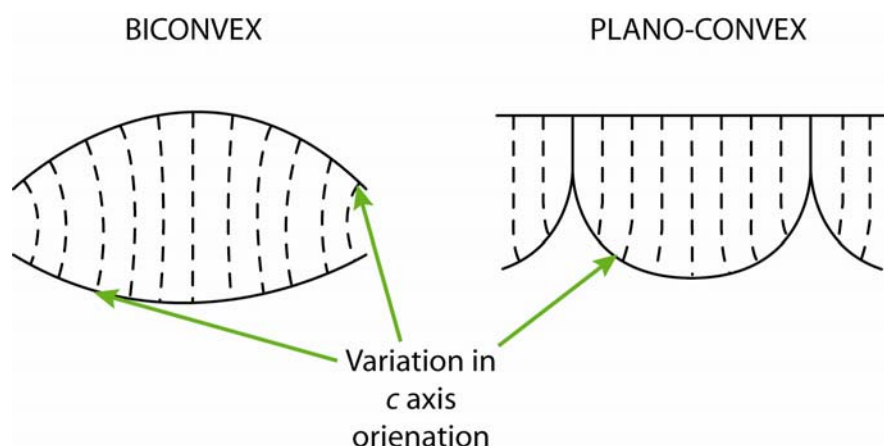


Figure 0.1 - Original microstructure of holochroal lenses.

Previous work (see Clarkson *et al.*, 2006 for review) has suggested that holochroal eyes functioned in a similar manner to the apposition eyes of modern arthropods. The findings of the present study reveal no evidence to suggest otherwise and given that no sublensar structures have been found yet, this comparison is not unreasonable.

Holochroal eyes do not show the same amount of diagenetic variation as the schizochroal lenses, this in itself reflects inherent differences in their original microstructure and/or composition. Nonetheless, the techniques used in the present study have been successful in providing a better understanding of the fine structures within the lenses in holochroal eyes.

EBSD and TEM have revealed considerable detail on the microstructure of lenses within schizochroal trilobite eyes. The present study confirms that the schizochroal eye does not consist of a single calcite crystal, but of a large number of micron scale sub-crystals that change in orientation across the lens towards both the outer and inner lens surfaces (Figure 0.2A). EBSD ChI scanning used in conjunction with EDS and EPMA have built upon the findings of Lee *et al.*, (2007a) to reveal a new model of schizochroal eye chemistry in which the schizochroal lenses consisted predominantly of HMC, with the controlled partitioning of magnesium for the creation of intralensar structures (Figure 0.2B). Moreover, optical modelling of the lenses has revealed that not only is this variation in chemistry a requirement for focusing light, but that the changing *c* axis orientation in the lenses enhances their focusing capabilities, as it would result in the production of extraordinary rays even when light enters the lens parallel to the lens axis. However, as light can enter the lens across a range of angles this *c* axis orientation is not essential in the formation of extraordinary rays. It is possibly that this microstructural arrangement is simply the result of biconvex lens growth by addition of trabeculae.

Determination of resolution and sensitivity of the eyes as well as eye parameter and F-number shows that the schizochroal eyes examined were optimised for life in a dim environment. All characteristics of the eyes: the large lenses; the separation of the lenses by sclera; the presence of the aplanatic surface and the change in refractive index by incorporation of the intralensar bowl, increase the amount of light that was transmitted to the photoreceptors (Figure 0.2C). It is argued that the overall eye structure was one of ommatidial type probably

consisting of optically isolated units. The ability of light/dark adaption cannot be determined as the lack of preservation of sub-lensar structures renders it impossible to determine the exact structure of the ommatidia or the possible presence of pigment cells, however based on comparison with modern animals, such as *Limulus*, it is likely that pigment was present.

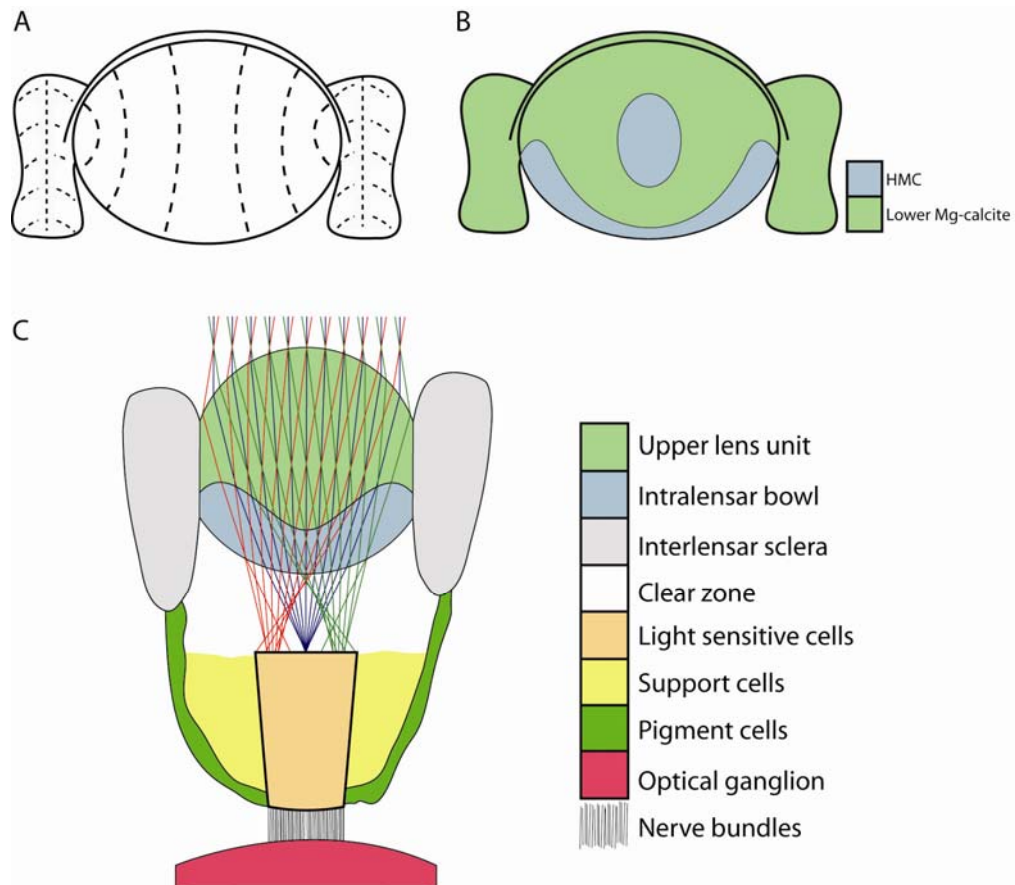


Figure 0.2 - Microstructure, chemistry and function of lenses in the schizochroal trilobite eye.

A. Original microstructure of schizochroal lenses determined using EBSD. Dashed lines indicate *c* axis orientation. **B.** Original chemistry of schizochroal lenses based on EDS, EPMA and ChI scanning. **C.** The function and inferred sub-lensar structure of the lens of *Phacops* sp. based on Code V modelling results.

Fortey and Chatterton (2003) argued that the presence of an ‘eye shade’ on the eye of the Devonian trilobite *Erbeochile erbeni* was indicative of a diurnal life habit, as such a feature is of little use in the dark. However, the findings of the present study suggest that the phacopids studied were active in dim light conditions. It is possible that the phacopid species examined in the present study represent nocturnal or crepuscular forms, and such a life habit could explain the extremely high eye parameter values of schizochroal eyes. The recent discovery, of a new species of *Erbenochile* (Chatterton and Gibb, 2010)

without an eyeshade, amongst those with eyeshades, suggests that this fauna may mark a transition in life habit of phacopids from nocturnal to diurnal.

The combinations of EBSD, EDS, EPMA and CL have made it possible to construct pathways showing the changes that take place to the original microstructure (Figure 0.3) and chemistry (Figure 0.4) during diagenesis. The presence of more than one stage of these sequences within a single eye highlights the sub-millimetre scale variability of diagenesis. The inability to superimpose these diagenetic pathways onto one another, despite microstructure indicating a fine scale of recrystallisation, shows how complex diagenesis can be and therefore how significant and unusual a find intralensar structures really are. The microstructure arrangement and chemical composition determined to be original (Figure 0.2A-B) are consistent across all genera analysed and are probably applicable across the Suborder Phacopina.

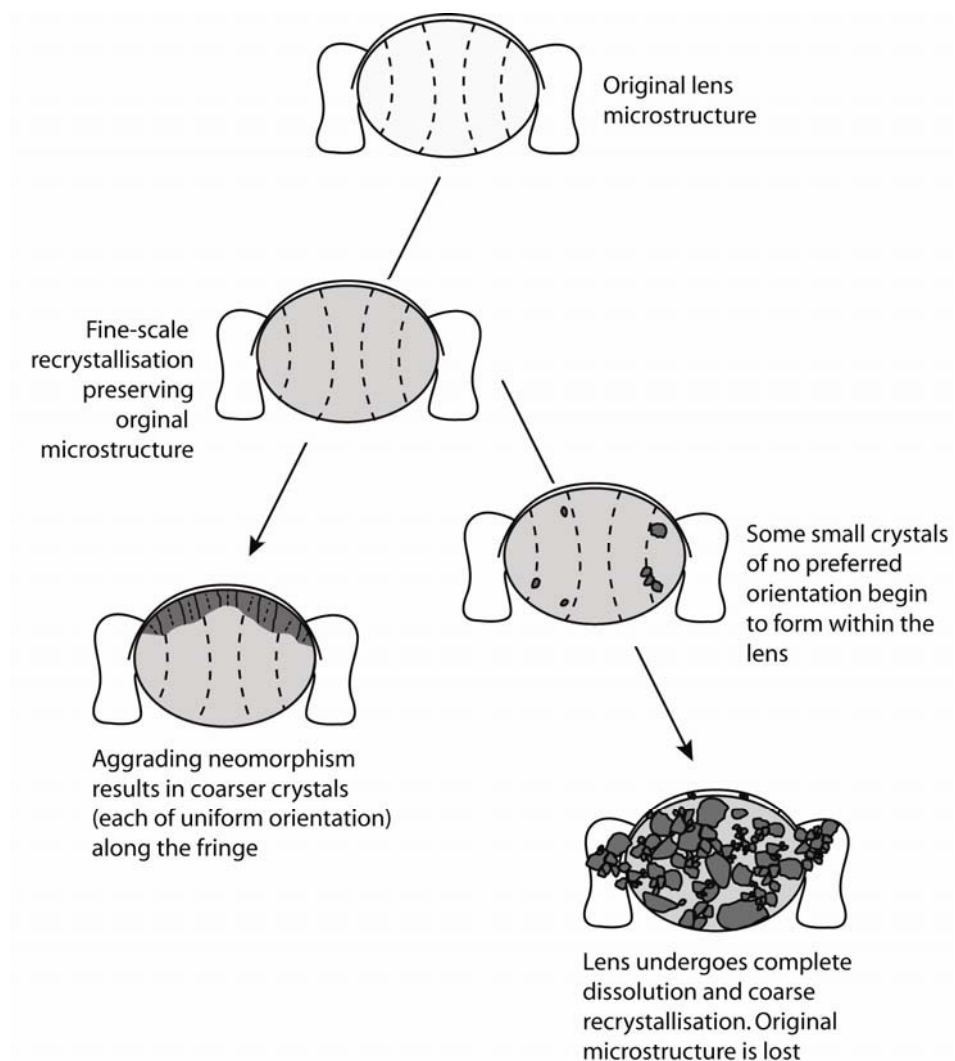


Figure 0.3 - Effects of diagenesis on original lens microstructure.

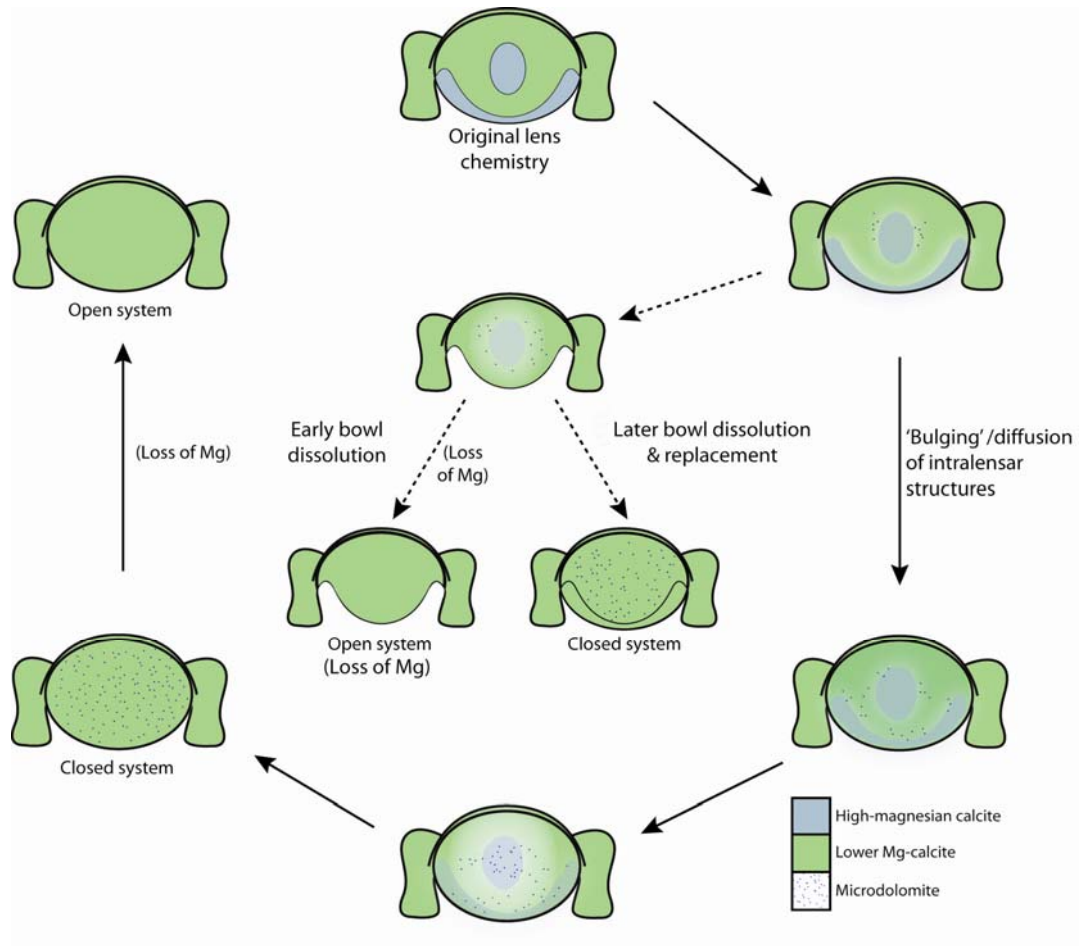


Figure 0.4 - Effects of diagenesis on original lens chemistry.

The understanding of trilobite eyes, particularly those of schizochroal type, which has been achieved through this work, has highlighted the degree of control that organisms can exhibit over the construction of their skeleton in terms of both crystal orientation and chemical composition. The ability to partition significant levels of magnesium from 'calcite seas' and concentrate this in certain areas of the lens provided the phacopids with the perfect dioptrics for an eye optimised, in all ways, for low light levels and capable of motion detection in the surrounding environment. This heightened sensitivity to variations in illumination would have allowed the phacopids to, in conjunction with other sensory organs such as tubercles and antennae, respond quickly to the approach of predators, and equally to target prey.

References

- ACEÑOLAZA, G. F., TORTELLO, M. F. & RÁBANO, I. 2001. The eyes of the early Tremadoc olenid trilobite *Jujuyaspis keideli* Kobayashi, 1936. *Journal of Paleontology*, 75, 346-350.
- ADDADI, L., JOESTER, D., NUDELMAN, F. & WEINER, S. 2006. Mollusk shell formation: A source of new concepts for understanding biomineralization processes. *Chemistry-a European Journal*, 12, 981-987.
- AHLBERG, P. 1995. Telephinid Trilobites from the Ordovician of Sweden. *Palaeontology*, 38, 259-285.
- AIZENBERG, J., ALBECK, S., WEINER, S. & ADDADI, L. 1994. Crystal Protein Interactions Studied by Overgrowth of Calcite on Biogenic Skeletal Elements. *Journal of Crystal Growth*, 142, 156-164.
- AIZENBERG, J. & HENDLER, G. 2004. Designing efficient microlens arrays: lessons from Nature. *Journal of materials chemistry*, 14, 2066-2072.
- AIZENBERG, J. & HENDLER, G. 2005. Learning from Marine Creatures How to Design Micro-Lenses. In: REIS, R. L. & WEINER, S. (eds.) *Learning from Nature How to Design New Implantable Biomaterials: From Biomineralization Fundamentals to Biomimetic Materials and Processing Routes*. Springer Netherlands.
- AIZENBERG, J., TKACHENKO, A., WEINER, S., ADDADI, L. & HENDLER, G. 2001. Calcitic microlenses as part of the photoreceptor system in brittlestars. *Nature*, 412, 819-822.
- ALAM, M. N., BLACKMAN, M. & PASHLEY, D. W. 1953. High-Angle Kikuchi Patterns. *Proceedings of the Royal Society of London Series A-Mathematical and Physical Sciences*, 221 (1145), 224-243.
- ALDRIDGE, R. J. 1986. Conodont palaeobiogeography and thermal maturation in the Caledonides. *Journal of the Geological Society*, 143, 177-184.
- ANDERSSON, A. & NILSSON, D. E. 1981. Fine structure and optical properties of an ostracode (Crustacea) nauplius eye. *Protoplasma*, 107, 361-374.
- ANGELIN, N. P. 1854. *Palaeontologica Scandinavica. I: Crustacea formationis transitionis*, Leipzig, Lund.

- ATCHISON, D. A. & SMITH, G. 2000. *Optics of the Human eye*, Edinburgh, Butterworth Heinemann.
- BARRANDE, J. 1846. *Notice préliminaire sur le système Silurien et les Trilobites de Bohême*, Hirschfeld: Leipzig.
- BARRANDE, J. 1852. *Système Silurien du Centre de la Bohême*, Prague and Paris.
- BATHURST, R. G. C. 1971. *Carbonate sediments and their diagenesis*, Amsterdam, Elsevier.
- BATTELLE, B. A. 2006. The eyes of *Limulus polyphemus* (Xiphosura, Chelicerata) and their afferent and efferent projections. *Arthropod Structure & Development*, 35, 261-274.
- BELKA, Z. 1991. Conodont colour alteration patterns in Devonian rocks of the eastern Anti-atlas, Morocco. *Journal of African Earth Sciences (and the Middle East)*, 12, 417-428.
- BERGSTROM, S. M. 1980. Conodonts as paleotemperature tools in Ordovician rocks of the Caledonides and adjacent areas in Scandinavia and the British Isles. *Geologiska Foereningen i Stockholm. Foerhandlingar*, 102, 377 - 392.
- BERGSTROM, S. M. 1990. Biostratigraphic and biogeographical significance of Middle and Upper Ordovician conodonts in the Girvan succession, South-West Scotland. *Courier Forschungsinstitut Senckenberg*, 118, 1-43.
- BERGSTROM, S. M., CHEN, X., GUTIERREZ-MARCO, J. C. & DRONOV, A. 2009. The new chronostratigraphic classification of the Ordovician System and its relations to major regional series and stages and to $\delta^{13}\text{C}$ chemostratigraphy. *Lethaia*, 42, 97-107.
- BESTMANN, M. & PRIOR, D. J. 2003. Intragranular dynamic recrystallization in naturally deformed calcite marble: diffusion accommodated grain boundary sliding as a result of subgrain rotation recrystallization. *Journal of Structural Geology*, 25, 1597-1613.
- BISCHOFF, W. D., BISHOP, F. C. & MACKENZIE, F. T. 1983. Biogenically Produced Magnesian Calcite Inhomogeneities in Chemical and Physical-Properties Comparison with Synthetic Phases. *American Mineralogist*, 68, 1183-1188.
- BLAKE, D. F., PEACOR, D. R. & ALLARD, L. F. 1984. Ultrastructural and Microanalytical Results from Echinoderm Calcite - Implications for Biomineralization and Diagenesis of Skeletal Material. *Micron and Microscopica Acta*, 15, 85-90.
- BRAITHWAITE, C. J. R. 1991. Dolomites, a Review of Origins, Geometry and Textures. *Transactions of the Royal Society of Edinburgh: Earth Sciences*, 82, 99-112.

- BRANDT, D. S. 2002. Ecdysial efficiency and evolutionary efficacy among marine arthropods: implications for trilobite survivorship. *Alcheringa*, 26, 399-421.
- BRONGNIART, A. 1822. *Historie naturelle des Crustacés fossils, sous les rapports zoologique et géologique, savoir les Trilobites. Les Crustacés proprement dits par A.-G.* Paris.
- BRONN, H. 1825. Ueber zwei Trilobiten-Arten zum Calymene-Geschlechte gehörig. *Zeitschrift für Mineralogie, Jahrgang 1825*, 317-321.
- BRUCKSCHEN, P., BRUHN, F., MEIJER, J., STEPHAN, A. & VEIZER, J. 1995. Diagenetic alteration of calcitic fossil shells: Proton microprobe (PIXE) as a trace element tool. *Nuclear Instruments and Methods in Physics Research Section B: Beam Interactions with Materials and Atoms*, 104, 427-431.
- BRUTHANSOVÁ, J. 2003. Exuviation of selected Bohemian Ordovician trilobites. *Special Papers in Palaeontology*, 70, 293-308.
- BRUTON, D. L. & HAAS, W. 1997. Functional morphology of Phacopinae (Trilobita) and the mechanics of enrolment. *Palaeontographica Abt. A*, 245, 1-43.
- BRUTON, D. L. & HAAS, W. 2003a. The puzzling eye of *Phacops*. *Special Papers in Palaeontology*, 70, 349-361.
- BRUTON, D. L. & HAAS, W. 2003b. Making *Phacops* Come Alive. *Special Papers in Palaeontology*, 70, 331-347.
- BRUTON, D. L. & HØYBERGET, M. 2006. A reconstruction of *Telephina bicuspis*, a pelagic trilobite from the Middle Ordovician of the Oslo Region, Norway. *Lethaia*, 39, 359-364.
- BRÜMMER, F., PFANNKUCHEN, M., BALTZ, A., HAUSER, T. & THIEL, V. 2008. Light inside sponges. *Journal of Experimental Marine Biology and Ecology*, 367, 61-64.
- BUSCHBECK, E., EHMER, B. & HOY, R. 1999. Chunk versus point sampling: Visual imaging in a small insect. *Science*, 286, 1178-1180.
- BUSCHBECK, E. K. 2005. The compound lens eye of Strepsiptera: morphological development of larvae and pupae. *Arthropod Structure & Development*, 34, 315-326.
- BUSCHBECK, E. K., EHMER, B. & HOY, R. R. 2003. The unusual visual system of the Strepsiptera: external eye and neuropils. *Journal of Comparative Physiology a-Neuroethology Sensory Neural and Behavioral Physiology*, 189, 617-630.
- CAMPBELL, K. S. W. 1975. The Functional Anatomy of Phacopid Trilobites: Musculature and Eyes. *Journal and Proceedings, Royal Society of New South Wales*, 108, 168-188.

- CAMPBENHAUSEN, C. von. 1967. The ability of *Limulus* to see visual patterns. *Journal of Experimental Biology*, 46, 557-570.
- CAVENEY, S. & MCINTYRE, P. 1981. Design of Graded-Index Lenses in the Superposition Eyes of Scarab Beetles. *Philosophical Transactions of the Royal Society of London. B, Biological Sciences*, 294, 589-632.
- CHATTERTON, B. D. & GIBB, S. L. 2010. Latest Early to Early Middle Devonian Trilobites from the *Erbenochile* bed, Jbel Issoumour, Southeastern Morocco. *Journal of Paleontology*, 84 (6), 1188-1205.
- CHATTERTON, B. D. & FORTEY, R. A. 2008. Linear clusters of articulated trilobites from Lower Ordovician (Arenig) strata at Bini Tinzoulin, North of Zagora, Southern Morocco. In: RÁBANO, I., GOZALO, R. & GARCÍA-BELLIDO, D. (eds.) *Advances in trilobite research*. Madrid: Instituto Geológico y Minero de España. pp. 73-78.
- CHATTERTON, B. D., FORTEY, R. A., BRETT, K. D., GIBB, S. L. & MCKELLAR, R. C. 2006. Trilobites from the upper Lower to Middle Devonian Timrhahhart Formation, Jbel Gara el Zguilma, southern Morocco. 25, 1-179.
- CHLUPÁČ, I. 1972. New Silurian and Lower Devonian phacopid trilobites from the Barrandian area (Czechoslovakia). *Časopis pro mineralogii a geologii*, 17, 395-401.
- CHLUPÁČ, I. 1977. The phacopid trilobites of the Silurian and Devonian of Czechoslovakia. *Rozpravy Ústředního Ústavu Geologického*, 43, 1-172.
- CHUGAEVA, M. N. 1964. Early and Middle Ordovician trilobites in the north-east of the USSR. In: CHUGAEVA, M. N., ROZMAN, K. H. S. & IVANOVA, V. A. (eds.) *Comparative biostratigraphy of Ordovician deposits in the north-east of the USSR*.: Transactions of the Academy of Sciences of the USSR Geological Institute.
- CLARKE, J. M. 1889. The Structure and Development of the Visual Area in the Trilobite, *Phacops rana*, Green. *Journal of Morphology*, 2, 253-270.
- CLARKSON, E. N. K. 1966. Schizochroal eyes and vision in some phacopid trilobites. *Palaeontology*, 9, 464-487.
- CLARKSON, E. N. K. 1967. Fine structure of the eye in two species of *Phacops* (Trilobita). *Palaeontology*, 10, 603-616.
- CLARKSON, E. N. K. 1975. The evolution of the eye in trilobites. *Fossils and Strata*, 4, 7-31.
- CLARKSON, E. N. K. 1979. The visual system of trilobites. *Palaeontology*, 22, 1-22.
- CLARKSON, E. N. K. & LEVI-SETTI, R. 1975. Trilobite eyes and the optics of Des Cartes and Huygens. *Nature*, 254, 663-667.

- CLARKSON, E. N. K. & TAYLOR, C. M. 1995. Ontogeny of the Trilobite *Olenus wahlenbergi* Westergard, 1922 from the Upper Cambrian Alum Shales of Andrarum, Skane, Sweden. *Transactions of the Royal Society of Edinburgh: Earth Sciences*, 86, 13-34.
- CLARKSON, E. N. K. & ZHANG, X. G. 1991. Ontogeny of the Carboniferous Trilobite *Paladin eichwaldi shunnerensis* (King 1914). *Transactions of the Royal Society of Edinburgh: Earth Sciences*, 82, 277-295.
- CLARKSON, E. N. K., LEVI-SETTI, R. & HORVATH, G. 2006. The eyes of trilobites: The oldest preserved visual system. *Arthropod Structure & Development*, 35, 247-259.
- COCKLE, P. 1999. Conodont Data in Relation to Time, Space and Environmental Relationships in the Silurian (Late Llandovery-Ludlow) Succession at Boree Creek (New South Wales, Australia). *Gabhandlungen Der Geologischen Bundesanstalt*, 54, 107-133, pls.1-5.
- COMPÈRE, P., THOREZ, A. & GOFFINET, G. 1998. Fine structural survey of old cuticle degradation during pre-ecdysis in two European Atlantic crabs. *Tissue and Cell*, 30, 41-56.
- CONWAY-MORRIS, S. 1998. *The Crucible of Creation: The Burgess Shale and the Rise of Animals*, Oxford, Oxford University Press.
- COWEN, R. & KELLEY, J. S. 1976. Stereoscopic Vision within Schizochroal Eye of Trilobites. *Nature*, 261, 130-131.
- ÇUBUKÇU, H. E., ERSOY, O., AYDAR, E. & ÇAKIR, U. 2008. WDS versus silicon drift detector EDS: A case report for the comparison of quantitative chemical analyses of natural silicate minerals. *Micron*, 39, 88-94.
- CUSACK, M., DAUPHIN, Y., CHUNG, P., PEREZ-HUERTA, A. & CUIF, J. P. 2008a. Multiscale structure of calcite fibres of the shell of the brachiopod *Terebratulina retusa*. *Journal of Structural Biology*, 164, 96-100.
- CUSACK, M., ENGLAND, J., DALBECK, P., TUDHOPE, A. W., FALLICK, A. E. & ALLISON, N. 2008b. Electron backscatter diffraction (EBSD) as a tool for detection of coral diagenesis. *Coral Reefs*, 27, 905-911.
- CUSACK, M., PEREZ-HUERTA, A. & DALBECK, P. 2007. Common crystallographic control in calcite biomineralization of bivalved shells. *Crystengcomm*, 9, 1215-1218.
- CUSACK, M., PÉREZ-HUERTA, A., DALBECK, P., CHUNG, P. & LEE, M. R. 2009. Comparison of calcite crystallographic texture in the shells of the rhynchonelliform brachiopod *Terebratulina retusa* and the bivalve mollusc *Mytilus edulis*. In: ROLLETT, A. D. (ed.) *Applications of Texture Analysis: Ceramic Transactions* John Wiley & Sons.
- CÖLFEN, H. 2007. Mesocrystals: Examples of Non-Classical Crystallization. In: BEHRENS, P. & BAEUERLEIN, E. (eds.) *Handbook of Biomineralization. Biomimetic and Bioinspired Chemistry*. Weinheim: John Wiley and Sons Ltd.

- DALBECK, P. & CUSACK, M. 2006. Crystallography (electron backscatter diffraction) and chemistry (electron probe microanalysis) of the avian eggshell. *Crystal Growth & Design*, 6, 2558-2562.
- DALINGWATER, J. E. 1973. Trilobite cuticle microstructure and composition. *Palaeontology*, 16, 827-839.
- DALINGWATER, J. E. & MILLER, J. 1977. The laminae and cuticular organisation of the trilobite *Asaphus raniceps*. *Palaeontology*, 20, 21-32.
- DESCARTES, R. 1637. *Oeuvres de DesCartes*.
- DICKSON, J. A. D. 2001a. Diagenesis and crystal caskets: Echinoderm Mg calcite transformation, Dry Canyon, New Mexico, USA. *Journal of Sedimentary Research*, 71, 764-777.
- DICKSON, J. A. D. 2001b. Transformation of echinoid Mg calcite skeletons by heating. *Geochimica Et Cosmochimica Acta*, 65, 443-454.
- DICKSON, J. A. D. 2002. Fossil Echinoderms As Monitor of the Mg/Ca Ratio of Phanerozoic Oceans. *Science*, 298, 1222-1224.
- DICKSON, J. A. D. 2004. Echinoderm skeletal preservation: Calcite-aragonite seas and the Mg/Ca ratio of phanerozoic oceans. *Journal of Sedimentary Research*, 74, 355-365.
- DOVE, P. M. 2010. The Rise of Skeletal Biominerals. *Elements*, 6, 37-42.
- DUDICH, E. 1931. Systematische und biologische Untersuchungen über die Kalkeinlagerungen des Crustaceenpanzers in polarisiertem Lichte. *Zoologica (Stuttgart)*, 30, 1-154.
- EDAX TSL Orientation representations. *OIMTM software users manual*.
- EICHWALD, E. 1825. *Observationes geognostico-zoologicae per Inghiam marisque Baltici Provincias nec non de Trilobites*, Casani.
- EICHWALD, E. 1858. Beitrag zur geographischen Verbreitung der fossilen Thiere Russlands. *Bulletin du la Societé Impériale des naturalistes de Moscou.*, 30- 193-242.
- EMMERICH, H. F. 1839. *De Trilobitis: dissertatio petrefactologica quam consensu et auctoritate amplissimi philosophorum ordinis in alma litterarum universitate Friderica Guilelma pro summis in philisophia honoribus*.
- EPSTEIN, A. G., EPSTEIN, J. B. & HARRIS, L. D. 1976. *Conodont color alteration: an index to organic metamorphism*.
- EXNER, S. 1891. *Die Physiologie der facettierten Augen von Krebsen und Insekten*, Leipzig und Wein, Deutiche.

- FARYNA, M., SZTWIERTNIA, K. & SIKORSKI, K. 2006. Simultaneous WDXS and EBSD investigations of dense PLZT ceramics. *Journal of the European Ceramic Society*, 26, 2967-2971.
- FEIST, R. 1991. The late Devonian trilobite crises. *Historical Biology: An International Journal of Paleobiology*, 5, 197 - 214.
- FLETCHER, H. O. 1950. Trilobites from the Silurian of New South Wales. *Records of the Australian Museum*, 22, 220-233.
- FOLK, R. L. 1965. Some aspects of recrystallization in ancient limestones. In: PRAY, L. C. & MURRAY, R. C. (eds.) *Dolomitization and Limestone Diagenesis: a Symposium*. Soc. Econ. Paleontologists Mineralogists.
- FORDYCE, D. & CRONIN, T. W. 1989. Comparison of Fossilized Schizochroal Compound Eyes of Phacopid Trilobites with Eyes of Modern Marine Crustaceans and Other Arthropods. *Journal of Crustacean Biology*, 9, 554-569.
- FORDYCE, D. & CRONIN, T. W. 1993. Trilobite Vision - a Comparison of Schizochroal and Holochroal Eyes with the Compound Eyes of Modern Arthropods. *Paleobiology*, 19, 288-303.
- FORTEY, R. A. 1975. The Ordovician trilobites of Spitsbergen. II. Asaphidae, Nileidae, Raphiophoridae and Telephinidae of the Valhallfonna Formation. *Skrifter Norsk Polarinstitut*, 162, 1-125, pls 1-41.
- FORTEY, R. A. 1985. Pelagic trilobites as an example of deducing the life habits of extinct arthropods. *Transactions of the Royal Society of Edinburgh: Earth Sciences*, 76, 219-230.
- FORTEY, R. A. 1997. Late Ordovician trilobites from southern Thailand. *Palaeontology*, 40, 397-449.
- FORTEY, R. A. & CHATTERTON, B. 2003. A Devonian trilobite with an eyeshade. *Science*, 301 (5640), 1689-1689.
- FORTEY, R. A. & CLARKSON, E. N. K. 1975. The function of the glabellar 'tubercle' in *Nileus* and other trilobites. *Lethaia*, 9, 101-106.
- FORTEY, R. A. & MORRIS, S. F. 1977. Variation in lens packing of *Phacops* (Trilobita). *Geological Magazine*, 114 (1), 25-32.
- FORTEY, R. A. & OWENS, R. M. 1975. Proetida - a new order of trilobites. *Fossils and Strata*, 4, 227-239.
- FORTEY, R. A. & OWENS, R. M. 1987. The Arenig Series in South Wales: stratigraphy and palaeontology. I. *Bulletin of the British Museum (Natural History) Geology*, 41, 69-307.
- FORTEY, R. A. & OWENS, R. M. 1999. Feedings habits in Trilobites. *Palaeontology*, 42, 429-465.
- FRANK, F. 1988. Orientation mapping. *Metallurgical and Materials Transactions A*, 19, 403-408.

- FRANK, R. M. 1965. An improved carbonate peels technique for high powered studies. *Journal of Sedimentary Petrology*, 335, 499-500.
- FROST, B. 1975. Eye movements in *Daphnia pulex* (De Geer). *Journal of Experimental Biology*, 62, 175-187.
- GÁL, J., HORVÁTH, G., CLARKSON, E. N. K. & HAIMAN, O. 2000. Image formation by bifocal lenses in a trilobite eye? *Vision Research*, 40, 843-853.
- GHOSH, G. 1999. Dispersion-equation coefficients for the refractive index and birefringence of calcite and quartz crystals. *Optics Communications*, 163, 95-102.
- GILLHAUS, A., RICHTER, D. K., MEIJER, J., NEUSER, R. D. & STEPHAN, A. 2001. Quantitative high resolution cathodoluminescence spectroscopy of diagenetic and hydrothermal dolomites. *Sedimentary Geology*, 140, 191-199.
- GOLDSTEIN, J. I., LYMAN, C. E. & WILLIAMS, D. B. 1989. The wavelength-dispersive spectrometer and its proposed use in the Analytical Electron Microscope. *Ultramicroscopy*, 28, 162-164.
- GRADSTEIN, F., OGG, J. & SMITH, A. 2004. *A Geological Time Scale*, Cambridge University Press.
- GREEN, J. M. 1832. Synopsis of the Trilobites of North America. *American Journal of Geology and Natural History*. 1 (12), 558-560, pl.14.
- GREINER, B. 2006. Adaptations for Nocturnal Vision in Insect Apposition Eyes. In: KWANG, W. J. (ed.) *International Review of Cytology*. Academic Press.
- GREINER, B., RIBI, W. A. & WARRANT, E. J. 2004. Retinal and optical adaptations for nocturnal vision in the halictid bee *Megalopta genalis*. *Cell and Tissue Research*, 316, 377-390.
- GRIESSHABER, E., NEUSER, R. D., BRAND, U. & SCHMAHL, W. W. 2009. Texture and microstructure of modern rhynchonellide brachiopod shells. In: ROLLETT, A. D. (ed.) *Applications of Texture Analysis: Ceramic Transactions*. John Wiley & Sons.
- GRIESSHABER, E., SCHMAHL, W. W., NEUSER, R., PETTKE, T., BLUM, M., MUTTERLOSE, J. & BRAND, U. 2007. Crystallographic texture and microstructure of terebratulide brachiopod shell calcite: An optimized materials design with hierarchical architecture. *American Mineralogist*, 92, 722-734.
- HADDING, A. 1913. Släktet Telephus Barr. *Geologiska Föreningens i Stockholm Förhandlingar*, 35, 25-50.
- HAN, R.-N. 2001. The eyes of Ordovician trilobite *Telephina convexa* Lu. *Acta Palaeontologica Sinica*, 40, 404-409.

- HARDIE, R. C. 1986. The photoreceptor array of the dipteran retina. *Trends in Neurosciences*, 9, 419-423.
- HARZSCH, S. & HAFNER, G. 2006. Evolution of eye development in arthropods: Phylogenetic aspects. *Arthropod Structure & Development*, 35, 319-340.
- HAWLE, I. & CORDA, A. J. C. 1847. Prodrum einer Monographie der Böhmischen Trilobiten. *Rozpr. Mat. Přír. K. České Náuk*, 5, 117-292.
- HEANEY, P. J., VICENZI, E. P., GIANNUZZI, L. A. & LIVI, K. J. T. 2001. Focused ion beam milling: A method of site-specific sample extraction for microanalysis of Earth and planetary materials. *American Mineralogist*, 86, 1094-1099.
- HELSEN, S. & KONIGSHOF, P. 1994. Conodont Thermal Alteration patterns in Paleozoic rocks from Belgium, Northern France and Western Germany. *Geological Magazine*, 131, 369-386.
- HENDLER, G. 1984. Brittlestar Color-Change and Phototaxis (Echinodermata - Ophiuroidea - Ophiocomidae). *Marine Ecology-Pubblicazioni Della Stazione Zoologica Di Napoli I*, 5, 379-401.
- HENDLER, G. & BYRNE, M. 1987. Fine-Structure of the Dorsal Arm Plate of *Ophiocoma Wendtii* - Evidence for a Photoreceptor System (Echinodermata, Ophiuroidea). *Zoomorphology*, 107, 261-272.
- HENNINGSMOEN, G. 1975. Moulting in trilobites. *Fossils and Strata*, 4, 179-200.
- HERZOG, E. D. & BARLOW Jr., R. B. 1991. Ultraviolet light from the nighttime sky enhances retinal sensitivity of *Limulus*. *Biological Bulletin*, 181, 321-322.
- HORVATH, G. 1989. Geometric optics of trilobite eyes: A theoretical study of the shape of the aspherical interface in the cornea of schizochroal eyes of phacopid trilobites. *Mathematical Biosciences*, 96, 79-94.
- HORVATH, G. & CLARKSON, E. N. K. 1993. Computational Reconstruction of the Probable Change of Form of the Corneal Lens and Maturation of Optics in the Post-ecdysial Development of the Schizochroal Eye of the Devonian Trilobite *Phacops rana milleri* Stewart 1927. *Journal of Theoretical Biology*, 160, 343-373.
- HORVÁTH, G., CLARKSON, E. N. K. & PIX, W. 1997. Survey of modern counterparts of schizochroal trilobite eyes: structural and functional similarities and differences. *Historical Biology*, 12, 229-263.
- HUMPHREYS, F. J., HUANG, Y., BROUGH, I. & HARRIS, C. 1999. Electron backscatter diffraction of grain and subgrain structures - resolution considerations. *Journal of Microscopy-Oxford*, 195, 212-216.
- HUYGENS, C. 1690. *Traité de la lumière*

- JELL, P. A. 1975. The abathochroal eye of *Pagetia*, a new type of trilobite eye. *Fossils and Strata*, 4.
- JONASOVA, K. & KOZMIK, Z. 2008. Eye evolution: Lens and cornea as an upgrade of animal visual system. *Seminars in Cell & Developmental Biology*, 19, 71-81.
- JONES, T. R. 1887. *Notes on some Silurian Ostracoda from Gothland.*, Stockholm.
- KAESLER, R. L. E. 1997. *Part O. Arthropoda 1. Trilobita Revised*, The Geological Society of America, Inc. and The University of Kansas, Boulder, Colorado, and Lawrence, Kansas.
- KALJO, D., HEINSALU, H., MENS, K., PUURA, I. & VIIRA, V. 1988. Cambrian-Ordovician Boundary beds at Tõnismägi, Tallinn, North Estonia. *Geological Magazine*, 125, 457-463.
- KEARNS, S. L. & ORR, P. J. 2009. Charge contrast imaging of exceptionally-preserved fossils. *Palaeontology*, 52, 673-680.
- KING, W. B. R. 1914. A new trilobite from the Millstone Grit of North Yorkshire. *Geological Magazine*, 63, 390-394.
- KIRSCHFELD, K. 1967. Die projektion der optischen umwelt auf das raster der rhabdomere im komplexauge von Musca. *Experimental Brain Research*, 3, 248-270.
- KIRSCHFELD, K. 1971. Acquisition and processing of optical data by compound eye of insects. *Naturwissenschaften*, 58, 201-209.
- KIRSCHFELD, K. 1974. The absolute sensitivity of lens and compound eyes. *Zeitschrift für Naturforschung. C, Journal of biosciences*, 29, 592-596.
- KLAJMON, K. 2008. The structure and composition of the exoskeleton of the growth stages of the Carboniferous trilobite *Paladin shunnerensis*. *Unpublished undergraduate dissertation*, 1-4.
- KLUG, C., SCHULZ, H. & DE BAETS, K. 2009. Red Devonian trilobites with green eyes from Morocco and the silicification of the trilobite exoskeleton. *Acta Palaeontologica Polonica*, 54, 117-123.
- KOBAYASHI, T. 1940. Lower Ordovician fossils from Caroline Creek, near Latrobe, Mersey River district, Tasmania. *Papers and Proceedings of the Royal Society of Tasmania* 1939, 67-76, pl. 12.
- KONTROVITZ, M. & PUCKETT, T. M. 1998. Ocular Shell Structures in Some Cretaceous Trachyleberid Ostracoda. *Micropaleontology*, 44, 201-206.
- KONTROVITZ, M. & SLACK, J. M. 1995. Ocular Shell Structures in Some Loxoconchid Ostracoda. *Micropaleontology*, 41, 369-374.
- LAND, M. F. 1981a. Optics and vision in invertebrates. In: Autrum, H. (ed.) *Handbook of sensory physiology*. Berlin: Springer. 471-592.

- LAND, M. F. 1981b. Optics of the Eyes of *Phronima* and Other Deep-Sea Amphipods. *Journal of Comparative Physiology*, 145, 209-226.
- LAND, M. F. & BURTON, F. A. 1979. Refractive-Index Gradient in the Crystalline Cones of the Eyes of a Euphausiid Crustacean. *Journal of Experimental Biology*, 82, 395-398.
- LAND, M. F. & NILSSON, D. 2002. *Animal Eyes*, Oxford University Press, Oxford. p.221.
- LANG, J., MAHDOUDI, M. L. & PASCAL, A. 1990. Sedimentation Calcrete Cycles in the Mesozoic Red Formations from the Central High Atlas (Telouet Area), Morocco. *Palaeogeography Palaeoclimatology Palaeoecology*, 81, 79-93.
- LASSEN, N. C. K. 1996. Automatic localisation of electron backscattering pattern bands from Hough transform. *Materials Science and Technology*, 12, 837-843.
- LEE, M. R. 2010. Transmission Electron Microscopy (TEM) of Earth and planetary materials: A review. *Mineralogical Magazine*, 74, 1-27.
- LEE, M. R., BLAND, P. A. & GRAHAM, G. 2003. Preparation of TEM samples by focused ion beam (FIB) techniques: applications to the study of clays and phyllosilicates in meteorites. *Mineralogical Magazine*, 67, 581-592.
- LEE, M. R., MARTIN, R. W., EDWARDS, P. R. & PARSONS, I. 2005a. Hyperspectral cathodoluminescence mapping of calcite and feldspar. *Geochimica et Cosmochimica Acta*, 69, A593-A593.
- LEE, M. R., MARTIN, R. W., TRAGER-COWAN, C. & EDWARDS, P. R. 2005b. Imaging of cathodoluminescence zoning in calcite by scanning electron microscopy and hyperspectral mapping. *Journal of Sedimentary Research*, 75, 313-322.
- LEE, M. R. & SMITH, C. L. 2006. Scanning transmission electron microscopy using a SEM: Applications to mineralogy and petrology. *Mineralogical Magazine*, 70, 579-590.
- LEE, M. R., TORNEY, C. & OWEN, A. W. 2007a. Magnesium-rich intralensar structures in schizochroal trilobite eyes. *Palaeontology*, 50, 1031-1037.
- LEE, M. R., BROWN, D. J., SMITH, C. L., HODSON, M. E., MACKENZIE, M. & HELLMANN, R. 2007b. Characterization of mineral surfaces using FIB and TEM: A case study of naturally weathered alkali feldspars. *American Mineralogist*, 92, 1383-1394.
- LEVI-SETTI, R. 1975. *Trilobites. A Photographic Atlas*, Chicago, The University of Chicago Press.
- LINDSTRÖM, G. 1901. Visual organs of the trilobites. *Kongliga Svenska Vetenskaps-Akademiens Handlingar*, 8, 1-89.

- LOHMANN, K. C. & MEYERS, W. J. 1977. Microdolomite Inclusions in Cloudy Prismatic Calcites: A Proposed Criterion for Former High-Magnesium Calcites. *Journal of Sedimentary Petrology*, 47, 1078-1088.
- LOWENSTAM, H. 1963. Biologic problems relating to the composition and diagenesis of sediments. In: DONNELLY, T. W. (ed.) *The Earth Sciences Problems and Progress in Current Research*. Chicago: Chicago University Press.
- LUQUET, G. & MARIN, F. 2004. Biomineralisations in crustaceans: storage strategies. *Comptes Rendus Palevol*, 3, 515-534.
- MACDONALD, J., FREER, A. & CUSACK, M. 2010. Alignment of Crystallographic c-Axis throughout the Four Distinct Microstructural Layers of the Oyster *Crassostrea gigas*. *Crystal Growth & Design*, 10, 1243-1246.
- MÄNNIL, R. 1858. *Estoniops* - a new genus of Phacopidae (Trilobita). *Eesti NSV Teaduste Akadeemia Toimetised*, 6, 385-388.
- MAREK, L. 1952. Contribution to the stratigraphy and fauna of the uppermost part of the Králův Dvůr Shales (Ashgillian). *Sborník Ústředního Ústavu Geologického*, 19, 429-455.
- MARSHALL, D. J. 1988. *Cathodoluminescence of Geological Materials*, Boston, Unwin Hyman Ltd.
- MCALLISTER, J. E. & BRAND, U. 1989. Geochemistry of Some Ordovician and Devonian Trilobite Cuticles from North-America. *Chemical Geology*, 78, 51-63.
- MCCORMICK, T. & FORTEY, R. A. 1998. Independent testing of a paleobiological hypothesis: the optical design of two Ordovician pelagic trilobites reveals their relative paleobathymetry. *Paleobiology*, 24, 235-253.
- MCCOY 1849. On the classification of some British fossil Crustacea with notices of some forms in the University collection at Cambridge. *Annals and Magazine of Natural History*, 2, 161-179, 330-335, 392-414.
- MCKELLAR, R. C. & CHATTERTON, B. D. E. 2009. Early and middle Devonian Phacopidae (Trilobita) of southern Morocco. *Palaeontographica Canadiana*, 28, 1-114.
- MCNAMARA, K. 1978. Paedomorphosis in Scottish Olenellid trilobites (Early Cambrian). *Paleontology*, 21, 635-655.
- MCNAMARA, K. J. & RUDKIN, D. M. 1984. Techniques of trilobite exuviation. *Lethaia*, 17, 153-173.
- MEDLIN, W. L. 1959. Thermoluminescent Properties of Calcite. *The Journal of Chemical Physics*, 30, 451-458.
- MEDLIN, W. L. 1968. The nature of traps and emission centers in thermoluminescent rock materials. In: MCDOUGALL, D. J. (ed.)

- Thermoluminescence of Geological Materials*. New York: Academic Press.
- MEYER-ROCHOW, V. B. & WALSH, S. 1978. The Eyes of Mesopelagic Crustaceans. III *Thysanopoda tricusidata* (Euphausiacea). *Cell and Tissue Research*, 195, 59-79.
- MILLER, J. & CLARKSON, E. N. K. 1980. Post-Ecdysial Development of the Cuticle and the Eye of the Devonian Trilobite *Phacops rana milleri* Stewart 1927. *Philosophical Transactions of the Royal Society of London Series B-Biological Sciences*, 288, 461-&.
- MOORE, R. C. (Ed.) 1959. *Treatise on Invertebrate Paleontology; Part O: Arthropoda Vol I[1], Arthropoda - General Features, Protarthropoda, Euarthropoda - General Features, Trilobitomorpha*, The Geological Society of America, Inc. and The University of Kansas, Boulder, Colorado, and Lawrence, Kansas.
- MØRK, M. B. E. & MOEN, K. 2007. Compaction microstructures in quartz grains and quartz cement in deeply buried reservoir sandstones using combined petrography and EBSD analysis. *Journal of Structural Geology*, 29, 1843-1854.
- MÜLLER, J. & TROSCHER, F. H. 1842. *System der Asteriden*, Braunschweig, Germany, Friedreich und Sohn.
- MYERS, J. H. & KONTROVITZ, M. 1988. Geometrical Optics of Some Ostracod Eyes. In: TETSURO HANAI, N. I. & KUNIHIRO, I. (eds.) *Developments in Palaeontology and Stratigraphy*. Elsevier.
- NEUSER, R. D. & RICHTER, D. K. 2007. Non-marine radiaxial fibrous calcites--examples of speleothems proved by electron backscatter diffraction. *Sedimentary Geology*, 194, 149-154.
- NILSSON, D. E. 1990. From cornea to retinal image in invertebrate eyes. *Trends in Neurosciences*, 13, 55-64.
- NILSSON, D. E. 1988. A new type of imaging optics in compound eyes. *Nature*, 332, 76-78.
- NILSSON, D. E. & NILSSON, H. L. 1981. A crustacean compound eye adapted for low light intensities (Isopoda). *Journal of Comparative Physiology A*, 143, 503-510.
- NISHIKAWA, S. & KIKUCHI, S. 1928a. Diffraction of Cathode Rays by Mica. *Nature*, 121, 1019-1020.
- NISHIKAWA, S. & KIKUCHI, S. 1928b. Diffraction of Cathode Rays by Calcite. *Nature*, 122, 726.
- OGATA, S., ISHIDA, J. & SASANO, T. 1994. Optical Sensor Array in an Artificial Compound Eye. *Optical Engineering*, 33, 3649-3655.
- OLLIVIER, F. J., SAMUELSON, D. A., BROOKS, D. E., LEWIS, P. A., KALLBERG, M. E. & KOMÁROMY, A. M. 2004. Comparative morphology of the

- tapetum lucidum (among selected species). *Veterinary Ophthalmology*, 7, 11-22.
- ÕPIK, A. A. 1937. Trilobiten aus Estland. Publications of the Geological Institutions of the University of Tartu. 52, 1-163, pl. 1 -26, figs. 1-42.
- ORA 2004. Code V: Imaging Optics. www.opticalres.com. Optical Research Associates.
- OTT, M. 2006. Visual accommodation in vertebrates: mechanisms, physiological response and stimuli. *Journal of Comparative Physiology a-Neuroethology Sensory Neural and Behavioral Physiology*, 192, 97-111.
- PAIN, S. 2009. Code red: How deep reef fish keep in touch. *New Scientist*.
- PARKER, A. 2003. In the blink of an eye. *Free Press, London*, 316pp.
- PRIOR, D. J., BOYLE, A. P., BRENNER, F., CHEADLE, M. C., DAY, A., LOPEZ, G., PERUZZO, L., POTTS, G. J., REDDY, S., SPIESS, R., TIMMS, N. E., TRIMBY, P., WHEELER, J. & ZETTERSTROM, L. 1999. The application of electron backscatter diffraction and orientation contrast imaging in the SEM to textural problems in rocks. *American Mineralogist*, 84, 1741-1759.
- PÉREZ-HUERTA, A. & CUSACK, M. 2009. Optimising electron backscatter diffraction of carbonate biominerals - resin type and carbon coating. *Microscopy & Microanalysis*, 15, 197-203.
- RANDLE, V. & CAUL, M. 1996. Representation of electron backscatter diffraction data. *Materials Science and Technology*, 12, 844-850.
- RAUE, L., KLEIN, H., RAABE, D. & FABRITIUS, H. 2009. Crystallographic textures from the exoskeleton of the lobster *Homarus americanus* and calculation of the mechanical properties of the calcite phase. In: ROLLETT, A. D. (ed.) *Applications of Texture Analysis: Ceramic Transactions*. John Wiley & Sons.
- RAYMOND, P. E. 1925. Some trilobites of the lower Middle Ordovician of eastern North America. *Bulletin of the Museum of Comparative Zoology, Harvard University*, 67, 1-180.
- REED, F. R. C. 1905. The classification of the Phacopidae. *Geological Magazine*, 2 (4), 172-178.
- REED, F. R. C. 1914. Notes on the Genus *Trinucleus* pt. 3. *Geological Magazine*, 51, 349-359, pl. 28-29.
- REED, H. H. 1970. *Rutley's Elements of Mineralogy*. Twenty-sixth Edition, Great Britain, Thomas Murby and Co.
- REED, R. M. & MILLIKEN, K. L. 2003. How to Overcome Imaging Problems Associated with Carbonate Minerals on SEM-Based

- Cathodoluminescence Systems. *Journal of Sedimentary Research*, 73, 328-332.
- REEDER, R. J. 1983. *Crystal chemistry of the rhombohedral carbonates*, Mineralogical Society of America, Washington.
- REEDER, R. J. 1992. Carbonates: Growth and Alteration Microstructures. In: BUSECK, P. R. (ed.) *Minerals and Reaction at the Atomic Scale: Transmission Electron Microscopy*. Chelsea, Michigan: Mineralogical Society of America.
- REEDER, R. J., FAGIOLOI, R. O. & MEYERS, W. J. 1990. Oscillatory zoning of Mn in solution-grown calcite crystals. *Earth Science Reviews*, 29, 39-46.
- RICHTER, R. & RICHTER, E. 1925. Unterlagen zum Fossilium Catalogus. Trilobita. II. *Senckenbergiana*, 7, 126.
- RIES, J. B. 2004. Effect of ambient Mg/Ca ratio on Mg fractionation in calcareous marine invertebrates: A record of the oceanic Mg/Ca ratio over the Phanerozoic. *Geology*, 32, 981-984.
- ROER, R. & DILLAMAN, R. 1984. The Structure and Calcification of the Crustacean Cuticle. *American Zoologist*, 24, 893-909.
- ROSS, R. J. J. 1967. Some Middle Ordovician brachiopods and trilobites from the Basin ranges, western United States. United. *States Geological Survey, Professional Paper*, 523D.
- ROWELL, A. J. & SCANLON, J. E. 1957. The Namurian of the north-west quarter of the Askrigg Block. *Proceedings of the Yorkshire Geological Society*, 31, 1-38.
- ROY, S. K. 1933. A new Devonian trilobite from southern Illinois. *Field Museum of Natural History Geological Series*, 5, 67-82.
- RUEDEMANN, R. 1916. The presence of a median eye in trilobites. *Bulletin of New York State Museum*, 189, 127-143.
- SALTER, J. W. 1864. A monograph of the British trilobites from the Cambrian, Silurian and Devonian formations. *Monographs of the Palaeontographical Society of London.*, 1-80, pl. 1-6.
- SCHMIDT, F. 1881. Revision der ostbaltischen silurischen Trilobiten nebst geognostische Übersicht des ostbaltischen Silurgebiets. Abt, 1 Phacopiden, Cheiruriden, und Encrinuriden. *Mem. Acad. imp. sci. St.-Petersbourg*, 30, 1-237, pl. 1-16.
- SCHOENEMANN, B. 2006. Cambrian view. *Palaeoworld*, 15, 307-314.
- SCHOENEMANN, B. 2007. Trilobite eyes and a new type of neural superposition eye in an ancient system. *Palaeontographica Abteilung A-Palaeozoologie-Stratigraphie*, 281, 63-91.

- SCHOENEMANN, B. & CLARKSON, E. N. K. 2008. Did The trabecula in phacopid lenses act as light-guides? In: RÁBANO, I., GOZALO, R. & GARCÍA-BELLIDO, D. (eds.) *Advances in trilobite research*. Madrid: Instituto Geológico y Minero de España.
- SCHOENEMANN, B. & CLARKSON, E. N. K. 2010. Modern functional principles in ancient eyes (eyes of phacopid trilobites). Poster Presentation. *International Palaeontological Congress*, London, 347.
- SCHOENEMANN, B., CLARKSON, E. N. K. & FRANZ, A. 2008. Sublensar capsules in phacopid eyes. In: RÁBANO, I., GOZALO, R. & GARCÍA-BELLIDO, D. (eds.) *Advances in trilobite research*. Madrid: Instituto Geológico y Minero de España.
- SCHOENEMANN, B., LIU, J.-N., SHU, D.-G., HAN, J. & ZHANG, Z.-F. 2009. A miniscule optimized visual system in the Lower Cambrian. *Lethaia*, 42, 265-273.
- SCHOENEMANN, B., CLARKSON, E. N. K., AHLBERG, P. & ÁLVAREZ, M. E. D. 2010. A tiny eye indicating a planktonic trilobite. *Palaeontology*, 53, 695-701.
- SCHULMAN, J. H., EVANS, L. W., GINTHER, R. J. & MURATA, K. J. 1947. The sensitized luminescence of manganese-activated calcite. *Journal of Applied Physics*, 18, 732-739.
- SCHÜNGEL, M. 1988. *Stratigraphie und Fazies der zentralen Gerlostein Mulde*. Univ. Bonn.
- SCOTT, J., DOCHERTY, F. T., MACKENZIE, M., SMITH, W., MILLER, B., COLLINS, C. L. & CRAVEN, A. J. 2006. Sample preparation for nanoanalytical electron microscopy using the FIB lift-out method and low energy ion milling. *Journal of Physics: Conference Series*, 26, 223.
- SIPPEL, R. F. & GLOVER, E. D. 1965. Structures in Carbonate Rocks Made Visible by Luminescence Petrography. *Science*, 150, 1283-1287.
- SLAVÍK, L. 2001. Lower Devonian conodonts from the KarlíkValley and Na Branžovech sections in the Barrandian area, Czech Republic, and their significance for Pragian conodont zonation. *Acta Geologica Polonica*, 51, 253-271.
- SLAVÍK, L. 2004. The Pragian-Emsian conodont successions of the Barrandian area: search of an alternative to the GSSP polygnathid-based correlation concept. *Geobios*, 37, 454-470.
- SLAVÍK, L., VALENZUELA-RIOS, J. I., HLADIL, J. & CARLS, P. 2007. Early pragian conodont-based correlations between the Barrandian area and the Spanish central Pyrenees. *Geological Journal*, 42, 499-512.
- SMITH, A. M. & GIRVAN, E. 2010. Understanding a bimineralic bryozoan: Skeletal structure and carbonate mineralogy of *Odontionella cyclops* (Foveolariidae: Cheilostomata: Bryozoa) in New Zealand. *Palaeogeography, Palaeoclimatology, Palaeoecology*, 289, 113-122.

- SMITH, A. M., NELSON, C. S. & SPENCER, H. G. 1998. Skeletal carbonate mineralogy of New Zealand bryozoans. *Marine Geology*, 151, 27-46.
- SMITH, J. V. & STENSTROM, R. C. 1965. Electron-excited luminescence as a petrological tool. *Journal of Geology*, 73, 627-635.
- SMITH, K. C. & MACAGNO, E. R. 1990. UV photoreceptors in the compound eye of *Daphnia magna* (Crustacea, Branchiopoda). A fourth spectral class in single ommatidia. *Journal of Comparative Physiology A: Neuroethology, Sensory, Neural, and Behavioral Physiology*, 166, 597-606.
- SNYDER, A. W. 1977. Acuity of Compound Eyes - Physical Limitations and Design. *Journal of Comparative Physiology*, 116, 161-182.
- SPEYER, S. E. 1985. Moulting in phacopid trilobites. *Transactions of the Royal Society of Edinburgh: Earth Sciences*, 76, 239-253.
- STEPHENSON, A. E., DEYOREO, J. J., WU, L., WU, K. J., HOYER, J. & DOVE, P. M. 2008. Peptides Enhance Magnesium Signature in Calcite: Insights into Origins of Vital Effects. *Science*, 322, 724.
- STOCKTON, W. L. & COWEN, R. 1976. Stereoscopic vision in one eye: paleophysiology of the schizochroal eye of trilobites. *Paleobiology*, 2, 304-315.
- STRUVE, W. 1970. Beiträge zur Kenntnis der Phacopina (Trilobita), 7: Phacops- Arten aus dem Rheinischen Devon. 1. *Senckenbergiana Lethaea*, 51, 133-189.
- STRUVE, W. 1972. Beiträge zur Kenntnis der Phacopina (Trilobita). 8. *Phacops*-Arten aus dem rheinischen Devon. 2. *Senckenbergiana lethaea*, 53, 383-403.
- STRUVE, W. 1990. [Paläozoologie III (1986-1990)]. *Courier Forschungsinstitut Senckenberg*, 127, 251-279.
- STÜRMER, W. & BERGSTRÖM, J. 1973. New Discoveries on Trilobites by X-rays. *Paläontologische Zeitschrift*, 47, 104.
- TANAKA, G. 2006. Functional morphology and light-gathering ability of podocopid ostracod eyes and the palaeontological implications. *Zoological Journal of the Linnean Society*, 147, 97-108.
- TANAKA, G., SIVETER, D. J. & PARKER, A. R. 2009. The Visual System and Paleocology of the Silurian Ostracod *Primitiopsis planifrons*. *Journal of Paleontology*, 83, 414-421.
- TAYLOR, J. R. A., HEBRANK, J. & KIER, W. M. 2007. Mechanical properties of the rigid and hydrostatic skeletons of molting blue crabs, *Callinectes sapidus* Rathbun. *Journal of Experimental Biology*, 210, 4272-4278.
- THIRY, M. & BENBRAHIM, M. 1990. Pedogenic Silicification in the Hamada Deposits on the Piedmont of Boudenib (Morocco). *Geodinamica Acta*, 4, 237-251.

- THOMAS, A. T. 1998. Variation in the eyes of the Silurian trilobites *Eophacops* and *Acaste* and its significance. *Palaeontology*, 41, 897-911.
- THOMAS, A. T. 2005. Developmental palaeobiology of trilobite eyes and its evolutionary significance. *Earth-Science Reviews*, 71, 77-93.
- TORNEY, C., LEE, M. R. & OWEN, A. W. 2008. An Electron backscatter Diffraction Study of *Geesops*: A Broader View of Trilobite Vision? In: RÁBANO, I., GOZALO, R. & GARCÍA-BELLIDO, D. (eds.) *Advances in trilobite research*. Madrid: Instituto Geológico y Minero de España. pp. 384-394.
- TORNEY, C., LEE, M. R. & OWEN, A. W. 2009. Peering into the eyes of Trilobites using EBSD. In: ROLLETT, A. D. (ed.) *Applications of Texture Analysis: Ceramic Transactions*. John Wiley & Sons. pp. 619-626.
- TOWE, K. M. 1967. Echinoderm Calcite - Single Crystal or Polycrystalline Aggregate. *Science*, 157, 1048-1050.
- TOWE, K. M. 1973. Trilobite Eyes: Calcified Lenses in vivo. *Science*, 179, 1007-1009.
- TREMEL, W., KÜTHER, J., BALZ, M., LOGES, N. & WOLF, S. E. 2007. Template Surfaces for the Formation of Calcium Carbonate. In: BEHRENS, P. & BAEUERLEIN, E. (eds.) *Handbook of Biomineralization. Biomimetic and Bioinspired Chemistry*. Weinheim: John Wiley and Sons Ltd.
- TUCKER, M. E. & WRIGHT, V. P. 1990. *Carbonate Sedimentology*, Oxford, Blackwell.
- VALCKE, S. L. A., PENNOCK, G. M., DRURY, M. R. & DE BRESSER, J. H. P. 2006. Electron backscattered diffraction as a tool to quantify subgrains in deformed calcite. *Journal of Microscopy-Oxford*, 224, 264-276.
- VALENTINE, J. L. & BROCK, G. A. 2003. A New Siphonotretid Brachiopod from the Silurian of Central-Western New South Wales, Australia. *Records of the Australian Museum*, 55, 231-244.
- VANDENBROUCKE, T. R. A., WILLIAMS, M., LENG, M., FORTEY, R. A., ANDREWS, J. E., TORNEY, C., PAGE, A. A., ARMSTRONG, H. A. & OWEN, A. W. 2010. Drilling the eyes out of trilobites: first results from stable isotope analyses of Ordovician *Carolinites*. Poster Presentation. *International Palaeontological Congress*. London.
- VANNIER, J., GARCÍA-BELLIDO, D. C., HU, S.-X. & CHEN, A.-L. 2009. Arthropod visual predators in the early pelagic ecosystem: evidence from the Burgess Shale and Chengjiang biotas. *Proceedings of the Royal Society of London B*, 276, 2567-2574.
- VICENZI, E. P. & HEANEY, P. J. 1999. Examining Martian alteration products using in situ TEM sectioning: A novel application of the focused ion beam (FIB) for the study of extraterrestrial material. In: Lunar and Planetary Science Conference, 1999.
- VODGES, A. W. 1980. A bibliography of Paleozoic Crustacea from 1698

- to 1889 including a list of North American species and a systematic arrangement of genera. *United States Geological Survey Bulletin*, 63, 1-177.
- VOGT, K. 1980. Die Spiegeloptik des Flußkrebsauges: The optical system of the Caryfish eye. *Journal of Comparative Physiology. A.*, 135, 1-19.
- VUKUSIC, P. & SAMBLES, J. R. 2003. Photonic structures in biology. *Nature*, 424, 852-855.
- WALCH, J. E. I. 1771. *Die naturgeschichte der verteinerungen, Dritter Theil. Zuerläuterung der Knorrischen Sammlung von Merkwürdigkeiten der Natur.*, Nürnberg.
- WANG, D., WALLACE, A. F., DE YOREO, J. J. & DOVE, P. M. 2009. Carboxylated molecules regulate magnesium content of amorphous calcium carbonates during calcification. *Proceedings of the National Academy of Sciences*, 106, 2151-21516.
- WATABE, N. 1965. Studies on shell formation: XI. Crystal--matrix relationships in the inner layers of mollusk shells. *Journal of Ultrastructure Research*, 12, 351-370.
- WATERMAN, T. H. 1954. Directional sensitivity of single ommatidia in the compound eyes of *Limulus*. *Proceedings of the National Academy of Sciences*, 40, 252-257.
- WEINER, S., TRAUB, W. & PARKER, S. B. 1984. Macromolecules in Mollusc Shells and Their Functions in Biomineralization [and Discussion]. *Philosophical Transactions of the Royal Society of London. B, Biological Sciences*, 304, 425-434.
- WELLER, J. M. 1936. Carboniferous trilobite genera. *Journal of Paleontology*, 10, 704-714.
- WENDT, J., BELKA, Z., KAUFMANN, B., KOSTREWA, R. & HAYER, J. 1997. The world's most spectacular carbonate mud mounds (Middle Devonian, Algerian Sahara). *Journal of Sedimentary Research*, 67, 424-436.
- WILLIAMS, D. B. & CARTER, C. B. 2009a. Imaging Strain Fields. *Transmission Electron Microscopy. A textbook for materials science*. Springer US.
- WILLIAMS, D. B. & CARTER, C. B. 2009b. Weak-Beam Dark-Field Microscopy. *Transmission Electron Microscopy. A textbook for materials science*. Springer US.
- WILMOT, N. V. & FALLICK, A. E. 1989. Original mineralogy of trilobite exoskeletons. *Palaeontology*, 32, 297-304.
- WOLLAST, R. & REINHARD-DERIE, D. 1977. Equilibrium and mechanism of dissolution of Mg-calcites. In: ANDERSEN, N. R. & MALAHOFF, A. (eds.) *The fate of fossil fuel CO₂ in the oceans*. New York and London: Plenum Press.

- YOUNG, S. & DOWNING, A. C. 1976. Receptive-Fields of Daphnia Ommatidia. *Journal of Experimental Biology*, 64, 185-202.
- ZHANG, X.-G. & CLARKSON, E. N. K. 1990. The eyes of Lower Cambrian Eodiscid trilobites. *Palaeontology*, 33, 911-932.

A

Specimen Log

Details of each specimen including taxonomy and stratigraphical occurrence are listed in the tables below. Museum specimen numbers and loan numbers are provided where applicable as well the institution from which the specimens were sourced.

Specimens were allocated numbers based on the order in which they were received for study. Thin section codes indicate the source location and genus of the sample. Where two or more sections were prepared for a single specimen letters T and B are used to indicate if the section was made at the top or bottom of the eye and L and R refer to which eye the section cuts (left/right). Where two or more specimens were encased in the same piece of rock, lower case letters were assigned to the different specimens.

E.g. 1: BB3aR = *Boeckops*/Bohemia/specimen 3a/ right eye

E.g. 2: G33RT = *Geesops*/Germany/specimen 33/right eye/ top

Thin sections labelled with G are *Geesops schlotheimi*, those with GG are *Geesops sparsinodosus*. Both species were sourced from the same locality.

Samples that were received already sectioned have a thin section code only. The codes, in cases that have previously been studied, were already assigned. To differentiate between these, additional letters indicating the genus were added.

All sections are cut in the horizontal plane unless otherwise stated in Table A.1; (V) indicates vertical, (T) indicates tangential and (O) indicates oblique.

Table A.1 - Taxonomic and locality source information for all specimens.

SPECIMEN NUMBER	THIN SECTION CODES	FAMILY	SPECIES	LOCALITY	
n/a	C1B	Telephinidae	<i>Carolinites sibericus</i>	Spitsbergen	Norway
n/a	C2.6		<i>Carolinites angustagena</i>		
n/a	TS1	Dalmanitidae	<i>Dalmanites</i> sp.	Unknown	
n/a	B5X1	Phacopidae	<i>Geesops schlotheimi</i>	Gees	Germany
001	RB1L	Phacopidae	<i>Reedops prospiciens</i>	Cikanka near Silvenec	Bohemia
002	RB2B RB2		<i>Reedops</i> cf. <i>cephalotes</i>	Darnil near Tikin	
003	BB3a BB3aR BB3b (V)		<i>Boeckops boeckii</i>	Branzovy near Lodenice	
004			<i>Nephranomma</i> cf. <i>modesta</i>	Cernka near Buborice	
005			<i>Reedops</i> cf. <i>stembergi</i>	Homolka near Velka	
006			<i>Reedops</i> (?) sp. cf. <i>cephalotes</i>	Branzovy near Lodenice	
007	RB7	Phacopidae	<i>Reedops cephalotes</i>	Srbsko "Biograf" quarry	Bohemia
008	PB8		<i>Phacops (Pedinopariops) superstes superstes</i>	Karlstejn, Hlubokr valley	
009			<i>Reedops</i> cf. <i>decorns</i>	Praha-Hlubocepy (Zvahr)	
010			<i>Phacops (pedinopariops) cf. degenor - superstes</i>	Cernika near Buborice	
011			<i>Reedops</i> cf. <i>decorus</i>	Cernika near Buborice	
012	RB12		Phacopidae	<i>Reedops bronni</i>	
013	RB13L	<i>Reedops</i> cf. <i>stembergi</i>		Praha-Podoli swimming pool	
014	RB14L	<i>Reedops cephalotes</i>		Konvarka (Praha-Smichor)	
015	LB1A	Phacopidae	<i>Ananaspis macdonaldi</i>	Borenore-Molong District	Australia
016	LB1B				
017	LB1C				
018		Phacopidae	<i>Geesops schlotheimi</i>	Gees, near Eifel	Germany
019					
020					
021	E21R E21L	Phacopidae	<i>Eldredgeops rana</i>	Theofird-Aekona Area, Ontario	Canada
022	E22B E22T			Martin-Marietta Quarry, Milan, Michigan	USA
023		Phacopidae	<i>Nyterops Nyter</i>	Meerbusch	Germany
024	OB24R OB24RB OB24L OB24LB	Dalmanitidae	<i>Odonotchile hausmanni</i>		Bohemia
025	PM25 (O)	Phacopidae	<i>Phacops</i> sp.	Tafilult	Morocco
026	PM26 (V)				
027	PM27				
028	PM28	Phacopidae	<i>Phacops</i> [=Barrandeops] <i>granulops</i>	Jbel Gara el Zguilma	Morocco
029	G29	Phacopidae	<i>Geesops schlotheimi</i>	Gees, near Eifel	Germany
030	G30				

SPECIMEN NUMBER	THIN SECTION CODES	FAMILY	SPECIES	LOCALITY		
031	G31R G31L					
032		Phacopidae Phacopidae	<i>Geesops schlotheimi</i>	Gees, near Eifel	Germany	
033	G33RT G33L					
034	G34LR					
035	G35 (T)					
036	G36R					
037	G37R					
038	G38L					
039	G39B (O) G39T (O)					
040	G40R (V)	Phacopidae	<i>Geesops schlotheimi</i>	Gees, near Eifel	Germany	
041						
042	G42R (V)					
043	CE43	Pterygometopidae	<i>Chasmops</i> sp.	Kunda-Aru Karjaar	Estonia	
044			<i>Achatella (Vironiaspis) kuckersianus</i>	Narva karjaar openpit		
045	EE45		<i>Estoniops exilis</i>	Narva karjaar		
046	EE46		<i>Estoniops exilis</i>	Kohtla kaevandus		
047	IE47R		<i>Ingriops trigonocephalus</i>	Paldiski		
048	IE48R	Pterygometopidae	<i>Ingriops</i> sp nov.	Vaike-Pakri Island	Estonia	
049		Pterygometopidae	<i>Pterygometopus sclerops</i>	Lonna joe paljand 1b	Estonia	
050			<i>Chasmops cf musei</i>	Torremae kraav		
051	CE51L					
052	CE52(R?)					
053	CE53					
054		Phacopidae	<i>Phacops</i> sp.	Near Erfoud	Morocco	
055	PM55					
056		Phacopidae	<i>Gessops sparsinodosus</i>	Salmer Weg, Gees, Eifel, Germany	Germany	
057						
058	GG58					
060	BM60	Phacopidae	<i>Barrandeops cf. granulops</i>	Hamar Laghdad, Tatilalt	Morocco	
061	BM61		<i>Barrandeops forteyi</i>	Boudib		
062	BM62					
063						
064		Phacopidae	<i>Acernaspis orestes</i>		Anticosti Island	
065	AM65	Phacopidae	<i>Austerops smoothops</i>	Zguilma locality	Morocco	
066		Proetidae	<i>Paladin eichwaldi shunnerensis</i>	Great Shunner Fell, North Yorkshire	England	

SPECIMEN NUMBER	THIN SECTION CODES	FAMILY	SPECIES	LOCALITY	
067					
068					
069		Proetidae	<i>Paladin eichwaldi shunnerensis</i>	Great Shunner Fell, North Yorkshire	England
070					
071					
072					
073					
074					
075					
076					
077		Proetidae	<i>Paladin eichwaldi shunnerensis</i>	Great Shunner Fell, North Yorkshire	England
078	PE78	Proetidae	<i>Paladin eichwaldi shunnerensis</i>	Great Shunner Fell, North Yorkshire	England
079	PE79				
080					
081	PE81				
082					
083	PE83				
084					
085	PE85				
086	PE86	Proetidae	<i>Paladin eichwaldi shunnerensis</i>	Great Shunner Fell, North Yorkshire	England
087	PE87				
088					
089					
090					
091	PE91				
092	PE92				
093	SS93				
094	SS94				
095	T95	Telephinidae	<i>Telephus mobergi</i>	Storsjön area , Jämtland Region	Sweden
096			<i>Telephus bicuspis</i>		
097	T97				
098	BM98	Phacopidae	<i>Barrandeops forteyi</i>	Boudib?	Morocco
099		Asaphidae?	<i>Asaphus?</i>	Torremae kraav?	Estonia

Table A.2 - Stratigraphical information for all specimens.

SPECIMEN NUMBER	THIN SECTION CODES	STRATIGRAPHY
n/a	C1B	Valhalfonne Formation
n/a	C2.6	Unit V4b from the Profilbekken Member, Valhalfonne Formation (type section)
n/a	TS1	Unknown
n/a	B5X1	Trilobitenfelder
001	RB1L	Silvenec ls. Facies (upper), Praha Fm. (layer no. 19)
002	RB2B RB2	Dvorce-Prokop Ls Facies, Praha Formation
003	BB3a BB3aR BB3b	Lodenice Ls. Facies, Praha Formation
004		Zlichor Ls. Facies, Zlichor Formation
005		Dvorce-Prokop Ls. Facies, Praha Formation (ca.20-30m above GSSP)
006		Slivenec Ls. Facies, Praha Formation
007	RB7	Lodenice Ls. Facies, Praha Formation
008	PB8	Daleje-Trebotor Formation, Daleje Shale
009		Zlichor Ls. Facies, Zlichor Formation
010		Zlichor and Daleje-Trebotor Formation (Intermediate layers)
011		Zlichor Ls. Zlichor Formation
012	RB12	Lodenice Ls. Facies, Praha Formation
013	RB13L	Silvenec and Dvorce-Prokop Ls. Facies, (Transition layers) Weathered "white beds", Praha Formation
014	RB14L	Dvorce-Prokop Ls. Facies, Praha Formation
015	LB1A	Boree Creek Formation
016	LB1B	
017	LB1C	
018		Trilobitenfelder
019		
020		
021	E21R E21L	Hamilton Group Formation
022	E22B E22T	Silica Formation (unit 7-9)
023		Curtum-Schichten
024	OB24R OB24RB OB24L OB24LB	Dvorce-Prokop Facies, Praha Formation
025	PM25	Teratine Formation, Merzonga Section, beds above Koneprusilts
026	PM26	
027	PM27	
028	PM28	Timrhanhart Formation, Leonaspis Couche

SPECIMEN NUMBER	THIN SECTION CODES	STRATIGRAPHY
029	G29	Trilobitenfelder
030	G30	
031	G31R G31L	Trilobitenfelder
032		
033	G33RT G33L	
034	G34LR	
035	G35	
036	G36R	
037	G37R	
038	G38L	
039	G39B G39T	
040	G40R	
041		
042	G42R	
043	CE43	
044		Kukruse lade
045	EE45	
046	EE46	
047	IE47R	Kunda lade
048	IE48R	Aseri lade Echinospaerites lk
049		BII/BIII panga al pinnast 0.05-0.10m
050		Oandu stage
051	CE51L	
052	CE52(R?)	
053	CE53	
054		Unknown
055	PM55	
056		'The Trench'
057		
058	GG58	
060	BM60	Red Cliff
061	BM61	
062	BM62	Psychopyge horizon, Tazoulart Formation
063		

SPECIMEN NUMBER	THIN SECTION CODES	STRATIGRAPHY
064		
065	AM65	Timrhanrhart Formation, ZGEE3 horizon
066		Shunner Fell Limestone, Namurian Millstone Grit
067		
068		
069		
070		
071		
072		
073		
074		
075		
076		
077		
078	PE78	
079	PE79	
080		
081	PE81	
082		
083	PE83	
084		
085	PE85	
086	PE86	
087	PE87	
088		
089		
090		
091	PE91	
092	PE92	
093	SS93	Upper Whitehouse Subgroup
094	SS94	
095	T95	Lower Anderson Shale (Hustedograptus teretiusculus biozone)
096		
097	T97	

SPECIMEN NUMBER	THIN SECTION CODES	STRATIGRAPHY
098	BM98	Tazoulart Formation
099		Oandu Stage

Table A.3 - Age data for all specimens.

SPECIMEN NUMBER	THIN SECTION CODES	AGE		EPOCH
n/a	C1B	Arenig	478.6±1.7 - ~466.5	Lower Ordovician
n/a	C2.6			
n/a	TS1	Unknown		
n/a	B5X1	Mid Eifelian	397.5±2.7 – 391.8±2.7	Middle Devonian
001	RB1L	Pragian	411.2±2.8 – 407.0±2.8	Lower Devonian
002	RB2B RB2	Pragian	411.2±2.8 – 407.0±2.8	
003	BB3a BB3aR BB3b	Pragian	411.2±2.8 – 407.0±2.8	
004		Lower Emsian	407.0±2.8 - ~401	Lower Devonian
005		Pragian	411.2±2.8 – 407.0±2.8	
006		Pragian	411.2±2.8 – 407.0±2.8	
007	RB7	Pragian	411.2±2.8 – 407.0±2.8	
008	PB8	Upper Emsian	~401 – 397.5±2.7	Lower Devonian
009		Lower Emsian	407.0±2.8 - ~401	
010		Emsian	407.0±2.8 – 397.5±2.7	
011		Lower Emsian	407.0±2.8 - ~401	
012	RB12	Pragian	411.2±2.8 – 407.0±2.8	Lower Devonian
013	RB13L	Pragian	411.2±2.8 – 407.0±2.8	
014	RB14L	Pragian	411.2±2.8 – 407.0±2.8	
015	LB1A	Silurian, upper Telychian - lowermost Sheinwoodian	428.2±2.3	Silurian
016	LB1B			
017	LB1C			
018		Mid Eifelian	397.5±2.7 – 391.8±2.7	Middle Devonian
019				
020				
021	E21R E21L	Givetian	397.5±2.7 – 385.3±2.6	Middle Devonian
022	E22B E22T		391.8±2.7 - 385.3±2.6	
023			Lower Givetian	
024	OB24R OB24RB OB24L OB24LB	Pragian	411.2±2.8 – 407.0±2.8	Lower Devonian
025	PM25	Eifelian	397.5±2.7 – 391.8±2.7	Middle Devonian

SPECIMEN NUMBER	THIN SECTION CODES	AGE		EPOCH
026	PM26			
027	PM27			
028	PM28	Upper Emsian	~401 – 397.5±2.7	Lower Devonian
029	G29	Mid Eifelian	~395 – 391.8±2.7	Middle Devonian
030	G30	Mid Eifelian	~395 – 391.8±2.7	Middle Devonian
031	G31R G31L			
032		Mid Eifelian	~395 – 391.8±2.7	Middle Devonian
033	G33RT G33L			
034	G34LR			
035	G35			
036	G36R			
037	G37R			
038	G38L			
039	G39B G39T			
040	G40R	Mid Eifelian	~395 – 391.8±2.7	Middle Devonian
041				
042	G42R			
043	CE43		488.3 – 443.7	Ordovician
044		Kukruse Stage-Sandbian	460.4 – 458.0	Upper Ordovician
045	EE45			
046	EE46			
047	IE47R	Kunda Stage-Darriwilian	467.2 – 463.9	Middle Ordovician
048	IE48R	Aseri Stage-Darriwilian	463.9 – 463.0	Middle Ordovician
049				Ordovician
050		Oandu Stage-Katian	455.8 – 545.5	Upper Ordovician
051	CE51L			
052	CE52(R?)			
053	CE53			
054			397.5 – 385.3	Middle Devonian
055	PM55			
056		Mid Eifelian	~395 – 391.8±2.7	Middle Devonian
057				
058	GG58			
060	BM60	Latest Emsian/earliest Eifelian	~397.5±2.7	Lower - Middle Devonian
061	BM61			

SPECIMEN NUMBER	THIN SECTION CODES	AGE		EPOCH
062	BM62	Upper Emsian	~401 – 397.5±2.7	Lower Devonian
063				
064				
065	AM65	Upper Emsian	~401 – 397.5±2.7	Lower Devonian
066		Namurian, Serpukhovian	326.4±1.6 – 318.1±1.3	Carboniferous
067				
068				
069				
070		Namurian, Serpukhovian	326.4±1.6 – 318.1±1.3	Carboniferous
071				
072				
073				
074				
075				
076				
077				
078	PE78	Namurian, Serpukhovian	326.4±1.6 – 318.1±1.3	Carboniferous
079	PE79			
080				
081	PE81			
082				
083	PE83			
084				
085	PE85			
086	PE86	Namurian, Serpukhovian	326.4±1.6 – 318.1±1.3	Carboniferous
087	PE87			
088				
089				
090		Upper Katian, Caradoc – Ashgill boundary	~451	Upper Ordovician
091	PE91			
092	PE92	Upper Darwillian Stage	~362	Middle Ordovician
093	SS93			
094	SS94			
095	T95			
096				

SPECIMEN NUMBER	THIN SECTION CODES	AGE		EPOCH
097	T97			
098	BM98	Upper Emsian	~401 – 397.5±2.7	Lower Devonian
099		Oandu Stage-Katian	455.8 – 545.5	Upper Ordovician

Table A.4 - Specimen Sources and Museum numbers.

SPECIMEN NUMBER	THIN SECTION CODES	LOAN NUMBER	MUSEUM NUMBER	INSTITUTION
n/a	C1B			Université Lille - Sciences et Technologies
n/a	C2.6			
n/a	TS3			Grant Institute, University of Edinburgh
n/a	B5X1			Universität Bonn
001	RB1L			Czech Geological Survey
002	RB2B RB2			
003	BB3a BB3aR BB3b			
004				
005				Czech Geological Survey
006				
007	RB7			
008	PB8			
009				
010				
011				Czech Geological Survey
012	RB12			
013	RB13L			
014	RB14L			
015	LB1A		NMV P312898	Museum Victoria
016	LB1B	IP2007/11	NMV P312899	
017	LB1C		NMV P312897	
018				Universität Bonn
019				
020				
021	E21R E21L			Royal Ontario Museum
022	E22B E22T		ROM 76 IP23	
023				Universität Bonn
024	OB24R OB24RB OB24L OB24LB		1963.15.69	Royal Museum of Scotland

SPECIMEN NUMBER	THIN SECTION CODES	LOAN NUMBER	MUSEUM NUMBER	INSTITUTION
025	PM25			Natural History Museum, London
026	PM26			
027	PM27			
028	PM28			
029	G29			Universität Bonn
030	G30			
031	G31R G31L			
032				
033	G33RT G33L			Universität Bonn
034	G34LR			
035	G35			
036	G36R			
037	G37R			
038	G38L			
039	G39B G39T			Universität Bonn
040	G40R			
041				
042	G42R			
043	CE43		337-361 (Neigla 2002)	Institute of Geology, Tallinn University of Technology
044			360-331 (Pärmaste 2000)	
045	EE45		360-332 (Pärmaste 2000)	
046	EE46		360-333	
047	IE47R		395-30 (Orviku, Karl 4.07.1927)	Institute of Geology, Tallinn University of Technology
048	IE48R		411-3 (Orviku, Karl 2.08.1928)	
049			438-401(=lon.79) (1963)	
050			553-1 (Männil, Ralf 1960)	Institute of Geology, Tallinn University of Technology
051	CE51L		553-2 (Männil, Ralf 1960)	
052	CE52(R?)		553-3 (Männil, Ralf 1960)	
053	CE53		553-4 (Männil, Ralf 1960)	
054				Purchased from Mr Wood's fossil shop, Edinburgh
055	PM55			
056				University of Oslo
057				
058	GG58			
060	BM60			Museum der Universität Zürich

SPECIMEN NUMBER	THIN SECTION CODES	LOAN NUMBER	MUSEUM NUMBER	INSTITUTION
061	BM61			
062	BM62			
063				
064				
065	AM65			
066				
067				
068				
069				
070				
071				
072				
073				
074				
075				
076				
077				
078	PE78			
079	PE79			
080				
081	PE81			
082				
083	PE83			
084				
085	PE85			
086	PE86			
087	PE87			
088				
089				
090				
091	PE91			
092	PE92			
093	SS93			
094	SS94			
095	T95			

SPECIMEN NUMBER	THIN SECTION CODES	LOAN NUMBER	MUSEUM NUMBER	INSTITUTION
096				
097	T97			
098	BM98			
099				Richard Fortey (personal collection)
				Institute of Geology, Tallinn University of Technology

Table A.5 – Analysis carried out on each specimen.
An ‘X’ indicates that the specimen was analysed by a particular method. ‘Opt’ and ‘Hyper.’
Correspond to optical CL and hyperspectral CL respectively.

SPECIMEN NUMBER	THIN SECTION CODES	TL	RL	CL		SEM IMAGING	EDS	EPMA	EBSD	TEM	CODE V
				OPT.	HYPER.						
n/a	C1B	X	X	X		X	X		X		
n/a	C2.6	X	X	X		X	X		X		X
n/a	TS3	X	X	X		X	X	X	X		
n/a	B5X1	X	X	X		X	X				
001	RB1L	X	X	X		X	X		X		
002	RB2B RB2	X	X	X		X	X		X		
003	BB3a BB3aR BB3b	X	X	X		X	X	X	X		X
004											
005											
006											
007	RB7	X	X	X		X	X		X		
008	PB8	X	X	X		X	X		X		
009											
010											
011											
012	RB12	X	X	X		X	X		X		
013	RB13L	X	X	X		X	X		X		
014	RB14L	X	X	X		X	X	X	X		
015	LB1A	X	X	X		X	X				
016	LB1B	X	X	X		X	X				
017	LB1C	X	X	X		X	X		X		X
018											
019											
020											
021	E21R E21L	X	X	X		X	X		X		
022	E22B E22T	X	X	X		X	X	X	X		

[illegible]

SPECIMEN NUMBER	THIN SECTION CODES	TL	RL	CL		SEM IMAGING	EDS	EPMA	EBSD	TEM	CODE V
				OPT.	HYPER.						
058	GG58	X	X	X		X	X		X		
060	BM60	X	X	X		X	X		X		
061	BM61	X	X	X							
062	BM62	X	X	X		X	X		X		
063											
064											
065	AM65	X	X	X		X	X	X	X		
066											
067											
068											
069											
070											
071											
072											
073											
074											
075											
076											
077											
078	PE78	X	X	X		X	X		X		X
079	PE79	X	X	X		X	X		X		
080											
081	PE81	X	X			X	X		X		
082											
083	PE83	X	X	X		X	X		X		
084											
085	PE85	X	X	X		X	X		X		
086	PE86	X	X			X	X				
087	PE87	X	X	X		X	X		X		
088											
089											
090											
091	PE91	X	X	X		X	X		X		
092	PE92	X	X	X		X	X		X		X
093	SS93	X	X	X		X	X		X		X

[illegible]

B

Point Counting Data

Lenses in schizochroal eyes as well as echinoderm fragments within the same acid etched thin sections were point counted for calcite, dolomite, pore space and other (non-carbonates or surface debris). Point counting provided information on the volume percentage of each constituent within an area counted. This data was normalised and the mole % of calcite and dolomite determined using information from Bischoff *et al.*, 1983. Values provide information on the present day dolomite concentration of the lenses and echinoderm fragments, which is a minimum value of the *in-vivo* magnesium content.

Table B.1 - Point counting of schizochroal lenses and echinoderm fragments.

SAMPLE		POINT COUNTS				
		<i>CALCITE</i>	<i>DOLOMITE</i>	<i>PORES</i>	<i>OTHER</i>	TOTAL
G41R	Lens 1	287	39	20	0	346
	Lens 1 repeat	146	20	8	0	174
	Lens 3	167	11	5	0	183
	Lens 3 repeat	118	17	5	1	141
G31R	Lens 1	104	15	1	1	121
R2B2	Lens 1 (base)	93	13	3	1	110
	Lens 1(top)	106	0	0	0	106
	Lens 4	114	10	5	4	133
TS3	Lens 1	116	17	3	0	136
	Lens 1 repeat	118	10	1	0	129
	Lens 2	120	17	0	1	138
IE48	Lens 1	110	0	1	1	112
	Lens 2	105	1	1	2	109
OB24LB	Lens 1	100	1	0	0	101
	Lens 2	110	9	2	0	121
	Lens 3	135	5	2	3	145
BB3aR	Lens 1	130	23	2	5	160
	Lens 2	110	16	1	0	127
	Lens 2 repeat	105	14	1	1	121
PM28	Lens 3	108	38	1	1	148
	Lens 4	75	32	0	1	108
AM65	Lens 2	75	26	0	6	107
	Lens 1	78	28	0	3	109
PM27	Lens 3 upper	90	34	2	0	126
	Lens 1	90	34	1	3	128
G41R	Crinoid ossicle (area 1)	175	10	10	5	200
	Crinoid ossicle (area 2)	140	8	5	10	163
	Echinoderm fragment	148	6	4	7	165

Table B.2 – Volume % values of schizochroal lenses and echinoderm fragments.

SAMPLE		VOLUME %				
		CALCITE	DOLOMITE	PORES	OTHER	TOTAL
G41R	Lens 1	82.95	11.27	5.78	0.00	100.00
	Lens 1 repeat	83.91	11.49	4.60	0.00	100.00
	Lens 3	91.26	6.01	2.73	0.00	100.00
	Lens 3 repeat	83.69	12.06	3.55	0.71	100.00
G31R	Lens 1	85.95	12.40	0.83	0.83	100.00
R2B2	Lens 1 (base)	84.55	11.82	2.73	0.91	100.00
	Lens 1(top)	100.00	0.00	0.00	0.00	100.00
	Lens 4	85.71	7.52	3.76	3.01	100.00
TS3	Lens 1	85.29	12.50	2.21	0.00	100.00
	Lens 1 repeat	91.47	7.75	0.78	0.00	100.00
	Lens 2	86.96	12.32	0.00	0.72	100.00
IE48	Lens 1	98.21	0.00	0.89	0.89	100.00
	Lens 2	96.33	0.92	0.92	1.83	100.00
OB24LB	Lens 1	99.01	0.99	0.00	0.00	100.00
	Lens 2	90.91	7.44	1.65	0.00	100.00
	Lens 3	93.10	3.45	1.38	2.07	100.00
BB3aR	Lens 1	81.25	14.38	1.25	3.13	100.00
	Lens 2	86.61	12.60	0.79	0.00	100.00
	Lens 2 repeat	86.78	11.57	0.83	0.83	100.00
PM28	Lens 3	72.97	25.68	0.68	0.68	100.00
	Lens 4	69.44	29.63	0.00	0.93	100.00
AM65	Lens 2	70.09	24.30	0.00	5.61	100.00
	Lens 1	71.56	25.69	0.00	2.75	100.00
PM27	Lens 3 upper	71.43	26.98	1.59	0.00	100.00
	Lens 1	70.31	26.56	0.78	2.34	100.00
G41R	Crinoid ossicle (area 1)	87.50	5.00	5.00	2.50	100.00
	Crinoid ossicle (area 2)	85.89	4.91	3.07	6.13	100.00
	Echinoderm fragment	89.70	3.64	2.42	4.24	100.00

Table B.3 – Mole % values of schizochroal lenses and echinoderm fragments.

SAMPLE		NORM. VOL. %		MOLE %	
		CALCITE	DOLOMITE	CALCITE	DOLOMITE
G41R	Lens 1	88.04	11.96	93.99	6.01
	Lens 1 repeat	87.95	12.05	93.94	6.06
	Lens 3	93.82	6.18	96.20	3.80
	Lens 3 repeat	87.41	12.59	93.67	6.33
G31R	Lens 1	87.39	12.61	923.66	6.34
R2B2	Lens 1 (base)	87.74	12.26	93.15	6.85
	Lens 1(top)	100.00	0.00	100.00	0.00
	Lens 4	91.94	8.06	95.50	4.50
TS3	Lens 1	87.22	12.78	92.86	7.14
	Lens 1 repeat	92.19	7.81	95.64	4.36
	Lens 2	87.59	12.41	93.07	6.93
IE48	Lens 1	100.00	0.00	100.00	0.00
	Lens 2	99.06	0.94	99.47	0.53
OB24LB	Lens 1	99.01	0.99	99.46	0.54
	Lens 2	92.44	7.56	95.78	4.22
	Lens 3	96.43	3.57	98.01	1.99
BB3aR	Lens 1	84.97	15.03	91.60	8.40
	Lens 2	87.30	12.70	92.91	7.09
	Lens 2 repeat	88.24	11.76	93.43	6.57
PM28	Lens 3	73.97	26.03	85.46	14.54
	Lens 4	70.09	29.91	83.29	16.71
AM65	Lens 2	74.26	25.74	85.62	14.38
	Lens 1	73.58	26.42	85.24	14.76
PM27	Lens 3 upper	72.58	27.42	84.68	15.32
	Lens 1	72.58	27.42	84.68	15.32
G41R	Crinoid ossicle (area 1)	94.59	5.41	96.98	3.02
	Crinoid ossicle (area 2)	94.59	5.41	96.98	3.02
	Echinoderm fragment	96.10	3.90	97.82	2.18

C

Microdolomite size distribution

Microdolomite size distribution was determined by point counting of SE imaging of acid etched thin sections. The number of crystals measured in each section varies due to differences in microdolomite abundance.

Standard deviation is given for the average crystal size (in microns) in each data set. Standard deviation is determined using the following equation:

$$\text{Standard deviation} = \sqrt{\text{Sum of (crystal size-mean size)}^2 / \text{total number of crystals measured}}$$

Each stage of this calculation is shown in the tables below.

C.1 *Austerops smoothops*

Table C.1 - Microdolomite crystal size distribution in AM65 Lens 2.

		CRYSTAL		CRYSTAL	<--	STANDARD	SIZE DISTRIBUTION		
SAMPLE	POINT	SIZE	AVERAGE	SIZE- MEAN	^2	DEVIATION	BIN	NO.	%
AM65 Lens 2	1	0.36	1.41	-1.05	1.11	1.12	0-1	16	53
	2	0.44		-0.97	0.95		1-2	9	30
	3	0.53		-0.88	0.78		2-3	1	3
	4	0.58		-0.83	0.69		3-4	3	10
	5	0.69		-0.73	0.53		4-5	0	0
	6	0.70		-0.71	0.51		5-6	1	3
	7	0.71		-0.70	0.49		6-7	0	0
	8	0.72		-0.70	0.48		7-8	0	0
	9	0.77		-0.64	0.41		8-9	0	0
	10	0.79		-0.62	0.39		9-10	0	0
	11	0.79		-0.62	0.38		10-11	0	0
	12	0.80		-0.62	0.38		11-12	0	0
	13	0.82		-0.59	0.35		>12	0	0
	14	0.88		-0.53	0.28				
	15	0.91		-0.50	0.25		TOTAL 30		
	16	0.94		-0.48	0.23				
	17	1.11		-0.31	0.10				
	18	1.17		-0.24	0.06				
	19	1.25		-0.17	0.03				
	20	1.35		-0.06	0.00				
	21	1.35		-0.06	0.00				
	22	1.51		0.09	0.01				
	23	1.71		0.30	0.09				
	24	1.74		0.32	0.10				
	25	1.83		0.41	0.17				
	26	2.84		1.43	2.04				
	27	3.15		1.74	3.02				
	28	3.20		1.79	3.20				
	29	3.25		1.84	3.38				
	30	5.53			4.12		16.95	1.12	

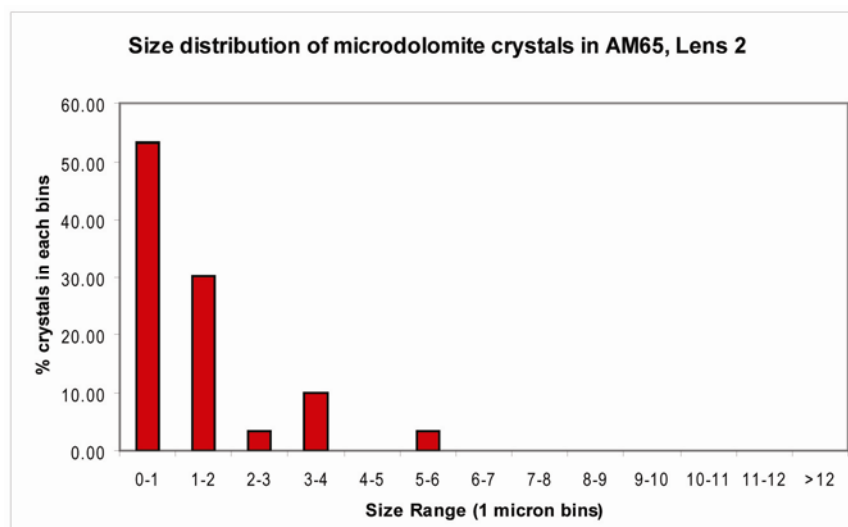


Figure C.1 - Size distribution of microdolomite crystals in AM65 Lens 2.

C.2 *Barrandeops granulops*

Table C.2 - Microdolomite crystal size distribution in PM28 Lens 3.

SAMPLE	POINT	CRYSTAL	AVERAGE	CRYSTAL	<--	STANDARD DEVIATION	SIZE DISTRIBUTION		
		SIZE		SIZE- MEAN	^2		BIN	NO.	%
PM28 Lens 3	1	0.35	2.10	-1.75	3.06	1.86	0-1	11	34
	2	0.38		-1.72	2.95		1-2	12	38
	3	0.53		-1.57	2.47		2-3	1	3
	4	0.64		-1.45	2.12		3-4	1	3
	5	0.66		-1.44	2.06		4-5	3	9
	6	0.68		-1.42	2.01		5-6	2	6
	7	0.69		-1.40	1.97		6-7	1	3
	8	0.73		-1.37	1.87		7-8	1	3
	9	0.74		-1.36	1.85		8-9	0	0
	10	0.88		-1.22	1.49		9-10	0	0
	11	0.96		-1.14	1.30		10-11	0	0
	12	1.06		-1.04	1.07		11-12	0	0
	13	1.07		-1.02	1.05		>12	0	0
	14	1.10		-1.00	1.00				
	15	1.18		-0.91	0.83		TOTAL 32		
	16	1.23		-0.86	0.75				
	17	1.43		-0.67	0.45				
	18	1.58		-0.51	0.26				
	19	1.70		-0.40	0.16				
	20	1.71		-0.38	0.15				
	21	1.72		-0.38	0.14				
	22	1.85		-0.24	0.06				
	23	1.94		-0.16	0.02				
	24	2.05		-0.05	0.00				
	25	3.01		0.92	0.84				
	26	4.02		1.92	3.68				
	27	4.26		2.16	4.66				
	28	4.35		2.25	5.07				
	29	5.39		3.29	10.84				
	30	5.87		3.78	14.27				
	31	6.28		4.18	17.51				
	32	7.06		4.96	24.60				

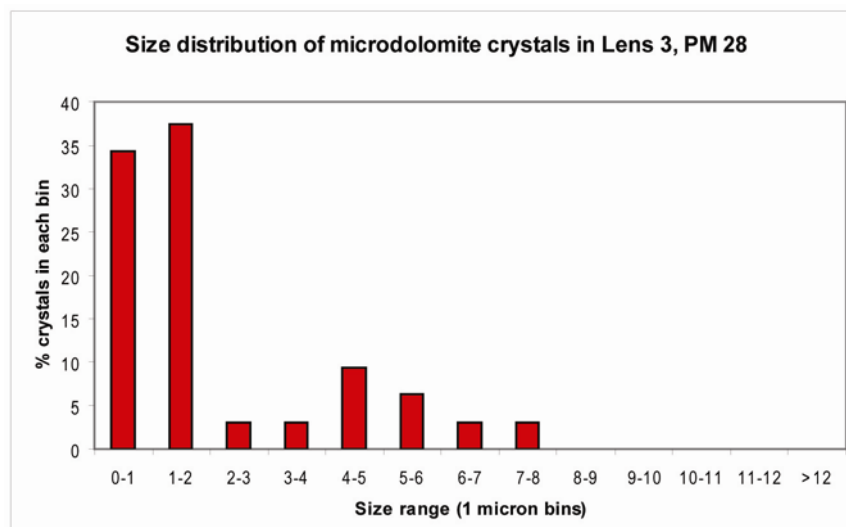
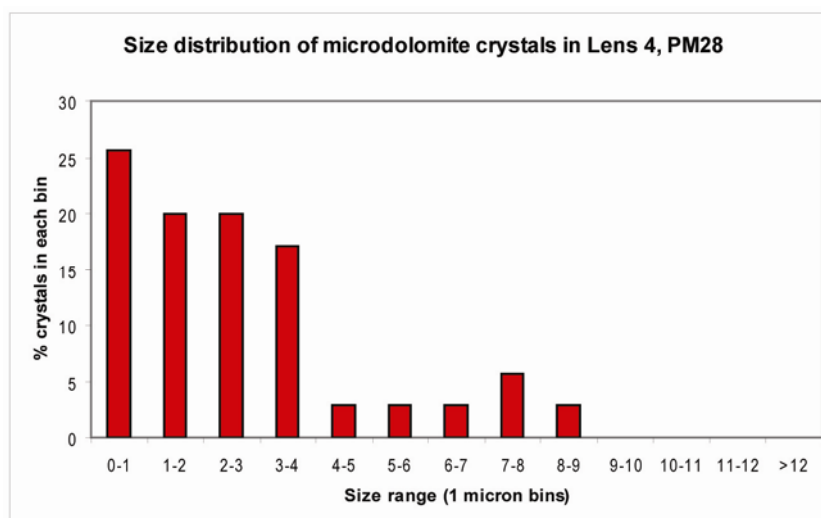


Figure C.2 - Size distribution of microdolomite crystals in PM28 Lens 3.

Table C.3 - Microdolomite crystal size distribution in PM28 Lens 4.

SAMPLE	POINT	CRYSTAL SIZE	AVERAGE	CRYSTAL SIZE- MEAN	<-- ^2	STANDARD DEVIATION	SIZE DISTRIBUTION		
							BIN	NO.	%
PM28 Lens 4	1	0.35	2.70	-2.35	5.50	2.13	0-1	9	26
	2	0.45		-2.25	5.06		1-2	7	20
	3	0.51		-2.19	4.80		2-3	7	20
	4	0.69		-2.01	4.05		3-4	6	17
	5	0.75		-1.95	3.81		4-5	1	3
	6	0.78		-1.92	3.68		5-6	1	3
	7	0.88		-1.82	3.31		6-7	1	3
	8	0.91		-1.79	3.19		7-8	2	6
	9	0.95		-1.75	3.05		8-9	1	3
	10	1.04		-1.66	2.77		9-10	0	0
	11	1.05		-1.65	2.71		10-11	0	0
	12	1.25		-1.45	2.09		11-12	0	0
	13	1.29		-1.41	1.98		>12	0	0
	14	1.29		-1.40	1.97				
	15	1.65		-1.05	1.10				
	16	1.76		-0.94	0.88		TOTAL	35	
	17	2.07		-0.62	0.39				
	18	2.08		-0.62	0.38				
	19	2.18		-0.52	0.27				
	20	2.48		-0.22	0.05				
	21	2.74		0.04	0.00				
	22	2.78		0.08	0.01				
	23	2.91		0.21	0.04				
	24	3.09		0.39	0.15				
	25	3.32		0.62	0.39				
	26	3.81		1.11	1.24				
	27	3.89		1.19	1.41				
	28	3.89		1.19	1.41				
	29	3.93		1.24	1.53				
	30	4.45		1.76	3.08				
	31	5.59		2.89	8.37				
	32	6.37		3.67	13.45				
	33	7.56		4.86	23.65				
	34	7.65		4.96	24.56				
	35	8.05		5.35	28.61				

**Figure C.3 - Size distribution of microdolomite crystals in PM28 Lens 4.**

C.3 Boeckops boeckii

Table C.4 - Microdolomite crystal size distribution in BB3aR Lens 1.

SAMPLE	POINT	CRYSTAL	AVERAGE	CRYSTAL	<--	STANDARD	SIZE DISTRIBUTION		
		SIZE		SIZE- MEAN	^2		DEVIATION	BIN	NO.
BB3aR Lens 1	1	0.48	5.52	-5.04	25.39	7.22	0-1	5	19
	2	0.53		-4.99	24.87		1-2	1	4
	3	0.71		-4.81	23.12		2-3	7	27
	4	0.73		-4.79	22.98		3-4	4	15
	5	0.87		-4.65	21.63		4-5	2	8
	6	1.41		-4.11	16.88		5-6	0	0
	7	2.25		-3.27	10.72		6-7	2	8
	8	2.32		-3.20	10.25		7-8	1	4
	9	2.58		-2.94	8.65		8-9	1	4
	10	2.74		-2.78	7.75		9-10	0	0
	11	2.78		-2.74	7.51		10-11	0	0
	12	2.78		-2.74	7.49		11-12	0	0
	13	2.97		-2.55	6.51		>12	3	12
	14	3.65		-1.87	3.49				
	15	3.67		-1.85	3.43		TOTAL 26		
	16	3.81		-1.71	2.92				
	17	3.83		-1.69	2.85				
	18	4.19		-1.33	1.76				
	19	4.75		-0.77	0.59				
	20	6.01		0.49	0.24				
	21	6.10		0.59	0.34				
	22	7.29		1.77	3.12				
	23	8.20		2.68	7.16				
	24	14.00		8.48	71.85				
	25	20.27		14.75	217.49				
	26	34.60		29.08	845.75				

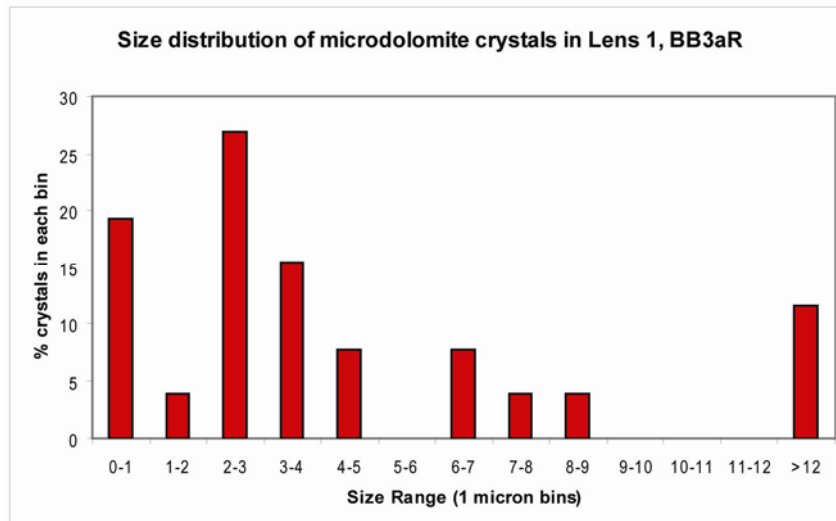
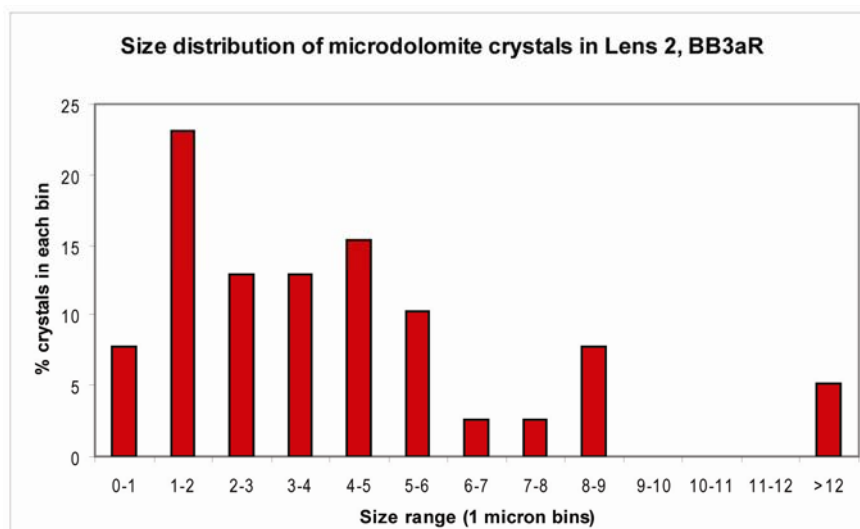


Figure C.4 - Size distribution of microdolomite crystals in BB3aR Lens 1.

Table C.5 - Microdolomite crystal size distribution in BB3aR Lens 2.

SAMPLE	POINT	CRYSTAL SIZE	AVERAGE	CRYSTAL SIZE- MEAN	<-- ^2	STANDARD DEVIATION	SIZE DISTRIBUTION		
							BIN	NO.	%
BB3aR Lens 2	1	0.55	4.04	-3.49	12.19	2.96	0-1	3	8
	2	0.78		-3.26	10.64		1-2	9	23
	3	0.82		-3.23	10.42		2-3	5	13
	4	1.04		-3.00	9.00		3-4	5	13
	5	1.05		-2.99	8.95		4-5	6	15
	6	1.18		-2.86	8.18		5-6	4	10
	7	1.41		-2.63	6.94		6-7	1	3
	8	1.51		-2.53	6.42		7-8	1	3
	9	1.66		-2.39	5.69		8-9	3	8
	10	1.67		-2.37	5.62		9-10	0	0
	11	1.79		-2.26	5.10		10-11	0	0
	12	1.83		-2.21	4.90		11-12	0	0
	13	2.08		-1.97	3.87		>12	2	5
	14	2.43		-1.61	2.61				
	15	2.85		-1.19	1.42		TOTAL 39		
	16	2.94		-1.11	1.23				
	17	2.96		-1.08	1.17				
	18	3.04		-1.01	1.01				
	19	3.19		-0.85	0.73				
	20	3.24		-0.80	0.65				
	21	3.59		-0.45	0.20				
	22	3.82		-0.23	0.05				
	23	4.07		0.02	0.00				
	24	4.10		0.06	0.00				
	25	4.24		0.19	0.04				
	26	4.35		0.31	0.10				
	27	4.46		0.41	0.17				
	28	4.56		0.52	0.27				
	29	5.24		1.20	1.43				
	30	5.47		1.42	2.02				
	31	5.49		1.45	2.10				
	32	5.66		1.61	2.61				
	33	6.93		2.88	8.32				
	34	7.31		3.27	10.68				
	35	8.11		4.07	16.57				
	36	8.27		4.23	17.86				
	37	8.36		4.32	18.62				
	38	12.80		8.76	76.74				
	39	12.86		8.82	77.71				

**Figure C.5 - Size distribution of microdolomite crystals in BB3aR Lens 2.**

C.4 Geesops schlotheimi

Table C.6 - Microdolomite crystal size distribution in G31R Lens 1.

SAMPLE	POINT	CRYSTAL SIZE	AVERAGE	CRYSTAL SIZE- MEAN	<-- ^2	STANDARD DEVIATION	SIZE DISTRIBUTION		
							BIN	NO.	%
G31R Lens 1	1	0.54		-2.42	5.85		0-1	7	16
	2	0.65		-2.30	5.30		1-2	11	26
	3	0.76		-2.20	4.84		2-3	9	21
	4	0.81		-2.15	4.62		3-4	10	23
	5	0.90		-2.05	4.21		4-5	1	2
	6	0.92		-2.03	4.14		5-6	1	2
	7	0.97		-1.99	3.94		6-7	1	2
	8	1.03		-1.93	3.73		7-8	0	0
	9	1.32		-1.63	2.67		8-9	0	0
	10	1.43		-1.53	2.33		9-10	1	2
	11	1.43		-1.53	2.33		10-11	1	2
	12	1.43		-1.52	2.32		11-12	1	2
	13	1.64		-1.32	1.73		>12	0	0
	14	1.67		-1.29	1.65				
	15	1.69		-1.27	1.60		TOTAL 43		
	16	1.82		-1.14	1.29				
	17	1.92		-1.03	1.07				
	18	1.96		-1.00	0.99				
	19	2.13		-0.83	0.69				
	20	2.22		-0.74	0.54				
	21	2.27		-0.69	0.47				
	22	2.32		-0.63	0.40				
	23	2.43		-0.53	0.28				
	24	2.48		-0.47	0.22				
	25	2.49		-0.47	0.22				
	26	2.51		-0.45	0.20				
	27	2.91		-0.05	0.00				
	28	3.04		0.08	0.01				
	29	3.08		0.12	0.01				
	30	3.14		0.18	0.03				
	31	3.18		0.22	0.05				
	32	3.22		0.27	0.07				
	33	3.27		0.32	0.10				
	34	3.66		0.71	0.50				
	35	3.84		0.89	0.79				
	36	3.90		0.95	0.90				
	37	3.91		0.96	0.91				
	38	4.88		1.92	3.70				
	39	5.40		2.44	5.95				
	40	6.26		3.30	10.91				
	41	9.56		6.61	43.65				
	42	10.19		7.24	52.39				
	43	11.92		2.96	8.97		80.37	2.45	

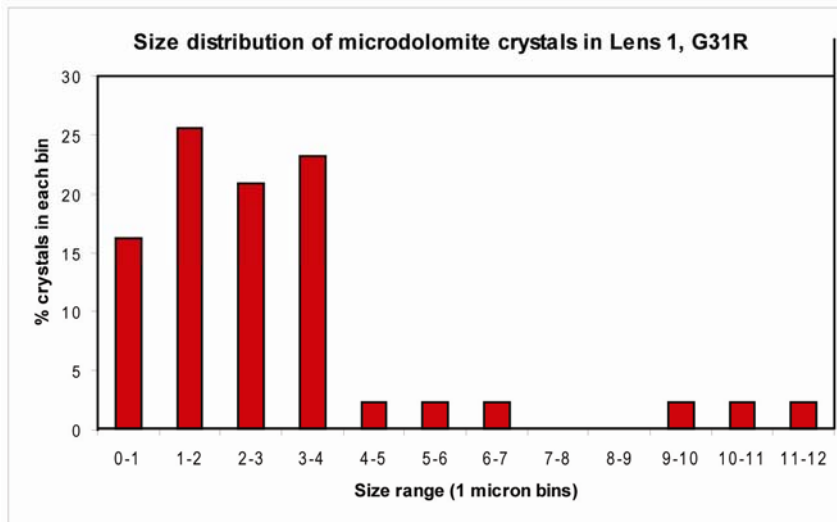


Figure C.6 - Size distribution of microdolomite crystals in G31R Lens 1.

Table C.7 - Microdolomite crystal size distribution in G41 Lens 1.

SAMPLE	POINT	CRYSTAL SIZE	AVERAGE	CRYSTAL SIZE- MEAN	<-- ^2	STANDARD DEVIATION	SIZE DISTRIBUTION		
							BIN	NO.	%
G41R Lens 1	1	0.68	2.27	-1.59	2.52	1.55	0-1	9	27
	2	0.77		-1.50	2.26		1-2	9	27
	3	0.80		-1.47	2.15		2-3	5	15
	4	0.82		-1.45	2.10		3-4	5	15
	5	0.88		-1.39	1.93		4-5	2	6
	6	0.90		-1.37	1.88		5-6	2	6
	7	0.93		-1.34	1.80		6-7	1	3
	8	0.97		-1.29	1.67		7-8	0	0
	9	0.98		-1.28	1.65		8-9	0	0
	10	1.06		-1.21	1.47		9-10	0	0
	11	1.08		-1.18	1.40		10-11	0	0
	12	1.12		-1.14	1.31		11-12	0	0
	13	1.27		-1.00	1.00		>12	0	0
	14	1.32		-0.95	0.90				
	15	1.55		-0.72	0.52		TOTAL	33	
	16	1.61		-0.66	0.43				
	17	1.66		-0.61	0.37				
	18	1.90		-0.37	0.13				
	19	2.03		-0.24	0.06				
	20	2.17		-0.10	0.01				
	21	2.58		0.31	0.10				
	22	2.69		0.42	0.18				
	23	2.71		0.44	0.19				
	24	3.03		0.76	0.58				
	25	3.09		0.82	0.68				
	26	3.28		1.01	1.03				
	27	3.30		1.03	1.07				
	28	3.31		1.04	1.09				
	29	4.06		1.80	3.23				
	30	4.77		2.50	6.24				
	31	5.06		2.79	7.81				
	32	5.93		3.66	13.40				
	33	6.53		4.26	18.16				

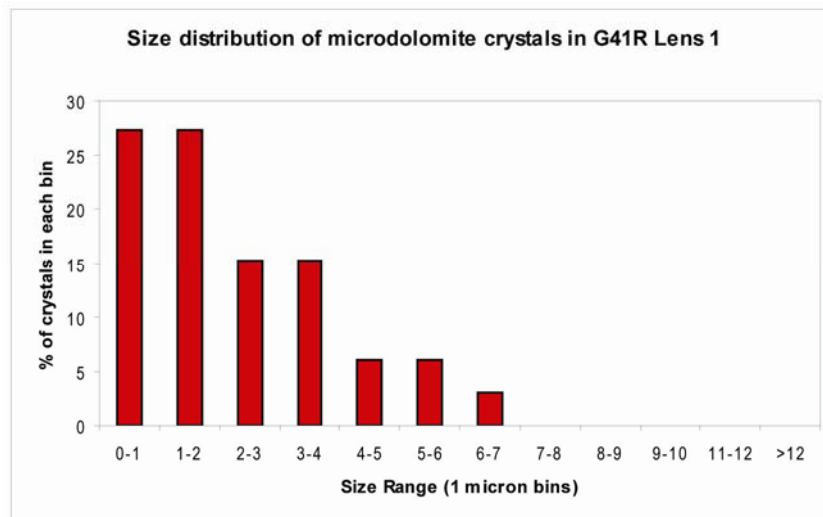


Figure C.7 - Size distribution of microdolomite crystals in G41R Lens 1.

C.5 *Odontochile hausmanni*

Table C.8 - Microdolomite crystal size distribution in OB24LB Lens 2.

SAMPLE	POINT	CRYSTAL SIZE	AVERAGE	CRYSTAL SIZE- MEAN	<-- ^2	STANDARD DEVIATION	SIZE DISTRIBUTION		
							BIN	NO.	%
OB24LB Lens 2	1	0.54	3.41	-2.87	8.24	2.57	0-1	3	18
	2	0.88		-2.53	6.40		1-2	4	24
	3	0.88		-2.52	6.38		2-3	3	18
	4	1.48		-1.93	3.72		3-4	1	6
	5	1.56		-1.85	3.41		4-5	3	18
	6	1.67		-1.74	3.03		5-6	0	0
	7	1.78		-1.63	2.65		6-7	0	0
	8	2.26		-1.15	1.32		7-8	2	12
	9	2.32		-1.09	1.18		8-9	0	0
	10	2.99		-0.42	0.17		9-10	1	6
	11	3.37		-0.03	0.00		10-11	0	0
	12	4.23		0.83	0.68		11-12	0	0
	13	4.54		1.13	1.29		>12	0	0
	14	4.98		1.58	2.48				
	15	7.12		3.71	13.78		TOTAL 17		
	16	7.63		4.23	17.87				
	17	9.69		6.28	39.45				

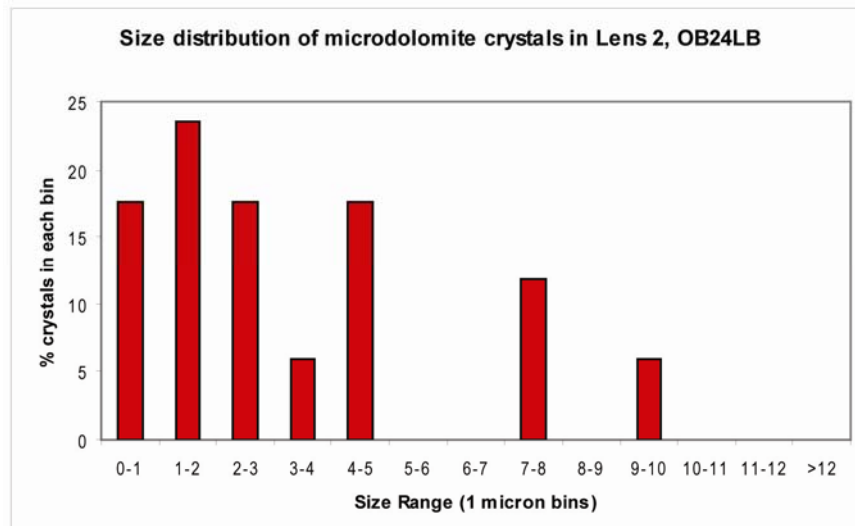


Figure C.8 - Size distribution of microdolomite crystals in OB24LB Lens 2.

Table C.9 - Microdolomite crystal size distribution in OB24LB Lens 3.

SAMPLE	POINT	CRYSTAL SIZE	AVERAGE	CRYSTAL SIZE- MEAN	<-- ^2	STANDARD DEVIATION	SIZE DISTRIBUTION		
							BIN	NO.	%
OB24LB Lens 3	1	0.69	2.35	-1.67	2.78	1.35	0-1	3	25
	2	0.78		-1.57	2.47		1-2	3	25
	3	0.98		-1.37	1.88		2-3	4	33
	4	1.68		-0.67	0.46		3-4	0	0
	5	1.78		-0.58	0.33		4-5	2	17
	6	1.93		-0.42	0.18		5-6	0	0
	7	2.22		-0.13	0.02		6-7	0	0
	8	2.64		0.29	0.08		7-8	0	0
	9	2.81		0.46	0.21		8-9	0	0
	10	2.93		0.57	0.33		9-10	0	0
	11	4.83		2.47	6.12		10-11	0	0
	12	4.98		2.62	6.87		11-12	0	0
							>12	0	0
							TOTAL		

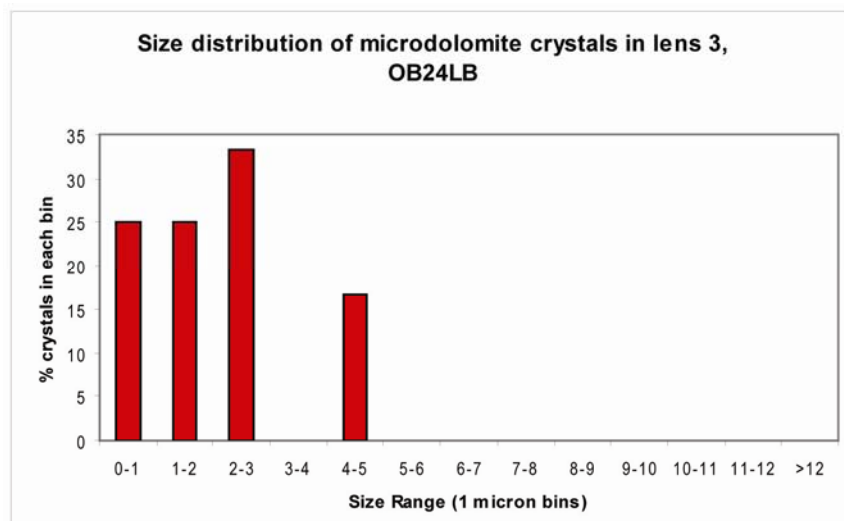


Figure C.9 - Size distribution of microdolomite crystals in OB24LB Lens 3.

C.6 *Phacops* sp.

Table C.10 - Microdolomite crystal size distribution in PM27 Lens 1.

SAMPLE	POINT	CRYSTAL SIZE	AVERAGE	CRYSTAL SIZE- MEAN	<-- ^2	STANDARD DEVIATION	SIZE DISTRIBUTION		
							BIN	NO.	%
PM27 Lens 1	1	0.48	1.16	-0.68	0.46	0.53	0-1	9	43
	2	0.52		-0.63	0.40		1-2	11	52
	3	0.57		-0.58	0.34		2-3	1	5
	4	0.62		-0.54	0.29		3-4	0	0
	5	0.63		-0.52	0.27		4-5	0	0
	6	0.69		-0.47	0.22		5-6	0	0
	7	0.76		-0.40	0.16		6-7	0	0
	8	0.84		-0.32	0.10		7-8	0	0
	9	0.96		-0.19	0.04		8-9	0	0
	10	1.07		-0.08	0.01		9-10	0	0
	11	1.11		-0.05	0.00		10-11	0	0
	12	1.19		0.04	0.00		11-12	0	0
	13	1.30		0.14	0.02		>12	0	0
	14	1.31		0.15	0.02				
	15	1.35		0.19	0.04		TOTAL 21		
	16	1.45		0.29	0.09				
	17	1.56		0.40	0.16				
	18	1.60		0.44	0.19				
	19	1.76		0.60	0.36				
	20	1.89		0.73	0.54				
	21	2.64		1.48	2.20				

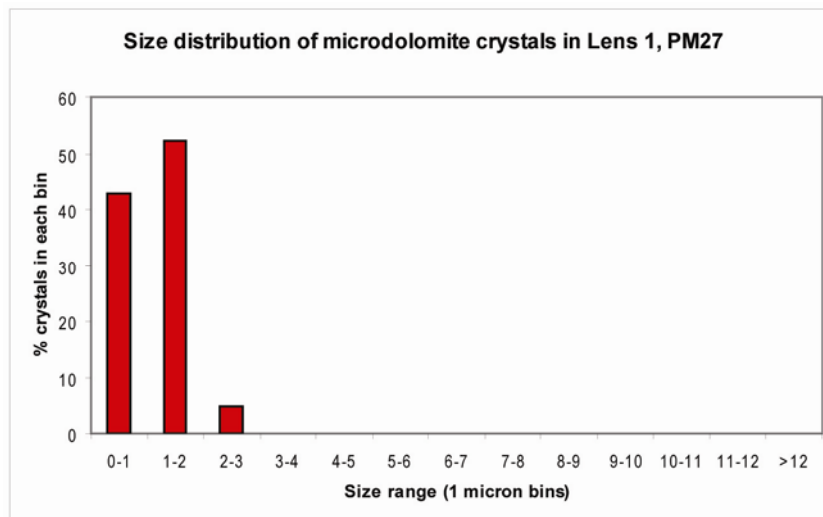


Figure C.10 - Size distribution of microdolomite crystals in PM27 Lens 1.

Table C.11 - Microdolomite crystal size distribution in PM27 Lens 3.

SAMPLE	POINT	CRYSTAL SIZE	AVERAGE	CRYSTAL SIZE- MEAN	<-- ^2	STANDARD DEVIATION	SIZE DISTRIBUTION		
							BIN	NO.	%
PM27 Lens 3	1	0.26	1.20	-0.93	0.87	0.97	0-1	40	63
	2	0.29		-0.91	0.82		1-2	14	22
	3	0.34		-0.85	0.73		2-3	6	9
	4	0.34		-0.85	0.73		3-4	2	3
	5	0.40		-0.80	0.64		4-5	1	2
	6	0.40		-0.79	0.63		5-6	1	2
	7	0.40		-0.79	0.63		6-7	0	0
	8	0.48		-0.72	0.51		7-8	0	0
	9	0.49		-0.71	0.51		8-9	0	0
	10	0.52		-0.68	0.46		9-10	0	0
	11	0.53		-0.67	0.45		10-11	0	0
	12	0.54		-0.65	0.43		11-12	0	0
	13	0.56		-0.64	0.41		>12	0	0
	14	0.56		-0.63	0.40				
	15	0.59		-0.61	0.37		TOTAL	64	
	16	0.60		-0.60	0.36				
	17	0.60		-0.59	0.35				
	18	0.61		-0.59	0.35				
	19	0.61		-0.59	0.34				
	20	0.62		-0.58	0.34				
	21	0.62		-0.58	0.34				
	22	0.63		-0.56	0.32				
	23	0.64		-0.56	0.32				
	24	0.68		-0.52	0.27				
	25	0.69		-0.51	0.26				
	26	0.69		-0.51	0.26				
	27	0.70		-0.49	0.24				
	28	0.71		-0.49	0.24				
	29	0.71		-0.48	0.23				
	30	0.72		-0.48	0.23				
	31	0.73		-0.47	0.22				
	32	0.75		-0.45	0.20				
	33	0.76		-0.44	0.19				
	34	0.79		-0.41	0.17				
	35	0.79		-0.40	0.16				
	36	0.82		-0.38	0.14				
	37	0.83		-0.37	0.14				
	38	0.92		-0.28	0.08				
	39	0.95		-0.24	0.06				
	40	0.97		-0.23	0.05				
	41	1.06		-0.13	0.02				
	42	1.08		-0.12	0.01				
	43	1.12		-0.08	0.01				
	44	1.15		-0.05	0.00				
	45	1.21		0.01	0.00				
	46	1.48		0.28	0.08				
	47	1.52		0.32	0.10				
	48	1.55		0.35	0.12				
	49	1.74		0.54	0.29				
	50	1.79		0.59	0.35				
	51	1.83		0.63	0.40				
	52	1.89		0.69	0.48				
	53	1.93		0.73	0.53				
	54	1.95		0.75	0.56				
	55	2.06		0.86	0.75				
	56	2.14		0.94	0.89				
	57	2.47		1.27	1.61				
	58	2.49		1.29	1.67				
	59	2.51		1.31	1.72				
	60	2.72		1.52	2.30				
	61	3.09		1.89	3.57				
	62	3.85		2.65	7.05				
	63	4.12		2.92	8.52				
	64	5.07		3.87	14.96				

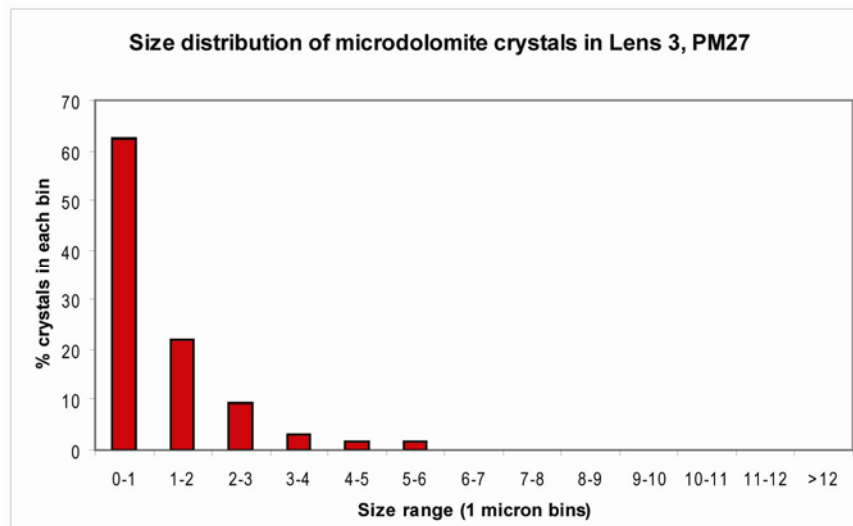


Figure C.11 - Size distribution of microdolomite crystals in PM27 Lens 3.

C.7 *Reedops cf. cephalotes*

Table C.12 - Microdolomite crystal size distribution in RB2B Lens 1.

		CRYSTAL		CRYSTAL	<--	STANDARD	SIZE DISTRIBUTION		
SAMPLE	POINT	SIZE	AVERAGE	SIZE- MEAN	^2	DEVIATION	BIN	NO.	%
RB2B Lens 1	1	0.44		-1.00	1.01		0-1	18	45
	2	0.47		-0.97	0.94		1-2	12	30
	3	0.51		-0.93	0.87		2-3	6	15
	4	0.53		-0.91	0.83		3-4	4	10
	5	0.59		-0.85	0.72		4-5	0	0
	6	0.65		-0.78	0.62		5-6	0	0
	7	0.66		-0.78	0.60		6-7	0	0
	8	0.66		-0.78	0.60		7-8	0	0
	9	0.72		-0.72	0.52		8-9	0	0
	10	0.72		-0.72	0.52		9-10	0	0
	11	0.73		-0.71	0.50		10-11	0	0
	12	0.74		-0.70	0.49		11-12	0	0
	13	0.79		-0.65	0.43		>12	0	0
	14	0.79		-0.64	0.41				
	15	0.86		-0.57	0.33		TOTAL 40		
	16	0.88		-0.56	0.31				
	17	0.89		-0.54	0.30				
	18	0.94		-0.50	0.25				
	19	1.16		-0.27	0.07				
	20	1.21		-0.23	0.05				
	21	1.22		-0.22	0.05				
	22	1.22		-0.22	0.05				
	23	1.24		-0.20	0.04				
	24	1.27		-0.16	0.03				
	25	1.29		-0.14	0.02				
	26	1.42		-0.02	0.00				
	27	1.84		0.40	0.16				
	28	1.85		0.41	0.17				
	29	1.88		0.44	0.19				
	30	1.92		0.48	0.23				
	31	2.11		0.67	0.45				
	32	2.20		0.77	0.59				
	33	2.40		0.96	0.93				
	34	2.51		1.07	1.14				
	35	2.58		1.14	1.30				
	36	2.69		1.25	1.57				
	37	3.15		1.71	2.93				
	38	3.19		1.75	3.06				
	39	3.20		1.76	3.09				
	40	3.41		1.97	3.88				
			1.44			0.87			

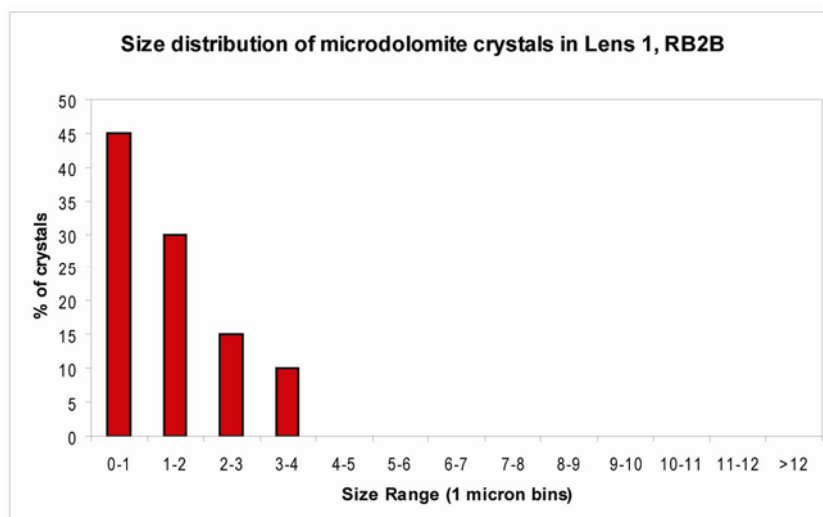


Figure C.12 - Size distribution of microdolomite crystals in RB2B Lens 1.

Table C.13 - Microdolomite crystal size distribution in RB2B Lens 4.

SAMPLE	POINT	CRYSTAL SIZE	AVERAGE	CRYSTAL SIZE- MEAN	<-- ^2	STANDARD DEVIATION	SIZE DISTRIBUTION		
							BIN	NO.	%
RB2B Lens 4	1	0.37	1.37	-1.00	0.99	0.76	0-1	5	38
	2	0.56		-0.81	0.65		1-2	5	38
	3	0.87		-0.50	0.25		2-3	3	23
	4	0.91		-0.46	0.21		3-4	0	0
	5	0.97		-0.40	0.16		4-5	0	0
	6	1.02		-0.35	0.12		5-6	0	0
	7	1.07		-0.30	0.09		6-7	0	0
	8	1.10		-0.27	0.07		7-8	0	0
	9	1.38		0.01	0.00		8-9	0	0
	10	1.67		0.30	0.09		9-10	0	0
	11	2.31		0.94	0.88		10-11	0	0
	12	2.63		1.26	1.58		11-12	0	0
	13	2.93		1.56	2.44		>12	0	0
							TOTAL	13	

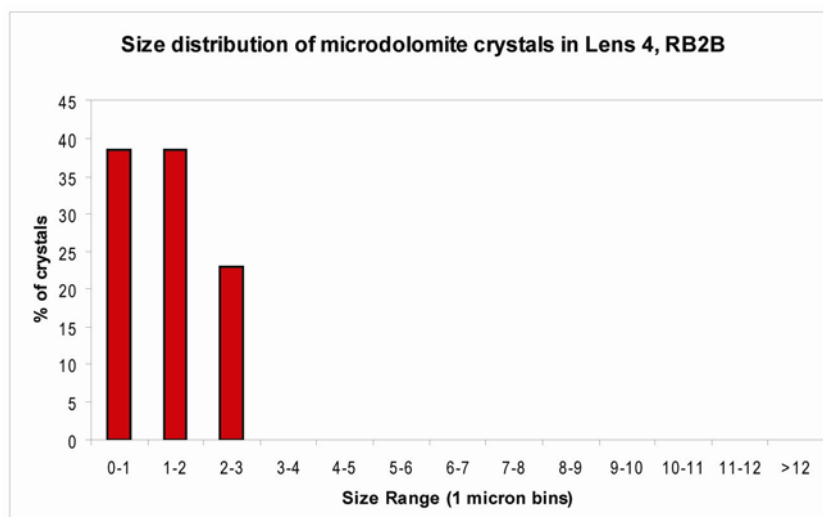


Figure C.13 - Size distribution of microdolomite crystals in RB2B Lens 4.

C.8 *Dalmanites* sp.

Table C.14 - Microdolomite crystal size distribution in TS1 Lens 1.

SAMPLE	POINT	CRYSTAL	AVERAGE	CRYSTAL	<--	STANDARD	SIZE DISTRIBUTION		
		SIZE		SIZE- MEAN	^2		DEVIATION	BIN	NO.
TS1 Lens 1	1	0.77	6.25	-5.48	30.04	6.10	0-1	1	3
	2	1.21		-5.04	25.40		1-2	5	17
	3	1.25		-5.01	25.08		2-3	4	13
	4	1.59		-4.66	21.75		3-4	7	23
	5	1.72		-4.53	20.54		4-5	2	7
	6	1.83		-4.43	19.60		5-6	2	7
	7	2.50		-3.75	14.09		6-7	0	0
	8	2.57		-3.68	13.58		7-8	1	3
	9	2.64		-3.61	13.05		8-9	0	0
	10	2.66		-3.60	12.93		9-10	2	7
	11	3.03		-3.22	10.39		10-11	0	0
	12	3.20		-3.05	9.29		11-12	1	3
	13	3.38		-2.87	8.24		>12	5	17
	14	3.51		-2.74	7.53				
	15	3.61		-2.64	6.98		TOTAL 30		
	16	3.78		-2.48	6.13				
	17	3.91		-2.34	5.50				
	18	4.03		-2.22	4.93				
	19	4.05		-2.20	4.84				
	20	5.42		-0.83	0.69				
	21	5.58		-0.67	0.45				
	22	7.80		1.55	2.39				
	23	9.16		2.91	8.48				
	24	9.51		3.25	10.59				
	25	11.98		5.73	32.84				
	26	13.04		6.78	46.03				
	27	14.12		7.86	61.86				
	28	14.46		8.21	67.33				
	29	15.99		9.74	94.84				
	30	29.29		23.04	530.67				

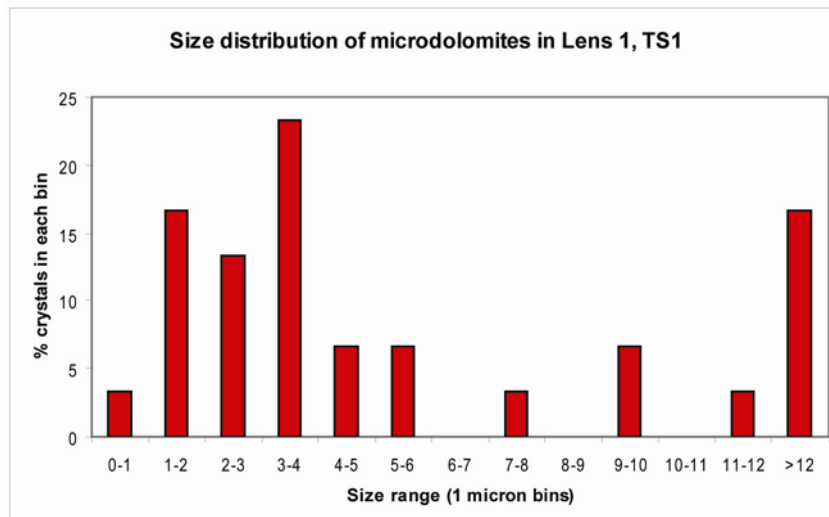


Figure C.14 - Size distribution of microdolomite crystals in TS1 Lens 1.

Table C.15 - Microdolomite crystal size distribution in TS1 Lens 2.

SAMPLE	POINT	CRYSTAL	AVERAGE	CRYSTAL	<--	STANDARD	SIZE DISTRIBUTION		
		SIZE		SIZE- MEAN	^2		DEVIATION	BIN	NO.
TS1 Lens 2	1	0.50	2.68	-2.18	4.76	2.79	0-1	3	15
	2	0.69		-2.00	3.99		1-2	7	35
	3	0.89		-1.80	3.23		2-3	4	20
	4	1.02		-1.67	2.78		3-4	3	15
	5	1.04		-1.65	2.72		4-5	2	10
	6	1.20		-1.49	2.21		5-6	0	0
	7	1.24		-1.44	2.08		6-7	0	0
	8	1.24		-1.44	2.07		7-8	0	0
	9	1.29		-1.39	1.93		8-9	0	0
	10	1.88		-0.81	0.65		9-10	0	0
	11	2.12		-0.56	0.32		10-11	0	0
	12	2.33		-0.35	0.12		11-12	0	0
	13	2.52		-0.16	0.03		>12	1	5
	14	2.86		0.17	0.03				
	15	3.01		0.33	0.11		TOTAL 20		
	16	3.35		0.66	0.44				
	17	3.91		1.22	1.50				
	18	4.45		1.76	3.11				
	19	4.50		1.81	3.29				
	20	13.65		10.97	120.26				

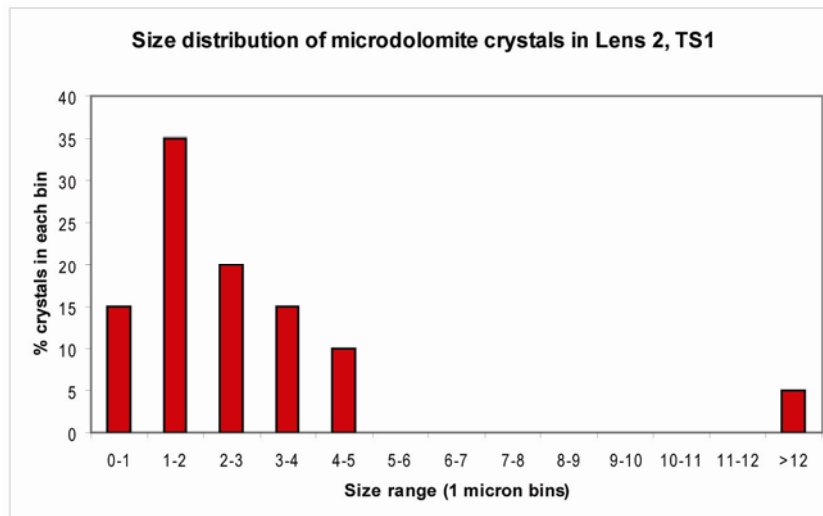
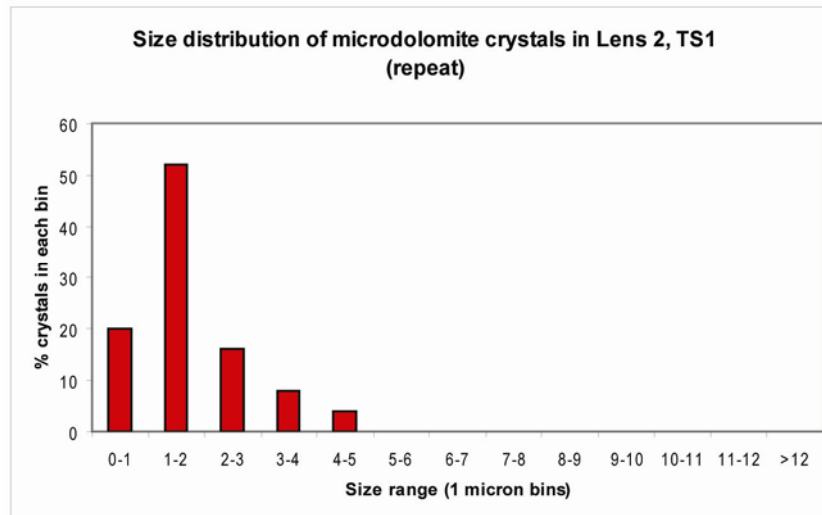
**Figure C.15 - Size distribution of microdolomite crystals in TS1 Lens 2.**

Table C.16 - Microdolomite crystal size distribution in TS1 Lens 2 repeat.

SAMPLE	POINT	CRYSTAL SIZE	AVERAGE	CRYSTAL SIZE- MEAN	<-- ^2	STANDARD DEVIATION	SIZE DISTRIBUTION		
							BIN	NO.	%
TS1 Lens2 repeat	1	0.64	1.90	-1.26	1.60	1.05	0-1	5	20
	2	0.69		-1.22	1.49		1-2	13	52
	3	0.74		-1.16	1.36		2-3	4	16
	4	0.78		-1.13	1.27		3-4	2	8
	5	0.98		-0.93	0.86		4-5	1	4
	6	1.02		-0.89	0.78		5-6	0	0
	7	1.03		-0.87	0.77		6-7	0	0
	8	1.12		-0.78	0.62		7-8	0	0
	9	1.15		-0.75	0.57		8-9	0	0
	10	1.51		-0.39	0.15		9-10	0	0
	11	1.52		-0.38	0.15		10-11	0	0
	12	1.79		-0.12	0.01		11-12	0	0
	13	1.80		-0.11	0.01		>12	0	0
	14	1.88		-0.03	0.00				
	15	1.90		-0.01	0.00		TOTAL	25	
	16	1.96		0.06	0.00				
	17	1.98		0.07	0.00				
	18	1.98		0.08	0.01				
	19	2.49		0.58	0.34				
	20	2.50		0.59	0.35				
	21	2.91		1.00	1.01				
	22	2.98		1.08	1.16				
	23	3.72		1.82	3.30				
	24	3.83		1.93	3.72				
	25	4.75		2.85	8.09				

**Figure C.16 - Size distribution of microdolomite crystals in TS1 Lens 2 (repeat).**

D

EDS Data

Quantitative EDS data was obtained using a Zeiss Sigma SEM. The spectrometers were calibrated for the elements of interest prior to analysis using the standards listed in section 2.4.

The following tables list all the raw data obtained. Values below the detection limits have been corrected in the main text but are left in the raw stated here.

[CD-ROM]

D.1 Holochroal Eye Results

Table D.1 – Weight % element EDS data for holochroal eyed trilobites.

SAMPLE	FEATURE	POINT	WEIGHT % ELEMENT				
			Ca	Mg	Sr	Fe	Mn
C1B	Lens 1	1	42.83	0.56	0.11	0.13	0.16
C1B	Lens 1	2	42.65	0.29	0.03	0.27	0.16
C1B	Lens 1	3	42.83	0.30	0.07	0.25	0.25
C1B	Lens 1	4	39.84	0.41	-0.03	0.21	0.24
C1B	Lens 1	5	42.17	0.48	0.04	0.10	0.26
C1B	Lens 2	1	43.07	0.30	0.04	0.24	0.29
C1B	Lens 2	2	42.68	0.38	0.21	0.08	0.21
C1B	Lens 2	3	42.87	0.35	0.10	0.23	0.17
C1B	Lens 2	4	42.13	0.37	0.11	0.26	0.26
C1B	Lens 2	5	42.48	0.26	0.02	0.14	0.17
C1B	Lens 4	1	42.63	0.35	0.05	0.17	0.18
C1B	Lens 4	2	42.30	0.42	0.14	0.13	0.23
C1B	Lens 4	3	41.25	0.29	0.14	0.22	0.34
C1B	Lens 4	4	40.35	0.35	0.05	0.32	0.19
C1B	Lens 4	5	40.52	0.26	0.06	1.25	0.17
SS93	Lens 1	1	36.02	0.28	0.04	0.03	1.86
SS93	Lens 1	2	35.82	0.34	0.05	0.07	1.68
SS93	Lens 1	3	35.53	0.26	0.07	0.03	1.83
SS93	Lens 1	4	36.01	0.25	0.02	0.12	1.59
SS93	Lens 1	5	36.14	0.19	0.00	0.06	1.96
SS93	Lens 2	1	36.23	0.23	-0.03	0.05	1.52
SS93	Lens 2	2	36.40	0.25	0.09	0.04	1.56
SS93	Lens 2	3	36.35	0.25	-0.04	0.13	1.62
SS93	Lens 2	4	36.30	0.17	0.08	0.03	1.64
SS93	Lens 2	5	35.87	0.15	0.04	0.08	2.03
SS93	Lens 3	1	36.05	0.19	-0.06	0.10	1.67
SS93	Lens 3	2	36.22	0.11	-0.11	0.14	1.54
SS93	Lens 3	3	36.36	0.17	-0.03	0.05	1.61
SS93	Lens 3	4	36.20	0.15	-0.04	0.15	1.50
SS93	Lens 3	5	35.93	0.23	0.12	0.14	1.75
PE79	Lens	1	30.65	1.68	0.04	0.24	0.11
PE79	Lens	2	31.06	1.56	0.14	0.34	0.01
PE79	Lens	3	31.58	0.70	0.07	0.68	0.10
PE79	Lens	4	31.17	0.92	0.06	0.60	0.08
PE79	Lens	5	30.84	1.41	0.19	0.21	0.07
PE79	Lens	6	30.73	1.54	0.21	0.30	0.11
PE79	Lens	7	31.21	0.97	0.09	0.55	0.09

SAMPLE	FEATURE	POINT	WEIGHT % ELEMENT				
			Ca	Mg	Sr	Fe	Mn
PE79	Lens	8	30.93	1.68	0.25	0.25	0.03
PE79	Lens	9	31.57	0.91	-0.01	0.54	0.03
PE79	Lens	10	31.28	0.78	0.08	0.62	0.01
PE79	Lens	11	30.70	1.68	0.20	0.17	0.08
PE79	Lens	12	30.92	1.90	0.25	0.09	0.03
PE79	Lens	13	31.16	1.47	0.18	0.27	0.02
PE79	Lens	14	31.57	0.78	-0.03	0.68	0.00
PE79	Lens	15	31.31	0.66	0.11	0.67	-0.04
PE79	Lens	16	31.44	0.57	0.04	0.56	0.22
PE79	Lens	17	31.44	0.51	0.05	0.70	0.17
PE79	Lens	18	31.46	0.48	0.01	0.67	0.11
PE79	Lens	19	31.85	0.41	0.01	0.84	0.12
PE79	Lens	20	31.30	0.45	0.04	0.96	0.07

Table D.2 – Weight % carbonate EDS data for holochroal eyed trilobites.

SAMPLE	FEATURE	POINT	WEIGHT % CARBONATE				
			Ca	Mg	Sr	Fe	Mn
C1B	Lens 1	1	106.95	1.94	0.19	0.27	0.33
C1B	Lens 1	2	106.50	1.01	0.05	0.56	0.33
C1B	Lens 1	3	106.95	1.04	0.12	0.52	0.52
C1B	Lens 1	4	99.48	1.42	-0.05	0.44	0.50
C1B	Lens 1	5	105.30	1.66	0.07	0.21	0.54
C1B	Lens 2	1	107.55	1.04	0.07	0.50	0.61
C1B	Lens 2	2	106.57	1.32	0.35	0.17	0.44
C1B	Lens 2	3	107.05	1.21	0.17	0.48	0.36
C1B	Lens 2	4	105.20	1.28	0.19	0.54	0.54
C1B	Lens 2	5	106.07	0.90	0.03	0.29	0.36
C1B	Lens 4	1	106.45	1.21	0.08	0.35	0.38
C1B	Lens 4	2	105.62	1.46	0.24	0.27	0.48
C1B	Lens 4	3	103.00	1.01	0.24	0.46	0.71
C1B	Lens 4	4	100.75	1.21	0.08	0.66	0.40
C1B	Lens 4	5	101.18	0.90	0.10	2.59	0.36
SS93	Lens 1	1	89.94	0.97	0.07	0.06	3.89
SS93	Lens 1	2	89.44	1.18	0.08	0.15	3.51
SS93	Lens 1	3	88.72	0.90	0.12	0.06	3.83
SS93	Lens 1	4	89.92	0.87	0.03	0.25	3.33
SS93	Lens 1	5	90.24	0.66	0.00	0.12	4.10
SS93	Lens 2	1	90.47	0.80	-0.05	0.10	3.18
SS93	Lens 2	2	90.89	0.87	0.15	0.08	3.26
SS93	Lens 2	3	90.77	0.87	-0.07	0.27	3.39

SAMPLE	FEATURE	POINT	WEIGHT % CARBONATE				
			Ca	Mg	Sr	Fe	Mn
SS93	Lens 2	4	90.64	0.59	0.13	0.06	3.43
SS93	Lens 2	5	89.57	0.52	0.07	0.17	4.25
SS93	Lens 3	1	90.02	0.66	-0.10	0.21	3.49
SS93	Lens 3	2	90.44	0.38	-0.19	0.29	3.22
SS93	Lens 3	3	90.79	0.59	-0.05	0.10	3.37
SS93	Lens 3	4	90.39	0.52	-0.07	0.31	3.14
SS93	Lens 3	5	89.72	0.80	0.20	0.29	3.66
PE79	Lens	1	76.53	5.83	0.07	0.50	0.23
PE79	Lens	2	77.56	5.41	0.24	0.71	0.02
PE79	Lens	3	78.86	2.43	0.12	1.41	0.21
PE79	Lens	4	77.83	3.19	0.10	1.24	0.17
PE79	Lens	5	77.01	4.89	0.32	0.44	0.15
PE79	Lens	6	76.73	5.34	0.35	0.62	0.23
PE79	Lens	7	77.93	3.36	0.15	1.14	0.19
PE79	Lens	8	77.23	5.83	0.42	0.52	0.06
PE79	Lens	9	78.83	3.16	-0.02	1.12	0.06
PE79	Lens	10	78.11	2.71	0.13	1.29	0.02
PE79	Lens	11	76.66	5.83	0.34	0.35	0.17
PE79	Lens	12	77.21	6.59	0.42	0.19	0.06
PE79	Lens	13	77.81	5.10	0.30	0.56	0.04
PE79	Lens	14	78.83	2.71	-0.05	1.41	0.00
PE79	Lens	15	78.18	2.29	0.19	1.39	-0.08
PE79	Lens	16	78.51	1.98	0.07	1.16	0.46
PE79	Lens	17	78.51	1.77	0.08	1.45	0.36
PE79	Lens	18	78.56	1.66	0.02	1.39	0.23
PE79	Lens	19	79.53	1.42	0.02	1.74	0.25
PE79	Lens	20	78.16	1.56	0.07	1.99	0.15

Table D.3 – Normalised Weight % carbonate EDS data for holochroal eyed trilobites.

SAMPLE	FEATURE	POINT	NORMALISED WEIGHT % CARBONATE				
			Ca	Mg	Sr	Fe	Mn
C1B	Lens 1	1	97.51	1.77	0.17	0.25	0.31
C1B	Lens 1	2	98.20	0.93	0.05	0.52	0.31
C1B	Lens 1	3	97.98	0.95	0.11	0.48	0.48
C1B	Lens 1	4	97.73	1.40	-0.05	0.43	0.49
C1B	Lens 1	5	97.70	1.54	0.06	0.19	0.50
C1B	Lens 2	1	97.98	0.95	0.06	0.45	0.55
C1B	Lens 2	2	97.91	1.21	0.33	0.15	0.40
C1B	Lens 2	3	97.97	1.11	0.15	0.44	0.33
C1B	Lens 2	4	97.63	1.19	0.17	0.50	0.50

SAMPLE	FEATURE	NORMALISED WEIGHT % CARBONATE					
		POINT	Ca	Mg	Sr	Fe	Mn
C1B	Lens 2	5	98.53	0.84	0.03	0.27	0.33
C1B	Lens 4	1	98.13	1.12	0.08	0.33	0.35
C1B	Lens 4	2	97.74	1.35	0.22	0.25	0.45
C1B	Lens 4	3	97.71	0.95	0.22	0.43	0.67
C1B	Lens 4	4	97.71	1.18	0.08	0.64	0.39
C1B	Lens 4	5	96.24	0.86	0.10	2.47	0.34
SS93	Lens 1	1	94.74	1.02	0.07	0.07	4.10
SS93	Lens 1	2	94.78	1.25	0.09	0.15	3.72
SS93	Lens 1	3	94.76	0.96	0.13	0.07	4.09
SS93	Lens 1	4	95.26	0.92	0.04	0.26	3.52
SS93	Lens 1	5	94.87	0.69	0.00	0.13	4.31
SS93	Lens 2	1	95.73	0.84	-0.05	0.11	3.37
SS93	Lens 2	2	95.42	0.91	0.16	0.09	3.43
SS93	Lens 2	3	95.32	0.91	-0.07	0.28	3.56
SS93	Lens 2	4	95.55	0.62	0.14	0.07	3.62
SS93	Lens 2	5	94.71	0.55	0.07	0.18	4.49
SS93	Lens 3	1	95.48	0.70	-0.11	0.22	3.71
SS93	Lens 3	2	96.06	0.41	-0.20	0.31	3.42
SS93	Lens 3	3	95.77	0.62	-0.05	0.11	3.55
SS93	Lens 3	4	95.86	0.55	-0.07	0.33	3.33
SS93	Lens 3	5	94.77	0.84	0.21	0.31	3.87
PE79	Lens	1	92.04	7.01	0.08	0.60	0.28
PE79	Lens	2	92.41	6.45	0.28	0.84	0.02
PE79	Lens	3	94.98	2.92	0.14	1.70	0.25
PE79	Lens	4	94.30	3.87	0.12	1.51	0.20
PE79	Lens	5	93.00	5.91	0.39	0.53	0.18
PE79	Lens	6	92.14	6.41	0.42	0.75	0.28
PE79	Lens	7	94.15	4.06	0.18	1.38	0.23
PE79	Lens	8	91.88	6.93	0.50	0.62	0.07
PE79	Lens	9	94.80	3.80	-0.02	1.35	0.08
PE79	Lens	10	94.96	3.29	0.16	1.56	0.03
PE79	Lens	11	91.98	6.99	0.40	0.42	0.20
PE79	Lens	12	91.40	7.80	0.50	0.22	0.07
PE79	Lens	13	92.84	6.08	0.36	0.67	0.05
PE79	Lens	14	95.10	3.26	-0.06	1.70	0.00
PE79	Lens	15	95.39	2.79	0.23	1.70	-0.10
PE79	Lens	16	95.54	2.41	0.08	1.41	0.56
PE79	Lens	17	95.54	2.15	0.10	1.77	0.43
PE79	Lens	18	95.97	2.03	0.02	1.70	0.28
PE79	Lens	19	95.86	1.71	0.02	2.10	0.30
PE79	Lens	20	95.40	1.91	0.08	2.43	0.18

Table D.4 – Mole % carbonate EDS data for holochroal eyed trilobites.

SAMPLE	FEATURE	MOLE % CARBONATE					
		POINT	Ca	Mg	Sr	Fe	Mn
C1B	Lens 1	1	97.31	2.10	0.11	0.21	0.27
C1B	Lens 1	2	98.15	1.10	0.03	0.45	0.27
C1B	Lens 1	3	97.97	1.13	0.07	0.41	0.42
C1B	Lens 1	4	97.58	1.66	-0.03	0.37	0.43
C1B	Lens 1	5	97.52	1.83	0.04	0.17	0.44
C1B	Lens 2	1	97.96	1.13	0.04	0.39	0.48
C1B	Lens 2	2	97.86	1.44	0.22	0.13	0.35
C1B	Lens 2	3	97.92	1.32	0.10	0.38	0.28
C1B	Lens 2	4	97.60	1.41	0.12	0.43	0.44
C1B	Lens 2	5	98.46	0.99	0.02	0.23	0.29
C1B	Lens 4	1	98.04	1.33	0.05	0.28	0.30
C1B	Lens 4	2	97.65	1.60	0.15	0.22	0.39
C1B	Lens 4	3	97.75	1.13	0.15	0.37	0.59
C1B	Lens 4	4	97.66	1.40	0.06	0.56	0.34
C1B	Lens 4	5	96.48	1.02	0.07	2.14	0.30
SS93	Lens 1	1	95.09	1.22	0.05	0.06	3.58
SS93	Lens 1	2	95.07	1.49	0.06	0.13	3.25
SS93	Lens 1	3	95.13	1.15	0.09	0.06	3.57
SS93	Lens 1	4	95.57	1.09	0.02	0.23	3.08
SS93	Lens 1	5	95.29	0.83	0.00	0.11	3.77
SS93	Lens 2	1	96.00	1.00	-0.04	0.10	2.94
SS93	Lens 2	2	95.74	1.08	0.11	0.08	2.99
SS93	Lens 2	3	95.61	1.08	-0.05	0.25	3.11
SS93	Lens 2	4	95.94	0.74	0.10	0.06	3.16
SS93	Lens 2	5	95.21	0.66	0.05	0.15	3.93
SS93	Lens 3	1	95.81	0.83	-0.07	0.19	3.24
SS93	Lens 3	2	96.39	0.48	-0.13	0.27	2.99
SS93	Lens 3	3	96.10	0.74	-0.04	0.09	3.10
SS93	Lens 3	4	96.20	0.66	-0.05	0.29	2.91
SS93	Lens 3	5	95.20	1.00	0.15	0.27	3.38
PE79	Lens	1	90.97	8.22	0.05	0.51	0.24
PE79	Lens	2	91.49	7.58	0.19	0.72	0.02
PE79	Lens	3	94.76	3.46	0.10	1.46	0.22
PE79	Lens	4	93.88	4.57	0.08	1.30	0.18
PE79	Lens	5	92.19	6.95	0.26	0.45	0.15
PE79	Lens	6	91.29	7.54	0.29	0.64	0.24
PE79	Lens	7	93.69	4.80	0.12	1.18	0.20
PE79	Lens	8	90.93	8.14	0.34	0.53	0.06
PE79	Lens	9	94.31	4.48	-0.01	1.16	0.07
PE79	Lens	10	94.63	3.89	0.11	1.35	0.02

SAMPLE	FEATURE	POINT	MOLE % CARBONATE				
			Ca	Mg	Sr	Fe	Mn
PE79	Lens	11	90.98	8.21	0.27	0.36	0.17
PE79	Lens	12	90.27	9.15	0.33	0.19	0.06
PE79	Lens	13	91.99	7.16	0.24	0.57	0.04
PE79	Lens	14	94.72	3.86	-0.04	1.46	0.00
PE79	Lens	15	95.17	3.31	0.15	1.46	-0.09
PE79	Lens	16	95.39	2.85	0.06	1.22	0.49
PE79	Lens	17	95.47	2.55	0.07	1.53	0.38
PE79	Lens	18	95.86	2.41	0.01	1.47	0.24
PE79	Lens	19	95.87	2.04	0.01	1.81	0.26
PE79	Lens	20	95.43	2.26	0.06	2.10	0.16

D.2 Schizochroal Eye Results

Table D.5 – Weight % element EDS data for schizochroal eyed trilobites.

SAMPLE	FEATURE	POINT	WEIGHT % ELEMENT				
			Ca	Mg	Sr	Fe	Mn
AM65	LENS	1	38.53	1.88	-0.28	0.11	0.03
AM65	LENS	2	39.61	1.84	-0.02	-0.06	0.06
AM65	LENS	3	38.62	2.24	0.18	0.11	-0.05
AM65	LENS	4	38.78	2.11	-0.06	0.04	0.07
AM65	LENS	5	39.19	1.78	0.14	0.17	0.09
AM65	LENS	6	38.88	1.86	0.02	0.23	0.09
AM65	LENS	7	39.56	1.60	-0.02	0.04	0.04
AM65	LENS	8	39.35	1.90	0.32	0.04	-0.01
AM65	LENS	9	38.57	2.95	0.09	0.13	-0.09
AM65	LENS	10	37.96	3.48	0.23	0.09	-0.14
AM65	LENS	11	38.12	2.54	0.14	0.06	-0.02
AM65	LENS	12	38.72	2.02	0.08	0.03	0.05
AM65	LENS	13	39.49	1.66	0.13	0.07	-0.01
AM65	LENS	14	38.77	2.02	0.22	-0.06	0.08
AM65	LENS	15	37.82	2.59	0.12	0.23	0.08
AM65	LENS	16	38.54	1.32	0.24	0.58	0.01
AM65	LENS	17	39.21	1.96	0.14	0.12	0.14
AM65	LENS	18	39.16	1.83	0.14	0.20	-0.08
AM65	LENS	19	38.88	1.95	0.09	0.19	0.13
AM65	LENS	20	39.14	2.11	0.01	0.01	-0.10
AM65	BOWL	1	38.86	0.44	-0.22	2.02	0.08
AM65	BOWL	2	39.03	0.43	-0.16	1.75	0.12
AM65	BOWL	3	39.95	0.37	-0.13	1.18	0.05
AM65	BOWL	4	38.98	0.33	-0.01	1.70	0.11

SAMPLE	FEATURE	WEIGHT % ELEMENT					
		POINT	Ca	Mg	Sr	Fe	Mn
AM65	BOWL	5	39.16	0.28	-0.07	1.90	-0.03
AM65	BOWL	6	39.05	0.32	0.05	1.60	0.03
AM65	BOWL	7	39.41	0.40	0.08	1.49	0.10
AM65	BOWL	8	39.24	0.37	0.08	1.51	0.15
AM65	BOWL	9	39.11	0.31	-0.29	1.62	0.02
AM65	BOWL	10	39.38	0.31	-0.08	1.77	0.06
E22B	LENS	1	40.31	0.35	-0.11	-0.01	0.04
E22B	LENS	2	40.58	0.37	-0.15	-0.05	0.13
E22B	LENS	3	40.73	0.39	-0.10	0.03	-0.05
E22B	LENS	4	40.12	0.54	-0.19	0.03	0.11
E22B	LENS	5	40.33	0.43	-0.10	-0.06	0.06
E22B	LENS	6	39.66	0.44	-0.05	-0.01	0.06
E22B	LENS	7	38.22	0.51	-0.20	0.04	0.02
E22B	LENS	8	38.44	0.57	-0.04	0.17	0.02
E22B	LENS	9	38.35	0.48	-0.20	0.10	0.01
E22B	LENS	10	38.12	0.51	-0.07	0.03	0.01
E22B	LENS	11	38.27	0.45	-0.16	0.11	0.06
E22B	LENS	12	38.25	0.55	-0.05	0.07	0.00
E22B	LENS	13	38.19	0.47	-0.34	-0.01	0.04
E22B	LENS	14	37.58	0.53	-0.28	0.04	0.02
E22B	LENS	15	38.23	0.40	-0.25	0.05	-0.01
E22B	LENS	16	38.31	0.45	-0.05	-0.05	0.06
E22B	LENS	17	37.91	0.62	-0.26	0.06	0.09
E22B	LENS	18	38.38	0.48	-0.08	0.02	0.05
E22B	LENS	19	36.67	0.48	-0.99	0.08	0.07
E22B	LENS	20	40.19	0.47	-0.48	0.06	0.00
E22B	LENS	21	40.21	0.55	-0.27	0.11	-0.04
E22B	LENS	22	40.39	0.59	-0.21	0.07	0.01
E22B	LENS	23	40.41	0.56	0.01	0.04	-0.06
E22B	LENS	24	40.51	0.48	-0.16	0.07	0.05
E22B	CORE	1	38.34	0.29	-0.07	0.13	0.00
E22B	CORE	2	38.76	0.33	-0.13	0.05	0.03
E22B	CORE	3	38.35	0.37	-0.10	0.01	0.07
E22B	BOWL	1	38.17	0.49	0.04	0.04	0.09
E22B	BOWL	2	38.32	0.44	-0.22	-0.04	-0.01
E22B	BOWL	3	38.49	0.43	-0.16	0.03	-0.02
E22B	BOWL	4	37.68	0.42	-0.07	0.03	-0.06
E22B	SCLERA	1	39.79	0.40	-0.13	-0.05	0.04
E22B	SCLERA	2	40.20	0.47	0.01	0.07	0.09
E22B	SCLERA	3	40.50	0.32	0.04	0.10	0.07
E22B	SCLERA	4	39.83	0.23	-0.15	0.08	0.06

SAMPLE	FEATURE	WEIGHT % ELEMENT					
		POINT	Ca	Mg	Sr	Fe	Mn
E22B	EXOSKELETON	1	38.12	0.36	0.08	0.01	-0.01
E22B	EXOSKELETON	2	37.96	0.38	-0.01	0.04	0.04
G33RT	LENS	1	38.30	0.55	0.21	-0.01	-0.01
G33RT	LENS	2	38.82	0.38	0.30	0.16	0.01
G33RT	LENS	3	38.07	0.48	-0.25	0.12	-0.01
G33RT	LENS	4	38.75	0.35	0.16	0.10	0.01
G33RT	LENS	5	38.12	0.27	0.15	-0.01	-0.05
G33RT	SCLERA	1	38.08	0.46	0.17	0.28	0.01
G33RT	SCLERA	2	38.03	0.50	0.20	0.13	-0.02
G33RT	EXOSKELETON	1	37.48	0.63	0.01	0.22	0.00
G33RT	EXOSKELETON	2	37.62	0.53	0.01	0.20	-0.06
PM28	LENS	1	40.04	2.13	0.29	0.20	-0.03
PM28	LENS	2	40.32	1.74	0.35	0.11	0.03
PM28	LENS	3	40.37	1.75	0.35	0.19	-0.06
PM28	LENS	4	40.09	1.47	0.23	0.26	-0.06
PM28	LENS	5	40.78	1.41	0.21	0.14	-0.09
PM28	LENS	6	39.31	1.47	0.37	0.07	0.01
PM28	LENS	7	40.90	1.09	0.43	-0.02	0.08
PM28	LENS	8	39.38	1.71	0.25	0.14	0.02
PM28	LENS	9	40.71	1.67	0.22	0.03	-0.09
PM28	LENS	10	40.73	1.35	0.26	0.17	-0.10
PM28	LENS	11	40.32	1.80	0.29	0.22	-0.03
PM28	LENS	12	39.77	1.08	0.22	0.18	0.07
PM28	LENS	13	40.39	1.90	0.23	-0.01	0.08
PM28	LENS	14	40.11	1.69	0.22	0.07	-0.05
PM28	LENS	15	39.19	1.98	0.20	0.42	0.03
TS1	LENS	1	38.23	0.56	-0.10	0.02	-0.02
TS1	LENS	2	38.64	0.49	-0.14	-0.04	0.03
TS1	LENS	3	36.28	2.23	-0.08	0.02	-0.04
TS1	LENS	4	38.25	0.53	-0.16	0.06	0.08
TS1	LENS	5	38.49	0.57	-0.10	-0.02	-0.03
TS1	LENS	6	38.07	0.49	-0.03	0.10	0.08
TS1	LENS	7	38.14	0.52	0.09	0.07	0.07
TS1	LENS	8	37.67	0.59	-0.11	0.01	0.05
TS1	LENS	9	38.27	0.60	-0.13	0.00	0.08
TS1	LENS	10	37.92	0.62	0.01	-0.02	0.00
TS1	LENS	11	37.87	0.48	0.02	-0.05	0.06
TS1	LENS	12	37.89	0.59	-0.12	0.00	0.01
TS1	LENS	13	38.09	0.49	0.02	-0.10	0.14
TS1	LENS	14	38.09	0.49	0.02	-0.10	0.14
TS1	SCLERA	1	38.21	0.45	-0.03	0.17	0.07

SAMPLE	FEATURE	WEIGHT % ELEMENT					
		POINT	Ca	Mg	Sr	Fe	Mn
TS1	SCLERA	2	38.59	0.51	-0.10	0.05	-0.13
TS1	SCLERA	3	38.27	0.54	-0.01	0.22	0.07
TS1	SCLERA	4	37.90	0.51	-0.13	0.21	0.05
TS1	SCLERA	5	37.81	0.54	-0.14	0.17	0.22
TS1	SCLERA	6	37.12	0.57	-0.03	0.28	-0.01
TS1	SCLERA	7	37.31	0.58	0.03	0.14	0.08
TS1	SCLERA	8	37.73	0.47	0.10	0.16	0.07
TS1	SCLERA	9	38.10	0.42	0.05	0.07	-0.05
TS1	SCLERA	10	37.40	0.54	-0.10	0.37	0.10

Table D.6 – Weight % carbonate EDS data for schizochroal eyed trilobites.

SAMPLE	FEATURE	POINT	WEIGHT % CARBONATE				
			CaCO ₃	MgCO ₃	SrCO ₃	FeCO ₃	MnCO ₃
AM65	LENS	1	96.21	6.52	-0.47	0.23	0.06
AM65	LENS	2	98.91	6.38	-0.03	-0.12	0.13
AM65	LENS	3	96.43	7.77	0.30	0.23	-0.10
AM65	LENS	4	96.83	7.32	-0.10	0.08	0.15
AM65	LENS	5	97.86	6.17	0.24	0.35	0.19
AM65	LENS	6	97.08	6.45	0.03	0.48	0.19
AM65	LENS	7	98.78	5.55	-0.03	0.08	0.08
AM65	LENS	8	98.26	6.59	0.54	0.08	-0.02
AM65	LENS	9	96.31	10.23	0.15	0.27	-0.19
AM65	LENS	10	94.79	12.07	0.39	0.19	-0.29
AM65	LENS	11	95.19	8.81	0.24	0.12	-0.04
AM65	LENS	12	96.68	7.01	0.13	0.06	0.10
AM65	LENS	13	98.61	5.76	0.22	0.15	-0.02
AM65	LENS	14	96.81	7.01	0.37	-0.12	0.17
AM65	LENS	15	94.44	8.98	0.20	0.48	0.17
AM65	LENS	16	96.23	4.58	0.40	1.20	0.02
AM65	LENS	17	97.91	6.80	0.24	0.25	0.29
AM65	LENS	18	97.78	6.35	0.24	0.41	-0.17
AM65	LENS	19	97.08	6.76	0.15	0.39	0.27
AM65	LENS	20	97.73	7.32	0.02	0.02	-0.21
AM65	BOWL	1	97.03	1.53	-0.37	4.19	0.17
AM65	BOWL	2	97.46	1.49	-0.27	3.63	0.25
AM65	BOWL	3	99.76	1.28	-0.22	2.45	0.10
AM65	BOWL	4	97.33	1.14	-0.02	3.53	0.23
AM65	BOWL	5	97.78	0.97	-0.12	3.94	-0.06
AM65	BOWL	6	97.51	1.11	0.08	3.32	0.06
AM65	BOWL	7	98.41	1.39	0.13	3.09	0.21

SAMPLE	FEATURE	POINT	WEIGHT % CARBONATE				
			CaCO ₃	MgCO ₃	SrCO ₃	FeCO ₃	MnCO ₃
AM65	BOWL	8	97.98	1.28	0.13	3.13	0.31
AM65	BOWL	9	97.66	1.08	-0.49	3.36	0.04
AM65	BOWL	10	98.33	1.08	-0.13	3.67	0.13
E22B	LENS	1	100.65	1.21	-0.19	-0.02	0.08
E22B	LENS	2	101.33	1.28	-0.25	-0.10	0.27
E22B	LENS	3	101.70	1.35	-0.17	0.06	-0.10
E22B	LENS	4	100.18	1.87	-0.32	0.06	0.23
E22B	LENS	5	100.70	1.49	-0.17	-0.12	0.13
E22B	LENS	6	99.03	1.53	-0.08	-0.02	0.13
E22B	LENS	7	95.44	1.77	-0.34	0.08	0.04
E22B	LENS	8	95.98	1.98	-0.07	0.35	0.04
E22B	LENS	9	95.76	1.66	-0.34	0.21	0.02
E22B	LENS	10	95.19	1.77	-0.12	0.06	0.02
E22B	LENS	11	95.56	1.56	-0.27	0.23	0.13
E22B	LENS	12	95.51	1.91	-0.08	0.15	0.00
E22B	LENS	13	95.36	1.63	-0.57	-0.02	0.08
E22B	LENS	14	93.84	1.84	-0.47	0.08	0.04
E22B	LENS	15	95.46	1.39	-0.42	0.10	-0.02
E22B	LENS	16	95.66	1.56	-0.08	-0.10	0.13
E22B	LENS	17	94.66	2.15	-0.44	0.12	0.19
E22B	LENS	18	95.84	1.66	-0.13	0.04	0.10
E22B	LENS	19	91.57	1.66	-1.67	0.17	0.15
E22B	LENS	20	100.35	1.63	-0.81	0.12	0.00
E22B	LENS	21	100.40	1.91	-0.45	0.23	-0.08
E22B	LENS	22	100.85	2.05	-0.35	0.15	0.02
E22B	LENS	23	100.90	1.94	0.02	0.08	-0.13
E22B	LENS	24	101.15	1.66	-0.27	0.15	0.10
E22B	CORE	1	95.74	1.01	-0.12	0.27	0.00
E22B	CORE	2	96.78	1.14	-0.22	0.10	0.06
E22B	CORE	3	95.76	1.28	-0.17	0.02	0.15
E22B	BOWL	1	95.31	1.70	0.07	0.08	0.19
E22B	BOWL	2	95.69	1.53	-0.37	-0.08	-0.02
E22B	BOWL	3	96.11	1.49	-0.27	0.06	-0.04
E22B	BOWL	4	94.09	1.46	-0.12	0.06	-0.13
E22B	SCLERA	1	99.36	1.39	-0.22	-0.10	0.08
E22B	SCLERA	2	100.38	1.63	0.02	0.15	0.19
E22B	SCLERA	3	101.13	1.11	0.07	0.21	0.15
E22B	SCLERA	4	99.46	0.80	-0.25	0.17	0.13
E22B	EXOSKELETON	1	95.19	1.25	0.13	0.02	-0.02
E22B	EXOSKELETON	2	94.79	1.32	-0.02	0.08	0.08
G33RT	LENS	1	95.64	1.91	0.35	-0.02	-0.02

SAMPLE	FEATURE	POINT	WEIGHT % CARBONATE				
			CaCO ₃	MgCO ₃	SrCO ₃	FeCO ₃	MnCO ₃
G33RT	LENS	2	96.93	1.32	0.51	0.33	0.02
G33RT	LENS	3	95.06	1.66	-0.42	0.25	-0.02
G33RT	LENS	4	96.76	1.21	0.27	0.21	0.02
G33RT	LENS	5	95.19	0.94	0.25	-0.02	-0.10
G33RT	SCLERA	1	95.09	1.60	0.29	0.58	0.02
G33RT	SCLERA	2	94.96	1.73	0.34	0.27	-0.04
G33RT	EXOSKELETON	1	93.59	2.19	0.02	0.46	0.00
G33RT	EXOSKELETON	2	93.94	1.84	0.02	0.41	-0.13
PM28	LENS	1	99.98	7.39	0.49	0.41	-0.06
PM28	LENS	2	100.68	6.04	0.59	0.23	0.06
PM28	LENS	3	100.80	6.07	0.59	0.39	-0.13
PM28	LENS	4	100.10	5.10	0.39	0.54	-0.13
PM28	LENS	5	101.83	4.89	0.35	0.29	-0.19
PM28	LENS	6	98.16	5.10	0.62	0.15	0.02
PM28	LENS	7	102.13	3.78	0.72	-0.04	0.17
PM28	LENS	8	98.33	5.93	0.42	0.29	0.04
PM28	LENS	9	101.65	5.79	0.37	0.06	-0.19
PM28	LENS	10	101.70	4.68	0.44	0.35	-0.21
PM28	LENS	11	100.68	6.24	0.49	0.46	-0.06
PM28	LENS	12	99.31	3.75	0.37	0.37	0.15
PM28	LENS	13	100.85	6.59	0.39	-0.02	0.17
PM28	LENS	14	100.15	5.86	0.37	0.15	-0.10
PM28	LENS	15	97.86	6.87	0.34	0.87	0.06
TS1	LENS	1	95.46	1.94	-0.17	0.04	-0.04
TS1	LENS	2	96.48	1.70	-0.24	-0.08	0.06
TS1	LENS	3	90.59	7.74	-0.13	0.04	-0.08
TS1	LENS	4	95.51	1.84	-0.27	0.12	0.17
TS1	LENS	5	96.11	1.98	-0.17	-0.04	-0.06
TS1	LENS	6	95.06	1.70	-0.05	0.21	0.17
TS1	LENS	7	95.24	1.80	0.15	0.15	0.15
TS1	LENS	8	94.06	2.05	-0.19	0.02	0.10
TS1	LENS	9	95.56	2.08	-0.22	0.00	0.17
TS1	LENS	10	94.69	2.15	0.02	-0.04	0.00
TS1	LENS	11	94.56	1.66	0.03	-0.10	0.13
TS1	LENS	12	94.61	2.05	-0.20	0.00	0.02
TS1	LENS	13	95.11	1.70	0.03	-0.21	0.29
TS1	LENS	14	95.11	1.70	0.03	-0.21	0.29
TS1	SCLERA	1	95.41	1.56	-0.05	0.35	0.15
TS1	SCLERA	2	96.36	1.77	-0.17	0.10	-0.27
TS1	SCLERA	3	95.56	1.87	-0.02	0.46	0.15
TS1	SCLERA	4	94.64	1.77	-0.22	0.44	0.10

SAMPLE	FEATURE	POINT	WEIGHT % CARBONATE				
			CaCO ₃	MgCO ₃	SrCO ₃	FeCO ₃	MnCO ₃
TS1	SCLERA	5	94.41	1.87	-0.24	0.35	0.46
TS1	SCLERA	6	92.69	1.98	-0.05	0.58	-0.02
TS1	SCLERA	7	93.16	2.01	0.05	0.29	0.17
TS1	SCLERA	8	94.21	1.63	0.17	0.33	0.15
TS1	SCLERA	9	95.14	1.46	0.08	0.15	-0.10
TS1	SCLERA	10	93.39	1.87	-0.17	0.77	0.21

Table D.7 – Normalised Weight % carbonate EDS data for schizochroal eyed trilobites.

SAMPLE	FEATURE	POINT	NORMALISED WEIGHT % CARBONATE				
			CaCO ₃	MgCO ₃	SrCO ₃	FeCO ₃	MnCO ₃
AM65	LENS	1	93.82	6.36	-0.46	0.22	0.06
AM65	LENS	2	93.97	6.06	-0.03	-0.12	0.12
AM65	LENS	3	92.17	7.43	0.29	0.22	-0.10
AM65	LENS	4	92.86	7.02	-0.10	0.08	0.14
AM65	LENS	5	93.37	5.89	0.23	0.34	0.18
AM65	LENS	6	93.14	6.19	0.03	0.46	0.18
AM65	LENS	7	94.56	5.31	-0.03	0.08	0.08
AM65	LENS	8	93.18	6.25	0.51	0.08	-0.02
AM65	LENS	9	90.20	9.58	0.14	0.25	-0.18
AM65	LENS	10	88.47	11.27	0.36	0.17	-0.27
AM65	LENS	11	91.25	8.45	0.23	0.12	-0.04
AM65	LENS	12	92.97	6.74	0.13	0.06	0.10
AM65	LENS	13	94.17	5.50	0.21	0.14	-0.02
AM65	LENS	14	92.88	6.72	0.36	-0.12	0.16
AM65	LENS	15	90.57	8.62	0.19	0.46	0.16
AM65	LENS	16	93.94	4.47	0.39	1.17	0.02
AM65	LENS	17	92.82	6.45	0.22	0.24	0.28
AM65	LENS	18	93.47	6.07	0.23	0.40	-0.16
AM65	LENS	19	92.76	6.46	0.14	0.38	0.26
AM65	LENS	20	93.19	6.98	0.02	0.02	-0.20
AM65	BOWL	1	94.62	1.49	-0.36	4.09	0.16
AM65	BOWL	2	95.02	1.45	-0.26	3.54	0.24
AM65	BOWL	3	96.50	1.24	-0.21	2.37	0.10
AM65	BOWL	4	95.22	1.12	-0.02	3.45	0.23
AM65	BOWL	5	95.38	0.95	-0.12	3.84	-0.06
AM65	BOWL	6	95.52	1.09	0.08	3.25	0.06
AM65	BOWL	7	95.33	1.34	0.13	2.99	0.20
AM65	BOWL	8	95.27	1.25	0.13	3.05	0.31

SAMPLE	FEATURE	POINT	NORMALISED WEIGHT % CARBONATE				
			CaCO ₃	MgCO ₃	SrCO ₃	FeCO ₃	MnCO ₃
AM65	BOWL	9	96.08	1.06	-0.48	3.31	0.04
AM65	BOWL	10	95.40	1.04	-0.13	3.56	0.12
E22B	LENS	1	98.93	1.19	-0.18	-0.02	0.08
E22B	LENS	2	98.83	1.25	-0.25	-0.10	0.27
E22B	LENS	3	98.89	1.32	-0.16	0.06	-0.10
E22B	LENS	4	98.19	1.84	-0.31	0.06	0.23
E22B	LENS	5	98.70	1.46	-0.17	-0.12	0.12
E22B	LENS	6	98.46	1.52	-0.08	-0.02	0.12
E22B	LENS	7	98.39	1.82	-0.35	0.09	0.04
E22B	LENS	8	97.66	2.01	-0.07	0.36	0.04
E22B	LENS	9	98.40	1.71	-0.35	0.21	0.02
E22B	LENS	10	98.21	1.83	-0.12	0.06	0.02
E22B	LENS	11	98.31	1.61	-0.28	0.23	0.13
E22B	LENS	12	97.98	1.96	-0.09	0.15	0.00
E22B	LENS	13	98.84	1.69	-0.59	-0.02	0.09
E22B	LENS	14	98.44	1.93	-0.49	0.09	0.04
E22B	LENS	15	98.91	1.44	-0.44	0.11	-0.02
E22B	LENS	16	98.46	1.61	-0.09	-0.11	0.13
E22B	LENS	17	97.91	2.22	-0.45	0.13	0.19
E22B	LENS	18	98.28	1.71	-0.14	0.04	0.11
E22B	LENS	19	99.66	1.81	-1.82	0.18	0.16
E22B	LENS	20	99.07	1.61	-0.80	0.12	0.00
E22B	LENS	21	98.43	1.87	-0.45	0.22	-0.08
E22B	LENS	22	98.19	1.99	-0.34	0.14	0.02
E22B	LENS	23	98.14	1.89	0.02	0.08	-0.12
E22B	LENS	24	98.40	1.62	-0.26	0.14	0.10
E22B	CORE	1	98.81	1.04	-0.12	0.28	0.00
E22B	CORE	2	98.88	1.17	-0.22	0.11	0.06
E22B	CORE	3	98.68	1.32	-0.17	0.02	0.15
E22B	BOWL	1	97.91	1.75	0.07	0.09	0.19
E22B	BOWL	2	98.91	1.58	-0.38	-0.09	-0.02
E22B	BOWL	3	98.72	1.53	-0.28	0.06	-0.04
E22B	BOWL	4	98.66	1.53	-0.12	0.07	-0.13
E22B	SCLERA	1	98.86	1.38	-0.22	-0.10	0.08
E22B	SCLERA	2	98.07	1.59	0.02	0.14	0.18
E22B	SCLERA	3	98.51	1.08	0.07	0.20	0.14
E22B	SCLERA	4	99.17	0.80	-0.25	0.17	0.13
E22B	EXOSKELETON	1	98.57	1.29	0.14	0.02	-0.02
E22B	EXOSKELETON	2	98.47	1.37	-0.02	0.09	0.09
G33RT	LENS	1	97.73	1.95	0.36	-0.02	-0.02
G33RT	LENS	2	97.80	1.33	0.51	0.33	0.02

SAMPLE	FEATURE	POINT	NORMALISED WEIGHT % CARBONATE				
			CaCO ₃	MgCO ₃	SrCO ₃	FeCO ₃	MnCO ₃
G33RT	LENS	3	98.48	1.72	-0.44	0.26	-0.02
G33RT	LENS	4	98.26	1.23	0.27	0.21	0.02
G33RT	LENS	5	98.89	0.97	0.26	-0.02	-0.11
G33RT	SCLERA	1	97.45	1.64	0.29	0.60	0.02
G33RT	SCLERA	2	97.64	1.78	0.35	0.28	-0.04
G33RT	EXOSKELETON	1	97.24	2.27	0.02	0.47	0.00
G33RT	EXOSKELETON	2	97.77	1.91	0.02	0.43	-0.13
PM28	LENS	1	92.40	6.83	0.45	0.38	-0.06
PM28	LENS	2	93.57	5.61	0.55	0.21	0.06
PM28	LENS	3	93.57	5.63	0.55	0.37	-0.12
PM28	LENS	4	94.43	4.81	0.37	0.51	-0.12
PM28	LENS	5	95.01	4.56	0.33	0.27	-0.18
PM28	LENS	6	94.34	4.90	0.60	0.14	0.02
PM28	LENS	7	95.66	3.54	0.68	-0.04	0.16
PM28	LENS	8	93.63	5.65	0.40	0.28	0.04
PM28	LENS	9	94.39	5.38	0.34	0.06	-0.17
PM28	LENS	10	95.08	4.38	0.41	0.33	-0.20
PM28	LENS	11	93.39	5.79	0.45	0.42	-0.06
PM28	LENS	12	95.54	3.60	0.36	0.36	0.14
PM28	LENS	13	93.40	6.10	0.36	-0.02	0.16
PM28	LENS	14	94.11	5.51	0.35	0.14	-0.10
PM28	LENS	15	92.32	6.48	0.32	0.82	0.06
TS1	LENS	1	98.18	2.00	-0.17	0.04	-0.04
TS1	LENS	2	98.53	1.74	-0.24	-0.08	0.06
TS1	LENS	3	92.30	7.88	-0.14	0.04	-0.09
TS1	LENS	4	98.09	1.89	-0.28	0.13	0.17
TS1	LENS	5	98.26	2.02	-0.17	-0.04	-0.06
TS1	LENS	6	97.92	1.75	-0.05	0.21	0.17
TS1	LENS	7	97.70	1.85	0.16	0.15	0.15
TS1	LENS	8	97.93	2.13	-0.19	0.02	0.11
TS1	LENS	9	97.92	2.13	-0.22	0.00	0.17
TS1	LENS	10	97.80	2.22	0.02	-0.04	0.00
TS1	LENS	11	98.21	1.73	0.03	-0.11	0.13
TS1	LENS	12	98.07	2.12	-0.21	0.00	0.02
TS1	LENS	13	98.12	1.75	0.03	-0.21	0.30
TS1	LENS	14	98.12	1.75	0.03	-0.21	0.30
TS1	SCLERA	1	97.94	1.60	-0.05	0.36	0.15
TS1	SCLERA	2	98.54	1.81	-0.17	0.11	-0.28
TS1	SCLERA	3	97.49	1.91	-0.02	0.47	0.15
TS1	SCLERA	4	97.84	1.83	-0.23	0.45	0.11
TS1	SCLERA	5	97.47	1.93	-0.24	0.36	0.48

SAMPLE	FEATURE	POINT	NORMALISED WEIGHT % CARBONATE				
			CaCO ₃	MgCO ₃	SrCO ₃	FeCO ₃	MnCO ₃
TS1	SCLERA	6	97.39	2.08	-0.05	0.61	-0.02
TS1	SCLERA	7	97.37	2.10	0.05	0.30	0.17
TS1	SCLERA	8	97.64	1.69	0.17	0.34	0.15
TS1	SCLERA	9	98.36	1.51	0.09	0.15	-0.11
TS1	SCLERA	10	97.21	1.95	-0.18	0.80	0.22

Table D.8 – Mole % carbonate EDS data for schizochroal eyed trilobites.

SAMPLE	FEATURE	POINT	MOLE % CARBONATE				
			CaCO ₃	MgCO ₃	SrCO ₃	FeCO ₃	MnCO ₃
AM65	LENS	1	92.61	7.45	-0.31	0.19	0.05
AM65	LENS	2	92.90	7.12	-0.02	-0.10	0.10
AM65	LENS	3	91.00	8.70	0.19	0.19	-0.09
AM65	LENS	4	91.65	8.22	-0.06	0.07	0.12
AM65	LENS	5	92.48	6.93	0.15	0.29	0.15
AM65	LENS	6	92.16	7.27	0.02	0.39	0.16
AM65	LENS	7	93.64	6.25	-0.02	0.07	0.07
AM65	LENS	8	92.26	7.35	0.34	0.07	-0.02
AM65	LENS	9	88.66	11.18	0.09	0.21	-0.15
AM65	LENS	10	86.73	13.11	0.24	0.15	-0.23
AM65	LENS	11	89.90	9.88	0.15	0.10	-0.03
AM65	LENS	12	91.87	7.90	0.09	0.05	0.09
AM65	LENS	13	93.29	6.47	0.14	0.12	-0.02
AM65	LENS	14	91.84	7.89	0.24	-0.10	0.14
AM65	LENS	15	89.26	10.08	0.13	0.39	0.14
AM65	LENS	16	93.43	5.28	0.27	1.01	0.02
AM65	LENS	17	91.84	7.57	0.15	0.20	0.24
AM65	LENS	18	92.52	7.13	0.15	0.34	-0.14
AM65	LENS	19	91.77	7.59	0.10	0.32	0.22
AM65	LENS	20	91.97	8.18	0.01	0.02	-0.17
AM65	BOWL	1	94.80	1.77	-0.25	3.54	0.14
AM65	BOWL	2	95.17	1.73	-0.18	3.06	0.21
AM65	BOWL	3	96.53	1.47	-0.14	2.05	0.09
AM65	BOWL	4	95.49	1.33	-0.01	2.99	0.20
AM65	BOWL	5	95.67	1.13	-0.08	3.33	-0.05
AM65	BOWL	6	95.78	1.29	0.06	2.82	0.05
AM65	BOWL	7	95.54	1.60	0.09	2.59	0.18
AM65	BOWL	8	95.52	1.49	0.09	2.64	0.27
AM65	BOWL	9	96.17	1.26	-0.33	2.86	0.04
AM65	BOWL	10	95.66	1.24	-0.09	3.09	0.11

SAMPLE	FEATURE	POINT	MOLE % CARBONATE				
			CaCO ₃	MgCO ₃	SrCO ₃	FeCO ₃	MnCO ₃
E22B	LENS	1	98.66	1.41	-0.12	-0.02	0.07
E22B	LENS	2	98.54	1.48	-0.17	-0.09	0.23
E22B	LENS	3	98.59	1.56	-0.11	0.05	-0.09
E22B	LENS	4	97.79	2.17	-0.21	0.05	0.20
E22B	LENS	5	98.38	1.73	-0.11	-0.11	0.11
E22B	LENS	6	98.17	1.80	-0.06	-0.02	0.11
E22B	LENS	7	97.97	2.16	-0.23	0.07	0.04
E22B	LENS	8	97.32	2.38	-0.05	0.31	0.04
E22B	LENS	9	98.01	2.02	-0.23	0.18	0.02
E22B	LENS	10	97.85	2.16	-0.08	0.06	0.02
E22B	LENS	11	97.97	1.90	-0.19	0.20	0.11
E22B	LENS	12	97.62	2.31	-0.06	0.13	0.00
E22B	LENS	13	98.35	2.00	-0.40	-0.02	0.08
E22B	LENS	14	97.94	2.28	-0.33	0.07	0.04
E22B	LENS	15	98.52	1.70	-0.29	0.09	-0.02
E22B	LENS	16	98.14	1.90	-0.06	-0.09	0.11
E22B	LENS	17	97.40	2.63	-0.31	0.11	0.17
E22B	LENS	18	97.94	2.02	-0.09	0.04	0.09
E22B	LENS	19	98.80	2.13	-1.22	0.15	0.14
E22B	LENS	20	98.53	1.90	-0.54	0.11	0.00
E22B	LENS	21	97.97	2.21	-0.30	0.19	-0.07
E22B	LENS	22	97.74	2.35	-0.23	0.12	0.02
E22B	LENS	23	97.79	2.23	0.01	0.07	-0.11
E22B	Lens	24	98.05	1.92	-0.18	0.12	0.09
E22B	CORE	1	98.61	1.23	-0.08	0.24	0.00
E22B	CORE	2	98.62	1.38	-0.15	0.09	0.06
E22B	CORE	3	98.40	1.57	-0.12	0.02	0.13
E22B	BOWL	1	97.64	2.07	0.05	0.07	0.17
E22B	BOWL	2	98.49	1.86	-0.26	-0.07	-0.02
E22B	BOWL	3	98.36	1.81	-0.19	0.06	-0.04
E22B	BOWL	4	98.33	1.81	-0.08	0.06	-0.11
E22B	SCLERA	1	98.53	1.63	-0.15	-0.09	0.07
E22B	SCLERA	2	97.82	1.89	0.01	0.12	0.16
E22B	SCLERA	3	98.38	1.28	0.04	0.17	0.12
E22B	SCLERA	4	98.98	0.94	-0.17	0.14	0.11
E22B	EXOSKELETON	1	98.37	1.53	0.09	0.02	-0.02
E22B	EXOSKELETON	2	98.24	1.62	-0.01	0.07	0.08
G33RT	LENS	1	97.48	2.31	0.24	-0.02	-0.02
G33RT	LENS	2	97.77	1.58	0.35	0.29	0.02
G33RT	LENS	3	98.05	2.04	-0.29	0.22	-0.02
G33RT	LENS	4	98.15	1.46	0.19	0.18	0.02

SAMPLE	FEATURE	POINT	MOLE % CARBONATE				
			CaCO ₃	MgCO ₃	SrCO ₃	FeCO ₃	MnCO ₃
G33RT	LENS	5	98.78	1.15	0.18	-0.02	-0.09
G33RT	SCLERA	1	97.33	1.94	0.20	0.51	0.02
G33RT	SCLERA	2	97.45	2.11	0.23	0.24	-0.04
G33RT	EXOSKELETON	1	96.89	2.69	0.01	0.41	0.00
G33RT	EXOSKELETON	2	97.47	2.26	0.01	0.37	-0.11
PM28	LENS	1	91.40	8.02	0.30	0.33	-0.05
PM28	LENS	2	92.80	6.60	0.37	0.18	0.05
PM28	LENS	3	92.79	6.63	0.37	0.31	-0.10
PM28	LENS	4	93.75	5.67	0.25	0.44	-0.10
PM28	LENS	5	94.32	5.38	0.22	0.23	-0.15
PM28	LENS	6	93.68	5.78	0.40	0.12	0.02
PM28	LENS	7	95.25	4.19	0.46	-0.03	0.14
PM28	LENS	8	92.81	6.65	0.27	0.24	0.03
PM28	LENS	9	93.54	6.33	0.23	0.05	-0.15
PM28	LENS	10	94.45	5.16	0.28	0.28	-0.17
PM28	LENS	11	92.57	6.81	0.30	0.36	-0.05
PM28	LENS	12	95.07	4.26	0.24	0.31	0.12
PM28	LENS	13	92.47	7.17	0.24	-0.02	0.13
PM28	LENS	14	93.25	6.48	0.23	0.12	-0.08
PM28	LENS	15	91.42	7.62	0.21	0.70	0.05
TS1	LENS	1	97.76	2.36	-0.12	0.04	-0.04
TS1	LENS	2	98.13	2.05	-0.16	-0.07	0.06
TS1	LENS	3	90.91	9.22	-0.09	0.04	-0.07
TS1	LENS	4	97.70	2.23	-0.19	0.11	0.15
TS1	LENS	5	97.82	2.39	-0.12	-0.04	-0.06
TS1	LENS	6	97.63	2.07	-0.04	0.18	0.15
TS1	LENS	7	97.45	2.19	0.11	0.13	0.13
TS1	LENS	8	97.50	2.52	-0.13	0.02	0.09
TS1	LENS	9	97.48	2.52	-0.15	0.00	0.15
TS1	LENS	10	97.40	2.63	0.01	-0.04	0.00
TS1	LENS	11	97.91	2.05	0.02	-0.09	0.11
TS1	LENS	12	97.62	2.51	-0.14	0.00	0.02
TS1	LENS	13	97.82	2.08	0.02	-0.18	0.26
TS1	LENS	14	97.82	2.08	0.02	-0.18	0.26
TS1	SCLERA	1	97.70	1.90	-0.04	0.31	0.13
TS1	SCLERA	2	98.13	2.14	-0.12	0.09	-0.24
TS1	SCLERA	3	97.22	2.26	-0.01	0.40	0.13
TS1	SCLERA	4	97.51	2.16	-0.15	0.39	0.09
TS1	SCLERA	5	97.15	2.29	-0.16	0.31	0.41
TS1	SCLERA	6	97.07	2.46	-0.04	0.53	-0.02
TS1	SCLERA	7	97.06	2.49	0.04	0.26	0.15

SAMPLE	FEATURE	POINT	MOLE % CARBONATE				
			CaCO ₃	MgCO ₃	SrCO ₃	FeCO ₃	MnCO ₃
TS1	SCLERA	8	97.45	2.00	0.12	0.30	0.13
TS1	SCLERA	9	98.12	1.78	0.06	0.13	-0.09
TS1	SCLERA	10	96.93	2.31	-0.12	0.69	0.19

D.3 Brittlestar DAP Results

Table D.9 - Weight % element EDS data for the Brittlestar DAP.

SAMPLE+ FEATURE	POINT	WEIGHT % ELEMENT				
		Ca	Mg	Sr	Fe	Mn
Lens	1	32.31	4.13	0.06	0.06	0.01
Lens	2	32.54	4.18	0.07	0.02	0.04
Lens	3	32.26	4.23	0.11	-0.03	0.06
Lens	4	32.45	4.28	0.06	0.09	0

Table D.10 - Weight % carbonate EDS data for the Brittlestar DAP.

SAMPLE+ FEATURE	POINT	WEIGHT % CARBONATE				
		CaCO ₃	MgCO ₃	SrCO ₃	FeCO ₃	MnCO ₃
Lens	1	80.68	14.33	0.10	0.12	0.02
Lens	2	81.25	14.50	0.12	0.04	0.08
Lens	3	80.55	14.67	0.19	-0.06	0.13
Lens	4	81.03	14.85	0.10	0.19	0.00

Table D.11 - Normalised weight % carbonate EDS data for the Brittlestar DAP.

SAMPLE+ FEATURE	POINT	NORMALISED WEIGHT % CARBONATE				
		CaCO ₃	MgCO ₃	SrCO ₃	FeCO ₃	MnCO ₃
Lens	1	84.70	15.04	0.11	0.13	0.02
Lens	2	84.64	15.10	0.12	0.04	0.09
Lens	3	84.37	15.37	0.19	-0.07	0.13
Lens	4	84.26	15.44	0.11	0.19	0.00

Table D.12 – Mole % carbonate EDS data for the Brittlestar DAP.

SAMPLE+ FEATURE	POINT	MOLE % CARBONATE				
		CaCO ₃	MgCO ₃	SrCO ₃	FeCO ₃	MnCO ₃
Lens	1	82.43	17.37	0.07	0.11	0.02
Lens	2	82.36	17.45	0.08	0.04	0.07
Lens	3	82.07	17.75	0.13	-0.05	0.11
Lens	4	81.94	17.82	0.07	0.16	0.00



EPMA Data

Based on the findings of EDS (section 5.1.5.1), a subset of samples of trilobites with schizochroal eyes were analysed by EPMA. Where a dash (-) has been entered, no data was collected for this particular element. 'Feature' refers to the location within the sample (i.e. lens, core, bowl, sclera etc). This was determined by the study of each thin section in reflected light after EPMA analysis; each point is identified by an area of damage (a burn mark) on the sample surface. Question marks following the feature name highlight uncertainty in it's exact location, e.g. where the point lies on or very close to the boundary between two features such as the lens base/cement boundary. Any uncertain points have been omitted from the summaries and averages in the results chapters to ensure an accurate determination of composition of each feature. Values below the detection limits have been put to zero for calculation of averages in the results chapters.

[CD-ROM]

E.1 Strathclyde EPMA Raw Data

Table E.1 - Weight % element EPMA data (Strathclyde) for trilobites with schizochroal eyes.

SAMPLE	FEATURE	DATA SET/ POINT	WEIGHT % ELEMENT					
			Ca	Mg	Sr	Fe	Mn	SUM
AM65 Lens 1 Traverse 1	Lens	1	24.90	0.24	0.01	1.02	0.07	26.25
AM65 Lens 1 Traverse 1	Lens	2	33.59	1.34	0.11	1.07	0.04	36.15
AM65 Lens 1 Traverse 1	Lens	3	27.27	3.76	0.14	0.79	0.06	32.02
AM65 Lens 1 Traverse 1	Lens	4	34.64	1.74	0.24	0.10	0.00	36.71
AM65 Lens 1 Traverse 1	Lens	5	35.02	1.41	0.22	0.04	0.00	36.69
AM65 Lens 1 Traverse 1	Lens	6	35.10	1.30	0.22	0.05	0.00	36.66
AM65 Lens 1 Traverse 1	Lens	7	34.85	1.76	0.20	0.02	0.05	36.89
AM65 Lens 1 Traverse 1	Lens	8	31.37	4.11	0.19	0.06	0.00	35.73
AM65 Lens 1 Traverse 1	Lens	9	35.61	1.40	0.22	0.09	0.02	37.34
AM65 Lens 1 Traverse 1	Lens	10	34.91	1.42	0.24	0.01	0.02	36.60
AM65 Lens 1 Traverse 1	Lens	11	35.32	1.36	0.21	0.02	0.01	36.91
AM65 Lens 1 Traverse 1	Lens	12	34.70	1.65	0.23	0.10	0.00	36.67
AM65 Lens 1 Traverse 1	Lens	13	34.38	1.60	0.23	0.05	0.05	36.31
AM65 Lens 1 Traverse 1	Lens	14	34.06	1.70	0.20	0.08	0.06	36.10
AM65 Lens 1 Traverse 1	Lens	15	32.00	2.22	0.19	0.18	0.08	34.67
AM65 Lens 1 Traverse 2	Lens	1	17.78	0.46	0.00	1.42	0.03	19.69
AM65 Lens 1 Traverse 2	Lens	2	31.55	0.35	0.03	1.40	0.15	33.48
AM65 Lens 1 Traverse 2	Lens	3	33.52	0.49	0.03	1.93	0.27	36.24
AM65 Lens 1 Traverse 2	Lens	4	34.99	2.10	0.26	0.12	0.02	37.49
AM65 Lens 1 Traverse 2	Lens	5	34.70	2.16	0.26	0.05	0.01	37.16
AM65 Lens 1 Traverse 2	Lens	6	34.63	2.26	0.31	0.03	0.03	37.25
AM65 Lens 1 Traverse 2	Lens	7	34.30	2.00	0.21	0.02	0.00	36.53
AM65 Lens 1 Traverse 2	Lens	8	35.25	1.62	0.20	0.08	0.03	37.17
AM65 Lens 1 Traverse 2	Lens	9	34.60	1.48	0.21	0.00	0.00	36.29
AM65 Lens 1 Traverse 2	Lens	10	30.36	3.56	0.15	0.22	0.02	34.30
AM65 Lens 1 Traverse 2	Lens	11	31.44	3.05	0.19	0.03	0.02	34.73
AM65 Lens 1 Traverse 2	Lens	12	34.20	1.61	0.26	0.01	0.06	36.14
AM65 Lens 1 Traverse 2	Lens	13	32.15	2.04	0.19	0.34	0.05	34.77
AM65 Lens 1 Traverse 2	Lens	14	34.79	1.25	0.22	0.19	0.05	36.49
AM65 Lens 1 Traverse 2	Lens	15	33.53	1.01	0.19	0.16	0.01	34.89
AM65 Lens 2 Traverse 1	Lens	1	34.22	1.66	0.20	0.11	0.09	36.28
AM65 Lens 2 Traverse 1	Lens	2	33.90	2.04	0.20	0.16	0.06	36.35
AM65 Lens 2 Traverse 1	Lens	3	34.68	1.81	0.23	0.04	0.05	36.80
AM65 Lens 2 Traverse 1	Lens	4	34.11	1.90	0.23	0.00	0.07	36.31
AM65 Lens 2 Traverse 1	Lens	5	33.73	2.06	0.24	0.05	0.02	36.09
AM65 Lens 2 Traverse 1	Lens	6	34.93	1.64	0.25	0.03	0.04	36.89
AM65 Lens 2 Traverse 1	Lens	7	34.15	2.20	0.25	0.00	0.05	36.65
AM65 Lens 2 Traverse 1	Lens	8	34.91	1.71	0.27	0.03	0.05	36.96
AM65 Lens 2 Traverse 1	Lens	9	33.95	1.95	0.24	0.00	0.00	36.14
AM65 Lens 2 Traverse 1	Lens	10	33.40	2.52	0.20	0.16	0.02	36.31
AM65 Lens 2 Traverse 1	Lens	11	35.79	1.47	0.25	0.02	0.05	37.58
AM65 Lens 2 Traverse 1	Lens	12	35.12	1.81	0.27	0.00	0.00	37.20
AM65 Lens 2 Traverse 1	Lens	13	33.22	2.27	0.23	0.00	0.03	35.75
AM65 Lens 2 Traverse 1	Lens	14	34.86	0.95	0.19	0.12	0.04	36.16
AM65 Lens 2 Traverse 1	Lens	15	34.16	1.67	0.24	0.13	0.03	36.22
AM65 Lens 2 Traverse 2	Lens	1	36.03	0.60	0.18	0.36	0.06	37.22
AM65 Lens 2 Traverse 2	Lens	2	35.23	1.43	0.27	0.23	0.06	37.22
AM65 Lens 2 Traverse 2	Lens	3	36.02	1.03	0.28	0.07	0.05	37.45
AM65 Lens 2 Traverse 2	Lens	4	33.47	2.08	0.26	0.04	0.01	35.86
AM65 Lens 2 Traverse 2	Lens	5	33.95	2.12	0.24	0.00	0.03	36.34
AM65 Lens 2 Traverse 2	Lens	6	33.62	1.91	0.26	0.01	0.00	35.79
AM65 Lens 2 Traverse 2	Lens	7	32.87	1.82	0.24	0.00	0.00	34.94
AM65 Lens 2 Traverse 2	Lens	8	34.66	1.37	0.19	0.07	0.00	36.28
AM65 Lens 2 Traverse 2	Lens	9	29.25	3.42	0.18	0.05	0.01	32.91
AM65 Lens 2 Traverse 2	Lens	10	30.68	3.61	0.26	0.04	0.00	34.59
AM65 Lens 2 Traverse 2	Lens	11	31.76	2.21	0.20	0.06	0.00	34.23
AM65 Lens 2 Traverse 2	Lens	12	28.50	3.99	0.23	0.16	0.06	32.94
AM65 Lens 2 Traverse 2	Lens	13	33.18	0.41	0.04	1.79	0.23	35.65

SAMPLE	FEATURE	DATA SET/ POINT	WEIGHT % ELEMENT					
			Ca	Mg	Sr	Fe	Mn	SUM
AM65 Lens 2 Traverse 2	Lens	14	26.63	0.32	0.00	1.46	0.05	28.46
AM65 Lens 2 Traverse 2	Lens	15	31.83	0.39	0.02	1.36	0.13	33.73
BB3aR Lens 2	Lens	1	40.08	0.15	-	0.00	0.06	40.29
BB3aR Lens 2	Lens	2	39.17	1.02	-	0.00	0.00	40.19
BB3aR Lens 2	Lens	3	40.17	0.33	-	0.00	0.00	40.50
BB3aR Lens 2	Lens	4	38.71	1.08	-	0.02	0.00	39.81
BB3aR Lens 2	Lens	5	39.84	0.41	-	0.00	0.03	40.28
BB3aR Lens 2	Lens	6	39.85	0.30	-	0.00	0.00	40.15
BB3aR Lens 2	Lens	7	40.13	0.20	-	0.03	0.02	40.38
BB3aR Lens 2	Lens	8	36.95	2.08	-	0.05	0.00	39.09
BB3aR Lens 2	Lens	9	39.50	0.57	-	0.01	0.00	40.07
BB3aR Lens 2	Lens	10	40.09	0.25	-	0.03	0.00	40.37
BB3aR Lens 2	Lens	11	38.27	1.20	-	0.00	0.02	39.49
BB3aR Lens 2	Lens	12	39.38	0.20	-	0.02	0.00	39.59
BB3aR Lens 2	Lens	13	39.87	0.23	-	0.02	0.00	40.12
BB3aR Lens 2	Lens	14	37.82	1.89	-	0.00	0.04	39.75
BB3aR Lens 2	Lens	15	39.26	0.71	-	0.01	0.01	39.98
BB3aR Lens 2	Lens	16	38.84	0.58	-	0.05	0.00	39.47
BB3aR Lens 2	Lens	17	38.81	1.05	-	0.00	0.00	39.87
BB3aR Lens 2	Lens	18	37.47	1.39	-	0.04	0.01	38.90
BB3aR Lens 2	Lens	19	39.74	0.11	-	0.00	0.00	39.85
BB3aR Lens 2	Lens	20	37.07	0.27	-	0.00	0.04	37.38
BB3aR Lens 2	Lens	21	39.85	0.28	-	0.03	0.00	40.17
BB3aR Lens 2	Lens	22	37.50	1.52	-	0.03	0.00	39.05
BB3aR Lens 2	Lens	23	39.64	0.40	-	0.01	0.00	40.05
BB3aR Lens 2	Lens	24	40.00	0.26	-	0.00	0.00	40.26
BB3aR Lens 2	Lens	25	39.90	0.28	-	0.03	0.00	40.21
BB3aR Lens 2	Lens	26	39.05	0.91	-	0.05	0.00	40.01
BB3aR Lens 2	Lens	27	39.64	0.34	-	0.00	0.00	39.98
BB3aR Lens 2	Lens	28	40.08	0.17	-	0.04	0.01	40.30
BB3aR Lens 2	Lens	29	40.00	0.15	-	0.03	0.02	40.19
BB3aR Lens 2	Lens	30	39.74	0.21	-	0.00	0.00	39.95
BB3aR Lens 2	Lens	31	39.88	0.27	-	0.00	0.00	40.15
BB3aR Lens 2	Lens	32	39.34	0.19	-	0.00	0.00	39.53
BB3aR Lens 2	Lens	33	39.32	0.36	-	0.02	0.00	39.70
BB3aR Lens 2	Lens	34	39.55	0.35	-	0.04	0.00	39.94
BB3aR Lens 2	Lens	35	39.06	0.13	-	0.01	0.00	39.20
BB3aR Lens 2	Lens	36	34.53	0.11	-	0.01	0.00	34.65
BB3aR Lens 2	Lens	37	39.47	0.15	-	0.08	0.00	39.70
BB3aR Lens 2	Lens	38	39.16	0.16	-	0.05	0.03	39.40
BB3aR Lens 2	Lens	39	36.59	1.06	-	0.08	0.05	37.78
BB3aR Lens 2	Lens	40	39.53	0.15	-	0.01	0.01	39.70
BB3aR Lens 2	Lens	41	39.61	0.17	-	0.00	0.00	39.79
BB3aR Lens 2	Lens	42	39.25	0.27	-	0.01	0.02	39.54
BB3aR Lens 2	Lens	43	27.00	9.49	-	0.00	0.00	36.49
BB3aR Lens 2	Lens	44	39.57	0.12	-	0.00	0.01	39.69
BB3aR Lens 2	Lens	45	39.50	0.17	-	0.09	0.04	39.80
BB3aR Lens 2	Lens	46	39.72	0.13	-	0.04	0.01	39.90
BB3aR Lens 2	Lens	47	38.83	0.32	-	0.00	0.00	39.15
BB3aR Lens 2	Lens	48	40.24	0.19	-	0.00	0.00	40.43
BB3aR Lens 2	Lens	49	39.54	0.31	-	0.03	0.00	39.88
BB3aR Lens 2	Lens	50	38.76	0.75	-	0.00	0.00	39.51
BB3aR Lens 2	Lens	51	39.45	0.19	-	0.00	0.00	39.64
BB3aR Lens 2	Lens	52	38.05	1.26	-	0.01	0.00	39.32
BB3aR Lens 2	Lens	53	37.23	1.64	-	0.01	0.00	38.88
BB3aR Lens 2	Lens	54	38.98	0.70	-	0.01	0.00	39.69
BB3aR Lens 2	Lens	55	39.46	0.18	-	0.00	0.04	39.67
BB3aR Lens 2	Lens	56	39.68	0.15	-	0.00	0.00	39.83
BB3aR Lens 2	Lens	57	38.58	0.13	-	0.01	0.00	38.72
BB3aR Lens 2	Lens	58	38.58	0.22	-	0.07	0.02	38.89
BB3aR Lens 2	Lens	59	38.08	0.99	-	0.00	0.02	39.09
BB3aR Lens 2	Lens	60	39.47	0.25	-	0.03	0.04	39.78
BB3aR Lens 2	Lens	61	39.69	0.26	-	0.00	0.00	39.95
BB3aR Lens 2	Lens	62	39.38	0.21	-	0.01	0.00	39.60
BB3aR Lens 2	Lens	63	35.46	2.73	-	0.06	0.02	38.27
BB3aR Lens 2	Lens	64	38.49	0.40	-	0.05	0.00	38.93
BB3aR Lens 2	Lens	65	39.72	0.13	-	0.06	0.05	39.95
BB3aR Lens 3	Lens	1	38.83	0.21	-	0.02	0.00	39.07
BB3aR Lens 3	Lens	2	39.52	0.17	-	0.00	0.04	39.74

SAMPLE	FEATURE	DATA SET/ POINT	WEIGHT % ELEMENT					
			Ca	Mg	Sr	Fe	Mn	SUM
BB3aR Lens 3	Lens	3	38.27	0.97	-	0.05	0.04	39.32
BB3aR Lens 3	Lens	4	38.17	1.11	-	0.05	0.02	39.34
BB3aR Lens 3	Lens	5	39.15	0.21	-	0.01	0.00	39.37
BB3aR Lens 3	Lens	6	35.55	1.65	-	0.00	0.00	37.20
BB3aR Lens 3	Lens	7	38.56	0.73	-	0.01	0.02	39.32
BB3aR Lens 3	Lens	8	37.89	0.23	-	0.00	0.01	38.13
BB3aR Lens 3	Lens	9	38.01	0.91	-	0.00	0.00	38.92
BB3aR Lens 3	Lens	10	36.52	0.66	-	0.00	0.01	37.19
BB3aR Lens 3	Lens	11	38.34	0.99	-	0.00	0.00	39.32
BB3aR Lens 3	Lens	12	39.54	0.06	-	0.01	0.00	39.60
BB3aR Lens 3	Lens	13	38.78	0.16	-	0.01	0.00	38.95
BB3aR Lens 3	Lens	14	39.54	0.13	-	0.00	0.02	39.70
BB3aR Lens 3	Lens	15	39.70	0.16	-	0.02	0.01	39.89
BB3aR Lens 3	Lens	16	39.42	0.38	-	0.03	0.02	39.85
BB3aR Lens 3	Lens	17	39.78	0.08	-	0.03	0.02	39.91
BB3aR Lens 3	Lens	18	39.97	0.13	-	0.04	0.00	40.13
BB3aR Lens 3	Lens	19	38.92	0.15	-	0.01	0.03	39.10
BB3aR Lens 3	Lens	20	38.57	0.29	-	0.02	0.01	38.89
BB3aR Lens 3	Lens	21	39.16	0.39	-	0.02	0.02	39.59
BB3aR Lens 3	Lens	22	38.87	0.76	-	0.03	0.02	39.68
BB3aR Lens 3	Lens	23	37.42	1.92	-	0.03	0.02	39.39
BB3aR Lens 3	Lens	24	33.92	0.23	-	0.00	0.00	34.16
BB3aR Lens 3	Lens	25	39.74	0.22	-	0.00	0.02	39.98
BB3aR Lens 3	Lens	26	37.56	0.24	-	0.03	0.00	37.82
BB3aR Lens 3	Lens	27	36.36	0.18	-	0.00	0.02	36.56
BB3aR Lens 3	Lens	28	37.10	1.17	-	0.02	0.01	38.30
BB3aR Lens 3	Lens	29	39.11	0.54	-	0.00	0.04	39.69
BB3aR Lens 3	Lens	30	38.82	0.15	-	0.00	0.02	39.00
BB3aR Lens 3	Lens	31	39.29	0.15	-	0.00	0.00	39.44
BB3aR Lens 3	Lens	32	39.13	0.41	-	0.06	0.00	39.60
BB3aR Lens 3	Lens	33	28.48	5.39	-	0.10	0.01	33.98
BB3aR Lens 3	Lens	34	38.47	0.51	-	0.03	0.00	39.01
BB3aR Lens 3	Lens	35	37.66	1.23	-	0.01	0.00	38.90
BB3aR Lens 3	Lens	36	38.29	0.68	-	0.02	0.00	39.00
BB3aR Lens 3	Lens	37	39.41	0.28	-	0.00	0.02	39.71
BB3aR Lens 3	Lens	38	38.45	0.16	-	0.84	0.04	39.48
BB3aR Lens 3	Lens	39	39.09	0.12	-	0.09	0.03	39.33
BB3aR Lens 3	Lens	40	38.25	0.13	-	0.01	0.05	38.44
BB3aR Lens 3	Lens	41	37.56	1.81	-	0.00	0.02	39.38
BB3aR Lens 3	Lens	42	39.84	0.15	-	0.03	0.01	40.04
BB3aR Lens 3	Lens	43	39.56	0.10	-	0.00	0.01	39.66
BB3aR Lens 3	Lens	44	39.38	0.18	-	0.04	0.02	39.62
BB3aR Lens 3	Lens	45	38.75	0.15	-	0.00	0.01	38.91
BB3aR Lens 3	Lens	46	39.33	0.14	-	0.05	0.00	39.51
BB3aR Lens 3	Lens	47	39.62	0.16	-	0.00	0.00	39.77
BB3aR Lens 3	Lens	48	37.23	0.14	-	0.02	0.00	37.39
BB3aR Lens 3	Lens	49	38.90	0.27	-	0.01	0.03	39.20
BB3aR Lens 3	Lens	50	39.07	0.36	-	0.01	0.00	39.44
BB3aR Lens 3	Lens	51	39.27	0.15	-	0.00	0.00	39.43
BB3aR Lens 3	Lens	52	37.58	1.85	-	0.06	0.00	39.49
BB3aR Lens 3	Lens	53	39.51	0.36	-	0.00	0.04	39.90
BB3aR Lens 3	Lens	54	39.16	1.15	-	0.06	0.00	40.36
BB3aR Lens 3	Lens	55	39.32	0.22	-	0.00	0.03	39.56
BB3aR Lens 3	Lens	56	30.48	0.14	-	0.01	0.01	30.65
BB3aR Lens 3	Lens	57	38.92	0.15	-	0.00	0.03	39.09
BB3aR Lens 3	Lens	58	34.08	0.03	-	0.05	0.01	34.17
BB3aR Lens 3	Lens	59	39.90	0.14	-	0.04	0.00	40.08
BB3aR Lens 3	Lens	60	39.85	0.17	-	0.00	0.00	40.02
BB3aR Lens 3	Lens	61	40.03	0.14	-	0.01	0.00	40.19
BB3aR Lens 3	Lens	62	39.89	0.13	-	0.00	0.02	40.04
BB3aR Lens 3	Lens	63	37.60	0.14	-	0.00	0.02	37.75
BB3aR Lens 3	Lens	64	39.87	0.17	-	0.00	0.02	40.06
BB3aR Lens 3	Lens	65	39.83	0.18	-	0.00	0.00	40.02
BB3aR Lens 3	Lens	66	39.85	0.14	-	0.00	0.01	40.00
BB3aR Lens 3	Lens	67	40.02	0.18	-	0.01	0.00	40.21
BB3aR Lens 3	Lens	68	37.47	2.09	-	0.02	0.00	39.58
BB3aR Lens 3	Lens	69	39.38	0.65	-	0.00	0.03	40.05
BB3aR Lens 3	Lens	70	39.80	0.15	-	0.00	0.00	39.94
BB3aR	Sclera	1	40.04	0.17	-	0.05	0.06	40.32
BB3aR	Sclera	2	39.31	0.18	-	0.00	0.01	39.50

SAMPLE	FEATURE	DATA SET/ POINT	WEIGHT % ELEMENT					
			Ca	Mg	Sr	Fe	Mn	SUM
BB3aR	Sclera	3	39.27	0.16	-	0.05	0.07	39.55
BB3aR	Sclera	4	39.47	0.15	-	0.07	0.03	39.71
BB3aR	Sclera	5	39.11	0.11	-	0.11	0.03	39.37
BB3aR	Sclera	6	17.63	0.05	-	0.03	0.00	17.71
BB3aR	Sclera	7	36.03	0.13	-	0.03	0.05	36.25
BB3aR	Sclera	8	34.82	0.11	-	0.03	0.01	34.97
BB3aR	Sclera	9	29.20	0.08	-	0.20	0.06	29.54
BB3aR	Sclera	10	38.05	0.12	-	0.09	0.05	38.30
BB3aR	Sclera	11	40.21	0.14	-	0.02	0.04	40.40
BB3aR	Sclera	12	39.95	0.17	-	0.04	0.01	40.17
BB3aR	Sclera	13	39.76	0.16	-	0.08	0.00	40.00
BB3aR	Sclera	14	40.02	0.16	-	0.01	0.00	40.19
BB3aR	Sclera	15	39.96	0.14	-	0.04	0.04	40.18
BB3aR	Sclera	16	39.95	0.12	-	0.14	0.04	40.25
BB3aR	Sclera	17	39.37	0.11	-	0.09	0.04	39.60
BB3aR	Cement	1	39.84	0.24	-	0.04	0.03	40.15
BB3aR	Cement	2	39.61	0.23	-	0.00	0.02	39.85
BB3aR	Cement	3	39.53	0.43	-	0.05	0.02	40.02
BB3aR	Cement	4	40.08	0.21	-	0.06	0.01	40.35
BB3aR	Cement	5	39.73	0.43	-	0.01	0.00	40.16
BB3aR	Cement	6	39.91	0.35	-	0.03	0.00	40.29
BB3aR	Cement	7	39.95	0.24	-	0.00	0.01	40.20
BB3aR	Cement	8	40.14	0.16	-	0.00	0.01	40.31
BB3aR	Cement	9	39.76	0.30	-	0.02	0.04	40.11
BB3aR	Cement	10	37.56	0.09	-	0.02	0.01	37.68
BB3aR	Cement	11	39.77	0.16	-	0.03	0.02	39.98
BB3aR	Cement	12	39.65	0.17	-	0.03	0.00	39.85
BB3aR	Cement	13	39.63	0.26	-	0.02	0.00	39.90
BB3aR	Cement	14	39.79	0.18	-	0.00	0.00	39.96
BB3aR	Cement	15	39.85	0.20	-	0.00	0.01	40.06
BB3aR	Cement	16	39.89	0.14	-	0.00	0.02	40.06
BB3aR	Cement	17	40.04	0.14	-	0.00	0.04	40.22
BB3aR	Cement	18	39.46	0.25	-	0.00	0.00	39.71
BB3aR	Cement	19	39.99	0.14	-	0.00	0.02	40.16
BB3aR	Cement	20	40.02	0.13	-	0.00	0.02	40.16
BB3aR	Cement	21	39.87	0.17	-	0.00	0.00	40.04
BB3aR	Cement	22	39.81	0.15	-	0.00	0.01	39.97
BB3aR	Cement	23	40.06	0.16	-	0.07	0.01	40.30
BB3aR	Cement	24	39.61	0.41	-	0.01	0.03	40.06
BB3aR	Cement	25	39.79	0.15	-	0.02	0.00	39.95
BB3aR	Cement	26	39.22	0.71	-	0.03	0.02	39.97
BB3aR	Cement	27	39.60	0.22	-	0.04	0.04	39.89
BB3aR	Cement	28	39.76	0.17	-	0.04	0.04	40.00
BB3aR	Cement	29	39.66	0.12	-	0.00	0.07	39.86
BB3aR	Cement	30	39.01	0.18	-	0.05	0.04	39.29
BB3aR	Cement	31	39.78	0.30	-	0.00	0.00	40.08
BB3aR	Cement	32	39.16	0.21	-	0.02	0.02	39.41
BB3aR	Cement	33	31.93	0.19	-	0.00	0.02	32.14
BB3aR	Cement	34	39.45	0.16	-	0.00	0.01	39.62
BB3aR	Cement	35	39.62	0.21	-	0.03	0.00	39.86
BB3aR	Cement	36	39.66	0.16	-	0.00	0.02	39.83
BB3aR	Cement	37	38.47	1.11	-	0.06	0.02	39.66
BB3aR	Cement	38	39.90	0.10	-	0.10	0.04	40.14
BB3aR	Cement	39	38.94	0.13	-	0.01	0.02	39.09
BB3aR	Cement	40	40.04	0.20	-	0.00	0.00	40.24
BB3aR	Cement	41	40.25	0.15	-	0.04	0.01	40.45
BB3aR	Cement	42	40.12	0.25	-	0.00	0.01	40.38
BB3aR	Cement	43	40.24	0.17	-	0.02	0.01	40.43
BB3aR	Cement	44	39.97	0.21	-	0.03	0.02	40.22
BB3aR	Cement	45	39.63	0.19	-	0.02	0.02	39.86
BB3aR	Cement	46	39.92	0.19	-	0.04	0.04	40.19
BB3aR	Cement	47	39.53	0.18	-	0.00	0.05	39.76
BB3aR	Cement	48	39.97	0.24	-	0.01	0.00	40.22
BB3aR	Cement	49	40.35	0.17	-	0.00	0.02	40.54
BB3aR	Cement	50	40.15	0.15	-	0.03	0.04	40.37
BB3aR	Cement	51	39.78	0.19	-	0.01	0.02	40.00
BB3aR	Cement	52	39.96	0.15	-	0.05	0.04	40.21
BB3aR	Cement	53	41.15	0.20	-	0.05	0.05	41.45
E22B Lens 1	Lens	1	18.72	0.51	-	-	-	19.23

SAMPLE	FEATURE	DATA SET/ POINT	WEIGHT % ELEMENT					
			Ca	Mg	Sr	Fe	Mn	SUM
E22B Lens 1	Lens	2	17.79	0.69	-	-	-	18.48
E22B Lens 1	Lens	3	37.81	0.40	-	-	-	38.21
E22B Lens 1	Lens	4	37.74	0.41	-	-	-	38.15
E22B Lens 1	Lens	5	36.65	0.32	-	-	-	36.97
E22B Lens 1	Lens	6	35.74	0.25	-	-	-	35.99
E22B Lens 1	Lens	7	37.29	0.35	-	-	-	37.64
E22B Lens 1	Lens	8	37.72	0.44	-	-	-	38.16
E22B Lens 1	Lens	9	37.53	0.38	-	-	-	37.91
E22B Lens 1	Lens	10	37.63	0.45	-	-	-	38.08
E22B Lens 1	Lens	11	38.00	0.37	-	-	-	38.37
E22B Lens 1	Lens	12	37.96	0.32	-	-	-	38.28
E22B Lens 1	Lens	13	38.11	0.25	-	-	-	38.36
E22B Lens 1	Lens	14	37.67	0.42	-	-	-	38.09
E22B Lens 1	Lens	15	37.62	0.43	-	-	-	38.05
E22B Lens 1	Lens	16	37.79	0.43	-	-	-	38.22
E22B Lens 1	Lens	17	32.48	0.27	-	-	-	32.75
E22B Lens 1	Lens	18	26.50	0.51	-	-	-	27.01
E22B Lens 1	Lens	19	37.40	0.27	-	-	-	37.67
E22B Lens 1	Lens	20	34.12	0.36	-	-	-	34.48
E22B Lens 1	Lens	21	17.50	0.73	-	-	-	18.23
E22B Lens 1	Lens	22	26.73	0.55	-	-	-	27.28
E22B Lens 1	Lens	23	36.73	0.31	-	-	-	37.04
E22B Lens 1	Lens	24	37.46	0.44	-	-	-	37.90
E22B Lens 1	Lens	25	37.35	0.45	-	-	-	37.80
E22B Lens 1	Lens	26	37.34	0.62	-	-	-	37.96
E22B Lens 1	Lens	27	37.52	0.51	-	-	-	38.03
E22B Lens 1	Lens	28	37.60	0.38	-	-	-	37.98
E22B Lens 1	Lens	29	37.81	0.41	-	-	-	38.22
E22B Lens 1	Lens	30	37.80	0.47	-	-	-	38.27
E22B Lens 1	Lens	31	37.08	0.54	-	-	-	37.62
E22B Lens 1	Lens	32	37.69	0.32	-	-	-	38.01
E22B Lens 1	Lens	33	37.59	0.36	-	-	-	37.95
E22B Lens 1	Lens	34	37.74	0.46	-	-	-	38.20
E22B Lens 1	Lens	35	37.66	0.44	-	-	-	38.10
E22B Lens 1	Lens	36	37.39	0.33	-	-	-	37.72
E22B Lens 1	Lens	37	35.39	0.20	-	-	-	35.59
E22B Lens 1	Lens	38	34.38	0.24	-	-	-	34.62
E22B Lens 1	Lens	39	35.80	0.34	-	-	-	36.14
E22B Lens 1	Lens	40	32.26	0.31	-	-	-	32.57
E22B Lens 1	Lens	41	37.90	0.28	-	-	-	38.18
E22B Lens 1	Lens	42	37.70	0.26	-	-	-	37.96
E22B Lens 1	Lens	43	37.76	0.22	-	-	-	37.98
E22B Lens 1	Lens	44	37.75	0.42	-	-	-	38.17
E22B Lens 1	Lens	45	37.20	0.70	-	-	-	37.90
E22B Lens 1	Lens	46	37.73	0.36	-	-	-	38.09
E22B Lens 1	Lens	47	37.82	0.34	-	-	-	38.16
E22B Lens 1	Lens	48	37.95	0.35	-	-	-	38.30
E22B Lens 1	Lens	49	37.99	0.26	-	-	-	38.25
E22B Lens 1	Lens	50	38.06	0.22	-	-	-	38.28
E22B Lens 1	Lens	51	38.06	0.22	-	-	-	38.28
E22B Lens 1	Lens	52	37.87	0.40	-	-	-	38.27
E22B Lens 1	Lens	53	37.59	0.38	-	-	-	37.97
E22B Lens 1	Lens	54	37.83	0.39	-	-	-	38.22
E22B Lens 1	Lens	55	37.11	0.41	-	-	-	37.52
E22B Lens 1	Lens	56	37.40	0.45	-	-	-	37.85
E22B Lens 1	Lens	57	37.90	0.27	-	-	-	38.17
E22B Lens 1	Lens	58	37.92	0.26	-	-	-	38.18
E22B Lens 1	Lens	59	37.75	0.31	-	-	-	38.06
E22B Lens 1	Lens	60	37.83	0.34	-	-	-	38.17
								0.00
E22B Lens 2	Lens	1	0.06	0.00	-	-	-	0.06
E22B Lens 2	Lens	2	0.11	0.00	-	-	-	0.11
E22B Lens 2	Lens	3	37.81	0.40	-	-	-	38.21
E22B Lens 2	Lens	4	37.53	0.52	-	-	-	38.05
E22B Lens 2	Lens	5	37.49	0.43	-	-	-	37.92
E22B Lens 2	Lens	6	37.58	0.32	-	-	-	37.90
E22B Lens 2	Lens	7	37.42	0.36	-	-	-	37.78
E22B Lens 2	Lens	8	33.67	0.43	-	-	-	34.10
E22B Lens 2	Lens	9	37.87	0.38	-	-	-	38.25
E22B Lens 2	Lens	10	37.45	0.43	-	-	-	37.88
E22B Lens 2	Lens	11	37.95	0.45	-	-	-	38.40

SAMPLE	FEATURE	DATA SET/ POINT	WEIGHT % ELEMENT					
			Ca	Mg	Sr	Fe	Mn	SUM
G33R Lens 1	Lens	1	29.69	0.53	-	-	-	30.22
G33R Lens 1	Lens	2	21.82	0.54	-	-	-	22.35
G33R Lens 1	Lens	3	33.79	0.24	-	-	-	34.03
G33R Lens 1	Lens	4	36.15	0.82	-	-	-	36.97
G33R Lens 1	Lens	5	36.31	0.36	-	-	-	36.67
G33R Lens 1	Lens	6	36.47	0.44	-	-	-	36.91
G33R Lens 1	Lens	7	36.36	0.26	-	-	-	36.62
G33R Lens 1	Lens	8	35.60	1.04	-	-	-	36.64
G33R Lens 1	Lens	9	34.76	2.09	-	-	-	36.84
G33R Lens 1	Lens	10	36.43	0.45	-	-	-	36.88
G33R Lens 1	Lens	11	34.73	1.16	-	-	-	35.89
G33R Lens 1	Lens	12	36.26	0.48	-	-	-	36.74
G33R Lens 1	Lens	13	36.29	0.40	-	-	-	36.69
G33R Lens 1	Lens	14	36.78	0.31	-	-	-	37.09
G33R Lens 1	Lens	15	36.37	0.47	-	-	-	36.84
G33R Lens 1	Lens	16	36.30	0.53	-	-	-	36.83
G33R Lens 1	Lens	17	36.10	0.44	-	-	-	36.54
G33R Lens 1	Lens	18	35.53	0.66	-	-	-	36.19
G33R Lens 1	Lens	19	35.96	0.48	-	-	-	36.43
G33R Lens 1	Lens	20	36.22	0.62	-	-	-	36.84
G33R Lens 1	Lens	21	35.77	0.65	-	-	-	36.42
G33R Lens 1	Lens	22	36.16	0.49	-	-	-	36.65
G33R Lens 1	Lens	23	35.17	0.44	-	-	-	35.61
G33R Lens 1	Lens	24	29.18	0.64	-	-	-	29.82
G33R Lens 1	Lens	25	35.23	0.32	-	-	-	35.55
G33R Lens 1	Lens	26	35.95	0.30	-	-	-	36.25
G33R Lens 1	Lens	27	36.07	0.31	-	-	-	36.38
G33R Lens 1	Lens	28	35.84	0.39	-	-	-	36.23
G33R Lens 1	Lens	29	35.57	0.46	-	-	-	36.03
G33R Lens 1	Lens	30	34.07	0.52	-	-	-	34.59
G33R Lens 1	Lens	31	34.50	0.44	-	-	-	34.94
G33R Lens 1	Lens	32	26.43	0.82	-	-	-	27.25
G33R Lens 1	Lens	33	32.11	0.49	-	-	-	32.60
G33R Lens 1	Lens	34	4.53	0.28	-	-	-	4.80
G33R Lens 1	Lens	35	10.57	0.51	-	-	-	11.08
G33R Lens 1	Lens	36	29.69	0.53	-	-	-	30.22
G33R Lens 1	Lens	37	21.82	0.54	-	-	-	22.35
G33R Lens 1	Lens	38	33.79	0.24	-	-	-	34.03
G33R Lens 1	Lens	39	36.15	0.82	-	-	-	36.97
G33R Lens 1	Lens	40	36.31	0.36	-	-	-	36.67
G33R Lens 1	Lens	41	36.47	0.44	-	-	-	36.91
G33R Lens 1	Lens	42	36.36	0.26	-	-	-	36.62
G33R Lens 1	Lens	43	35.60	1.04	-	-	-	36.64
G33R Lens 1	Lens	44	34.76	2.09	-	-	-	36.84
G33R Lens 1	Lens	45	36.43	0.45	-	-	-	36.88
G33R Lens 1	Lens	46	34.73	1.16	-	-	-	35.89
G33R Lens 1	Lens	47	36.26	0.48	-	-	-	36.74
G33R Lens 1	Lens	48	36.29	0.40	-	-	-	36.69
G33R Lens 1	Lens	49	36.78	0.31	-	-	-	37.09
G33R Lens 1	Lens	50	36.37	0.47	-	-	-	36.84
G33R Lens 1	Lens	51	36.30	0.53	-	-	-	36.83
G33R Lens 1	Lens	52	36.10	0.44	-	-	-	36.54
G33R Lens 1	Lens	53	35.53	0.66	-	-	-	36.19
G33R Lens 1	Lens	54	35.96	0.48	-	-	-	36.43
G33R Lens 1	Lens	55	36.22	0.62	-	-	-	36.84
G33R Lens 1	Lens	56	35.77	0.65	-	-	-	36.42
G33R Lens 1	Lens	57	36.16	0.49	-	-	-	36.65
G33R Lens 1	Lens	58	35.17	0.44	-	-	-	35.61
G33R Lens 1	Lens	59	29.18	0.64	-	-	-	29.82
G33R Lens 1	Lens	60	35.23	0.32	-	-	-	35.55
G33R Lens 1	Lens	61	35.95	0.30	-	-	-	36.25
G33R Lens 1	Lens	62	36.07	0.31	-	-	-	36.38
G33R Lens 1	Lens	63	35.84	0.39	-	-	-	36.23
G33R Lens 1	Lens	64	35.57	0.46	-	-	-	36.03
G33R Lens 1	Lens	65	34.07	0.52	-	-	-	34.59
G33R Lens 1	Lens	66	34.50	0.44	-	-	-	34.94
G33R Lens 1	Lens	67	26.43	0.82	-	-	-	27.25
G33R Lens 1	Lens	68	32.11	0.49	-	-	-	32.60
G33R Lens 1	Lens	69	27.87	0.37	-	-	-	28.24
G33R Lens 1	Lens	70	36.07	0.33	-	-	-	36.40

SAMPLE	FEATURE	DATA SET/ POINT	WEIGHT % ELEMENT					
			Ca	Mg	Sr	Fe	Mn	SUM
G33R Lens 1	Lens	71	36.35	0.30	-	-	-	36.65
G33R Lens 1	Lens	72	36.32	0.37	-	-	-	36.68
G33R Lens 1	Lens	73	36.22	0.29	-	-	-	36.51
G33R Lens 1	Lens	74	36.49	0.39	-	-	-	36.87
G33R Lens 1	Lens	75	36.31	0.37	-	-	-	36.67
G33R Lens 1	Lens	76	36.48	0.57	-	-	-	37.05
G33R Lens 1	Lens	77	36.59	0.40	-	-	-	36.98
G33R Lens 1	Lens	78	35.76	0.35	-	-	-	36.12
G33R Lens 1	Lens	79	36.64	0.44	-	-	-	37.08
G33R Lens 1	Lens	80	36.01	0.65	-	-	-	36.66
G33R Lens 1	Lens	81	36.13	0.48	-	-	-	36.61
G33R Lens 1	Lens	82	35.75	0.71	-	-	-	36.46
G33R Lens 1	Lens	83	36.26	0.47	-	-	-	36.73
G33R Lens 1	Lens	84	36.57	0.63	-	-	-	37.20
G33R Lens 1	Lens	85	36.08	0.66	-	-	-	36.74
G33R Lens 1	Lens	86	36.12	0.67	-	-	-	36.79
G33R Lens 1	Lens	87	36.50	0.52	-	-	-	37.02
G33R Lens 1	Lens	88	35.96	1.11	-	-	-	37.06
G33R Lens 1	Lens	89	35.96	0.45	-	-	-	36.40
G33R Lens 1	Lens	90	35.17	0.56	-	-	-	35.72
G33R Lens 1	Lens	91	35.10	0.39	-	-	-	35.49
G33R Lens 1	Lens	92	35.98	0.57	-	-	-	36.55
G33R Lens 1	Lens	93	36.61	0.58	-	-	-	37.19
G33R Lens 1	Lens	94	35.97	0.38	-	-	-	36.34
G33R Lens 1	Lens	95	36.45	0.43	-	-	-	36.88
G33R Lens 1	Lens	96	36.43	0.41	-	-	-	36.85
G33R Lens 1	Lens	97	36.52	0.42	-	-	-	36.94
G33R Lens 1	Lens	98	36.61	0.33	-	-	-	36.94
G33R Lens 1	Lens	99	36.33	0.32	-	-	-	36.65
G33R Lens 1	Lens	100	36.31	0.36	-	-	-	36.68
G33R Lens 1	Lens	101	36.20	0.39	-	-	-	36.58
G33R Lens 1	Lens	102	36.56	0.40	-	-	-	36.96
G33R Lens 1	Lens	103	36.69	0.41	-	-	-	37.09
G42R Lens 1 Traverse 1	Lens	1	40.16	0.43	0.15	0.14	0.00	40.88
G42R Lens 1 Traverse 1	Lens	2	40.19	0.40	0.17	0.13	0.02	40.90
G42R Lens 1 Traverse 1	Lens	3	39.01	0.41	0.17	0.13	0.05	39.77
G42R Lens 1 Traverse 1	Lens	4	37.50	0.30	0.19	0.16	0.01	38.15
G42R Lens 1 Traverse 1	Lens	5	38.32	0.32	0.20	0.13	0.01	38.98
G42R Lens 1 Traverse 1	Lens	6	38.16	0.36	0.21	0.19	0.00	38.91
G42R Lens 1 Traverse 1	Lens	7	39.63	0.36	0.25	0.10	0.03	40.38
G42R Lens 1 Traverse 1	Lens	8	39.24	0.49	0.21	0.12	0.04	40.08
G42R Lens 1 Traverse 1	Lens	9	38.46	0.69	0.16	0.21	0.01	39.54
G42R Lens 1 Traverse 1	Lens	10	38.78	0.88	0.21	0.13	0.03	40.01
G42R Lens 1 Traverse 1	Lens	11	38.15	1.11	0.20	0.18	0.05	39.69
G42R Lens 1 Traverse 1	Lens	12	38.76	0.50	0.18	0.16	0.00	39.60
G42R Lens 1 Traverse 1	Lens	13	39.00	0.35	0.21	0.08	0.04	39.68
G42R Lens 1 Traverse 1	Lens	14	38.31	0.79	0.16	0.15	0.09	39.50
G42R Lens 1 Traverse 1	Lens	15	39.29	0.34	0.19	0.15	0.05	40.02
G42R Lens 1 Traverse 1	Lens	16	38.82	0.49	0.23	0.07	0.05	39.67
G42R Lens 1 Traverse 1	Lens	17	37.82	1.41	0.19	0.15	0.06	39.63
G42R Lens 1 Traverse 1	Lens	18	37.86	0.97	0.18	0.26	0.01	39.28
G42R Lens 1 Traverse 1	Lens	19	34.66	0.81	0.15	0.15	0.00	35.78
G42R Lens 1 Traverse 1	Lens	20	38.84	0.79	0.19	0.18	0.00	40.01
G42R Lens 1 Traverse 1	Lens	21	39.01	0.36	0.14	0.10	0.01	39.61
G42R Lens 1 Traverse 1	Lens	22	38.46	0.74	0.16	0.13	0.03	39.52
G42R Lens 1 Traverse 1	Lens	23	40.18	0.41	0.21	0.10	0.03	40.93
G42R Lens 1 Traverse 1	Lens	24	38.25	0.46	0.19	0.17	0.00	39.07
G42R Lens 1 Traverse 1	Lens	25	39.34	0.36	0.21	0.11	0.04	40.05
G42R Lens 1 Traverse 1	Lens	26	39.53	0.37	0.19	0.14	0.00	40.22
G42R Lens 1 Traverse 1	Lens	27	38.48	0.35	0.22	0.14	0.01	39.21
G42R Lens 1 Traverse 1	Lens	28	39.05	0.43	0.20	0.15	0.02	39.84
G42R Lens 1 Traverse 1	Lens	29	39.23	0.39	0.21	0.12	0.02	39.97
G42R Lens 1 Traverse 1	Lens	30	39.55	0.42	0.21	0.17	0.01	40.37
G42R Lens 1 Traverse 2	Lens	1	38.86	0.59	0.19	0.09	0.03	39.76
G42R Lens 1 Traverse 2	Lens	2	38.46	1.11	0.18	0.20	0.06	40.00
G42R Lens 1 Traverse 2	Lens	3	40.12	0.31	0.14	0.13	0.01	40.70
G42R Lens 1 Traverse 2	Lens	4	37.97	0.69	0.14	0.21	0.00	39.01
G42R Lens 1 Traverse 2	Lens	5	20.93	3.08	0.16	0.47	0.06	24.69
G42R Lens 1 Traverse 2	Lens	6	38.80	0.34	0.18	0.14	0.03	39.49

SAMPLE	FEATURE	DATA SET/ POINT	WEIGHT % ELEMENT					
			Ca	Mg	Sr	Fe	Mn	SUM
G42R Lens 1 Traverse 2	Lens	7	40.21	0.33	0.20	0.13	0.03	40.89
G42R Lens 1 Traverse 2	Lens	8	38.91	0.86	0.19	0.12	0.01	40.08
G42R Lens 1 Traverse 2	Lens	9	39.55	0.38	0.28	0.11	0.04	40.36
G42R Lens 1 Traverse 2	Lens	10	38.45	0.89	0.21	0.20	0.06	39.81
G42R Lens 1 Traverse 2	Lens	11	40.47	0.35	0.23	0.14	0.02	41.20
G42R Lens 1 Traverse 2	Lens	12	39.61	0.67	0.17	0.07	0.05	40.57
G42R Lens 1 Traverse 2	Lens	13	38.37	0.66	0.20	0.13	0.05	39.41
G42R Lens 1 Traverse 2	Lens	14	38.10	0.96	0.17	0.15	0.03	39.41
G42R Lens 1 Traverse 2	Lens	15	38.44	0.72	0.19	0.08	0.02	39.45
G42R Lens 3 Traverse 1	Lens	1	39.69	0.47	0.23	0.12	0.02	40.52
G42R Lens 3 Traverse 1	Lens	2	40.29	0.41	0.22	0.21	0.05	41.17
G42R Lens 3 Traverse 1	Lens	3	38.03	0.37	0.20	0.13	0.01	38.75
G42R Lens 3 Traverse 1	Lens	4	38.49	0.39	0.16	0.14	0.02	39.19
G42R Lens 3 Traverse 1	Lens	5	40.23	0.40	0.25	0.11	0.05	41.03
G42R Lens 3 Traverse 1	Lens	6	40.05	0.49	0.19	0.11	0.05	40.88
G42R Lens 3 Traverse 1	Lens	7	39.78	0.50	0.18	0.11	0.00	40.57
G42R Lens 3 Traverse 1	Lens	8	39.77	0.52	0.23	0.15	0.04	40.70
G42R Lens 3 Traverse 1	Lens	9	39.89	0.52	0.19	0.15	0.00	40.74
G42R Lens 3 Traverse 1	Lens	10	39.43	0.45	0.18	0.15	0.04	40.24
G42R Lens 3 Traverse 1	Lens	11	39.50	0.54	0.21	0.13	0.06	40.43
G42R Lens 3 Traverse 1	Lens	12	39.79	0.37	0.30	0.13	0.00	40.59
G42R Lens 3 Traverse 1	Lens	13	40.07	0.27	0.38	0.09	0.00	40.81
G42R Lens 3 Traverse 1	Lens	14	39.94	0.51	0.15	0.08	0.01	40.70
G42R Lens 3 Traverse 1	Lens	15	40.06	0.48	0.20	0.15	0.02	40.91
G42R Lens 3 Traverse 1	Lens	16	40.14	0.40	0.22	0.09	0.03	40.87
G42R Lens 3 Traverse 1	Lens	17	39.83	0.47	0.24	0.15	0.06	40.75
G42R Lens 3 Traverse 1	Lens	18	39.73	0.61	0.22	0.08	0.04	40.67
G42R Lens 3 Traverse 1	Lens	19	39.87	0.51	0.20	0.17	0.05	40.80
G42R Lens 3 Traverse 1	Lens	20	39.83	0.46	0.27	0.12	0.07	40.75
G42R Lens 3 Traverse 1	Lens	21	39.96	0.56	0.21	0.13	0.00	40.86
G42R Lens 3 Traverse 1	Lens	22	39.81	0.37	0.21	0.15	0.02	40.56
G42R Lens 3 Traverse 1	Lens	23	38.43	0.33	0.20	0.19	0.02	39.17
G42R Lens 3 Traverse 1	Lens	24	38.49	0.40	0.19	0.18	0.02	39.29
G42R Lens 3 Traverse 1	Lens	25	38.66	0.41	0.21	0.14	0.00	39.41
G42R Lens 3 Traverse 2	Lens	1	34.39	0.52	0.19	0.14	0.02	35.26
G42R Lens 3 Traverse 2	Lens	2	35.30	0.46	0.20	0.11	0.00	36.07
G42R Lens 3 Traverse 2	Lens	3	38.56	0.37	0.18	0.18	0.00	39.28
G42R Lens 3 Traverse 2	Lens	4	39.38	0.35	0.18	0.17	0.03	40.12
G42R Lens 3 Traverse 2	Lens	5	39.34	0.46	0.25	0.14	0.00	40.19
G42R Lens 3 Traverse 2	Lens	6	34.57	0.55	0.20	0.14	0.00	35.47
G42R Lens 3 Traverse 2	Lens	7	34.24	0.52	0.18	0.13	0.00	35.07
G42R Lens 3 Traverse 2	Lens	8	36.84	0.52	0.25	0.16	0.02	37.78
G42R Lens 3 Traverse 2	Lens	9	35.58	0.55	0.21	0.10	0.00	36.45
G42R Lens 3 Traverse 2	Lens	10	40.40	0.46	0.21	0.12	0.06	41.25
G42R Lens 3 Traverse 2	Lens	11	40.02	0.66	0.21	0.12	0.06	41.07
G42R Lens 3 Traverse 2	Lens	12	38.65	0.43	0.31	0.05	0.00	39.44
G42R Lens 3 Traverse 2	Lens	13	36.64	0.37	0.37	0.11	0.00	37.50
G42R Lens 3 Traverse 2	Lens	14	40.99	0.54	0.13	0.12	0.05	41.82
G42R Lens 3 Traverse 2	Lens	15	36.89	0.51	0.18	0.10	0.05	37.73
G42R Lens 3 Traverse 2	Lens	16	35.65	0.40	0.21	0.04	0.04	36.34
G42R Lens 3 Traverse 2	Lens	17	37.80	0.57	0.21	0.16	0.02	38.75
G42R Lens 3 Traverse 2	Lens	18	36.09	0.62	0.22	0.13	0.00	37.06
G42R Lens 3 Traverse 2	Lens	19	32.36	0.52	0.21	0.11	0.04	33.25
G42R Lens 3 Traverse 2	Lens	20	33.95	0.48	0.24	0.07	0.04	34.77
G42R Lens 3 Traverse 2	Lens	21	34.95	0.58	0.19	0.11	0.02	35.85
G42R Lens 3 Traverse 2	Lens	22	35.51	0.40	0.25	0.10	0.00	36.27
G42R Lens 3 Traverse 2	Lens	23	39.01	0.30	0.18	0.21	0.05	39.75
G42R Lens 3 Traverse 2	Lens	24	40.18	0.43	0.22	0.11	0.02	40.96
G42R Lens 3 Traverse 2	Lens	25	40.23	0.42	0.21	0.14	0.03	41.03
G42R Lens 2 Traverse 1	Lens	1	39.07	0.29	0.26	0.09	0.05	39.75
G42R Lens 2 Traverse 1	Lens	2	39.25	0.38	0.17	0.09	0.00	39.89
G42R Lens 2 Traverse 1	Lens	3	37.99	1.23	0.21	0.23	0.00	39.66
G42R Lens 2 Traverse 1	Lens	4	36.75	0.54	0.18	0.19	0.06	37.73
G42R Lens 2 Traverse 1	Lens	5	39.25	0.46	0.17	0.16	0.07	40.09
G42R Lens 2 Traverse 1	Lens	6	39.58	0.36	0.19	0.10	0.05	40.28
G42R Lens 2 Traverse 1	Lens	7	38.64	0.45	0.25	0.11	0.00	39.46
G42R Lens 2 Traverse 1	Lens	8	40.24	0.48	0.16	0.12	0.02	41.02
G42R Lens 2 Traverse 1	Lens	9	32.51	0.49	0.18	0.11	0.01	33.30

SAMPLE	FEATURE	DATA SET/ POINT	WEIGHT % ELEMENT					
			Ca	Mg	Sr	Fe	Mn	SUM
G42R Lens 2 Traverse 1	Lens	10	32.78	0.47	0.15	0.12	0.03	33.56
G42R Lens 2 Traverse 1	Lens	11	39.57	0.35	0.38	0.07	0.00	40.37
G42R Lens 2 Traverse 1	Lens	12	40.35	0.48	0.29	0.12	0.04	41.27
G42R Lens 2 Traverse 1	Lens	13	40.39	0.36	0.27	0.13	0.04	41.20
G42R Lens 2 Traverse 1	Lens	14	40.51	0.47	0.20	0.12	0.02	41.32
G42R Lens 2 Traverse 1	Lens	15	40.90	0.39	0.31	0.09	0.01	41.69
G42R Lens 2 Traverse 1	Lens	16	40.63	0.39	0.30	0.12	0.00	41.44
G42R Lens 2 Traverse 1	Lens	17	37.72	0.41	0.22	0.19	0.03	38.57
G42R Lens 2 Traverse 1	Lens	18	35.44	0.59	0.15	1.16	0.01	37.36
G42R Lens 2 Traverse 1	Lens	19	36.71	0.48	0.16	0.33	0.06	37.73
G42R Lens 2 Traverse 1	Lens	20	34.93	0.51	0.11	0.49	0.02	36.07
G42R Lens 2 Traverse 1	Lens	21	34.06	0.58	0.09	0.43	0.03	35.20
G42R Lens 2 Traverse 1	Lens	22	19.12	0.69	0.04	0.63	0.03	20.51
G42R Lens 2 Traverse 1	Lens	23	35.76	1.05	0.14	0.96	0.06	37.97
G42R Lens 2 Traverse 1	Lens	24	33.95	0.33	0.14	0.21	0.00	34.63
G42R Lens 2 Traverse 1	Lens	25	5.30	0.58	0.00	1.00	0.05	6.94
G42R Lens 2 Traverse 1	Lens	26	39.17	0.80	0.19	0.17	0.03	40.36
G42R Lens 2 Traverse 1	Lens	27	39.66	0.48	0.22	0.09	0.04	40.49
G42R Lens 2 Traverse 1	Lens	28	37.99	1.17	0.20	0.17	0.00	39.53
G42R Lens 2 Traverse 1	Lens	29	39.43	0.26	0.17	0.05	0.02	39.93
G42R Lens 2 Traverse 1	Lens	30	38.94	0.88	0.15	0.21	0.05	40.23
G42R	Sclera	1	40.62	0.33	0.21	0.07	0.00	41.23
G42R	Sclera	2	39.24	0.79	0.21	0.14	0.05	40.42
G42R	Sclera	3	40.30	0.40	0.23	0.15	0.03	41.09
G42R	Sclera	4	40.29	0.52	0.23	0.13	0.01	41.17
G42R	Sclera	5	40.39	0.35	0.36	0.07	0.00	41.16
G42R	Sclera	6	40.61	0.42	0.29	0.06	0.02	41.40
G42R	Sclera	7	40.06	0.52	0.29	0.10	0.00	40.97
G42R	Sclera	8	40.31	0.52	0.19	0.11	0.00	41.13
G42R	Sclera	9	40.80	0.46	0.25	0.08	0.02	41.61
G42R	Sclera	10	40.53	0.45	0.25	0.16	0.03	41.40
G42R	Sclera	11	39.87	0.63	0.30	0.13	0.04	40.97
G42R	Sclera	12	40.57	0.44	0.27	0.13	0.00	41.42
G42R	Sclera	13	40.39	0.48	0.21	0.10	0.03	41.21
G42R	Sclera	14	39.24	0.44	0.18	0.23	0.03	40.12
G42R	Sclera	15	36.61	0.55	0.09	0.42	0.01	37.69
G42R	Sclera	16	35.54	0.69	0.13	0.67	0.00	37.02
G42R	Sclera	17	38.61	0.49	0.17	0.26	0.02	39.55
G42R	Sclera	18	37.36	0.45	0.17	0.26	0.04	38.27
G42R	Sclera	19	33.31	0.57	0.09	0.47	0.01	34.45
G42R	Sclera	20	24.37	1.44	0.03	2.92	0.04	28.80
G42R	Sclera	21	36.02	0.58	0.08	0.49	0.04	37.22
G42R	Sclera	22	36.70	0.48	0.14	0.29	0.02	37.63
G42R	Sclera	23	34.26	0.72	0.13	0.89	0.05	36.05
G42R	Sclera	24	26.78	0.23	0.13	0.20	0.00	27.34
G42R	Sclera	25	34.83	0.32	0.17	0.16	0.07	35.54
G42R	Crinoid	1	37.52	0.68	0.16	0.13	0.00	38.50
G42R	Crinoid	2	37.01	0.51	0.22	0.21	0.03	37.97
G42R	Crinoid	3	37.54	0.99	0.19	0.13	0.00	38.85
G42R	Crinoid	4	29.97	0.80	0.09	0.75	0.01	31.61
G42R	Crinoid	5	37.69	0.53	0.17	0.15	0.03	38.58
G42R	Crinoid	6	36.16	0.53	0.15	0.32	0.05	37.20
G42R	Crinoid	7	37.21	0.44	0.15	0.09	0.01	37.89
G42R	Crinoid	8	37.28	0.48	0.15	0.23	0.04	38.17
G42R	Crinoid	9	33.08	0.44	0.10	0.18	0.02	33.82
G42R	Crinoid	10	38.58	0.50	0.19	0.14	0.07	39.47
G42R	Crinoid	11	37.30	0.49	0.13	0.12	0.05	38.10
G42R	Crinoid	12	38.25	0.45	0.16	0.12	0.00	38.97
G42R	Crinoid	13	38.47	0.58	0.24	0.16	0.03	39.48
G42R	Crinoid	14	34.49	0.51	0.14	0.37	0.04	35.54
G42R	Crinoid	15	34.38	0.41	0.13	0.20	0.02	35.15
G42R	Crinoid	16	38.27	0.57	0.18	0.16	0.00	39.17
G42R	Crinoid	17	38.50	0.56	0.11	0.15	0.02	39.34
G42R	Crinoid	18	36.10	0.53	0.17	0.29	0.01	37.10
G42R	Crinoid	19	34.86	0.64	0.16	0.40	0.06	36.13
G42R	Crinoid	20	37.68	0.50	0.17	0.19	0.02	38.56
G42R	Crinoid	21	36.50	0.45	0.14	0.27	0.04	37.40
G42R	Crinoid	22	37.03	0.53	0.17	0.25	0.00	37.99
G42R	Crinoid	23	39.41	0.39	0.24	0.16	0.06	40.27

SAMPLE	FEATURE	DATA SET/ POINT	WEIGHT % ELEMENT					
			Ca	Mg	Sr	Fe	Mn	SUM
G42R	Crinoid	24	38.55	0.46	0.20	0.13	0.00	39.33
G42R	Crinoid	25	36.16	0.86	0.16	0.22	0.01	37.40
PM28 (Lens 1)	Lens	1	35.49	0.64	-	1.67	0.05	37.85
PM28 (Lens 1)	Lens	2	34.81	2.36	-	0.15	0.00	37.32
PM28 (Lens 1)	Lens	3	36.78	1.45	-	0.19	0.00	38.42
PM28 (Lens 1)	Lens	4	36.36	1.91	-	0.02	0.00	38.28
PM28 (Lens 1)	Lens	5	36.35	1.87	-	0.04	0.03	38.29
PM28 (Lens 1)	Lens	6	36.12	2.02	-	0.02	0.04	38.20
PM28 (Lens 1)	Lens	7	35.94	1.79	-	0.00	0.01	37.75
PM28 (Lens 1)	Lens	8	34.68	2.64	-	0.05	0.01	37.38
PM28 (Lens 1)	Lens	9	36.35	1.93	-	0.01	0.02	38.31
PM28 (Lens 1)	Lens	10	34.57	2.34	-	0.05	0.02	36.98
PM28 (Lens 1)	Lens	11	36.27	1.48	-	0.00	0.00	37.75
PM28 (Lens 1)	Lens	12	35.95	1.93	-	0.05	0.00	37.93
PM28 (Lens 1)	Lens	13	36.04	1.66	-	0.31	0.00	38.01
PM28 (Lens 1)	Bowl?	14	37.20	0.24	-	1.20	0.00	38.63
PM28 (Lens 1)	Bowl?	15	37.36	0.24	-	1.24	0.04	38.88
PM28 Lens 1 (traverse 2)	Lens	1	37.78	0.26	-	1.49	0.07	39.59
PM28 Lens 1 (traverse 2)	Lens	2	37.70	0.25	-	1.17	0.08	39.20
PM28 Lens 1 (traverse 2)	Lens	3	36.78	1.69	-	0.30	0.03	38.80
PM28 Lens 1 (traverse 2)	Lens	4	36.56	1.92	-	0.01	0.01	38.50
PM28 Lens 1 (traverse 2)	Lens	5	36.70	1.45	-	0.00	0.04	38.18
PM28 Lens 1 (traverse 2)	Lens	6	34.94	2.28	-	0.02	0.04	37.27
PM28 Lens 1 (traverse 2)	Lens	7	36.78	2.03	-	0.01	0.00	38.82
PM28 Lens 1 (traverse 2)	Lens	8	34.85	2.60	-	0.03	0.01	37.49
PM28 Lens 1 (traverse 2)	Lens	9	36.18	1.79	-	0.05	0.00	38.02
PM28 Lens 1 (traverse 2)	Lens	10	36.30	2.05	-	0.01	0.00	38.37
PM28 Lens 1 (traverse 2)	Lens	11	36.66	1.87	-	0.05	0.01	38.59
PM28 Lens 1 (traverse 2)	Lens	12	36.63	1.95	-	0.04	0.00	38.62
PM28 Lens 1 (traverse 2)	Lens	13	37.05	1.43	-	0.21	0.01	38.70
PM28 Lens 1 (traverse 2)	Lens	14	35.16	2.38	-	0.20	0.00	37.74
PM28 Lens 1 (traverse 2)	Lens	15	35.90	0.68	-	1.62	0.05	38.25
PM28 Lens 2 (traverse 1)	Lens	1	35.78	1.37	-	0.00	0.02	37.17
PM28 Lens 2 (traverse 1)	Lens	2	36.15	1.87	-	0.06	0.03	38.11
PM28 Lens 2 (traverse 1)	Lens	3	36.75	1.77	-	0.04	0.04	38.60
PM28 Lens 2 (traverse 1)	Lens	4	35.53	2.48	-	0.00	0.06	38.07
PM28 Lens 2 (traverse 1)	Lens	5	36.45	1.80	-	0.00	0.00	38.24
PM28 Lens 2 (traverse 1)	Lens	6	35.07	2.26	-	0.01	0.02	37.37
PM28 Lens 2 (traverse 1)	Lens	7	36.55	2.20	-	0.01	0.00	38.75
PM28 Lens 2 (traverse 1)	Lens	8	35.18	2.73	-	0.01	0.01	37.93
PM28 Lens 2 (traverse 1)	Lens	9	36.73	1.80	-	0.00	0.02	38.55
PM28 Lens 2 (traverse 1)	Lens	10	35.99	2.22	-	0.02	0.02	38.25
PM28 Lens 2 (traverse 1)	Lens	11	35.69	2.20	-	0.07	0.03	37.99
PM28 Lens 2 (traverse 1)	Lens	12	36.68	1.01	-	0.92	0.05	38.65
PM28 Lens 2 (traverse 1)	Lens	13	38.12	0.21	-	1.08	0.02	39.42
PM28 Lens 2 (traverse 1)	Lens	14	30.46	0.41	-	2.32	0.09	33.28
PM28 Lens 2 (traverse 1)	Lens	15	8.71	2.37	-	14.68	0.00	25.75
PM28 Lens 2 (traverse 2)	Lens	1	37.06	0.30	-	1.16	0.05	38.56
PM28 Lens 2 (traverse 2)	Lens	2	37.24	0.48	-	1.20	0.07	38.99
PM28 Lens 2 (traverse 2)	Lens	3	35.78	1.64	-	0.32	0.07	37.80
PM28 Lens 2 (traverse 2)	Lens	4	37.47	1.38	-	0.14	0.00	38.99
PM28 Lens 2 (traverse 2)	Lens	5	36.19	1.92	-	0.11	0.04	38.25
PM28 Lens 2 (traverse 2)	Lens	6	36.33	1.87	-	0.02	0.01	38.23
PM28 Lens 2 (traverse 2)	Lens	7	36.89	1.89	-	0.05	0.04	38.86
PM28 Lens 2 (traverse 2)	Lens	8	36.90	1.51	-	0.13	0.02	38.56
PM28 Lens 2 (traverse 2)	Lens	9	36.17	1.97	-	0.08	0.06	38.28
PM28 Lens 2 (traverse 2)	Lens	10	37.69	1.18	-	0.00	0.03	38.90
PM28 Lens 2 (traverse 2)	Lens	11	35.00	2.47	-	0.03	0.00	37.50
PM28 Lens 2 (traverse 2)	Lens	12	34.50	2.21	-	0.01	0.03	36.74
PM28 Lens 2 (traverse 2)	Lens	13	35.76	2.08	-	0.29	0.01	38.14
PM28 Lens 2 (traverse 2)	Lens	14	36.67	0.38	-	1.31	0.07	38.43
PM28 Lens 2 (traverse 2)	Cement ?	15	36.54	0.24	-	0.89	0.05	37.72
PM28 Lens 3 (taverse 1)	Lens	1	32.78	2.57	-	0.02	0.02	35.38
PM28 Lens 3 (taverse 1)	Lens	2	37.19	1.21	-	0.03	0.03	38.46
PM28 Lens 3 (taverse 1)	Lens	3	36.34	2.11	-	0.05	0.05	38.55
PM28 Lens 3 (taverse 1)	Lens	4	35.88	1.71	-	0.04	0.00	37.63

SAMPLE	FEATURE	DATA SET/ POINT	WEIGHT % ELEMENT					
			Ca	Mg	Sr	Fe	Mn	SUM
PM28 Lens 3 (taverse 1)	Lens	5	36.30	1.93	-	0.07	0.01	38.30
PM28 Lens 3 (taverse 1)	Lens	6	37.17	1.68	-	0.02	0.00	38.87
PM28 Lens 3 (taverse 1)	Lens	7	36.52	2.24	-	0.04	0.03	38.83
PM28 Lens 3 (taverse 1)	Lens	8	36.46	2.00	-	0.01	0.00	38.47
PM28 Lens 3 (taverse 1)	Lens	9	34.90	2.80	-	0.03	0.00	37.72
PM28 Lens 3 (taverse 1)	Lens	10	35.38	2.89	-	0.03	0.00	38.30
PM28 Lens 3 (taverse 1)	Lens	11	35.08	1.88	-	0.25	0.01	37.22
PM28 Lens 3 (taverse 1)	Lens	12	36.01	1.89	-	0.76	0.03	38.69
PM28 Lens 3 (taverse 1)	Lens	13	31.23	0.20	-	1.74	0.06	33.22
PM28 Lens 3 (taverse 1)	Lens	14	33.18	0.28	-	1.77	0.09	35.32
PM28 Lens 3 (taverse 1)	Lens	15	35.88	0.26	-	1.17	0.02	37.33
PM28 Lens 3 (taverse 1)	Lens	16	36.00	1.72	-	0.74	0.11	38.57
PM28 Lens 3 (taverse 1)	Lens	17	35.90	2.16	-	0.21	0.05	38.32
PM28 Lens 3 (taverse 1)	Lens	18	36.70	1.87	-	0.04	0.00	38.61
PM28 Lens 3 (taverse 1)	Lens	19	35.94	1.63	-	0.06	0.01	37.64
PM28 Lens 3 (taverse 1)	Lens	20	35.44	1.82	-	0.00	0.00	37.27
PM28 Lens 3 (traverse 2)	Lens	1	36.72	1.92	-	0.08	0.00	38.71
PM28 Lens 3 (traverse 2)	Lens	2	36.67	2.08	-	0.07	0.00	38.82
PM28 Lens 3 (traverse 2)	Lens	3	37.17	1.46	-	0.10	0.00	38.73
PM28 Lens 3 (traverse 2)	Lens	4	38.01	1.23	-	0.00	0.00	39.24
PM28 Lens 3 (traverse 2)	Lens	5	37.90	1.34	-	0.01	0.03	39.28
PM28 Lens 3 (traverse 2)	Lens	6	34.44	2.95	-	0.04	0.00	37.45
PM28 Lens 3 (traverse 2)	Lens	7	37.44	1.72	-	0.08	0.00	39.24
PM28 Lens 3 (traverse 2)	Lens	8	38.05	0.96	-	0.10	0.00	39.11
PM28 Lens 3 (traverse 2)	Lens	9	37.17	1.78	-	0.07	0.04	39.05
PM28 Lens 3 (traverse 2)	Lens	10	36.67	1.95	-	0.01	0.00	38.63
PM28 Lens 3 (traverse 2)	Lens	11	35.38	2.29	-	0.31	0.03	38.00
PM28 Lens 3 (traverse 2)	Lens	12	35.63	2.04	-	0.02	0.03	37.73
PM28 Lens 3 (traverse 2)	Lens	13	36.34	2.17	-	0.05	0.00	38.55
PM28 Lens 3 (traverse 2)	Lens	14	35.90	2.02	-	0.34	0.06	38.32
PM28 Lens 3 (traverse 2)	Lens	15	36.78	1.41	-	0.53	0.09	38.80

Table E.2 - Weight % carbonate EPMA data (Strathclyde) for trilobites with schizochroal eyes.

SAMPLE	FEATURE	DATA SET/ POINT	WEIGHT % CARBONATE					
			Ca	Mg	Sr	Fe	Mn	SUM
AM65 Lens 1 Traverse 1	Lens	1	62.19	0.82	0.02	2.12	0.15	65.30
AM65 Lens 1 Traverse 1	Lens	2	83.88	4.64	0.19	2.21	0.09	91.01
AM65 Lens 1 Traverse 1	Lens	3	68.09	13.04	0.24	1.64	0.12	83.13
AM65 Lens 1 Traverse 1	Lens	4	86.51	6.02	0.40	0.20	0.00	93.13
AM65 Lens 1 Traverse 1	Lens	5	87.46	4.89	0.37	0.08	0.00	92.80
AM65 Lens 1 Traverse 1	Lens	6	87.63	4.52	0.36	0.09	0.00	92.61
AM65 Lens 1 Traverse 1	Lens	7	87.03	6.11	0.34	0.05	0.11	93.63
AM65 Lens 1 Traverse 1	Lens	8	78.34	14.25	0.32	0.13	0.00	93.04
AM65 Lens 1 Traverse 1	Lens	9	88.91	4.84	0.37	0.19	0.04	94.36
AM65 Lens 1 Traverse 1	Lens	10	87.18	4.91	0.40	0.03	0.04	92.55
AM65 Lens 1 Traverse 1	Lens	11	88.18	4.73	0.35	0.04	0.01	93.32
AM65 Lens 1 Traverse 1	Lens	12	86.64	5.72	0.38	0.21	0.00	92.94
AM65 Lens 1 Traverse 1	Lens	13	85.85	5.54	0.38	0.11	0.10	91.98
AM65 Lens 1 Traverse 1	Lens	14	85.05	5.90	0.33	0.16	0.13	91.58
AM65 Lens 1 Traverse 1	Lens	15	79.90	7.70	0.33	0.37	0.17	88.45
AM65 Lens 1 Traverse 2	Lens	1	44.39	1.60	0.00	2.94	0.07	49.00
AM65 Lens 1 Traverse 2	Lens	2	78.78	1.23	0.05	2.90	0.31	83.27
AM65 Lens 1 Traverse 2	Lens	3	83.69	1.70	0.05	4.00	0.57	90.02
AM65 Lens 1 Traverse 2	Lens	4	87.38	7.29	0.44	0.24	0.03	95.39
AM65 Lens 1 Traverse 2	Lens	5	86.63	7.50	0.43	0.09	0.01	94.67
AM65 Lens 1 Traverse 2	Lens	6	86.47	7.83	0.52	0.05	0.06	94.94
AM65 Lens 1 Traverse 2	Lens	7	85.64	6.95	0.36	0.04	0.00	92.98
AM65 Lens 1 Traverse 2	Lens	8	88.02	5.61	0.33	0.16	0.07	94.19
AM65 Lens 1 Traverse 2	Lens	9	86.39	5.13	0.36	0.00	0.00	91.87

SAMPLE	FEATURE	DATA SET/ POINT	WEIGHT % CARBONATE					
			Ca	Mg	Sr	Fe	Mn	SUM
AM65 Lens 1 Traverse 2	Lens	10	75.81	12.36	0.25	0.45	0.03	88.90
AM65 Lens 1 Traverse 2	Lens	11	78.51	10.59	0.32	0.07	0.03	89.52
AM65 Lens 1 Traverse 2	Lens	12	85.40	5.59	0.43	0.02	0.12	91.56
AM65 Lens 1 Traverse 2	Lens	13	80.28	7.06	0.32	0.71	0.09	88.47
AM65 Lens 1 Traverse 2	Lens	14	86.86	4.33	0.38	0.39	0.10	92.06
AM65 Lens 1 Traverse 2	Lens	15	83.72	3.49	0.31	0.32	0.02	87.87
AM65 Lens 2 Traverse 1	Lens	1	85.44	5.74	0.34	0.23	0.19	91.95
AM65 Lens 2 Traverse 1	Lens	2	84.65	7.07	0.34	0.33	0.12	92.50
AM65 Lens 2 Traverse 1	Lens	3	86.61	6.26	0.38	0.08	0.10	93.43
AM65 Lens 2 Traverse 1	Lens	4	85.17	6.60	0.39	0.01	0.14	92.31
AM65 Lens 2 Traverse 1	Lens	5	84.22	7.14	0.40	0.10	0.05	91.91
AM65 Lens 2 Traverse 1	Lens	6	87.21	5.69	0.42	0.07	0.08	93.48
AM65 Lens 2 Traverse 1	Lens	7	85.27	7.62	0.42	0.00	0.10	93.42
AM65 Lens 2 Traverse 1	Lens	8	87.16	5.92	0.45	0.05	0.10	93.69
AM65 Lens 2 Traverse 1	Lens	9	84.78	6.76	0.40	0.00	0.01	91.95
AM65 Lens 2 Traverse 1	Lens	10	83.40	8.73	0.34	0.34	0.04	92.86
AM65 Lens 2 Traverse 1	Lens	11	89.37	5.11	0.42	0.04	0.11	95.05
AM65 Lens 2 Traverse 1	Lens	12	87.70	6.29	0.45	0.00	0.00	94.43
AM65 Lens 2 Traverse 1	Lens	13	82.94	7.88	0.39	0.00	0.05	91.27
AM65 Lens 2 Traverse 1	Lens	14	87.03	3.31	0.32	0.26	0.08	91.00
AM65 Lens 2 Traverse 1	Lens	15	85.29	5.78	0.40	0.27	0.07	91.79
AM65 Lens 2 Traverse 2	Lens	1	89.95	2.07	0.30	0.74	0.13	93.19
AM65 Lens 2 Traverse 2	Lens	2	87.98	4.97	0.45	0.48	0.12	94.00
AM65 Lens 2 Traverse 2	Lens	3	89.94	3.57	0.47	0.15	0.11	94.24
AM65 Lens 2 Traverse 2	Lens	4	83.58	7.22	0.43	0.07	0.03	91.34
AM65 Lens 2 Traverse 2	Lens	5	84.76	7.36	0.41	0.00	0.07	92.59
AM65 Lens 2 Traverse 2	Lens	6	83.94	6.61	0.43	0.01	0.00	91.00
AM65 Lens 2 Traverse 2	Lens	7	82.09	6.32	0.41	0.00	0.00	88.82
AM65 Lens 2 Traverse 2	Lens	8	86.53	4.76	0.32	0.15	0.00	91.75
AM65 Lens 2 Traverse 2	Lens	9	73.03	11.87	0.30	0.11	0.02	85.33
AM65 Lens 2 Traverse 2	Lens	10	76.61	12.53	0.44	0.09	0.00	89.66
AM65 Lens 2 Traverse 2	Lens	11	79.30	7.66	0.34	0.13	0.00	87.43
AM65 Lens 2 Traverse 2	Lens	12	71.16	13.84	0.38	0.33	0.13	85.85
AM65 Lens 2 Traverse 2	Lens	13	82.85	1.41	0.07	3.72	0.49	88.53
AM65 Lens 2 Traverse 2	Lens	14	66.50	1.11	0.00	3.02	0.11	70.74
AM65 Lens 2 Traverse 2	Lens	15	79.49	1.36	0.03	2.82	0.27	83.97
BB3aR Lens 2	Lens	1	100.08	0.53	0.00	0.00	0.13	100.73
BB3aR Lens 2	Lens	2	97.80	3.53	0.00	0.00	0.01	101.34
BB3aR Lens 2	Lens	3	100.30	1.14	0.00	0.00	0.00	101.45
BB3aR Lens 2	Lens	4	96.66	3.75	0.00	0.05	0.00	100.45
BB3aR Lens 2	Lens	5	99.48	1.42	0.00	0.00	0.05	100.95
BB3aR Lens 2	Lens	6	99.50	1.05	0.00	0.00	0.00	100.56
BB3aR Lens 2	Lens	7	100.20	0.69	0.00	0.06	0.04	100.99
BB3aR Lens 2	Lens	8	92.26	7.23	0.00	0.11	0.00	99.60
BB3aR Lens 2	Lens	9	98.63	1.96	0.00	0.01	0.00	100.60
BB3aR Lens 2	Lens	10	100.09	0.88	0.00	0.07	0.00	101.04
BB3aR Lens 2	Lens	11	95.56	4.16	0.00	0.00	0.05	99.76
BB3aR Lens 2	Lens	12	98.32	0.69	0.00	0.03	0.00	99.04
BB3aR Lens 2	Lens	13	99.55	0.80	0.00	0.03	0.01	100.38
BB3aR Lens 2	Lens	14	94.44	6.57	0.00	0.00	0.07	101.08
BB3aR Lens 2	Lens	15	98.03	2.47	0.00	0.01	0.01	100.52
BB3aR Lens 2	Lens	16	96.99	2.02	0.00	0.09	0.00	99.11
BB3aR Lens 2	Lens	17	96.92	3.65	0.00	0.01	0.00	100.57
BB3aR Lens 2	Lens	18	93.56	4.81	0.00	0.07	0.03	98.46
BB3aR Lens 2	Lens	19	99.24	0.36	0.00	0.00	0.00	99.60
BB3aR Lens 2	Lens	20	92.57	0.93	0.00	0.00	0.08	93.59
BB3aR Lens 2	Lens	21	99.52	0.98	0.00	0.07	0.00	100.56
BB3aR Lens 2	Lens	22	93.63	5.27	0.00	0.07	0.00	98.97
BB3aR Lens 2	Lens	23	98.98	1.40	0.00	0.01	0.00	100.39
BB3aR Lens 2	Lens	24	99.89	0.89	0.00	0.00	0.00	100.78

SAMPLE	FEATURE	DATA SET/ POINT	WEIGHT % CARBONATE					
			Ca	Mg	Sr	Fe	Mn	SUM
BB3aR Lens 2	Lens	25	99.64	0.97	0.00	0.05	0.00	100.66
BB3aR Lens 2	Lens	26	97.52	3.15	0.00	0.11	0.00	100.77
BB3aR Lens 2	Lens	27	98.99	1.17	0.00	0.00	0.00	100.16
BB3aR Lens 2	Lens	28	100.08	0.60	0.00	0.07	0.02	100.77
BB3aR Lens 2	Lens	29	99.88	0.52	0.00	0.05	0.04	100.49
BB3aR Lens 2	Lens	30	99.22	0.72	0.00	0.00	0.01	99.95
BB3aR Lens 2	Lens	31	99.59	0.92	0.00	0.00	0.00	100.52
BB3aR Lens 2	Lens	32	98.22	0.66	0.00	0.00	0.00	98.89
BB3aR Lens 2	Lens	33	98.17	1.25	0.00	0.05	0.00	99.47
BB3aR Lens 2	Lens	34	98.76	1.22	0.00	0.09	0.00	100.07
BB3aR Lens 2	Lens	35	97.53	0.45	0.00	0.02	0.00	98.00
BB3aR Lens 2	Lens	36	86.22	0.39	0.00	0.02	0.00	86.63
BB3aR Lens 2	Lens	37	98.56	0.53	0.00	0.16	0.00	99.25
BB3aR Lens 2	Lens	38	97.78	0.56	0.00	0.09	0.06	98.50
BB3aR Lens 2	Lens	39	91.36	3.69	0.00	0.16	0.10	95.31
BB3aR Lens 2	Lens	40	98.70	0.53	0.00	0.01	0.02	99.26
BB3aR Lens 2	Lens	41	98.91	0.59	0.00	0.00	0.01	99.51
BB3aR Lens 2	Lens	42	98.00	0.94	0.00	0.02	0.04	98.99
BB3aR Lens 2	Lens	43	67.41	32.93	0.00	0.00	0.00	100.35
BB3aR Lens 2	Lens	44	98.80	0.41	0.00	0.00	0.02	99.22
BB3aR Lens 2	Lens	45	98.63	0.60	0.00	0.18	0.09	99.50
BB3aR Lens 2	Lens	46	99.18	0.46	0.00	0.08	0.01	99.73
BB3aR Lens 2	Lens	47	96.96	1.09	0.00	0.00	0.00	98.06
BB3aR Lens 2	Lens	48	100.48	0.66	0.00	0.00	0.00	101.15
BB3aR Lens 2	Lens	49	98.73	1.08	0.00	0.07	0.00	99.88
BB3aR Lens 2	Lens	50	96.78	2.60	0.00	0.00	0.00	99.38
BB3aR Lens 2	Lens	51	98.50	0.66	0.00	0.00	0.00	99.17
BB3aR Lens 2	Lens	52	95.00	4.38	0.00	0.03	0.00	99.40
BB3aR Lens 2	Lens	53	92.96	5.69	0.00	0.03	0.00	98.68
BB3aR Lens 2	Lens	54	97.34	2.41	0.00	0.03	0.00	99.78
BB3aR Lens 2	Lens	55	98.52	0.62	0.00	0.00	0.08	99.23
BB3aR Lens 2	Lens	56	99.08	0.53	0.00	0.00	0.00	99.61
BB3aR Lens 2	Lens	57	96.33	0.44	0.00	0.02	0.00	96.79
BB3aR Lens 2	Lens	58	96.32	0.77	0.00	0.15	0.04	97.28
BB3aR Lens 2	Lens	59	95.08	3.42	0.00	0.00	0.05	98.55
BB3aR Lens 2	Lens	60	98.55	0.85	0.00	0.07	0.08	99.55
BB3aR Lens 2	Lens	61	99.11	0.91	0.00	0.00	0.00	100.01
BB3aR Lens 2	Lens	62	98.32	0.74	0.00	0.01	0.00	99.07
BB3aR Lens 2	Lens	63	88.55	9.47	0.00	0.12	0.03	98.18
BB3aR Lens 2	Lens	64	96.10	1.38	0.00	0.11	0.00	97.58
BB3aR Lens 2	Lens	65	99.18	0.45	0.00	0.12	0.09	99.85
BB3aR Lens 3	Lens	1	96.96	0.73	0.00	0.05	0.00	97.75
BB3aR Lens 3	Lens	2	98.69	0.60	0.00	0.00	0.09	99.38
BB3aR Lens 3	Lens	3	95.57	3.35	0.00	0.10	0.07	99.10
BB3aR Lens 3	Lens	4	95.31	3.84	0.00	0.09	0.04	99.28
BB3aR Lens 3	Lens	5	97.76	0.73	0.00	0.01	0.00	98.50
BB3aR Lens 3	Lens	6	88.76	5.73	0.00	0.00	0.00	94.49
BB3aR Lens 3	Lens	7	96.29	2.54	0.00	0.01	0.04	98.88
BB3aR Lens 3	Lens	8	94.60	0.81	0.00	0.00	0.02	95.44
BB3aR Lens 3	Lens	9	94.91	3.15	0.00	0.00	0.00	98.06
BB3aR Lens 3	Lens	10	91.19	2.29	0.00	0.00	0.02	93.50
BB3aR Lens 3	Lens	11	95.73	3.42	0.00	0.00	0.00	99.15
BB3aR Lens 3	Lens	12	98.72	0.19	0.00	0.02	0.00	98.93
BB3aR Lens 3	Lens	13	96.83	0.55	0.00	0.02	0.00	97.40
BB3aR Lens 3	Lens	14	98.74	0.46	0.00	0.00	0.04	99.25
BB3aR Lens 3	Lens	15	99.14	0.56	0.00	0.04	0.01	99.76
BB3aR Lens 3	Lens	16	98.43	1.32	0.00	0.07	0.04	99.86
BB3aR Lens 3	Lens	17	99.32	0.27	0.00	0.07	0.05	99.70
BB3aR Lens 3	Lens	18	99.80	0.45	0.00	0.07	0.00	100.32
BB3aR Lens 3	Lens	19	97.17	0.50	0.00	0.02	0.06	97.76
BB3aR Lens 3	Lens	20	96.32	0.99	0.00	0.05	0.02	97.38
BB3aR Lens 3	Lens	21	97.78	1.36	0.00	0.04	0.05	99.22

SAMPLE	FEATURE	DATA SET/ POINT	WEIGHT % CARBONATE					
			Ca	Mg	Sr	Fe	Mn	SUM
BB3aR Lens 3	Lens	22	97.06	2.64	0.00	0.07	0.04	99.79
BB3aR Lens 3	Lens	23	93.43	6.67	0.00	0.07	0.05	100.21
BB3aR Lens 3	Lens	24	84.71	0.81	0.00	0.00	0.00	85.52
BB3aR Lens 3	Lens	25	99.22	0.76	0.00	0.01	0.05	100.04
BB3aR Lens 3	Lens	26	93.79	0.82	0.00	0.06	0.00	94.66
BB3aR Lens 3	Lens	27	90.79	0.63	0.00	0.00	0.04	91.45
BB3aR Lens 3	Lens	28	92.65	4.07	0.00	0.04	0.01	96.77
BB3aR Lens 3	Lens	29	97.66	1.87	0.00	0.00	0.09	99.62
BB3aR Lens 3	Lens	30	96.94	0.52	0.00	0.00	0.05	97.51
BB3aR Lens 3	Lens	31	98.10	0.51	0.00	0.00	0.00	98.62
BB3aR Lens 3	Lens	32	97.71	1.41	0.00	0.13	0.00	99.25
BB3aR Lens 3	Lens	33	71.12	18.69	0.00	0.21	0.02	90.04
BB3aR Lens 3	Lens	34	96.05	1.76	0.00	0.07	0.00	97.88
BB3aR Lens 3	Lens	35	94.04	4.26	0.00	0.03	0.00	98.32
BB3aR Lens 3	Lens	36	95.62	2.36	0.00	0.05	0.00	98.02
BB3aR Lens 3	Lens	37	98.41	0.96	0.00	0.00	0.04	99.41
BB3aR Lens 3	Lens	38	96.00	0.54	0.00	1.74	0.08	98.36
BB3aR Lens 3	Lens	39	97.61	0.42	0.00	0.18	0.07	98.28
BB3aR Lens 3	Lens	40	95.50	0.45	0.00	0.02	0.11	96.09
BB3aR Lens 3	Lens	41	93.78	6.26	0.00	0.00	0.04	100.08
BB3aR Lens 3	Lens	42	99.49	0.52	0.00	0.07	0.02	100.10
BB3aR Lens 3	Lens	43	98.77	0.33	0.00	0.00	0.02	99.13
BB3aR Lens 3	Lens	44	98.34	0.61	0.00	0.07	0.05	99.08
BB3aR Lens 3	Lens	45	96.75	0.52	0.00	0.00	0.02	97.29
BB3aR Lens 3	Lens	46	98.21	0.47	0.00	0.09	0.00	98.78
BB3aR Lens 3	Lens	47	98.92	0.54	0.00	0.00	0.00	99.46
BB3aR Lens 3	Lens	48	92.97	0.50	0.00	0.03	0.00	93.50
BB3aR Lens 3	Lens	49	97.13	0.92	0.00	0.02	0.06	98.14
BB3aR Lens 3	Lens	50	97.56	1.23	0.00	0.02	0.00	98.81
BB3aR Lens 3	Lens	51	98.06	0.53	0.00	0.00	0.00	98.59
BB3aR Lens 3	Lens	52	93.85	6.40	0.00	0.12	0.01	100.38
BB3aR Lens 3	Lens	53	98.65	1.26	0.00	0.00	0.07	99.98
BB3aR Lens 3	Lens	54	97.78	3.99	0.00	0.12	0.00	101.88
BB3aR Lens 3	Lens	55	98.17	0.75	0.00	0.00	0.05	98.98
BB3aR Lens 3	Lens	56	76.11	0.50	0.00	0.02	0.02	76.65
BB3aR Lens 3	Lens	57	97.18	0.51	0.00	0.00	0.05	97.74
BB3aR Lens 3	Lens	58	85.09	0.11	0.00	0.10	0.01	85.32
BB3aR Lens 3	Lens	59	99.63	0.48	0.00	0.09	0.00	100.20
BB3aR Lens 3	Lens	60	99.50	0.58	0.00	0.00	0.01	100.09
BB3aR Lens 3	Lens	61	99.96	0.50	0.00	0.03	0.00	100.49
BB3aR Lens 3	Lens	62	99.60	0.43	0.00	0.00	0.05	100.08
BB3aR Lens 3	Lens	63	93.87	0.48	0.00	0.00	0.03	94.38
BB3aR Lens 3	Lens	64	99.56	0.58	0.00	0.00	0.05	100.18
BB3aR Lens 3	Lens	65	99.46	0.64	0.00	0.00	0.00	100.10
BB3aR Lens 3	Lens	66	99.51	0.49	0.00	0.00	0.02	100.02
BB3aR Lens 3	Lens	67	99.94	0.61	0.00	0.02	0.00	100.57
BB3aR Lens 3	Lens	68	93.55	7.26	0.00	0.04	0.00	100.85
BB3aR Lens 3	Lens	69	98.33	2.24	0.00	0.00	0.06	100.63
BB3aR Lens 3	Lens	70	99.37	0.51	0.00	0.00	0.00	99.87
BB3aR	Sclera	1	99.98	0.60	0.00	0.11	0.12	100.81
BB3aR	Sclera	2	98.14	0.63	0.00	0.01	0.01	98.80
BB3aR	Sclera	3	98.05	0.57	0.00	0.10	0.14	98.86
BB3aR	Sclera	4	98.56	0.51	0.00	0.14	0.06	99.27
BB3aR	Sclera	5	97.66	0.39	0.00	0.23	0.07	98.34
BB3aR	Sclera	6	44.02	0.16	0.00	0.07	0.00	44.25
BB3aR	Sclera	7	89.97	0.45	0.00	0.07	0.11	90.61
BB3aR	Sclera	8	86.94	0.38	0.00	0.06	0.03	87.41
BB3aR	Sclera	9	72.92	0.28	0.00	0.42	0.12	73.73
BB3aR	Sclera	10	95.01	0.43	0.00	0.18	0.10	95.71
BB3aR	Sclera	11	100.40	0.48	0.00	0.03	0.09	101.00
BB3aR	Sclera	12	99.76	0.60	0.00	0.07	0.02	100.45
BB3aR	Sclera	13	99.29	0.55	0.00	0.16	0.00	100.00

SAMPLE	FEATURE	DATA SET/ POINT	WEIGHT % CARBONATE					
			Ca	Mg	Sr	Fe	Mn	SUM
BB3aR	Sclera	14	99.94	0.54	0.00	0.02	0.00	100.50
BB3aR	Sclera	15	99.79	0.50	0.00	0.09	0.07	100.44
BB3aR	Sclera	16	99.76	0.40	0.00	0.29	0.08	100.54
BB3aR	Sclera	17	98.31	0.37	0.00	0.18	0.07	98.94
BB3aR	Cement	1	99.48	0.84	0.00	0.07	0.06	100.45
BB3aR	Cement	2	98.91	0.78	0.00	0.00	0.04	99.72
BB3aR	Cement	3	98.70	1.47	0.00	0.11	0.04	100.32
BB3aR	Cement	4	100.07	0.71	0.00	0.12	0.02	100.93
BB3aR	Cement	5	99.19	1.48	0.00	0.01	0.00	100.69
BB3aR	Cement	6	99.65	1.20	0.00	0.07	0.00	100.92
BB3aR	Cement	7	99.75	0.83	0.00	0.00	0.02	100.60
BB3aR	Cement	8	100.23	0.54	0.00	0.00	0.02	100.80
BB3aR	Cement	9	99.27	1.03	0.00	0.04	0.08	100.42
BB3aR	Cement	10	93.78	0.31	0.00	0.04	0.03	94.16
BB3aR	Cement	11	99.31	0.54	0.00	0.05	0.05	99.96
BB3aR	Cement	12	99.00	0.58	0.00	0.07	0.00	99.64
BB3aR	Cement	13	98.94	0.89	0.00	0.03	0.00	99.87
BB3aR	Cement	14	99.35	0.61	0.00	0.00	0.00	99.96
BB3aR	Cement	15	99.51	0.70	0.00	0.00	0.02	100.23
BB3aR	Cement	16	99.61	0.49	0.00	0.00	0.05	100.15
BB3aR	Cement	17	99.98	0.49	0.00	0.00	0.07	100.55
BB3aR	Cement	18	98.53	0.87	0.00	0.00	0.00	99.40
BB3aR	Cement	19	99.87	0.49	0.00	0.00	0.05	100.41
BB3aR	Cement	20	99.92	0.45	0.00	0.00	0.03	100.41
BB3aR	Cement	21	99.56	0.59	0.00	0.00	0.00	100.15
BB3aR	Cement	22	99.41	0.51	0.00	0.00	0.01	99.93
BB3aR	Cement	23	100.04	0.54	0.00	0.14	0.02	100.74
BB3aR	Cement	24	98.90	1.44	0.00	0.01	0.07	100.41
BB3aR	Cement	25	99.35	0.51	0.00	0.04	0.00	99.90
BB3aR	Cement	26	97.93	2.45	0.00	0.05	0.04	100.47
BB3aR	Cement	27	98.87	0.78	0.00	0.08	0.07	99.80
BB3aR	Cement	28	99.28	0.58	0.00	0.08	0.08	100.01
BB3aR	Cement	29	99.04	0.43	0.00	0.00	0.15	99.62
BB3aR	Cement	30	97.41	0.63	0.00	0.11	0.08	98.24
BB3aR	Cement	31	99.34	1.02	0.00	0.00	0.00	100.36
BB3aR	Cement	32	97.79	0.73	0.00	0.04	0.05	98.60
BB3aR	Cement	33	79.74	0.67	0.00	0.00	0.03	80.44
BB3aR	Cement	34	98.51	0.54	0.00	0.00	0.02	99.07
BB3aR	Cement	35	98.93	0.71	0.00	0.06	0.00	99.71
BB3aR	Cement	36	99.03	0.55	0.00	0.00	0.03	99.61
BB3aR	Cement	37	96.07	3.84	0.00	0.12	0.04	100.07
BB3aR	Cement	38	99.63	0.35	0.00	0.21	0.09	100.28
BB3aR	Cement	39	97.22	0.45	0.00	0.02	0.04	97.73
BB3aR	Cement	40	99.99	0.69	0.00	0.00	0.00	100.67
BB3aR	Cement	41	100.50	0.50	0.00	0.09	0.02	101.12
BB3aR	Cement	42	100.19	0.85	0.00	0.00	0.03	101.06
BB3aR	Cement	43	100.47	0.57	0.00	0.04	0.02	101.11
BB3aR	Cement	44	99.80	0.72	0.00	0.05	0.03	100.60
BB3aR	Cement	45	98.96	0.66	0.00	0.04	0.05	99.70
BB3aR	Cement	46	99.68	0.65	0.00	0.09	0.09	100.49
BB3aR	Cement	47	98.71	0.63	0.00	0.01	0.09	99.44
BB3aR	Cement	48	99.81	0.84	0.00	0.02	0.00	100.67
BB3aR	Cement	49	100.76	0.59	0.00	0.00	0.04	101.38
BB3aR	Cement	50	100.25	0.53	0.00	0.05	0.09	100.92
BB3aR	Cement	51	99.33	0.67	0.00	0.01	0.04	100.05
BB3aR	Cement	52	99.79	0.53	0.00	0.11	0.09	100.51
BB3aR	Cement	53	102.75	0.69	0.00	0.11	0.10	103.65
E22B Lens 1	Lens	1	46.74	1.77	0.00	0.00	0.00	48.51
E22B Lens 1	Lens	2	44.42	2.39	0.00	0.00	0.00	46.82
E22B Lens 1	Lens	3	94.41	1.39	0.00	0.00	0.00	95.80
E22B Lens 1	Lens	4	94.24	1.42	0.00	0.00	0.00	95.66

SAMPLE	FEATURE	DATA SET/ POINT	WEIGHT % CARBONATE					
			Ca	Mg	Sr	Fe	Mn	SUM
E22B Lens 1	Lens	5	91.52	1.11	0.00	0.00	0.00	92.63
E22B Lens 1	Lens	6	89.24	0.87	0.00	0.00	0.00	90.11
E22B Lens 1	Lens	7	93.11	1.21	0.00	0.00	0.00	94.33
E22B Lens 1	Lens	8	94.19	1.53	0.00	0.00	0.00	95.71
E22B Lens 1	Lens	9	93.71	1.32	0.00	0.00	0.00	95.03
E22B Lens 1	Lens	10	93.96	1.56	0.00	0.00	0.00	95.52
E22B Lens 1	Lens	11	94.89	1.28	0.00	0.00	0.00	96.17
E22B Lens 1	Lens	12	94.79	1.11	0.00	0.00	0.00	95.90
E22B Lens 1	Lens	13	95.16	0.87	0.00	0.00	0.00	96.03
E22B Lens 1	Lens	14	94.06	1.46	0.00	0.00	0.00	95.52
E22B Lens 1	Lens	15	93.94	1.49	0.00	0.00	0.00	95.43
E22B Lens 1	Lens	16	94.36	1.49	0.00	0.00	0.00	95.85
E22B Lens 1	Lens	17	81.10	0.94	0.00	0.00	0.00	82.04
E22B Lens 1	Lens	18	66.17	1.77	0.00	0.00	0.00	67.94
E22B Lens 1	Lens	19	93.39	0.94	0.00	0.00	0.00	94.32
E22B Lens 1	Lens	20	85.20	1.25	0.00	0.00	0.00	86.45
E22B Lens 1	Lens	21	43.70	2.53	0.00	0.00	0.00	46.23
E22B Lens 1	Lens	22	66.74	1.91	0.00	0.00	0.00	68.65
E22B Lens 1	Lens	23	91.72	1.08	0.00	0.00	0.00	92.79
E22B Lens 1	Lens	24	93.54	1.53	0.00	0.00	0.00	95.06
E22B Lens 1	Lens	25	93.26	1.56	0.00	0.00	0.00	94.82
E22B Lens 1	Lens	26	93.24	2.15	0.00	0.00	0.00	95.39
E22B Lens 1	Lens	27	93.69	1.77	0.00	0.00	0.00	95.46
E22B Lens 1	Lens	28	93.89	1.32	0.00	0.00	0.00	95.21
E22B Lens 1	Lens	29	94.41	1.42	0.00	0.00	0.00	95.83
E22B Lens 1	Lens	30	94.39	1.63	0.00	0.00	0.00	96.02
E22B Lens 1	Lens	31	92.59	1.87	0.00	0.00	0.00	94.46
E22B Lens 1	Lens	32	94.11	1.11	0.00	0.00	0.00	95.22
E22B Lens 1	Lens	33	93.86	1.25	0.00	0.00	0.00	95.11
E22B Lens 1	Lens	34	94.24	1.60	0.00	0.00	0.00	95.83
E22B Lens 1	Lens	35	94.04	1.53	0.00	0.00	0.00	95.56
E22B Lens 1	Lens	36	93.36	1.14	0.00	0.00	0.00	94.51
E22B Lens 1	Lens	37	88.37	0.69	0.00	0.00	0.00	89.06
E22B Lens 1	Lens	38	85.85	0.83	0.00	0.00	0.00	86.68
E22B Lens 1	Lens	39	89.39	1.18	0.00	0.00	0.00	90.57
E22B Lens 1	Lens	40	80.55	1.08	0.00	0.00	0.00	81.63
E22B Lens 1	Lens	41	94.64	0.97	0.00	0.00	0.00	95.61
E22B Lens 1	Lens	42	94.14	0.90	0.00	0.00	0.00	95.04
E22B Lens 1	Lens	43	94.29	0.76	0.00	0.00	0.00	95.05
E22B Lens 1	Lens	44	94.26	1.46	0.00	0.00	0.00	95.72
E22B Lens 1	Lens	45	92.89	2.43	0.00	0.00	0.00	95.32
E22B Lens 1	Lens	46	94.21	1.25	0.00	0.00	0.00	95.46
E22B Lens 1	Lens	47	94.44	1.18	0.00	0.00	0.00	95.62
E22B Lens 1	Lens	48	94.76	1.21	0.00	0.00	0.00	95.98
E22B Lens 1	Lens	49	94.86	0.90	0.00	0.00	0.00	95.76
E22B Lens 1	Lens	50	95.04	0.76	0.00	0.00	0.00	95.80
E22B Lens 1	Lens	51	95.04	0.76	0.00	0.00	0.00	95.80
E22B Lens 1	Lens	52	94.56	1.39	0.00	0.00	0.00	95.95
E22B Lens 1	Lens	53	93.86	1.32	0.00	0.00	0.00	95.18
E22B Lens 1	Lens	54	94.46	1.35	0.00	0.00	0.00	95.81
E22B Lens 1	Lens	55	92.66	1.42	0.00	0.00	0.00	94.09
E22B Lens 1	Lens	56	93.39	1.56	0.00	0.00	0.00	94.95
E22B Lens 1	Lens	57	94.64	0.94	0.00	0.00	0.00	95.57
E22B Lens 1	Lens	58	94.69	0.90	0.00	0.00	0.00	95.59
E22B Lens 1	Lens	59	94.26	1.08	0.00	0.00	0.00	95.34
E22B Lens 1	Lens	60	94.46	1.18	0.00	0.00	0.00	95.64
E22B Lens 2	Lens	1	0.15	0.00	0.00	0.00	0.00	0.15
E22B Lens 2	Lens	2	0.27	0.00	0.00	0.00	0.00	0.27
E22B Lens 2	Lens	3	94.41	1.39	0.00	0.00	0.00	95.80
E22B Lens 2	Lens	4	93.71	1.80	0.00	0.00	0.00	95.52
E22B Lens 2	Lens	5	93.61	1.49	0.00	0.00	0.00	95.10
E22B Lens 2	Lens	6	93.84	1.11	0.00	0.00	0.00	94.95

SAMPLE	FEATURE	DATA SET/ POINT	WEIGHT % CARBONATE					
			Ca	Mg	Sr	Fe	Mn	SUM
E22B Lens 2	Lens	7	93.44	1.25	0.00	0.00	0.00	94.69
E22B Lens 2	Lens	8	84.07	1.49	0.00	0.00	0.00	85.57
E22B Lens 2	Lens	9	94.56	1.32	0.00	0.00	0.00	95.88
E22B Lens 2	Lens	10	93.51	1.49	0.00	0.00	0.00	95.00
E22B Lens 2	Lens	11	94.76	1.56	0.00	0.00	0.00	96.32
G33R Lens 1	Lens	1	74.13	1.83	0.00	0.00	0.00	75.97
G33R Lens 1	Lens	2	54.48	1.86	0.00	0.00	0.00	56.34
G33R Lens 1	Lens	3	84.37	0.83	0.00	0.00	0.00	85.20
G33R Lens 1	Lens	4	90.27	2.83	0.00	0.00	0.00	93.10
G33R Lens 1	Lens	5	90.67	1.23	0.00	0.00	0.00	91.90
G33R Lens 1	Lens	6	91.06	1.53	0.00	0.00	0.00	92.59
G33R Lens 1	Lens	7	90.79	0.91	0.00	0.00	0.00	91.70
G33R Lens 1	Lens	8	88.90	3.60	0.00	0.00	0.00	92.49
G33R Lens 1	Lens	9	86.79	7.24	0.00	0.00	0.00	94.02
G33R Lens 1	Lens	10	90.96	1.55	0.00	0.00	0.00	92.51
G33R Lens 1	Lens	11	86.72	4.02	0.00	0.00	0.00	90.73
G33R Lens 1	Lens	12	90.54	1.66	0.00	0.00	0.00	92.20
G33R Lens 1	Lens	13	90.60	1.40	0.00	0.00	0.00	92.00
G33R Lens 1	Lens	14	91.84	1.07	0.00	0.00	0.00	92.91
G33R Lens 1	Lens	15	90.82	1.62	0.00	0.00	0.00	92.44
G33R Lens 1	Lens	16	90.65	1.82	0.00	0.00	0.00	92.47
G33R Lens 1	Lens	17	90.13	1.54	0.00	0.00	0.00	91.67
G33R Lens 1	Lens	18	88.73	2.27	0.00	0.00	0.00	91.00
G33R Lens 1	Lens	19	89.78	1.65	0.00	0.00	0.00	91.44
G33R Lens 1	Lens	20	90.44	2.15	0.00	0.00	0.00	92.60
G33R Lens 1	Lens	21	89.32	2.26	0.00	0.00	0.00	91.58
G33R Lens 1	Lens	22	90.28	1.70	0.00	0.00	0.00	91.98
G33R Lens 1	Lens	23	87.82	1.51	0.00	0.00	0.00	89.33
G33R Lens 1	Lens	24	72.85	2.23	0.00	0.00	0.00	75.09
G33R Lens 1	Lens	25	87.97	1.12	0.00	0.00	0.00	89.09
G33R Lens 1	Lens	26	89.76	1.03	0.00	0.00	0.00	90.79
G33R Lens 1	Lens	27	90.07	1.06	0.00	0.00	0.00	91.12
G33R Lens 1	Lens	28	89.50	1.36	0.00	0.00	0.00	90.85
G33R Lens 1	Lens	29	88.82	1.59	0.00	0.00	0.00	90.41
G33R Lens 1	Lens	30	85.07	1.82	0.00	0.00	0.00	86.89
G33R Lens 1	Lens	31	86.15	1.51	0.00	0.00	0.00	87.66
G33R Lens 1	Lens	32	66.00	2.85	0.00	0.00	0.00	68.85
G33R Lens 1	Lens	33	80.18	1.69	0.00	0.00	0.00	81.87
G33R Lens 1	Lens	34	11.30	0.96	0.00	0.00	0.00	12.26
G33R Lens 1	Lens	35	26.40	1.78	0.00	0.00	0.00	28.17
G33R Lens 1	Lens	36	74.13	1.83	0.00	0.00	0.00	75.97
G33R Lens 1	Lens	37	54.48	1.86	0.00	0.00	0.00	56.34
G33R Lens 1	Lens	38	84.37	0.83	0.00	0.00	0.00	85.20
G33R Lens 1	Lens	39	90.27	2.83	0.00	0.00	0.00	93.10
G33R Lens 1	Lens	40	90.67	1.23	0.00	0.00	0.00	91.90
G33R Lens 1	Lens	41	91.06	1.53	0.00	0.00	0.00	92.59
G33R Lens 1	Lens	42	90.79	0.91	0.00	0.00	0.00	91.70
G33R Lens 1	Lens	43	88.90	3.60	0.00	0.00	0.00	92.49
G33R Lens 1	Lens	44	86.79	7.24	0.00	0.00	0.00	94.02
G33R Lens 1	Lens	45	90.96	1.55	0.00	0.00	0.00	92.51
G33R Lens 1	Lens	46	86.72	4.02	0.00	0.00	0.00	90.73
G33R Lens 1	Lens	47	90.54	1.66	0.00	0.00	0.00	92.20
G33R Lens 1	Lens	48	90.60	1.40	0.00	0.00	0.00	92.00
G33R Lens 1	Lens	49	91.84	1.07	0.00	0.00	0.00	92.91
G33R Lens 1	Lens	50	90.82	1.62	0.00	0.00	0.00	92.44
G33R Lens 1	Lens	51	90.65	1.82	0.00	0.00	0.00	92.47
G33R Lens 1	Lens	52	90.13	1.54	0.00	0.00	0.00	91.67
G33R Lens 1	Lens	53	88.73	2.27	0.00	0.00	0.00	91.00
G33R Lens 1	Lens	54	89.78	1.65	0.00	0.00	0.00	91.44
G33R Lens 1	Lens	55	90.44	2.15	0.00	0.00	0.00	92.60
G33R Lens 1	Lens	56	89.32	2.26	0.00	0.00	0.00	91.58
G33R Lens 1	Lens	57	90.28	1.70	0.00	0.00	0.00	91.98

SAMPLE	FEATURE	DATA SET/ POINT	WEIGHT % CARBONATE					
			Ca	Mg	Sr	Fe	Mn	SUM
G33R Lens 1	Lens	58	87.82	1.51	0.00	0.00	0.00	89.33
G33R Lens 1	Lens	59	72.85	2.23	0.00	0.00	0.00	75.09
G33R Lens 1	Lens	60	87.97	1.12	0.00	0.00	0.00	89.09
G33R Lens 1	Lens	61	89.76	1.03	0.00	0.00	0.00	90.79
G33R Lens 1	Lens	62	90.07	1.06	0.00	0.00	0.00	91.12
G33R Lens 1	Lens	63	89.50	1.36	0.00	0.00	0.00	90.85
G33R Lens 1	Lens	64	88.82	1.59	0.00	0.00	0.00	90.41
G33R Lens 1	Lens	65	85.07	1.82	0.00	0.00	0.00	86.89
G33R Lens 1	Lens	66	86.15	1.51	0.00	0.00	0.00	87.66
G33R Lens 1	Lens	67	66.00	2.85	0.00	0.00	0.00	68.85
G33R Lens 1	Lens	68	80.18	1.69	0.00	0.00	0.00	81.87
G33R Lens 1	Lens	69	69.60	1.27	0.00	0.00	0.00	70.86
G33R Lens 1	Lens	70	90.06	1.16	0.00	0.00	0.00	91.21
G33R Lens 1	Lens	71	90.76	1.03	0.00	0.00	0.00	91.79
G33R Lens 1	Lens	72	90.69	1.27	0.00	0.00	0.00	91.95
G33R Lens 1	Lens	73	90.44	1.01	0.00	0.00	0.00	91.45
G33R Lens 1	Lens	74	91.11	1.34	0.00	0.00	0.00	92.45
G33R Lens 1	Lens	75	90.66	1.27	0.00	0.00	0.00	91.93
G33R Lens 1	Lens	76	91.08	1.99	0.00	0.00	0.00	93.07
G33R Lens 1	Lens	77	91.36	1.37	0.00	0.00	0.00	92.73
G33R Lens 1	Lens	78	89.30	1.22	0.00	0.00	0.00	90.52
G33R Lens 1	Lens	79	91.49	1.54	0.00	0.00	0.00	93.03
G33R Lens 1	Lens	80	89.91	2.27	0.00	0.00	0.00	92.17
G33R Lens 1	Lens	81	90.21	1.67	0.00	0.00	0.00	91.88
G33R Lens 1	Lens	82	89.26	2.47	0.00	0.00	0.00	91.73
G33R Lens 1	Lens	83	90.55	1.63	0.00	0.00	0.00	92.18
G33R Lens 1	Lens	84	91.31	2.18	0.00	0.00	0.00	93.49
G33R Lens 1	Lens	85	90.09	2.30	0.00	0.00	0.00	92.39
G33R Lens 1	Lens	86	90.20	2.33	0.00	0.00	0.00	92.53
G33R Lens 1	Lens	87	91.15	1.79	0.00	0.00	0.00	92.94
G33R Lens 1	Lens	88	89.79	3.84	0.00	0.00	0.00	93.62
G33R Lens 1	Lens	89	89.78	1.55	0.00	0.00	0.00	91.33
G33R Lens 1	Lens	90	87.81	1.93	0.00	0.00	0.00	89.73
G33R Lens 1	Lens	91	87.65	1.34	0.00	0.00	0.00	88.99
G33R Lens 1	Lens	92	89.85	1.96	0.00	0.00	0.00	91.81
G33R Lens 1	Lens	93	91.41	2.00	0.00	0.00	0.00	93.41
G33R Lens 1	Lens	94	89.80	1.30	0.00	0.00	0.00	91.11
G33R Lens 1	Lens	95	91.01	1.50	0.00	0.00	0.00	92.52
G33R Lens 1	Lens	96	90.97	1.44	0.00	0.00	0.00	92.40
G33R Lens 1	Lens	97	91.20	1.46	0.00	0.00	0.00	92.65
G33R Lens 1	Lens	98	91.41	1.16	0.00	0.00	0.00	92.57
G33R Lens 1	Lens	99	90.71	1.11	0.00	0.00	0.00	91.82
G33R Lens 1	Lens	100	90.67	1.26	0.00	0.00	0.00	91.93
G33R Lens 1	Lens	101	90.38	1.34	0.00	0.00	0.00	91.72
G33R Lens 1	Lens	102	91.28	1.39	0.00	0.00	0.00	92.67
G33R Lens 1	Lens	103	91.60	1.42	0.00	0.00	0.00	93.02
G42R Lens 1 Traverse 1	Lens	1	100.27	1.49	0.26	0.28	0.00	102.30
G42R Lens 1 Traverse 1	Lens	2	100.34	1.38	0.28	0.27	0.04	102.32
G42R Lens 1 Traverse 1	Lens	3	97.41	1.44	0.29	0.27	0.10	99.50
G42R Lens 1 Traverse 1	Lens	4	93.63	1.03	0.31	0.32	0.02	95.32
G42R Lens 1 Traverse 1	Lens	5	95.68	1.12	0.34	0.27	0.02	97.43
G42R Lens 1 Traverse 1	Lens	6	95.30	1.23	0.35	0.38	0.00	97.26
G42R Lens 1 Traverse 1	Lens	7	98.96	1.26	0.42	0.21	0.07	100.92
G42R Lens 1 Traverse 1	Lens	8	97.97	1.69	0.35	0.24	0.08	100.32
G42R Lens 1 Traverse 1	Lens	9	96.04	2.40	0.27	0.43	0.02	99.17
G42R Lens 1 Traverse 1	Lens	10	96.83	3.04	0.35	0.27	0.05	100.53
G42R Lens 1 Traverse 1	Lens	11	95.26	3.85	0.34	0.37	0.11	99.92
G42R Lens 1 Traverse 1	Lens	12	96.78	1.74	0.30	0.33	0.00	99.15
G42R Lens 1 Traverse 1	Lens	13	97.38	1.22	0.36	0.16	0.08	99.20
G42R Lens 1 Traverse 1	Lens	14	95.67	2.72	0.27	0.32	0.19	99.17
G42R Lens 1 Traverse 1	Lens	15	98.11	1.17	0.31	0.32	0.11	100.01
G42R Lens 1 Traverse 1	Lens	16	96.94	1.70	0.39	0.15	0.11	99.29

SAMPLE	FEATURE	DATA SET/ POINT	WEIGHT % CARBONATE					
			Ca	Mg	Sr	Fe	Mn	SUM
G42R Lens 1 Traverse 1	Lens	17	94.43	4.90	0.32	0.31	0.12	100.08
G42R Lens 1 Traverse 1	Lens	18	94.53	3.37	0.30	0.55	0.02	98.77
G42R Lens 1 Traverse 1	Lens	19	86.55	2.82	0.26	0.31	0.01	89.95
G42R Lens 1 Traverse 1	Lens	20	96.97	2.75	0.33	0.38	0.01	100.44
G42R Lens 1 Traverse 1	Lens	21	97.40	1.26	0.23	0.20	0.02	99.11
G42R Lens 1 Traverse 1	Lens	22	96.04	2.56	0.28	0.26	0.06	99.20
G42R Lens 1 Traverse 1	Lens	23	100.33	1.42	0.36	0.21	0.06	102.38
G42R Lens 1 Traverse 1	Lens	24	95.52	1.60	0.32	0.36	0.00	97.79
G42R Lens 1 Traverse 1	Lens	25	98.23	1.23	0.35	0.22	0.08	100.11
G42R Lens 1 Traverse 1	Lens	26	98.70	1.27	0.32	0.29	0.00	100.58
G42R Lens 1 Traverse 1	Lens	27	96.07	1.22	0.38	0.29	0.02	97.99
G42R Lens 1 Traverse 1	Lens	28	97.50	1.48	0.33	0.32	0.04	99.66
G42R Lens 1 Traverse 1	Lens	29	97.97	1.36	0.36	0.24	0.04	99.96
G42R Lens 1 Traverse 1	Lens	30	98.75	1.47	0.35	0.36	0.03	100.96
G42R Lens 1 Traverse 2	Lens	1	97.02	2.06	0.33	0.18	0.05	99.65
G42R Lens 1 Traverse 2	Lens	2	96.02	3.83	0.30	0.41	0.13	100.70
G42R Lens 1 Traverse 2	Lens	3	100.17	1.07	0.23	0.27	0.03	101.76
G42R Lens 1 Traverse 2	Lens	4	94.82	2.39	0.23	0.44	0.01	97.89
G42R Lens 1 Traverse 2	Lens	5	52.25	10.67	0.27	0.97	0.12	64.28
G42R Lens 1 Traverse 2	Lens	6	96.88	1.19	0.30	0.29	0.06	98.72
G42R Lens 1 Traverse 2	Lens	7	100.39	1.13	0.33	0.28	0.06	102.20
G42R Lens 1 Traverse 2	Lens	8	97.15	2.98	0.32	0.24	0.01	100.70
G42R Lens 1 Traverse 2	Lens	9	98.76	1.33	0.48	0.23	0.08	100.87
G42R Lens 1 Traverse 2	Lens	10	96.01	3.10	0.35	0.42	0.12	100.00
G42R Lens 1 Traverse 2	Lens	11	101.06	1.20	0.38	0.29	0.03	102.96
G42R Lens 1 Traverse 2	Lens	12	98.91	2.33	0.28	0.15	0.11	101.78
G42R Lens 1 Traverse 2	Lens	13	95.82	2.28	0.33	0.26	0.11	98.80
G42R Lens 1 Traverse 2	Lens	14	95.14	3.34	0.29	0.31	0.05	99.13
G42R Lens 1 Traverse 2	Lens	15	95.98	2.51	0.31	0.16	0.05	99.01
G42R Lens 3 Traverse 1	Lens	1	99.12	1.62	0.38	0.25	0.03	101.40
G42R Lens 3 Traverse 1	Lens	2	100.61	1.44	0.36	0.43	0.09	102.93
G42R Lens 3 Traverse 1	Lens	3	94.97	1.28	0.34	0.27	0.03	96.88
G42R Lens 3 Traverse 1	Lens	4	96.10	1.36	0.27	0.28	0.03	98.05
G42R Lens 3 Traverse 1	Lens	5	100.44	1.39	0.42	0.22	0.09	102.57
G42R Lens 3 Traverse 1	Lens	6	100.01	1.69	0.32	0.23	0.10	102.34
G42R Lens 3 Traverse 1	Lens	7	99.33	1.75	0.30	0.22	0.00	101.61
G42R Lens 3 Traverse 1	Lens	8	99.30	1.81	0.38	0.30	0.08	101.87
G42R Lens 3 Traverse 1	Lens	9	99.60	1.81	0.32	0.30	0.00	102.03
G42R Lens 3 Traverse 1	Lens	10	98.44	1.55	0.30	0.31	0.08	100.69
G42R Lens 3 Traverse 1	Lens	11	98.62	1.87	0.35	0.26	0.13	101.23
G42R Lens 3 Traverse 1	Lens	12	99.35	1.28	0.51	0.26	0.01	101.41
G42R Lens 3 Traverse 1	Lens	13	100.05	0.94	0.63	0.19	0.01	101.83
G42R Lens 3 Traverse 1	Lens	14	99.73	1.77	0.26	0.17	0.02	101.95
G42R Lens 3 Traverse 1	Lens	15	100.03	1.65	0.34	0.31	0.04	102.37
G42R Lens 3 Traverse 1	Lens	16	100.23	1.37	0.37	0.18	0.05	102.21
G42R Lens 3 Traverse 1	Lens	17	99.46	1.62	0.40	0.30	0.13	101.92
G42R Lens 3 Traverse 1	Lens	18	99.20	2.11	0.36	0.17	0.08	101.92
G42R Lens 3 Traverse 1	Lens	19	99.56	1.76	0.34	0.34	0.11	102.11
G42R Lens 3 Traverse 1	Lens	20	99.46	1.60	0.45	0.25	0.14	101.90
G42R Lens 3 Traverse 1	Lens	21	99.78	1.93	0.35	0.27	0.01	102.34
G42R Lens 3 Traverse 1	Lens	22	99.41	1.27	0.36	0.30	0.05	101.39
G42R Lens 3 Traverse 1	Lens	23	95.96	1.15	0.34	0.40	0.03	97.88
G42R Lens 3 Traverse 1	Lens	24	96.12	1.40	0.32	0.37	0.04	98.25
G42R Lens 3 Traverse 1	Lens	25	96.52	1.40	0.35	0.29	0.00	98.57
G42R Lens 3 Traverse 2	Lens	1	85.87	1.81	0.32	0.29	0.04	88.33
G42R Lens 3 Traverse 2	Lens	2	88.14	1.61	0.34	0.23	0.00	90.32
G42R Lens 3 Traverse 2	Lens	3	96.28	1.27	0.30	0.37	0.00	98.21
G42R Lens 3 Traverse 2	Lens	4	98.34	1.21	0.29	0.36	0.07	100.28
G42R Lens 3 Traverse 2	Lens	5	98.23	1.58	0.42	0.30	0.00	100.53
G42R Lens 3 Traverse 2	Lens	6	86.32	1.92	0.34	0.29	0.00	88.87

SAMPLE	FEATURE	DATA SET/ POINT	WEIGHT % CARBONATE					
			Ca	Mg	Sr	Fe	Mn	SUM
G42R Lens 3 Traverse 2	Lens	7	85.51	1.80	0.30	0.27	0.00	87.87
G42R Lens 3 Traverse 2	Lens	8	91.99	1.81	0.41	0.33	0.04	94.58
G42R Lens 3 Traverse 2	Lens	9	88.83	1.92	0.36	0.21	0.00	91.33
G42R Lens 3 Traverse 2	Lens	10	100.88	1.59	0.35	0.25	0.13	103.20
G42R Lens 3 Traverse 2	Lens	11	99.94	2.29	0.35	0.25	0.13	102.96
G42R Lens 3 Traverse 2	Lens	12	96.51	1.49	0.52	0.11	0.00	98.63
G42R Lens 3 Traverse 2	Lens	13	91.49	1.29	0.62	0.23	0.00	93.64
G42R Lens 3 Traverse 2	Lens	14	102.36	1.87	0.22	0.24	0.10	104.78
G42R Lens 3 Traverse 2	Lens	15	92.10	1.78	0.31	0.20	0.11	94.50
G42R Lens 3 Traverse 2	Lens	16	89.02	1.38	0.35	0.09	0.08	90.92
G42R Lens 3 Traverse 2	Lens	17	94.38	1.97	0.35	0.32	0.05	97.07
G42R Lens 3 Traverse 2	Lens	18	90.11	2.16	0.37	0.27	0.00	92.91
G42R Lens 3 Traverse 2	Lens	19	80.81	1.81	0.36	0.23	0.08	83.29
G42R Lens 3 Traverse 2	Lens	20	84.78	1.65	0.41	0.14	0.08	87.04
G42R Lens 3 Traverse 2	Lens	21	87.27	2.03	0.32	0.22	0.05	89.87
G42R Lens 3 Traverse 2	Lens	22	88.67	1.40	0.42	0.21	0.00	90.70
G42R Lens 3 Traverse 2	Lens	23	97.41	1.05	0.30	0.44	0.10	99.30
G42R Lens 3 Traverse 2	Lens	24	100.33	1.51	0.37	0.23	0.03	102.47
G42R Lens 3 Traverse 2	Lens	25	100.45	1.45	0.35	0.29	0.07	102.61
G42R Lens 2 Traverse 1	Lens	1	97.55	1.02	0.43	0.18	0.10	99.28
G42R Lens 2 Traverse 1	Lens	2	98.01	1.31	0.29	0.18	0.00	99.79
G42R Lens 2 Traverse 1	Lens	3	94.87	4.26	0.35	0.48	0.00	99.97
G42R Lens 2 Traverse 1	Lens	4	91.77	1.87	0.31	0.40	0.13	94.49
G42R Lens 2 Traverse 1	Lens	5	98.00	1.58	0.29	0.32	0.14	100.32
G42R Lens 2 Traverse 1	Lens	6	98.82	1.25	0.32	0.21	0.10	100.70
G42R Lens 2 Traverse 1	Lens	7	96.49	1.57	0.42	0.23	0.00	98.72
G42R Lens 2 Traverse 1	Lens	8	100.49	1.67	0.27	0.25	0.04	102.72
G42R Lens 2 Traverse 1	Lens	9	81.18	1.70	0.29	0.23	0.01	83.42
G42R Lens 2 Traverse 1	Lens	10	81.85	1.64	0.26	0.25	0.07	84.07
G42R Lens 2 Traverse 1	Lens	11	98.80	1.21	0.64	0.15	0.00	100.80
G42R Lens 2 Traverse 1	Lens	12	100.75	1.67	0.48	0.24	0.08	103.23
G42R Lens 2 Traverse 1	Lens	13	100.84	1.26	0.46	0.27	0.09	102.92
G42R Lens 2 Traverse 1	Lens	14	101.16	1.62	0.33	0.25	0.04	103.40
G42R Lens 2 Traverse 1	Lens	15	102.12	1.34	0.52	0.19	0.02	104.18
G42R Lens 2 Traverse 1	Lens	16	101.45	1.35	0.51	0.24	0.00	103.56
G42R Lens 2 Traverse 1	Lens	17	94.18	1.42	0.37	0.40	0.07	96.44
G42R Lens 2 Traverse 1	Lens	18	88.48	2.06	0.25	2.41	0.02	93.23
G42R Lens 2 Traverse 1	Lens	19	91.66	1.65	0.28	0.69	0.12	94.39
G42R Lens 2 Traverse 1	Lens	20	87.23	1.78	0.19	1.02	0.04	90.25
G42R Lens 2 Traverse 1	Lens	21	85.06	2.01	0.16	0.90	0.06	88.18
G42R Lens 2 Traverse 1	Lens	22	47.75	2.38	0.07	1.30	0.06	51.56
G42R Lens 2 Traverse 1	Lens	23	89.29	3.65	0.23	1.99	0.12	95.28
G42R Lens 2 Traverse 1	Lens	24	84.78	1.16	0.24	0.43	0.00	86.60
G42R Lens 2 Traverse 1	Lens	25	13.24	2.02	0.00	2.08	0.11	17.44
G42R Lens 2 Traverse 1	Lens	26	97.82	2.79	0.31	0.34	0.06	101.32
G42R Lens 2 Traverse 1	Lens	27	99.03	1.68	0.37	0.18	0.09	101.35
G42R Lens 2 Traverse 1	Lens	28	94.86	4.06	0.34	0.35	0.00	99.61
G42R Lens 2 Traverse 1	Lens	29	98.46	0.90	0.29	0.10	0.04	99.78
G42R Lens 2 Traverse 1	Lens	30	97.23	3.04	0.26	0.43	0.11	101.06
G42R	Sclera	1	101.43	1.16	0.35	0.14	0.01	103.09
G42R	Sclera	2	97.98	2.74	0.35	0.28	0.10	101.44
G42R	Sclera	3	100.62	1.37	0.38	0.30	0.06	102.74
G42R	Sclera	4	100.60	1.80	0.38	0.27	0.03	103.07
G42R	Sclera	5	100.85	1.20	0.60	0.14	0.00	102.79
G42R	Sclera	6	101.41	1.45	0.48	0.13	0.05	103.52
G42R	Sclera	7	100.03	1.82	0.49	0.21	0.00	102.54
G42R	Sclera	8	100.66	1.80	0.32	0.23	0.00	103.01
G42R	Sclera	9	101.88	1.60	0.43	0.16	0.05	104.11
G42R	Sclera	10	101.20	1.55	0.41	0.32	0.05	103.53
G42R	Sclera	11	99.57	2.19	0.51	0.27	0.08	102.61
G42R	Sclera	12	101.31	1.52	0.46	0.28	0.00	103.56

SAMPLE	FEATURE	DATA SET/ POINT	WEIGHT % CARBONATE					
			Ca	Mg	Sr	Fe	Mn	SUM
G42R	Sclera	13	100.86	1.68	0.35	0.20	0.06	103.15
G42R	Sclera	14	97.98	1.53	0.31	0.48	0.05	100.35
G42R	Sclera	15	91.41	1.91	0.15	0.88	0.03	94.38
G42R	Sclera	16	88.73	2.38	0.21	1.39	0.00	92.72
G42R	Sclera	17	96.42	1.70	0.29	0.53	0.05	98.98
G42R	Sclera	18	93.28	1.55	0.29	0.55	0.08	95.74
G42R	Sclera	19	83.17	1.98	0.14	0.98	0.02	86.29
G42R	Sclera	20	60.84	4.98	0.05	6.06	0.09	72.02
G42R	Sclera	21	89.94	2.02	0.14	1.02	0.08	93.21
G42R	Sclera	22	91.65	1.67	0.24	0.60	0.03	94.18
G42R	Sclera	23	85.55	2.49	0.22	1.85	0.09	90.21
G42R	Sclera	24	66.88	0.80	0.21	0.41	0.00	68.30
G42R	Sclera	25	86.97	1.11	0.29	0.32	0.14	88.82
G42R	Crinoid	1	93.69	2.37	0.27	0.28	0.00	96.62
G42R	Crinoid	2	92.42	1.75	0.36	0.44	0.06	95.02
G42R	Crinoid	3	93.73	3.43	0.32	0.27	0.00	97.75
G42R	Crinoid	4	74.84	2.77	0.14	1.56	0.01	79.32
G42R	Crinoid	5	94.12	1.85	0.29	0.32	0.05	96.63
G42R	Crinoid	6	90.29	1.82	0.25	0.66	0.11	93.13
G42R	Crinoid	7	92.91	1.53	0.25	0.18	0.01	94.88
G42R	Crinoid	8	93.09	1.65	0.25	0.47	0.08	95.55
G42R	Crinoid	9	82.59	1.52	0.17	0.37	0.04	84.70
G42R	Crinoid	10	96.34	1.72	0.32	0.29	0.15	98.81
G42R	Crinoid	11	93.15	1.71	0.22	0.24	0.11	95.43
G42R	Crinoid	12	95.50	1.55	0.28	0.25	0.00	97.57
G42R	Crinoid	13	96.07	2.01	0.41	0.33	0.05	98.87
G42R	Crinoid	14	86.11	1.75	0.24	0.76	0.09	88.95
G42R	Crinoid	15	85.85	1.43	0.22	0.42	0.05	87.97
G42R	Crinoid	16	95.57	1.96	0.30	0.33	0.00	98.16
G42R	Crinoid	17	96.12	1.95	0.19	0.31	0.05	98.61
G42R	Crinoid	18	90.15	1.82	0.29	0.61	0.02	92.89
G42R	Crinoid	19	87.05	2.23	0.27	0.83	0.13	90.51
G42R	Crinoid	20	94.08	1.75	0.28	0.40	0.04	96.55
G42R	Crinoid	21	91.14	1.55	0.24	0.57	0.08	93.57
G42R	Crinoid	22	92.47	1.84	0.28	0.52	0.00	95.13
G42R	Crinoid	23	98.42	1.35	0.40	0.34	0.13	100.64
G42R	Crinoid	24	96.26	1.59	0.34	0.26	0.00	98.45
G42R	Crinoid	25	90.28	2.98	0.27	0.45	0.01	93.99
PM28 (Lens 1)	Lens	1	88.61	2.21	0.00	3.47	0.10	94.39
PM28 (Lens 1)	Lens	2	86.92	8.19	0.00	0.31	0.00	95.42
PM28 (Lens 1)	Lens	3	91.83	5.04	0.00	0.39	0.01	97.27
PM28 (Lens 1)	Lens	4	90.79	6.61	0.00	0.03	0.00	97.44
PM28 (Lens 1)	Lens	5	90.76	6.48	0.00	0.09	0.06	97.38
PM28 (Lens 1)	Lens	6	90.19	7.00	0.00	0.05	0.07	97.31
PM28 (Lens 1)	Lens	7	89.74	6.22	0.00	0.00	0.03	96.00
PM28 (Lens 1)	Lens	8	86.61	9.16	0.00	0.09	0.03	95.89
PM28 (Lens 1)	Lens	9	90.76	6.69	0.00	0.03	0.04	97.52
PM28 (Lens 1)	Lens	10	86.31	8.11	0.00	0.10	0.05	94.58
PM28 (Lens 1)	Lens	11	90.56	5.14	0.00	0.00	0.00	95.70
PM28 (Lens 1)	Lens	12	89.77	6.69	0.00	0.11	0.00	96.57
PM28 (Lens 1)	Lens	13	89.99	5.74	0.00	0.65	0.00	96.38
PM28 (Lens 1)	Bowl?	14	92.88	0.82	0.00	2.49	0.00	96.18
PM28 (Lens 1)	Bowl?	15	93.30	0.83	0.00	2.56	0.09	96.77
PM28 Lens 1 (traverse 2)	Lens	1	94.34	0.88	0.00	3.09	0.14	98.45
PM28 Lens 1 (traverse 2)	Lens	2	94.12	0.88	0.00	2.43	0.16	97.59
PM28 Lens 1 (traverse 2)	Lens	3	91.85	5.85	0.00	0.61	0.06	98.37
PM28 Lens 1 (traverse 2)	Lens	4	91.29	6.66	0.00	0.02	0.03	97.99
PM28 Lens 1 (traverse 2)	Lens	5	91.63	5.02	0.00	0.00	0.07	96.73
PM28 Lens 1 (traverse 2)	Lens	6	87.25	7.90	0.00	0.03	0.09	95.26
PM28 Lens 1 (traverse 2)	Lens	7	91.83	7.03	0.00	0.03	0.00	98.90

SAMPLE	FEATURE	DATA SET/ POINT	WEIGHT % CARBONATE					
			Ca	Mg	Sr	Fe	Mn	SUM
PM28 Lens 1 (traverse 2)	Lens	8	87.02	9.03	0.00	0.06	0.01	96.13
PM28 Lens 1 (traverse 2)	Lens	9	90.35	6.20	0.00	0.11	0.00	96.66
PM28 Lens 1 (traverse 2)	Lens	10	90.64	7.11	0.00	0.03	0.01	97.78
PM28 Lens 1 (traverse 2)	Lens	11	91.55	6.49	0.00	0.10	0.03	98.16
PM28 Lens 1 (traverse 2)	Lens	12	91.46	6.78	0.00	0.08	0.00	98.33
PM28 Lens 1 (traverse 2)	Lens	13	92.51	4.97	0.00	0.43	0.02	97.93
PM28 Lens 1 (traverse 2)	Lens	14	87.79	8.25	0.00	0.41	0.00	96.46
PM28 Lens 1 (traverse 2)	Lens	15	89.64	2.36	0.00	3.36	0.10	95.46
PM28 Lens 2 (traverse 1)	Lens	1	89.35	4.73	0.00	0.00	0.04	94.13
PM28 Lens 2 (traverse 1)	Lens	2	90.25	6.48	0.00	0.12	0.07	96.93
PM28 Lens 2 (traverse 1)	Lens	3	91.76	6.15	0.00	0.08	0.08	98.07
PM28 Lens 2 (traverse 1)	Lens	4	88.72	8.61	0.00	0.00	0.12	97.44
PM28 Lens 2 (traverse 1)	Lens	5	91.00	6.23	0.00	0.00	0.00	97.23
PM28 Lens 2 (traverse 1)	Lens	6	87.57	7.85	0.00	0.02	0.05	95.48
PM28 Lens 2 (traverse 1)	Lens	7	91.26	7.61	0.00	0.03	0.00	98.90
PM28 Lens 2 (traverse 1)	Lens	8	87.84	9.47	0.00	0.03	0.02	97.36
PM28 Lens 2 (traverse 1)	Lens	9	91.71	6.25	0.00	0.00	0.05	98.01
PM28 Lens 2 (traverse 1)	Lens	10	89.86	7.70	0.00	0.05	0.03	97.64
PM28 Lens 2 (traverse 1)	Lens	11	89.11	7.64	0.00	0.15	0.07	96.97
PM28 Lens 2 (traverse 1)	Lens	12	91.60	3.49	0.00	1.90	0.10	97.08
PM28 Lens 2 (traverse 1)	Lens	13	95.17	0.72	0.00	2.23	0.04	98.17
PM28 Lens 2 (traverse 1)	Lens	14	76.05	1.42	0.00	4.81	0.18	82.47
PM28 Lens 2 (traverse 1)	Lens	15	21.74	8.21	0.00	30.44	0.00	60.40
PM28 Lens 2 (traverse 2)	Lens	1	92.53	1.05	0.00	2.40	0.09	96.07
PM28 Lens 2 (traverse 2)	Lens	2	92.98	1.67	0.00	2.48	0.15	97.28
PM28 Lens 2 (traverse 2)	Lens	3	89.34	5.69	0.00	0.66	0.14	95.83
PM28 Lens 2 (traverse 2)	Lens	4	93.57	4.77	0.00	0.29	0.00	98.64
PM28 Lens 2 (traverse 2)	Lens	5	90.37	6.65	0.00	0.22	0.08	97.32
PM28 Lens 2 (traverse 2)	Lens	6	90.73	6.47	0.00	0.05	0.02	97.26
PM28 Lens 2 (traverse 2)	Lens	7	92.10	6.56	0.00	0.09	0.09	98.84
PM28 Lens 2 (traverse 2)	Lens	8	92.14	5.25	0.00	0.26	0.04	97.69
PM28 Lens 2 (traverse 2)	Lens	9	90.32	6.85	0.00	0.17	0.12	97.45
PM28 Lens 2 (traverse 2)	Lens	10	94.11	4.08	0.00	0.00	0.06	98.25
PM28 Lens 2 (traverse 2)	Lens	11	87.39	8.57	0.00	0.07	0.00	96.03
PM28 Lens 2 (traverse 2)	Lens	12	86.13	7.66	0.00	0.01	0.05	93.86
PM28 Lens 2 (traverse 2)	Lens	13	89.28	7.21	0.00	0.61	0.02	97.12
PM28 Lens 2 (traverse 2)	Lens	14	91.57	1.30	0.00	2.71	0.15	95.73
PM28 Lens 2 (traverse 2)	Cement ?	15	91.24	0.82	0.00	1.85	0.11	94.01
PM28 Lens 3 (traverse 1)	Lens	1	81.85	8.90	0.00	0.04	0.04	90.83
PM28 Lens 3 (traverse 1)	Lens	2	92.87	4.19	0.00	0.07	0.06	97.19
PM28 Lens 3 (traverse 1)	Lens	3	90.74	7.33	0.00	0.09	0.11	98.27
PM28 Lens 3 (traverse 1)	Lens	4	89.59	5.93	0.00	0.09	0.00	95.60
PM28 Lens 3 (traverse 1)	Lens	5	90.64	6.68	0.00	0.14	0.02	97.48
PM28 Lens 3 (traverse 1)	Lens	6	92.81	5.83	0.00	0.04	0.00	98.68
PM28 Lens 3 (traverse 1)	Lens	7	91.20	7.78	0.00	0.09	0.05	99.12
PM28 Lens 3 (traverse 1)	Lens	8	91.04	6.94	0.00	0.02	0.00	98.00
PM28 Lens 3 (traverse 1)	Lens	9	87.14	9.70	0.00	0.06	0.00	96.90
PM28 Lens 3 (traverse 1)	Lens	10	88.33	10.02	0.00	0.06	0.00	98.42
PM28 Lens 3 (traverse 1)	Lens	11	87.60	6.51	0.00	0.53	0.01	94.66
PM28 Lens 3 (traverse 1)	Lens	12	89.91	6.54	0.00	1.58	0.06	98.10
PM28 Lens 3 (traverse 1)	Lens	13	77.98	0.68	0.00	3.61	0.12	82.39
PM28 Lens 3 (traverse 1)	Lens	14	82.85	0.97	0.00	3.68	0.19	87.69
PM28 Lens 3 (traverse 1)	Lens	15	89.60	0.88	0.00	2.42	0.05	92.95
PM28 Lens 3 (traverse 1)	Lens	16	89.88	5.97	0.00	1.54	0.24	97.62
PM28 Lens 3 (traverse 1)	Lens	17	89.65	7.49	0.00	0.43	0.09	97.67
PM28 Lens 3 (traverse 1)	Lens	18	91.64	6.49	0.00	0.09	0.00	98.21
PM28 Lens 3 (traverse 1)	Lens	19	89.75	5.64	0.00	0.12	0.02	95.54
PM28 Lens 3 (traverse 1)	Lens	20	88.50	6.31	0.00	0.01	0.01	94.83
PM28 Lens 3 (traverse 2)	Lens	1	91.68	6.64	0.00	0.17	0.00	98.50

SAMPLE	FEATURE	DATA SET/ POINT	WEIGHT % CARBONATE					
			Ca	Mg	Sr	Fe	Mn	SUM
PM28 Lens 3 (traverse 2)	Lens	2	91.57	7.21	0.00	0.14	0.00	98.92
PM28 Lens 3 (traverse 2)	Lens	3	92.82	5.06	0.00	0.21	0.00	98.08
PM28 Lens 3 (traverse 2)	Lens	4	94.91	4.28	0.00	0.00	0.00	99.19
PM28 Lens 3 (traverse 2)	Lens	5	94.64	4.65	0.00	0.02	0.06	99.38
PM28 Lens 3 (traverse 2)	Lens	6	86.01	10.25	0.00	0.09	0.01	96.35
PM28 Lens 3 (traverse 2)	Lens	7	93.48	5.96	0.00	0.17	0.01	99.61
PM28 Lens 3 (traverse 2)	Lens	8	95.00	3.33	0.00	0.21	0.00	98.54
PM28 Lens 3 (traverse 2)	Lens	9	92.81	6.16	0.00	0.15	0.07	99.19
PM28 Lens 3 (traverse 2)	Lens	10	91.56	6.75	0.00	0.03	0.00	98.34
PM28 Lens 3 (traverse 2)	Lens	11	88.33	7.93	0.00	0.64	0.05	96.95
PM28 Lens 3 (traverse 2)	Lens	12	88.97	7.09	0.00	0.05	0.07	96.17
PM28 Lens 3 (traverse 2)	Lens	13	90.73	7.52	0.00	0.09	0.00	98.35
PM28 Lens 3 (traverse 2)	Lens	14	89.64	7.02	0.00	0.70	0.12	97.48
PM28 Lens 3 (traverse 2)	Lens	15	91.84	4.88	0.00	1.09	0.18	97.99

Table E.3 - Normalised weight % carbonate EPMA data (Strathclyde) for trilobites with schizochroal eyes.

SAMPLE	FEATURE	DATA SET/ POINT	NORMALISED WEIGHT % CARBONATE				
			Ca	Mg	Sr	Fe	Mn
AM65 Lens 1 Traverse 1	Lens	1	95.23	1.26	0.03	3.25	0.23
AM65 Lens 1 Traverse 1	Lens	2	92.17	5.10	0.21	2.43	0.10
AM65 Lens 1 Traverse 1	Lens	3	81.91	15.69	0.29	1.97	0.14
AM65 Lens 1 Traverse 1	Lens	4	92.89	6.47	0.43	0.22	0.00
AM65 Lens 1 Traverse 1	Lens	5	94.24	5.27	0.40	0.09	0.00
AM65 Lens 1 Traverse 1	Lens	6	94.62	4.88	0.39	0.10	0.00
AM65 Lens 1 Traverse 1	Lens	7	92.95	6.52	0.36	0.05	0.11
AM65 Lens 1 Traverse 1	Lens	8	84.20	15.31	0.34	0.14	0.00
AM65 Lens 1 Traverse 1	Lens	9	94.23	5.13	0.39	0.21	0.04
AM65 Lens 1 Traverse 1	Lens	10	94.20	5.30	0.43	0.03	0.04
AM65 Lens 1 Traverse 1	Lens	11	94.50	5.07	0.38	0.05	0.01
AM65 Lens 1 Traverse 1	Lens	12	93.21	6.15	0.41	0.23	0.00
AM65 Lens 1 Traverse 1	Lens	13	93.34	6.02	0.41	0.12	0.11
AM65 Lens 1 Traverse 1	Lens	14	92.87	6.45	0.36	0.17	0.14
AM65 Lens 1 Traverse 1	Lens	15	90.33	8.70	0.37	0.41	0.19
AM65 Lens 1 Traverse 2	Lens	1	90.59	3.27	0.00	6.00	0.14
AM65 Lens 1 Traverse 2	Lens	2	94.61	1.47	0.05	3.49	0.38
AM65 Lens 1 Traverse 2	Lens	3	92.97	1.89	0.05	4.45	0.63
AM65 Lens 1 Traverse 2	Lens	4	91.61	7.65	0.46	0.25	0.03
AM65 Lens 1 Traverse 2	Lens	5	91.51	7.92	0.46	0.10	0.01
AM65 Lens 1 Traverse 2	Lens	6	91.08	8.24	0.55	0.06	0.07
AM65 Lens 1 Traverse 2	Lens	7	92.10	7.47	0.38	0.04	0.00
AM65 Lens 1 Traverse 2	Lens	8	93.45	5.96	0.35	0.17	0.07
AM65 Lens 1 Traverse 2	Lens	9	94.03	5.58	0.39	0.00	0.00
AM65 Lens 1 Traverse 2	Lens	10	85.28	13.91	0.28	0.50	0.04
AM65 Lens 1 Traverse 2	Lens	11	87.70	11.83	0.36	0.08	0.04
AM65 Lens 1 Traverse 2	Lens	12	93.27	6.11	0.47	0.02	0.13
AM65 Lens 1 Traverse 2	Lens	13	90.75	7.98	0.36	0.80	0.11
AM65 Lens 1 Traverse 2	Lens	14	94.36	4.70	0.41	0.42	0.11
AM65 Lens 1 Traverse 2	Lens	15	95.28	3.97	0.35	0.37	0.03
AM65 Lens 2 Traverse 1	Lens	1	92.92	6.24	0.37	0.25	0.21
AM65 Lens 2 Traverse 1	Lens	2	91.51	7.64	0.37	0.36	0.12
AM65 Lens 2 Traverse 1	Lens	3	92.69	6.70	0.41	0.08	0.11
AM65 Lens 2 Traverse 1	Lens	4	92.27	7.15	0.43	0.01	0.15
AM65 Lens 2 Traverse 1	Lens	5	91.64	7.77	0.43	0.11	0.05
AM65 Lens 2 Traverse 1	Lens	6	93.30	6.09	0.45	0.08	0.09
AM65 Lens 2 Traverse 1	Lens	7	91.28	8.16	0.45	0.00	0.11

SAMPLE	FEATURE	DATA SET/ POINT	NORMALISED WEIGHT % CARBONATE				
			Ca	Mg	Sr	Fe	Mn
AM65 Lens 2 Traverse 1	Lens	8	93.03	6.32	0.48	0.06	0.11
AM65 Lens 2 Traverse 1	Lens	9	92.20	7.35	0.44	0.00	0.01
AM65 Lens 2 Traverse 1	Lens	10	89.82	9.40	0.37	0.37	0.05
AM65 Lens 2 Traverse 1	Lens	11	94.03	5.38	0.44	0.04	0.11
AM65 Lens 2 Traverse 1	Lens	12	92.87	6.66	0.47	0.00	0.00
AM65 Lens 2 Traverse 1	Lens	13	90.87	8.64	0.43	0.00	0.06
AM65 Lens 2 Traverse 1	Lens	14	95.64	3.64	0.35	0.28	0.09
AM65 Lens 2 Traverse 1	Lens	15	92.91	6.29	0.43	0.29	0.07
AM65 Lens 2 Traverse 2	Lens	1	96.52	2.22	0.33	0.79	0.14
AM65 Lens 2 Traverse 2	Lens	2	93.59	5.29	0.48	0.51	0.12
AM65 Lens 2 Traverse 2	Lens	3	95.43	3.79	0.50	0.16	0.11
AM65 Lens 2 Traverse 2	Lens	4	91.51	7.90	0.48	0.08	0.03
AM65 Lens 2 Traverse 2	Lens	5	91.54	7.95	0.44	0.00	0.07
AM65 Lens 2 Traverse 2	Lens	6	92.25	7.27	0.48	0.01	0.00
AM65 Lens 2 Traverse 2	Lens	7	92.42	7.12	0.46	0.00	0.00
AM65 Lens 2 Traverse 2	Lens	8	94.31	5.18	0.35	0.16	0.00
AM65 Lens 2 Traverse 2	Lens	9	85.58	13.91	0.36	0.12	0.03
AM65 Lens 2 Traverse 2	Lens	10	85.44	13.97	0.49	0.10	0.00
AM65 Lens 2 Traverse 2	Lens	11	90.71	8.76	0.39	0.15	0.00
AM65 Lens 2 Traverse 2	Lens	12	82.89	16.13	0.45	0.39	0.15
AM65 Lens 2 Traverse 2	Lens	13	93.58	1.59	0.07	4.20	0.55
AM65 Lens 2 Traverse 2	Lens	14	94.01	1.56	0.00	4.27	0.16
AM65 Lens 2 Traverse 2	Lens	15	94.66	1.62	0.04	3.35	0.32
BB3aR Lens 2	Lens	1	99.35	0.52	0.00	0.00	0.13
BB3aR Lens 2	Lens	2	96.51	3.48	0.00	0.00	0.01
BB3aR Lens 2	Lens	3	98.87	1.13	0.00	0.00	0.00
BB3aR Lens 2	Lens	4	96.22	3.73	0.00	0.05	0.00
BB3aR Lens 2	Lens	5	98.54	1.41	0.00	0.00	0.05
BB3aR Lens 2	Lens	6	98.95	1.05	0.00	0.00	0.00
BB3aR Lens 2	Lens	7	99.21	0.69	0.00	0.06	0.04
BB3aR Lens 2	Lens	8	92.63	7.25	0.00	0.11	0.00
BB3aR Lens 2	Lens	9	98.04	1.95	0.00	0.01	0.00
BB3aR Lens 2	Lens	10	99.06	0.87	0.00	0.07	0.00
BB3aR Lens 2	Lens	11	95.78	4.17	0.00	0.00	0.05
BB3aR Lens 2	Lens	12	99.28	0.69	0.00	0.03	0.00
BB3aR Lens 2	Lens	13	99.17	0.79	0.00	0.03	0.01
BB3aR Lens 2	Lens	14	93.43	6.50	0.00	0.00	0.07
BB3aR Lens 2	Lens	15	97.52	2.45	0.00	0.01	0.01
BB3aR Lens 2	Lens	16	97.87	2.04	0.00	0.09	0.00
BB3aR Lens 2	Lens	17	96.37	3.62	0.00	0.01	0.00
BB3aR Lens 2	Lens	18	95.01	4.88	0.00	0.08	0.03
BB3aR Lens 2	Lens	19	99.63	0.37	0.00	0.00	0.00
BB3aR Lens 2	Lens	20	98.92	1.00	0.00	0.00	0.09
BB3aR Lens 2	Lens	21	98.96	0.97	0.00	0.07	0.00
BB3aR Lens 2	Lens	22	94.61	5.32	0.00	0.07	0.00
BB3aR Lens 2	Lens	23	98.60	1.39	0.00	0.01	0.00
BB3aR Lens 2	Lens	24	99.12	0.88	0.00	0.00	0.00
BB3aR Lens 2	Lens	25	98.98	0.96	0.00	0.05	0.00
BB3aR Lens 2	Lens	26	96.77	3.12	0.00	0.10	0.00
BB3aR Lens 2	Lens	27	98.83	1.17	0.00	0.00	0.00
BB3aR Lens 2	Lens	28	99.32	0.59	0.00	0.07	0.02
BB3aR Lens 2	Lens	29	99.39	0.52	0.00	0.05	0.04
BB3aR Lens 2	Lens	30	99.27	0.72	0.00	0.00	0.01
BB3aR Lens 2	Lens	31	99.08	0.92	0.00	0.00	0.00
BB3aR Lens 2	Lens	32	99.33	0.67	0.00	0.00	0.00
BB3aR Lens 2	Lens	33	98.69	1.26	0.00	0.05	0.00
BB3aR Lens 2	Lens	34	98.69	1.22	0.00	0.08	0.00
BB3aR Lens 2	Lens	35	99.52	0.46	0.00	0.02	0.00
BB3aR Lens 2	Lens	36	99.53	0.45	0.00	0.03	0.00
BB3aR Lens 2	Lens	37	99.30	0.53	0.00	0.16	0.00
BB3aR Lens 2	Lens	38	99.28	0.57	0.00	0.09	0.06

SAMPLE	FEATURE	DATA SET/ POINT	NORMALISED WEIGHT % CARBONATE				
			Ca	Mg	Sr	Fe	Mn
BB3aR Lens 2	Lens	39	95.85	3.87	0.00	0.17	0.11
BB3aR Lens 2	Lens	40	99.44	0.53	0.00	0.01	0.02
BB3aR Lens 2	Lens	41	99.40	0.59	0.00	0.00	0.01
BB3aR Lens 2	Lens	42	99.00	0.95	0.00	0.02	0.04
BB3aR Lens 2	Lens	43	67.18	32.82	0.00	0.00	0.00
BB3aR Lens 2	Lens	44	99.57	0.41	0.00	0.00	0.02
BB3aR Lens 2	Lens	45	99.13	0.60	0.00	0.18	0.09
BB3aR Lens 2	Lens	46	99.45	0.46	0.00	0.08	0.01
BB3aR Lens 2	Lens	47	98.88	1.11	0.00	0.00	0.00
BB3aR Lens 2	Lens	48	99.35	0.65	0.00	0.00	0.00
BB3aR Lens 2	Lens	49	98.85	1.08	0.00	0.07	0.00
BB3aR Lens 2	Lens	50	97.38	2.62	0.00	0.00	0.00
BB3aR Lens 2	Lens	51	99.33	0.67	0.00	0.00	0.00
BB3aR Lens 2	Lens	52	95.57	4.40	0.00	0.03	0.00
BB3aR Lens 2	Lens	53	94.20	5.77	0.00	0.03	0.00
BB3aR Lens 2	Lens	54	97.55	2.42	0.00	0.03	0.00
BB3aR Lens 2	Lens	55	99.29	0.63	0.00	0.00	0.08
BB3aR Lens 2	Lens	56	99.47	0.53	0.00	0.00	0.00
BB3aR Lens 2	Lens	57	99.53	0.45	0.00	0.02	0.00
BB3aR Lens 2	Lens	58	99.02	0.79	0.00	0.16	0.04
BB3aR Lens 2	Lens	59	96.48	3.47	0.00	0.00	0.05
BB3aR Lens 2	Lens	60	99.00	0.86	0.00	0.07	0.08
BB3aR Lens 2	Lens	61	99.09	0.91	0.00	0.00	0.00
BB3aR Lens 2	Lens	62	99.25	0.74	0.00	0.01	0.00
BB3aR Lens 2	Lens	63	90.20	9.65	0.00	0.12	0.03
BB3aR Lens 2	Lens	64	98.48	1.41	0.00	0.11	0.00
BB3aR Lens 2	Lens	65	99.33	0.45	0.00	0.12	0.09
BB3aR Lens 3	Lens	1	99.20	0.75	0.00	0.05	0.00
BB3aR Lens 3	Lens	2	99.31	0.60	0.00	0.00	0.09
BB3aR Lens 3	Lens	3	96.44	3.38	0.00	0.10	0.07
BB3aR Lens 3	Lens	4	96.00	3.87	0.00	0.09	0.04
BB3aR Lens 3	Lens	5	99.24	0.74	0.00	0.01	0.00
BB3aR Lens 3	Lens	6	93.93	6.07	0.00	0.00	0.00
BB3aR Lens 3	Lens	7	97.38	2.57	0.00	0.01	0.04
BB3aR Lens 3	Lens	8	99.13	0.85	0.00	0.00	0.02
BB3aR Lens 3	Lens	9	96.78	3.22	0.00	0.00	0.00
BB3aR Lens 3	Lens	10	97.53	2.45	0.00	0.00	0.02
BB3aR Lens 3	Lens	11	96.55	3.45	0.00	0.00	0.00
BB3aR Lens 3	Lens	12	99.79	0.19	0.00	0.02	0.00
BB3aR Lens 3	Lens	13	99.41	0.57	0.00	0.02	0.00
BB3aR Lens 3	Lens	14	99.49	0.47	0.00	0.00	0.04
BB3aR Lens 3	Lens	15	99.38	0.56	0.00	0.04	0.01
BB3aR Lens 3	Lens	16	98.57	1.32	0.00	0.07	0.04
BB3aR Lens 3	Lens	17	99.62	0.27	0.00	0.07	0.05
BB3aR Lens 3	Lens	18	99.48	0.45	0.00	0.07	0.00
BB3aR Lens 3	Lens	19	99.40	0.51	0.00	0.02	0.06
BB3aR Lens 3	Lens	20	98.91	1.02	0.00	0.05	0.02
BB3aR Lens 3	Lens	21	98.55	1.37	0.00	0.04	0.05
BB3aR Lens 3	Lens	22	97.26	2.64	0.00	0.07	0.04
BB3aR Lens 3	Lens	23	93.23	6.66	0.00	0.07	0.05
BB3aR Lens 3	Lens	24	99.05	0.95	0.00	0.00	0.00
BB3aR Lens 3	Lens	25	99.18	0.76	0.00	0.01	0.05
BB3aR Lens 3	Lens	26	99.08	0.86	0.00	0.06	0.00
BB3aR Lens 3	Lens	27	99.27	0.69	0.00	0.00	0.04
BB3aR Lens 3	Lens	28	95.74	4.20	0.00	0.05	0.01
BB3aR Lens 3	Lens	29	98.03	1.88	0.00	0.00	0.09
BB3aR Lens 3	Lens	30	99.42	0.53	0.00	0.00	0.05
BB3aR Lens 3	Lens	31	99.48	0.52	0.00	0.00	0.00
BB3aR Lens 3	Lens	32	98.45	1.42	0.00	0.13	0.00
BB3aR Lens 3	Lens	33	78.99	20.76	0.00	0.23	0.03
BB3aR Lens 3	Lens	34	98.13	1.80	0.00	0.07	0.00
BB3aR Lens 3	Lens	35	95.64	4.33	0.00	0.03	0.00

SAMPLE	FEATURE	DATA SET/ POINT	NORMALISED WEIGHT % CARBONATE				
			Ca	Mg	Sr	Fe	Mn
BB3aR Lens 3	Lens	36	97.54	2.41	0.00	0.05	0.00
BB3aR Lens 3	Lens	37	99.00	0.97	0.00	0.00	0.04
BB3aR Lens 3	Lens	38	97.61	0.55	0.00	1.77	0.08
BB3aR Lens 3	Lens	39	99.32	0.43	0.00	0.19	0.07
BB3aR Lens 3	Lens	40	99.39	0.47	0.00	0.02	0.12
BB3aR Lens 3	Lens	41	93.70	6.26	0.00	0.00	0.04
BB3aR Lens 3	Lens	42	99.39	0.52	0.00	0.07	0.02
BB3aR Lens 3	Lens	43	99.64	0.34	0.00	0.00	0.02
BB3aR Lens 3	Lens	44	99.26	0.62	0.00	0.08	0.05
BB3aR Lens 3	Lens	45	99.45	0.53	0.00	0.00	0.02
BB3aR Lens 3	Lens	46	99.43	0.48	0.00	0.09	0.00
BB3aR Lens 3	Lens	47	99.46	0.54	0.00	0.00	0.00
BB3aR Lens 3	Lens	48	99.44	0.53	0.00	0.03	0.00
BB3aR Lens 3	Lens	49	98.98	0.94	0.00	0.02	0.06
BB3aR Lens 3	Lens	50	98.73	1.25	0.00	0.02	0.00
BB3aR Lens 3	Lens	51	99.46	0.54	0.00	0.00	0.00
BB3aR Lens 3	Lens	52	93.50	6.38	0.00	0.12	0.01
BB3aR Lens 3	Lens	53	98.67	1.26	0.00	0.00	0.07
BB3aR Lens 3	Lens	54	95.97	3.92	0.00	0.11	0.00
BB3aR Lens 3	Lens	55	99.19	0.76	0.00	0.00	0.05
BB3aR Lens 3	Lens	56	99.29	0.65	0.00	0.03	0.03
BB3aR Lens 3	Lens	57	99.42	0.52	0.00	0.00	0.06
BB3aR Lens 3	Lens	58	99.73	0.13	0.00	0.12	0.01
BB3aR Lens 3	Lens	59	99.43	0.48	0.00	0.09	0.00
BB3aR Lens 3	Lens	60	99.41	0.58	0.00	0.00	0.01
BB3aR Lens 3	Lens	61	99.48	0.50	0.00	0.03	0.00
BB3aR Lens 3	Lens	62	99.52	0.43	0.00	0.00	0.05
BB3aR Lens 3	Lens	63	99.46	0.51	0.00	0.00	0.03
BB3aR Lens 3	Lens	64	99.38	0.57	0.00	0.00	0.05
BB3aR Lens 3	Lens	65	99.36	0.64	0.00	0.00	0.00
BB3aR Lens 3	Lens	66	99.49	0.49	0.00	0.00	0.02
BB3aR Lens 3	Lens	67	99.37	0.61	0.00	0.02	0.00
BB3aR Lens 3	Lens	68	92.77	7.20	0.00	0.04	0.00
BB3aR Lens 3	Lens	69	97.72	2.22	0.00	0.00	0.06
BB3aR Lens 3	Lens	70	99.49	0.51	0.00	0.00	0.00
BB3aR	Sclera	1	99.18	0.60	0.00	0.11	0.12
BB3aR	Sclera	2	99.34	0.64	0.00	0.01	0.01
BB3aR	Sclera	3	99.18	0.57	0.00	0.10	0.15
BB3aR	Sclera	4	99.29	0.51	0.00	0.14	0.06
BB3aR	Sclera	5	99.31	0.39	0.00	0.23	0.07
BB3aR	Sclera	6	99.47	0.37	0.00	0.16	0.00
BB3aR	Sclera	7	99.30	0.50	0.00	0.08	0.12
BB3aR	Sclera	8	99.46	0.44	0.00	0.07	0.03
BB3aR	Sclera	9	98.90	0.38	0.00	0.57	0.16
BB3aR	Sclera	10	99.26	0.45	0.00	0.18	0.10
BB3aR	Sclera	11	99.41	0.47	0.00	0.03	0.08
BB3aR	Sclera	12	99.31	0.59	0.00	0.07	0.02
BB3aR	Sclera	13	99.29	0.55	0.00	0.16	0.00
BB3aR	Sclera	14	99.44	0.54	0.00	0.02	0.00
BB3aR	Sclera	15	99.35	0.49	0.00	0.08	0.07
BB3aR	Sclera	16	99.23	0.40	0.00	0.29	0.08
BB3aR	Sclera	17	99.37	0.38	0.00	0.18	0.07
BB3aR	Cement	1	99.03	0.84	0.00	0.07	0.06
BB3aR	Cement	2	99.18	0.78	0.00	0.00	0.04
BB3aR	Cement	3	98.39	1.47	0.00	0.11	0.04
BB3aR	Cement	4	99.15	0.70	0.00	0.12	0.02
BB3aR	Cement	5	98.52	1.47	0.00	0.01	0.00
BB3aR	Cement	6	98.74	1.19	0.00	0.07	0.00
BB3aR	Cement	7	99.16	0.82	0.00	0.00	0.02
BB3aR	Cement	8	99.44	0.54	0.00	0.00	0.02
BB3aR	Cement	9	98.86	1.03	0.00	0.04	0.08

SAMPLE	FEATURE	DATA SET/ POINT	NORMALISED WEIGHT % CARBONATE				
			Ca	Mg	Sr	Fe	Mn
BB3aR	Cement	10	99.60	0.33	0.00	0.04	0.03
BB3aR	Cement	11	99.36	0.54	0.00	0.05	0.05
BB3aR	Cement	12	99.35	0.58	0.00	0.07	0.00
BB3aR	Cement	13	99.07	0.90	0.00	0.03	0.00
BB3aR	Cement	14	99.39	0.61	0.00	0.00	0.00
BB3aR	Cement	15	99.28	0.70	0.00	0.00	0.02
BB3aR	Cement	16	99.46	0.49	0.00	0.00	0.05
BB3aR	Cement	17	99.44	0.49	0.00	0.00	0.07
BB3aR	Cement	18	99.13	0.87	0.00	0.00	0.00
BB3aR	Cement	19	99.46	0.49	0.00	0.00	0.05
BB3aR	Cement	20	99.52	0.45	0.00	0.00	0.03
BB3aR	Cement	21	99.41	0.59	0.00	0.00	0.00
BB3aR	Cement	22	99.47	0.51	0.00	0.00	0.01
BB3aR	Cement	23	99.30	0.54	0.00	0.14	0.02
BB3aR	Cement	24	98.49	1.43	0.00	0.01	0.07
BB3aR	Cement	25	99.45	0.51	0.00	0.04	0.00
BB3aR	Cement	26	97.47	2.44	0.00	0.05	0.04
BB3aR	Cement	27	99.07	0.78	0.00	0.08	0.07
BB3aR	Cement	28	99.27	0.58	0.00	0.08	0.08
BB3aR	Cement	29	99.42	0.43	0.00	0.00	0.15
BB3aR	Cement	30	99.16	0.65	0.00	0.11	0.08
BB3aR	Cement	31	98.98	1.02	0.00	0.00	0.00
BB3aR	Cement	32	99.17	0.74	0.00	0.04	0.05
BB3aR	Cement	33	99.13	0.83	0.00	0.00	0.04
BB3aR	Cement	34	99.43	0.54	0.00	0.00	0.02
BB3aR	Cement	35	99.22	0.72	0.00	0.06	0.00
BB3aR	Cement	36	99.41	0.55	0.00	0.00	0.03
BB3aR	Cement	37	96.00	3.84	0.00	0.12	0.04
BB3aR	Cement	38	99.35	0.35	0.00	0.21	0.09
BB3aR	Cement	39	99.48	0.46	0.00	0.02	0.04
BB3aR	Cement	40	99.32	0.68	0.00	0.00	0.00
BB3aR	Cement	41	99.39	0.50	0.00	0.09	0.02
BB3aR	Cement	42	99.13	0.84	0.00	0.00	0.03
BB3aR	Cement	43	99.38	0.57	0.00	0.03	0.02
BB3aR	Cement	44	99.20	0.72	0.00	0.05	0.03
BB3aR	Cement	45	99.25	0.66	0.00	0.04	0.05
BB3aR	Cement	46	99.19	0.64	0.00	0.08	0.09
BB3aR	Cement	47	99.27	0.63	0.00	0.01	0.09
BB3aR	Cement	48	99.15	0.83	0.00	0.02	0.00
BB3aR	Cement	49	99.38	0.58	0.00	0.00	0.04
BB3aR	Cement	50	99.34	0.52	0.00	0.05	0.08
BB3aR	Cement	51	99.28	0.67	0.00	0.01	0.04
BB3aR	Cement	52	99.28	0.52	0.00	0.11	0.09
BB3aR	Cement	53	99.13	0.67	0.00	0.11	0.09
E22B Lens 1	Lens	1	96.35	3.65	0.00	0.00	0.00
E22B Lens 1	Lens	2	94.89	5.11	0.00	0.00	0.00
E22B Lens 1	Lens	3	98.55	1.45	0.00	0.00	0.00
E22B Lens 1	Lens	4	98.51	1.49	0.00	0.00	0.00
E22B Lens 1	Lens	5	98.80	1.20	0.00	0.00	0.00
E22B Lens 1	Lens	6	99.04	0.96	0.00	0.00	0.00
E22B Lens 1	Lens	7	98.71	1.29	0.00	0.00	0.00
E22B Lens 1	Lens	8	98.41	1.59	0.00	0.00	0.00
E22B Lens 1	Lens	9	98.61	1.39	0.00	0.00	0.00
E22B Lens 1	Lens	10	98.37	1.63	0.00	0.00	0.00
E22B Lens 1	Lens	11	98.67	1.33	0.00	0.00	0.00
E22B Lens 1	Lens	12	98.84	1.16	0.00	0.00	0.00
E22B Lens 1	Lens	13	99.10	0.90	0.00	0.00	0.00
E22B Lens 1	Lens	14	98.47	1.53	0.00	0.00	0.00
E22B Lens 1	Lens	15	98.44	1.56	0.00	0.00	0.00
E22B Lens 1	Lens	16	98.44	1.56	0.00	0.00	0.00
E22B Lens 1	Lens	17	98.86	1.14	0.00	0.00	0.00
E22B Lens 1	Lens	18	97.40	2.60	0.00	0.00	0.00

SAMPLE	FEATURE	DATA SET/ POINT	NORMALISED WEIGHT % CARBONATE				
			Ca	Mg	Sr	Fe	Mn
E22B Lens 1	Lens	19	99.01	0.99	0.00	0.00	0.00
E22B Lens 1	Lens	20	98.56	1.44	0.00	0.00	0.00
E22B Lens 1	Lens	21	94.52	5.48	0.00	0.00	0.00
E22B Lens 1	Lens	22	97.22	2.78	0.00	0.00	0.00
E22B Lens 1	Lens	23	98.84	1.16	0.00	0.00	0.00
E22B Lens 1	Lens	24	98.39	1.61	0.00	0.00	0.00
E22B Lens 1	Lens	25	98.35	1.65	0.00	0.00	0.00
E22B Lens 1	Lens	26	97.75	2.25	0.00	0.00	0.00
E22B Lens 1	Lens	27	98.15	1.85	0.00	0.00	0.00
E22B Lens 1	Lens	28	98.62	1.38	0.00	0.00	0.00
E22B Lens 1	Lens	29	98.52	1.48	0.00	0.00	0.00
E22B Lens 1	Lens	30	98.30	1.70	0.00	0.00	0.00
E22B Lens 1	Lens	31	98.02	1.98	0.00	0.00	0.00
E22B Lens 1	Lens	32	98.83	1.17	0.00	0.00	0.00
E22B Lens 1	Lens	33	98.69	1.31	0.00	0.00	0.00
E22B Lens 1	Lens	34	98.34	1.66	0.00	0.00	0.00
E22B Lens 1	Lens	35	98.40	1.60	0.00	0.00	0.00
E22B Lens 1	Lens	36	98.79	1.21	0.00	0.00	0.00
E22B Lens 1	Lens	37	99.22	0.78	0.00	0.00	0.00
E22B Lens 1	Lens	38	99.04	0.96	0.00	0.00	0.00
E22B Lens 1	Lens	39	98.70	1.30	0.00	0.00	0.00
E22B Lens 1	Lens	40	98.68	1.32	0.00	0.00	0.00
E22B Lens 1	Lens	41	98.98	1.02	0.00	0.00	0.00
E22B Lens 1	Lens	42	99.05	0.95	0.00	0.00	0.00
E22B Lens 1	Lens	43	99.20	0.80	0.00	0.00	0.00
E22B Lens 1	Lens	44	98.48	1.52	0.00	0.00	0.00
E22B Lens 1	Lens	45	97.45	2.55	0.00	0.00	0.00
E22B Lens 1	Lens	46	98.69	1.31	0.00	0.00	0.00
E22B Lens 1	Lens	47	98.77	1.23	0.00	0.00	0.00
E22B Lens 1	Lens	48	98.74	1.26	0.00	0.00	0.00
E22B Lens 1	Lens	49	99.06	0.94	0.00	0.00	0.00
E22B Lens 1	Lens	50	99.20	0.80	0.00	0.00	0.00
E22B Lens 1	Lens	51	99.20	0.80	0.00	0.00	0.00
E22B Lens 1	Lens	52	98.55	1.45	0.00	0.00	0.00
E22B Lens 1	Lens	53	98.62	1.38	0.00	0.00	0.00
E22B Lens 1	Lens	54	98.59	1.41	0.00	0.00	0.00
E22B Lens 1	Lens	55	98.49	1.51	0.00	0.00	0.00
E22B Lens 1	Lens	56	98.36	1.64	0.00	0.00	0.00
E22B Lens 1	Lens	57	99.02	0.98	0.00	0.00	0.00
E22B Lens 1	Lens	58	99.06	0.94	0.00	0.00	0.00
E22B Lens 1	Lens	59	98.87	1.13	0.00	0.00	0.00
E22B Lens 1	Lens	60	98.77	1.23	0.00	0.00	0.00
E22B Lens 2	Lens	1	100.00	0.00	0.00	0.00	0.00
E22B Lens 2	Lens	2	100.00	0.00	0.00	0.00	0.00
E22B Lens 2	Lens	3	98.55	1.45	0.00	0.00	0.00
E22B Lens 2	Lens	4	98.11	1.89	0.00	0.00	0.00
E22B Lens 2	Lens	5	98.43	1.57	0.00	0.00	0.00
E22B Lens 2	Lens	6	98.83	1.17	0.00	0.00	0.00
E22B Lens 2	Lens	7	98.68	1.32	0.00	0.00	0.00
E22B Lens 2	Lens	8	98.26	1.74	0.00	0.00	0.00
E22B Lens 2	Lens	9	98.63	1.37	0.00	0.00	0.00
E22B Lens 2	Lens	10	98.43	1.57	0.00	0.00	0.00
E22B Lens 2	Lens	11	98.38	1.62	0.00	0.00	0.00
G33R Lens 1	Lens	1	97.58	2.42	0.00	0.00	0.00
G33R Lens 1	Lens	2	96.71	3.29	0.00	0.00	0.00
G33R Lens 1	Lens	3	99.03	0.97	0.00	0.00	0.00
G33R Lens 1	Lens	4	96.96	3.04	0.00	0.00	0.00
G33R Lens 1	Lens	5	98.66	1.34	0.00	0.00	0.00
G33R Lens 1	Lens	6	98.35	1.65	0.00	0.00	0.00
G33R Lens 1	Lens	7	99.01	0.99	0.00	0.00	0.00
G33R Lens 1	Lens	8	96.11	3.89	0.00	0.00	0.00

SAMPLE	FEATURE	DATA SET/ POINT	NORMALISED WEIGHT % CARBONATE				
			Ca	Mg	Sr	Fe	Mn
G33R Lens 1	Lens	9	92.30	7.70	0.00	0.00	0.00
G33R Lens 1	Lens	10	98.32	1.68	0.00	0.00	0.00
G33R Lens 1	Lens	11	95.57	4.43	0.00	0.00	0.00
G33R Lens 1	Lens	12	98.20	1.80	0.00	0.00	0.00
G33R Lens 1	Lens	13	98.48	1.52	0.00	0.00	0.00
G33R Lens 1	Lens	14	98.85	1.15	0.00	0.00	0.00
G33R Lens 1	Lens	15	98.24	1.76	0.00	0.00	0.00
G33R Lens 1	Lens	16	98.03	1.97	0.00	0.00	0.00
G33R Lens 1	Lens	17	98.32	1.68	0.00	0.00	0.00
G33R Lens 1	Lens	18	97.50	2.50	0.00	0.00	0.00
G33R Lens 1	Lens	19	98.19	1.81	0.00	0.00	0.00
G33R Lens 1	Lens	20	97.67	2.33	0.00	0.00	0.00
G33R Lens 1	Lens	21	97.53	2.47	0.00	0.00	0.00
G33R Lens 1	Lens	22	98.16	1.84	0.00	0.00	0.00
G33R Lens 1	Lens	23	98.31	1.69	0.00	0.00	0.00
G33R Lens 1	Lens	24	97.03	2.97	0.00	0.00	0.00
G33R Lens 1	Lens	25	98.75	1.25	0.00	0.00	0.00
G33R Lens 1	Lens	26	98.86	1.14	0.00	0.00	0.00
G33R Lens 1	Lens	27	98.84	1.16	0.00	0.00	0.00
G33R Lens 1	Lens	28	98.51	1.49	0.00	0.00	0.00
G33R Lens 1	Lens	29	98.24	1.76	0.00	0.00	0.00
G33R Lens 1	Lens	30	97.91	2.09	0.00	0.00	0.00
G33R Lens 1	Lens	31	98.27	1.73	0.00	0.00	0.00
G33R Lens 1	Lens	32	95.86	4.14	0.00	0.00	0.00
G33R Lens 1	Lens	33	97.94	2.06	0.00	0.00	0.00
G33R Lens 1	Lens	34	92.19	7.81	0.00	0.00	0.00
G33R Lens 1	Lens	35	93.70	6.30	0.00	0.00	0.00
G33R Lens 1	Lens	36	97.58	2.42	0.00	0.00	0.00
G33R Lens 1	Lens	37	96.71	3.29	0.00	0.00	0.00
G33R Lens 1	Lens	38	99.03	0.97	0.00	0.00	0.00
G33R Lens 1	Lens	39	96.96	3.04	0.00	0.00	0.00
G33R Lens 1	Lens	40	98.66	1.34	0.00	0.00	0.00
G33R Lens 1	Lens	41	98.35	1.65	0.00	0.00	0.00
G33R Lens 1	Lens	42	99.01	0.99	0.00	0.00	0.00
G33R Lens 1	Lens	43	96.11	3.89	0.00	0.00	0.00
G33R Lens 1	Lens	44	92.30	7.70	0.00	0.00	0.00
G33R Lens 1	Lens	45	98.32	1.68	0.00	0.00	0.00
G33R Lens 1	Lens	46	95.57	4.43	0.00	0.00	0.00
G33R Lens 1	Lens	47	98.20	1.80	0.00	0.00	0.00
G33R Lens 1	Lens	48	98.48	1.52	0.00	0.00	0.00
G33R Lens 1	Lens	49	98.85	1.15	0.00	0.00	0.00
G33R Lens 1	Lens	50	98.24	1.76	0.00	0.00	0.00
G33R Lens 1	Lens	51	98.03	1.97	0.00	0.00	0.00
G33R Lens 1	Lens	52	98.32	1.68	0.00	0.00	0.00
G33R Lens 1	Lens	53	97.50	2.50	0.00	0.00	0.00
G33R Lens 1	Lens	54	98.19	1.81	0.00	0.00	0.00
G33R Lens 1	Lens	55	97.67	2.33	0.00	0.00	0.00
G33R Lens 1	Lens	56	97.53	2.47	0.00	0.00	0.00
G33R Lens 1	Lens	57	98.16	1.84	0.00	0.00	0.00
G33R Lens 1	Lens	58	98.31	1.69	0.00	0.00	0.00
G33R Lens 1	Lens	59	97.03	2.97	0.00	0.00	0.00
G33R Lens 1	Lens	60	98.75	1.25	0.00	0.00	0.00
G33R Lens 1	Lens	61	98.86	1.14	0.00	0.00	0.00
G33R Lens 1	Lens	62	98.84	1.16	0.00	0.00	0.00
G33R Lens 1	Lens	63	98.51	1.49	0.00	0.00	0.00
G33R Lens 1	Lens	64	98.24	1.76	0.00	0.00	0.00
G33R Lens 1	Lens	65	97.91	2.09	0.00	0.00	0.00
G33R Lens 1	Lens	66	98.27	1.73	0.00	0.00	0.00
G33R Lens 1	Lens	67	95.86	4.14	0.00	0.00	0.00
G33R Lens 1	Lens	68	97.94	2.06	0.00	0.00	0.00
G33R Lens 1	Lens	69	98.21	1.79	0.00	0.00	0.00
G33R Lens 1	Lens	70	98.73	1.27	0.00	0.00	0.00
G33R Lens 1	Lens	71	98.88	1.12	0.00	0.00	0.00

SAMPLE	FEATURE	DATA SET/ POINT	NORMALISED WEIGHT % CARBONATE				
			Ca	Mg	Sr	Fe	Mn
G33R Lens 1	Lens	72	98.62	1.38	0.00	0.00	0.00
G33R Lens 1	Lens	73	98.90	1.10	0.00	0.00	0.00
G33R Lens 1	Lens	74	98.55	1.45	0.00	0.00	0.00
G33R Lens 1	Lens	75	98.62	1.38	0.00	0.00	0.00
G33R Lens 1	Lens	76	97.86	2.14	0.00	0.00	0.00
G33R Lens 1	Lens	77	98.52	1.48	0.00	0.00	0.00
G33R Lens 1	Lens	78	98.66	1.34	0.00	0.00	0.00
G33R Lens 1	Lens	79	98.34	1.66	0.00	0.00	0.00
G33R Lens 1	Lens	80	97.54	2.46	0.00	0.00	0.00
G33R Lens 1	Lens	81	98.18	1.82	0.00	0.00	0.00
G33R Lens 1	Lens	82	97.31	2.69	0.00	0.00	0.00
G33R Lens 1	Lens	83	98.24	1.76	0.00	0.00	0.00
G33R Lens 1	Lens	84	97.67	2.33	0.00	0.00	0.00
G33R Lens 1	Lens	85	97.51	2.49	0.00	0.00	0.00
G33R Lens 1	Lens	86	97.48	2.52	0.00	0.00	0.00
G33R Lens 1	Lens	87	98.08	1.92	0.00	0.00	0.00
G33R Lens 1	Lens	88	95.90	4.10	0.00	0.00	0.00
G33R Lens 1	Lens	89	98.30	1.70	0.00	0.00	0.00
G33R Lens 1	Lens	90	97.85	2.15	0.00	0.00	0.00
G33R Lens 1	Lens	91	98.50	1.50	0.00	0.00	0.00
G33R Lens 1	Lens	92	97.87	2.13	0.00	0.00	0.00
G33R Lens 1	Lens	93	97.86	2.14	0.00	0.00	0.00
G33R Lens 1	Lens	94	98.57	1.43	0.00	0.00	0.00
G33R Lens 1	Lens	95	98.38	1.62	0.00	0.00	0.00
G33R Lens 1	Lens	96	98.45	1.55	0.00	0.00	0.00
G33R Lens 1	Lens	97	98.43	1.57	0.00	0.00	0.00
G33R Lens 1	Lens	98	98.75	1.25	0.00	0.00	0.00
G33R Lens 1	Lens	99	98.79	1.21	0.00	0.00	0.00
G33R Lens 1	Lens	100	98.63	1.37	0.00	0.00	0.00
G33R Lens 1	Lens	101	98.54	1.46	0.00	0.00	0.00
G33R Lens 1	Lens	102	98.50	1.50	0.00	0.00	0.00
G33R Lens 1	Lens	103	98.47	1.53	0.00	0.00	0.00
G42R Lens 1 Traverse 1	Lens	1	98.02	1.45	0.25	0.28	0.00
G42R Lens 1 Traverse 1	Lens	2	98.07	1.35	0.27	0.26	0.04
G42R Lens 1 Traverse 1	Lens	3	97.90	1.44	0.29	0.27	0.10
G42R Lens 1 Traverse 1	Lens	4	98.23	1.08	0.33	0.34	0.02
G42R Lens 1 Traverse 1	Lens	5	98.20	1.15	0.35	0.28	0.02
G42R Lens 1 Traverse 1	Lens	6	97.98	1.27	0.36	0.39	0.00
G42R Lens 1 Traverse 1	Lens	7	98.06	1.25	0.41	0.21	0.07
G42R Lens 1 Traverse 1	Lens	8	97.65	1.69	0.35	0.24	0.08
G42R Lens 1 Traverse 1	Lens	9	96.85	2.42	0.28	0.43	0.02
G42R Lens 1 Traverse 1	Lens	10	96.32	3.02	0.34	0.26	0.05
G42R Lens 1 Traverse 1	Lens	11	95.33	3.85	0.34	0.37	0.11
G42R Lens 1 Traverse 1	Lens	12	97.61	1.76	0.30	0.33	0.00
G42R Lens 1 Traverse 1	Lens	13	98.16	1.23	0.36	0.16	0.08
G42R Lens 1 Traverse 1	Lens	14	96.47	2.75	0.28	0.32	0.19
G42R Lens 1 Traverse 1	Lens	15	98.10	1.17	0.31	0.32	0.11
G42R Lens 1 Traverse 1	Lens	16	97.64	1.72	0.39	0.15	0.11
G42R Lens 1 Traverse 1	Lens	17	94.35	4.90	0.32	0.31	0.11
G42R Lens 1 Traverse 1	Lens	18	95.71	3.41	0.31	0.55	0.02
G42R Lens 1 Traverse 1	Lens	19	96.23	3.13	0.28	0.35	0.01
G42R Lens 1 Traverse 1	Lens	20	96.55	2.74	0.32	0.38	0.01
G42R Lens 1 Traverse 1	Lens	21	98.28	1.27	0.23	0.20	0.02
G42R Lens 1 Traverse 1	Lens	22	96.82	2.58	0.28	0.26	0.06
G42R Lens 1 Traverse 1	Lens	23	98.00	1.39	0.35	0.20	0.06
G42R Lens 1 Traverse 1	Lens	24	97.67	1.64	0.33	0.36	0.00
G42R Lens 1 Traverse 1	Lens	25	98.12	1.23	0.35	0.22	0.08
G42R Lens 1 Traverse 1	Lens	26	98.13	1.26	0.31	0.29	0.00
G42R Lens 1 Traverse 1	Lens	27	98.04	1.25	0.39	0.30	0.02
G42R Lens 1 Traverse 1	Lens	28	97.83	1.48	0.33	0.32	0.04
G42R Lens 1 Traverse 1	Lens	29	98.00	1.36	0.36	0.24	0.04
G42R Lens 1 Traverse 1	Lens	30	97.81	1.46	0.35	0.36	0.03

SAMPLE	FEATURE	DATA SET/ POINT	NORMALISED WEIGHT % CARBONATE				
			Ca	Mg	Sr	Fe	Mn
G42R Lens 1 Traverse 2	Lens	1	97.37	2.07	0.33	0.18	0.05
G42R Lens 1 Traverse 2	Lens	2	95.36	3.81	0.30	0.41	0.13
G42R Lens 1 Traverse 2	Lens	3	98.44	1.05	0.22	0.26	0.03
G42R Lens 1 Traverse 2	Lens	4	96.86	2.45	0.24	0.45	0.01
G42R Lens 1 Traverse 2	Lens	5	81.28	16.60	0.42	1.51	0.19
G42R Lens 1 Traverse 2	Lens	6	98.13	1.21	0.30	0.30	0.06
G42R Lens 1 Traverse 2	Lens	7	98.23	1.11	0.33	0.27	0.06
G42R Lens 1 Traverse 2	Lens	8	96.47	2.96	0.32	0.24	0.01
G42R Lens 1 Traverse 2	Lens	9	97.91	1.32	0.47	0.23	0.07
G42R Lens 1 Traverse 2	Lens	10	96.01	3.10	0.35	0.42	0.12
G42R Lens 1 Traverse 2	Lens	11	98.15	1.17	0.37	0.28	0.03
G42R Lens 1 Traverse 2	Lens	12	97.18	2.29	0.27	0.15	0.11
G42R Lens 1 Traverse 2	Lens	13	96.98	2.31	0.34	0.26	0.11
G42R Lens 1 Traverse 2	Lens	14	95.97	3.37	0.29	0.31	0.05
G42R Lens 1 Traverse 2	Lens	15	96.93	2.54	0.31	0.17	0.05
G42R Lens 3 Traverse 1	Lens	1	97.75	1.60	0.37	0.25	0.03
G42R Lens 3 Traverse 1	Lens	2	97.74	1.40	0.35	0.42	0.09
G42R Lens 3 Traverse 1	Lens	3	98.03	1.32	0.35	0.27	0.03
G42R Lens 3 Traverse 1	Lens	4	98.01	1.39	0.28	0.29	0.03
G42R Lens 3 Traverse 1	Lens	5	97.93	1.35	0.41	0.21	0.09
G42R Lens 3 Traverse 1	Lens	6	97.72	1.65	0.31	0.23	0.10
G42R Lens 3 Traverse 1	Lens	7	97.76	1.72	0.30	0.22	0.00
G42R Lens 3 Traverse 1	Lens	8	97.47	1.77	0.37	0.30	0.08
G42R Lens 3 Traverse 1	Lens	9	97.62	1.77	0.32	0.29	0.00
G42R Lens 3 Traverse 1	Lens	10	97.77	1.54	0.30	0.31	0.07
G42R Lens 3 Traverse 1	Lens	11	97.42	1.85	0.35	0.26	0.13
G42R Lens 3 Traverse 1	Lens	12	97.96	1.27	0.50	0.26	0.01
G42R Lens 3 Traverse 1	Lens	13	98.25	0.93	0.62	0.19	0.01
G42R Lens 3 Traverse 1	Lens	14	97.83	1.73	0.25	0.17	0.02
G42R Lens 3 Traverse 1	Lens	15	97.72	1.61	0.33	0.30	0.04
G42R Lens 3 Traverse 1	Lens	16	98.06	1.34	0.37	0.18	0.05
G42R Lens 3 Traverse 1	Lens	17	97.59	1.59	0.40	0.30	0.13
G42R Lens 3 Traverse 1	Lens	18	97.33	2.07	0.36	0.16	0.08
G42R Lens 3 Traverse 1	Lens	19	97.50	1.72	0.33	0.34	0.11
G42R Lens 3 Traverse 1	Lens	20	97.61	1.57	0.44	0.24	0.14
G42R Lens 3 Traverse 1	Lens	21	97.50	1.89	0.34	0.26	0.01
G42R Lens 3 Traverse 1	Lens	22	98.04	1.26	0.36	0.30	0.05
G42R Lens 3 Traverse 1	Lens	23	98.04	1.18	0.35	0.40	0.03
G42R Lens 3 Traverse 1	Lens	24	97.83	1.43	0.32	0.38	0.04
G42R Lens 3 Traverse 1	Lens	25	97.92	1.43	0.35	0.29	0.00
G42R Lens 3 Traverse 2	Lens	1	97.21	2.05	0.36	0.33	0.05
G42R Lens 3 Traverse 2	Lens	2	97.59	1.78	0.37	0.26	0.00
G42R Lens 3 Traverse 2	Lens	3	98.03	1.29	0.31	0.37	0.00
G42R Lens 3 Traverse 2	Lens	4	98.07	1.21	0.29	0.36	0.07
G42R Lens 3 Traverse 2	Lens	5	97.71	1.57	0.42	0.30	0.00
G42R Lens 3 Traverse 2	Lens	6	97.13	2.16	0.38	0.33	0.00
G42R Lens 3 Traverse 2	Lens	7	97.31	2.04	0.34	0.30	0.00
G42R Lens 3 Traverse 2	Lens	8	97.27	1.91	0.44	0.34	0.04
G42R Lens 3 Traverse 2	Lens	9	97.27	2.10	0.39	0.23	0.00
G42R Lens 3 Traverse 2	Lens	10	97.76	1.54	0.34	0.24	0.13
G42R Lens 3 Traverse 2	Lens	11	97.07	2.22	0.34	0.24	0.12
G42R Lens 3 Traverse 2	Lens	12	97.86	1.51	0.52	0.11	0.00
G42R Lens 3 Traverse 2	Lens	13	97.71	1.38	0.67	0.25	0.00
G42R Lens 3 Traverse 2	Lens	14	97.69	1.78	0.21	0.23	0.09
G42R Lens 3 Traverse 2	Lens	15	97.46	1.89	0.33	0.21	0.11
G42R Lens 3 Traverse 2	Lens	16	97.91	1.52	0.39	0.10	0.09
G42R Lens 3 Traverse 2	Lens	17	97.22	2.03	0.36	0.33	0.05
G42R Lens 3 Traverse 2	Lens	18	96.99	2.32	0.40	0.29	0.00
G42R Lens 3 Traverse 2	Lens	19	97.02	2.17	0.43	0.28	0.10
G42R Lens 3 Traverse 2	Lens	20	97.40	1.89	0.47	0.16	0.09

SAMPLE	FEATURE	DATA SET/ POINT	NORMALISED WEIGHT % CARBONATE				
			Ca	Mg	Sr	Fe	Mn
G42R Lens 3 Traverse 2	Lens	21	97.10	2.25	0.35	0.24	0.05
G42R Lens 3 Traverse 2	Lens	22	97.76	1.55	0.47	0.23	0.00
G42R Lens 3 Traverse 2	Lens	23	98.10	1.05	0.30	0.44	0.10
G42R Lens 3 Traverse 2	Lens	24	97.92	1.47	0.36	0.22	0.03
G42R Lens 3 Traverse 2	Lens	25	97.89	1.41	0.34	0.29	0.07
G42R Lens 2 Traverse 1	Lens	1	98.26	1.02	0.43	0.18	0.10
G42R Lens 2 Traverse 1	Lens	2	98.22	1.31	0.29	0.18	0.00
G42R Lens 2 Traverse 1	Lens	3	94.90	4.26	0.35	0.48	0.00
G42R Lens 2 Traverse 1	Lens	4	97.12	1.98	0.33	0.42	0.14
G42R Lens 2 Traverse 1	Lens	5	97.68	1.57	0.29	0.32	0.14
G42R Lens 2 Traverse 1	Lens	6	98.13	1.24	0.32	0.21	0.10
G42R Lens 2 Traverse 1	Lens	7	97.75	1.59	0.42	0.24	0.00
G42R Lens 2 Traverse 1	Lens	8	97.83	1.63	0.26	0.24	0.04
G42R Lens 2 Traverse 1	Lens	9	97.31	2.04	0.35	0.28	0.02
G42R Lens 2 Traverse 1	Lens	10	97.36	1.96	0.30	0.30	0.08
G42R Lens 2 Traverse 1	Lens	11	98.02	1.20	0.63	0.15	0.00
G42R Lens 2 Traverse 1	Lens	12	97.60	1.62	0.47	0.23	0.08
G42R Lens 2 Traverse 1	Lens	13	97.98	1.22	0.45	0.27	0.09
G42R Lens 2 Traverse 1	Lens	14	97.83	1.57	0.32	0.24	0.03
G42R Lens 2 Traverse 1	Lens	15	98.02	1.28	0.49	0.19	0.02
G42R Lens 2 Traverse 1	Lens	16	97.97	1.30	0.49	0.23	0.00
G42R Lens 2 Traverse 1	Lens	17	97.66	1.47	0.39	0.41	0.07
G42R Lens 2 Traverse 1	Lens	18	94.91	2.21	0.27	2.59	0.02
G42R Lens 2 Traverse 1	Lens	19	97.11	1.75	0.29	0.73	0.12
G42R Lens 2 Traverse 1	Lens	20	96.65	1.97	0.21	1.13	0.04
G42R Lens 2 Traverse 1	Lens	21	96.45	2.28	0.18	1.02	0.07
G42R Lens 2 Traverse 1	Lens	22	92.61	4.61	0.14	2.52	0.11
G42R Lens 2 Traverse 1	Lens	23	93.71	3.83	0.24	2.09	0.13
G42R Lens 2 Traverse 1	Lens	24	97.89	1.34	0.27	0.49	0.00
G42R Lens 2 Traverse 1	Lens	25	75.92	11.55	0.00	11.90	0.62
G42R Lens 2 Traverse 1	Lens	26	96.54	2.75	0.31	0.34	0.06
G42R Lens 2 Traverse 1	Lens	27	97.72	1.66	0.36	0.17	0.09
G42R Lens 2 Traverse 1	Lens	28	95.23	4.08	0.34	0.35	0.00
G42R Lens 2 Traverse 1	Lens	29	98.67	0.90	0.29	0.10	0.04
G42R Lens 2 Traverse 1	Lens	30	96.21	3.01	0.26	0.42	0.11
G42R	Sclera	1	98.40	1.12	0.34	0.13	0.01
G42R	Sclera	2	96.59	2.70	0.34	0.28	0.10
G42R	Sclera	3	97.94	1.33	0.37	0.30	0.06
G42R	Sclera	4	97.60	1.74	0.37	0.26	0.03
G42R	Sclera	5	98.11	1.17	0.58	0.14	0.00
G42R	Sclera	6	97.96	1.40	0.47	0.12	0.05
G42R	Sclera	7	97.55	1.77	0.47	0.20	0.00
G42R	Sclera	8	97.72	1.75	0.31	0.23	0.00
G42R	Sclera	9	97.85	1.54	0.41	0.15	0.05
G42R	Sclera	10	97.74	1.50	0.40	0.31	0.05
G42R	Sclera	11	97.03	2.14	0.50	0.26	0.07
G42R	Sclera	12	97.82	1.47	0.44	0.27	0.00
G42R	Sclera	13	97.78	1.62	0.34	0.19	0.06
G42R	Sclera	14	97.64	1.52	0.31	0.48	0.05
G42R	Sclera	15	96.85	2.03	0.16	0.93	0.03
G42R	Sclera	16	95.70	2.57	0.23	1.50	0.00
G42R	Sclera	17	97.41	1.71	0.29	0.54	0.05
G42R	Sclera	18	97.43	1.62	0.30	0.57	0.08
G42R	Sclera	19	96.38	2.29	0.17	1.13	0.03
G42R	Sclera	20	84.48	6.91	0.07	8.42	0.12
G42R	Sclera	21	96.49	2.17	0.15	1.10	0.09
G42R	Sclera	22	97.31	1.77	0.25	0.63	0.03
G42R	Sclera	23	94.83	2.76	0.25	2.05	0.10
G42R	Sclera	24	97.92	1.18	0.31	0.60	0.00
G42R	Sclera	25	97.91	1.25	0.32	0.36	0.16

SAMPLE	FEATURE	DATA SET/ POINT	NORMALISED WEIGHT % CARBONATE				
			Ca	Mg	Sr	Fe	Mn
G42R	Crinoid	1	96.97	2.46	0.28	0.29	0.00
G42R	Crinoid	2	97.26	1.84	0.38	0.46	0.06
G42R	Crinoid	3	95.89	3.51	0.33	0.28	0.00
G42R	Crinoid	4	94.35	3.49	0.18	1.96	0.02
G42R	Crinoid	5	97.40	1.92	0.30	0.33	0.05
G42R	Crinoid	6	96.95	1.96	0.27	0.71	0.11
G42R	Crinoid	7	97.92	1.62	0.26	0.19	0.01
G42R	Crinoid	8	97.43	1.73	0.27	0.49	0.08
G42R	Crinoid	9	97.51	1.80	0.20	0.44	0.05
G42R	Crinoid	10	97.50	1.74	0.32	0.29	0.15
G42R	Crinoid	11	97.61	1.79	0.23	0.25	0.12
G42R	Crinoid	12	97.88	1.59	0.28	0.25	0.00
G42R	Crinoid	13	97.17	2.03	0.41	0.33	0.05
G42R	Crinoid	14	96.81	1.97	0.27	0.85	0.10
G42R	Crinoid	15	97.59	1.62	0.25	0.48	0.05
G42R	Crinoid	16	97.37	2.00	0.30	0.34	0.00
G42R	Crinoid	17	97.47	1.97	0.19	0.31	0.05
G42R	Crinoid	18	97.05	1.96	0.31	0.65	0.02
G42R	Crinoid	19	96.18	2.46	0.30	0.91	0.15
G42R	Crinoid	20	97.45	1.81	0.29	0.41	0.04
G42R	Crinoid	21	97.40	1.65	0.26	0.61	0.08
G42R	Crinoid	22	97.21	1.94	0.30	0.55	0.00
G42R	Crinoid	23	97.79	1.34	0.39	0.34	0.13
G42R	Crinoid	24	97.78	1.61	0.34	0.26	0.00
G42R	Crinoid	25	96.06	3.17	0.29	0.47	0.01
PM28 (Lens 1)	Lens	1	93.88	2.34	0.00	3.67	0.11
PM28 (Lens 1)	Lens	2	91.09	8.59	0.00	0.33	0.00
PM28 (Lens 1)	Lens	3	94.41	5.18	0.00	0.40	0.01
PM28 (Lens 1)	Lens	4	93.18	6.79	0.00	0.03	0.00
PM28 (Lens 1)	Lens	5	93.20	6.65	0.00	0.09	0.06
PM28 (Lens 1)	Lens	6	92.68	7.19	0.00	0.05	0.08
PM28 (Lens 1)	Lens	7	93.49	6.48	0.00	0.00	0.03
PM28 (Lens 1)	Lens	8	90.32	9.55	0.00	0.10	0.03
PM28 (Lens 1)	Lens	9	93.07	6.86	0.00	0.03	0.04
PM28 (Lens 1)	Lens	10	91.26	8.57	0.00	0.11	0.05
PM28 (Lens 1)	Lens	11	94.62	5.38	0.00	0.00	0.00
PM28 (Lens 1)	Lens	12	92.96	6.93	0.00	0.11	0.00
PM28 (Lens 1)	Lens	13	93.37	5.96	0.00	0.68	0.00
PM28 (Lens 1)	Bowl?	14	96.56	0.85	0.00	2.59	0.00
PM28 (Lens 1)	Bowl?	15	96.41	0.85	0.00	2.65	0.09
PM28 Lens 1 (traverse 2)	Lens	1	95.83	0.90	0.00	3.14	0.14
PM28 Lens 1 (traverse 2)	Lens	2	96.45	0.90	0.00	2.49	0.16
PM28 Lens 1 (traverse 2)	Lens	3	93.37	5.94	0.00	0.62	0.06
PM28 Lens 1 (traverse 2)	Lens	4	93.16	6.79	0.00	0.02	0.03
PM28 Lens 1 (traverse 2)	Lens	5	94.73	5.19	0.00	0.00	0.08
PM28 Lens 1 (traverse 2)	Lens	6	91.59	8.29	0.00	0.03	0.09
PM28 Lens 1 (traverse 2)	Lens	7	92.86	7.11	0.00	0.03	0.00
PM28 Lens 1 (traverse 2)	Lens	8	90.53	9.40	0.00	0.06	0.01
PM28 Lens 1 (traverse 2)	Lens	9	93.47	6.42	0.00	0.11	0.00
PM28 Lens 1 (traverse 2)	Lens	10	92.69	7.27	0.00	0.03	0.01
PM28 Lens 1 (traverse 2)	Lens	11	93.26	6.61	0.00	0.10	0.03
PM28 Lens 1 (traverse 2)	Lens	12	93.02	6.89	0.00	0.08	0.00
PM28 Lens 1 (traverse 2)	Lens	13	94.47	5.07	0.00	0.44	0.02
PM28 Lens 1 (traverse 2)	Lens	14	91.01	8.56	0.00	0.43	0.00
PM28 Lens 1 (traverse 2)	Lens	15	93.90	2.47	0.00	3.52	0.11
PM28 Lens 2 (traverse 1)	Lens	1	94.93	5.03	0.00	0.00	0.04
PM28 Lens 2 (traverse 1)	Lens	2	93.11	6.69	0.00	0.13	0.07
PM28 Lens 2 (traverse 1)	Lens	3	93.57	6.27	0.00	0.08	0.08
PM28 Lens 2 (traverse 1)	Lens	4	91.05	8.83	0.00	0.00	0.12
PM28 Lens 2 (traverse 1)	Lens	5	93.60	6.40	0.00	0.00	0.00

SAMPLE	FEATURE	DATA SET/ POINT	NORMALISED WEIGHT % CARBONATE				
			Ca	Mg	Sr	Fe	Mn
PM28 Lens 2 (traverse 1)	Lens	6	91.71	8.22	0.00	0.02	0.05
PM28 Lens 2 (traverse 1)	Lens	7	92.27	7.70	0.00	0.03	0.00
PM28 Lens 2 (traverse 1)	Lens	8	90.22	9.73	0.00	0.03	0.02
PM28 Lens 2 (traverse 1)	Lens	9	93.57	6.38	0.00	0.00	0.05
PM28 Lens 2 (traverse 1)	Lens	10	92.03	7.89	0.00	0.05	0.03
PM28 Lens 2 (traverse 1)	Lens	11	91.90	7.88	0.00	0.15	0.07
PM28 Lens 2 (traverse 1)	Lens	12	94.35	3.59	0.00	1.96	0.10
PM28 Lens 2 (traverse 1)	Lens	13	96.95	0.74	0.00	2.28	0.04
PM28 Lens 2 (traverse 1)	Lens	14	92.22	1.72	0.00	5.84	0.22
PM28 Lens 2 (traverse 1)	Lens	15	36.00	13.59	0.00	50.41	0.00
PM28 Lens 2 (traverse 2)	Lens	1	96.31	1.09	0.00	2.50	0.10
PM28 Lens 2 (traverse 2)	Lens	2	95.58	1.72	0.00	2.55	0.16
PM28 Lens 2 (traverse 2)	Lens	3	93.22	5.94	0.00	0.69	0.15
PM28 Lens 2 (traverse 2)	Lens	4	94.87	4.84	0.00	0.30	0.00
PM28 Lens 2 (traverse 2)	Lens	5	92.86	6.84	0.00	0.23	0.08
PM28 Lens 2 (traverse 2)	Lens	6	93.28	6.65	0.00	0.05	0.02
PM28 Lens 2 (traverse 2)	Lens	7	93.18	6.63	0.00	0.09	0.09
PM28 Lens 2 (traverse 2)	Lens	8	94.32	5.37	0.00	0.27	0.04
PM28 Lens 2 (traverse 2)	Lens	9	92.68	7.03	0.00	0.17	0.12
PM28 Lens 2 (traverse 2)	Lens	10	95.78	4.16	0.00	0.00	0.06
PM28 Lens 2 (traverse 2)	Lens	11	91.00	8.93	0.00	0.07	0.00
PM28 Lens 2 (traverse 2)	Lens	12	91.77	8.16	0.00	0.01	0.06
PM28 Lens 2 (traverse 2)	Lens	13	91.93	7.42	0.00	0.63	0.02
PM28 Lens 2 (traverse 2)	Lens	14	95.66	1.36	0.00	2.83	0.16
PM28 Lens 2 (traverse 2)	Cement ?	15	97.05	0.87	0.00	1.96	0.12
PM28 Lens 3 (taverse 1)	Lens	1	90.12	9.80	0.00	0.04	0.04
PM28 Lens 3 (taverse 1)	Lens	2	95.55	4.31	0.00	0.07	0.06
PM28 Lens 3 (taverse 1)	Lens	3	92.34	7.45	0.00	0.09	0.11
PM28 Lens 3 (taverse 1)	Lens	4	93.71	6.20	0.00	0.09	0.00
PM28 Lens 3 (taverse 1)	Lens	5	92.98	6.85	0.00	0.14	0.02
PM28 Lens 3 (taverse 1)	Lens	6	94.05	5.91	0.00	0.04	0.00
PM28 Lens 3 (taverse 1)	Lens	7	92.01	7.85	0.00	0.09	0.05
PM28 Lens 3 (taverse 1)	Lens	8	92.90	7.08	0.00	0.02	0.00
PM28 Lens 3 (taverse 1)	Lens	9	89.93	10.01	0.00	0.06	0.00
PM28 Lens 3 (taverse 1)	Lens	10	89.75	10.19	0.00	0.06	0.00
PM28 Lens 3 (taverse 1)	Lens	11	92.55	6.88	0.00	0.56	0.01
PM28 Lens 3 (taverse 1)	Lens	12	91.66	6.67	0.00	1.62	0.06
PM28 Lens 3 (taverse 1)	Lens	13	94.64	0.83	0.00	4.38	0.15
PM28 Lens 3 (taverse 1)	Lens	14	94.48	1.11	0.00	4.19	0.21
PM28 Lens 3 (taverse 1)	Lens	15	96.39	0.95	0.00	2.60	0.05
PM28 Lens 3 (taverse 1)	Lens	16	92.07	6.11	0.00	1.57	0.24
PM28 Lens 3 (taverse 1)	Lens	17	91.79	7.67	0.00	0.44	0.10
PM28 Lens 3 (taverse 1)	Lens	18	93.31	6.60	0.00	0.09	0.00
PM28 Lens 3 (taverse 1)	Lens	19	93.95	5.90	0.00	0.13	0.02
PM28 Lens 3 (taverse 1)	Lens	20	93.33	6.65	0.00	0.01	0.01
PM28 Lens 3 (traverse 2)	Lens	1	93.08	6.74	0.00	0.17	0.00
PM28 Lens 3 (traverse 2)	Lens	2	92.57	7.29	0.00	0.14	0.00
PM28 Lens 3 (traverse 2)	Lens	3	94.63	5.16	0.00	0.21	0.00
PM28 Lens 3 (traverse 2)	Lens	4	95.68	4.31	0.00	0.00	0.00
PM28 Lens 3 (traverse 2)	Lens	5	95.23	4.68	0.00	0.02	0.06
PM28 Lens 3 (traverse 2)	Lens	6	89.26	10.63	0.00	0.09	0.01
PM28 Lens 3 (traverse 2)	Lens	7	93.84	5.98	0.00	0.17	0.01
PM28 Lens 3 (traverse 2)	Lens	8	96.41	3.38	0.00	0.21	0.00
PM28 Lens 3 (traverse 2)	Lens	9	93.57	6.21	0.00	0.15	0.07
PM28 Lens 3 (traverse 2)	Lens	10	93.11	6.87	0.00	0.03	0.00
PM28 Lens 3 (traverse 2)	Lens	11	91.11	8.18	0.00	0.66	0.06
PM28 Lens 3 (traverse 2)	Lens	12	92.51	7.37	0.00	0.05	0.07
PM28 Lens 3 (traverse 2)	Lens	13	92.25	7.65	0.00	0.09	0.00
PM28 Lens 3 (traverse 2)	Lens	14	91.95	7.20	0.00	0.72	0.12
PM28 Lens 3 (traverse 2)	Lens	15	93.73	4.98	0.00	1.11	0.18

Table E.4 - Mole % carbonate EPMA data (Strathclyde) for trilobites with schizochroal eyes.

SAMPLE	FEATURE	DATA SET/ POINT	MOLE % CARBONATE				
			Ca	Mg	Sr	Fe	Mn
AM65 Lens 1 Traverse 1	Lens	1	95.5	1.5	0.0	2.8	0.2
AM65 Lens 1 Traverse 1	Lens	2	91.7	6.0	0.1	2.1	0.1
AM65 Lens 1 Traverse 1	Lens	3	79.9	18.2	0.2	1.7	0.1
AM65 Lens 1 Traverse 1	Lens	4	91.9	7.6	0.3	0.2	0.0
AM65 Lens 1 Traverse 1	Lens	5	93.5	6.2	0.3	0.1	0.0
AM65 Lens 1 Traverse 1	Lens	6	93.9	5.8	0.3	0.1	0.0
AM65 Lens 1 Traverse 1	Lens	7	92.0	7.7	0.2	0.0	0.1
AM65 Lens 1 Traverse 1	Lens	8	82.0	17.7	0.2	0.1	0.0
AM65 Lens 1 Traverse 1	Lens	9	93.5	6.0	0.3	0.2	0.0
AM65 Lens 1 Traverse 1	Lens	10	93.4	6.2	0.3	0.0	0.0
AM65 Lens 1 Traverse 1	Lens	11	93.7	6.0	0.3	0.0	0.0
AM65 Lens 1 Traverse 1	Lens	12	92.3	7.2	0.3	0.2	0.0
AM65 Lens 1 Traverse 1	Lens	13	92.4	7.1	0.3	0.1	0.1
AM65 Lens 1 Traverse 1	Lens	14	91.9	7.6	0.2	0.1	0.1
AM65 Lens 1 Traverse 1	Lens	15	89.1	10.2	0.2	0.4	0.2
AM65 Lens 1 Traverse 2	Lens	1	90.8	3.9	0.0	5.2	0.1
AM65 Lens 1 Traverse 2	Lens	2	94.9	1.8	0.0	3.0	0.3
AM65 Lens 1 Traverse 2	Lens	3	93.3	2.3	0.0	3.9	0.6
AM65 Lens 1 Traverse 2	Lens	4	90.5	9.0	0.3	0.2	0.0
AM65 Lens 1 Traverse 2	Lens	5	90.3	9.3	0.3	0.1	0.0
AM65 Lens 1 Traverse 2	Lens	6	89.9	9.7	0.4	0.0	0.1
AM65 Lens 1 Traverse 2	Lens	7	90.9	8.8	0.3	0.0	0.0
AM65 Lens 1 Traverse 2	Lens	8	92.6	7.0	0.2	0.1	0.1
AM65 Lens 1 Traverse 2	Lens	9	93.2	6.6	0.3	0.0	0.0
AM65 Lens 1 Traverse 2	Lens	10	83.2	16.1	0.2	0.4	0.0
AM65 Lens 1 Traverse 2	Lens	11	85.9	13.8	0.2	0.1	0.0
AM65 Lens 1 Traverse 2	Lens	12	92.4	7.2	0.3	0.0	0.1
AM65 Lens 1 Traverse 2	Lens	13	89.6	9.4	0.2	0.7	0.1
AM65 Lens 1 Traverse 2	Lens	14	93.7	5.5	0.3	0.4	0.1
AM65 Lens 1 Traverse 2	Lens	15	94.7	4.7	0.2	0.3	0.0
AM65 Lens 2 Traverse 1	Lens	1	92.0	7.3	0.2	0.2	0.2
AM65 Lens 2 Traverse 1	Lens	2	90.4	9.0	0.2	0.3	0.1
AM65 Lens 2 Traverse 1	Lens	3	91.7	7.9	0.3	0.1	0.1
AM65 Lens 2 Traverse 1	Lens	4	91.2	8.4	0.3	0.0	0.1
AM65 Lens 2 Traverse 1	Lens	5	90.5	9.1	0.3	0.1	0.0
AM65 Lens 2 Traverse 1	Lens	6	92.4	7.2	0.3	0.1	0.1
AM65 Lens 2 Traverse 1	Lens	7	90.0	9.6	0.3	0.0	0.1
AM65 Lens 2 Traverse 1	Lens	8	92.1	7.4	0.3	0.0	0.1
AM65 Lens 2 Traverse 1	Lens	9	91.1	8.6	0.3	0.0	0.0
AM65 Lens 2 Traverse 1	Lens	10	88.4	11.0	0.2	0.3	0.0
AM65 Lens 2 Traverse 1	Lens	11	93.2	6.3	0.3	0.0	0.1
AM65 Lens 2 Traverse 1	Lens	12	91.9	7.8	0.3	0.0	0.0
AM65 Lens 2 Traverse 1	Lens	13	89.6	10.1	0.3	0.0	0.1
AM65 Lens 2 Traverse 1	Lens	14	95.1	4.3	0.2	0.2	0.1
AM65 Lens 2 Traverse 1	Lens	15	92.0	7.4	0.3	0.2	0.1
AM65 Lens 2 Traverse 2	Lens	1	96.3	2.6	0.2	0.7	0.1
AM65 Lens 2 Traverse 2	Lens	2	92.9	6.2	0.3	0.4	0.1
AM65 Lens 2 Traverse 2	Lens	3	94.9	4.5	0.3	0.1	0.1
AM65 Lens 2 Traverse 2	Lens	4	90.3	9.3	0.3	0.1	0.0
AM65 Lens 2 Traverse 2	Lens	5	90.3	9.3	0.3	0.0	0.1
AM65 Lens 2 Traverse 2	Lens	6	91.1	8.5	0.3	0.0	0.0
AM65 Lens 2 Traverse 2	Lens	7	91.3	8.3	0.3	0.0	0.0
AM65 Lens 2 Traverse 2	Lens	8	93.5	6.1	0.2	0.1	0.0

SAMPLE	FEATURE	DATA SET/ POINT	MOLE % CARBONATE				
			Ca	Mg	Sr	Fe	Mn
AM65 Lens 2 Traverse 2	Lens	9	83.5	16.1	0.2	0.1	0.0
AM65 Lens 2 Traverse 2	Lens	10	83.4	16.2	0.3	0.1	0.0
AM65 Lens 2 Traverse 2	Lens	11	89.4	10.2	0.3	0.1	0.0
AM65 Lens 2 Traverse 2	Lens	12	80.6	18.6	0.3	0.3	0.1
AM65 Lens 2 Traverse 2	Lens	13	93.9	1.9	0.1	3.6	0.5
AM65 Lens 2 Traverse 2	Lens	14	94.3	1.9	0.0	3.7	0.1
AM65 Lens 2 Traverse 2	Lens	15	94.9	1.9	0.0	2.9	0.3
BB3aR Lens 2	Lens	1	99.3	0.6	0.0	0.0	0.1
BB3aR Lens 2	Lens	2	95.9	4.1	0.0	0.0	0.0
BB3aR Lens 2	Lens	3	98.7	1.3	0.0	0.0	0.0
BB3aR Lens 2	Lens	4	95.6	4.4	0.0	0.0	0.0
BB3aR Lens 2	Lens	5	98.3	1.7	0.0	0.0	0.0
BB3aR Lens 2	Lens	6	98.8	1.2	0.0	0.0	0.0
BB3aR Lens 2	Lens	7	99.1	0.8	0.0	0.1	0.0
BB3aR Lens 2	Lens	8	91.4	8.5	0.0	0.1	0.0
BB3aR Lens 2	Lens	9	97.7	2.3	0.0	0.0	0.0
BB3aR Lens 2	Lens	10	98.9	1.0	0.0	0.1	0.0
BB3aR Lens 2	Lens	11	95.0	4.9	0.0	0.0	0.0
BB3aR Lens 2	Lens	12	99.2	0.8	0.0	0.0	0.0
BB3aR Lens 2	Lens	13	99.0	0.9	0.0	0.0	0.0
BB3aR Lens 2	Lens	14	92.3	7.6	0.0	0.0	0.1
BB3aR Lens 2	Lens	15	97.1	2.9	0.0	0.0	0.0
BB3aR Lens 2	Lens	16	97.5	2.4	0.0	0.1	0.0
BB3aR Lens 2	Lens	17	95.7	4.3	0.0	0.0	0.0
BB3aR Lens 2	Lens	18	94.2	5.7	0.0	0.1	0.0
BB3aR Lens 2	Lens	19	99.6	0.4	0.0	0.0	0.0
BB3aR Lens 2	Lens	20	98.7	1.2	0.0	0.0	0.1
BB3aR Lens 2	Lens	21	98.8	1.2	0.0	0.1	0.0
BB3aR Lens 2	Lens	22	93.7	6.3	0.0	0.1	0.0
BB3aR Lens 2	Lens	23	98.3	1.6	0.0	0.0	0.0
BB3aR Lens 2	Lens	24	99.0	1.0	0.0	0.0	0.0
BB3aR Lens 2	Lens	25	98.8	1.1	0.0	0.0	0.0
BB3aR Lens 2	Lens	26	96.2	3.7	0.0	0.1	0.0
BB3aR Lens 2	Lens	27	98.6	1.4	0.0	0.0	0.0
BB3aR Lens 2	Lens	28	99.2	0.7	0.0	0.1	0.0
BB3aR Lens 2	Lens	29	99.3	0.6	0.0	0.0	0.0
BB3aR Lens 2	Lens	30	99.1	0.9	0.0	0.0	0.0
BB3aR Lens 2	Lens	31	98.9	1.1	0.0	0.0	0.0
BB3aR Lens 2	Lens	32	99.2	0.8	0.0	0.0	0.0
BB3aR Lens 2	Lens	33	98.5	1.5	0.0	0.0	0.0
BB3aR Lens 2	Lens	34	98.5	1.4	0.0	0.1	0.0
BB3aR Lens 2	Lens	35	99.4	0.5	0.0	0.0	0.0
BB3aR Lens 2	Lens	36	99.4	0.5	0.0	0.0	0.0
BB3aR Lens 2	Lens	37	99.2	0.6	0.0	0.1	0.0
BB3aR Lens 2	Lens	38	99.2	0.7	0.0	0.1	0.1
BB3aR Lens 2	Lens	39	95.2	4.6	0.0	0.1	0.1
BB3aR Lens 2	Lens	40	99.3	0.6	0.0	0.0	0.0
BB3aR Lens 2	Lens	41	99.3	0.7	0.0	0.0	0.0
BB3aR Lens 2	Lens	42	98.8	1.1	0.0	0.0	0.0
BB3aR Lens 2	Lens	43	63.3	36.7	0.0	0.0	0.0
BB3aR Lens 2	Lens	44	99.5	0.5	0.0	0.0	0.0
BB3aR Lens 2	Lens	45	99.1	0.7	0.0	0.2	0.1
BB3aR Lens 2	Lens	46	99.4	0.5	0.0	0.1	0.0
BB3aR Lens 2	Lens	47	98.7	1.3	0.0	0.0	0.0
BB3aR Lens 2	Lens	48	99.2	0.8	0.0	0.0	0.0
BB3aR Lens 2	Lens	49	98.7	1.3	0.0	0.1	0.0
BB3aR Lens 2	Lens	50	96.9	3.1	0.0	0.0	0.0
BB3aR Lens 2	Lens	51	99.2	0.8	0.0	0.0	0.0
BB3aR Lens 2	Lens	52	94.8	5.2	0.0	0.0	0.0
BB3aR Lens 2	Lens	53	93.2	6.8	0.0	0.0	0.0
BB3aR Lens 2	Lens	54	97.1	2.9	0.0	0.0	0.0
BB3aR Lens 2	Lens	55	99.2	0.7	0.0	0.0	0.1

SAMPLE	FEATURE	DATA SET/ POINT	MOLE % CARBONATE				
			Ca	Mg	Sr	Fe	Mn
BB3aR Lens 2	Lens	56	99.4	0.6	0.0	0.0	0.0
BB3aR Lens 2	Lens	57	99.4	0.5	0.0	0.0	0.0
BB3aR Lens 2	Lens	58	98.9	0.9	0.0	0.1	0.0
BB3aR Lens 2	Lens	59	95.9	4.1	0.0	0.0	0.0
BB3aR Lens 2	Lens	60	98.9	1.0	0.0	0.1	0.1
BB3aR Lens 2	Lens	61	98.9	1.1	0.0	0.0	0.0
BB3aR Lens 2	Lens	62	99.1	0.9	0.0	0.0	0.0
BB3aR Lens 2	Lens	63	88.6	11.3	0.0	0.1	0.0
BB3aR Lens 2	Lens	64	98.2	1.7	0.0	0.1	0.0
BB3aR Lens 2	Lens	65	99.3	0.5	0.0	0.1	0.1
BB3aR Lens 3	Lens	1	99.1	0.9	0.0	0.0	0.0
BB3aR Lens 3	Lens	2	99.2	0.7	0.0	0.0	0.1
BB3aR Lens 3	Lens	3	95.9	4.0	0.0	0.1	0.1
BB3aR Lens 3	Lens	4	95.3	4.6	0.0	0.1	0.0
BB3aR Lens 3	Lens	5	99.1	0.9	0.0	0.0	0.0
BB3aR Lens 3	Lens	6	92.9	7.1	0.0	0.0	0.0
BB3aR Lens 3	Lens	7	96.9	3.0	0.0	0.0	0.0
BB3aR Lens 3	Lens	8	99.0	1.0	0.0	0.0	0.0
BB3aR Lens 3	Lens	9	96.2	3.8	0.0	0.0	0.0
BB3aR Lens 3	Lens	10	97.1	2.9	0.0	0.0	0.0
BB3aR Lens 3	Lens	11	95.9	4.1	0.0	0.0	0.0
BB3aR Lens 3	Lens	12	99.8	0.2	0.0	0.0	0.0
BB3aR Lens 3	Lens	13	99.3	0.7	0.0	0.0	0.0
BB3aR Lens 3	Lens	14	99.4	0.6	0.0	0.0	0.0
BB3aR Lens 3	Lens	15	99.3	0.7	0.0	0.0	0.0
BB3aR Lens 3	Lens	16	98.3	1.6	0.0	0.1	0.0
BB3aR Lens 3	Lens	17	99.6	0.3	0.0	0.1	0.0
BB3aR Lens 3	Lens	18	99.4	0.5	0.0	0.1	0.0
BB3aR Lens 3	Lens	19	99.3	0.6	0.0	0.0	0.1
BB3aR Lens 3	Lens	20	98.7	1.2	0.0	0.0	0.0
BB3aR Lens 3	Lens	21	98.3	1.6	0.0	0.0	0.0
BB3aR Lens 3	Lens	22	96.8	3.1	0.0	0.1	0.0
BB3aR Lens 3	Lens	23	92.1	7.8	0.0	0.1	0.0
BB3aR Lens 3	Lens	24	98.9	1.1	0.0	0.0	0.0
BB3aR Lens 3	Lens	25	99.0	0.9	0.0	0.0	0.0
BB3aR Lens 3	Lens	26	98.9	1.0	0.0	0.1	0.0
BB3aR Lens 3	Lens	27	99.2	0.8	0.0	0.0	0.0
BB3aR Lens 3	Lens	28	95.0	4.9	0.0	0.0	0.0
BB3aR Lens 3	Lens	29	97.7	2.2	0.0	0.0	0.1
BB3aR Lens 3	Lens	30	99.3	0.6	0.0	0.0	0.0
BB3aR Lens 3	Lens	31	99.4	0.6	0.0	0.0	0.0
BB3aR Lens 3	Lens	32	98.2	1.7	0.0	0.1	0.0
BB3aR Lens 3	Lens	33	76.1	23.7	0.0	0.2	0.0
BB3aR Lens 3	Lens	34	97.8	2.1	0.0	0.1	0.0
BB3aR Lens 3	Lens	35	94.9	5.1	0.0	0.0	0.0
BB3aR Lens 3	Lens	36	97.1	2.8	0.0	0.0	0.0
BB3aR Lens 3	Lens	37	98.8	1.1	0.0	0.0	0.0
BB3aR Lens 3	Lens	38	97.8	0.6	0.0	1.5	0.1
BB3aR Lens 3	Lens	39	99.3	0.5	0.0	0.2	0.1
BB3aR Lens 3	Lens	40	99.3	0.6	0.0	0.0	0.1
BB3aR Lens 3	Lens	41	92.6	7.3	0.0	0.0	0.0
BB3aR Lens 3	Lens	42	99.3	0.6	0.0	0.1	0.0
BB3aR Lens 3	Lens	43	99.6	0.4	0.0	0.0	0.0
BB3aR Lens 3	Lens	44	99.2	0.7	0.0	0.1	0.0
BB3aR Lens 3	Lens	45	99.3	0.6	0.0	0.0	0.0
BB3aR Lens 3	Lens	46	99.4	0.6	0.0	0.1	0.0
BB3aR Lens 3	Lens	47	99.4	0.6	0.0	0.0	0.0
BB3aR Lens 3	Lens	48	99.3	0.6	0.0	0.0	0.0
BB3aR Lens 3	Lens	49	98.8	1.1	0.0	0.0	0.1
BB3aR Lens 3	Lens	50	98.5	1.5	0.0	0.0	0.0
BB3aR Lens 3	Lens	51	99.4	0.6	0.0	0.0	0.0
BB3aR Lens 3	Lens	52	92.4	7.5	0.0	0.1	0.0

SAMPLE	FEATURE	DATA SET/ POINT	MOLE % CARBONATE				
			Ca	Mg	Sr	Fe	Mn
BB3aR Lens 3	Lens	53	98.4	1.5	0.0	0.0	0.1
BB3aR Lens 3	Lens	54	95.3	4.6	0.0	0.1	0.0
BB3aR Lens 3	Lens	55	99.1	0.9	0.0	0.0	0.0
BB3aR Lens 3	Lens	56	99.2	0.8	0.0	0.0	0.0
BB3aR Lens 3	Lens	57	99.3	0.6	0.0	0.0	0.0
BB3aR Lens 3	Lens	58	99.7	0.2	0.0	0.1	0.0
BB3aR Lens 3	Lens	59	99.4	0.6	0.0	0.1	0.0
BB3aR Lens 3	Lens	60	99.3	0.7	0.0	0.0	0.0
BB3aR Lens 3	Lens	61	99.4	0.6	0.0	0.0	0.0
BB3aR Lens 3	Lens	62	99.4	0.5	0.0	0.0	0.0
BB3aR Lens 3	Lens	63	99.4	0.6	0.0	0.0	0.0
BB3aR Lens 3	Lens	64	99.3	0.7	0.0	0.0	0.0
BB3aR Lens 3	Lens	65	99.2	0.8	0.0	0.0	0.0
BB3aR Lens 3	Lens	66	99.4	0.6	0.0	0.0	0.0
BB3aR Lens 3	Lens	67	99.3	0.7	0.0	0.0	0.0
BB3aR Lens 3	Lens	68	91.5	8.4	0.0	0.0	0.0
BB3aR Lens 3	Lens	69	97.3	2.6	0.0	0.0	0.1
BB3aR Lens 3	Lens	70	99.4	0.6	0.0	0.0	0.0
BB3aR	Sclera	1	99.1	0.7	0.0	0.1	0.1
BB3aR	Sclera	2	99.2	0.8	0.0	0.0	0.0
BB3aR	Sclera	3	99.1	0.7	0.0	0.1	0.1
BB3aR	Sclera	4	99.2	0.6	0.0	0.1	0.1
BB3aR	Sclera	5	99.3	0.5	0.0	0.2	0.1
BB3aR	Sclera	6	99.4	0.4	0.0	0.1	0.0
BB3aR	Sclera	7	99.2	0.6	0.0	0.1	0.1
BB3aR	Sclera	8	99.4	0.5	0.0	0.1	0.0
BB3aR	Sclera	9	98.9	0.4	0.0	0.5	0.1
BB3aR	Sclera	10	99.2	0.5	0.0	0.2	0.1
BB3aR	Sclera	11	99.3	0.6	0.0	0.0	0.1
BB3aR	Sclera	12	99.2	0.7	0.0	0.1	0.0
BB3aR	Sclera	13	99.2	0.7	0.0	0.1	0.0
BB3aR	Sclera	14	99.3	0.6	0.0	0.0	0.0
BB3aR	Sclera	15	99.3	0.6	0.0	0.1	0.1
BB3aR	Sclera	16	99.2	0.5	0.0	0.2	0.1
BB3aR	Sclera	17	99.3	0.4	0.0	0.2	0.1
BB3aR	Cement	1	98.9	1.0	0.0	0.1	0.1
BB3aR	Cement	2	99.0	0.9	0.0	0.0	0.0
BB3aR	Cement	3	98.1	1.7	0.0	0.1	0.0
BB3aR	Cement	4	99.0	0.8	0.0	0.1	0.0
BB3aR	Cement	5	98.2	1.7	0.0	0.0	0.0
BB3aR	Cement	6	98.5	1.4	0.0	0.1	0.0
BB3aR	Cement	7	99.0	1.0	0.0	0.0	0.0
BB3aR	Cement	8	99.3	0.6	0.0	0.0	0.0
BB3aR	Cement	9	98.7	1.2	0.0	0.0	0.1
BB3aR	Cement	10	99.5	0.4	0.0	0.0	0.0
BB3aR	Cement	11	99.3	0.6	0.0	0.0	0.0
BB3aR	Cement	12	99.3	0.7	0.0	0.1	0.0
BB3aR	Cement	13	98.9	1.1	0.0	0.0	0.0
BB3aR	Cement	14	99.3	0.7	0.0	0.0	0.0
BB3aR	Cement	15	99.2	0.8	0.0	0.0	0.0
BB3aR	Cement	16	99.4	0.6	0.0	0.0	0.0
BB3aR	Cement	17	99.4	0.6	0.0	0.0	0.1
BB3aR	Cement	18	99.0	1.0	0.0	0.0	0.0
BB3aR	Cement	19	99.4	0.6	0.0	0.0	0.0
BB3aR	Cement	20	99.4	0.5	0.0	0.0	0.0
BB3aR	Cement	21	99.3	0.7	0.0	0.0	0.0
BB3aR	Cement	22	99.4	0.6	0.0	0.0	0.0
BB3aR	Cement	23	99.2	0.6	0.0	0.1	0.0
BB3aR	Cement	24	98.2	1.7	0.0	0.0	0.1
BB3aR	Cement	25	99.4	0.6	0.0	0.0	0.0
BB3aR	Cement	26	97.0	2.9	0.0	0.0	0.0

SAMPLE	FEATURE	DATA SET/ POINT	MOLE % CARBONATE				
			Ca	Mg	Sr	Fe	Mn
BB3aR	Cement	27	98.9	0.9	0.0	0.1	0.1
BB3aR	Cement	28	99.2	0.7	0.0	0.1	0.1
BB3aR	Cement	29	99.4	0.5	0.0	0.0	0.1
BB3aR	Cement	30	99.1	0.8	0.0	0.1	0.1
BB3aR	Cement	31	98.8	1.2	0.0	0.0	0.0
BB3aR	Cement	32	99.0	0.9	0.0	0.0	0.0
BB3aR	Cement	33	99.0	1.0	0.0	0.0	0.0
BB3aR	Cement	34	99.3	0.6	0.0	0.0	0.0
BB3aR	Cement	35	99.1	0.8	0.0	0.1	0.0
BB3aR	Cement	36	99.3	0.7	0.0	0.0	0.0
BB3aR	Cement	37	95.3	4.5	0.0	0.1	0.0
BB3aR	Cement	38	99.3	0.4	0.0	0.2	0.1
BB3aR	Cement	39	99.4	0.5	0.0	0.0	0.0
BB3aR	Cement	40	99.2	0.8	0.0	0.0	0.0
BB3aR	Cement	41	99.3	0.6	0.0	0.1	0.0
BB3aR	Cement	42	99.0	1.0	0.0	0.0	0.0
BB3aR	Cement	43	99.3	0.7	0.0	0.0	0.0
BB3aR	Cement	44	99.1	0.9	0.0	0.0	0.0
BB3aR	Cement	45	99.1	0.8	0.0	0.0	0.0
BB3aR	Cement	46	99.1	0.8	0.0	0.1	0.1
BB3aR	Cement	47	99.2	0.7	0.0	0.0	0.1
BB3aR	Cement	48	99.0	1.0	0.0	0.0	0.0
BB3aR	Cement	49	99.3	0.7	0.0	0.0	0.0
BB3aR	Cement	50	99.3	0.6	0.0	0.0	0.1
BB3aR	Cement	51	99.2	0.8	0.0	0.0	0.0
BB3aR	Cement	52	99.2	0.6	0.0	0.1	0.1
BB3aR	Cement	53	99.0	0.8	0.0	0.1	0.1
E22B Lens 1	Lens	1	95.7	4.3	0.0	0.0	0.0
E22B Lens 1	Lens	2	94.0	6.0	0.0	0.0	0.0
E22B Lens 1	Lens	3	98.3	1.7	0.0	0.0	0.0
E22B Lens 1	Lens	4	98.2	1.8	0.0	0.0	0.0
E22B Lens 1	Lens	5	98.6	1.4	0.0	0.0	0.0
E22B Lens 1	Lens	6	98.9	1.1	0.0	0.0	0.0
E22B Lens 1	Lens	7	98.5	1.5	0.0	0.0	0.0
E22B Lens 1	Lens	8	98.1	1.9	0.0	0.0	0.0
E22B Lens 1	Lens	9	98.4	1.6	0.0	0.0	0.0
E22B Lens 1	Lens	10	98.1	1.9	0.0	0.0	0.0
E22B Lens 1	Lens	11	98.4	1.6	0.0	0.0	0.0
E22B Lens 1	Lens	12	98.6	1.4	0.0	0.0	0.0
E22B Lens 1	Lens	13	98.9	1.1	0.0	0.0	0.0
E22B Lens 1	Lens	14	98.2	1.8	0.0	0.0	0.0
E22B Lens 1	Lens	15	98.1	1.9	0.0	0.0	0.0
E22B Lens 1	Lens	16	98.2	1.8	0.0	0.0	0.0
E22B Lens 1	Lens	17	98.6	1.4	0.0	0.0	0.0
E22B Lens 1	Lens	18	96.9	3.1	0.0	0.0	0.0
E22B Lens 1	Lens	19	98.8	1.2	0.0	0.0	0.0
E22B Lens 1	Lens	20	98.3	1.7	0.0	0.0	0.0
E22B Lens 1	Lens	21	93.6	6.4	0.0	0.0	0.0
E22B Lens 1	Lens	22	96.7	3.3	0.0	0.0	0.0
E22B Lens 1	Lens	23	98.6	1.4	0.0	0.0	0.0
E22B Lens 1	Lens	24	98.1	1.9	0.0	0.0	0.0
E22B Lens 1	Lens	25	98.1	1.9	0.0	0.0	0.0
E22B Lens 1	Lens	26	97.3	2.7	0.0	0.0	0.0
E22B Lens 1	Lens	27	97.8	2.2	0.0	0.0	0.0
E22B Lens 1	Lens	28	98.4	1.6	0.0	0.0	0.0
E22B Lens 1	Lens	29	98.2	1.8	0.0	0.0	0.0
E22B Lens 1	Lens	30	98.0	2.0	0.0	0.0	0.0
E22B Lens 1	Lens	31	97.7	2.3	0.0	0.0	0.0
E22B Lens 1	Lens	32	98.6	1.4	0.0	0.0	0.0
E22B Lens 1	Lens	33	98.4	1.6	0.0	0.0	0.0
E22B Lens 1	Lens	34	98.0	2.0	0.0	0.0	0.0
E22B Lens 1	Lens	35	98.1	1.9	0.0	0.0	0.0

SAMPLE	FEATURE	DATA SET/ POINT	MOLE % CARBONATE				
			Ca	Mg	Sr	Fe	Mn
E22B Lens 1	Lens	36	98.6	1.4	0.0	0.0	0.0
E22B Lens 1	Lens	37	99.1	0.9	0.0	0.0	0.0
E22B Lens 1	Lens	38	98.9	1.1	0.0	0.0	0.0
E22B Lens 1	Lens	39	98.5	1.5	0.0	0.0	0.0
E22B Lens 1	Lens	40	98.4	1.6	0.0	0.0	0.0
E22B Lens 1	Lens	41	98.8	1.2	0.0	0.0	0.0
E22B Lens 1	Lens	42	98.9	1.1	0.0	0.0	0.0
E22B Lens 1	Lens	43	99.0	1.0	0.0	0.0	0.0
E22B Lens 1	Lens	44	98.2	1.8	0.0	0.0	0.0
E22B Lens 1	Lens	45	97.0	3.0	0.0	0.0	0.0
E22B Lens 1	Lens	46	98.5	1.5	0.0	0.0	0.0
E22B Lens 1	Lens	47	98.5	1.5	0.0	0.0	0.0
E22B Lens 1	Lens	48	98.5	1.5	0.0	0.0	0.0
E22B Lens 1	Lens	49	98.9	1.1	0.0	0.0	0.0
E22B Lens 1	Lens	50	99.1	0.9	0.0	0.0	0.0
E22B Lens 1	Lens	51	99.1	0.9	0.0	0.0	0.0
E22B Lens 1	Lens	52	98.3	1.7	0.0	0.0	0.0
E22B Lens 1	Lens	53	98.4	1.6	0.0	0.0	0.0
E22B Lens 1	Lens	54	98.3	1.7	0.0	0.0	0.0
E22B Lens 1	Lens	55	98.2	1.8	0.0	0.0	0.0
E22B Lens 1	Lens	56	98.1	1.9	0.0	0.0	0.0
E22B Lens 1	Lens	57	98.8	1.2	0.0	0.0	0.0
E22B Lens 1	Lens	58	98.9	1.1	0.0	0.0	0.0
E22B Lens 1	Lens	59	98.7	1.3	0.0	0.0	0.0
E22B Lens 1	Lens	60	98.5	1.5	0.0	0.0	0.0
E22B Lens 2	Lens	1	100.0	0.0	0.0	0.0	0.0
E22B Lens 2	Lens	2	100.0	0.0	0.0	0.0	0.0
E22B Lens 2	Lens	3	98.3	1.7	0.0	0.0	0.0
E22B Lens 2	Lens	4	97.8	2.2	0.0	0.0	0.0
E22B Lens 2	Lens	5	98.1	1.9	0.0	0.0	0.0
E22B Lens 2	Lens	6	98.6	1.4	0.0	0.0	0.0
E22B Lens 2	Lens	7	98.4	1.6	0.0	0.0	0.0
E22B Lens 2	Lens	8	97.9	2.1	0.0	0.0	0.0
E22B Lens 2	Lens	9	98.4	1.6	0.0	0.0	0.0
E22B Lens 2	Lens	10	98.1	1.9	0.0	0.0	0.0
E22B Lens 2	Lens	11	98.1	1.9	0.0	0.0	0.0
G33R Lens 1	Lens	1	97.1	2.9	0.0	0.0	0.0
G33R Lens 1	Lens	2	96.1	3.9	0.0	0.0	0.0
G33R Lens 1	Lens	3	98.8	1.2	0.0	0.0	0.0
G33R Lens 1	Lens	4	96.4	3.6	0.0	0.0	0.0
G33R Lens 1	Lens	5	98.4	1.6	0.0	0.0	0.0
G33R Lens 1	Lens	6	98.0	2.0	0.0	0.0	0.0
G33R Lens 1	Lens	7	98.8	1.2	0.0	0.0	0.0
G33R Lens 1	Lens	8	95.4	4.6	0.0	0.0	0.0
G33R Lens 1	Lens	9	91.0	9.0	0.0	0.0	0.0
G33R Lens 1	Lens	10	98.0	2.0	0.0	0.0	0.0
G33R Lens 1	Lens	11	94.8	5.2	0.0	0.0	0.0
G33R Lens 1	Lens	12	97.9	2.1	0.0	0.0	0.0
G33R Lens 1	Lens	13	98.2	1.8	0.0	0.0	0.0
G33R Lens 1	Lens	14	98.6	1.4	0.0	0.0	0.0
G33R Lens 1	Lens	15	97.9	2.1	0.0	0.0	0.0
G33R Lens 1	Lens	16	97.7	2.3	0.0	0.0	0.0
G33R Lens 1	Lens	17	98.0	2.0	0.0	0.0	0.0
G33R Lens 1	Lens	18	97.0	3.0	0.0	0.0	0.0
G33R Lens 1	Lens	19	97.9	2.1	0.0	0.0	0.0
G33R Lens 1	Lens	20	97.3	2.7	0.0	0.0	0.0
G33R Lens 1	Lens	21	97.1	2.9	0.0	0.0	0.0
G33R Lens 1	Lens	22	97.8	2.2	0.0	0.0	0.0
G33R Lens 1	Lens	23	98.0	2.0	0.0	0.0	0.0
G33R Lens 1	Lens	24	96.5	3.5	0.0	0.0	0.0
G33R Lens 1	Lens	25	98.5	1.5	0.0	0.0	0.0

SAMPLE	FEATURE	DATA SET/ POINT	MOLE % CARBONATE				
			Ca	Mg	Sr	Fe	Mn
G33R Lens 1	Lens	26	98.7	1.3	0.0	0.0	0.0
G33R Lens 1	Lens	27	98.6	1.4	0.0	0.0	0.0
G33R Lens 1	Lens	28	98.2	1.8	0.0	0.0	0.0
G33R Lens 1	Lens	29	97.9	2.1	0.0	0.0	0.0
G33R Lens 1	Lens	30	97.5	2.5	0.0	0.0	0.0
G33R Lens 1	Lens	31	98.0	2.0	0.0	0.0	0.0
G33R Lens 1	Lens	32	95.1	4.9	0.0	0.0	0.0
G33R Lens 1	Lens	33	97.6	2.4	0.0	0.0	0.0
G33R Lens 1	Lens	34	90.9	9.1	0.0	0.0	0.0
G33R Lens 1	Lens	35	92.6	7.4	0.0	0.0	0.0
G33R Lens 1	Lens	36	97.1	2.9	0.0	0.0	0.0
G33R Lens 1	Lens	37	96.1	3.9	0.0	0.0	0.0
G33R Lens 1	Lens	38	98.8	1.2	0.0	0.0	0.0
G33R Lens 1	Lens	39	96.4	3.6	0.0	0.0	0.0
G33R Lens 1	Lens	40	98.4	1.6	0.0	0.0	0.0
G33R Lens 1	Lens	41	98.0	2.0	0.0	0.0	0.0
G33R Lens 1	Lens	42	98.8	1.2	0.0	0.0	0.0
G33R Lens 1	Lens	43	95.4	4.6	0.0	0.0	0.0
G33R Lens 1	Lens	44	91.0	9.0	0.0	0.0	0.0
G33R Lens 1	Lens	45	98.0	2.0	0.0	0.0	0.0
G33R Lens 1	Lens	46	94.8	5.2	0.0	0.0	0.0
G33R Lens 1	Lens	47	97.9	2.1	0.0	0.0	0.0
G33R Lens 1	Lens	48	98.2	1.8	0.0	0.0	0.0
G33R Lens 1	Lens	49	98.6	1.4	0.0	0.0	0.0
G33R Lens 1	Lens	50	97.9	2.1	0.0	0.0	0.0
G33R Lens 1	Lens	51	97.7	2.3	0.0	0.0	0.0
G33R Lens 1	Lens	52	98.0	2.0	0.0	0.0	0.0
G33R Lens 1	Lens	53	97.0	3.0	0.0	0.0	0.0
G33R Lens 1	Lens	54	97.9	2.1	0.0	0.0	0.0
G33R Lens 1	Lens	55	97.3	2.7	0.0	0.0	0.0
G33R Lens 1	Lens	56	97.1	2.9	0.0	0.0	0.0
G33R Lens 1	Lens	57	97.8	2.2	0.0	0.0	0.0
G33R Lens 1	Lens	58	98.0	2.0	0.0	0.0	0.0
G33R Lens 1	Lens	59	96.5	3.5	0.0	0.0	0.0
G33R Lens 1	Lens	60	98.5	1.5	0.0	0.0	0.0
G33R Lens 1	Lens	61	98.7	1.3	0.0	0.0	0.0
G33R Lens 1	Lens	62	98.6	1.4	0.0	0.0	0.0
G33R Lens 1	Lens	63	98.2	1.8	0.0	0.0	0.0
G33R Lens 1	Lens	64	97.9	2.1	0.0	0.0	0.0
G33R Lens 1	Lens	65	97.5	2.5	0.0	0.0	0.0
G33R Lens 1	Lens	66	98.0	2.0	0.0	0.0	0.0
G33R Lens 1	Lens	67	95.1	4.9	0.0	0.0	0.0
G33R Lens 1	Lens	68	97.6	2.4	0.0	0.0	0.0
G33R Lens 1	Lens	69	97.9	2.1	0.0	0.0	0.0
G33R Lens 1	Lens	70	98.5	1.5	0.0	0.0	0.0
G33R Lens 1	Lens	71	98.7	1.3	0.0	0.0	0.0
G33R Lens 1	Lens	72	98.4	1.6	0.0	0.0	0.0
G33R Lens 1	Lens	73	98.7	1.3	0.0	0.0	0.0
G33R Lens 1	Lens	74	98.3	1.7	0.0	0.0	0.0
G33R Lens 1	Lens	75	98.4	1.6	0.0	0.0	0.0
G33R Lens 1	Lens	76	97.5	2.5	0.0	0.0	0.0
G33R Lens 1	Lens	77	98.2	1.8	0.0	0.0	0.0
G33R Lens 1	Lens	78	98.4	1.6	0.0	0.0	0.0
G33R Lens 1	Lens	79	98.0	2.0	0.0	0.0	0.0
G33R Lens 1	Lens	80	97.1	2.9	0.0	0.0	0.0
G33R Lens 1	Lens	81	97.8	2.2	0.0	0.0	0.0
G33R Lens 1	Lens	82	96.8	3.2	0.0	0.0	0.0
G33R Lens 1	Lens	83	97.9	2.1	0.0	0.0	0.0
G33R Lens 1	Lens	84	97.2	2.8	0.0	0.0	0.0
G33R Lens 1	Lens	85	97.1	2.9	0.0	0.0	0.0
G33R Lens 1	Lens	86	97.0	3.0	0.0	0.0	0.0
G33R Lens 1	Lens	87	97.7	2.3	0.0	0.0	0.0
G33R Lens 1	Lens	88	95.2	4.8	0.0	0.0	0.0

SAMPLE	FEATURE	DATA SET/ POINT	MOLE % CARBONATE				
			Ca	Mg	Sr	Fe	Mn
G33R Lens 1	Lens	89	98.0	2.0	0.0	0.0	0.0
G33R Lens 1	Lens	90	97.5	2.5	0.0	0.0	0.0
G33R Lens 1	Lens	91	98.2	1.8	0.0	0.0	0.0
G33R Lens 1	Lens	92	97.5	2.5	0.0	0.0	0.0
G33R Lens 1	Lens	93	97.5	2.5	0.0	0.0	0.0
G33R Lens 1	Lens	94	98.3	1.7	0.0	0.0	0.0
G33R Lens 1	Lens	95	98.1	1.9	0.0	0.0	0.0
G33R Lens 1	Lens	96	98.2	1.8	0.0	0.0	0.0
G33R Lens 1	Lens	97	98.1	1.9	0.0	0.0	0.0
G33R Lens 1	Lens	98	98.5	1.5	0.0	0.0	0.0
G33R Lens 1	Lens	99	98.6	1.4	0.0	0.0	0.0
G33R Lens 1	Lens	100	98.4	1.6	0.0	0.0	0.0
G33R Lens 1	Lens	101	98.3	1.7	0.0	0.0	0.0
G33R Lens 1	Lens	102	98.2	1.8	0.0	0.0	0.0
G33R Lens 1	Lens	103	98.2	1.8	0.0	0.0	0.0
G42R Lens 1 Traverse 1	Lens	1	97.9	1.7	0.2	0.2	0.0
G42R Lens 1 Traverse 1	Lens	2	97.9	1.6	0.2	0.2	0.0
G42R Lens 1 Traverse 1	Lens	3	97.8	1.7	0.2	0.2	0.1
G42R Lens 1 Traverse 1	Lens	4	98.2	1.3	0.2	0.3	0.0
G42R Lens 1 Traverse 1	Lens	5	98.1	1.4	0.2	0.2	0.0
G42R Lens 1 Traverse 1	Lens	6	97.9	1.5	0.2	0.3	0.0
G42R Lens 1 Traverse 1	Lens	7	98.0	1.5	0.3	0.2	0.1
G42R Lens 1 Traverse 1	Lens	8	97.5	2.0	0.2	0.2	0.1
G42R Lens 1 Traverse 1	Lens	9	96.6	2.9	0.2	0.4	0.0
G42R Lens 1 Traverse 1	Lens	10	95.9	3.6	0.2	0.2	0.0
G42R Lens 1 Traverse 1	Lens	11	94.8	4.5	0.2	0.3	0.1
G42R Lens 1 Traverse 1	Lens	12	97.4	2.1	0.2	0.3	0.0
G42R Lens 1 Traverse 1	Lens	13	98.1	1.5	0.2	0.1	0.1
G42R Lens 1 Traverse 1	Lens	14	96.1	3.2	0.2	0.3	0.2
G42R Lens 1 Traverse 1	Lens	15	98.0	1.4	0.2	0.3	0.1
G42R Lens 1 Traverse 1	Lens	16	97.5	2.0	0.3	0.1	0.1
G42R Lens 1 Traverse 1	Lens	17	93.6	5.8	0.2	0.3	0.1
G42R Lens 1 Traverse 1	Lens	18	95.3	4.0	0.2	0.5	0.0
G42R Lens 1 Traverse 1	Lens	19	95.8	3.7	0.2	0.3	0.0
G42R Lens 1 Traverse 1	Lens	20	96.2	3.2	0.2	0.3	0.0
G42R Lens 1 Traverse 1	Lens	21	98.2	1.5	0.2	0.2	0.0
G42R Lens 1 Traverse 1	Lens	22	96.5	3.1	0.2	0.2	0.1
G42R Lens 1 Traverse 1	Lens	23	97.9	1.6	0.2	0.2	0.1
G42R Lens 1 Traverse 1	Lens	24	97.5	1.9	0.2	0.3	0.0
G42R Lens 1 Traverse 1	Lens	25	98.0	1.5	0.2	0.2	0.1
G42R Lens 1 Traverse 1	Lens	26	98.0	1.5	0.2	0.3	0.0
G42R Lens 1 Traverse 1	Lens	27	98.0	1.5	0.3	0.3	0.0
G42R Lens 1 Traverse 1	Lens	28	97.7	1.8	0.2	0.3	0.0
G42R Lens 1 Traverse 1	Lens	29	97.9	1.6	0.2	0.2	0.0
G42R Lens 1 Traverse 1	Lens	30	97.7	1.7	0.2	0.3	0.0
G42R Lens 1 Traverse 2	Lens	1	97.1	2.4	0.2	0.2	0.0
G42R Lens 1 Traverse 2	Lens	2	94.8	4.5	0.2	0.4	0.1
G42R Lens 1 Traverse 2	Lens	3	98.4	1.2	0.2	0.2	0.0
G42R Lens 1 Traverse 2	Lens	4	96.6	2.9	0.2	0.4	0.0
G42R Lens 1 Traverse 2	Lens	5	79.1	19.2	0.3	1.3	0.2
G42R Lens 1 Traverse 2	Lens	6	98.1	1.4	0.2	0.3	0.1
G42R Lens 1 Traverse 2	Lens	7	98.2	1.3	0.2	0.2	0.1
G42R Lens 1 Traverse 2	Lens	8	96.1	3.5	0.2	0.2	0.0
G42R Lens 1 Traverse 2	Lens	9	97.9	1.6	0.3	0.2	0.1
G42R Lens 1 Traverse 2	Lens	10	95.6	3.7	0.2	0.4	0.1
G42R Lens 1 Traverse 2	Lens	11	98.1	1.4	0.2	0.2	0.0
G42R Lens 1 Traverse 2	Lens	12	96.9	2.7	0.2	0.1	0.1
G42R Lens 1 Traverse 2	Lens	13	96.7	2.7	0.2	0.2	0.1
G42R Lens 1 Traverse 2	Lens	14	95.5	4.0	0.2	0.3	0.0
G42R Lens 1 Traverse 2	Lens	15	96.6	3.0	0.2	0.1	0.0

SAMPLE	FEATURE	DATA SET/ POINT	MOLE % CARBONATE				
			Ca	Mg	Sr	Fe	Mn
G42R Lens 3 Traverse 1	Lens	1	97.6	1.9	0.3	0.2	0.0
G42R Lens 3 Traverse 1	Lens	2	97.7	1.7	0.2	0.4	0.1
G42R Lens 3 Traverse 1	Lens	3	97.9	1.6	0.2	0.2	0.0
G42R Lens 3 Traverse 1	Lens	4	97.9	1.6	0.2	0.2	0.0
G42R Lens 3 Traverse 1	Lens	5	97.9	1.6	0.3	0.2	0.1
G42R Lens 3 Traverse 1	Lens	6	97.6	2.0	0.2	0.2	0.1
G42R Lens 3 Traverse 1	Lens	7	97.6	2.0	0.2	0.2	0.0
G42R Lens 3 Traverse 1	Lens	8	97.3	2.1	0.3	0.3	0.1
G42R Lens 3 Traverse 1	Lens	9	97.4	2.1	0.2	0.3	0.0
G42R Lens 3 Traverse 1	Lens	10	97.6	1.8	0.2	0.3	0.1
G42R Lens 3 Traverse 1	Lens	11	97.2	2.2	0.2	0.2	0.1
G42R Lens 3 Traverse 1	Lens	12	97.9	1.5	0.3	0.2	0.0
G42R Lens 3 Traverse 1	Lens	13	98.3	1.1	0.4	0.2	0.0
G42R Lens 3 Traverse 1	Lens	14	97.6	2.1	0.2	0.1	0.0
G42R Lens 3 Traverse 1	Lens	15	97.6	1.9	0.2	0.3	0.0
G42R Lens 3 Traverse 1	Lens	16	98.0	1.6	0.2	0.2	0.0
G42R Lens 3 Traverse 1	Lens	17	97.5	1.9	0.3	0.3	0.1
G42R Lens 3 Traverse 1	Lens	18	97.1	2.5	0.2	0.1	0.1
G42R Lens 3 Traverse 1	Lens	19	97.3	2.0	0.2	0.3	0.1
G42R Lens 3 Traverse 1	Lens	20	97.5	1.9	0.3	0.2	0.1
G42R Lens 3 Traverse 1	Lens	21	97.3	2.2	0.2	0.2	0.0
G42R Lens 3 Traverse 1	Lens	22	98.0	1.5	0.2	0.3	0.0
G42R Lens 3 Traverse 1	Lens	23	98.0	1.4	0.2	0.3	0.0
G42R Lens 3 Traverse 1	Lens	24	97.7	1.7	0.2	0.3	0.0
G42R Lens 3 Traverse 1	Lens	25	97.8	1.7	0.2	0.3	0.0
G42R Lens 3 Traverse 2	Lens	1	97.0	2.4	0.2	0.3	0.0
G42R Lens 3 Traverse 2	Lens	2	97.4	2.1	0.3	0.2	0.0
G42R Lens 3 Traverse 2	Lens	3	97.9	1.5	0.2	0.3	0.0
G42R Lens 3 Traverse 2	Lens	4	98.0	1.4	0.2	0.3	0.1
G42R Lens 3 Traverse 2	Lens	5	97.6	1.9	0.3	0.3	0.0
G42R Lens 3 Traverse 2	Lens	6	96.9	2.6	0.3	0.3	0.0
G42R Lens 3 Traverse 2	Lens	7	97.1	2.4	0.2	0.3	0.0
G42R Lens 3 Traverse 2	Lens	8	97.1	2.3	0.3	0.3	0.0
G42R Lens 3 Traverse 2	Lens	9	97.0	2.5	0.3	0.2	0.0
G42R Lens 3 Traverse 2	Lens	10	97.6	1.8	0.2	0.2	0.1
G42R Lens 3 Traverse 2	Lens	11	96.8	2.6	0.2	0.2	0.1
G42R Lens 3 Traverse 2	Lens	12	97.8	1.8	0.4	0.1	0.0
G42R Lens 3 Traverse 2	Lens	13	97.7	1.6	0.5	0.2	0.0
G42R Lens 3 Traverse 2	Lens	14	97.5	2.1	0.1	0.2	0.1
G42R Lens 3 Traverse 2	Lens	15	97.3	2.2	0.2	0.2	0.1
G42R Lens 3 Traverse 2	Lens	16	97.8	1.8	0.3	0.1	0.1
G42R Lens 3 Traverse 2	Lens	17	97.0	2.4	0.2	0.3	0.0
G42R Lens 3 Traverse 2	Lens	18	96.7	2.7	0.3	0.2	0.0
G42R Lens 3 Traverse 2	Lens	19	96.8	2.6	0.3	0.2	0.1
G42R Lens 3 Traverse 2	Lens	20	97.2	2.2	0.3	0.1	0.1
G42R Lens 3 Traverse 2	Lens	21	96.8	2.7	0.2	0.2	0.0
G42R Lens 3 Traverse 2	Lens	22	97.7	1.8	0.3	0.2	0.0
G42R Lens 3 Traverse 2	Lens	23	98.1	1.3	0.2	0.4	0.1
G42R Lens 3 Traverse 2	Lens	24	97.8	1.7	0.2	0.2	0.0
G42R Lens 3 Traverse 2	Lens	25	97.8	1.7	0.2	0.2	0.1
G42R Lens 2 Traverse 1	Lens	1	98.2	1.2	0.3	0.2	0.1
G42R Lens 2 Traverse 1	Lens	2	98.1	1.6	0.2	0.2	0.0
G42R Lens 2 Traverse 1	Lens	3	94.3	5.0	0.2	0.4	0.0
G42R Lens 2 Traverse 1	Lens	4	96.9	2.3	0.2	0.4	0.1
G42R Lens 2 Traverse 1	Lens	5	97.5	1.9	0.2	0.3	0.1
G42R Lens 2 Traverse 1	Lens	6	98.0	1.5	0.2	0.2	0.1
G42R Lens 2 Traverse 1	Lens	7	97.6	1.9	0.3	0.2	0.0
G42R Lens 2 Traverse 1	Lens	8	97.7	1.9	0.2	0.2	0.0
G42R Lens 2 Traverse 1	Lens	9	97.1	2.4	0.2	0.2	0.0
G42R Lens 2 Traverse 1	Lens	10	97.1	2.3	0.2	0.3	0.1
G42R Lens 2 Traverse 1	Lens	11	98.0	1.4	0.4	0.1	0.0

SAMPLE	FEATURE	DATA SET/ POINT	MOLE % CARBONATE				
			Ca	Mg	Sr	Fe	Mn
G42R Lens 2 Traverse 1	Lens	12	97.5	1.9	0.3	0.2	0.1
G42R Lens 2 Traverse 1	Lens	13	97.9	1.5	0.3	0.2	0.1
G42R Lens 2 Traverse 1	Lens	14	97.7	1.9	0.2	0.2	0.0
G42R Lens 2 Traverse 1	Lens	15	98.0	1.5	0.3	0.2	0.0
G42R Lens 2 Traverse 1	Lens	16	97.9	1.5	0.3	0.2	0.0
G42R Lens 2 Traverse 1	Lens	17	97.6	1.7	0.3	0.4	0.1
G42R Lens 2 Traverse 1	Lens	18	94.9	2.6	0.2	2.2	0.0
G42R Lens 2 Traverse 1	Lens	19	97.0	2.1	0.2	0.6	0.1
G42R Lens 2 Traverse 1	Lens	20	96.5	2.3	0.1	1.0	0.0
G42R Lens 2 Traverse 1	Lens	21	96.2	2.7	0.1	0.9	0.1
G42R Lens 2 Traverse 1	Lens	22	92.2	5.4	0.1	2.2	0.1
G42R Lens 2 Traverse 1	Lens	23	93.4	4.5	0.2	1.8	0.1
G42R Lens 2 Traverse 1	Lens	24	97.8	1.6	0.2	0.4	0.0
G42R Lens 2 Traverse 1	Lens	25	75.6	13.7	0.0	10.2	0.5
G42R Lens 2 Traverse 1	Lens	26	96.2	3.3	0.2	0.3	0.1
G42R Lens 2 Traverse 1	Lens	27	97.6	2.0	0.2	0.2	0.1
G42R Lens 2 Traverse 1	Lens	28	94.7	4.8	0.2	0.3	0.0
G42R Lens 2 Traverse 1	Lens	29	98.6	1.1	0.2	0.1	0.0
G42R Lens 2 Traverse 1	Lens	30	95.8	3.6	0.2	0.4	0.1
G42R	Sclera	1	98.3	1.3	0.2	0.1	0.0
G42R	Sclera	2	96.3	3.2	0.2	0.2	0.1
G42R	Sclera	3	97.9	1.6	0.2	0.3	0.0
G42R	Sclera	4	97.4	2.1	0.3	0.2	0.0
G42R	Sclera	5	98.1	1.4	0.4	0.1	0.0
G42R	Sclera	6	97.9	1.7	0.3	0.1	0.0
G42R	Sclera	7	97.4	2.1	0.3	0.2	0.0
G42R	Sclera	8	97.5	2.1	0.2	0.2	0.0
G42R	Sclera	9	97.7	1.8	0.3	0.1	0.0
G42R	Sclera	10	97.6	1.8	0.3	0.3	0.0
G42R	Sclera	11	96.8	2.5	0.3	0.2	0.1
G42R	Sclera	12	97.7	1.7	0.3	0.2	0.0
G42R	Sclera	13	97.6	1.9	0.2	0.2	0.0
G42R	Sclera	14	97.5	1.8	0.2	0.4	0.0
G42R	Sclera	15	96.7	2.4	0.1	0.8	0.0
G42R	Sclera	16	95.5	3.0	0.2	1.3	0.0
G42R	Sclera	17	97.3	2.0	0.2	0.5	0.0
G42R	Sclera	18	97.3	1.9	0.2	0.5	0.1
G42R	Sclera	19	96.2	2.7	0.1	1.0	0.0
G42R	Sclera	20	84.4	8.2	0.0	7.3	0.1
G42R	Sclera	21	96.3	2.6	0.1	0.9	0.1
G42R	Sclera	22	97.2	2.1	0.2	0.5	0.0
G42R	Sclera	23	94.7	3.3	0.2	1.8	0.1
G42R	Sclera	24	97.9	1.4	0.2	0.5	0.0
G42R	Sclera	25	97.9	1.5	0.2	0.3	0.1
G42R	Crinoid	1	96.7	2.9	0.2	0.2	0.0
G42R	Crinoid	2	97.1	2.2	0.3	0.4	0.1
G42R	Crinoid	3	95.4	4.1	0.2	0.2	0.0
G42R	Crinoid	4	94.0	4.1	0.1	1.7	0.0
G42R	Crinoid	5	97.2	2.3	0.2	0.3	0.0
G42R	Crinoid	6	96.8	2.3	0.2	0.6	0.1
G42R	Crinoid	7	97.7	1.9	0.2	0.2	0.0
G42R	Crinoid	8	97.3	2.1	0.2	0.4	0.1
G42R	Crinoid	9	97.3	2.1	0.1	0.4	0.0
G42R	Crinoid	10	97.3	2.1	0.2	0.3	0.1
G42R	Crinoid	11	97.4	2.1	0.2	0.2	0.1
G42R	Crinoid	12	97.7	1.9	0.2	0.2	0.0
G42R	Crinoid	13	97.0	2.4	0.3	0.3	0.0
G42R	Crinoid	14	96.7	2.3	0.2	0.7	0.1
G42R	Crinoid	15	97.4	1.9	0.2	0.4	0.0
G42R	Crinoid	16	97.1	2.4	0.2	0.3	0.0
G42R	Crinoid	17	97.2	2.3	0.1	0.3	0.0

SAMPLE	FEATURE	DATA SET/ POINT	MOLE % CARBONATE				
			Ca	Mg	Sr	Fe	Mn
G42R	Crinoid	18	96.9	2.3	0.2	0.6	0.0
G42R	Crinoid	19	96.0	2.9	0.2	0.8	0.1
G42R	Crinoid	20	97.3	2.1	0.2	0.4	0.0
G42R	Crinoid	21	97.3	2.0	0.2	0.5	0.1
G42R	Crinoid	22	97.0	2.3	0.2	0.5	0.0
G42R	Crinoid	23	97.7	1.6	0.3	0.3	0.1
G42R	Crinoid	24	97.6	1.9	0.2	0.2	0.0
G42R	Crinoid	25	95.6	3.7	0.2	0.4	0.0
PM28 (Lens 1)	Lens	1	94.0	2.8	0.0	3.2	0.1
PM28 (Lens 1)	Lens	2	89.7	10.0	0.0	0.3	0.0
PM28 (Lens 1)	Lens	3	93.6	6.1	0.0	0.3	0.0
PM28 (Lens 1)	Lens	4	92.0	8.0	0.0	0.0	0.0
PM28 (Lens 1)	Lens	5	92.1	7.8	0.0	0.1	0.1
PM28 (Lens 1)	Lens	6	91.5	8.4	0.0	0.0	0.1
PM28 (Lens 1)	Lens	7	92.4	7.6	0.0	0.0	0.0
PM28 (Lens 1)	Lens	8	88.7	11.1	0.0	0.1	0.0
PM28 (Lens 1)	Lens	9	91.9	8.0	0.0	0.0	0.0
PM28 (Lens 1)	Lens	10	89.8	10.0	0.0	0.1	0.0
PM28 (Lens 1)	Lens	11	93.7	6.3	0.0	0.0	0.0
PM28 (Lens 1)	Lens	12	91.8	8.1	0.0	0.1	0.0
PM28 (Lens 1)	Lens	13	92.4	7.0	0.0	0.6	0.0
PM28 (Lens 1)	Bowl?	14	96.8	1.0	0.0	2.2	0.0
PM28 (Lens 1)	Bowl?	15	96.6	1.0	0.0	2.3	0.1
PM28 Lens 1 (traverse 2)	Lens	1	96.1	1.1	0.0	2.7	0.1
PM28 Lens 1 (traverse 2)	Lens	2	96.6	1.1	0.0	2.2	0.1
PM28 Lens 1 (traverse 2)	Lens	3	92.4	7.0	0.0	0.5	0.1
PM28 Lens 1 (traverse 2)	Lens	4	92.0	8.0	0.0	0.0	0.0
PM28 Lens 1 (traverse 2)	Lens	5	93.8	6.1	0.0	0.0	0.1
PM28 Lens 1 (traverse 2)	Lens	6	90.2	9.7	0.0	0.0	0.1
PM28 Lens 1 (traverse 2)	Lens	7	91.6	8.3	0.0	0.0	0.0
PM28 Lens 1 (traverse 2)	Lens	8	89.0	11.0	0.0	0.1	0.0
PM28 Lens 1 (traverse 2)	Lens	9	92.4	7.5	0.0	0.1	0.0
PM28 Lens 1 (traverse 2)	Lens	10	91.5	8.5	0.0	0.0	0.0
PM28 Lens 1 (traverse 2)	Lens	11	92.1	7.8	0.0	0.1	0.0
PM28 Lens 1 (traverse 2)	Lens	12	91.8	8.1	0.0	0.1	0.0
PM28 Lens 1 (traverse 2)	Lens	13	93.6	6.0	0.0	0.4	0.0
PM28 Lens 1 (traverse 2)	Lens	14	89.6	10.0	0.0	0.4	0.0
PM28 Lens 1 (traverse 2)	Lens	15	93.9	2.9	0.0	3.0	0.1
PM28 Lens 2 (traverse 1)	Lens	1	94.0	5.9	0.0	0.0	0.0
PM28 Lens 2 (traverse 1)	Lens	2	92.0	7.8	0.0	0.1	0.1
PM28 Lens 2 (traverse 1)	Lens	3	92.5	7.4	0.0	0.1	0.1
PM28 Lens 2 (traverse 1)	Lens	4	89.6	10.3	0.0	0.0	0.1
PM28 Lens 2 (traverse 1)	Lens	5	92.5	7.5	0.0	0.0	0.0
PM28 Lens 2 (traverse 1)	Lens	6	90.3	9.6	0.0	0.0	0.0
PM28 Lens 2 (traverse 1)	Lens	7	91.0	9.0	0.0	0.0	0.0
PM28 Lens 2 (traverse 1)	Lens	8	88.6	11.3	0.0	0.0	0.0
PM28 Lens 2 (traverse 1)	Lens	9	92.5	7.5	0.0	0.0	0.0
PM28 Lens 2 (traverse 1)	Lens	10	90.7	9.2	0.0	0.0	0.0
PM28 Lens 2 (traverse 1)	Lens	11	90.6	9.2	0.0	0.1	0.1
PM28 Lens 2 (traverse 1)	Lens	12	94.0	4.2	0.0	1.7	0.1
PM28 Lens 2 (traverse 1)	Lens	13	97.1	0.9	0.0	2.0	0.0
PM28 Lens 2 (traverse 1)	Lens	14	92.7	2.1	0.0	5.1	0.2
PM28 Lens 2 (traverse 1)	Lens	15	37.6	16.9	0.0	45.5	0.0
PM28 Lens 2 (traverse 2)	Lens	1	96.5	1.3	0.0	2.2	0.1
PM28 Lens 2 (traverse 2)	Lens	2	95.6	2.0	0.0	2.2	0.1
PM28 Lens 2 (traverse 2)	Lens	3	92.3	7.0	0.0	0.6	0.1
PM28 Lens 2 (traverse 2)	Lens	4	94.1	5.7	0.0	0.3	0.0
PM28 Lens 2 (traverse 2)	Lens	5	91.7	8.0	0.0	0.2	0.1
PM28 Lens 2 (traverse 2)	Lens	6	92.1	7.8	0.0	0.0	0.0

SAMPLE	FEATURE	DATA SET/ POINT	MOLE % CARBONATE				
			Ca	Mg	Sr	Fe	Mn
PM28 Lens 2 (traverse 2)	Lens	7	92.1	7.8	0.0	0.1	0.1
PM28 Lens 2 (traverse 2)	Lens	8	93.4	6.3	0.0	0.2	0.0
PM28 Lens 2 (traverse 2)	Lens	9	91.5	8.2	0.0	0.1	0.1
PM28 Lens 2 (traverse 2)	Lens	10	95.0	4.9	0.0	0.0	0.1
PM28 Lens 2 (traverse 2)	Lens	11	89.5	10.4	0.0	0.1	0.0
PM28 Lens 2 (traverse 2)	Lens	12	90.4	9.5	0.0	0.0	0.0
PM28 Lens 2 (traverse 2)	Lens	13	90.7	8.7	0.0	0.5	0.0
PM28 Lens 2 (traverse 2)	Lens	14	95.8	1.6	0.0	2.4	0.1
PM28 Lens 2 (traverse 2)	Cement ?	15	97.2	1.0	0.0	1.7	0.1
PM28 Lens 3 (taverse 1)	Lens	1	88.5	11.4	0.0	0.0	0.0
PM28 Lens 3 (taverse 1)	Lens	2	94.8	5.1	0.0	0.1	0.1
PM28 Lens 3 (taverse 1)	Lens	3	91.1	8.7	0.0	0.1	0.1
PM28 Lens 3 (taverse 1)	Lens	4	92.6	7.3	0.0	0.1	0.0
PM28 Lens 3 (taverse 1)	Lens	5	91.8	8.0	0.0	0.1	0.0
PM28 Lens 3 (taverse 1)	Lens	6	93.0	6.9	0.0	0.0	0.0
PM28 Lens 3 (taverse 1)	Lens	7	90.7	9.2	0.0	0.1	0.0
PM28 Lens 3 (taverse 1)	Lens	8	91.7	8.3	0.0	0.0	0.0
PM28 Lens 3 (taverse 1)	Lens	9	88.3	11.7	0.0	0.1	0.0
PM28 Lens 3 (taverse 1)	Lens	10	88.1	11.9	0.0	0.1	0.0
PM28 Lens 3 (taverse 1)	Lens	11	91.4	8.1	0.0	0.5	0.0
PM28 Lens 3 (taverse 1)	Lens	12	90.7	7.8	0.0	1.4	0.1
PM28 Lens 3 (taverse 1)	Lens	13	95.1	1.0	0.0	3.8	0.1
PM28 Lens 3 (taverse 1)	Lens	14	94.9	1.3	0.0	3.6	0.2
PM28 Lens 3 (taverse 1)	Lens	15	96.6	1.1	0.0	2.3	0.0
PM28 Lens 3 (taverse 1)	Lens	16	91.3	7.2	0.0	1.3	0.2
PM28 Lens 3 (taverse 1)	Lens	17	90.6	9.0	0.0	0.4	0.1
PM28 Lens 3 (taverse 1)	Lens	18	92.2	7.7	0.0	0.1	0.0
PM28 Lens 3 (taverse 1)	Lens	19	92.9	6.9	0.0	0.1	0.0
PM28 Lens 3 (taverse 1)	Lens	20	92.2	7.8	0.0	0.0	0.0
PM28 Lens 3 (traverse 2)	Lens	1	91.9	7.9	0.0	0.1	0.0
PM28 Lens 3 (traverse 2)	Lens	2	91.3	8.5	0.0	0.1	0.0
PM28 Lens 3 (traverse 2)	Lens	3	93.8	6.1	0.0	0.2	0.0
PM28 Lens 3 (traverse 2)	Lens	4	94.9	5.1	0.0	0.0	0.0
PM28 Lens 3 (traverse 2)	Lens	5	94.4	5.5	0.0	0.0	0.1
PM28 Lens 3 (traverse 2)	Lens	6	87.5	12.4	0.0	0.1	0.0
PM28 Lens 3 (traverse 2)	Lens	7	92.8	7.0	0.0	0.1	0.0
PM28 Lens 3 (traverse 2)	Lens	8	95.8	4.0	0.0	0.2	0.0
PM28 Lens 3 (traverse 2)	Lens	9	92.5	7.3	0.0	0.1	0.1
PM28 Lens 3 (traverse 2)	Lens	10	91.9	8.0	0.0	0.0	0.0
PM28 Lens 3 (traverse 2)	Lens	11	89.8	9.6	0.0	0.6	0.0
PM28 Lens 3 (traverse 2)	Lens	12	91.3	8.6	0.0	0.0	0.1
PM28 Lens 3 (traverse 2)	Lens	13	91.0	9.0	0.0	0.1	0.0
PM28 Lens 3 (traverse 2)	Lens	14	90.8	8.4	0.0	0.6	0.1
PM28 Lens 3 (traverse 2)	Lens	15	93.0	5.9	0.0	1.0	0.2

E. 2 Edinburgh EPMA Raw Data

Table E.5 - Weight % element EPMA data (Edinburgh) for trilobites with schizochroal eyes.

SAMPLE	FEATURE	DATA SET/ POINT	WEIGHT % ELEMENT					
			Ca	Mg	Sr	Fe	Mn	SUM
BB3aR cement	Cement	1 / 1	38.35	0.34	0.02	0.01	0.01	38.74
BB3aR cement	Cement	1 / 2	38.82	0.03	0.01	0.01	0.02	38.89
BB3aR cement	Cement	1 / 3	38.53	0.02	0.00	-0.01	0.01	38.55
BB3aR cement	Cement	1 / 4	38.41	0.29	0.03	0.00	0.01	38.74
BB3aR cement	Cement	1 / 5	38.74	0.45	0.04	0.01	-0.03	39.20

SAMPLE	FEATURE	DATA SET/ POINT	WEIGHT % ELEMENT					
			Ca	Mg	Sr	Fe	Mn	SUM
BB3aR cement	Cement	1 / 6	38.97	0.34	0.09	0.03	0.01	39.43
BB3aR cement	Cement	1 / 7	38.27	0.18	0.02	0.00	0.00	38.47
BB3aR cement	Cement	1 / 8	39.03	0.25	0.02	0.02	0.00	39.32
BB3aR cement	Cement	1 / 9	39.11	0.20	0.01	0.02	0.02	39.36
BB3aR cement	Cement	1 / 10	39.30	0.10	0.01	0.00	-0.01	39.40
BB3aR cement	Cement	1 / 11	39.30	0.08	0.01	0.00	0.02	39.41
BB3aR cement	Cement	1 / 12	39.07	0.16	0.03	0.00	0.01	39.27
BB3aR cement	Cement	1 / 13	38.61	0.17	0.03	0.00	0.01	38.81
BB3aR cement	Cement	1 / 14	38.90	0.29	0.03	0.01	0.01	39.23
BB3aR cement	Cement	1 / 15	38.98	0.17	0.04	0.01	0.02	39.22
BB3aR Lens 2b diagonal traverse	Lens	1 / 1	38.74	0.28	0.03	0.01	0.02	39.08
BB3aR Lens 2b diagonal traverse	Lens	1 / 2	37.89	0.09	0.03	0.00	0.01	38.03
BB3aR Lens 2b diagonal traverse	Lens	1 / 3	39.91	0.85	0.04	0.00	-0.01	40.80
BB3aR Lens 2b diagonal traverse	Lens	1 / 4	38.49	3.17	0.06	-0.01	-0.01	41.70
BB3aR Lens 2b diagonal traverse	Lens	1 / 5	38.82	0.10	0.03	0.00	0.00	38.96
BB3aR Lens 2b diagonal traverse	Lens	1 / 6	39.21	0.09	0.03	0.00	0.01	39.34
BB3aR Lens 2b diagonal traverse	Lens	1 / 7	37.70	0.12	0.05	-0.01	0.00	37.86
BB3aR Lens 2b diagonal traverse	Lens	1 / 8	35.45	3.09	0.05	-0.01	0.00	38.59
BB3aR Lens 2b diagonal traverse	Lens	1 / 9	37.66	0.16	0.03	0.01	-0.01	37.85
BB3aR Lens 2b diagonal traverse	Lens	1 / 10	38.37	0.19	0.04	0.00	0.00	38.61
BB3aR Lens 2b diagonal traverse	Lens	1 / 11	32.27	0.08	0.00	-0.01	-0.01	32.33
BB3aR Lens 2b diagonal traverse	Lens	1 / 12	37.79	1.69	0.05	0.02	0.01	39.55
BB3aR Lens 2b diagonal traverse	Lens	1 / 13	37.89	0.22	0.02	0.00	0.00	38.13
BB3aR vertical traverse	Resin	1 / 1	38.74	0.10	0.01	0.07	0.04	38.95
BB3aR vertical traverse	Resin	1 / 2	38.85	0.14	0.02	0.02	0.00	39.03
BB3aR vertical traverse	Lens	1 / 3	38.04	0.14	0.03	0.01	-0.01	38.22
BB3aR vertical traverse	Lens	1 / 4	40.30	0.16	0.04	0.00	-0.01	40.49
BB3aR vertical traverse	Lens	1 / 5	38.10	0.10	0.06	-0.01	-0.02	38.23
BB3aR vertical traverse	Lens	1 / 6	38.87	0.23	0.06	-0.01	0.00	39.15
BB3aR vertical traverse	Lens	1 / 7	37.96	0.30	0.06	0.01	0.00	38.33
BB3aR vertical traverse	Lens	1 / 8	38.10	0.15	0.04	0.01	0.01	38.30
BB3aR vertical traverse	Lens	1 / 9	40.09	0.16	0.04	0.00	-0.01	40.28
BB3aR vertical traverse	Lens	1 / 10	38.86	0.09	0.03	0.01	0.00	38.98
BB3aR vertical traverse	Lens	1 / 11	38.24	0.35	0.03	0.00	0.01	38.62
BB3aR vertical traverse	Lens	1 / 12	38.74	0.08	0.01	0.01	0.00	38.84
BB3aR vertical traverse	Lens	1 / 13	38.70	0.06	0.03	0.00	0.01	38.80
BB3aR vertical traverse	Lens	1 / 14	35.58	0.14	-0.01	0.00	0.00	35.72
BB3aR vertical traverse	Lens	1 / 15	39.27	0.72	0.02	-0.01	-0.01	39.99
BB3aR vertical traverse	Lens	1 / 16	30.81	1.21	0.05	0.00	0.00	32.07
BB3aR vertical traverse	Lens	1 / 17	39.02	0.29	0.01	0.00	0.01	39.33
BB3aR vertical traverse	Lens	1 / 18	39.36	0.18	0.00	0.00	0.00	39.55
BB3aR vertical traverse	Lens	1 / 19	20.30	5.38	0.02	0.01	0.00	25.70
BB3aR vertical traverse	Lens	1 / 20	38.87	0.16	0.03	0.01	-0.01	39.06
BB3aR vertical traverse	Lens/Matrix	1 / 21	36.92	0.26	0.03	0.00	0.00	37.21
BB3aR vertical traverse	Matrix	1 / 22	39.02	0.22	0.03	-0.01	0.00	39.25
BB3aR vertical traverse	Matrix	1 / 23	39.33	0.16	0.01	0.00	-0.01	39.49
BB3aR vertical traverse	Matrix	1 / 24	37.91	0.26	0.00	0.00	0.01	38.18
BB3aR vertical traverse	Matrix	1 / 25	38.45	0.20	0.04	0.00	0.00	38.69
BB3aR vertical traverse	Matrix	1 / 26	38.68	0.09	0.03	0.00	0.01	38.80
BB3aR vertical traverse	Matrix	1 / 27	38.88	0.28	0.03	-0.01	0.02	39.19
BB3aR horizontal traverse	Sclera	2 / 1	38.94	0.16	0.01	0.02	0.04	39.17
BB3aR horizontal traverse	Sclera	2 / 2	39.48	0.11	0.01	0.09	0.07	39.76
BB3aR horizontal traverse	Sclera	2 / 3	38.55	0.17	0.01	0.02	0.01	38.76
BB3aR horizontal traverse	Sclera	2 / 4	38.29	0.12	0.01	0.07	0.07	38.56
BB3aR horizontal traverse	Lens	2 / 5	35.33	0.11	0.02	0.08	0.03	35.58
BB3aR horizontal traverse	Lens	2 / 6	39.26	0.12	0.01	0.01	0.04	39.45
BB3aR horizontal traverse	Lens	2 / 7	36.75	0.13	0.03	0.01	0.18	37.10
BB3aR horizontal traverse	Lens	2 / 8	38.66	0.11	0.04	0.05	0.04	38.89
BB3aR horizontal traverse	Lens	2 / 9	36.82	0.38	0.03	0.02	0.01	37.25
BB3aR horizontal traverse	Lens	2 / 10	35.02	0.04	0.02	0.01	0.01	35.09
BB3aR horizontal traverse	Lens	2 / 11	39.13	0.14	0.01	0.00	-0.01	39.26
BB3aR horizontal traverse	Lens	2 / 12	39.40	0.24	0.02	0.00	0.01	39.67
BB3aR horizontal traverse	Lens	2 / 13	35.21	0.19	0.04	-0.01	0.02	35.45
BB3aR horizontal traverse	Lens	2 / 14	37.50	0.24	0.03	0.01	0.00	37.78
BB3aR horizontal traverse	Lens	2 / 15	38.73	0.14	0.04	0.01	0.02	38.93
BB3aR horizontal traverse	Lens	2 / 16	22.41	0.02	0.00	0.08	0.01	22.52
BB3aR horizontal traverse	Lens	2 / 17	28.48	0.01	-0.01	0.11	0.01	28.60
BB3aR horizontal traverse	Lens	2 / 18	37.51	0.08	0.03	0.05	0.00	37.68

SAMPLE	FEATURE	DATA SET/ POINT	WEIGHT % ELEMENT					
			Ca	Mg	Sr	Fe	Mn	SUM
BB3aR horizontal traverse	Lens	2 / 19	39.79	0.20	0.01	0.00	0.00	40.00
BB3aR horizontal traverse	Lens	2 / 20	39.32	0.16	0.02	0.02	0.01	39.52
BB3aR horizontal traverse	Lens	2 / 21	36.35	0.22	0.03	0.01	0.00	36.61
BB3aR horizontal traverse	Lens	2 / 22	38.99	0.34	0.03	0.00	-0.01	39.34
BB3aR horizontal traverse	Lens	2 / 23	39.24	0.22	0.03	0.10	0.01	39.60
BB3aR horizontal traverse	Lens	2 / 24	39.67	0.12	0.04	0.20	0.02	40.04
BB3aR horizontal traverse	Lens	2 / 25	39.08	0.11	0.03	0.18	0.03	39.43
BB3aR horizontal traverse	Lens	2 / 26	39.12	0.20	0.03	0.00	0.00	39.35
BB3aR horizontal traverse	Lens	2 / 27	38.44	0.38	0.03	0.00	0.00	38.85
BB3aR horizontal traverse	Lens	2 / 28	38.35	0.34	0.02	0.00	0.01	38.72
BB3aR horizontal traverse	Lens	2 / 29	24.47	5.02	0.00	0.11	0.00	29.61
BB3aR horizontal traverse	Lens	2 / 30	39.22	0.24	0.02	0.00	0.00	39.48
BB3aR horizontal traverse	Lens	2 / 31	35.19	6.82	0.04	0.00	0.02	42.07
BB3aR horizontal traverse	Lens/Sclera	2 / 32	38.62	0.16	0.04	0.38	0.09	39.28
BB3aR horizontal traverse	Sclera	2 / 33	38.08	0.11	0.03	0.11	0.08	38.42
BB3aR horizontal traverse	Sclera	2 / 34	38.16	0.19	0.02	0.04	0.03	38.44
BB3aR sclera of lens 1	Sclera	1 / 1	40.20	0.15	0.02	0.13	0.01	40.51
BB3aR sclera of lens 2	Sclera	1 / 2	38.86	0.18	0.01	0.04	0.03	39.12
BB3aR sclera of lens 3	Sclera	1 / 3	37.98	0.22	0.01	0.04	0.01	38.28
BB3aR sclera of lens 4	Sclera	1 / 4	38.23	0.11	0.06	0.19	0.02	38.61
BB3aR sclera of lens 5	Sclera	1 / 5	38.56	0.19	0.01	0.02	0.03	38.81
BB3aR exoskeleton	E'skeleton	2 / 1	38.88	0.13	0.04	0.10	0.09	39.23
BB3aR exoskeleton	E'skeleton	2 / 2	39.44	0.13	0.03	0.00	0.02	39.62
BB3aR exoskeleton	E'skeleton	2 / 3	39.02	0.08	0.01	0.07	0.03	39.22
BB3aR exoskeleton	E'skeleton	2 / 4	38.62	0.33	0.03	0.00	0.01	38.98
BB3aR exoskeleton	E'skeleton	2 / 5	38.97	0.21	0.03	0.01	0.03	39.24
BB3aR exoskeleton	E'skeleton	2 / 6	38.79	0.16	0.01	0.04	0.03	39.02
BB3aR exoskeleton	E'skeleton	2 / 7	38.85	0.21	0.03	0.03	0.02	39.15
BB3aR exoskeleton	E'skeleton	2 / 8	38.91	0.12	0.02	0.02	0.03	39.11
BB3aR exoskeleton	E'skeleton	2 / 9	40.18	0.19	0.02	0.01	0.00	40.40
BB3aR exoskeleton	E'skeleton	2 / 10	38.18	0.33	0.01	0.01	0.00	38.52
BB3aR exoskeleton	E'skeleton	2 / 11	38.04	0.11	0.03	0.14	0.14	38.46
BB3aR exoskeleton	E'skeleton	2 / 12	39.83	0.11	0.02	0.09	0.06	40.11
BB3aR exoskeleton	E'skeleton	2 / 13	39.31	0.17	0.03	0.02	0.03	39.54
BB3aR exoskeleton	E'skeleton	2 / 14	38.25	0.14	0.02	0.03	0.01	38.45
BB3aR exoskeleton	E'skeleton	2 / 15	38.66	0.20	0.01	0.02	0.00	38.89
BB3aR exoskeleton	E'skeleton	2 / 16	39.46	0.18	0.02	0.03	0.05	39.75
BB3aR exoskeleton	E'skeleton	2 / 17	38.97	0.12	0.00	0.00	0.03	39.13
BB3aR exoskeleton	E'skeleton	2 / 18	39.66	0.20	0.02	0.04	0.03	39.94
E22B Lens 1 vertical traverse	Matrix	1 / 1	32.80	0.35	0.02	0.39	0.03	33.58
E22B Lens 1 vertical traverse	Cornea	1 / 2	37.03	0.16	0.02	0.06	0.06	37.34
E22B Lens 1 vertical traverse	Lens	1 / 3	38.66	0.34	0.01	0.04	0.03	39.08
E22B Lens 1 vertical traverse	Lens	1 / 4	37.95	0.60	0.07	0.00	0.00	38.62
E22B Lens 1 vertical traverse	Lens	1 / 5	39.00	0.38	0.05	0.00	0.02	39.46
E22B Lens 1 vertical traverse	Lens	1 / 6	38.27	0.45	0.04	0.01	0.02	38.79
E22B Lens 1 vertical traverse	Lens	1 / 7	38.26	0.13	0.01	-0.01	0.03	38.41
E22B Lens 1 vertical traverse	Core	1 / 8	31.72	0.14	0.00	0.00	0.01	31.87
E22B Lens 1 vertical traverse	Core	1 / 9	38.67	0.44	0.07	0.00	0.01	39.18
E22B Lens 1 vertical traverse	Core	1 / 10	39.01	0.39	0.03	0.00	0.03	39.46
E22B Lens 1 vertical traverse	Core	1 / 11	39.00	0.27	0.03	0.02	0.06	39.38
E22B Lens 1 vertical traverse	Core	1 / 12	38.27	0.27	0.02	0.00	0.07	38.63
E22B Lens 1 vertical traverse	Core	1 / 13	38.83	0.24	0.02	0.00	0.07	39.16
E22B Lens 1 vertical traverse	Core	1 / 14	38.77	0.20	0.00	0.01	0.10	39.08
E22B Lens 1 vertical traverse	Lens	1 / 15	38.40	0.44	0.06	0.00	0.02	38.93
E22B Lens 1 vertical traverse	Lens	1 / 16	36.51	0.52	0.03	0.00	0.03	37.08
E22B Lens 1 vertical traverse	Matrix	1 / 17	39.11	0.51	0.03	0.01	0.03	39.69
E22B Lens 1 vertical traverse	Matrix	1 / 18	6.71	0.32	-0.02	0.20	0.02	7.23
E22B Lens 1 vertical traverse	Matrix	1 / 19	38.23	0.29	0.00	0.33	0.05	38.90
E22B Lens 1 horizontal traverse	Sclera	2 / 1	38.17	0.34	0.03	0.05	0.04	38.62
E22B Lens 1 horizontal traverse	Sclera	2 / 2	38.62	0.30	0.04	0.04	0.04	39.05
E22B Lens 1 horizontal traverse	Sclera	2 / 3	38.44	0.30	0.03	0.05	0.03	38.85
E22B Lens 1 horizontal traverse	Sclera/Lens	2 / 4	39.08	0.26	0.02	0.05	0.06	39.47
E22B Lens 1 horizontal traverse	Bowl	2 / 5	38.51	0.59	0.02	0.04	0.04	39.21
E22B Lens 1 horizontal traverse	Bowl	2 / 6	39.13	0.37	0.02	0.03	0.04	39.59
E22B Lens 1 horizontal traverse	Lens	2 / 7	38.32	0.30	0.02	0.01	0.05	38.70
E22B Lens 1 horizontal traverse	Lens	2 / 8	38.48	0.25	0.03	0.01	0.04	38.81
E22B Lens 1 horizontal traverse	Core	2 / 9	37.90	0.48	0.02	0.00	0.03	38.43

SAMPLE	FEATURE	DATA SET/ POINT	WEIGHT % ELEMENT					
			Ca	Mg	Sr	Fe	Mn	SUM
E22B Lens 1 horizontal traverse	Core	2 / 10	38.79	0.24	0.03	0.01	0.02	39.09
E22B Lens 1 horizontal traverse	Core	2 / 11	39.13	0.28	0.01	-0.01	0.05	39.47
E22B Lens 1 horizontal traverse	Core	2 / 12	39.36	0.28	0.01	0.00	0.06	39.72
E22B Lens 1 horizontal traverse	Core	2 / 13	38.70	0.35	0.06	0.01	0.05	39.16
E22B Lens 1 horizontal traverse	Core	2 / 14	38.15	0.50	0.03	0.01	0.01	38.70
E22B Lens 1 horizontal traverse	Core	2 / 15	38.12	0.50	0.05	0.00	0.04	38.70
E22B Lens 1 horizontal traverse	Lens	2 / 16	38.87	0.51	0.03	0.00	0.07	39.48
E22B Lens 1 horizontal traverse	Lens	2 / 17	38.73	0.59	0.03	-0.01	0.03	39.37
E22B Lens 1 horizontal traverse	Bowl	2 / 18	37.68	0.55	0.05	-0.02	0.05	38.32
E22B Lens 1 horizontal traverse	Bowl	2 / 19	35.13	0.55	0.03	0.21	0.07	36.00
E22B Lens 1 horizontal traverse	Sclera	2 / 20	38.52	0.24	0.03	0.05	0.07	38.91
E22B Lens 1 horizontal traverse	Sclera	2 / 21	39.66	0.33	0.04	0.06	0.06	40.14
E22B Lens 1 horizontal traverse	Sclera	2 / 22	38.62	0.34	0.04	0.05	0.04	39.09
E22B Lens 1 horizontal traverse	Sclera	2 / 23	38.16	0.38	0.04	0.03	0.03	38.65
E22B Lens 1 horizontal traverse	Sclera	2 / 24	38.34	0.48	0.06	0.03	0.04	38.96
E22B Lens 1 horizontal traverse	Sclera	2 / 25	38.69	0.35	0.04	0.03	0.05	39.16
E22B exoskeleton	E'skeleton	3 / 1	38.16	0.37	0.05	0.05	0.05	38.68
E22B exoskeleton	E'skeleton	3 / 2	38.13	0.39	0.04	0.04	0.04	38.63
E22B exoskeleton	E'skeleton	3 / 3	39.07	0.41	0.03	0.01	0.02	39.54
E22B exoskeleton	E'skeleton	3 / 4	38.17	0.44	0.06	0.00	0.04	38.71
E22B exoskeleton	E'skeleton	3 / 5	38.60	0.34	0.03	0.02	0.04	39.03
E22B exoskeleton	E'skeleton	3 / 6	38.82	0.37	0.03	0.02	0.05	39.29
E22B exoskeleton	E'skeleton	3 / 7	38.42	0.37	0.05	0.03	0.04	38.90
E22B exoskeleton	E'skeleton	3 / 8	38.56	0.29	0.04	0.04	0.05	38.99
E22B exoskeleton	E'skeleton	3 / 9	38.13	0.28	0.03	0.02	0.06	38.52
E22B exoskeleton	E'skeleton	3 / 10	37.78	0.32	0.04	0.07	0.06	38.26
E22B exoskeleton	E'skeleton	3 / 11	37.91	0.34	0.04	0.01	0.08	38.38
E22B exoskeleton	E'skeleton	3 / 12	39.22	0.29	0.05	0.06	0.07	39.69
E22B Lens 3 vertical traverse	Resin	1 / 1	0.10	0.00	-0.01	0.00	0.00	0.09
E22B Lens 3 vertical traverse	Resin	1 / 2	0.12	0.00	0.00	0.00	-0.01	0.10
E22B Lens 3 vertical traverse	Lens	1 / 3	38.53	0.33	0.02	0.05	0.12	39.04
E22B Lens 3 vertical traverse	Lens	1 / 4	35.84	0.77	0.04	0.00	0.01	36.67
E22B Lens 3 vertical traverse	Lens	1 / 5	38.60	0.43	0.05	0.00	0.02	39.11
E22B Lens 3 vertical traverse	Lens	1 / 6	39.01	0.39	0.05	0.01	0.03	39.49
E22B Lens 3 vertical traverse	Lens	1 / 7	38.51	0.43	0.04	0.01	0.01	39.00
E22B Lens 3 vertical traverse	Core	1 / 8	37.79	0.43	0.04	0.01	0.00	38.27
E22B Lens 3 vertical traverse	Core	1 / 9	38.68	0.41	0.04	-0.01	0.04	39.15
E22B Lens 3 vertical traverse	Core	1 / 10	37.96	0.54	0.07	0.01	0.01	38.59
E22B Lens 3 vertical traverse	Core	1 / 11	39.17	0.23	0.00	-0.01	0.09	39.49
E22B Lens 3 vertical traverse	Core	1 / 12	38.94	0.37	0.03	0.01	0.03	39.36
E22B Lens 3 vertical traverse	Core	1 / 13	38.56	0.29	0.01	0.00	0.09	38.95
E22B Lens 3 vertical traverse	Core	1 / 14	39.08	0.47	0.04	0.00	0.03	39.62
E22B Lens 3 vertical traverse	Lens	1 / 15	38.07	0.47	0.05	0.01	0.02	38.61
E22B Lens 3 vertical traverse	Lens Base	1 / 16	13.15	0.55	0.01	0.38	0.00	14.09
E22B Lens 3 vertical traverse	Matrix	1 / 17	38.03	0.50	-0.01	0.13	0.10	38.75
E22B Lens 3 vertical traverse	Matrix	1 / 18	39.94	0.52	0.03	0.03	0.03	40.54
E22B Lens 3 horizontal traverse	Sclera	2 / 1	38.96	0.33	0.04	0.05	0.05	39.43
E22B Lens 3 horizontal traverse	Sclera	2 / 2	38.89	0.34	0.02	0.02	0.04	39.31
E22B Lens 3 horizontal traverse	Sclera	2 / 3	39.55	0.32	0.04	0.05	0.06	40.03
E22B Lens 3 horizontal traverse	Sclera	2 / 4	38.89	0.25	0.03	0.09	0.05	39.31
E22B Lens 3 horizontal traverse	Bowl	2 / 5	38.11	0.40	0.04	0.01	0.04	38.60
E22B Lens 3 horizontal traverse	Bowl	2 / 6	39.24	0.35	0.02	0.00	0.12	39.71
E22B Lens 3 horizontal traverse	Lens	2 / 7	38.87	0.46	0.02	0.01	0.03	39.39
E22B Lens 3 horizontal traverse	Lens	2 / 8	38.36	0.34	-0.01	0.00	0.03	38.73
E22B Lens 3 horizontal traverse	Lens	2 / 9	37.91	0.35	0.01	-0.01	0.03	38.29
E22B Lens 3 horizontal traverse	Core	2 / 10	38.13	0.53	0.04	0.01	0.01	38.72
E22B Lens 3 horizontal traverse	Core	2 / 11	38.55	0.31	0.01	-0.01	0.08	38.93
E22B Lens 3 horizontal traverse	Core	2 / 12	38.30	0.36	0.03	-0.01	0.07	38.76
E22B Lens 3 horizontal traverse	Core	2 / 13	38.96	0.30	0.01	0.01	0.06	39.35
E22B Lens 3 horizontal traverse	Core	2 / 14	38.20	0.50	0.04	0.00	0.04	38.78
E22B Lens 3 horizontal traverse	Core	2 / 15	38.94	0.39	0.04	0.00	0.02	39.38
E22B Lens 3 horizontal traverse	Lens	2 / 16	36.18	0.47	0.06	0.00	0.01	36.73
E22B Lens 3 horizontal traverse	Lens	2 / 17	38.47	0.37	0.03	0.00	0.03	38.89
E22B Lens 3 horizontal traverse	Lens	2 / 18	37.63	0.38	0.04	-0.01	0.03	38.07
E22B Lens 3 horizontal traverse	Bowl	2 / 19	38.58	0.68	0.00	-0.01	0.04	39.29
E22B Lens 3 horizontal traverse	Bowl	2 / 20	37.34	0.39	0.06	0.01	0.04	37.85
E22B Lens 3 horizontal traverse	Sclera	2 / 21	38.36	0.24	0.04	0.08	0.05	38.77
E22B Lens 3 horizontal traverse	Sclera	2 / 22	38.46	0.43	0.04	0.02	0.05	38.99

SAMPLE	FEATURE	DATA SET/ POINT	WEIGHT % ELEMENT					
			Ca	Mg	Sr	Fe	Mn	SUM
E22B Lens 3 horizontal traverse	Sclera	2 / 23	38.30	0.39	0.05	0.04	0.02	38.80
E22B Lens 3 horizontal traverse	Sclera	2 / 24	39.13	0.38	0.03	0.04	0.03	39.60
E22B Lens 3 horizontal traverse	Sclera	2 / 25	39.68	0.42	0.04	0.04	0.05	40.23
G33R Lens 1 vertical traverse	Resin	1 / 1	0.06	0.01	0.00	0.01	0.00	0.08
G33R Lens 1 vertical traverse	Resin	1 / 2	34.07	0.11	0.19	0.15	0.04	34.56
G33R Lens 1 vertical traverse	Resin	1 / 3	38.14	0.17	0.14	0.09	0.03	38.56
G33R Lens 1 vertical traverse	Resin	1 / 4	38.18	0.18	0.17	0.11	0.04	38.69
G33R Lens 1 vertical traverse	Lens	1 / 5	36.68	0.44	0.18	0.17	0.07	37.55
G33R Lens 1 vertical traverse	Lens	1 / 6	36.20	1.05	0.22	0.25	0.06	37.78
G33R Lens 1 vertical traverse	Lens	1 / 7	37.66	0.40	0.12	0.26	0.06	38.50
G33R Lens 1 vertical traverse	Lens	1 / 8	30.25	0.26	0.12	0.15	0.05	30.82
G33R Lens 1 vertical traverse	Lens	1 / 9	38.52	0.45	0.07	0.30	0.06	39.41
G33R Lens 1 vertical traverse	Lens	1 / 10	37.93	0.34	0.25	0.17	0.06	38.75
G33R Lens 1 vertical traverse	Lens	1 / 11	37.54	0.27	0.22	0.12	0.06	38.20
G33R Lens 1 vertical traverse	Lens	1 / 12	34.27	0.31	0.20	0.25	0.10	35.15
G33R Lens 1 vertical traverse	Lens	1 / 13	37.86	0.58	0.19	0.16	0.01	38.81
G33R Lens 1 vertical traverse	Lens	1 / 14	38.81	0.54	0.25	0.17	0.01	39.78
G33R Lens 1 vertical traverse	Lens	1 / 15	37.48	0.62	0.14	0.20	0.03	38.48
G33R Lens 1 vertical traverse	Cement	1 / 16	26.57	0.72	0.13	0.38	0.03	27.82
G33R Lens 1 vertical traverse	Cement	1 / 17	33.05	0.76	0.12	0.59	0.03	34.54
G33R Lens 1 vertical traverse	Cement	1 / 18	32.36	0.60	0.05	0.23	0.03	33.28
G33R Lens 1 vertical traverse	Cement	1 / 19	7.10	0.11	0.05	0.09	0.01	7.35
G33R Lens 1 vertical traverse	Matrix	1 / 20	36.24	0.65	0.15	0.32	0.04	37.40
G33R Lens 1 horizontal traverse	Lens	2 / 1	37.43	0.42	0.14	0.16	0.06	38.19
G33R Lens 1 horizontal traverse	Lens	2 / 2	38.03	0.37	0.14	0.15	0.02	38.71
G33R Lens 1 horizontal traverse	Lens	2 / 3	38.97	0.27	0.16	0.14	0.05	39.60
G33R Lens 1 horizontal traverse	Lens	2 / 4	37.50	0.11	0.06	0.29	0.19	38.15
G33R Lens 1 horizontal traverse	Lens	2 / 5	39.00	0.18	0.11	0.29	0.05	39.64
G33R Lens 1 horizontal traverse	Lens	2 / 6	37.33	0.36	0.28	0.15	0.05	38.17
G33R Lens 1 horizontal traverse	Lens	2 / 7	37.75	1.32	0.19	0.51	0.06	39.84
G33R Lens 1 horizontal traverse	Lens	2 / 8	37.72	0.37	0.21	0.15	0.02	38.47
G33R Lens 1 horizontal traverse	Lens	2 / 9	37.31	0.39	0.19	0.19	0.06	38.14
G33R Lens 1 horizontal traverse	Lens	2 / 10	37.43	0.20	0.18	0.21	0.07	38.08
G33R Lens 1 horizontal traverse	Lens	2 / 11	37.01	0.42	0.13	0.20	0.06	37.81
G33R Lens 1 horizontal traverse	Lens	2 / 12	37.18	0.34	0.18	0.13	0.03	37.86
G33R Lens 1 horizontal traverse	Lens	2 / 13	34.93	0.10	0.47	0.02	0.02	35.54
G33R sclera	Sclera	3 / 1	38.54	0.39	0.14	0.17	0.06	39.31
G33R sclera	Sclera	3 / 2	40.26	0.48	0.23	0.14	0.04	41.14
G33R sclera	Sclera	3 / 3	38.74	0.45	0.29	0.14	0.02	39.64
G33R sclera	Sclera	3 / 4	39.70	0.32	0.21	0.20	0.04	40.46
G33R sclera	Sclera	3 / 5	38.81	0.58	0.24	0.12	0.04	39.79
G33R sclera	Sclera	3 / 6	39.77	0.38	0.25	0.11	0.05	40.57
G33R sclera	Sclera	3 / 7	39.35	0.42	0.21	0.20	0.03	40.20
G33R sclera	Sclera	3 / 8	38.77	0.66	0.21	0.15	0.03	39.82
G33R sclera	Sclera	3 / 9	38.79	0.48	0.17	0.18	0.04	39.66
G33R sclera	Sclera	3 / 10	38.60	0.46	0.24	0.12	0.03	39.45
G33R sclera	Sclera	3 / 11	39.20	0.73	0.24	0.17	0.04	40.37
G33R sclera	Sclera	3 / 12	38.31	0.34	0.18	0.14	0.05	39.02
PM28 Lens 3 vertical traverse	Resin	1 / 1	0.02	0.00	0.01	0.00	0.00	0.04
PM28 Lens 3 vertical traverse	Resin	1 / 2	0.02	0.00	-0.01	-0.01	0.00	0.02
PM28 Lens 3 vertical traverse	Resin	1 / 3	0.03	0.00	-0.01	0.00	0.00	0.01
PM28 Lens 3 vertical traverse	Lens	1 / 4	30.87	1.37	0.21	0.01	0.03	32.48
PM28 Lens 3 vertical traverse	Lens	1 / 5	38.42	0.47	0.20	0.03	0.02	39.13
PM28 Lens 3 vertical traverse	Lens	1 / 6	23.97	2.20	0.16	0.08	0.02	26.44
PM28 Lens 3 vertical traverse	Lens	1 / 7	34.92	1.54	0.23	0.01	0.02	36.71
PM28 Lens 3 vertical traverse	Lens	1 / 8	36.14	1.76	0.32	0.02	0.01	38.25
PM28 Lens 3 vertical traverse	Lens	1 / 9	37.08	1.62	0.24	0.01	0.01	38.97
PM28 Lens 3 vertical traverse	Lens	1 / 10	37.17	1.95	0.22	0.04	0.00	39.38
PM28 Lens 3 vertical traverse	Lens	1 / 11	36.28	1.36	0.26	0.02	-0.01	37.92
PM28 Lens 3 vertical traverse	Lens	1 / 12	33.88	2.33	0.25	0.04	0.00	36.51
PM28 Lens 3 vertical traverse	Lens	1 / 13	37.37	0.20	0.04	1.48	0.08	39.17
PM28 Lens 3 vertical traverse	Bowl?	1 / 14	38.25	0.15	0.03	1.00	0.05	39.49
PM28 Lens 3 vertical traverse	Lens	1 / 15	27.54	0.19	0.02	4.14	0.04	31.94
PM28 Lens 3 vertical traverse	Matrix	1 / 16	33.39	0.33	0.02	1.53	0.19	35.46
PM28 Lens 3 vertical traverse	Matrix	1 / 17	5.28	0.21	-0.01	0.32	0.01	5.81
PM28 Lens 3 vertical traverse	Matrix	1 / 18	3.49	2.81	-0.01	4.64	0.02	10.95

SAMPLE	FEATURE	DATA SET/ POINT	WEIGHT % ELEMENT					
			Ca	Mg	Sr	Fe	Mn	SUM
PM28 Lens 3 horizontal traverse	Lens	2 / 1	33.01	0.40	0.03	2.04	0.07	35.55
PM28 Lens 3 horizontal traverse	Lens	2 / 2	35.94	1.49	0.25	0.07	0.00	37.75
PM28 Lens 3 horizontal traverse	Lens	2 / 3	33.14	2.00	0.22	0.21	0.02	35.60
PM28 Lens 3 horizontal traverse	Lens	2 / 4	35.98	2.17	0.21	0.02	0.01	38.40
PM28 Lens 3 horizontal traverse	Lens	2 / 5	36.69	1.06	0.22	0.02	0.01	38.00
PM28 Lens 3 horizontal traverse	Lens	2 / 6	33.89	0.77	0.19	0.01	0.00	34.87
PM28 Lens 3 horizontal traverse	Lens	2 / 7	30.58	0.84	0.24	0.02	-0.01	31.67
PM28 Lens 3 horizontal traverse	Lens	2 / 8	37.48	1.07	0.24	0.00	0.00	38.80
PM28 Lens 3 horizontal traverse	Lens	2 / 9	27.96	1.17	0.19	0.01	-0.01	29.31
PM28 Lens 3 horizontal traverse	Lens	2 / 10	36.75	1.39	0.23	0.00	0.00	38.38
PM28 Lens 3 horizontal traverse	Lens	2 / 11	36.90	1.10	0.22	0.01	0.01	38.24
PM28 Lens 3 horizontal traverse	Lens	2 / 12	29.94	4.36	0.24	0.02	0.02	34.58
PM28 Lens 3 horizontal traverse	Lens	2 / 13	37.02	0.91	0.25	0.01	0.02	38.21
PM28 Lens 3 horizontal traverse	Lens	2 / 14	36.34	2.23	0.22	0.04	0.03	38.87
PM28 Lens 3 horizontal traverse	Lens	2 / 15	37.34	1.92	0.17	0.23	0.05	39.71
PM28 Lens 5 vertical traverse	Resin	1 / 1	-0.01	0.00	-0.01	0.01	0.01	0.01
PM28 Lens 5 vertical traverse	Resin	1 / 2	-0.01	0.00	0.01	0.00	0.00	0.00
PM28 Lens 5 vertical traverse	Lens	1 / 3	37.87	0.81	0.25	0.06	0.17	39.15
PM28 Lens 5 vertical traverse	Lens	1 / 4	38.88	0.12	0.23	0.04	0.14	39.42
PM28 Lens 5 vertical traverse	Lens	1 / 5	38.17	1.04	0.22	0.09	0.23	39.75
PM28 Lens 5 vertical traverse	Lens	1 / 6	37.56	0.89	0.28	0.07	0.25	39.05
PM28 Lens 5 vertical traverse	Lens	1 / 7	38.01	0.69	0.18	0.03	0.04	38.95
PM28 Lens 5 vertical traverse	Lens	1 / 8	36.24	1.34	0.17	0.13	0.04	37.92
PM28 Lens 5 vertical traverse	Lens	1 / 9	38.00	0.31	0.18	0.27	0.10	38.85
PM28 Lens 5 vertical traverse	Lens	1 / 10	34.84	1.55	0.22	-0.01	-0.01	36.59
PM28 Lens 5 vertical traverse	Lens	1 / 11	37.37	2.09	0.21	0.00	0.00	39.68
PM28 Lens 5 vertical traverse	Lens	1 / 12	35.21	1.41	0.17	0.10	0.00	36.88
PM28 Lens 5 vertical traverse	Lens	1 / 13	37.09	1.98	0.19	0.01	0.00	39.26
PM28 Lens 5 vertical traverse	Lens	1 / 14	36.46	2.29	0.22	0.06	0.03	39.05
PM28 Lens 5 vertical traverse	Lens	1 / 15	36.08	4.08	0.26	0.04	0.00	40.46
PM28 Lens 5 vertical traverse	Lens	1 / 16	34.56	3.26	0.19	1.13	0.12	39.26
PM28 Lens 5 vertical traverse	Lens	1 / 17	34.78	0.23	0.03	1.47	0.13	36.63
PM28 Lens 5 vertical traverse	Matrix	1 / 18	36.11	0.30	0.02	0.89	0.11	37.43
PM28 Lens 5 vertical traverse	Matrix	1 / 19	35.61	0.14	0.03	0.91	0.06	36.74
PM28 Lens 5 vertical traverse	Matrix	1 / 20	36.66	0.26	0.05	1.30	0.09	38.36
PM28 Lens 5 vertical traverse	Matrix	1 / 21	28.84	0.20	0.01	1.00	0.06	30.11
PM28 Lens 5 vertical traverse	Matrix	1 / 22	6.95	0.85	0.03	2.65	0.93	11.41
PM28 Lens 5 horizontal traverse	Lens	2 / 1	36.08	0.51	0.05	1.43	0.58	38.65
PM28 Lens 5 horizontal traverse	Lens	2 / 2	36.39	1.20	0.21	0.29	0.07	38.16
PM28 Lens 5 horizontal traverse	Lens	2 / 3	32.20	2.43	0.23	0.19	0.01	35.05
PM28 Lens 5 horizontal traverse	Lens	2 / 4	38.00	0.43	0.16	0.32	0.06	38.97
PM28 Lens 5 horizontal traverse	Lens	2 / 5	38.37	0.33	0.16	0.27	0.04	39.18
PM28 Lens 5 horizontal traverse	Lens	2 / 6	32.65	0.70	0.14	0.18	0.05	33.72
PM28 Lens 5 horizontal traverse	Lens	2 / 7	38.58	0.58	0.18	0.07	0.02	39.43
PM28 Lens 5 horizontal traverse	Lens	2 / 8	36.06	5.09	0.21	0.00	0.00	41.37
PM28 Lens 5 horizontal traverse	Lens	2 / 9	37.18	0.68	0.22	-0.01	0.00	38.08
PM28 Lens 5 horizontal traverse	Lens	2 / 10	36.90	1.15	0.22	0.01	-0.01	38.27
PM28 Lens 5 horizontal traverse	Lens	2 / 11	31.03	1.42	0.21	0.03	0.01	32.70
PM28 Lens 5 horizontal traverse	Lens	2 / 12	36.49	1.08	0.19	0.00	-0.01	37.76
PM28 Lens 5 horizontal traverse	Lens	2 / 13	36.67	1.43	0.18	0.04	0.00	38.32
PM28 Lens 5 horizontal traverse	Lens	2 / 14	34.52	1.90	0.20	0.23	0.04	36.88
PM28 Lens 5 horizontal traverse	Lens	2 / 15	37.20	2.24	0.22	0.13	0.01	39.80
PM28 Lens 5 horizontal traverse	Lens	2 / 16	30.82	5.58	0.25	0.08	0.01	36.74
PM28 Lens 5 horizontal traverse	Lens	2 / 17	38.04	1.38	0.20	0.14	0.03	39.80
TS1 Lens 4 vertical traverse	Resin	1 / 1	0.02	0.00	0.00	0.01	0.00	0.03
TS1 Lens 4 vertical traverse	Resin	1 / 2	0.02	0.00	-0.01	0.00	0.00	0.01
TS1 Lens 4 vertical traverse	Lens	1 / 3	37.89	0.45	0.04	0.08	0.04	38.50
TS1 Lens 4 vertical traverse	Lens	1 / 4	38.48	0.49	0.05	0.02	0.02	39.06
TS1 Lens 4 vertical traverse	Lens	1 / 5	15.47	0.23	0.06	0.02	-0.01	15.78
TS1 Lens 4 vertical traverse	Lens	1 / 6	27.88	2.66	0.08	0.07	0.00	30.70
TS1 Lens 4 vertical traverse	Lens	1 / 7	39.19	0.15	0.07	0.12	0.03	39.56
TS1 Lens 4 vertical traverse	Lens	1 / 8	33.85	4.55	0.06	0.97	0.07	39.51
TS1 Lens 4 vertical traverse	Lens	1 / 9	38.65	0.10	0.07	0.13	0.06	39.02
TS1 Lens 4 vertical traverse	Lens	1 / 10	38.18	0.72	0.04	0.18	0.05	39.17
TS1 Lens 4 vertical traverse	Core	1 / 11	38.37	0.12	0.06	0.12	0.03	38.69
TS1 Lens 4 vertical traverse	Core	1 / 12	37.96	0.12	0.07	0.09	0.05	38.28
TS1 Lens 4 vertical traverse	Core	1 / 13	38.77	0.15	0.05	0.20	0.06	39.23
TS1 Lens 4 vertical traverse	Core	1 / 14	37.81	0.21	0.04	0.20	0.05	38.32

SAMPLE	FEATURE	DATA SET/ POINT	WEIGHT % ELEMENT					
			Ca	Mg	Sr	Fe	Mn	SUM
TS1 Lens 4 vertical traverse	Core	1 / 15	34.71	2.12	0.05	0.35	0.06	37.28
TS1 Lens 4 vertical traverse	Core	1 / 16	38.23	0.19	0.06	0.16	0.06	38.69
TS1 Lens 4 vertical traverse	Lens	1 / 17	35.11	2.58	0.06	0.39	0.04	38.18
TS1 Lens 4 vertical traverse	Lens	1 / 18	29.36	0.42	0.05	0.08	0.04	29.95
TS1 Lens 4 vertical traverse	Lens	1 / 19	38.06	3.41	0.07	0.55	0.08	42.17
TS1 Lens 4 vertical traverse	Lens	1 / 20	38.45	0.94	0.07	0.73	0.09	40.28
TS1 Lens 4 vertical traverse	Matrix?	1 / 21	37.67	0.50	0.06	0.12	0.05	38.40
TS1 Lens 4 vertical traverse	Matrix?	1 / 22	36.29	0.69	0.02	0.40	0.05	37.47
TS1 Lens 4 horizontal traverse	Sclera	2 / 1	38.26	0.42	0.08	0.29	0.07	39.12
TS1 Lens 4 horizontal traverse	Sclera	2 / 2	38.57	0.45	0.09	0.10	0.02	39.23
TS1 Lens 4 horizontal traverse	Sclera	2 / 3	39.63	0.41	0.09	0.27	0.04	40.43
TS1 Lens 4 horizontal traverse	Lens	2 / 4	38.06	0.31	0.08	0.27	0.04	38.76
TS1 Lens 4 horizontal traverse	Lens	2 / 5	38.01	0.44	0.05	0.12	0.02	38.64
TS1 Lens 4 horizontal traverse	Lens	2 / 6	37.05	0.80	0.05	0.01	0.02	37.93
TS1 Lens 4 horizontal traverse	Lens	2 / 7	38.46	0.44	0.04	0.00	0.02	38.97
TS1 Lens 4 horizontal traverse	Lens	2 / 8	38.96	0.52	0.06	0.04	0.03	39.60
TS1 Lens 4 horizontal traverse	Lens	2 / 9	37.89	0.47	0.11	0.05	0.04	38.56
TS1 Lens 4 horizontal traverse	Lens	2 / 10	37.56	0.39	0.06	0.01	0.03	38.05
TS1 Lens 4 horizontal traverse	Lens	2 / 11	37.84	0.39	0.05	0.02	0.02	38.33
TS1 Lens 4 horizontal traverse	Lens	2 / 12	37.47	0.67	0.06	0.01	0.01	38.23
TS1 Lens 4 horizontal traverse	Lens	2 / 13	38.14	0.25	0.06	0.01	0.02	38.49
TS1 Lens 4 horizontal traverse	Core	2 / 14	38.20	0.31	0.04	0.05	0.02	38.61
TS1 Lens 4 horizontal traverse	Core	2 / 15	38.57	0.21	0.04	0.24	0.10	39.16
TS1 Lens 4 horizontal traverse	Core	2 / 16	38.15	0.20	0.04	0.25	0.07	38.71
TS1 Lens 4 horizontal traverse	Lens	2 / 17	37.94	0.08	0.04	0.12	0.03	38.22
TS1 Lens 4 horizontal traverse	Lens	2 / 18	39.06	0.21	0.06	0.18	0.02	39.54
TS1 Lens 4 horizontal traverse	Lens	2 / 19	40.14	0.11	0.07	0.12	0.06	40.50
TS1 Lens 4 horizontal traverse	Lens	2 / 20	37.34	0.78	0.08	0.07	0.03	38.31
TS1 Lens 4 horizontal traverse	Lens	2 / 21	38.54	0.56	0.04	0.08	0.03	39.24
TS1 Lens 4 horizontal traverse	Lens	2 / 22	36.81	0.17	0.07	0.01	0.02	37.07
TS1 Lens 4 horizontal traverse	Lens	2 / 23	38.28	0.21	0.07	0.01	0.01	38.57
TS1 Lens 4 horizontal traverse	Lens	2 / 24	37.51	0.33	0.07	0.02	0.02	37.96
TS1 Lens 4 horizontal traverse	Lens	2 / 25	38.61	0.31	0.06	0.03	0.03	39.04
TS1 Lens 4 horizontal traverse	Lens	2 / 26	38.59	0.61	0.06	0.18	0.08	39.52
TS1 Lens 4 horizontal traverse	Lens/Sclera	2 / 27	35.34	0.73	0.06	0.05	0.04	36.21
TS1 Lens 4 horizontal traverse	Sclera	2 / 28	37.10	1.66	0.06	0.20	0.11	39.13
TS1 Lens 4 horizontal traverse	Sclera	2 / 29	38.97	0.37	0.06	0.08	0.02	39.50
TS1 Lens 4 horizontal traverse	Sclera	2 / 30	38.45	0.48	0.08	0.14	0.03	39.18
TS1 Lens 4 horizontal traverse	Sclera	2 / 31	39.44	0.42	0.07	0.20	0.04	40.17
TS1 Lens 5 vertical traverse	Resin	1 / 1	0.04	0.00	0.01	0.00	0.01	0.06
TS1 Lens 5 vertical traverse	Resin	1 / 2	0.03	0.01	0.00	0.00	-0.01	0.02
TS1 Lens 5 vertical traverse	Lens	1 / 3	38.30	0.56	0.08	0.27	0.07	39.28
TS1 Lens 5 vertical traverse	Lens	1 / 4	39.18	0.49	0.05	0.02	0.03	39.77
TS1 Lens 5 vertical traverse	Core	1 / 5	37.27	0.64	0.05	0.16	0.06	38.18
TS1 Lens 5 vertical traverse	Core	1 / 6	39.27	0.13	0.07	0.19	0.08	39.74
TS1 Lens 5 vertical traverse	Core	1 / 7	24.19	1.93	0.03	0.62	0.07	26.83
TS1 Lens 5 vertical traverse	Core	1 / 8	39.27	0.47	0.09	0.27	0.10	40.20
TS1 Lens 5 vertical traverse	Core	1 / 9	38.57	0.12	0.07	0.12	0.10	38.98
TS1 Lens 5 vertical traverse	Core	1 / 10	37.03	0.54	0.07	0.16	0.08	37.88
TS1 Lens 5 vertical traverse	Core	1 / 11	36.72	7.93	0.06	1.70	0.18	46.59
TS1 Lens 5 vertical traverse	Core	1 / 12	38.21	0.56	0.07	0.24	0.13	39.20
TS1 Lens 5 vertical traverse	Core	1 / 13	26.83	0.81	0.06	0.29	0.12	28.11
TS1 Lens 5 vertical traverse	Core	1 / 14	38.53	1.17	0.04	0.38	0.09	40.22
TS1 Lens 5 vertical traverse	Core	1 / 15	38.22	0.19	0.06	0.24	0.12	38.83
TS1 Lens 5 vertical traverse	Core	1 / 16	39.68	0.33	0.06	0.28	0.12	40.47
TS1 Lens 5 vertical traverse	Core	1 / 17	38.19	0.73	0.07	0.11	0.05	39.15
TS1 Lens 5 vertical traverse	Core/Lens	1 / 18	38.20	0.30	0.05	0.03	0.04	38.62
TS1 Lens 5 vertical traverse	Bowl	1 / 19	39.61	0.55	0.08	0.11	0.08	40.43
TS1 Lens 5 vertical traverse	Bowl	1 / 20	36.50	0.47	0.08	0.54	0.16	37.74
TS1 Lens 5 vertical traverse	Matrix	1 / 21	38.81	0.41	0.10	0.21	0.05	39.58
TS1 Lens 5 vertical traverse	Matrix	1 / 22	29.11	0.69	0.07	1.06	0.04	30.96
TS1 Lens 5 vertical traverse	Matrix	1 / 23	38.06	0.38	0.07	0.30	0.03	38.85
TS1 Lens 5 vertical traverse	Matrix	1 / 24	37.23	0.44	0.05	0.28	0.04	38.05
TS1 Lens 5 vertical traverse	Matrix	1 / 25	39.06	0.65	0.04	0.38	0.06	40.19
TS1 Lens 5 horizontal traverse	Sclera	2 / 1	38.69	0.63	0.11	0.31	0.08	39.82
TS1 Lens 5 horizontal traverse	Sclera	2 / 2	38.17	0.60	0.11	0.34	0.13	39.35
TS1 Lens 5 horizontal traverse	Lens	2 / 3	38.30	0.56	0.08	0.36	0.15	39.45
TS1 Lens 5 horizontal traverse	Lens	2 / 4	36.95	0.36	0.10	0.08	0.04	37.53

SAMPLE	FEATURE	DATA SET/ POINT	WEIGHT % ELEMENT					
			Ca	Mg	Sr	Fe	Mn	SUM
TS1 Lens 5 horizontal traverse	Lens	2 / 5	37.47	0.34	0.05	0.01	0.02	37.90
TS1 Lens 5 horizontal traverse	Lens	2 / 6	38.57	0.50	0.06	0.13	0.04	39.30
TS1 Lens 5 horizontal traverse	Lens	2 / 7	37.78	0.52	0.05	0.05	0.04	38.44
TS1 Lens 5 horizontal traverse	Lens	2 / 8	39.58	0.34	0.04	0.01	0.02	39.99
TS1 Lens 5 horizontal traverse	Lens	2 / 9	38.76	0.45	0.08	0.01	0.01	39.30
TS1 Lens 5 horizontal traverse	Core	2 / 10	39.44	0.52	0.06	0.02	0.02	40.05
TS1 Lens 5 horizontal traverse	Core	2 / 11	38.64	0.21	0.08	0.01	0.02	38.97
TS1 Lens 5 horizontal traverse	Core	2 / 12	38.90	0.50	0.06	0.04	0.02	39.52
TS1 Lens 5 horizontal traverse	Core	2 / 13	38.04	0.37	0.06	0.03	0.03	38.53
TS1 Lens 5 horizontal traverse	Core	2 / 14	34.66	0.40	0.07	0.27	0.09	35.49
TS1 Lens 5 horizontal traverse	Core	2 / 15	33.97	7.69	0.03	1.89	0.20	43.78
TS1 Lens 5 horizontal traverse	Core	2 / 16	38.59	0.16	0.07	0.15	0.16	39.13
TS1 Lens 5 horizontal traverse	Core	2 / 17	38.13	0.34	0.06	0.29	0.12	38.94
TS1 Lens 5 horizontal traverse	Core	2 / 18	38.30	0.09	0.04	0.09	0.08	38.60
TS1 Lens 5 horizontal traverse	Core	2 / 19	27.09	1.29	0.05	0.29	0.09	28.81
TS1 Lens 5 horizontal traverse	Lens	2 / 20	39.14	0.41	0.04	0.09	0.09	39.78
TS1 Lens 5 horizontal traverse	Lens	2 / 21	39.16	1.64	0.05	0.13	0.07	41.05
TS1 Lens 5 horizontal traverse	Lens	2 / 22	34.23	0.43	0.03	0.04	0.04	34.79
TS1 Lens 5 horizontal traverse	Lens	2 / 23	38.25	0.50	0.09	0.02	0.01	38.87
TS1 Lens 5 horizontal traverse	Lens	2 / 24	38.31	0.46	0.04	0.02	0.05	38.89
TS1 Lens 5 horizontal traverse	Lens	2 / 25	36.96	0.46	0.07	0.02	0.03	37.53
TS1 Lens 5 horizontal traverse	Lens	2 / 26	36.88	0.66	0.06	0.08	0.04	37.72
TS1 Lens 5 horizontal traverse	Lens/Sclera	2 / 27	38.28	0.49	0.06	0.02	0.00	38.84
TS1 Lens 5 horizontal traverse	Sclera	2 / 28	37.31	0.71	0.06	0.01	0.01	38.11
TS1 Lens 5 horizontal traverse	Sclera	2 / 29	38.15	0.60	0.14	0.24	0.04	39.16
TS1 Lens 5 horizontal traverse	Sclera	2 / 30	37.69	0.67	0.10	0.24	0.04	38.74
TS1 sclera	Sclera	3 / 1	38.54	0.72	0.11	0.20	0.05	39.62
TS1 sclera	Sclera	3 / 2	37.91	0.56	0.09	0.21	0.06	38.82
TS1 sclera	Sclera	3 / 3	38.82	0.46	0.08	0.22	0.06	39.63
TS1 sclera	Sclera	3 / 4	39.17	0.37	0.10	0.26	0.05	39.93
TS1 sclera	Sclera	3 / 5	38.28	0.46	0.08	0.28	0.07	39.16
TS1 sclera	Sclera	3 / 6	39.74	0.56	0.06	0.11	0.05	40.53
TS1 sclera	Sclera	3 / 7	38.02	0.50	0.07	0.22	0.09	38.90
TS1 sclera	Sclera	3 / 8	38.14	0.58	0.10	0.15	0.02	39.00
TS1 sclera	Sclera	3 / 9	38.01	0.47	0.07	0.22	0.07	38.84

Table E.6 - Weight % carbonate EPMA data (Edinburgh) for trilobites with schizochroal eyes.

SAMPLE	FEATURE	DATA SET/ POINT	WEIGHT % CARBONATE					
			Ca	Mg	Sr	Fe	Mn	SUM
BB3aR cement	Cement	1 / 1	95.77	1.19	0.03	0.02	0.02	97.03
BB3aR cement	Cement	1 / 2	96.93	0.10	0.02	0.02	0.03	97.10
BB3aR cement	Cement	1 / 3	96.21	0.07	0.00	-0.02	0.02	96.28
BB3aR cement	Cement	1 / 4	95.91	0.99	0.05	0.00	0.02	96.98
BB3aR cement	Cement	1 / 5	96.73	1.54	0.07	0.02	-0.07	98.29
BB3aR cement	Cement	1 / 6	97.30	1.18	0.15	0.06	0.01	98.70
BB3aR cement	Cement	1 / 7	95.56	0.62	0.03	0.01	0.01	96.23
BB3aR cement	Cement	1 / 8	97.45	0.88	0.03	0.04	0.00	98.40
BB3aR cement	Cement	1 / 9	97.67	0.68	0.02	0.05	0.04	98.46
BB3aR cement	Cement	1 / 10	98.14	0.34	0.02	0.00	-0.02	98.47
BB3aR cement	Cement	1 / 11	98.14	0.29	0.02	0.00	0.04	98.48
BB3aR cement	Cement	1 / 12	97.56	0.57	0.05	0.00	0.02	98.20
BB3aR cement	Cement	1 / 13	96.40	0.58	0.04	0.01	0.01	97.05
BB3aR cement	Cement	1 / 14	97.13	1.00	0.05	0.01	0.02	98.22
BB3aR cement	Cement	1 / 15	97.32	0.60	0.07	0.01	0.04	98.05
BB3aR Lens 2b diagonal traverse	Lens	1 / 1	96.73	0.99	0.06	0.02	0.03	97.83
BB3aR Lens 2b diagonal traverse	Lens	1 / 2	94.62	0.32	0.06	0.00	0.03	95.02
BB3aR Lens 2b diagonal traverse	Lens	1 / 3	99.66	2.95	0.08	0.00	-0.01	102.67
BB3aR Lens 2b diagonal traverse	Lens	1 / 4	96.11	11.00	0.10	-0.02	-0.01	107.17
BB3aR Lens 2b diagonal traverse	Lens	1 / 5	96.93	0.36	0.05	0.00	0.00	97.35
BB3aR Lens 2b diagonal traverse	Lens	1 / 6	97.91	0.32	0.05	0.00	0.03	98.30
BB3aR Lens 2b diagonal traverse	Lens	1 / 7	94.13	0.43	0.09	-0.01	0.00	94.62
BB3aR Lens 2b diagonal traverse	Lens	1 / 8	88.53	10.73	0.09	-0.02	0.01	99.33
BB3aR Lens 2b diagonal traverse	Lens	1 / 9	94.04	0.54	0.05	0.01	-0.01	94.63

SAMPLE	FEATURE	DATA SET/ POINT	WEIGHT % CARBONATE					
			Ca	Mg	Sr	Fe	Mn	SUM
BB3aR Lens 2b diagonal traverse	Lens	1 / 10	95.81	0.67	0.07	-0.01	0.00	96.55
BB3aR Lens 2b diagonal traverse	Lens	1 / 11	80.57	0.29	0.00	-0.02	-0.02	80.82
BB3aR Lens 2b diagonal traverse	Lens	1 / 12	94.36	5.87	0.08	0.04	0.02	100.36
BB3aR Lens 2b diagonal traverse	Lens	1 / 13	94.61	0.78	0.04	-0.01	0.00	95.41
BB3aR vertical traverse	Resin	1 / 1	96.73	0.35	0.02	0.14	0.07	97.32
BB3aR vertical traverse	Resin	1 / 2	97.01	0.47	0.03	0.05	0.01	97.57
BB3aR vertical traverse	Lens	1 / 3	94.99	0.49	0.06	0.02	-0.01	95.54
BB3aR vertical traverse	Lens	1 / 4	100.63	0.54	0.06	0.01	-0.01	101.23
BB3aR vertical traverse	Lens	1 / 5	95.14	0.34	0.10	-0.03	-0.03	95.51
BB3aR vertical traverse	Lens	1 / 6	97.07	0.79	0.09	-0.01	0.01	97.94
BB3aR vertical traverse	Lens	1 / 7	94.80	1.04	0.10	0.02	-0.01	95.94
BB3aR vertical traverse	Lens	1 / 8	95.13	0.52	0.06	0.01	0.01	95.74
BB3aR vertical traverse	Lens	1 / 9	100.09	0.56	0.06	0.01	-0.02	100.70
BB3aR vertical traverse	Lens	1 / 10	97.02	0.30	0.05	0.02	-0.01	97.38
BB3aR vertical traverse	Lens	1 / 11	95.48	1.21	0.05	-0.01	0.02	96.75
BB3aR vertical traverse	Lens	1 / 12	96.72	0.27	0.03	0.02	0.00	97.04
BB3aR vertical traverse	Lens	1 / 13	96.64	0.21	0.06	0.00	0.01	96.92
BB3aR vertical traverse	Lens	1 / 14	88.84	0.49	-0.01	0.00	0.01	89.33
BB3aR vertical traverse	Lens	1 / 15	98.07	2.50	0.04	-0.02	-0.02	100.56
BB3aR vertical traverse	Lens	1 / 16	76.93	4.20	0.09	0.00	0.00	81.22
BB3aR vertical traverse	Lens	1 / 17	97.43	1.00	0.02	-0.01	0.02	98.47
BB3aR vertical traverse	Lens	1 / 18	98.29	0.63	0.00	0.01	0.00	98.94
BB3aR vertical traverse	Lens	1 / 19	50.69	18.65	0.03	0.02	0.00	69.37
BB3aR vertical traverse	Lens	1 / 20	97.06	0.56	0.04	0.01	-0.01	97.66
BB3aR vertical traverse	Lens/Matrix	1 / 21	92.18	0.92	0.05	0.00	0.01	93.15
BB3aR vertical traverse	Matrix	1 / 22	97.42	0.77	0.05	-0.02	-0.01	98.21
BB3aR vertical traverse	Matrix	1 / 23	98.21	0.55	0.02	0.00	-0.01	98.76
BB3aR vertical traverse	Matrix	1 / 24	94.67	0.91	0.00	0.00	0.02	95.59
BB3aR vertical traverse	Matrix	1 / 25	96.02	0.70	0.07	-0.01	0.01	96.78
BB3aR vertical traverse	Matrix	1 / 26	96.59	0.30	0.04	0.00	0.01	96.94
BB3aR vertical traverse	Matrix	1 / 27	97.08	0.96	0.04	-0.01	0.04	98.10
BB3aR horizontal traverse	Sclera	2 / 1	97.23	0.56	0.02	0.04	0.09	97.94
BB3aR horizontal traverse	Sclera	2 / 2	98.59	0.37	0.01	0.18	0.15	99.30
BB3aR horizontal traverse	Sclera	2 / 3	96.25	0.59	0.02	0.04	0.02	96.93
BB3aR horizontal traverse	Sclera	2 / 4	95.61	0.43	0.02	0.14	0.15	96.35
BB3aR horizontal traverse	Lens	2 / 5	88.21	0.38	0.04	0.17	0.07	88.88
BB3aR horizontal traverse	Lens	2 / 6	98.03	0.43	0.01	0.03	0.09	98.59
BB3aR horizontal traverse	Lens	2 / 7	91.76	0.46	0.04	0.02	0.38	92.66
BB3aR horizontal traverse	Lens	2 / 8	96.52	0.37	0.06	0.11	0.09	97.15
BB3aR horizontal traverse	Lens	2 / 9	91.94	1.32	0.05	0.03	0.02	93.35
BB3aR horizontal traverse	Lens	2 / 10	87.43	0.13	0.03	0.03	0.01	87.63
BB3aR horizontal traverse	Lens	2 / 11	97.71	0.48	0.02	-0.01	-0.03	98.16
BB3aR horizontal traverse	Lens	2 / 12	98.38	0.84	0.03	0.00	0.01	99.28
BB3aR horizontal traverse	Lens	2 / 13	87.93	0.66	0.07	-0.01	0.04	88.68
BB3aR horizontal traverse	Lens	2 / 14	93.65	0.84	0.05	0.01	-0.01	94.55
BB3aR horizontal traverse	Lens	2 / 15	96.70	0.47	0.06	0.03	0.04	97.30
BB3aR horizontal traverse	Lens	2 / 16	55.95	0.06	0.01	0.18	0.01	56.20
BB3aR horizontal traverse	Lens	2 / 17	71.11	0.03	-0.01	0.22	0.03	71.37
BB3aR horizontal traverse	Lens	2 / 18	93.67	0.29	0.05	0.10	0.01	94.13
BB3aR horizontal traverse	Lens	2 / 19	99.36	0.70	0.02	0.00	0.00	100.07
BB3aR horizontal traverse	Lens	2 / 20	98.17	0.56	0.04	0.04	0.01	98.82
BB3aR horizontal traverse	Lens	2 / 21	90.77	0.77	0.05	0.01	0.00	91.61
BB3aR horizontal traverse	Lens	2 / 22	97.35	1.17	0.06	-0.01	-0.02	98.55
BB3aR horizontal traverse	Lens	2 / 23	97.99	0.76	0.04	0.20	0.02	99.02
BB3aR horizontal traverse	Lens	2 / 24	99.06	0.42	0.06	0.41	0.03	99.98
BB3aR horizontal traverse	Lens	2 / 25	97.59	0.37	0.05	0.38	0.06	98.46
BB3aR horizontal traverse	Lens	2 / 26	97.69	0.70	0.05	0.00	-0.01	98.43
BB3aR horizontal traverse	Lens	2 / 27	95.98	1.32	0.05	0.00	0.01	97.35
BB3aR horizontal traverse	Lens	2 / 28	95.76	1.19	0.03	-0.01	0.02	96.99
BB3aR horizontal traverse	Lens	2 / 29	61.11	17.43	0.01	0.23	0.00	78.76
BB3aR horizontal traverse	Lens	2 / 30	97.93	0.82	0.03	0.00	0.00	98.78
BB3aR horizontal traverse	Lens	2 / 31	87.88	23.66	0.07	0.00	0.04	111.64
BB3aR horizontal traverse	Lens/Sclera	2 / 32	96.42	0.56	0.07	0.78	0.19	98.02
BB3aR horizontal traverse	Sclera	2 / 33	95.10	0.38	0.05	0.23	0.17	95.94
BB3aR horizontal traverse	Sclera	2 / 34	95.28	0.66	0.04	0.08	0.06	96.12
BB3aR sclera of lens 1	Sclera	1 / 1	100.37	0.52	0.03	0.28	0.03	101.23
BB3aR sclera of lens 2	Sclera	1 / 2	97.04	0.63	0.01	0.08	0.07	97.83
BB3aR sclera of lens 3	Sclera	1 / 3	94.84	0.78	0.02	0.09	0.03	95.76

SAMPLE	FEATURE	DATA SET/ POINT	WEIGHT % CARBONATE					
			Ca	Mg	Sr	Fe	Mn	SUM
BB3aR sclera of lens 4	Sclera	1 / 4	95.47	0.37	0.10	0.39	0.04	96.37
BB3aR sclera of lens 5	Sclera	1 / 5	96.30	0.67	0.02	0.03	0.06	97.08
BB3aR exoskeleton	E'skeleton	2 / 1	97.07	0.43	0.07	0.22	0.18	97.98
BB3aR exoskeleton	E'skeleton	2 / 2	98.48	0.45	0.05	0.01	0.04	99.02
BB3aR exoskeleton	E'skeleton	2 / 3	97.44	0.28	0.02	0.15	0.06	97.96
BB3aR exoskeleton	E'skeleton	2 / 4	96.42	1.13	0.05	0.01	0.02	97.62
BB3aR exoskeleton	E'skeleton	2 / 5	97.30	0.71	0.05	0.02	0.06	98.14
BB3aR exoskeleton	E'skeleton	2 / 6	96.85	0.54	0.02	0.09	0.06	97.56
BB3aR exoskeleton	E'skeleton	2 / 7	97.02	0.74	0.05	0.07	0.05	97.92
BB3aR exoskeleton	E'skeleton	2 / 8	97.17	0.40	0.04	0.05	0.06	97.72
BB3aR exoskeleton	E'skeleton	2 / 9	100.34	0.67	0.03	0.01	0.00	101.05
BB3aR exoskeleton	E'skeleton	2 / 10	95.33	1.14	0.02	0.02	-0.01	96.50
BB3aR exoskeleton	E'skeleton	2 / 11	94.99	0.38	0.05	0.29	0.29	96.01
BB3aR exoskeleton	E'skeleton	2 / 12	99.46	0.37	0.03	0.19	0.13	100.18
BB3aR exoskeleton	E'skeleton	2 / 13	98.15	0.57	0.04	0.04	0.06	98.86
BB3aR exoskeleton	E'skeleton	2 / 14	95.51	0.47	0.04	0.06	0.03	96.10
BB3aR exoskeleton	E'skeleton	2 / 15	96.54	0.69	0.02	0.03	0.01	97.29
BB3aR exoskeleton	E'skeleton	2 / 16	98.54	0.61	0.04	0.07	0.11	99.36
BB3aR exoskeleton	E'skeleton	2 / 17	97.31	0.43	0.00	-0.01	0.07	97.80
BB3aR exoskeleton	E'skeleton	2 / 18	99.03	0.68	0.03	0.08	0.05	99.87
E22B Lens 1 vertical traverse	Matrix	1 / 1	81.90	1.21	0.03	0.80	0.06	84.00
E22B Lens 1 vertical traverse	Cornea	1 / 2	92.47	0.56	0.04	0.13	0.12	93.32
E22B Lens 1 vertical traverse	Lens	1 / 3	96.54	1.18	0.02	0.08	0.07	97.88
E22B Lens 1 vertical traverse	Lens	1 / 4	94.77	2.09	0.11	-0.01	0.01	96.96
E22B Lens 1 vertical traverse	Lens	1 / 5	97.38	1.32	0.09	0.01	0.05	98.84
E22B Lens 1 vertical traverse	Lens	1 / 6	95.57	1.57	0.06	0.01	0.04	97.25
E22B Lens 1 vertical traverse	Lens	1 / 7	95.54	0.43	0.01	-0.02	0.06	96.03
E22B Lens 1 vertical traverse	Core	1 / 8	79.20	0.48	-0.01	-0.01	0.03	79.70
E22B Lens 1 vertical traverse	Core	1 / 9	96.56	1.54	0.11	-0.01	0.01	98.21
E22B Lens 1 vertical traverse	Core	1 / 10	97.40	1.35	0.06	0.00	0.07	98.88
E22B Lens 1 vertical traverse	Core	1 / 11	97.39	0.95	0.05	0.04	0.12	98.54
E22B Lens 1 vertical traverse	Core	1 / 12	95.55	0.95	0.03	0.00	0.15	96.69
E22B Lens 1 vertical traverse	Core	1 / 13	96.95	0.83	0.03	0.01	0.14	97.97
E22B Lens 1 vertical traverse	Core	1 / 14	96.81	0.69	0.01	0.03	0.21	97.73
E22B Lens 1 vertical traverse	Lens	1 / 15	95.88	1.54	0.11	0.00	0.05	97.58
E22B Lens 1 vertical traverse	Lens	1 / 16	91.17	1.80	0.06	-0.01	0.06	93.07
E22B Lens 1 vertical traverse	Matrix	1 / 17	97.67	1.76	0.06	0.02	0.06	99.56
E22B Lens 1 vertical traverse	Matrix	1 / 18	16.75	1.12	-0.03	0.41	0.03	18.29
E22B Lens 1 vertical traverse	Matrix	1 / 19	95.46	1.01	0.00	0.68	0.09	97.26
E22B Lens 1 horizontal traverse	Sclera	2 / 1	95.31	1.17	0.05	0.10	0.07	96.71
E22B Lens 1 horizontal traverse	Sclera	2 / 2	96.43	1.03	0.08	0.09	0.09	97.71
E22B Lens 1 horizontal traverse	Sclera	2 / 3	95.99	1.03	0.05	0.11	0.06	97.24
E22B Lens 1 horizontal traverse	Sclera/Lens	2 / 4	97.58	0.89	0.04	0.11	0.12	98.73
E22B Lens 1 horizontal traverse	Bowl	2 / 5	96.15	2.05	0.04	0.09	0.09	98.42
E22B Lens 1 horizontal traverse	Bowl	2 / 6	97.71	1.30	0.03	0.06	0.08	99.18
E22B Lens 1 horizontal traverse	Lens	2 / 7	95.69	1.05	0.04	0.01	0.10	96.88
E22B Lens 1 horizontal traverse	Lens	2 / 8	96.10	0.86	0.04	0.02	0.09	97.11
E22B Lens 1 horizontal traverse	Core	2 / 9	94.64	1.66	0.04	0.00	0.07	96.40
E22B Lens 1 horizontal traverse	Core	2 / 10	96.85	0.84	0.05	0.02	0.05	97.80
E22B Lens 1 horizontal traverse	Core	2 / 11	97.70	0.96	0.02	-0.02	0.11	98.78
E22B Lens 1 horizontal traverse	Core	2 / 12	98.29	0.97	0.03	0.01	0.12	99.41
E22B Lens 1 horizontal traverse	Core	2 / 13	96.63	1.20	0.09	0.03	0.11	98.06
E22B Lens 1 horizontal traverse	Core	2 / 14	95.27	1.73	0.05	0.01	0.03	97.09
E22B Lens 1 horizontal traverse	Core	2 / 15	95.18	1.72	0.09	0.00	0.08	97.06
E22B Lens 1 horizontal traverse	Lens	2 / 16	97.07	1.77	0.04	0.01	0.14	99.03
E22B Lens 1 horizontal traverse	Lens	2 / 17	96.71	2.03	0.05	-0.02	0.06	98.84
E22B Lens 1 horizontal traverse	Bowl	2 / 18	94.09	1.92	0.09	-0.03	0.10	96.17
E22B Lens 1 horizontal traverse	Bowl	2 / 19	87.73	1.92	0.05	0.44	0.14	90.28
E22B Lens 1 horizontal traverse	Sclera	2 / 20	96.19	0.83	0.05	0.11	0.15	97.33
E22B Lens 1 horizontal traverse	Sclera	2 / 21	99.03	1.13	0.06	0.12	0.13	100.46
E22B Lens 1 horizontal traverse	Sclera	2 / 22	96.43	1.17	0.07	0.10	0.09	97.87
E22B Lens 1 horizontal traverse	Sclera	2 / 23	95.30	1.30	0.07	0.07	0.06	96.80
E22B Lens 1 horizontal traverse	Sclera	2 / 24	95.74	1.67	0.11	0.07	0.08	97.67
E22B Lens 1 horizontal traverse	Sclera	2 / 25	96.61	1.21	0.07	0.06	0.11	98.05
E22B exoskeleton	E'skeleton	3 / 1	95.29	1.30	0.08	0.10	0.10	96.87
E22B exoskeleton	E'skeleton	3 / 2	95.20	1.34	0.07	0.08	0.08	96.76
E22B exoskeleton	E'skeleton	3 / 3	97.55	1.43	0.05	0.02	0.03	99.09

SAMPLE	FEATURE	DATA SET/ POINT	WEIGHT % CARBONATE					
			Ca	Mg	Sr	Fe	Mn	SUM
E22B exoskeleton	E'skeleton	3 / 4	95.32	1.52	0.10	0.00	0.08	97.02
E22B exoskeleton	E'skeleton	3 / 5	96.39	1.18	0.05	0.04	0.08	97.75
E22B exoskeleton	E'skeleton	3 / 6	96.94	1.29	0.05	0.05	0.10	98.42
E22B exoskeleton	E'skeleton	3 / 7	95.94	1.27	0.08	0.06	0.07	97.43
E22B exoskeleton	E'skeleton	3 / 8	96.29	1.00	0.07	0.09	0.11	97.56
E22B exoskeleton	E'skeleton	3 / 9	95.22	0.98	0.04	0.03	0.12	96.40
E22B exoskeleton	E'skeleton	3 / 10	94.33	1.10	0.07	0.14	0.12	95.76
E22B exoskeleton	E'skeleton	3 / 11	94.66	1.17	0.07	0.02	0.16	96.08
E22B exoskeleton	E'skeleton	3 / 12	97.93	1.01	0.08	0.12	0.15	99.30
E22B Lens 3 vertical traverse	Resin	1 / 1	0.25	0.00	-0.01	0.00	-0.01	0.23
E22B Lens 3 vertical traverse	Resin	1 / 2	0.29	0.00	-0.01	-0.01	-0.01	0.27
E22B Lens 3 vertical traverse	Lens	1 / 3	96.20	1.13	0.04	0.10	0.24	97.72
E22B Lens 3 vertical traverse	Lens	1 / 4	89.49	2.68	0.07	0.01	0.02	92.27
E22B Lens 3 vertical traverse	Lens	1 / 5	96.38	1.49	0.09	0.00	0.05	98.01
E22B Lens 3 vertical traverse	Lens	1 / 6	97.41	1.34	0.09	0.02	0.06	98.92
E22B Lens 3 vertical traverse	Lens	1 / 7	96.16	1.51	0.07	0.01	0.01	97.77
E22B Lens 3 vertical traverse	Core	1 / 8	94.37	1.49	0.06	0.01	0.01	95.95
E22B Lens 3 vertical traverse	Core	1 / 9	96.57	1.42	0.06	-0.01	0.09	98.12
E22B Lens 3 vertical traverse	Core	1 / 10	94.79	1.87	0.11	0.02	0.03	96.82
E22B Lens 3 vertical traverse	Core	1 / 11	97.81	0.81	0.01	-0.01	0.18	98.80
E22B Lens 3 vertical traverse	Core	1 / 12	97.23	1.28	0.04	0.01	0.06	98.62
E22B Lens 3 vertical traverse	Core	1 / 13	96.29	0.99	0.02	0.01	0.18	97.49
E22B Lens 3 vertical traverse	Core	1 / 14	97.58	1.64	0.07	-0.01	0.06	99.35
E22B Lens 3 vertical traverse	Lens	1 / 15	95.05	1.62	0.08	0.02	0.05	96.82
E22B Lens 3 vertical traverse	Lens Base	1 / 16	32.85	1.90	0.01	0.79	-0.01	35.54
E22B Lens 3 vertical traverse	Matrix	1 / 17	94.97	1.72	-0.01	0.27	0.21	97.16
E22B Lens 3 vertical traverse	Matrix	1 / 18	99.72	1.81	0.04	0.05	0.07	101.69
E22B Lens 3 horizontal traverse	Sclera	2 / 1	97.29	1.15	0.07	0.10	0.11	98.71
E22B Lens 3 horizontal traverse	Sclera	2 / 2	97.11	1.17	0.04	0.03	0.09	98.45
E22B Lens 3 horizontal traverse	Sclera	2 / 3	98.76	1.12	0.08	0.10	0.13	100.19
E22B Lens 3 horizontal traverse	Sclera	2 / 4	97.12	0.87	0.05	0.18	0.11	98.33
E22B Lens 3 horizontal traverse	Bowl	2 / 5	95.17	1.39	0.07	0.02	0.08	96.73
E22B Lens 3 horizontal traverse	Bowl	2 / 6	97.97	1.20	0.03	0.00	0.25	99.44
E22B Lens 3 horizontal traverse	Lens	2 / 7	97.05	1.59	0.04	0.02	0.07	98.77
E22B Lens 3 horizontal traverse	Lens	2 / 8	95.79	1.18	-0.01	0.01	0.06	97.03
E22B Lens 3 horizontal traverse	Lens	2 / 9	94.66	1.23	0.01	-0.01	0.06	95.95
E22B Lens 3 horizontal traverse	Core	2 / 10	95.21	1.82	0.07	0.02	0.02	97.15
E22B Lens 3 horizontal traverse	Core	2 / 11	96.25	1.07	0.01	-0.03	0.17	97.47
E22B Lens 3 horizontal traverse	Core	2 / 12	95.64	1.25	0.05	-0.01	0.14	97.07
E22B Lens 3 horizontal traverse	Core	2 / 13	97.29	1.04	0.02	0.03	0.12	98.50
E22B Lens 3 horizontal traverse	Core	2 / 14	95.38	1.73	0.07	0.00	0.09	97.28
E22B Lens 3 horizontal traverse	Core	2 / 15	97.23	1.35	0.06	0.00	0.04	98.68
E22B Lens 3 horizontal traverse	Lens	2 / 16	90.34	1.65	0.10	0.00	0.03	92.12
E22B Lens 3 horizontal traverse	Lens	2 / 17	96.05	1.28	0.05	0.00	0.05	97.43
E22B Lens 3 horizontal traverse	Lens	2 / 18	93.97	1.33	0.06	-0.02	0.05	95.40
E22B Lens 3 horizontal traverse	Bowl	2 / 19	96.34	2.37	0.01	-0.02	0.07	98.77
E22B Lens 3 horizontal traverse	Bowl	2 / 20	93.25	1.37	0.10	0.03	0.08	94.83
E22B Lens 3 horizontal traverse	Sclera	2 / 21	95.79	0.85	0.07	0.16	0.11	96.97
E22B Lens 3 horizontal traverse	Sclera	2 / 22	96.02	1.49	0.07	0.05	0.10	97.72
E22B Lens 3 horizontal traverse	Sclera	2 / 23	95.62	1.36	0.09	0.07	0.04	97.19
E22B Lens 3 horizontal traverse	Sclera	2 / 24	97.71	1.31	0.05	0.08	0.06	99.20
E22B Lens 3 horizontal traverse	Sclera	2 / 25	99.08	1.47	0.07	0.09	0.10	100.80
G33R Lens 1 vertical traverse	Resin	1 / 1	0.16	0.02	0.00	0.01	0.00	0.20
G33R Lens 1 vertical traverse	Resin	1 / 2	85.08	0.37	0.32	0.31	0.08	86.16
G33R Lens 1 vertical traverse	Resin	1 / 3	95.24	0.58	0.23	0.18	0.07	96.30
G33R Lens 1 vertical traverse	Resin	1 / 4	95.34	0.64	0.29	0.23	0.09	96.59
G33R Lens 1 vertical traverse	Lens	1 / 5	91.60	1.53	0.30	0.36	0.14	93.93
G33R Lens 1 vertical traverse	Lens	1 / 6	90.39	3.62	0.38	0.53	0.12	95.04
G33R Lens 1 vertical traverse	Lens	1 / 7	94.03	1.39	0.20	0.55	0.12	96.29
G33R Lens 1 vertical traverse	Lens	1 / 8	75.52	0.91	0.20	0.31	0.10	77.05
G33R Lens 1 vertical traverse	Lens	1 / 9	96.18	1.57	0.12	0.62	0.13	98.63
G33R Lens 1 vertical traverse	Lens	1 / 10	94.71	1.17	0.43	0.34	0.13	96.79
G33R Lens 1 vertical traverse	Lens	1 / 11	93.74	0.93	0.37	0.24	0.12	95.41
G33R Lens 1 vertical traverse	Lens	1 / 12	85.58	1.09	0.34	0.52	0.22	87.75
G33R Lens 1 vertical traverse	Lens	1 / 13	94.53	2.03	0.32	0.34	0.03	97.25
G33R Lens 1 vertical traverse	Lens	1 / 14	96.92	1.86	0.42	0.36	0.03	99.58
G33R Lens 1 vertical traverse	Lens	1 / 15	93.59	2.14	0.24	0.42	0.07	96.46
G33R Lens 1 vertical traverse	Cement	1 / 16	66.34	2.48	0.21	0.78	0.07	69.89

SAMPLE	FEATURE	DATA SET/ POINT	WEIGHT % CARBONATE					
			Ca	Mg	Sr	Fe	Mn	SUM
G33R Lens 1 vertical traverse	Cement	1 / 17	82.52	2.64	0.19	1.22	0.07	86.64
G33R Lens 1 vertical traverse	Cement	1 / 18	80.81	2.08	0.09	0.49	0.06	83.52
G33R Lens 1 vertical traverse	Cement	1 / 19	17.72	0.37	0.08	0.18	0.02	18.38
G33R Lens 1 vertical traverse	Matrix	1 / 20	90.49	2.27	0.25	0.65	0.09	93.75
G33R Lens 1 horizontal traverse	Lens	2 / 1	93.45	1.45	0.23	0.32	0.12	95.57
G33R Lens 1 horizontal traverse	Lens	2 / 2	94.97	1.27	0.23	0.32	0.04	96.83
G33R Lens 1 horizontal traverse	Lens	2 / 3	97.31	0.95	0.27	0.30	0.11	98.94
G33R Lens 1 horizontal traverse	Lens	2 / 4	93.65	0.39	0.10	0.60	0.39	95.13
G33R Lens 1 horizontal traverse	Lens	2 / 5	97.39	0.61	0.19	0.61	0.11	98.92
G33R Lens 1 horizontal traverse	Lens	2 / 6	93.21	1.24	0.48	0.31	0.11	95.35
G33R Lens 1 horizontal traverse	Lens	2 / 7	94.26	4.59	0.32	1.06	0.13	100.37
G33R Lens 1 horizontal traverse	Lens	2 / 8	94.19	1.29	0.35	0.32	0.03	96.19
G33R Lens 1 horizontal traverse	Lens	2 / 9	93.16	1.37	0.31	0.40	0.12	95.37
G33R Lens 1 horizontal traverse	Lens	2 / 10	93.45	0.69	0.29	0.43	0.15	95.01
G33R Lens 1 horizontal traverse	Lens	2 / 11	92.41	1.45	0.21	0.42	0.12	94.61
G33R Lens 1 horizontal traverse	Lens	2 / 12	92.85	1.17	0.31	0.26	0.07	94.65
G33R Lens 1 horizontal traverse	Lens	2 / 13	87.22	0.34	0.80	0.04	0.04	88.44
G33R sclera	Sclera	3 / 1	96.24	1.35	0.23	0.36	0.13	98.32
G33R sclera	Sclera	3 / 2	100.52	1.68	0.38	0.29	0.08	102.95
G33R sclera	Sclera	3 / 3	96.73	1.56	0.48	0.30	0.05	99.11
G33R sclera	Sclera	3 / 4	99.13	1.10	0.35	0.41	0.08	101.07
G33R sclera	Sclera	3 / 5	96.91	2.01	0.41	0.25	0.09	99.66
G33R sclera	Sclera	3 / 6	99.29	1.33	0.43	0.23	0.11	101.39
G33R sclera	Sclera	3 / 7	98.26	1.46	0.35	0.41	0.06	100.53
G33R sclera	Sclera	3 / 8	96.81	2.29	0.36	0.31	0.06	99.83
G33R sclera	Sclera	3 / 9	96.85	1.68	0.29	0.37	0.09	99.27
G33R sclera	Sclera	3 / 10	96.38	1.59	0.40	0.26	0.07	98.70
G33R sclera	Sclera	3 / 11	97.88	2.51	0.40	0.36	0.08	101.23
G33R sclera	Sclera	3 / 12	95.67	1.19	0.30	0.28	0.11	97.55
PM28 Lens 3 vertical traverse	Resin	1 / 1	0.05	0.00	0.02	0.01	0.00	0.08
PM28 Lens 3 vertical traverse	Resin	1 / 2	0.06	0.00	-0.01	-0.01	0.00	0.05
PM28 Lens 3 vertical traverse	Resin	1 / 3	0.07	0.00	-0.02	0.00	-0.01	0.04
PM28 Lens 3 vertical traverse	Lens	1 / 4	77.07	4.76	0.35	0.02	0.05	82.25
PM28 Lens 3 vertical traverse	Lens	1 / 5	95.92	1.62	0.33	0.07	0.05	97.98
PM28 Lens 3 vertical traverse	Lens	1 / 6	59.85	7.63	0.27	0.17	0.05	67.98
PM28 Lens 3 vertical traverse	Lens	1 / 7	87.20	5.33	0.38	0.02	0.04	92.98
PM28 Lens 3 vertical traverse	Lens	1 / 8	90.24	6.10	0.53	0.05	0.03	96.96
PM28 Lens 3 vertical traverse	Lens	1 / 9	92.58	5.63	0.41	0.03	0.02	98.68
PM28 Lens 3 vertical traverse	Lens	1 / 10	92.81	6.78	0.37	0.09	0.00	100.04
PM28 Lens 3 vertical traverse	Lens	1 / 11	90.60	4.72	0.44	0.04	-0.02	95.79
PM28 Lens 3 vertical traverse	Lens	1 / 12	84.61	8.08	0.43	0.09	0.00	93.21
PM28 Lens 3 vertical traverse	Lens	1 / 13	93.31	0.70	0.07	3.07	0.16	97.31
PM28 Lens 3 vertical traverse	Bowl?	1 / 14	95.50	0.54	0.05	2.08	0.11	98.28
PM28 Lens 3 vertical traverse	Lens	1 / 15	68.77	0.67	0.04	8.58	0.09	78.16
PM28 Lens 3 vertical traverse	Matrix	1 / 16	83.37	1.16	0.03	3.18	0.39	88.13
PM28 Lens 3 vertical traverse	Matrix	1 / 17	13.20	0.71	-0.02	0.66	0.02	14.57
PM28 Lens 3 vertical traverse	Matrix	1 / 18	8.73	9.76	-0.01	9.62	0.03	28.13
PM28 Lens 3 horizontal traverse	Lens	2 / 1	82.42	1.37	0.05	4.24	0.15	88.23
PM28 Lens 3 horizontal traverse	Lens	2 / 2	89.74	5.15	0.42	0.14	0.00	95.47
PM28 Lens 3 horizontal traverse	Lens	2 / 3	82.76	6.94	0.36	0.44	0.05	90.55
PM28 Lens 3 horizontal traverse	Lens	2 / 4	89.84	7.52	0.36	0.05	0.03	97.81
PM28 Lens 3 horizontal traverse	Lens	2 / 5	91.62	3.66	0.38	0.03	0.02	95.71
PM28 Lens 3 horizontal traverse	Lens	2 / 6	84.63	2.68	0.33	0.03	0.00	87.66
PM28 Lens 3 horizontal traverse	Lens	2 / 7	76.36	2.91	0.40	0.05	-0.01	79.70
PM28 Lens 3 horizontal traverse	Lens	2 / 8	93.60	3.72	0.40	0.00	0.01	97.73
PM28 Lens 3 horizontal traverse	Lens	2 / 9	69.82	4.04	0.32	0.01	-0.02	74.17
PM28 Lens 3 horizontal traverse	Lens	2 / 10	91.77	4.82	0.39	0.01	0.01	96.99
PM28 Lens 3 horizontal traverse	Lens	2 / 11	92.14	3.83	0.37	0.01	0.03	96.38
PM28 Lens 3 horizontal traverse	Lens	2 / 12	74.76	15.13	0.41	0.04	0.04	90.38
PM28 Lens 3 horizontal traverse	Lens	2 / 13	92.44	3.15	0.42	0.03	0.03	96.07
PM28 Lens 3 horizontal traverse	Lens	2 / 14	90.75	7.74	0.37	0.08	0.07	99.01
PM28 Lens 3 horizontal traverse	Lens	2 / 15	93.23	6.66	0.29	0.48	0.11	100.77
PM28 Lens 5 vertical traverse	Resin	1 / 1	-0.01	0.01	-0.01	0.01	0.02	0.02
PM28 Lens 5 vertical traverse	Resin	1 / 2	-0.02	0.00	0.01	0.00	-0.01	-0.02
PM28 Lens 5 vertical traverse	Lens	1 / 3	94.57	2.80	0.41	0.12	0.35	98.24
PM28 Lens 5 vertical traverse	Lens	1 / 4	97.09	0.42	0.38	0.09	0.30	98.28

SAMPLE	FEATURE	DATA SET/ POINT	WEIGHT % CARBONATE					
			Ca	Mg	Sr	Fe	Mn	SUM
PM28 Lens 5 vertical traverse	Lens	1 / 5	95.31	3.62	0.37	0.19	0.47	99.96
PM28 Lens 5 vertical traverse	Lens	1 / 6	93.78	3.08	0.47	0.15	0.53	98.01
PM28 Lens 5 vertical traverse	Lens	1 / 7	94.91	2.40	0.30	0.06	0.09	97.76
PM28 Lens 5 vertical traverse	Lens	1 / 8	90.49	4.64	0.29	0.27	0.08	95.78
PM28 Lens 5 vertical traverse	Lens	1 / 9	94.87	1.06	0.30	0.56	0.20	97.00
PM28 Lens 5 vertical traverse	Lens	1 / 10	87.00	5.39	0.37	-0.02	-0.02	92.71
PM28 Lens 5 vertical traverse	Lens	1 / 11	93.32	7.25	0.36	0.01	0.00	100.93
PM28 Lens 5 vertical traverse	Lens	1 / 12	87.92	4.87	0.28	0.20	-0.01	93.28
PM28 Lens 5 vertical traverse	Lens	1 / 13	92.61	6.85	0.32	0.02	-0.01	99.79
PM28 Lens 5 vertical traverse	Lens	1 / 14	91.03	7.95	0.37	0.12	0.05	99.52
PM28 Lens 5 vertical traverse	Lens	1 / 15	90.08	14.16	0.43	0.09	0.01	104.77
PM28 Lens 5 vertical traverse	Lens	1 / 16	86.29	11.30	0.32	2.34	0.26	100.51
PM28 Lens 5 vertical traverse	Lens	1 / 17	86.85	0.80	0.04	3.05	0.26	91.00
PM28 Lens 5 vertical traverse	Matrix	1 / 18	90.18	1.03	0.04	1.85	0.22	93.32
PM28 Lens 5 vertical traverse	Matrix	1 / 19	88.91	0.47	0.05	1.88	0.13	91.45
PM28 Lens 5 vertical traverse	Matrix	1 / 20	91.54	0.89	0.08	2.70	0.20	95.40
PM28 Lens 5 vertical traverse	Matrix	1 / 21	72.01	0.68	0.02	2.08	0.13	74.92
PM28 Lens 5 vertical traverse	Matrix	1 / 22	17.35	2.93	0.06	5.49	1.95	27.79
PM28 Lens 5 horizontal traverse	Lens	2 / 1	90.09	1.76	0.09	2.97	1.22	96.13
PM28 Lens 5 horizontal traverse	Lens	2 / 2	90.88	4.18	0.36	0.59	0.14	96.14
PM28 Lens 5 horizontal traverse	Lens	2 / 3	80.40	8.42	0.39	0.39	0.02	89.62
PM28 Lens 5 horizontal traverse	Lens	2 / 4	94.89	1.49	0.27	0.66	0.13	97.43
PM28 Lens 5 horizontal traverse	Lens	2 / 5	95.81	1.15	0.27	0.57	0.09	97.89
PM28 Lens 5 horizontal traverse	Lens	2 / 6	81.53	2.42	0.24	0.38	0.10	84.66
PM28 Lens 5 horizontal traverse	Lens	2 / 7	96.33	2.02	0.31	0.14	0.05	98.85
PM28 Lens 5 horizontal traverse	Lens	2 / 8	90.05	17.64	0.36	0.01	0.00	108.06
PM28 Lens 5 horizontal traverse	Lens	2 / 9	92.85	2.35	0.38	-0.01	0.00	95.56
PM28 Lens 5 horizontal traverse	Lens	2 / 10	92.15	4.00	0.36	0.02	-0.02	96.52
PM28 Lens 5 horizontal traverse	Lens	2 / 11	77.49	4.91	0.35	0.06	0.02	82.83
PM28 Lens 5 horizontal traverse	Lens	2 / 12	91.13	3.75	0.31	0.01	-0.01	95.19
PM28 Lens 5 horizontal traverse	Lens	2 / 13	91.56	4.97	0.31	0.08	-0.01	96.92
PM28 Lens 5 horizontal traverse	Lens	2 / 14	86.19	6.59	0.33	0.47	0.09	93.67
PM28 Lens 5 horizontal traverse	Lens	2 / 15	92.89	7.78	0.37	0.27	0.02	101.33
PM28 Lens 5 horizontal traverse	Lens	2 / 16	76.96	19.37	0.42	0.16	0.02	96.93
PM28 Lens 5 horizontal traverse	Lens	2 / 17	95.00	4.79	0.34	0.29	0.07	100.48
TS1 Lens 4 vertical traverse	Resin	1 / 1	0.05	0.01	0.00	0.01	0.00	0.07
TS1 Lens 4 vertical traverse	Resin	1 / 2	0.05	0.00	-0.01	0.01	-0.01	0.04
TS1 Lens 4 vertical traverse	Lens	1 / 3	94.62	1.55	0.07	0.16	0.08	96.48
TS1 Lens 4 vertical traverse	Lens	1 / 4	96.09	1.71	0.09	0.03	0.05	97.96
TS1 Lens 4 vertical traverse	Lens	1 / 5	38.64	0.79	0.10	0.05	-0.01	39.56
TS1 Lens 4 vertical traverse	Lens	1 / 6	69.61	9.24	0.14	0.14	0.01	79.14
TS1 Lens 4 vertical traverse	Lens	1 / 7	97.86	0.51	0.12	0.25	0.06	98.80
TS1 Lens 4 vertical traverse	Lens	1 / 8	84.53	15.79	0.10	2.01	0.16	102.58
TS1 Lens 4 vertical traverse	Lens	1 / 9	96.51	0.36	0.12	0.28	0.13	97.40
TS1 Lens 4 vertical traverse	Lens	1 / 10	95.33	2.51	0.07	0.38	0.10	98.39
TS1 Lens 4 vertical traverse	Core	1 / 11	95.80	0.40	0.09	0.24	0.07	96.61
TS1 Lens 4 vertical traverse	Core	1 / 12	94.78	0.41	0.11	0.18	0.11	95.59
TS1 Lens 4 vertical traverse	Core	1 / 13	96.82	0.54	0.08	0.41	0.12	97.97
TS1 Lens 4 vertical traverse	Core	1 / 14	94.42	0.73	0.08	0.41	0.11	95.75
TS1 Lens 4 vertical traverse	Core	1 / 15	86.66	7.37	0.08	0.72	0.12	94.95
TS1 Lens 4 vertical traverse	Core	1 / 16	95.46	0.67	0.10	0.33	0.12	96.67
TS1 Lens 4 vertical traverse	Lens	1 / 17	87.67	8.96	0.10	0.81	0.08	97.62
TS1 Lens 4 vertical traverse	Lens	1 / 18	73.31	1.45	0.08	0.17	0.09	75.09
TS1 Lens 4 vertical traverse	Lens	1 / 19	95.04	11.82	0.12	1.14	0.17	108.29
TS1 Lens 4 vertical traverse	Lens	1 / 20	96.01	3.27	0.11	1.52	0.18	101.09
TS1 Lens 4 vertical traverse	Matrix?	1 / 21	94.06	1.74	0.10	0.24	0.10	96.25
TS1 Lens 4 vertical traverse	Matrix?	1 / 22	90.62	2.40	0.04	0.84	0.11	94.01
TS1 Lens 4 horizontal traverse	Sclera	2 / 1	95.53	1.46	0.14	0.61	0.14	97.88
TS1 Lens 4 horizontal traverse	Sclera	2 / 2	96.31	1.57	0.15	0.21	0.04	98.28
TS1 Lens 4 horizontal traverse	Sclera	2 / 3	98.96	1.43	0.14	0.55	0.08	101.17
TS1 Lens 4 horizontal traverse	Lens	2 / 4	95.03	1.07	0.14	0.55	0.09	96.88
TS1 Lens 4 horizontal traverse	Lens	2 / 5	94.90	1.52	0.08	0.25	0.05	96.80
TS1 Lens 4 horizontal traverse	Lens	2 / 6	92.51	2.76	0.09	0.02	0.05	95.43
TS1 Lens 4 horizontal traverse	Lens	2 / 7	96.03	1.54	0.07	0.01	0.04	97.69
TS1 Lens 4 horizontal traverse	Lens	2 / 8	97.29	1.80	0.09	0.08	0.05	99.31
TS1 Lens 4 horizontal traverse	Lens	2 / 9	94.61	1.61	0.18	0.11	0.09	96.60
TS1 Lens 4 horizontal traverse	Lens	2 / 10	93.78	1.35	0.11	0.02	0.05	95.31
TS1 Lens 4 horizontal traverse	Lens	2 / 11	94.49	1.35	0.09	0.05	0.05	96.02

SAMPLE	FEATURE	DATA SET/ POINT	WEIGHT % CARBONATE					
			Ca	Mg	Sr	Fe	Mn	SUM
TS1 Lens 4 horizontal traverse	Lens	2 / 12	93.56	2.33	0.11	0.03	0.03	96.05
TS1 Lens 4 horizontal traverse	Lens	2 / 13	95.24	0.88	0.10	0.02	0.04	96.29
TS1 Lens 4 horizontal traverse	Core	2 / 14	95.37	1.06	0.07	0.10	0.04	96.65
TS1 Lens 4 horizontal traverse	Core	2 / 15	96.30	0.71	0.07	0.51	0.21	97.80
TS1 Lens 4 horizontal traverse	Core	2 / 16	95.25	0.69	0.07	0.51	0.15	96.68
TS1 Lens 4 horizontal traverse	Lens	2 / 17	94.74	0.29	0.07	0.25	0.06	95.41
TS1 Lens 4 horizontal traverse	Lens	2 / 18	97.54	0.74	0.11	0.36	0.04	98.80
TS1 Lens 4 horizontal traverse	Lens	2 / 19	100.23	0.39	0.12	0.24	0.12	101.11
TS1 Lens 4 horizontal traverse	Lens	2 / 20	93.25	2.72	0.13	0.15	0.06	96.31
TS1 Lens 4 horizontal traverse	Lens	2 / 21	96.23	1.94	0.08	0.16	0.05	98.46
TS1 Lens 4 horizontal traverse	Lens	2 / 22	91.91	0.58	0.11	0.02	0.05	92.67
TS1 Lens 4 horizontal traverse	Lens	2 / 23	95.58	0.72	0.11	0.02	0.03	96.46
TS1 Lens 4 horizontal traverse	Lens	2 / 24	93.67	1.13	0.12	0.05	0.05	95.02
TS1 Lens 4 horizontal traverse	Lens	2 / 25	96.41	1.08	0.10	0.06	0.07	97.72
TS1 Lens 4 horizontal traverse	Lens	2 / 26	96.35	2.12	0.10	0.38	0.17	99.12
TS1 Lens 4 horizontal traverse	Lens/Sclera	2 / 27	88.25	2.52	0.10	0.10	0.08	91.04
TS1 Lens 4 horizontal traverse	Sclera	2 / 28	92.65	5.75	0.10	0.41	0.24	99.15
TS1 Lens 4 horizontal traverse	Sclera	2 / 29	97.30	1.27	0.10	0.17	0.04	98.90
TS1 Lens 4 horizontal traverse	Sclera	2 / 30	96.02	1.66	0.14	0.29	0.06	98.16
TS1 Lens 4 horizontal traverse	Sclera	2 / 31	98.47	1.46	0.12	0.43	0.08	100.56
TS1 Lens 5 vertical traverse	Resin	1 / 1	0.10	0.01	0.01	0.01	0.02	0.14
TS1 Lens 5 vertical traverse	Resin	1 / 2	0.07	0.02	0.00	0.00	-0.01	0.07
TS1 Lens 5 vertical traverse	Lens	1 / 3	95.65	1.93	0.13	0.56	0.14	98.41
TS1 Lens 5 vertical traverse	Lens	1 / 4	97.83	1.70	0.09	0.03	0.07	99.73
TS1 Lens 5 vertical traverse	Core	1 / 5	93.07	2.21	0.09	0.33	0.12	95.82
TS1 Lens 5 vertical traverse	Core	1 / 6	98.06	0.46	0.11	0.38	0.18	99.19
TS1 Lens 5 vertical traverse	Core	1 / 7	60.39	6.68	0.06	1.28	0.15	68.56
TS1 Lens 5 vertical traverse	Core	1 / 8	98.05	1.63	0.14	0.57	0.22	100.60
TS1 Lens 5 vertical traverse	Core	1 / 9	96.30	0.41	0.12	0.26	0.22	97.31
TS1 Lens 5 vertical traverse	Core	1 / 10	92.47	1.87	0.12	0.33	0.17	94.96
TS1 Lens 5 vertical traverse	Core	1 / 11	91.68	27.51	0.11	3.53	0.37	123.20
TS1 Lens 5 vertical traverse	Core	1 / 12	95.41	1.96	0.11	0.49	0.26	98.23
TS1 Lens 5 vertical traverse	Core	1 / 13	66.99	2.80	0.10	0.61	0.26	70.76
TS1 Lens 5 vertical traverse	Core	1 / 14	96.21	4.07	0.07	0.79	0.18	101.33
TS1 Lens 5 vertical traverse	Core	1 / 15	95.44	0.66	0.10	0.50	0.25	96.95
TS1 Lens 5 vertical traverse	Core	1 / 16	99.09	1.15	0.10	0.58	0.25	101.15
TS1 Lens 5 vertical traverse	Core	1 / 17	95.35	2.55	0.12	0.23	0.10	98.34
TS1 Lens 5 vertical traverse	Core/Lens	1 / 18	95.39	1.03	0.09	0.06	0.08	96.65
TS1 Lens 5 vertical traverse	Bowl	1 / 19	98.91	1.90	0.14	0.22	0.16	101.33
TS1 Lens 5 vertical traverse	Bowl	1 / 20	91.14	1.62	0.13	1.12	0.34	94.34
TS1 Lens 5 vertical traverse	Matrix	1 / 21	96.91	1.42	0.16	0.45	0.10	99.04
TS1 Lens 5 vertical traverse	Matrix	1 / 22	72.68	2.40	0.11	2.20	0.08	77.47
TS1 Lens 5 vertical traverse	Matrix	1 / 23	95.04	1.32	0.11	0.63	0.07	97.17
TS1 Lens 5 vertical traverse	Matrix	1 / 24	92.96	1.54	0.09	0.58	0.09	95.26
TS1 Lens 5 vertical traverse	Matrix	1 / 25	97.54	2.25	0.07	0.79	0.12	100.77
TS1 Lens 5 horizontal traverse	Sclera	2 / 1	96.61	2.19	0.18	0.65	0.16	99.79
TS1 Lens 5 horizontal traverse	Sclera	2 / 2	95.31	2.09	0.18	0.70	0.27	98.55
TS1 Lens 5 horizontal traverse	Lens	2 / 3	95.63	1.94	0.13	0.74	0.32	98.76
TS1 Lens 5 horizontal traverse	Lens	2 / 4	92.28	1.25	0.16	0.16	0.08	93.94
TS1 Lens 5 horizontal traverse	Lens	2 / 5	93.57	1.18	0.09	0.02	0.05	94.91
TS1 Lens 5 horizontal traverse	Lens	2 / 6	96.32	1.72	0.11	0.26	0.08	98.49
TS1 Lens 5 horizontal traverse	Lens	2 / 7	94.35	1.81	0.08	0.10	0.08	96.42
TS1 Lens 5 horizontal traverse	Lens	2 / 8	98.84	1.16	0.06	0.02	0.05	100.14
TS1 Lens 5 horizontal traverse	Lens	2 / 9	96.78	1.55	0.13	0.02	0.03	98.50
TS1 Lens 5 horizontal traverse	Core	2 / 10	98.48	1.80	0.09	0.04	0.04	100.45
TS1 Lens 5 horizontal traverse	Core	2 / 11	96.50	0.74	0.13	0.02	0.05	97.44
TS1 Lens 5 horizontal traverse	Core	2 / 12	97.14	1.73	0.10	0.08	0.05	99.10
TS1 Lens 5 horizontal traverse	Core	2 / 13	94.97	1.29	0.10	0.05	0.07	96.49
TS1 Lens 5 horizontal traverse	Core	2 / 14	86.54	1.40	0.11	0.57	0.20	88.81
TS1 Lens 5 horizontal traverse	Core	2 / 15	84.83	26.67	0.04	3.92	0.41	115.88
TS1 Lens 5 horizontal traverse	Core	2 / 16	96.36	0.54	0.12	0.32	0.34	97.67
TS1 Lens 5 horizontal traverse	Core	2 / 17	95.21	1.18	0.10	0.60	0.26	97.35
TS1 Lens 5 horizontal traverse	Core	2 / 18	95.63	0.32	0.06	0.19	0.16	96.37
TS1 Lens 5 horizontal traverse	Core	2 / 19	67.64	4.46	0.09	0.59	0.19	72.98
TS1 Lens 5 horizontal traverse	Lens	2 / 20	97.74	1.42	0.07	0.19	0.18	99.61
TS1 Lens 5 horizontal traverse	Lens	2 / 21	97.78	5.67	0.09	0.27	0.15	103.96
TS1 Lens 5 horizontal traverse	Lens	2 / 22	85.48	1.51	0.05	0.09	0.09	87.23
TS1 Lens 5 horizontal traverse	Lens	2 / 23	95.51	1.74	0.15	0.04	0.03	97.47
TS1 Lens 5 horizontal traverse	Lens	2 / 24	95.65	1.61	0.07	0.04	0.11	97.49

SAMPLE	FEATURE	DATA SET/ POINT	WEIGHT % CARBONATE					
			Ca	Mg	Sr	Fe	Mn	SUM
TS1 Lens 5 horizontal traverse	Lens	2 / 25	92.28	1.58	0.12	0.04	0.06	94.08
TS1 Lens 5 horizontal traverse	Lens	2 / 26	92.09	2.30	0.10	0.17	0.08	94.74
TS1 Lens 5 horizontal traverse	Lens/Sclera	2 / 27	95.58	1.69	0.10	0.04	0.01	97.41
TS1 Lens 5 horizontal traverse	Sclera	2 / 28	93.17	2.47	0.11	0.02	0.03	95.80
TS1 Lens 5 horizontal traverse	Sclera	2 / 29	95.26	2.07	0.24	0.49	0.07	98.13
TS1 Lens 5 horizontal traverse	Sclera	2 / 30	94.12	2.32	0.16	0.50	0.09	97.20
TS1 sclera	Sclera	3 / 1	96.22	2.49	0.19	0.41	0.11	99.43
TS1 sclera	Sclera	3 / 2	94.66	1.93	0.16	0.43	0.13	97.30
TS1 sclera	Sclera	3 / 3	96.94	1.58	0.13	0.45	0.12	99.22
TS1 sclera	Sclera	3 / 4	97.80	1.27	0.16	0.53	0.10	99.86
TS1 sclera	Sclera	3 / 5	95.58	1.58	0.13	0.58	0.15	98.02
TS1 sclera	Sclera	3 / 6	99.24	1.96	0.10	0.22	0.11	101.63
TS1 sclera	Sclera	3 / 7	94.94	1.73	0.12	0.46	0.18	97.44
TS1 sclera	Sclera	3 / 8	95.24	2.02	0.17	0.31	0.05	97.79
TS1 sclera	Sclera	3 / 9	94.92	1.64	0.11	0.45	0.15	97.26

Table E.7 - Normalised weight % carbonate EPMA data (Edinburgh) for trilobites with schizochroal eyes.

SAMPLE	FEATURE	DATA SET/ POINT	NORMALISED WEIGHT % CARBONATE				
			Ca	Mg	Sr	Fe	Mn
BB3aR cement	Cement	1 / 1	98.69	1.23	0.03	0.02	0.02
BB3aR cement	Cement	1 / 2	99.82	0.10	0.03	0.02	0.04
BB3aR cement	Cement	1 / 3	99.93	0.07	0.00	-0.02	0.02
BB3aR cement	Cement	1 / 4	98.90	1.02	0.05	0.00	0.02
BB3aR cement	Cement	1 / 5	98.41	1.57	0.07	0.02	-0.07
BB3aR cement	Cement	1 / 6	98.58	1.20	0.15	0.06	0.01
BB3aR cement	Cement	1 / 7	99.31	0.65	0.03	0.01	0.01
BB3aR cement	Cement	1 / 8	99.03	0.89	0.03	0.04	0.00
BB3aR cement	Cement	1 / 9	99.20	0.69	0.02	0.05	0.04
BB3aR cement	Cement	1 / 10	99.67	0.35	0.02	-0.01	-0.02
BB3aR cement	Cement	1 / 11	99.65	0.29	0.02	0.00	0.04
BB3aR cement	Cement	1 / 12	99.35	0.58	0.05	0.00	0.02
BB3aR cement	Cement	1 / 13	99.33	0.60	0.05	0.01	0.01
BB3aR cement	Cement	1 / 14	98.90	1.02	0.05	0.01	0.02
BB3aR cement	Cement	1 / 15	99.26	0.61	0.07	0.01	0.05
BB3aR Lens 2b diagonal traverse	Lens	1 / 1	98.88	1.01	0.06	0.02	0.03
BB3aR Lens 2b diagonal traverse	Lens	1 / 2	99.58	0.34	0.06	-0.01	0.03
BB3aR Lens 2b diagonal traverse	Lens	1 / 3	97.07	2.87	0.07	0.00	-0.01
BB3aR Lens 2b diagonal traverse	Lens	1 / 4	89.68	10.26	0.09	-0.02	-0.01
BB3aR Lens 2b diagonal traverse	Lens	1 / 5	99.57	0.37	0.06	0.00	0.00
BB3aR Lens 2b diagonal traverse	Lens	1 / 6	99.60	0.32	0.05	0.00	0.03
BB3aR Lens 2b diagonal traverse	Lens	1 / 7	99.48	0.45	0.09	-0.02	0.00
BB3aR Lens 2b diagonal traverse	Lens	1 / 8	89.12	10.80	0.09	-0.02	0.01
BB3aR Lens 2b diagonal traverse	Lens	1 / 9	99.37	0.57	0.06	0.02	-0.02
BB3aR Lens 2b diagonal traverse	Lens	1 / 10	99.23	0.69	0.08	-0.01	0.00
BB3aR Lens 2b diagonal traverse	Lens	1 / 11	99.68	0.36	0.00	-0.02	-0.03
BB3aR Lens 2b diagonal traverse	Lens	1 / 12	94.02	5.85	0.08	0.04	0.02
BB3aR Lens 2b diagonal traverse	Lens	1 / 13	99.16	0.82	0.04	-0.01	0.00
BB3aR vertical traverse	Resin	1 / 1	99.40	0.36	0.02	0.15	0.08
BB3aR vertical traverse	Resin	1 / 2	99.43	0.48	0.03	0.05	0.01
BB3aR vertical traverse	Lens	1 / 3	99.42	0.52	0.06	0.02	-0.01
BB3aR vertical traverse	Lens	1 / 4	99.41	0.53	0.06	0.01	-0.01
BB3aR vertical traverse	Lens	1 / 5	99.61	0.35	0.10	-0.03	-0.04
BB3aR vertical traverse	Lens	1 / 6	99.11	0.81	0.10	-0.02	0.01
BB3aR vertical traverse	Lens	1 / 7	98.80	1.08	0.10	0.02	-0.01
BB3aR vertical traverse	Lens	1 / 8	99.37	0.54	0.06	0.01	0.01
BB3aR vertical traverse	Lens	1 / 9	99.40	0.55	0.06	0.01	-0.02
BB3aR vertical traverse	Lens	1 / 10	99.63	0.31	0.05	0.02	-0.01
BB3aR vertical traverse	Lens	1 / 11	98.68	1.25	0.05	-0.01	0.02
BB3aR vertical traverse	Lens	1 / 12	99.67	0.28	0.03	0.02	0.00
BB3aR vertical traverse	Lens	1 / 13	99.71	0.22	0.06	0.00	0.01

SAMPLE	FEATURE	DATA SET/ POINT	NORMALISED WEIGHT % CARBONATE				
			Ca	Mg	Sr	Fe	Mn
BB3aR vertical traverse	Lens	1 / 14	99.45	0.55	-0.02	0.00	0.01
BB3aR vertical traverse	Lens	1 / 15	97.53	2.48	0.04	-0.02	-0.02
BB3aR vertical traverse	Lens	1 / 16	94.72	5.17	0.11	0.00	0.00
BB3aR vertical traverse	Lens	1 / 17	98.95	1.02	0.02	-0.01	0.02
BB3aR vertical traverse	Lens	1 / 18	99.35	0.64	0.00	0.01	0.00
BB3aR vertical traverse	Lens	1 / 19	73.06	26.88	0.04	0.02	-0.01
BB3aR vertical traverse	Lens	1 / 20	99.38	0.57	0.04	0.02	-0.01
BB3aR vertical traverse	Lens/Matrix	1 / 21	98.96	0.98	0.05	0.00	0.01
BB3aR vertical traverse	Matrix	1 / 22	99.20	0.78	0.05	-0.02	-0.01
BB3aR vertical traverse	Matrix	1 / 23	99.45	0.55	0.02	0.00	-0.01
BB3aR vertical traverse	Matrix	1 / 24	99.03	0.95	0.00	0.00	0.02
BB3aR vertical traverse	Matrix	1 / 25	99.21	0.72	0.07	-0.01	0.01
BB3aR vertical traverse	Matrix	1 / 26	99.63	0.31	0.05	0.00	0.01
BB3aR vertical traverse	Matrix	1 / 27	98.96	0.98	0.04	-0.01	0.04
BB3aR horizontal traverse	Sclera	2 / 1	99.28	0.57	0.02	0.04	0.09
BB3aR horizontal traverse	Sclera	2 / 2	99.28	0.38	0.01	0.18	0.15
BB3aR horizontal traverse	Sclera	2 / 3	99.30	0.61	0.02	0.04	0.02
BB3aR horizontal traverse	Sclera	2 / 4	99.24	0.44	0.02	0.15	0.15
BB3aR horizontal traverse	Lens	2 / 5	99.25	0.43	0.05	0.19	0.08
BB3aR horizontal traverse	Lens	2 / 6	99.43	0.44	0.01	0.03	0.09
BB3aR horizontal traverse	Lens	2 / 7	99.03	0.50	0.05	0.02	0.41
BB3aR horizontal traverse	Lens	2 / 8	99.36	0.38	0.06	0.11	0.09
BB3aR horizontal traverse	Lens	2 / 9	98.49	1.41	0.05	0.03	0.02
BB3aR horizontal traverse	Lens	2 / 10	99.78	0.15	0.03	0.03	0.02
BB3aR horizontal traverse	Lens	2 / 11	99.54	0.48	0.02	-0.01	-0.03
BB3aR horizontal traverse	Lens	2 / 12	99.10	0.85	0.03	0.00	0.01
BB3aR horizontal traverse	Lens	2 / 13	99.15	0.75	0.07	-0.02	0.04
BB3aR horizontal traverse	Lens	2 / 14	99.05	0.89	0.06	0.01	-0.01
BB3aR horizontal traverse	Lens	2 / 15	99.38	0.49	0.06	0.03	0.04
BB3aR horizontal traverse	Lens	2 / 16	99.55	0.10	0.01	0.31	0.02
BB3aR horizontal traverse	Lens	2 / 17	99.63	0.04	-0.02	0.31	0.04
BB3aR horizontal traverse	Lens	2 / 18	99.51	0.31	0.06	0.11	0.01
BB3aR horizontal traverse	Lens	2 / 19	99.29	0.70	0.02	0.00	0.00
BB3aR horizontal traverse	Lens	2 / 20	99.35	0.56	0.04	0.04	0.01
BB3aR horizontal traverse	Lens	2 / 21	99.08	0.84	0.06	0.01	0.01
BB3aR horizontal traverse	Lens	2 / 22	98.78	1.19	0.06	-0.01	-0.02
BB3aR horizontal traverse	Lens	2 / 23	98.97	0.77	0.04	0.21	0.02
BB3aR horizontal traverse	Lens	2 / 24	99.07	0.42	0.06	0.41	0.03
BB3aR horizontal traverse	Lens	2 / 25	99.12	0.37	0.05	0.39	0.06
BB3aR horizontal traverse	Lens	2 / 26	99.25	0.71	0.05	0.00	-0.01
BB3aR horizontal traverse	Lens	2 / 27	98.60	1.35	0.05	0.00	0.01
BB3aR horizontal traverse	Lens	2 / 28	98.73	1.22	0.03	-0.01	0.02
BB3aR horizontal traverse	Lens	2 / 29	77.59	22.13	0.01	0.29	0.00
BB3aR horizontal traverse	Lens	2 / 30	99.14	0.83	0.03	0.00	0.00
BB3aR horizontal traverse	Lens	2 / 31	78.72	21.19	0.06	0.00	0.04
BB3aR horizontal traverse	Lens/Sclera	2 / 32	98.37	0.57	0.07	0.79	0.19
BB3aR horizontal traverse	Sclera	2 / 33	99.12	0.40	0.06	0.24	0.18
BB3aR horizontal traverse	Sclera	2 / 34	99.12	0.69	0.04	0.09	0.06
BB3aR sclera of lens 1	Sclera	1 / 1	99.15	0.51	0.03	0.27	0.03
BB3aR sclera of lens 2	Sclera	1 / 2	99.19	0.64	0.01	0.08	0.07
BB3aR sclera of lens 3	Sclera	1 / 3	99.05	0.81	0.02	0.09	0.03
BB3aR sclera of lens 4	Sclera	1 / 4	99.07	0.39	0.10	0.41	0.04
BB3aR sclera of lens 5	Sclera	1 / 5	99.19	0.69	0.02	0.04	0.07
BB3aR exoskeleton	E'skeleton	2 / 1	99.08	0.44	0.07	0.22	0.19
BB3aR exoskeleton	E'skeleton	2 / 2	99.45	0.45	0.05	0.01	0.04
BB3aR exoskeleton	E'skeleton	2 / 3	99.48	0.29	0.02	0.16	0.06
BB3aR exoskeleton	E'skeleton	2 / 4	98.77	1.16	0.05	0.01	0.02
BB3aR exoskeleton	E'skeleton	2 / 5	99.14	0.73	0.05	0.02	0.06
BB3aR exoskeleton	E'skeleton	2 / 6	99.28	0.55	0.02	0.09	0.06
BB3aR exoskeleton	E'skeleton	2 / 7	99.08	0.76	0.05	0.07	0.05
BB3aR exoskeleton	E'skeleton	2 / 8	99.43	0.41	0.04	0.05	0.07
BB3aR exoskeleton	E'skeleton	2 / 9	99.30	0.66	0.03	0.01	0.00
BB3aR exoskeleton	E'skeleton	2 / 10	98.78	1.18	0.02	0.02	-0.01
BB3aR exoskeleton	E'skeleton	2 / 11	98.94	0.40	0.06	0.31	0.30
BB3aR exoskeleton	E'skeleton	2 / 12	99.27	0.37	0.03	0.19	0.13
BB3aR exoskeleton	E'skeleton	2 / 13	99.28	0.58	0.04	0.04	0.06
BB3aR exoskeleton	E'skeleton	2 / 14	99.38	0.49	0.04	0.06	0.03
BB3aR exoskeleton	E'skeleton	2 / 15	99.23	0.71	0.02	0.03	0.01

SAMPLE	FEATURE	DATA SET/ POINT	NORMALISED WEIGHT % CARBONATE				
			Ca	Mg	Sr	Fe	Mn
BB3aR exoskeleton	E'skeleton	2 / 16	99.17	0.61	0.04	0.07	0.11
BB3aR exoskeleton	E'skeleton	2 / 17	99.50	0.44	0.00	-0.01	0.07
BB3aR exoskeleton	E'skeleton	2 / 18	99.15	0.68	0.03	0.08	0.05
E22B Lens 1 vertical traverse	Matrix	1 / 1	97.49	1.44	0.04	0.95	0.08
E22B Lens 1 vertical traverse	Cornea	1 / 2	99.09	0.60	0.04	0.14	0.13
E22B Lens 1 vertical traverse	Lens	1 / 3	98.63	1.20	0.02	0.08	0.07
E22B Lens 1 vertical traverse	Lens	1 / 4	97.73	2.15	0.11	-0.01	0.01
E22B Lens 1 vertical traverse	Lens	1 / 5	98.52	1.34	0.09	0.01	0.05
E22B Lens 1 vertical traverse	Lens	1 / 6	98.26	1.62	0.06	0.01	0.04
E22B Lens 1 vertical traverse	Lens	1 / 7	99.50	0.45	0.01	-0.02	0.06
E22B Lens 1 vertical traverse	Core	1 / 8	99.37	0.61	-0.01	-0.01	0.04
E22B Lens 1 vertical traverse	Core	1 / 9	98.32	1.57	0.11	-0.01	0.01
E22B Lens 1 vertical traverse	Core	1 / 10	98.51	1.37	0.06	0.00	0.07
E22B Lens 1 vertical traverse	Core	1 / 11	98.83	0.96	0.05	0.04	0.12
E22B Lens 1 vertical traverse	Core	1 / 12	98.82	0.98	0.03	0.00	0.16
E22B Lens 1 vertical traverse	Core	1 / 13	98.96	0.85	0.04	0.01	0.15
E22B Lens 1 vertical traverse	Core	1 / 14	99.05	0.70	0.01	0.03	0.21
E22B Lens 1 vertical traverse	Lens	1 / 15	98.26	1.58	0.11	0.00	0.05
E22B Lens 1 vertical traverse	Lens	1 / 16	97.96	1.93	0.06	-0.01	0.06
E22B Lens 1 vertical traverse	Matrix	1 / 17	98.10	1.77	0.06	0.02	0.06
E22B Lens 1 vertical traverse	Matrix	1 / 18	91.60	6.11	-0.16	2.27	0.18
E22B Lens 1 vertical traverse	Matrix	1 / 19	98.16	1.04	0.00	0.70	0.10
E22B Lens 1 horizontal traverse	Sclera	2 / 1	98.56	1.21	0.05	0.10	0.08
E22B Lens 1 horizontal traverse	Sclera	2 / 2	98.68	1.05	0.08	0.09	0.09
E22B Lens 1 horizontal traverse	Sclera	2 / 3	98.72	1.06	0.05	0.12	0.06
E22B Lens 1 horizontal traverse	Sclera/Lens	2 / 4	98.84	0.90	0.04	0.11	0.12
E22B Lens 1 horizontal traverse	Bowl	2 / 5	97.69	2.08	0.04	0.09	0.09
E22B Lens 1 horizontal traverse	Bowl	2 / 6	98.52	1.31	0.03	0.06	0.08
E22B Lens 1 horizontal traverse	Lens	2 / 7	98.76	1.08	0.04	0.01	0.10
E22B Lens 1 horizontal traverse	Lens	2 / 8	98.96	0.89	0.05	0.02	0.09
E22B Lens 1 horizontal traverse	Core	2 / 9	98.17	1.72	0.04	0.00	0.07
E22B Lens 1 horizontal traverse	Core	2 / 10	99.02	0.86	0.05	0.02	0.05
E22B Lens 1 horizontal traverse	Core	2 / 11	98.91	0.97	0.02	-0.02	0.12
E22B Lens 1 horizontal traverse	Core	2 / 12	98.87	0.98	0.03	0.01	0.12
E22B Lens 1 horizontal traverse	Core	2 / 13	98.54	1.23	0.10	0.03	0.11
E22B Lens 1 horizontal traverse	Core	2 / 14	98.13	1.78	0.05	0.01	0.03
E22B Lens 1 horizontal traverse	Core	2 / 15	98.06	1.78	0.09	0.00	0.08
E22B Lens 1 horizontal traverse	Lens	2 / 16	98.02	1.79	0.05	0.01	0.15
E22B Lens 1 horizontal traverse	Lens	2 / 17	97.84	2.06	0.05	-0.02	0.07
E22B Lens 1 horizontal traverse	Bowl	2 / 18	97.84	2.00	0.09	-0.03	0.10
E22B Lens 1 horizontal traverse	Bowl	2 / 19	97.17	2.13	0.06	0.49	0.15
E22B Lens 1 horizontal traverse	Sclera	2 / 20	98.83	0.85	0.05	0.11	0.16
E22B Lens 1 horizontal traverse	Sclera	2 / 21	98.57	1.12	0.06	0.11	0.13
E22B Lens 1 horizontal traverse	Sclera	2 / 22	98.52	1.20	0.08	0.11	0.09
E22B Lens 1 horizontal traverse	Sclera	2 / 23	98.45	1.35	0.07	0.07	0.06
E22B Lens 1 horizontal traverse	Sclera	2 / 24	98.02	1.71	0.11	0.07	0.09
E22B Lens 1 horizontal traverse	Sclera	2 / 25	98.54	1.23	0.07	0.06	0.11
E22B exoskeleton	E'skeleton	3 / 1	98.37	1.34	0.08	0.10	0.11
E22B exoskeleton	E'skeleton	3 / 2	98.39	1.38	0.07	0.08	0.08
E22B exoskeleton	E'skeleton	3 / 3	98.44	1.45	0.05	0.02	0.03
E22B exoskeleton	E'skeleton	3 / 4	98.24	1.57	0.11	0.00	0.08
E22B exoskeleton	E'skeleton	3 / 5	98.61	1.21	0.05	0.05	0.08
E22B exoskeleton	E'skeleton	3 / 6	98.49	1.31	0.05	0.05	0.10
E22B exoskeleton	E'skeleton	3 / 7	98.47	1.31	0.08	0.07	0.08
E22B exoskeleton	E'skeleton	3 / 8	98.70	1.03	0.07	0.09	0.11
E22B exoskeleton	E'skeleton	3 / 9	98.78	1.01	0.04	0.04	0.12
E22B exoskeleton	E'skeleton	3 / 10	98.51	1.15	0.07	0.15	0.12
E22B exoskeleton	E'skeleton	3 / 11	98.52	1.22	0.08	0.02	0.17
E22B exoskeleton	E'skeleton	3 / 12	98.62	1.02	0.08	0.12	0.16
E22B Lens 3 vertical traverse	Resin	1 / 1	108.71	-1.05	-4.14	-0.45	-3.07
E22B Lens 3 vertical traverse	Resin	1 / 2	108.49	1.69	-2.21	-3.11	-4.86
E22B Lens 3 vertical traverse	Lens	1 / 3	98.45	1.16	0.04	0.11	0.25
E22B Lens 3 vertical traverse	Lens	1 / 4	96.98	2.90	0.08	0.01	0.03
E22B Lens 3 vertical traverse	Lens	1 / 5	98.34	1.52	0.09	0.00	0.05
E22B Lens 3 vertical traverse	Lens	1 / 6	98.47	1.36	0.09	0.02	0.07
E22B Lens 3 vertical traverse	Lens	1 / 7	98.36	1.54	0.08	0.01	0.01
E22B Lens 3 vertical traverse	Core	1 / 8	98.36	1.55	0.07	0.01	0.01

SAMPLE	FEATURE	DATA SET/ POINT	NORMALISED WEIGHT % CARBONATE				
			Ca	Mg	Sr	Fe	Mn
E22B Lens 3 vertical traverse	Core	1 / 9	98.42	1.45	0.06	-0.01	0.09
E22B Lens 3 vertical traverse	Core	1 / 10	97.90	1.93	0.12	0.02	0.03
E22B Lens 3 vertical traverse	Core	1 / 11	98.99	0.82	0.01	-0.01	0.19
E22B Lens 3 vertical traverse	Core	1 / 12	98.59	1.29	0.04	0.01	0.06
E22B Lens 3 vertical traverse	Core	1 / 13	98.77	1.02	0.02	0.01	0.18
E22B Lens 3 vertical traverse	Core	1 / 14	98.22	1.65	0.07	-0.01	0.06
E22B Lens 3 vertical traverse	Lens	1 / 15	98.18	1.67	0.08	0.02	0.05
E22B Lens 3 vertical traverse	Lens Base	1 / 16	92.41	5.34	0.03	2.24	-0.02
E22B Lens 3 vertical traverse	Matrix	1 / 17	97.74	1.77	-0.01	0.28	0.21
E22B Lens 3 vertical traverse	Matrix	1 / 18	98.06	1.78	0.04	0.05	0.07
E22B Lens 3 horizontal traverse	Sclera	2 / 1	98.55	1.16	0.07	0.10	0.11
E22B Lens 3 horizontal traverse	Sclera	2 / 2	98.64	1.19	0.04	0.03	0.10
E22B Lens 3 horizontal traverse	Sclera	2 / 3	98.58	1.12	0.08	0.10	0.13
E22B Lens 3 horizontal traverse	Sclera	2 / 4	98.77	0.89	0.05	0.18	0.11
E22B Lens 3 horizontal traverse	Bowl	2 / 5	98.38	1.44	0.07	0.03	0.08
E22B Lens 3 horizontal traverse	Bowl	2 / 6	98.52	1.21	0.03	0.00	0.25
E22B Lens 3 horizontal traverse	Lens	2 / 7	98.26	1.61	0.04	0.02	0.07
E22B Lens 3 horizontal traverse	Lens	2 / 8	98.72	1.22	-0.01	0.01	0.06
E22B Lens 3 horizontal traverse	Lens	2 / 9	98.65	1.28	0.01	-0.01	0.06
E22B Lens 3 horizontal traverse	Core	2 / 10	98.01	1.87	0.08	0.02	0.02
E22B Lens 3 horizontal traverse	Core	2 / 11	98.75	1.09	0.01	-0.03	0.17
E22B Lens 3 horizontal traverse	Core	2 / 12	98.53	1.28	0.06	-0.01	0.15
E22B Lens 3 horizontal traverse	Core	2 / 13	98.77	1.06	0.02	0.03	0.12
E22B Lens 3 horizontal traverse	Core	2 / 14	98.05	1.78	0.07	0.00	0.09
E22B Lens 3 horizontal traverse	Core	2 / 15	98.53	1.37	0.06	0.00	0.04
E22B Lens 3 horizontal traverse	Lens	2 / 16	98.07	1.79	0.11	0.00	0.03
E22B Lens 3 horizontal traverse	Lens	2 / 17	98.58	1.31	0.05	0.00	0.05
E22B Lens 3 horizontal traverse	Lens	2 / 18	98.50	1.39	0.06	-0.02	0.06
E22B Lens 3 horizontal traverse	Bowl	2 / 19	97.54	2.40	0.01	-0.02	0.07
E22B Lens 3 horizontal traverse	Bowl	2 / 20	98.34	1.44	0.10	0.03	0.08
E22B Lens 3 horizontal traverse	Sclera	2 / 21	98.78	0.87	0.07	0.16	0.11
E22B Lens 3 horizontal traverse	Sclera	2 / 22	98.26	1.52	0.07	0.05	0.10
E22B Lens 3 horizontal traverse	Sclera	2 / 23	98.39	1.40	0.09	0.08	0.05
E22B Lens 3 horizontal traverse	Sclera	2 / 24	98.49	1.32	0.05	0.08	0.06
E22B Lens 3 horizontal traverse	Sclera	2 / 25	98.29	1.45	0.07	0.09	0.10
G33R Lens 1 vertical traverse	Resin	1 / 1	79.53	10.56	2.02	6.11	1.78
G33R Lens 1 vertical traverse	Resin	1 / 2	98.74	0.43	0.37	0.36	0.09
G33R Lens 1 vertical traverse	Resin	1 / 3	98.91	0.60	0.24	0.18	0.07
G33R Lens 1 vertical traverse	Resin	1 / 4	98.70	0.66	0.30	0.24	0.10
G33R Lens 1 vertical traverse	Lens	1 / 5	97.52	1.62	0.32	0.38	0.15
G33R Lens 1 vertical traverse	Lens	1 / 6	95.11	3.81	0.40	0.55	0.12
G33R Lens 1 vertical traverse	Lens	1 / 7	97.66	1.44	0.21	0.57	0.13
G33R Lens 1 vertical traverse	Lens	1 / 8	98.02	1.19	0.26	0.41	0.12
G33R Lens 1 vertical traverse	Lens	1 / 9	97.52	1.60	0.12	0.63	0.14
G33R Lens 1 vertical traverse	Lens	1 / 10	97.86	1.21	0.44	0.36	0.13
G33R Lens 1 vertical traverse	Lens	1 / 11	98.26	0.97	0.39	0.25	0.13
G33R Lens 1 vertical traverse	Lens	1 / 12	97.53	1.24	0.39	0.59	0.25
G33R Lens 1 vertical traverse	Lens	1 / 13	97.20	2.08	0.33	0.35	0.03
G33R Lens 1 vertical traverse	Lens	1 / 14	97.32	1.87	0.42	0.36	0.03
G33R Lens 1 vertical traverse	Lens	1 / 15	97.03	2.22	0.25	0.43	0.07
G33R Lens 1 vertical traverse	Cement	1 / 16	94.92	3.55	0.31	1.12	0.10
G33R Lens 1 vertical traverse	Cement	1 / 17	95.25	3.05	0.22	1.40	0.08
G33R Lens 1 vertical traverse	Cement	1 / 18	96.75	2.50	0.11	0.58	0.07
G33R Lens 1 vertical traverse	Cement	1 / 19	96.42	2.03	0.45	1.00	0.09
G33R Lens 1 vertical traverse	Matrix	1 / 20	96.53	2.42	0.27	0.70	0.09
G33R Lens 1 horizontal traverse	Lens	2 / 1	97.79	1.51	0.24	0.34	0.12
G33R Lens 1 horizontal traverse	Lens	2 / 2	98.09	1.31	0.24	0.33	0.04
G33R Lens 1 horizontal traverse	Lens	2 / 3	98.36	0.96	0.27	0.30	0.11
G33R Lens 1 horizontal traverse	Lens	2 / 4	98.44	0.41	0.10	0.63	0.41
G33R Lens 1 horizontal traverse	Lens	2 / 5	98.46	0.62	0.19	0.62	0.11
G33R Lens 1 horizontal traverse	Lens	2 / 6	97.76	1.30	0.50	0.33	0.12
G33R Lens 1 horizontal traverse	Lens	2 / 7	93.92	4.58	0.32	1.06	0.13
G33R Lens 1 horizontal traverse	Lens	2 / 8	97.93	1.34	0.36	0.33	0.03
G33R Lens 1 horizontal traverse	Lens	2 / 9	97.69	1.43	0.33	0.42	0.13
G33R Lens 1 horizontal traverse	Lens	2 / 10	98.36	0.72	0.31	0.45	0.15
G33R Lens 1 horizontal traverse	Lens	2 / 11	97.68	1.53	0.22	0.44	0.12
G33R Lens 1 horizontal traverse	Lens	2 / 12	98.10	1.23	0.33	0.27	0.07
G33R Lens 1 horizontal traverse	Lens	2 / 13	98.62	0.38	0.90	0.05	0.05

SAMPLE	FEATURE	DATA SET/ POINT	NORMALISED WEIGHT % CARBONATE				
			Ca	Mg	Sr	Fe	Mn
G33R sclera	Sclera	3 / 1	97.89	1.38	0.24	0.37	0.13
G33R sclera	Sclera	3 / 2	97.65	1.63	0.37	0.28	0.08
G33R sclera	Sclera	3 / 3	97.60	1.57	0.49	0.30	0.05
G33R sclera	Sclera	3 / 4	98.08	1.09	0.35	0.41	0.08
G33R sclera	Sclera	3 / 5	97.23	2.02	0.41	0.25	0.09
G33R sclera	Sclera	3 / 6	97.93	1.31	0.42	0.23	0.11
G33R sclera	Sclera	3 / 7	97.74	1.45	0.35	0.41	0.06
G33R sclera	Sclera	3 / 8	96.97	2.30	0.36	0.31	0.06
G33R sclera	Sclera	3 / 9	97.56	1.69	0.29	0.37	0.09
G33R sclera	Sclera	3 / 10	97.64	1.62	0.41	0.26	0.07
G33R sclera	Sclera	3 / 11	96.69	2.48	0.40	0.35	0.08
G33R sclera	Sclera	3 / 12	98.07	1.22	0.30	0.29	0.11
PM28 Lens 3 vertical traverse	Resin	1 / 1	66.49	2.54	19.55	9.12	2.30
PM28 Lens 3 vertical traverse	Resin	1 / 2	125.99	9.85	-19.14	-23.56	6.85
PM28 Lens 3 vertical traverse	Resin	1 / 3	180.25	-8.82	-52.24	5.27	-24.46
PM28 Lens 3 vertical traverse	Lens	1 / 4	93.70	5.79	0.42	0.02	0.06
PM28 Lens 3 vertical traverse	Lens	1 / 5	97.90	1.65	0.34	0.07	0.05
PM28 Lens 3 vertical traverse	Lens	1 / 6	88.05	11.22	0.40	0.25	0.07
PM28 Lens 3 vertical traverse	Lens	1 / 7	93.79	5.74	0.41	0.02	0.04
PM28 Lens 3 vertical traverse	Lens	1 / 8	93.07	6.30	0.55	0.05	0.03
PM28 Lens 3 vertical traverse	Lens	1 / 9	93.82	5.71	0.42	0.03	0.02
PM28 Lens 3 vertical traverse	Lens	1 / 10	92.77	6.77	0.37	0.09	0.00
PM28 Lens 3 vertical traverse	Lens	1 / 11	94.59	4.93	0.46	0.04	-0.02
PM28 Lens 3 vertical traverse	Lens	1 / 12	90.78	8.66	0.46	0.10	0.00
PM28 Lens 3 vertical traverse	Lens	1 / 13	95.89	0.72	0.07	3.15	0.17
PM28 Lens 3 vertical traverse	Bowl?	1 / 14	97.18	0.55	0.05	2.11	0.11
PM28 Lens 3 vertical traverse	Lens	1 / 15	87.99	0.86	0.05	10.98	0.12
PM28 Lens 3 vertical traverse	Matrix	1 / 16	94.60	1.31	0.03	3.61	0.45
PM28 Lens 3 vertical traverse	Matrix	1 / 17	90.57	4.89	-0.12	4.53	0.13
PM28 Lens 3 vertical traverse	Matrix	1 / 18	31.03	34.69	-0.05	34.20	0.12
PM28 Lens 3 horizontal traverse	Lens	2 / 1	93.42	1.55	0.05	4.80	0.17
PM28 Lens 3 horizontal traverse	Lens	2 / 2	94.00	5.40	0.44	0.15	0.00
PM28 Lens 3 horizontal traverse	Lens	2 / 3	91.39	7.67	0.40	0.48	0.05
PM28 Lens 3 horizontal traverse	Lens	2 / 4	91.86	7.69	0.37	0.05	0.03
PM28 Lens 3 horizontal traverse	Lens	2 / 5	95.73	3.83	0.39	0.03	0.02
PM28 Lens 3 horizontal traverse	Lens	2 / 6	96.54	3.05	0.37	0.03	0.00
PM28 Lens 3 horizontal traverse	Lens	2 / 7	95.81	3.65	0.50	0.06	-0.02
PM28 Lens 3 horizontal traverse	Lens	2 / 8	95.77	3.81	0.41	0.00	0.01
PM28 Lens 3 horizontal traverse	Lens	2 / 9	94.14	5.45	0.43	0.02	-0.03
PM28 Lens 3 horizontal traverse	Lens	2 / 10	94.62	4.96	0.40	0.01	0.01
PM28 Lens 3 horizontal traverse	Lens	2 / 11	95.60	3.97	0.38	0.01	0.03
PM28 Lens 3 horizontal traverse	Lens	2 / 12	82.72	16.74	0.46	0.04	0.04
PM28 Lens 3 horizontal traverse	Lens	2 / 13	96.22	3.28	0.44	0.03	0.03
PM28 Lens 3 horizontal traverse	Lens	2 / 14	91.65	7.82	0.37	0.09	0.07
PM28 Lens 3 horizontal traverse	Lens	2 / 15	92.52	6.61	0.29	0.48	0.11
PM28 Lens 5 vertical traverse	Resin	1 / 1	-76.52	57.40	-66.08	83.91	101.30
PM28 Lens 5 vertical traverse	Resin	1 / 2	135.40	4.04	-68.76	-4.84	34.16
PM28 Lens 5 vertical traverse	Lens	1 / 3	96.26	2.84	0.42	0.12	0.35
PM28 Lens 5 vertical traverse	Lens	1 / 4	98.78	0.43	0.39	0.09	0.31
PM28 Lens 5 vertical traverse	Lens	1 / 5	95.35	3.62	0.37	0.19	0.47
PM28 Lens 5 vertical traverse	Lens	1 / 6	95.69	3.14	0.48	0.15	0.54
PM28 Lens 5 vertical traverse	Lens	1 / 7	97.08	2.45	0.30	0.06	0.09
PM28 Lens 5 vertical traverse	Lens	1 / 8	94.48	4.84	0.31	0.29	0.09
PM28 Lens 5 vertical traverse	Lens	1 / 9	97.81	1.09	0.31	0.58	0.21
PM28 Lens 5 vertical traverse	Lens	1 / 10	93.84	5.81	0.40	-0.02	-0.02
PM28 Lens 5 vertical traverse	Lens	1 / 11	92.46	7.18	0.36	0.01	0.00
PM28 Lens 5 vertical traverse	Lens	1 / 12	94.26	5.23	0.30	0.22	-0.01
PM28 Lens 5 vertical traverse	Lens	1 / 13	92.80	6.87	0.32	0.02	-0.01
PM28 Lens 5 vertical traverse	Lens	1 / 14	91.47	7.98	0.37	0.12	0.06
PM28 Lens 5 vertical traverse	Lens	1 / 15	85.98	13.51	0.41	0.08	0.01
PM28 Lens 5 vertical traverse	Lens	1 / 16	85.85	11.25	0.32	2.32	0.26
PM28 Lens 5 vertical traverse	Lens	1 / 17	95.44	0.88	0.05	3.35	0.29
PM28 Lens 5 vertical traverse	Matrix	1 / 18	96.63	1.10	0.04	1.99	0.24
PM28 Lens 5 vertical traverse	Matrix	1 / 19	97.22	0.52	0.06	2.06	0.14
PM28 Lens 5 vertical traverse	Matrix	1 / 20	95.95	0.93	0.08	2.83	0.20
PM28 Lens 5 vertical traverse	Matrix	1 / 21	96.11	0.91	0.03	2.78	0.17
PM28 Lens 5 vertical traverse	Matrix	1 / 22	62.45	10.55	0.20	19.77	7.02

SAMPLE	FEATURE	DATA SET/ POINT	NORMALISED WEIGHT % CARBONATE				
			Ca	Mg	Sr	Fe	Mn
PM28 Lens 5 horizontal traverse	Lens	2 / 1	93.72	1.83	0.09	3.09	1.27
PM28 Lens 5 horizontal traverse	Lens	2 / 2	94.53	4.34	0.37	0.62	0.14
PM28 Lens 5 horizontal traverse	Lens	2 / 3	89.72	9.39	0.43	0.44	0.02
PM28 Lens 5 horizontal traverse	Lens	2 / 4	97.38	1.53	0.27	0.68	0.13
PM28 Lens 5 horizontal traverse	Lens	2 / 5	97.88	1.18	0.28	0.58	0.10
PM28 Lens 5 horizontal traverse	Lens	2 / 6	96.30	2.86	0.28	0.45	0.12
PM28 Lens 5 horizontal traverse	Lens	2 / 7	97.46	2.04	0.31	0.14	0.05
PM28 Lens 5 horizontal traverse	Lens	2 / 8	83.33	16.32	0.33	0.01	0.00
PM28 Lens 5 horizontal traverse	Lens	2 / 9	97.16	2.46	0.40	-0.01	0.00
PM28 Lens 5 horizontal traverse	Lens	2 / 10	95.47	4.15	0.38	0.02	-0.02
PM28 Lens 5 horizontal traverse	Lens	2 / 11	93.56	5.93	0.42	0.07	0.02
PM28 Lens 5 horizontal traverse	Lens	2 / 12	95.73	3.94	0.33	0.01	-0.01
PM28 Lens 5 horizontal traverse	Lens	2 / 13	94.47	5.13	0.32	0.08	-0.01
PM28 Lens 5 horizontal traverse	Lens	2 / 14	92.01	7.04	0.35	0.50	0.09
PM28 Lens 5 horizontal traverse	Lens	2 / 15	91.67	7.68	0.36	0.27	0.02
PM28 Lens 5 horizontal traverse	Lens	2 / 16	79.40	19.98	0.44	0.16	0.02
PM28 Lens 5 horizontal traverse	Lens	2 / 17	94.54	4.77	0.34	0.29	0.07
TS1 Lens 4 vertical traverse	Resin	1 / 1	67.00	15.19	2.77	16.19	-1.15
TS1 Lens 4 vertical traverse	Resin	1 / 2	133.27	-5.50	-29.83	18.64	-16.58
TS1 Lens 4 vertical traverse	Lens	1 / 3	98.07	1.60	0.08	0.17	0.08
TS1 Lens 4 vertical traverse	Lens	1 / 4	98.09	1.74	0.09	0.03	0.05
TS1 Lens 4 vertical traverse	Lens	1 / 5	97.67	1.99	0.26	0.12	-0.03
TS1 Lens 4 vertical traverse	Lens	1 / 6	87.96	11.68	0.18	0.18	0.01
TS1 Lens 4 vertical traverse	Lens	1 / 7	99.05	0.52	0.13	0.25	0.06
TS1 Lens 4 vertical traverse	Lens	1 / 8	82.40	15.39	0.10	1.95	0.15
TS1 Lens 4 vertical traverse	Lens	1 / 9	99.09	0.37	0.13	0.29	0.14
TS1 Lens 4 vertical traverse	Lens	1 / 10	96.89	2.56	0.07	0.39	0.10
TS1 Lens 4 vertical traverse	Core	1 / 11	99.16	0.42	0.10	0.25	0.07
TS1 Lens 4 vertical traverse	Core	1 / 12	99.15	0.43	0.12	0.19	0.12
TS1 Lens 4 vertical traverse	Core	1 / 13	98.82	0.55	0.09	0.42	0.12
TS1 Lens 4 vertical traverse	Core	1 / 14	98.61	0.77	0.08	0.43	0.12
TS1 Lens 4 vertical traverse	Core	1 / 15	91.27	7.76	0.09	0.76	0.12
TS1 Lens 4 vertical traverse	Core	1 / 16	98.75	0.69	0.10	0.34	0.12
TS1 Lens 4 vertical traverse	Lens	1 / 17	89.80	9.18	0.10	0.83	0.08
TS1 Lens 4 vertical traverse	Lens	1 / 18	97.62	1.93	0.11	0.22	0.12
TS1 Lens 4 vertical traverse	Lens	1 / 19	87.77	10.92	0.11	1.06	0.15
TS1 Lens 4 vertical traverse	Lens	1 / 20	94.97	3.23	0.11	1.51	0.18
TS1 Lens 4 vertical traverse	Matrix?	1 / 21	97.73	1.81	0.11	0.25	0.10
TS1 Lens 4 vertical traverse	Matrix?	1 / 22	96.39	2.55	0.04	0.89	0.12
TS1 Lens 4 horizontal traverse	Sclera	2 / 1	97.61	1.49	0.14	0.62	0.14
TS1 Lens 4 horizontal traverse	Sclera	2 / 2	98.00	1.59	0.15	0.21	0.04
TS1 Lens 4 horizontal traverse	Sclera	2 / 3	97.82	1.42	0.14	0.55	0.08
TS1 Lens 4 horizontal traverse	Lens	2 / 4	98.09	1.11	0.14	0.57	0.09
TS1 Lens 4 horizontal traverse	Lens	2 / 5	98.04	1.57	0.08	0.26	0.05
TS1 Lens 4 horizontal traverse	Lens	2 / 6	96.95	2.89	0.10	0.02	0.05
TS1 Lens 4 horizontal traverse	Lens	2 / 7	98.30	1.57	0.08	0.01	0.04
TS1 Lens 4 horizontal traverse	Lens	2 / 8	97.96	1.81	0.09	0.08	0.05
TS1 Lens 4 horizontal traverse	Lens	2 / 9	97.94	1.67	0.18	0.12	0.09
TS1 Lens 4 horizontal traverse	Lens	2 / 10	98.40	1.41	0.11	0.02	0.06
TS1 Lens 4 horizontal traverse	Lens	2 / 11	98.41	1.40	0.09	0.05	0.05
TS1 Lens 4 horizontal traverse	Lens	2 / 12	97.41	2.43	0.11	0.03	0.03
TS1 Lens 4 horizontal traverse	Lens	2 / 13	98.92	0.92	0.10	0.02	0.04
TS1 Lens 4 horizontal traverse	Core	2 / 14	98.68	1.10	0.07	0.11	0.04
TS1 Lens 4 horizontal traverse	Core	2 / 15	98.47	0.73	0.07	0.52	0.21
TS1 Lens 4 horizontal traverse	Core	2 / 16	98.52	0.72	0.08	0.53	0.15
TS1 Lens 4 horizontal traverse	Lens	2 / 17	99.30	0.31	0.07	0.26	0.06
TS1 Lens 4 horizontal traverse	Lens	2 / 18	98.73	0.75	0.11	0.37	0.04
TS1 Lens 4 horizontal traverse	Lens	2 / 19	99.13	0.39	0.12	0.24	0.12
TS1 Lens 4 horizontal traverse	Lens	2 / 20	96.82	2.82	0.13	0.16	0.07
TS1 Lens 4 horizontal traverse	Lens	2 / 21	97.74	1.97	0.08	0.17	0.05
TS1 Lens 4 horizontal traverse	Lens	2 / 22	99.18	0.63	0.12	0.02	0.05
TS1 Lens 4 horizontal traverse	Lens	2 / 23	99.09	0.75	0.12	0.02	0.03
TS1 Lens 4 horizontal traverse	Lens	2 / 24	98.58	1.19	0.13	0.05	0.05
TS1 Lens 4 horizontal traverse	Lens	2 / 25	98.66	1.10	0.10	0.06	0.07
TS1 Lens 4 horizontal traverse	Lens	2 / 26	97.20	2.14	0.10	0.38	0.17
TS1 Lens 4 horizontal traverse	Lens/Sclera	2 / 27	96.94	2.76	0.11	0.11	0.09
TS1 Lens 4 horizontal traverse	Sclera	2 / 28	93.44	5.80	0.10	0.42	0.24
TS1 Lens 4 horizontal traverse	Sclera	2 / 29	98.39	1.29	0.10	0.17	0.04

SAMPLE	FEATURE	DATA SET/ POINT	NORMALISED WEIGHT % CARBONATE				
			Ca	Mg	Sr	Fe	Mn
TS1 Lens 4 horizontal traverse	Sclera	2 / 30	97.81	1.69	0.14	0.29	0.06
TS1 Lens 4 horizontal traverse	Sclera	2 / 31	97.93	1.46	0.12	0.42	0.07
TS1 Lens 5 vertical traverse	Resin	1 / 1	67.65	8.65	7.94	5.17	10.58
TS1 Lens 5 vertical traverse	Resin	1 / 2	98.22	25.71	-5.76	-2.96	-15.21
TS1 Lens 5 vertical traverse	Lens	1 / 3	97.19	1.96	0.13	0.57	0.14
TS1 Lens 5 vertical traverse	Lens	1 / 4	98.10	1.71	0.09	0.03	0.07
TS1 Lens 5 vertical traverse	Core	1 / 5	97.13	2.31	0.09	0.34	0.13
TS1 Lens 5 vertical traverse	Core	1 / 6	98.86	0.46	0.12	0.39	0.18
TS1 Lens 5 vertical traverse	Core	1 / 7	88.09	9.75	0.08	1.87	0.21
TS1 Lens 5 vertical traverse	Core	1 / 8	97.46	1.62	0.14	0.56	0.21
TS1 Lens 5 vertical traverse	Core	1 / 9	98.96	0.42	0.13	0.26	0.22
TS1 Lens 5 vertical traverse	Core	1 / 10	97.38	1.97	0.13	0.34	0.18
TS1 Lens 5 vertical traverse	Core	1 / 11	74.42	22.33	0.09	2.86	0.30
TS1 Lens 5 vertical traverse	Core	1 / 12	97.13	1.99	0.11	0.50	0.27
TS1 Lens 5 vertical traverse	Core	1 / 13	94.67	3.96	0.15	0.86	0.36
TS1 Lens 5 vertical traverse	Core	1 / 14	94.95	4.01	0.07	0.78	0.18
TS1 Lens 5 vertical traverse	Core	1 / 15	98.44	0.69	0.10	0.52	0.26
TS1 Lens 5 vertical traverse	Core	1 / 16	97.96	1.13	0.10	0.57	0.24
TS1 Lens 5 vertical traverse	Core	1 / 17	96.96	2.59	0.12	0.23	0.10
TS1 Lens 5 vertical traverse	Core/Lens	1 / 18	98.69	1.06	0.10	0.07	0.08
TS1 Lens 5 vertical traverse	Bowl	1 / 19	97.61	1.88	0.13	0.22	0.16
TS1 Lens 5 vertical traverse	Bowl	1 / 20	96.61	1.71	0.14	1.19	0.36
TS1 Lens 5 vertical traverse	Matrix	1 / 21	97.85	1.44	0.17	0.45	0.10
TS1 Lens 5 vertical traverse	Matrix	1 / 22	93.82	3.09	0.14	2.84	0.11
TS1 Lens 5 vertical traverse	Matrix	1 / 23	97.80	1.36	0.11	0.65	0.07
TS1 Lens 5 vertical traverse	Matrix	1 / 24	97.58	1.62	0.09	0.61	0.09
TS1 Lens 5 vertical traverse	Matrix	1 / 25	96.79	2.23	0.07	0.79	0.12
TS1 Lens 5 horizontal traverse	Sclera	2 / 1	96.81	2.19	0.18	0.65	0.16
TS1 Lens 5 horizontal traverse	Sclera	2 / 2	96.71	2.12	0.19	0.71	0.27
TS1 Lens 5 horizontal traverse	Lens	2 / 3	96.83	1.97	0.13	0.75	0.32
TS1 Lens 5 horizontal traverse	Lens	2 / 4	98.23	1.33	0.17	0.17	0.09
TS1 Lens 5 horizontal traverse	Lens	2 / 5	98.59	1.25	0.09	0.02	0.05
TS1 Lens 5 horizontal traverse	Lens	2 / 6	97.79	1.75	0.11	0.27	0.08
TS1 Lens 5 horizontal traverse	Lens	2 / 7	97.85	1.88	0.09	0.11	0.09
TS1 Lens 5 horizontal traverse	Lens	2 / 8	98.71	1.16	0.06	0.02	0.05
TS1 Lens 5 horizontal traverse	Lens	2 / 9	98.25	1.57	0.13	0.02	0.03
TS1 Lens 5 horizontal traverse	Core	2 / 10	98.04	1.79	0.09	0.04	0.04
TS1 Lens 5 horizontal traverse	Core	2 / 11	99.03	0.76	0.14	0.02	0.05
TS1 Lens 5 horizontal traverse	Core	2 / 12	98.02	1.75	0.10	0.08	0.05
TS1 Lens 5 horizontal traverse	Core	2 / 13	98.43	1.34	0.11	0.06	0.07
TS1 Lens 5 horizontal traverse	Core	2 / 14	97.44	1.57	0.13	0.64	0.22
TS1 Lens 5 horizontal traverse	Core	2 / 15	73.21	23.02	0.04	3.39	0.35
TS1 Lens 5 horizontal traverse	Core	2 / 16	98.65	0.56	0.12	0.32	0.35
TS1 Lens 5 horizontal traverse	Core	2 / 17	97.81	1.21	0.11	0.61	0.27
TS1 Lens 5 horizontal traverse	Core	2 / 18	99.23	0.34	0.06	0.20	0.17
TS1 Lens 5 horizontal traverse	Core	2 / 19	92.69	6.11	0.12	0.81	0.27
TS1 Lens 5 horizontal traverse	Lens	2 / 20	98.12	1.43	0.07	0.19	0.19
TS1 Lens 5 horizontal traverse	Lens	2 / 21	94.06	5.46	0.08	0.26	0.15
TS1 Lens 5 horizontal traverse	Lens	2 / 22	98.00	1.73	0.06	0.11	0.11
TS1 Lens 5 horizontal traverse	Lens	2 / 23	97.98	1.79	0.16	0.04	0.03
TS1 Lens 5 horizontal traverse	Lens	2 / 24	98.11	1.65	0.08	0.05	0.11
TS1 Lens 5 horizontal traverse	Lens	2 / 25	98.08	1.68	0.13	0.05	0.06
TS1 Lens 5 horizontal traverse	Lens	2 / 26	97.20	2.43	0.11	0.17	0.08
TS1 Lens 5 horizontal traverse	Lens/Sclera	2 / 27	98.12	1.74	0.10	0.04	0.01
TS1 Lens 5 horizontal traverse	Sclera	2 / 28	97.26	2.58	0.11	0.03	0.03
TS1 Lens 5 horizontal traverse	Sclera	2 / 29	97.07	2.11	0.24	0.50	0.07
TS1 Lens 5 horizontal traverse	Sclera	2 / 30	96.84	2.39	0.17	0.51	0.10
TS1 sclera	Sclera	3 / 1	96.78	2.51	0.19	0.41	0.11
TS1 sclera	Sclera	3 / 2	97.29	1.98	0.16	0.44	0.13
TS1 sclera	Sclera	3 / 3	97.70	1.60	0.13	0.45	0.12
TS1 sclera	Sclera	3 / 4	97.93	1.27	0.16	0.53	0.10
TS1 sclera	Sclera	3 / 5	97.51	1.62	0.14	0.59	0.15
TS1 sclera	Sclera	3 / 6	97.65	1.93	0.10	0.22	0.11
TS1 sclera	Sclera	3 / 7	97.44	1.78	0.12	0.48	0.19
TS1 sclera	Sclera	3 / 8	97.39	2.07	0.18	0.31	0.05
TS1 sclera	Sclera	3 / 9	97.58	1.69	0.11	0.46	0.15

Table E.8 - Mole % carbonate EPMA data (Edinburgh) for trilobites with schizochroal eyes.

SAMPLE	FEATURE	DATA SET/ POINT	MOLE % CARBONATE				
			Ca	Mg	Sr	Fe	Mn
BB3aR cement	Cement	1 / 1	98.48	1.46	0.02	0.02	0.02
BB3aR cement	Cement	1 / 2	99.82	0.12	0.02	0.02	0.03
BB3aR cement	Cement	1 / 3	99.91	0.08	0.00	-0.02	0.02
BB3aR cement	Cement	1 / 4	98.73	1.21	0.04	0.00	0.02
BB3aR cement	Cement	1 / 5	98.13	1.86	0.05	0.01	-0.06
BB3aR cement	Cement	1 / 6	98.41	1.42	0.10	0.05	0.01
BB3aR cement	Cement	1 / 7	99.20	0.77	0.02	0.01	0.01
BB3aR cement	Cement	1 / 8	98.89	1.06	0.02	0.04	0.00
BB3aR cement	Cement	1 / 9	99.09	0.82	0.01	0.04	0.04
BB3aR cement	Cement	1 / 10	99.60	0.41	0.01	0.00	-0.02
BB3aR cement	Cement	1 / 11	99.61	0.35	0.01	0.00	0.03
BB3aR cement	Cement	1 / 12	99.26	0.69	0.03	0.00	0.02
BB3aR cement	Cement	1 / 13	99.24	0.71	0.03	0.01	0.01
BB3aR cement	Cement	1 / 14	98.73	1.21	0.03	0.01	0.02
BB3aR cement	Cement	1 / 15	99.17	0.72	0.05	0.01	0.04
BB3aR Lens 2b diagonal traverse	Lens	1 / 1	98.72	1.19	0.04	0.01	0.03
BB3aR Lens 2b diagonal traverse	Lens	1 / 2	99.54	0.40	0.04	0.00	0.03
BB3aR Lens 2b diagonal traverse	Lens	1 / 3	96.57	3.39	0.05	0.00	-0.01
BB3aR Lens 2b diagonal traverse	Lens	1 / 4	88.01	11.95	0.06	-0.02	-0.01
BB3aR Lens 2b diagonal traverse	Lens	1 / 5	99.51	0.44	0.04	0.00	0.00
BB3aR Lens 2b diagonal traverse	Lens	1 / 6	99.56	0.38	0.04	0.00	0.02
BB3aR Lens 2b diagonal traverse	Lens	1 / 7	99.42	0.53	0.06	-0.01	0.00
BB3aR Lens 2b diagonal traverse	Lens	1 / 8	87.38	12.57	0.06	-0.02	0.01
BB3aR Lens 2b diagonal traverse	Lens	1 / 9	99.28	0.68	0.04	0.01	-0.01
BB3aR Lens 2b diagonal traverse	Lens	1 / 10	99.13	0.82	0.05	0.00	0.00
BB3aR Lens 2b diagonal traverse	Lens	1 / 11	99.61	0.43	0.00	-0.02	-0.02
BB3aR Lens 2b diagonal traverse	Lens	1 / 12	93.03	6.87	0.05	0.03	0.02
BB3aR Lens 2b diagonal traverse	Lens	1 / 13	99.01	0.97	0.03	-0.01	0.00
BB3aR vertical traverse	Resin	1 / 1	99.37	0.43	0.01	0.13	0.07
BB3aR vertical traverse	Resin	1 / 2	99.36	0.57	0.02	0.04	0.01
BB3aR vertical traverse	Lens	1 / 3	99.34	0.61	0.04	0.02	-0.01
BB3aR vertical traverse	Lens	1 / 4	99.33	0.63	0.04	0.01	-0.01
BB3aR vertical traverse	Lens	1 / 5	99.57	0.42	0.07	-0.03	-0.03
BB3aR vertical traverse	Lens	1 / 6	98.99	0.95	0.07	-0.01	0.01
BB3aR vertical traverse	Lens	1 / 7	98.64	1.28	0.07	0.02	-0.01
BB3aR vertical traverse	Lens	1 / 8	99.29	0.64	0.04	0.01	0.01
BB3aR vertical traverse	Lens	1 / 9	99.31	0.66	0.04	0.01	-0.02
BB3aR vertical traverse	Lens	1 / 10	99.59	0.36	0.04	0.01	-0.01
BB3aR vertical traverse	Lens	1 / 11	98.47	1.48	0.03	-0.01	0.02
BB3aR vertical traverse	Lens	1 / 12	99.63	0.33	0.02	0.02	0.00
BB3aR vertical traverse	Lens	1 / 13	99.69	0.26	0.04	0.00	0.01
BB3aR vertical traverse	Lens	1 / 14	99.35	0.65	-0.01	0.00	0.01
BB3aR vertical traverse	Lens	1 / 15	97.08	2.94	0.02	-0.02	-0.02
BB3aR vertical traverse	Lens	1 / 16	93.84	6.08	0.07	0.00	0.00
BB3aR vertical traverse	Lens	1 / 17	98.77	1.21	0.02	-0.01	0.02
BB3aR vertical traverse	Lens	1 / 18	99.23	0.76	0.00	0.01	0.00
BB3aR vertical traverse	Lens	1 / 19	69.58	30.39	0.03	0.02	-0.01
BB3aR vertical traverse	Lens	1 / 20	99.29	0.67	0.03	0.01	-0.01
BB3aR vertical traverse	Lens/Matrix	1 / 21	98.79	1.17	0.03	0.00	0.01
BB3aR vertical traverse	Matrix	1 / 22	99.07	0.92	0.03	-0.02	0.00
BB3aR vertical traverse	Matrix	1 / 23	99.35	0.66	0.01	0.00	-0.01
BB3aR vertical traverse	Matrix	1 / 24	98.86	1.13	0.00	0.00	0.01
BB3aR vertical traverse	Matrix	1 / 25	99.10	0.86	0.05	-0.01	0.01
BB3aR vertical traverse	Matrix	1 / 26	99.59	0.37	0.03	0.00	0.01
BB3aR vertical traverse	Matrix	1 / 27	98.79	1.16	0.03	-0.01	0.03
BB3aR horizontal traverse	Sclera	2 / 1	99.20	0.68	0.01	0.04	0.08
BB3aR horizontal traverse	Sclera	2 / 2	99.26	0.45	0.01	0.16	0.13
BB3aR horizontal traverse	Sclera	2 / 3	99.20	0.72	0.02	0.04	0.02
BB3aR horizontal traverse	Sclera	2 / 4	99.20	0.53	0.01	0.13	0.13
BB3aR horizontal traverse	Lens	2 / 5	99.22	0.51	0.03	0.17	0.07
BB3aR horizontal traverse	Lens	2 / 6	99.37	0.52	0.01	0.03	0.08
BB3aR horizontal traverse	Lens	2 / 7	99.01	0.59	0.03	0.02	0.35
BB3aR horizontal traverse	Lens	2 / 8	99.33	0.45	0.04	0.10	0.08
BB3aR horizontal traverse	Lens	2 / 9	98.25	1.67	0.03	0.03	0.02

SAMPLE	FEATURE	DATA SET/ POINT	MOLE % CARBONATE				
			Ca	Mg	Sr	Fe	Mn
BB3aR horizontal traverse	Lens	2 / 10	99.76	0.18	0.02	0.02	0.01
BB3aR horizontal traverse	Lens	2 / 11	99.45	0.57	0.01	-0.01	-0.02
BB3aR horizontal traverse	Lens	2 / 12	98.96	1.01	0.02	0.00	0.01
BB3aR horizontal traverse	Lens	2 / 13	99.04	0.88	0.05	-0.01	0.04
BB3aR horizontal traverse	Lens	2 / 14	98.90	1.06	0.04	0.01	-0.01
BB3aR horizontal traverse	Lens	2 / 15	99.32	0.58	0.04	0.02	0.04
BB3aR horizontal traverse	Lens	2 / 16	99.58	0.12	0.01	0.27	0.02
BB3aR horizontal traverse	Lens	2 / 17	99.66	0.05	-0.01	0.27	0.03
BB3aR horizontal traverse	Lens	2 / 18	99.49	0.37	0.04	0.10	0.01
BB3aR horizontal traverse	Lens	2 / 19	99.16	0.83	0.01	0.00	0.00
BB3aR horizontal traverse	Lens	2 / 20	99.26	0.67	0.02	0.04	0.01
BB3aR horizontal traverse	Lens	2 / 21	98.95	1.00	0.04	0.01	0.00
BB3aR horizontal traverse	Lens	2 / 22	98.58	1.40	0.04	-0.01	-0.02
BB3aR horizontal traverse	Lens	2 / 23	98.87	0.91	0.03	0.18	0.02
BB3aR horizontal traverse	Lens	2 / 24	99.08	0.50	0.04	0.35	0.03
BB3aR horizontal traverse	Lens	2 / 25	99.13	0.45	0.04	0.34	0.05
BB3aR horizontal traverse	Lens	2 / 26	99.13	0.84	0.03	0.00	-0.01
BB3aR horizontal traverse	Lens	2 / 27	98.36	1.60	0.03	0.00	0.01
BB3aR horizontal traverse	Lens	2 / 28	98.52	1.45	0.02	-0.01	0.02
BB3aR horizontal traverse	Lens	2 / 29	74.53	25.23	0.00	0.24	0.00
BB3aR horizontal traverse	Lens	2 / 30	98.99	0.98	0.02	0.00	0.00
BB3aR horizontal traverse	Lens	2 / 31	75.73	24.20	0.04	0.00	0.03
BB3aR horizontal traverse	Lens/Sclera	2 / 32	98.42	0.68	0.05	0.69	0.16
BB3aR horizontal traverse	Sclera	2 / 33	99.12	0.47	0.04	0.21	0.16
BB3aR horizontal traverse	Sclera	2 / 34	99.03	0.82	0.03	0.08	0.05
BB3aR sclera of lens 1	Sclera	1 / 1	99.11	0.61	0.02	0.24	0.02
BB3aR sclera of lens 2	Sclera	1 / 2	99.10	0.76	0.01	0.07	0.06
BB3aR sclera of lens 3	Sclera	1 / 3	98.92	0.96	0.02	0.08	0.03
BB3aR sclera of lens 4	Sclera	1 / 4	99.09	0.46	0.07	0.35	0.03
BB3aR sclera of lens 5	Sclera	1 / 5	99.09	0.82	0.01	0.03	0.06
BB3aR exoskeleton	E'skeleton	2 / 1	99.07	0.53	0.05	0.19	0.16
BB3aR exoskeleton	E'skeleton	2 / 2	99.39	0.54	0.03	0.01	0.03
BB3aR exoskeleton	E'skeleton	2 / 3	99.46	0.34	0.01	0.14	0.05
BB3aR exoskeleton	E'skeleton	2 / 4	98.57	1.37	0.03	0.00	0.02
BB3aR exoskeleton	E'skeleton	2 / 5	99.04	0.86	0.03	0.01	0.05
BB3aR exoskeleton	E'skeleton	2 / 6	99.20	0.65	0.01	0.08	0.05
BB3aR exoskeleton	E'skeleton	2 / 7	98.97	0.90	0.03	0.06	0.04
BB3aR exoskeleton	E'skeleton	2 / 8	99.38	0.49	0.03	0.04	0.06
BB3aR exoskeleton	E'skeleton	2 / 9	99.19	0.78	0.02	0.01	0.00
BB3aR exoskeleton	E'skeleton	2 / 10	98.58	1.40	0.01	0.02	-0.01
BB3aR exoskeleton	E'skeleton	2 / 11	98.96	0.47	0.04	0.26	0.26
BB3aR exoskeleton	E'skeleton	2 / 12	99.26	0.44	0.02	0.17	0.12
BB3aR exoskeleton	E'skeleton	2 / 13	99.20	0.69	0.03	0.03	0.05
BB3aR exoskeleton	E'skeleton	2 / 14	99.32	0.58	0.03	0.05	0.03
BB3aR exoskeleton	E'skeleton	2 / 15	99.11	0.85	0.01	0.03	0.00
BB3aR exoskeleton	E'skeleton	2 / 16	99.09	0.73	0.03	0.06	0.09
BB3aR exoskeleton	E'skeleton	2 / 17	99.43	0.52	0.00	-0.01	0.06
BB3aR exoskeleton	E'skeleton	2 / 18	99.05	0.81	0.02	0.07	0.05
E22B Lens 1 vertical traverse	Matrix	1 / 1	97.38	1.70	0.03	0.82	0.07
E22B Lens 1 vertical traverse	Cornea	1 / 2	99.03	0.71	0.03	0.12	0.11
E22B Lens 1 vertical traverse	Lens	1 / 3	98.43	1.43	0.01	0.07	0.06
E22B Lens 1 vertical traverse	Lens	1 / 4	97.38	2.55	0.08	-0.01	0.01
E22B Lens 1 vertical traverse	Lens	1 / 5	98.31	1.59	0.06	0.00	0.04
E22B Lens 1 vertical traverse	Lens	1 / 6	97.99	1.92	0.04	0.01	0.04
E22B Lens 1 vertical traverse	Lens	1 / 7	99.42	0.54	0.01	-0.02	0.05
E22B Lens 1 vertical traverse	Core	1 / 8	99.26	0.72	-0.01	-0.01	0.03
E22B Lens 1 vertical traverse	Core	1 / 9	98.07	1.86	0.08	-0.01	0.01
E22B Lens 1 vertical traverse	Core	1 / 10	98.28	1.62	0.04	0.00	0.06
E22B Lens 1 vertical traverse	Core	1 / 11	98.69	1.14	0.04	0.03	0.10
E22B Lens 1 vertical traverse	Core	1 / 12	98.67	1.16	0.02	0.00	0.14
E22B Lens 1 vertical traverse	Core	1 / 13	98.83	1.01	0.02	0.01	0.13
E22B Lens 1 vertical traverse	Core	1 / 14	98.95	0.83	0.00	0.02	0.18
E22B Lens 1 vertical traverse	Lens	1 / 15	98.01	1.87	0.07	0.00	0.05
E22B Lens 1 vertical traverse	Lens	1 / 16	97.63	2.28	0.04	-0.01	0.06
E22B Lens 1 vertical traverse	Matrix	1 / 17	97.80	2.09	0.04	0.02	0.05
E22B Lens 1 vertical traverse	Matrix	1 / 18	90.82	7.19	-0.11	1.94	0.16
E22B Lens 1 vertical traverse	Matrix	1 / 19	98.07	1.24	0.00	0.61	0.08

SAMPLE	FEATURE	DATA SET/ POINT	MOLE % CARBONATE				
			Ca	Mg	Sr	Fe	Mn
E22B Lens 1 horizontal traverse	Sclera	2 / 1	98.38	1.43	0.04	0.09	0.07
E22B Lens 1 horizontal traverse	Sclera	2 / 2	98.54	1.25	0.05	0.08	0.08
E22B Lens 1 horizontal traverse	Sclera	2 / 3	98.56	1.26	0.03	0.10	0.05
E22B Lens 1 horizontal traverse	Sclera/Lens	2 / 4	98.71	1.06	0.02	0.09	0.10
E22B Lens 1 horizontal traverse	Bowl	2 / 5	97.35	2.46	0.03	0.07	0.08
E22B Lens 1 horizontal traverse	Bowl	2 / 6	98.30	1.55	0.02	0.05	0.07
E22B Lens 1 horizontal traverse	Lens	2 / 7	98.59	1.28	0.03	0.01	0.09
E22B Lens 1 horizontal traverse	Lens	2 / 8	98.82	1.06	0.03	0.01	0.08
E22B Lens 1 horizontal traverse	Core	2 / 9	97.88	2.03	0.03	0.00	0.06
E22B Lens 1 horizontal traverse	Core	2 / 10	98.89	1.01	0.03	0.02	0.04
E22B Lens 1 horizontal traverse	Core	2 / 11	98.74	1.15	0.01	-0.01	0.10
E22B Lens 1 horizontal traverse	Core	2 / 12	98.71	1.16	0.02	0.01	0.10
E22B Lens 1 horizontal traverse	Core	2 / 13	98.36	1.45	0.07	0.02	0.10
E22B Lens 1 horizontal traverse	Core	2 / 14	97.82	2.11	0.04	0.01	0.02
E22B Lens 1 horizontal traverse	Core	2 / 15	97.77	2.10	0.06	0.00	0.07
E22B Lens 1 horizontal traverse	Lens	2 / 16	97.72	2.11	0.03	0.01	0.13
E22B Lens 1 horizontal traverse	Lens	2 / 17	97.49	2.43	0.03	-0.01	0.06
E22B Lens 1 horizontal traverse	Bowl	2 / 18	97.51	2.36	0.06	-0.03	0.09
E22B Lens 1 horizontal traverse	Bowl	2 / 19	96.89	2.52	0.04	0.42	0.13
E22B Lens 1 horizontal traverse	Sclera	2 / 20	98.73	1.01	0.03	0.09	0.14
E22B Lens 1 horizontal traverse	Sclera	2 / 21	98.41	1.33	0.04	0.10	0.11
E22B Lens 1 horizontal traverse	Sclera	2 / 22	98.35	1.42	0.05	0.09	0.08
E22B Lens 1 horizontal traverse	Sclera	2 / 23	98.24	1.60	0.05	0.06	0.06
E22B Lens 1 horizontal traverse	Sclera	2 / 24	97.77	2.02	0.07	0.06	0.07
E22B Lens 1 horizontal traverse	Sclera	2 / 25	98.35	1.46	0.04	0.05	0.09
E22B exoskeleton	E'skeleton	3 / 1	98.18	1.59	0.06	0.08	0.09
E22B exoskeleton	E'skeleton	3 / 2	98.18	1.63	0.05	0.07	0.07
E22B exoskeleton	E'skeleton	3 / 3	98.20	1.71	0.04	0.02	0.03
E22B exoskeleton	E'skeleton	3 / 4	98.00	1.86	0.07	0.00	0.07
E22B exoskeleton	E'skeleton	3 / 5	98.42	1.44	0.04	0.04	0.07
E22B exoskeleton	E'skeleton	3 / 6	98.29	1.55	0.03	0.04	0.09
E22B exoskeleton	E'skeleton	3 / 7	98.27	1.55	0.05	0.06	0.07
E22B exoskeleton	E'skeleton	3 / 8	98.56	1.22	0.05	0.08	0.09
E22B exoskeleton	E'skeleton	3 / 9	98.63	1.20	0.03	0.03	0.11
E22B exoskeleton	E'skeleton	3 / 10	98.35	1.36	0.05	0.13	0.11
E22B exoskeleton	E'skeleton	3 / 11	98.34	1.44	0.05	0.02	0.15
E22B exoskeleton	E'skeleton	3 / 12	98.49	1.21	0.06	0.10	0.14
E22B Lens 3 vertical traverse	Resin	1 / 1	107.00	-1.22	-2.76	-0.38	-2.63
E22B Lens 3 vertical traverse	Resin	1 / 2	106.28	1.97	-1.47	-2.63	-4.15
E22B Lens 3 vertical traverse	Lens	1 / 3	98.29	1.37	0.03	0.09	0.21
E22B Lens 3 vertical traverse	Lens	1 / 4	96.49	3.43	0.05	0.01	0.02
E22B Lens 3 vertical traverse	Lens	1 / 5	98.09	1.80	0.06	0.00	0.05
E22B Lens 3 vertical traverse	Lens	1 / 6	98.26	1.61	0.06	0.02	0.06
E22B Lens 3 vertical traverse	Lens	1 / 7	98.10	1.83	0.05	0.01	0.01
E22B Lens 3 vertical traverse	Core	1 / 8	98.10	1.83	0.05	0.01	0.01
E22B Lens 3 vertical traverse	Core	1 / 9	98.18	1.71	0.04	-0.01	0.08
E22B Lens 3 vertical traverse	Core	1 / 10	97.59	2.28	0.08	0.02	0.02
E22B Lens 3 vertical traverse	Core	1 / 11	98.87	0.98	0.00	-0.01	0.16
E22B Lens 3 vertical traverse	Core	1 / 12	98.38	1.53	0.03	0.01	0.05
E22B Lens 3 vertical traverse	Core	1 / 13	98.61	1.20	0.01	0.01	0.16
E22B Lens 3 vertical traverse	Core	1 / 14	97.95	1.96	0.05	0.00	0.05
E22B Lens 3 vertical traverse	Lens	1 / 15	97.90	1.98	0.05	0.02	0.04
E22B Lens 3 vertical traverse	Lens Base	1 / 16	91.78	6.29	0.02	1.92	-0.01
E22B Lens 3 vertical traverse	Matrix	1 / 17	97.48	2.10	-0.01	0.24	0.19
E22B Lens 3 vertical traverse	Matrix	1 / 18	97.77	2.10	0.03	0.04	0.06
E22B Lens 3 horizontal traverse	Sclera	2 / 1	98.39	1.38	0.05	0.09	0.10
E22B Lens 3 horizontal traverse	Sclera	2 / 2	98.45	1.41	0.02	0.03	0.08
E22B Lens 3 horizontal traverse	Sclera	2 / 3	98.42	1.33	0.05	0.08	0.12
E22B Lens 3 horizontal traverse	Sclera	2 / 4	98.66	1.05	0.03	0.16	0.10
E22B Lens 3 horizontal traverse	Bowl	2 / 5	98.16	1.70	0.05	0.02	0.07
E22B Lens 3 horizontal traverse	Bowl	2 / 6	98.34	1.43	0.02	0.00	0.22
E22B Lens 3 horizontal traverse	Lens	2 / 7	97.99	1.90	0.03	0.01	0.06
E22B Lens 3 horizontal traverse	Lens	2 / 8	98.50	1.44	-0.01	0.01	0.06
E22B Lens 3 horizontal traverse	Lens	2 / 9	98.43	1.52	0.01	-0.01	0.05
E22B Lens 3 horizontal traverse	Core	2 / 10	97.69	2.22	0.05	0.02	0.02
E22B Lens 3 horizontal traverse	Core	2 / 11	98.57	1.30	0.01	-0.03	0.15
E22B Lens 3 horizontal traverse	Core	2 / 12	98.32	1.52	0.04	-0.01	0.13
E22B Lens 3 horizontal traverse	Core	2 / 13	98.60	1.25	0.02	0.02	0.10

SAMPLE	FEATURE	DATA SET/ POINT	MOLE % CARBONATE				
			Ca	Mg	Sr	Fe	Mn
E22B Lens 3 horizontal traverse	Core	2 / 14	97.76	2.11	0.05	0.00	0.08
E22B Lens 3 horizontal traverse	Core	2 / 15	98.30	1.63	0.04	0.00	0.03
E22B Lens 3 horizontal traverse	Lens	2 / 16	97.78	2.12	0.07	0.00	0.02
E22B Lens 3 horizontal traverse	Lens	2 / 17	98.36	1.56	0.03	0.00	0.05
E22B Lens 3 horizontal traverse	Lens	2 / 18	98.27	1.65	0.04	-0.01	0.05
E22B Lens 3 horizontal traverse	Bowl	2 / 19	97.11	2.84	0.00	-0.02	0.06
E22B Lens 3 horizontal traverse	Bowl	2 / 20	98.12	1.71	0.07	0.03	0.07
E22B Lens 3 horizontal traverse	Sclera	2 / 21	98.68	1.04	0.05	0.14	0.10
E22B Lens 3 horizontal traverse	Sclera	2 / 22	98.02	1.80	0.05	0.04	0.09
E22B Lens 3 horizontal traverse	Sclera	2 / 23	98.18	1.66	0.06	0.07	0.04
E22B Lens 3 horizontal traverse	Sclera	2 / 24	98.28	1.57	0.03	0.07	0.05
E22B Lens 3 horizontal traverse	Sclera	2 / 25	98.07	1.72	0.05	0.07	0.09
G33R Lens 1 vertical traverse	Resin	1 / 1	79.32	12.51	1.36	5.26	1.54
G33R Lens 1 vertical traverse	Resin	1 / 2	98.84	0.51	0.25	0.31	0.08
G33R Lens 1 vertical traverse	Resin	1 / 3	98.90	0.71	0.16	0.16	0.06
G33R Lens 1 vertical traverse	Resin	1 / 4	98.72	0.78	0.20	0.21	0.08
G33R Lens 1 vertical traverse	Lens	1 / 5	97.39	1.93	0.22	0.33	0.13
G33R Lens 1 vertical traverse	Lens	1 / 6	94.64	4.51	0.27	0.48	0.11
G33R Lens 1 vertical traverse	Lens	1 / 7	97.55	1.71	0.14	0.49	0.11
G33R Lens 1 vertical traverse	Lens	1 / 8	97.96	1.41	0.18	0.35	0.11
G33R Lens 1 vertical traverse	Lens	1 / 9	97.37	1.89	0.08	0.54	0.12
G33R Lens 1 vertical traverse	Lens	1 / 10	97.84	1.43	0.30	0.31	0.12
G33R Lens 1 vertical traverse	Lens	1 / 11	98.25	1.15	0.26	0.22	0.11
G33R Lens 1 vertical traverse	Lens	1 / 12	97.53	1.47	0.27	0.51	0.22
G33R Lens 1 vertical traverse	Lens	1 / 13	96.98	2.47	0.23	0.30	0.03
G33R Lens 1 vertical traverse	Lens	1 / 14	97.16	2.22	0.29	0.31	0.02
G33R Lens 1 vertical traverse	Lens	1 / 15	96.77	2.63	0.17	0.37	0.06
G33R Lens 1 vertical traverse	Cement	1 / 16	94.54	4.20	0.21	0.96	0.09
G33R Lens 1 vertical traverse	Cement	1 / 17	94.97	3.61	0.15	1.21	0.07
G33R Lens 1 vertical traverse	Cement	1 / 18	96.42	2.95	0.07	0.50	0.06
G33R Lens 1 vertical traverse	Cement	1 / 19	96.34	2.41	0.30	0.87	0.08
G33R Lens 1 vertical traverse	Matrix	1 / 20	96.28	2.86	0.18	0.60	0.08
G33R Lens 1 horizontal traverse	Lens	2 / 1	97.65	1.79	0.16	0.29	0.10
G33R Lens 1 horizontal traverse	Lens	2 / 2	97.97	1.55	0.16	0.28	0.03
G33R Lens 1 horizontal traverse	Lens	2 / 3	98.32	1.14	0.18	0.26	0.09
G33R Lens 1 horizontal traverse	Lens	2 / 4	98.54	0.49	0.07	0.54	0.36
G33R Lens 1 horizontal traverse	Lens	2 / 5	98.50	0.74	0.13	0.53	0.10
G33R Lens 1 horizontal traverse	Lens	2 / 6	97.74	1.54	0.34	0.28	0.10
G33R Lens 1 horizontal traverse	Lens	2 / 7	93.36	5.40	0.21	0.91	0.12
G33R Lens 1 horizontal traverse	Lens	2 / 8	97.85	1.59	0.25	0.29	0.03
G33R Lens 1 horizontal traverse	Lens	2 / 9	97.60	1.70	0.22	0.36	0.11
G33R Lens 1 horizontal traverse	Lens	2 / 10	98.41	0.86	0.21	0.39	0.13
G33R Lens 1 horizontal traverse	Lens	2 / 11	97.54	1.82	0.15	0.38	0.11
G33R Lens 1 horizontal traverse	Lens	2 / 12	98.02	1.46	0.22	0.24	0.06
G33R Lens 1 horizontal traverse	Lens	2 / 13	98.85	0.45	0.61	0.04	0.04
G33R sclera	Sclera	3 / 1	97.77	1.63	0.16	0.32	0.12
G33R sclera	Sclera	3 / 2	97.51	1.93	0.25	0.24	0.07
G33R sclera	Sclera	3 / 3	97.51	1.86	0.33	0.26	0.04
G33R sclera	Sclera	3 / 4	98.05	1.29	0.24	0.35	0.07
G33R sclera	Sclera	3 / 5	97.04	2.39	0.28	0.22	0.08
G33R sclera	Sclera	3 / 6	97.87	1.55	0.29	0.20	0.10
G33R sclera	Sclera	3 / 7	97.64	1.72	0.24	0.35	0.05
G33R sclera	Sclera	3 / 8	96.72	2.72	0.24	0.27	0.05
G33R sclera	Sclera	3 / 9	97.40	2.01	0.19	0.32	0.08
G33R sclera	Sclera	3 / 10	97.52	1.92	0.28	0.22	0.06
G33R sclera	Sclera	3 / 11	96.42	2.94	0.27	0.30	0.07
G33R sclera	Sclera	3 / 12	97.99	1.45	0.21	0.25	0.10
PM28 Lens 3 vertical traverse	Resin	1 / 1	71.77	3.26	14.31	8.51	2.16
PM28 Lens 3 vertical traverse	Resin	1 / 2	114.20	10.60	-11.76	-18.45	5.41
PM28 Lens 3 vertical traverse	Resin	1 / 3	153.25	-8.90	-30.11	3.87	-18.11
PM28 Lens 3 vertical traverse	Lens	1 / 4	92.83	6.81	0.29	0.02	0.06
PM28 Lens 3 vertical traverse	Lens	1 / 5	97.72	1.95	0.23	0.06	0.04
PM28 Lens 3 vertical traverse	Lens	1 / 6	86.39	13.07	0.27	0.22	0.06
PM28 Lens 3 vertical traverse	Lens	1 / 7	92.92	6.75	0.28	0.02	0.03
PM28 Lens 3 vertical traverse	Lens	1 / 8	92.16	7.40	0.37	0.05	0.03
PM28 Lens 3 vertical traverse	Lens	1 / 9	92.96	6.71	0.28	0.03	0.02
PM28 Lens 3 vertical traverse	Lens	1 / 10	91.72	7.95	0.25	0.08	0.00

SAMPLE	FEATURE	DATA SET/ POINT	MOLE % CARBONATE				
			Ca	Mg	Sr	Fe	Mn
PM28 Lens 3 vertical traverse	Lens	1 / 11	93.86	5.81	0.31	0.03	-0.02
PM28 Lens 3 vertical traverse	Lens	1 / 12	89.47	10.14	0.31	0.08	0.00
PM28 Lens 3 vertical traverse	Lens	1 / 13	96.22	0.85	0.05	2.73	0.15
PM28 Lens 3 vertical traverse	Bowl?	1 / 14	97.39	0.65	0.04	1.83	0.10
PM28 Lens 3 vertical traverse	Lens	1 / 15	89.21	1.04	0.04	9.61	0.10
PM28 Lens 3 vertical traverse	Matrix	1 / 16	94.90	1.56	0.02	3.13	0.39
PM28 Lens 3 vertical traverse	Matrix	1 / 17	90.28	5.79	-0.08	3.90	0.11
PM28 Lens 3 vertical traverse	Matrix	1 / 18	30.47	40.44	-0.03	29.01	0.11
PM28 Lens 3 horizontal traverse	Lens	2 / 1	93.80	1.85	0.04	4.17	0.14
PM28 Lens 3 horizontal traverse	Lens	2 / 2	93.21	6.35	0.30	0.13	0.00
PM28 Lens 3 horizontal traverse	Lens	2 / 3	90.28	8.99	0.27	0.41	0.04
PM28 Lens 3 horizontal traverse	Lens	2 / 4	90.67	9.01	0.25	0.04	0.03
PM28 Lens 3 horizontal traverse	Lens	2 / 5	95.17	4.52	0.27	0.03	0.01
PM28 Lens 3 horizontal traverse	Lens	2 / 6	96.11	3.61	0.25	0.02	0.00
PM28 Lens 3 horizontal traverse	Lens	2 / 7	95.32	4.31	0.34	0.05	-0.01
PM28 Lens 3 horizontal traverse	Lens	2 / 8	95.22	4.50	0.28	0.00	0.01
PM28 Lens 3 horizontal traverse	Lens	2 / 9	93.31	6.41	0.29	0.01	-0.03
PM28 Lens 3 horizontal traverse	Lens	2 / 10	93.87	5.85	0.27	0.00	0.01
PM28 Lens 3 horizontal traverse	Lens	2 / 11	95.02	4.69	0.26	0.01	0.02
PM28 Lens 3 horizontal traverse	Lens	2 / 12	80.33	19.30	0.30	0.04	0.03
PM28 Lens 3 horizontal traverse	Lens	2 / 13	95.78	3.87	0.30	0.03	0.03
PM28 Lens 3 horizontal traverse	Lens	2 / 14	90.46	9.16	0.25	0.07	0.06
PM28 Lens 3 horizontal traverse	Lens	2 / 15	91.54	7.77	0.19	0.41	0.09
PM28 Lens 5 vertical traverse	Resin	1 / 1	-71.17	63.38	-41.67	67.43	82.04
PM28 Lens 5 vertical traverse	Resin	1 / 2	113.64	4.03	-39.13	-3.51	24.96
PM28 Lens 5 vertical traverse	Lens	1 / 3	95.94	3.37	0.29	0.10	0.31
PM28 Lens 5 vertical traverse	Lens	1 / 4	98.88	0.51	0.26	0.08	0.27
PM28 Lens 5 vertical traverse	Lens	1 / 5	94.90	4.28	0.25	0.16	0.41
PM28 Lens 5 vertical traverse	Lens	1 / 6	95.36	3.71	0.32	0.13	0.47
PM28 Lens 5 vertical traverse	Lens	1 / 7	96.75	2.90	0.21	0.05	0.08
PM28 Lens 5 vertical traverse	Lens	1 / 8	93.77	5.71	0.21	0.25	0.07
PM28 Lens 5 vertical traverse	Lens	1 / 9	97.81	1.29	0.21	0.50	0.18
PM28 Lens 5 vertical traverse	Lens	1 / 10	92.94	6.83	0.27	-0.02	-0.02
PM28 Lens 5 vertical traverse	Lens	1 / 11	91.34	8.42	0.24	0.00	0.00
PM28 Lens 5 vertical traverse	Lens	1 / 12	93.47	6.15	0.20	0.19	0.00
PM28 Lens 5 vertical traverse	Lens	1 / 13	91.72	8.06	0.21	0.02	-0.01
PM28 Lens 5 vertical traverse	Lens	1 / 14	90.25	9.35	0.25	0.10	0.05
PM28 Lens 5 vertical traverse	Lens	1 / 15	83.98	15.67	0.27	0.07	0.01
PM28 Lens 5 vertical traverse	Lens	1 / 16	84.46	13.13	0.21	1.98	0.22
PM28 Lens 5 vertical traverse	Lens	1 / 17	95.76	1.05	0.03	2.90	0.25
PM28 Lens 5 vertical traverse	Matrix	1 / 18	96.73	1.31	0.03	1.72	0.21
PM28 Lens 5 vertical traverse	Matrix	1 / 19	97.44	0.62	0.04	1.78	0.12
PM28 Lens 5 vertical traverse	Matrix	1 / 20	96.21	1.11	0.06	2.45	0.18
PM28 Lens 5 vertical traverse	Matrix	1 / 21	96.34	1.08	0.02	2.40	0.15
PM28 Lens 5 vertical traverse	Matrix	1 / 22	63.52	12.75	0.14	17.37	6.22
PM28 Lens 5 horizontal traverse	Lens	2 / 1	93.97	2.18	0.06	2.67	1.11
PM28 Lens 5 horizontal traverse	Lens	2 / 2	93.97	5.13	0.25	0.53	0.12
PM28 Lens 5 horizontal traverse	Lens	2 / 3	88.34	10.98	0.29	0.37	0.02
PM28 Lens 5 horizontal traverse	Lens	2 / 4	97.30	1.82	0.18	0.59	0.11
PM28 Lens 5 horizontal traverse	Lens	2 / 5	97.84	1.40	0.19	0.50	0.08
PM28 Lens 5 horizontal traverse	Lens	2 / 6	95.94	3.38	0.19	0.39	0.10
PM28 Lens 5 horizontal traverse	Lens	2 / 7	97.21	2.42	0.21	0.12	0.04
PM28 Lens 5 horizontal traverse	Lens	2 / 8	80.95	18.82	0.22	0.01	0.00
PM28 Lens 5 horizontal traverse	Lens	2 / 9	96.84	2.91	0.27	-0.01	0.00
PM28 Lens 5 horizontal traverse	Lens	2 / 10	94.85	4.89	0.25	0.02	-0.02
PM28 Lens 5 horizontal traverse	Lens	2 / 11	92.67	6.97	0.28	0.06	0.02
PM28 Lens 5 horizontal traverse	Lens	2 / 12	95.13	4.65	0.22	0.00	-0.01
PM28 Lens 5 horizontal traverse	Lens	2 / 13	93.68	6.04	0.22	0.07	-0.01
PM28 Lens 5 horizontal traverse	Lens	2 / 14	90.99	8.26	0.24	0.43	0.08
PM28 Lens 5 horizontal traverse	Lens	2 / 15	90.51	9.00	0.24	0.23	0.01
PM28 Lens 5 horizontal traverse	Lens	2 / 16	76.66	22.90	0.29	0.13	0.02
PM28 Lens 5 horizontal traverse	Lens	2 / 17	93.85	5.62	0.23	0.24	0.06
TS1 Lens 4 vertical traverse	Resin	1 / 1	67.07	18.06	1.88	14.00	-1.00
TS1 Lens 4 vertical traverse	Resin	1 / 2	123.19	-6.03	-18.69	14.88	-13.35
TS1 Lens 4 vertical traverse	Lens	1 / 3	97.83	1.90	0.05	0.15	0.07
TS1 Lens 4 vertical traverse	Lens	1 / 4	97.81	2.06	0.06	0.03	0.04
TS1 Lens 4 vertical traverse	Lens	1 / 5	97.40	2.35	0.17	0.10	-0.03

SAMPLE	FEATURE	DATA SET/ POINT	MOLE % CARBONATE				
			Ca	Mg	Sr	Fe	Mn
TS1 Lens 4 vertical traverse	Lens	1 / 6	86.15	13.58	0.12	0.15	0.01
TS1 Lens 4 vertical traverse	Lens	1 / 7	99.03	0.62	0.08	0.22	0.05
TS1 Lens 4 vertical traverse	Lens	1 / 8	80.34	17.82	0.06	1.65	0.13
TS1 Lens 4 vertical traverse	Lens	1 / 9	99.12	0.43	0.08	0.25	0.12
TS1 Lens 4 vertical traverse	Lens	1 / 10	96.51	3.02	0.05	0.33	0.09
TS1 Lens 4 vertical traverse	Core	1 / 11	99.16	0.50	0.07	0.22	0.06
TS1 Lens 4 vertical traverse	Core	1 / 12	99.15	0.50	0.08	0.16	0.10
TS1 Lens 4 vertical traverse	Core	1 / 13	98.82	0.65	0.06	0.37	0.10
TS1 Lens 4 vertical traverse	Core	1 / 14	98.56	0.91	0.05	0.37	0.10
TS1 Lens 4 vertical traverse	Core	1 / 15	90.10	9.09	0.06	0.65	0.10
TS1 Lens 4 vertical traverse	Core	1 / 16	98.71	0.82	0.07	0.30	0.11
TS1 Lens 4 vertical traverse	Lens	1 / 17	88.42	10.73	0.07	0.71	0.07
TS1 Lens 4 vertical traverse	Lens	1 / 18	97.35	2.28	0.07	0.19	0.11
TS1 Lens 4 vertical traverse	Lens	1 / 19	86.18	12.72	0.07	0.90	0.13
TS1 Lens 4 vertical traverse	Lens	1 / 20	94.65	3.82	0.07	1.30	0.16
TS1 Lens 4 vertical traverse	Matrix?	1 / 21	97.48	2.15	0.07	0.22	0.09
TS1 Lens 4 vertical traverse	Matrix?	1 / 22	96.08	3.02	0.03	0.77	0.10
TS1 Lens 4 horizontal traverse	Sclera	2 / 1	97.48	1.77	0.10	0.53	0.12
TS1 Lens 4 horizontal traverse	Sclera	2 / 2	97.79	1.89	0.10	0.18	0.04
TS1 Lens 4 horizontal traverse	Sclera	2 / 3	97.69	1.68	0.10	0.47	0.07
TS1 Lens 4 horizontal traverse	Lens	2 / 4	98.02	1.31	0.10	0.49	0.08
TS1 Lens 4 horizontal traverse	Lens	2 / 5	97.82	1.86	0.06	0.22	0.05
TS1 Lens 4 horizontal traverse	Lens	2 / 6	96.46	3.42	0.06	0.01	0.04
TS1 Lens 4 horizontal traverse	Lens	2 / 7	98.04	1.86	0.05	0.01	0.04
TS1 Lens 4 horizontal traverse	Lens	2 / 8	97.68	2.14	0.06	0.07	0.05
TS1 Lens 4 horizontal traverse	Lens	2 / 9	97.72	1.98	0.12	0.10	0.08
TS1 Lens 4 horizontal traverse	Lens	2 / 10	98.18	1.67	0.08	0.02	0.05
TS1 Lens 4 horizontal traverse	Lens	2 / 11	98.19	1.66	0.06	0.04	0.04
TS1 Lens 4 horizontal traverse	Lens	2 / 12	97.01	2.87	0.08	0.02	0.02
TS1 Lens 4 horizontal traverse	Lens	2 / 13	98.79	1.09	0.07	0.02	0.03
TS1 Lens 4 horizontal traverse	Core	2 / 14	98.52	1.31	0.05	0.09	0.03
TS1 Lens 4 horizontal traverse	Core	2 / 15	98.45	0.86	0.05	0.45	0.19
TS1 Lens 4 horizontal traverse	Core	2 / 16	98.51	0.85	0.05	0.46	0.13
TS1 Lens 4 horizontal traverse	Lens	2 / 17	99.31	0.36	0.05	0.23	0.06
TS1 Lens 4 horizontal traverse	Lens	2 / 18	98.68	0.89	0.07	0.32	0.04
TS1 Lens 4 horizontal traverse	Lens	2 / 19	99.14	0.46	0.08	0.21	0.11
TS1 Lens 4 horizontal traverse	Lens	2 / 20	96.38	3.34	0.09	0.14	0.06
TS1 Lens 4 horizontal traverse	Lens	2 / 21	97.43	2.33	0.05	0.14	0.05
TS1 Lens 4 horizontal traverse	Lens	2 / 22	99.11	0.74	0.08	0.02	0.04
TS1 Lens 4 horizontal traverse	Lens	2 / 23	99.00	0.89	0.08	0.01	0.03
TS1 Lens 4 horizontal traverse	Lens	2 / 24	98.42	1.41	0.09	0.05	0.04
TS1 Lens 4 horizontal traverse	Lens	2 / 25	98.51	1.31	0.07	0.05	0.06
TS1 Lens 4 horizontal traverse	Lens	2 / 26	96.92	2.53	0.07	0.33	0.15
TS1 Lens 4 horizontal traverse	Lens/Sclera	2 / 27	96.50	3.27	0.07	0.09	0.07
TS1 Lens 4 horizontal traverse	Sclera	2 / 28	92.55	6.82	0.07	0.36	0.21
TS1 Lens 4 horizontal traverse	Sclera	2 / 29	98.22	1.53	0.07	0.15	0.04
TS1 Lens 4 horizontal traverse	Sclera	2 / 30	97.59	2.00	0.09	0.25	0.05
TS1 Lens 4 horizontal traverse	Sclera	2 / 31	97.76	1.73	0.08	0.36	0.07
TS1 Lens 5 vertical traverse	Resin	1 / 1	69.75	10.59	5.55	4.61	9.50
TS1 Lens 5 vertical traverse	Resin	1 / 2	90.08	27.99	-3.58	-2.34	-12.14
TS1 Lens 5 vertical traverse	Lens	1 / 3	96.97	2.33	0.09	0.49	0.12
TS1 Lens 5 vertical traverse	Lens	1 / 4	97.83	2.02	0.06	0.03	0.06
TS1 Lens 5 vertical traverse	Core	1 / 5	96.80	2.73	0.06	0.29	0.11
TS1 Lens 5 vertical traverse	Core	1 / 6	98.89	0.55	0.08	0.33	0.15
TS1 Lens 5 vertical traverse	Core	1 / 7	86.77	11.40	0.06	1.59	0.18
TS1 Lens 5 vertical traverse	Core	1 / 8	97.32	1.92	0.10	0.49	0.19
TS1 Lens 5 vertical traverse	Core	1 / 9	98.99	0.50	0.09	0.23	0.19
TS1 Lens 5 vertical traverse	Core	1 / 10	97.13	2.34	0.09	0.30	0.15
TS1 Lens 5 vertical traverse	Core	1 / 11	71.75	25.56	0.06	2.38	0.25
TS1 Lens 5 vertical traverse	Core	1 / 12	96.90	2.36	0.08	0.43	0.23
TS1 Lens 5 vertical traverse	Core	1 / 13	94.17	4.68	0.10	0.73	0.32
TS1 Lens 5 vertical traverse	Core	1 / 14	94.39	4.74	0.05	0.67	0.16
TS1 Lens 5 vertical traverse	Core	1 / 15	98.45	0.81	0.07	0.45	0.22
TS1 Lens 5 vertical traverse	Core	1 / 16	97.89	1.34	0.07	0.49	0.21
TS1 Lens 5 vertical traverse	Core	1 / 17	96.57	3.06	0.08	0.20	0.09
TS1 Lens 5 vertical traverse	Core/Lens	1 / 18	98.54	1.26	0.06	0.06	0.07
TS1 Lens 5 vertical traverse	Bowl	1 / 19	97.36	2.22	0.09	0.19	0.14
TS1 Lens 5 vertical traverse	Bowl	1 / 20	96.54	2.03	0.09	1.02	0.31
TS1 Lens 5 vertical traverse	Matrix	1 / 21	97.71	1.71	0.11	0.39	0.09

SAMPLE	FEATURE	DATA SET/ POINT	MOLE % CARBONATE				
			Ca	Mg	Sr	Fe	Mn
TS1 Lens 5 vertical traverse	Matrix	1 / 22	93.70	3.67	0.10	2.45	0.09
TS1 Lens 5 vertical traverse	Matrix	1 / 23	97.69	1.61	0.08	0.56	0.06
TS1 Lens 5 vertical traverse	Matrix	1 / 24	97.41	1.92	0.06	0.53	0.08
TS1 Lens 5 vertical traverse	Matrix	1 / 25	96.53	2.64	0.05	0.68	0.10
TS1 Lens 5 horizontal traverse	Sclera	2 / 1	96.58	2.60	0.12	0.56	0.14
TS1 Lens 5 horizontal traverse	Sclera	2 / 2	96.51	2.51	0.13	0.61	0.24
TS1 Lens 5 horizontal traverse	Lens	2 / 3	96.65	2.33	0.09	0.65	0.28
TS1 Lens 5 horizontal traverse	Lens	2 / 4	98.08	1.58	0.12	0.15	0.08
TS1 Lens 5 horizontal traverse	Lens	2 / 5	98.40	1.48	0.06	0.02	0.04
TS1 Lens 5 horizontal traverse	Lens	2 / 6	97.56	2.07	0.07	0.23	0.07
TS1 Lens 5 horizontal traverse	Lens	2 / 7	97.55	2.22	0.06	0.09	0.07
TS1 Lens 5 horizontal traverse	Lens	2 / 8	98.52	1.38	0.04	0.02	0.04
TS1 Lens 5 horizontal traverse	Lens	2 / 9	98.01	1.86	0.09	0.02	0.02
TS1 Lens 5 horizontal traverse	Core	2 / 10	97.75	2.12	0.06	0.03	0.03
TS1 Lens 5 horizontal traverse	Core	2 / 11	98.95	0.90	0.09	0.02	0.05
TS1 Lens 5 horizontal traverse	Core	2 / 12	97.75	2.07	0.07	0.07	0.04
TS1 Lens 5 horizontal traverse	Core	2 / 13	98.23	1.58	0.07	0.05	0.06
TS1 Lens 5 horizontal traverse	Core	2 / 14	97.31	1.86	0.09	0.55	0.19
TS1 Lens 5 horizontal traverse	Core	2 / 15	70.54	26.33	0.02	2.82	0.30
TS1 Lens 5 horizontal traverse	Core	2 / 16	98.67	0.66	0.08	0.28	0.30
TS1 Lens 5 horizontal traverse	Core	2 / 17	97.73	1.43	0.07	0.53	0.23
TS1 Lens 5 horizontal traverse	Core	2 / 18	99.24	0.40	0.04	0.17	0.15
TS1 Lens 5 horizontal traverse	Core	2 / 19	91.81	7.18	0.08	0.70	0.23
TS1 Lens 5 horizontal traverse	Lens	2 / 20	97.93	1.69	0.05	0.17	0.16
TS1 Lens 5 horizontal traverse	Lens	2 / 21	93.18	6.42	0.06	0.22	0.13
TS1 Lens 5 horizontal traverse	Lens	2 / 22	97.73	2.05	0.04	0.09	0.09
TS1 Lens 5 horizontal traverse	Lens	2 / 23	97.72	2.12	0.11	0.04	0.03
TS1 Lens 5 horizontal traverse	Lens	2 / 24	97.85	1.96	0.05	0.04	0.10
TS1 Lens 5 horizontal traverse	Lens	2 / 25	97.83	1.99	0.09	0.04	0.05
TS1 Lens 5 horizontal traverse	Lens	2 / 26	96.83	2.88	0.07	0.15	0.07
TS1 Lens 5 horizontal traverse	Lens/Sclera	2 / 27	97.83	2.06	0.07	0.04	0.01
TS1 Lens 5 horizontal traverse	Sclera	2 / 28	96.83	3.05	0.07	0.02	0.03
TS1 Lens 5 horizontal traverse	Sclera	2 / 29	96.84	2.50	0.16	0.43	0.07
TS1 Lens 5 horizontal traverse	Sclera	2 / 30	96.54	2.83	0.11	0.44	0.08
TS1 sclera	Sclera	3 / 1	96.45	2.97	0.13	0.35	0.10
TS1 sclera	Sclera	3 / 2	97.05	2.35	0.11	0.38	0.11
TS1 sclera	Sclera	3 / 3	97.53	1.89	0.09	0.39	0.10
TS1 sclera	Sclera	3 / 4	97.83	1.51	0.11	0.46	0.09
TS1 sclera	Sclera	3 / 5	97.35	1.92	0.09	0.51	0.13
TS1 sclera	Sclera	3 / 6	97.37	2.28	0.07	0.19	0.09
TS1 sclera	Sclera	3 / 7	97.24	2.10	0.08	0.41	0.16
TS1 sclera	Sclera	3 / 8	97.11	2.45	0.12	0.27	0.04
TS1 sclera	Sclera	3 / 9	97.39	2.00	0.08	0.40	0.13



Code V Data

Surface curvatures of all lenses were determined prior to Code V modelling by the method outlined in section 2.8. The tables below detail all information input to Code V prior to modelling and all results obtained for trilobites, brittlestars and ostracods.

Several data input terms (Table F.1 and Table F.2) require explanation:

Scale: this relates to the scale used in determining surface curvatures of the lenses. Dependant on the scale of the x and y axes on the image from which surface curvature was determined. This has no bearing on the results obtained from Code V, which in the text and the results table below are expressed as microns.

r, k, A, B and C: these are the mathematical functions used to express the surface shape. r is the radius of curvature, k is the conic constant; A, B and C are polynomial expressions.

Y-semi-A: This value is equivalent to half the diameter of the lens.

EPD: The entrance pupil diameter is, in 2-dimensions, the width along the lens aperture which light enters. In many cases, this is equal to the lens diameter. In some cases this value may be less than the diameter of the lens. This was necessary to overcome glitches in the software, which prevented the production of spot diagrams.

FOV: The field of view of the lenses is expressed as an angle 'about' the lens axis, i.e. a FOV of 18° is $\pm 9^\circ$ about the lens axis. Determined using the method outlined in section 2.8.2.2.

The ‘relative aberration’ of each system (Table F.4) refers to the aberration of the paraxial rays and is the aberration of the lens expressed as a percentage of the EPD of the lens.

The ‘receptor area’ values indicated in Table F.4 are equal to the total aberration created by the lens for all ray types; this assumes that the receptor(s) are positioned to accept all light entering the lens.

F.1 Input Data

Table F.1. - Code V data input; surface types and characteristics.

SAMPLE	SURFACE	SURFACE TYPE	SCALE (input only)	r	k	A	B	C
Phacops (PM27)	Outer surface	CONIC	um	165.40	0.0169			
	Bowl	ASPHERIC		-38.98	-1.6910	1.40E-07	1.13E-13	6.50E-18
	Lens base	SPHERE		-186.53				
Ingriops (IE48)	Outer surface	CONIC	mm	0.1533	-0.0005			
	Lens base	ASPHERIC		-0.0751	-5.0812	1.00E-07	1.66E-13	1.0E+21
	Hypothetical bowl base	SPHERE		-0.1533				
Boeckops (BB3aR)	Outer surface	CONIC	um	319.79	-0.28			
	Lens base	CONIC		-310.41	-0.52			
Geesops (G42)	Outer surface	SPHERE	mm	0.1477				
	Lens base	SPHERE		-0.1395				
Ananaspis (LB1C)	Outer surface	SPHERE	um	189.73				
	Lens base	SPHERE		-171.18				
Odontochile (OB24RB)	Outer surface	SPHERE	mm	-0.1515				
	Lens base	SPHERE		0.1217				
Paladin (Adult) (PE78)	Outer surface	SPHERE	mm	176500.00				
	Lens base	SPHERE		-0.0426				
Paladin (Juvenile) (PE92)	Outer surface	ASPHERIC	um	20.75	-0.3027	-2.40E-9	2.63E-13	
	Lens base	CONIC		-26.27	0.0264			
Symphysops (SS93)	Outer surface	SPHERE	mm	10000.0000				
	Lens base	SPHERE		-0.1219				
Telephina (T95)	Outer surface	CONIC	mm/10	-0.0116	-0.0016			
	Lens base	CONIC		0.0261	7.0024			
Carolinites (C2.6)	Outer surface	CONIC	mm	-0.0640	2.4837			
	Lens base	CONIC		0.0500	-0.6683			

SAMPLE	SURFACE	SURFACE TYPE	SCALE (input only)	r	k	A	B	C
Brittlestar (shape 1)	Epidermis	SPHERIC	mm	0.005				
	Outer surface	SPHERE		0.0256				
	Lens base	ASPHERIC		0.0000	3.3295	-5.09E-15		
Brittlestar (shape 2)	Epidermis	SPHERIC	µm x10	Infinity				
	Outer surface	CONIC		251.51	-0.2682	-2.41E-09	2.63E-12	-7.33E-19
	Lens base	ASPHERIC		188.40	0.0500	-2.81E-07	1.85E-12	2.13E-16
Ostracod	Outer surface	CONIC	um	-0.4835	112.8800			
	Lens base	CONIC		0.0666	-0.3050			
	Tapetum	CONIC		0.0666	-0.3050			

Table F.2 - Code V input data continued; surface thicknesses and apertures, and FOV angles.

SAMPLE	SURFACE	THICKNESS	Y-Semi A	EPD (MICRONS)	FOV +/- (DEGREES)
Phacops (PM27)	Outer surface	266.40	154.50	270	9.0
	Bowl	64.10			
	Lens base				
Ingriops (IE48)	Outer surface	0.1773	0.1475	250	4.4
	Lens base	0.0700			
	Hypothetical bowl base				
Boeckops (BB3aR)	Outer surface	369.1	264.5	500	10 (E)
	Lens base				
Geesops (G42)	Outer surface	0.1778	0.1000	200	2.8
	Lens base				
Ananaspis (LB1C)	Outer surface	186.40	244.10	250	8.6
	Lens base				
Odontochile (OB24RB)	Outer surface	0.1339	0.0807	150	2.0
	Lens base				
Paladin (Adult) (PE78)	Outer surface	0.0764	0.3830	60	3.1
	Lens base				
Paladin (Juvenile) (PE92)	Outer surface	42.2300	23.27	40	1.2
	Lens base				
Symphysops (SS93)	Outer surface	0.1431	0.7270	175	4.2
	Lens base				

SAMPLE	SURFACE	THICKNESS	Y-Semi A	EPD (MICRONS)	FOV +/- (DEGREES)
Telephina (T95)	Outer surface	0.0084	0.0084	170	6.7
	Lens base				
Carolinites (C2.6)	Outer surface	0.0625	0.0304	60	3.0
	Lens base				
Brittlestar (shape 1)	Epidermis	0.0050	0.0235	40	5.0
	Outer surface	0.0305			
	Lens base				
Brittlestar (shape 2)	Epidermis	50.00	174.10	35	5.0
	Outer surface	297.80			
	Lens base				
Ostracod	Outer surface	0.0452	0.0425	85	2.0
	Lens base				
	Tapetum				

F.2 Results

Table F.3 - Code V modelling results; back and effective focal lengths and F-numbers.

GENUS	RAY TYPE	LENS	BOWL	BFL (μm)	EFL (μm)	F-NUMBER
Phacops (PM27)	Ordinary	LMC	-	162	328	1.21
	Ordinary	HMC	-	420	586	2.17
	Ordinary	LMC	HMC	173	339	1.26
	Extraordinary	LMC	HMC	333	499	1.85
	Ord-Ext	LMC	HMC	114	280	1.04
	Ext-Ord	LMC	HMC	267	433	1.60
	Ordinary	HMC	LMC	163	329	1.22
	Extraordinary	HMC	LMC	425	591	2.19
	Ord-Ext	HMC	LMC	121	287	1.06
	Ext-Ord	HMC	LMC	256	422	1.56
Ingriops (IE48)	Paraxial	LMC		200	247	0.99
	Ordinary	LMC		197	244	0.97
	Ordinary	HMC		189	236	0.94
	Ord-Ext	LMC	HMC	40	167	0.67
Boeckops (BB3aR)	Ordinary	LMC		346	512	1.02
	Ordinary	HMC		339	505	1.02
Geesops (G40)	Ordinary	LMC		168	233	1.17
	Ordinary	HMC		164	230	1.15

GENUS	RAY TYPE	LENS	BOWL	BFL (μm)	EFL (μm)	F-NUMBER
Ananaspis (LB1C)	Ordinary	LMC		202	275	1.10
	Ordinary	HMC		192	266	1.06
Odontochile (OB24RB)	Ordinary	LMC		201	216	1.44
	Ordinary	HMC		195	209	1.39
Paladin ADULT (PE78)	Ordinary	LMC		115	115	1.92
	Extraordinary	LMC		191	191	2.94
	Paraxial	LMC		117	117	1.95
Paladin JUVENILE (PE92)	Ordinary	LMC		24	45	1.14
	Extraordinary	LMC		23	45	1.13
	Paraxial	LMC		24	46	1.14
Carolinites (C2.6)	Ordinary	LMC		69	91	1.52
	Extraordinary	LMC		126	149	2.48
	Paraxial	LMC		71	94	1.57
Symphysops (SS93)	Ordinary	LMC		309	309	2.13
	Extraordinary	LMC		584	584	4.03
	Paraxial	LMC		324	324	2.23
Telephina (T95)	Ordinary	LMC		219	223	1.33
	Extraordinary	LMC		392	396	2.36
	Paraxial	LMC		223	227	1.35
Brittlestar (shape 1)	Paraxial	HMC		14	29	0.74
	Extraordinary	HMC		52	68	1.69
Brittlestar (shape 1) with epidermis	Paraxial	HMC		19	35	0.88
	Extraordinary	HMC		76	92	2.33
Brittlestar (shape 2)	Paraxial	HMC		17	27	0.79
	Extraordinary	HMC		45	56	1.60
Brittlestar (shape 2) with epidermis	Paraxial	HMC		22	33	0.93
	Extraordinary	HMC		52	63	1.80
Ostracod	Paraxial	LMC		168	179	2.10
	Extraordinary	LMC		305	316	3.71
	Ordinary	LMC		168	179	2.10
with tapetum	Ordinary	LMC		75	85	1.00

Table F.4 - Code V modelling results continued; aberration values and approximate receptor areas.

GENUS	RAY TYPE	LENS	BOWL	CENTRAL ABERRATION (RMS)	RELATIVE ABERRATION (%)	RECEPTOR AREA
Phacops (PM27)	Ordinary	LMC		40	15	132
	Ordinary	HMC		22	8	178

GENUS	RAY TYPE	LENS	BOWL	CENTRAL ABERRATION (RMS)	RELATIVE ABERRATION (%)	RECEPTOR AREA
	Ordinary	LMC	HMC	18	7	123
	Extraordinary	LMC	HMC	10	4	188
	Ord-Ext	LMC	HMC	1	0	143
	Ext-Ord	LMC	HMC	62	23	205
	Ordinary	HMC	LMC	16	6	133
	Extraordinary	HMC	LMC	32	12	215
	Ord-Ext	HMC	LMC	3	1	126
	Ext-Ord	HMC	LMC	85	31	234
Ingriops (IE48)	Paraxial	LMC		56	22	24
	Ordinary	LMC		54	22	114
	Ordinary	HMC		57	23	109
	Ord-Ext	LMC	HMC	11	5	28
Boeckops (BB3aR)	Ordinary	LMC		93	19	237
	Ordinary	HMC		92	19	250
Geesops (G40)	Ordinary	LMC		16	8	99
	Ordinary	HMC		16	8	103
Anaspis (LB1C)	Ordinary	LMC		50	20	120
	Ordinary	HMC		49	20	142
Odontochile (OB24RB)	Ordinary	LMC		13	9	54
	Ordinary	HMC		13	9	58
Paladin ADULT (PE78)	Ordinary	LMC		24	40	50
	Extraordinary	LMC		29	45	53
	Paraxial	LMC		25	41	25
Paladin JUVENILE (PE92)	Ordinary	LMC		9	21	17
	Extraordinary	LMC		9	22	17
	Paraxial	LMC		9	22	9
Carolinites (C2.6)	Ordinary	LMC		5	9	40
	Extraordinary	LMC		5	9	58
	Paraxial	LMC		6	9	6
Symphysops (SS93)	Ordinary	LMC		22	13	193
	Extraordinary	LMC		6	3	178
	Paraxial	LMC		18	11	18
Telephina (T95)	Ordinary	LMC		8	4	105
	Extraordinary	LMC		7	4	120
	Paraxial	LMC		8	4	8
Brittlestar (shape 1)	Paraxial	HMC		2	5	2
	Extraordinary	HMC		5	13	21
Brittlestar (shape 1) with epidermis	Paraxial	HMC		4	11	7
	Extraordinary	HMC		17	34	30

GENUS	RAY TYPE	LENS	BOWL	CENTRAL ABERRATION (RMS)	RELATIVE ABERRATION (%)	RECEPTOR AREA
Brittlestar (shape 2)	Paraxial	HMC		5	14	5
	Extraordinary	HMC		13	36	12
Brittlestar (shape 1) with epidermis	Paraxial	HMC		7	21	17
	Extraordinary	HMC		15	43	32
Ostracod	Paraxial	LMC		9	10	9
	Extraordinary	LMC		7	8	47
	Ordinary	LMC		9	10	39
with tapetum	Ordinary	LMC		4	5	12